ISSN 1580-3155 Pages 1–250 ■ Year 2022, Vol. 69, No. 1

Slovensko kemijsko društvo
Slovenian Chemical Society

Acta Chimica Slovenica

1

69/2022

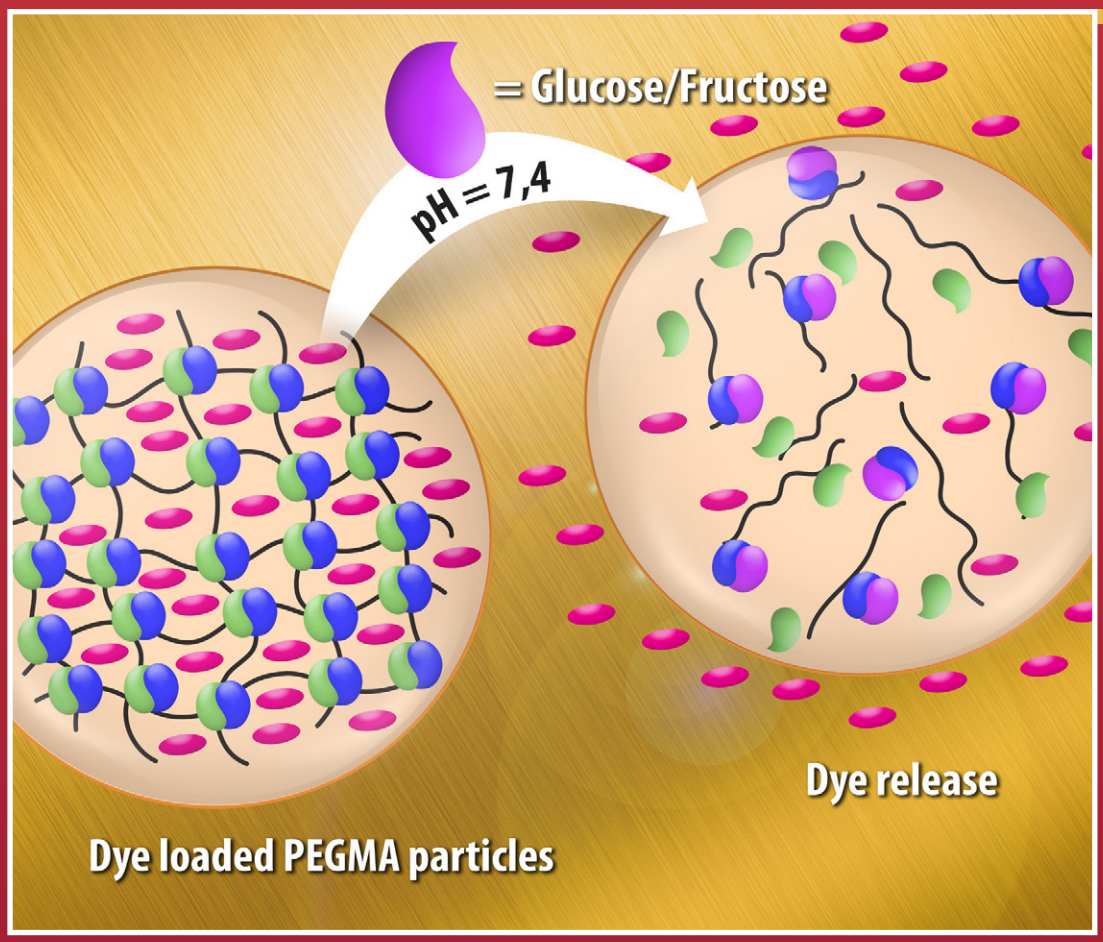

http://acta.chem-soc.si

EDITOR-IN-CHIEF

KSENIJA KOGEJ
University of Ljubjana, Facuty of Chemstry and Chemical Technology, Večna pot 113, SI-1000 Ljubljana, Slovenija
E-mail: ACSi@fkkt.uni-lj.si, Telephone: (+386)-1-479-8538

ASSOCIATE EDITORS

Alen Albreht, *National Institute of Chemistry, Slovenia*
Aleš Berlec, *Jožef Stefan Institute, Slovenia*
Janez Cerkovnik, *University of Ljubljana, Slovenia*
Mirela Dragomir, *Jožef Stefan Institute, Slovenia*
Ksenija Kogej, *University of Ljubljana, Slovenia*
Krištof Kranjc, *University of Ljubljana, Slovenia*
Matjaž Kristl, *University of Maribor, Slovenia*
Franc Perdih, *University of Ljubljana, Slovenia*
Aleš Ručigaj, *University of Ljubljana, Slovenia*
Helena Prosen, *University of Ljubljana, Slovenia*
Irena Vovk, *National Institute of Chemistry, Slovenia*

ADMINISTRATIVE ASSISTANT

Marjana Gantar Albreht, *National Institute of Chemistry, Slovenia*

EDITORIAL BOARD

Wolfgang Buchberger, *Johannes Kepler University, Austria*
Alojz Demšar, *University of Ljubljana, Slovenia*
Stanislav Gobec, *University of Ljubljana, Slovenia*
Marko Goličnik, *University of Ljubljana, Slovenia*
Günter Grampp, *Graz University of Technology, Austria*
Wojciech Grochala, *University of Warsaw, Poland*
Danijel Kikelj, *University of Ljubljana*
Janez Košmrlj, *University of Ljubljana, Slovenia*
Blaž Likozar, *National Institute of Chemistry, Slovenia*
Mahesh K. Lakshman, *The City College and The City University of New York, USA*
Janez Mavri, *National Institute of Chemistry, Slovenia*
Friedrich Srienc, *University of Minnesota, USA*
Walter Steiner, *Graz University of Technology, Austria*
Jurij Svete, *University of Ljubljana, Slovenia*
David Šarlah, *University of Illinois at Urbana-Champaign, USA; Università degli Studi di Pavia, Italy*
Ivan Švancara, *University of Pardubice, Czech Republic*
Jiri Pinkas, *Masaryk University Brno, Czech Republic*
Gašper Tavčar, *Jožef Stefan Institute, Slovenia*
Ennio Zangrando, *University of Trieste, Italy*

ADVISORY EDITORIAL BOARD

Chairman
Branko Stanovnik, Slovenia

Members
Udo A. Th. Brinkman, The Netherlands
Attilio Cesaro, Italy
Vida Hudnik, Slovenia
Venčeslav Kaučič, Slovenia
Željko Knez, Slovenia
Radovan Komel, Slovenia
Stane Pejovnik, Slovenia
Anton Perdih, Slovenia
Slavko Pečar, Slovenia
Andrej Petrič, Slovenia
Boris Pihlar, Slovenia
Milan Randić, Des Moines, USA
Jože Škerjanc, Slovenia
Đurđa Vasić-Rački, Croatia
Marjan Veber, Slovenia
Gorazd Vesnaver, Slovenia
Jure Zupan, Slovenia
Boris Žemva, Slovenia
Majda Žigon, Slovenia

Acta Chimica Slovenica is indexed in: *Academic Search Complete, Central & Eastern European Academic Source, Chemical Abstracts Plus, Chemical Engineering Collection (India), Chemistry Citation Index Expanded, Current Contents (Physical, Chemical and Earth Sciences), Digitalna knjižnica Slovenije (dLib.si), DOAJ, ISI Alerting Services, PubMed, Science Citation Index Expanded, SciFinder (CAS), Scopus and Web of Science.* Impact factor for 2020 is IF = 1.735.

Articles in this journal are published under the Creative Commons Attribution 4.0 International License

Izdaja – Published by:
SLOVENSKO KEMIJSKO DRUŠTVO – SLOVENIAN CHEMICAL SOCIETY
Naslov redakcije in uprave – Address of the Editorial Board and Administration
Hajdrihova 19, SI-1000 Ljubljana, Slovenija
Tel.: (+386)-1-476-0252; Fax: (+386)-1-476-0300; E-mail: chem.soc@ki.si

Izdajanje sofinancirajo – Financially supported by:
National Institute of Chemistry, Ljubljana, Slovenia
Jožef Stefan Institute, Ljubljana, Slovenia
Faculty of Chemistry and Chemical Technology, University of Ljubljana, Slovenia
Faculty of Chemistry and Chemical Engineering, University of Maribor, Slovenia

Acta Chimica Slovenica izhaja štirikrat letno v elektronski obliki na spletni strani http://*acta.chem-soc.si*. V primeru posvečenih številk izhaja revija tudi v tiskani obliki v omejenem številu izvodov.

Acta Chimica Slovenica appears quarterly in electronic form on the web site *http://acta.chem-soc.si*. In case of dedicated issues, a limited number of printed copies are issued as well.

Transakcijski račun: 02053-0013322846 Bank Account No.: SI56020530013322846-Nova Ljubljanska banka d. d., Trg republike 2, SI-1520 Ljubljana, Slovenia, SWIFT Code: LJBA SI 2X

Oblikovanje ovitka – Design cover: KULT, oblikovalski studio, Simon KAJTNA, s. p. Grafična priprava za tisk: OSITO, Laura Jankovič, s.p.

Graphical Contents

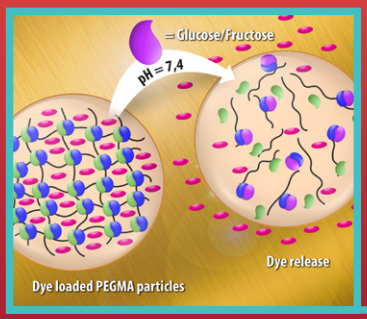

Acta Chimica Slovenica
Year 2022, Vol. 69, No. 1

SCIENTIFIC PAPER

1–12 Analytical chemistry

Fabrication of Zirconium Silicate Reinforced Superhydrophobic Coating for the Evaluation of Corrosion-Resistance

Mubarak Ali Muhamath Basha and Sathiya Srinivasan

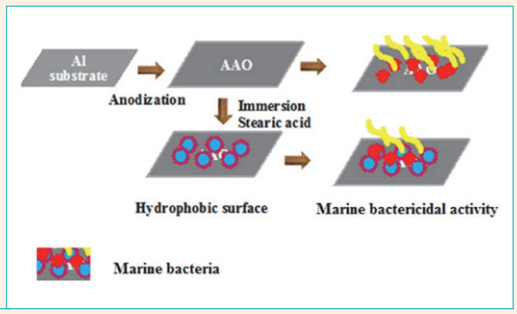

13–29 Organic chemistry

Synthesis of Fused Quinoline Derivatives with Antiproliferative Activities and Tyrosine Kinases, Pim-1 Kinase Inhibitions

Rafat Milad Mohareb, Rehab Ali Ibrahim, Amira Mohamed Elmetwally and Marwa Soliman Gamaan

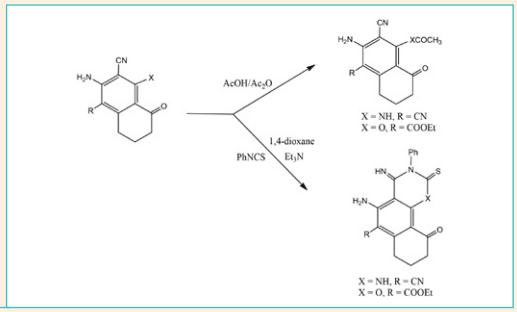

30–38 Organic chemistry

Glucose-Decorated Silica-Molybdate Complex: A Novel Catalyst for Facile Synthesis of Pyrano[2,3-d]-Pyrimidine Derivatives

Arezoo Pourkazemi, Negin Asaadi, Mahnaz Farahi, Ali Zarnegaryan and Bahador Karami

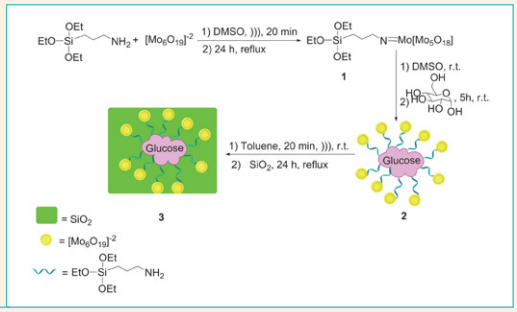

39–48 Organic chemistry

Synthesis of Glucose/Fructose Sensitive Poly(ethylene glycol) Methyl Ether Methacrylate Particles with Novel Boronate Ester Bridge Crosslinker and their Dye Release Applications

Şeküre Yildirim, Hasan Akyildiz and Zeynep Çetinkaya

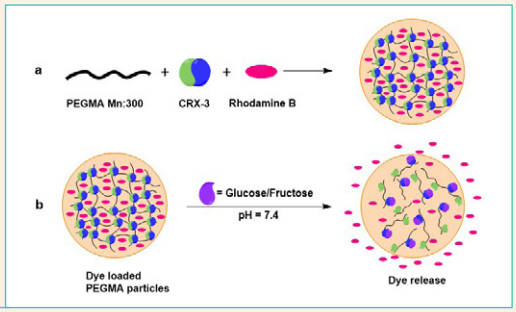

49–59 Analytical chemistry

Proposal of an HPLC/UV/FLD Screening Method for the Simultaneous Determination of Ten Antibiotics in Environmental Waters

Idalia Francisca Carmona-Alvarado, María de la Luz Salazar-Cavazos, Noemí Waksman de Torres, Aurora de Jesús Garza-Juárez, Lidia Naccha-Torres, Jose Francisco Islas and Norma Cavazos-Rocha

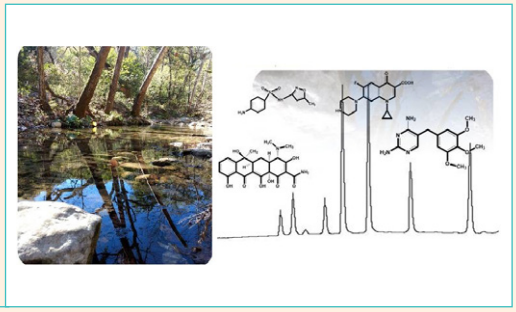

60–72 General chemistry

The Effect of Heuristics on the Reasoning of the Pre-Service Science Teachers on the Topic of Melting and Boiling Point

Gülen Önal Karakoyun and Erol Asiltürk

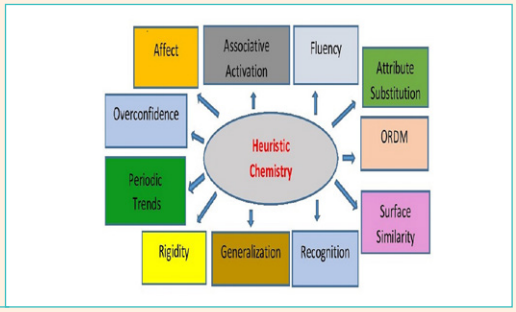

73–80 Organic chemistry

Synthesis of the New 1-(7-Methoxy-1-benzofuran-2-yl)-3-(4-methylphenyl)prop-2-en-1-one and Controlling of Spectroscopic, Optical and Conductivity Properties by Concentration

Demet Coskun, Mehmet Fatih Coskun and Bayram Gunduz

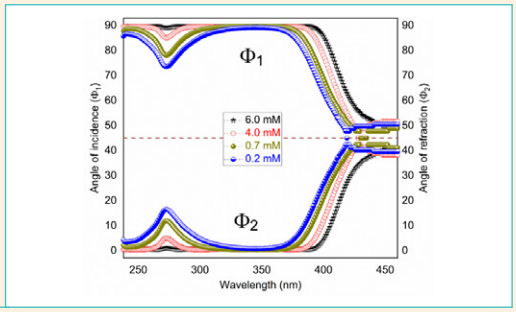

81–90 Biochemistry and molecular biology

Effects of Individual and Co-exposure of Copper Oxide Nanoparticles and Copper Sulphate on Nile Tilapia *Oreochromis niloticus*: Nanoparticles Enhance Pesticide Biochemical Toxicity

Özgür Fırat, Rabia Erol and Özge Fırat

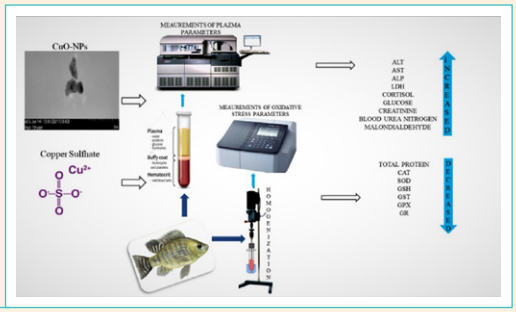

91–97 Organic chemistry

A Facile Synthesis of Bioactive Five- and Six-membered *N*-heterocyclic Aromatic Compounds Using $AlCoFe_2O_4$ as a Green Catalyst

Fatemeh Mostaghni, Homa Shafiekhani and Nosrat Madadi Mahani

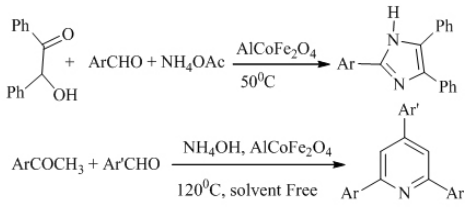

98–107 Applied chemistry

Synthesis and Application of Silica Supported Calix[4] arene Derivative as a New Processing Aid Agent for Reducing Hysteresis of Tread Rubber Compounds Used in Low Rolling Resistance Tires

Seyedeh Nazanin Sadat-Mansouri, Nasrin Hamrahjou, Saeed Taghvaei-Ganjali and Reza Zadmard

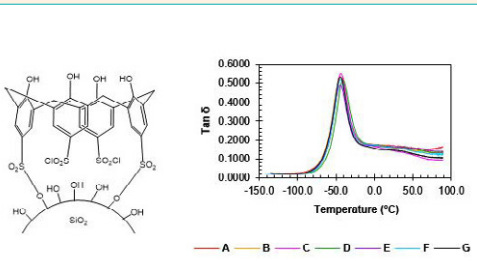

108–115 Analytical chemistry

A Novel Solid-State PVC-Membrane Potentiometric Dopamine-Selective Sensor Based on Molecular Imprinted Polymer

Nurşen Dere, Zuhal Yolcu and Murat Yolcu

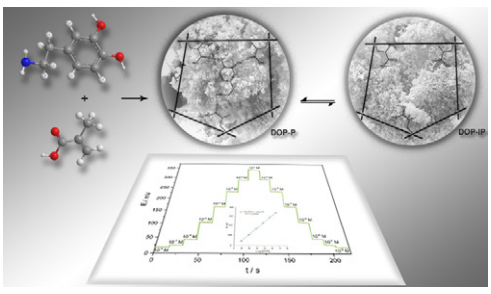

116–124 Organic chemistry

Combustion Synthesis of Nano Fe_2O_3 and its Utilization as a Catalyst for the Synthesis of N^{α}-Protected Acyl Thioureas and Study of Anti-bacterial Activities

Raghavendra Mahadevaiah, Lalithamba Haraluru Shankraiah and Latha Haraluru Kamalamma Eshwaraiah

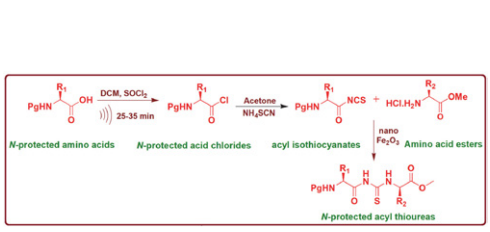

125–132 Analytical chemistry

Acetyl Cellulose Film with 18-crown-6 Ether for Colorimetric Phosgene Detection

Martin Lobotka, Vladimír Pitschmann and Zbyněk Kobliha

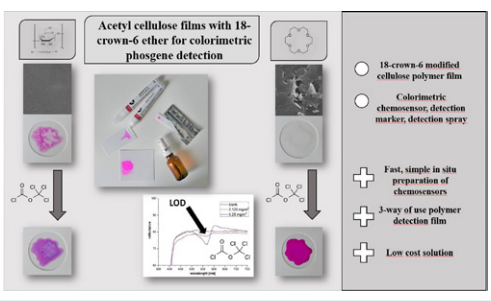

133–146 Inorganic chemistry

Modulation of Cerium Carbonate Crystal Growth by Polyvinylpyrrolidone using Density Functional Theory

Deyun Sun, Yanhong Hu, Mao Tang, Ze Hu, Peng Liu, Zhaogang Liu and Jinxiu Wu

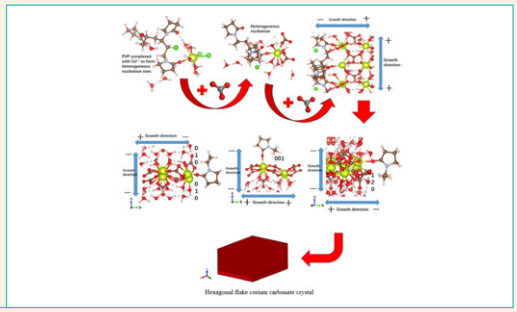

147–156 Inorganic chemistry

Synthesis, Structure, Thermal Decomposition and Computational Calculation of Heterodinuclear Ni^{II} – Zn^{II} Complexes

Yaprak Gürsoy Tuncer, Hasan Nazır, Kübra Gürpınar, Ingrid Svoboda, Nurdane Yılmaz, Orhan Atakol and Emine Kübra İnal

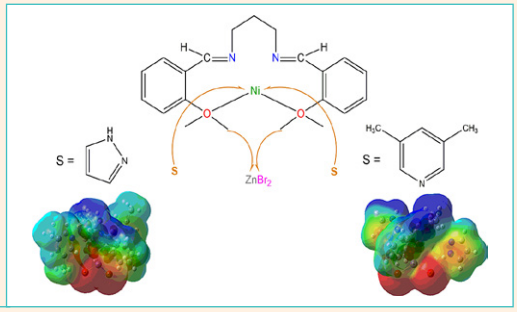

157–166 Inorganic chemistry

Synthesis, Characterization, X-Ray Crystal Structures and Antibacterial Activity of Zinc(II) and Vanadium(V) Complexes Derived from 5-Bromo-2-((2-(methylamino) ethylimino)methyl)phenol

Cheng Liu

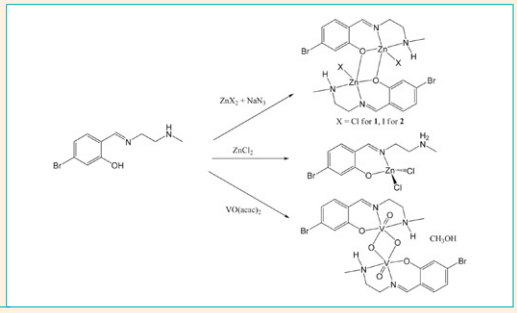

167–186 Chemical education

The Students' Perceptions Using *3DChemMol* Molecular Editor for Construction and Editing of Molecular Models

Danica Dolničar, Bojana Boh Podgornik and Vesna Ferk Savec

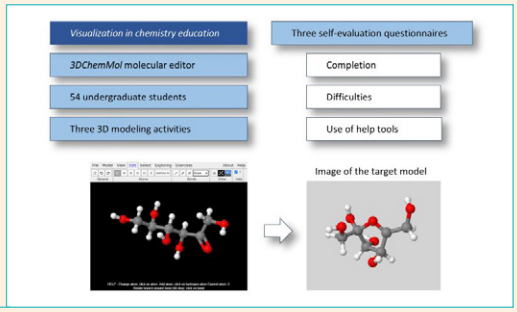

187–199 Organic chemistry

Synthesis of New Regioisomers of 5-Nitro-1,4-Naphthoquinone, Evaluation of Antioxidant and Catalase Inhibition Activities

Aesha F. SH. Abdassalam, Nahide Gulsah Deniz, Cigdem Sayil, Mustafa Ozyurek, Emin Ahmet Yesil and Huseyin Salihoglu

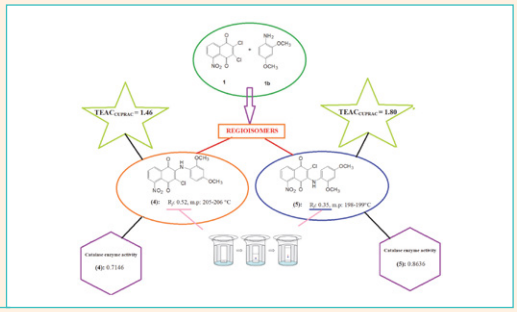

200–216 Inorganic chemistry

Metal Based Bioactive Nitrogen and Oxygen Donor Mono and Bis Schiff Bases: Design, Synthesis, Spectral Characterization, Computational Analysis and Antibacterial Screening

Sajjad Hussain Sumrra, Wardha Zafar, Sabaahatul Ain Malik, Khalid Mahmood, Syed Salman Shafqat and Saira Arif

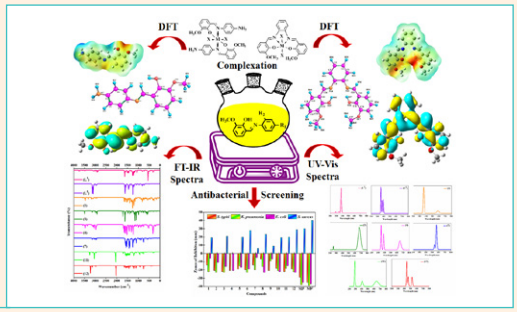

217–226 Materials science

Metal and Non-Metal Modified Titania: the Effect of Phase Composition and Surface Area on Photocatalytic Activity

Boštjan Žener, Lev Matoh, Martin Reli, Andrijana Sever Škapin and Romana Cerc Korošec

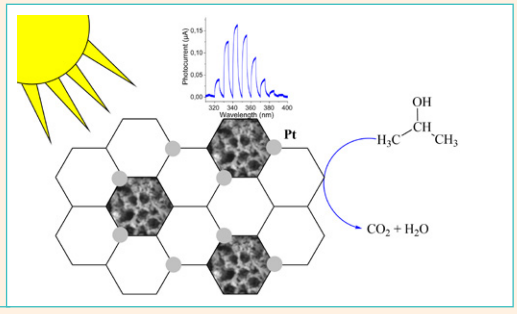

227–234 General chemistry

Synthesis, Crystal Structure and Separation Performance of *p-tert*-butyl(tetradecyloxy)calix[6]arene

Wei Zhang, Zhi-qiang Cai, Xiao-min Shuai, Wei Li, Qiu-chen Huang, Ruo-nan Chen, Qi-qi Zang, Fei-fei Li and Tao Sun

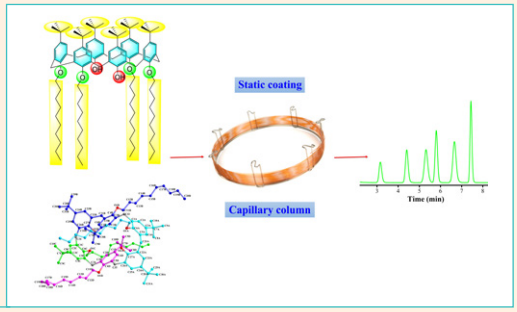

235–242 Inorganic chemistry

Two Oxidovanadium(V) Complexes with Hydrazone Ligands: Synthesis, Crystal Structures and Catalytic Oxidation Property

Yan Lei

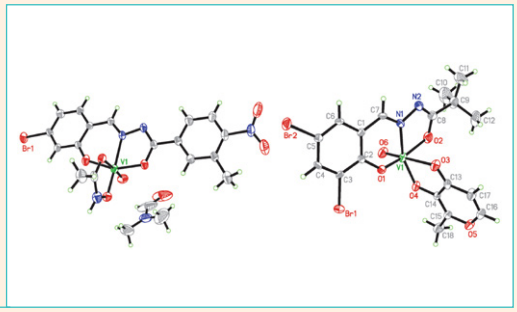

243–250 Organic chemistry

Crystallography and DFT Studies of Synthesized Tetraketones

Elma Veljović, Krešimir Molčanov, Mirsada Salihović, Una Glamočlija, Amar Osmanović, Nevzeta Ljubijankić and Selma Špirtović-Halilović

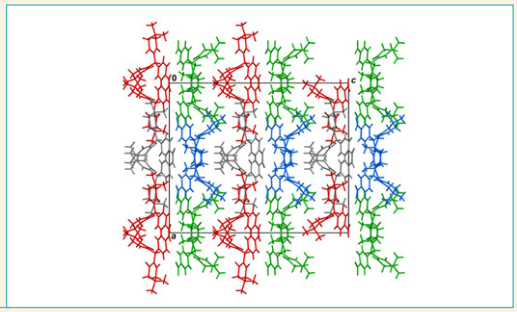

Scientific paper

Fabrication of Zirconium Silicate Reinforced Superhydrophobic Coating for the Evaluation of Corrosion-Resistance

Mubarak Ali Muhamath Basha[1,*] and Sathiya Srinivasan[1]

Department of Chemistry, Chikkaiah Naicker College, Erode-638004. Tamilnadu, India

** Corresponding author: E-mail: mubarakscience@gmail.com*

Received: 07-19-2021

Abstract

The present work investigates on anodisation of aluminium in 1.0 M sodium oxalate and methodically evaluates the influence of zirconium silicate as an additive. The effect of additive upon structure, morphology, micro hardness and composition of the coating formed under various anodising conditions has been examined comprehensively. The surface of the coating was modified by stearic acid and its immersion time was optimized. The dependence of surface morphology, kinetic parameters, and microstructural characteristics of the coating on electrolyte /additive concentration, anodising time, and the temperature has also been inspected. X-ray diffraction (XRD), Scanning Electron Microscopy (SEM) combined with EDAX studies indicates the beneficial role of zirconium silicate towards the formation of crystalline coating with improved corrosion-resistant characteristics. The static water contact angle on the surface-modified coatings was 122° ± 0.4°. This contact angle of super hydrophobic coating has been improved by KOH treatment (152.76° ± 0.4°) which is obtained under optimized conditions exhibit the corrosion resistance ($1.68 \times 10^8\ \Omega\ cm^{-1}$) which is nearly 8 times higher than that of bare aluminium ($8.36 \times 10^1\ \Omega\ cm^{-1}$). The efficacies of the surface-modified coatings against bacteria that are commonly encountered in marine (Desulfovibrio desulfuricans) and medical applications (Staphylococcus aureus and Escherichia coli) are also demonstrated.

Keywords: Anodisation; aluminium; sodium oxalate; corrosion resistance.

1. Introduction

Aluminium is selected for their optimal combination of physical and mechanical properties.[1] Another benefit, which may be just as significant from an environmental standpoint, is that aluminium components may be recycled with relatively little energy use.[2] In damp environments, however, this thin layer is reactive and susceptible to corrosion and contamination.[3] Anodisation of aluminium is a well-established and easy method in comparison with micro-arc discharge oxidation (MDO), gas flame spray, plasma thermal spray, physical vapour deposition, and high-temperature glass enamelling methods to progress the applicability of aluminium.[4–5] Since, anodisation is an electrochemical process, its conditions (voltage, time, temperature) and composition of electrolytes together, play a central role in the characteristics of the coating.

In this connection, numerous investigations devoted to exploring the relationship between the composition of the electrolytes (e.g., sulfuric acid, chromic acid, phosphoric acid, or oxalic acid) and anodic behaviour of aluminium. However, because the acid molecules confined within the holes may cause more corrosion, the porous type oxide layer is not desirable for corrosion prevention.[6] To resolve this issue, the weak electrolytes are preferred. To enhance further the corrosion resistance, abrasion resistance, and electrical insulation of the oxide coating and to increase the coating thickness, additive salts have been added into the electrolytic solution as investigated by numerous studies.[7–9] Scarcely, reports are available upon the use of zirconium silicate as an additive for anodisation of aluminium, except for our earlier study on aluminium anodisation with Lithium sulphate-zirconium silicate bath, [10] which illustrated that significant enhancement in corrosion protection and micro hardness behaviour of nanocomposite coatings.

Super hydrophobicity, found on many natural surfaces, the most classic example being the lotus leaf, has inspired researchers around the world for its unique charac-

teristics such as self-cleaning,[11] water repellence,[12] anti-icing,[13] anti-corrosion,[14] and oil-water separation.[15] The presence of a low energy layer over a rough hierarchical structure is crucial for constructing a hydrophobic surface.[16] So far, a large number of approaches have been successfully used to develop superhydrophobic surfaces, including chemical vapour deposition,[17] chemical etching,[18] sol-gel,[19] solution immersion,[20] hydrothermal synthesis,[21] and laser fabrication,[22] etc., Anodisation is an effective technique to fine-tune the surface morphology trough constructing superhydrophobic surface.[23] Preparation of the superhydrophobic surface of the aluminium substrate by anodisation in phosphoric acid followed by low-temperature plasma treatment is reported.[24] Investigation about a superhydrophobic surface on aluminium alloy via anodising in an electrolyte consisting of sulfuric acid, oxalic acid, and sodium chloride, followed by polypropylene coating is also attempted successfully.[25] Heretofore, researchers coated an anodized aluminium alloy surface with RF-sputtered polytetrafluoroethylene to generate a superhydrophobic surface.[26] In terms of real-world applications, fabricating hydrophobic aluminium alloy surfaces with superior corrosion resistance and chemical stability is critical.[27]

In this regard, herein we report the anodic behaviour of aluminium in the presence and absence of a zirconium silicate additive using sodium oxalate as an electrolyte. The parameters such as the concentration of the electrolyte/additive, voltage, temperature, etc., were studied to establish the correlation with growth kinetic parameters namely thickness and growth rate. The anodic coating formed which was immersed in stearic acid for surface modification and the immersion time was varied for optimization. We have also studied the mechanical properties, microstructural characterisation, chemical composition, and electrochemical corrosion behaviour of the coating which is prepared with and without the addition of zirconium silicate additive in non-conventional weak electrolyte namely sodium oxalate followed by surface modification of anodic coating. Further, we have also carried out the corrosion behaviour of anodic layer and surface modified anodic layer formed under various experimental conditions are determined by Tafel polarization and electrochemical impedance spectroscopy (EIS) analyses.

2. Experimental Methods

2. 1. Materials

Sodium oxalate, zirconium silicate, sulphuric acid, sodium chloride, chromic acid, phosphoric acid, per chloric acid, ethanol, stearic acid, and acetone were purchased from Aldrich chemicals (Aldrich, India). All of the chemicals used were analytical grade and were used as received. Deionized water was used in all of the studies.

2. 2. Preparation of Anodic Coating

High purity aluminium (99.999% pure, AL104, Mettler-Toledo International. Inc.) The plate of thickness 0.5 mm was used for this investigation. Surface pre-treatment is a successive step involved in the process of anodisation. The surface pre-treatment process was accomplished by following the procedure reported elsewhere.[28] Aluminium was cleaned and degreased with the use of ultrasonicator by using acetone, water and ethanol as a medium. The surface cleaned aluminium samples were subjected to the thermal annealing process at 450 °C for 30 min.

The etching process is performed by immersing the samples in 5% sodium hydroxide for 2 min at room temperature (35° ± 1 °C) to cast off the native oxide layer. The resulted aluminium samples were subjected to electro polishing in a mixture consists of perchloricacid:ethanol (1: 3) under an applied voltage of 20 V, which is maintained for 3 min. The pre-treated samples thus obtained were used for anodising studies in a two-electrode configuration using a direct current power supply (Aplab Model: 05 A/30 V and 0–1 A/120 V) and we determined the weight of every specimen. Graphite sheet is used as a cathode and the sample to be anodised acts as an anode in an electrolytic bath comprising 1.0 M sodium oxalate with and without zirconium silicate additive. The anodised coatings obtained from the bath containing zirconium silicate concentration of 0, 0.1 g/L, 0.2 g/L, 0.3 g/L to 0.4 g/L are designated as SO, Zr1, Zr2, Zr3 and Zr4 respectively. Anodised specimens were cleaned with de-ionized water pursued by drying in the N_2 atmosphere and their weight is determined. 1 cm^2 working surface is used for the study and the rest of the surface was insulated using an epoxy resin. All the experimental studies were carried out in aerated and stirred conditions. These experiments were repeated in triplicate to acquire accurate results. The anodic coating formed under an optimized condition was immersed in stearic acid for surface modification at various time intervals such as 15 and 30 min. These two samples are designated as SA1 and SA2. The steps involved in the process is schematically depicted in Scheme S1.

2. 3. Characterisation of Anodic Coating

The crystalline nature of the coating was examined using a Philips X-Pert X-ray Diffractometer (XRD) with the use of CuKa radiation of wavelength, λ = 1.54 Å with Step Size [° 2θ] 0.0300. Scanning Electron Microscope (SEM, FEI - QUANTA-FEG 250, Japan) is used to examine the surface morphologies of the coating. Field emission scanning electron microscope and energy-dispersive X-ray spectroscopic studies were carried out to analyse the microstructure and elemental composition of the coatings. Vickers micro hardness indenter is used to quantify the micro hardness of the specimen. (Tester MH6, USA). Thickness tester (Touchstone1) is employed for measuring the coating thickness non-destructively. Contact Angle associated with SA1 and SA2 surfaces was measured with a

contact angle measuring system (OCA20, Data physics Corporation, Germany) under ambient temperature. All the measurements were conducted at five positions on each sample with 4 μL DI water droplets. To evaluate the durability of the Zr3, SA1 and SA2 samples, the influences of exposure to air at room temperature (35º ± 1 ºC) were systematically investigated.

2. 4. Preparation of Superhydrophobic Coating

To examine the corrosion resistance of the superhydrophobic coatings were carried out for optimized Zr3 (Zirconium silicate), SA1 (stearic acid) and SA2 (stearic acid & KOH) samples for comparison. The SA1 was prepared by using the Zr3 sample immersed in stearic acid 3g/L for 15 min. To further enhance the super hydrophobicity, KOH treatment was applied to prepare by using the SA1 immersed in stearic acid 10 g/L KOH for 30 min (SA2).

2. 5. Evaluation of Corrosion Resistance

Tafel polarisation investigations and electrochemical impedance spectroscopy (EIS) in 3.5 percent NaCl (using an electrochemical workstation (600TM Potentiostat/ Galvanostat, Inc.) are used to examine the coatings' electrochemical corrosion behaviour. These studies were executed in the three-electrode configuration that consists of Ag/AgCl/saturated KCl as a reference electrode, a platinum wire as a counter electrode, and aluminium as a working electrode. Fully aerated conditions are maintained during the experiments. Tafel polarisation studies were performed by applying potential in the range of +2 V to –2 V with a scan rate of 1 mV/s. Using the method of extrapolation of anodic and cathodic sections, current density associated with corrosion (I_{corr}) and the resistance offered for charge transfer reaction (R_P) is determined and tabulated as shown in Table. 1. R_p is determined with the use of Stern-Geary equation as follows,[29]

$$R_P = \frac{b_a b_c}{2.303\, I_{corr}\,(b_a + b_c)} \quad (1)$$

Where in I_{corr} signifies corrosion current density, cathodic/anodic Tafel constants as (b_a and b_c). I_{corr} and E_{corr} are obtained from the intercept of Tafel slopes. EIS plots are recorded at frequencies between 100 kHz and 0.01 Hz with 12 points per decade. The amplitude of the sinusoidal potential signal was set as 5 mV. The impedance spectra obtained were analysed by fitting with an appropriate Randel's equivalent circuit.

2. 6. Marine Bacterial Studies

The marine bacteria used in this study were the sulphate reducing strains of Desulfovibrio desulfuricans (ATCC#14563). The bacterium was cultured at 37 °C in a modified Postgate's C medium used for enrichment culture, which contained 35 g NaCl, 0.5 g KH_2PO_4, 0.06 g $CaCl_2$ $2H_2O$, 2 g $MgSO_4$ $7H_2O$, 1 g yeast extract, 0.004 g $FeSO_4$ $7H_2O$, and 0.3 g sodium citrate in 1 L deionized water. The medium was autoclaved at 121°C and 20 psi for 15 min.[30–31] after the stipulated period (7 days), the SA1 and SA2 were washed twice with phosphate-buffered saline (19 PBS, pH 7.4). The cells were detected by live/dead staining. 200 mL of dye mixture (100 mL acridine orange, green fluorescence in live cells, and 100 mL ethidium bromide, red fluorescence in dead cells in distilled water) was mixed with 2 mL cell suspension in a well plate. The suspension was studied right away using an Olympus Ti-Eclipse inverted fluorescence microscope to record the data under the magnification of 400 x of the instrument.

3. Results and Discussion

3. 1. Anodising Process Optimization Studies

A methodical comprehensive evaluation of the influence of the composition of the additive into the electrolyte, period of anodisation process, and anodising temperature upon morphology and kinetics of the coating has been carried out to comprehend the fundamental mechanism behind the formation of the highly corrosion-resistive layer. To recognize the role of additive towards tuning the microstructural features, morphology, micro-hardness, and corrosion resistance of the coating was carried out in sodium oxalate in the presence and absence of zirconium silicate. The optimal concentration of sodium oxalate was kept as 1.0 M.

3. 1. 1. Effect of Zirconium Silicate Concentration Additive

The formation and properties of the coating are greatly manipulated by the concentration of zirconium silicate as illustrated by Fig S1a, wherein the concentration of zirconium silicate is varied from 0.1 g/L to 0.4 g/L in 1.0 M sodium oxalate at constant voltage of 55 V and temperature (35° ± 1° C). This behavior could be explained due to the existence of two competing reactions, namely oxide coating growth and its dissolution. Based on an earlier study, a sequence of reactions occurs during the anodisation process together with the combination of metal ions with OH and SiO_3 to form Al $(OH)_3$ and Al_2 $(SiO_3)_3$. In the current report, the presence of zirconium silicate (0.3 g/L) leads to develop the coating with a high thickness (82 μm).

The coating obtained using sodium oxalate without additive results in poor growth performance (thickness: 70 μm; growth rate: 0.9 μm/min). From Fig. S1a, it is intended that the zirconium silicate concentration directly impacts the thickness (growth rate: 1.2 μm/min) of the coating.

Therefore, to throw the light about the kinetics of the coating, zirconium silicate concentration is varied from 0.1 g/L to 0.4 g/L (0.1 g/L, 0.2 g/L, 0.3 and 0.4 g/L) and exploration is directed towards to develop the coating uniformly. When the concentration of zirconium silicate increases from 0.1 g/L to 0.4 g/L, the silicate ion concentration increases and these ions interact with $Al_2(SiO_3)_3$. The credible rationale behind this performance is strongly related to the presence of zirconium silicate additive resulting in non-uniform cooling near the anode surface.

The coating thickness has been increased when zirconium silicate is added into the sodium oxalate solution. At this juncture, anodic coating with more thickness is favoured rather than thin oxide coating and the incorporation of ZrO_2 into the oxide layer is high. So the thickness of the coating also upsurges. Owing to pitting attack on pre-formed barrier oxide which is formed under the low zirconium silicate concentration (< 0.1 g/L), the surface becomes non-uniform. However, when the additive concentration exceeds optimum, the dissolution rate of the coating by anodisation dominates over its formation.

When the concentration of zirconium silicate is increased beyond the optimal level (0.3 g/L) ease of access and inner movement of the oxygen ions (O^{2-}) or hydroxide ions (OH−) towards the Al/Aluminium oxide interface improves, which react with Al^{3+} ions that are shifted around outwards from aluminium surfaces. This tendency results in declined growth parameters because the entire specimen is being surrounded by an oxide layer. From the results, it is inferred that the rate of deposition, morphological properties, and thickness of the coating which strongly depends on zirconium silicate additive concentration. This observation is analogous to previous studies wherein aluminium anodisation is carried out in weak electrolyte with the addition of silicate material.[13–14]

3. 1. 2. Effect of Anodisation Voltage

Fig. S1b depicts the influence of anodisation voltage on growth kinetics which is evaluated by carrying out anodisation at constant temperature and optimized zirconium silicate additive concentration on varying voltage from 45 V to 65 V. From the results, it can be construed that the thickness and growth rate characteristics go linearly with voltage up to 55 V and started to decline after that. Since the oxidation occurs at a slow rate, the coating thickness (62 μm) at a lower voltage (45 V), has been formed with deprived mechanical properties. When voltage maintained is optimal (55 V), the system can afford more driving force for the ions needed for the growth, and it makes it likely to increase the incorporation of ZrO_2 into the oxide coating. However, at the higher voltage (65 V), growth parameters are decreased significantly owing to both local joule heat effect and of the presence of more number of Zr^{2+} ions that competes with aluminium oxide deposition. In addition to this, dissociation of sodium oxalate has also been accelerated at higher applied voltage. The pH of the solution is increased from 8 to 9 due to the release of Na^+ ions that in sequence favours the coating dissolution. When the anodising voltage is 65 V, there is a high degree of hydration and ion incorporation into the anodic coating.

3. 1. 3. Effect of Temperature

Fig. S1c illustrates the influence of anodising temperature on the properties of the coating when anodisation is carried out at a constant voltage of 55 V under zirconium silicate concentration at various temperatures (20° to 35 °C). When anodisation is carried out at low temperature (at 20 °C), both rates of deposition of oxide coating and its dissolution are slowed down. Therefore, at this low temperature (≤ 20 °C), the desired thickness is not achieved. When the temperature of the electrolyte increased (35° ± 1 °C) the growth properties of the coating condition, the heat produced is not disseminated efficiently and distributed uniformly throughout the electrolyte. The nucleation and the growth of the coating are not favoured and afterward, the coating starts to dissolve chemically. Ultimately, burning or breaking of the coating in the highly heated solution which leads to a decrease in thickness. It is worth mentioning that unlike conventional sulphuric acid anodisation, the process employed here does not require ice-cold conditions, thereby making the process simple. Since anodisation temperature straightforwardly influences the rate of mass transfer of O^{2-} and Al^{3+} ions and inward diffusion of O^{2-} ions are assisted when the temperature is increased beyond room temperature.

3. 1. 4. Effect of Process Dduration

Fig. S1d shows the effect of duration 30 min, 60 min, 90 min of anodising process on coating properties when the reaction is carried out under applied voltage of 55 V at 30 °C using electrolyte bath comprising 0.3 g/L zirconium silicate additive in 1.0 M sodium oxalate. At the beginning step, anodised layers formation prevail over the chemical dissolution of it and in compliance with Faradays' law growth kinetics of the anodised layer which is a linear dependence on anodising period. As the duration of the anodising process is prolonged beyond 30 min, aluminium reacted with oxide ions and there is a weight gain in the coating because the rate of deposition is directly proportional to process duration. This oxide coating continues to grow up to a definite period (60 min) to cover the entire surface. Accordingly, when anodisation is performed for 90 min, the thickness of the coating went down attributable for cracking or breaking of the coating. Inefficient dissipation of the amount of heat evolved during the process

is the underlying reason for this behaviour. For example, the thickness of the coating is determined to be 60 μm, 70 μm and 68 μm for 30 min, 60 min, and 90 min respectively. These results exemplify the significance of the optimal duration of the anodising process. Based on the aforementioned studies and observations, the anodisation process carried out at room temperature (35° ± 1 °C) using 1.0 M sodium oxalate and 0.3 g/L zirconium silicate bath under an applied voltage of 55V for 65 min is determined to be the optimal condition.

3. 2. Micro-structural Analysis

3. 2. 1. XRD

Fig.1 shows the X-ray diffraction pattern of aluminium without additive (SO) and with additives for Zr1, Zr2, Zr3 and Zr4 samples. The pristine SO shows peaks at 17° (101), 18° (102), 23° (106), 26° (113), 30° (204), 42° (109), 51° (204), 62° (325), 87° (204) and 95° (204) which confirmed the presence of monoclinic structure. However, the addition of zirconium silicate at a constant current density exhibits the peaks located at 38°, 63° and 74° with preferred orientation of (109), (326) and (337) respectively. In the case of other additive concentration, there is little variability in peak position and depicted clearly in Fig. 2. The observed peaks are well-matched with the standard data (JCPDS card No: 88-1609). The δ-Al_2O_3 phase is observed for these compositions. Based on the anodising conditions, the coatings formed are mainly crystalline. It is found that the coatings after the addition of additives show some traces of zirconia and alumina. Using the Debye-Scherer equation, the average crystalline size for SO, Zr1, Zr2, Zr3 and Zr4 were 26.8 nm, 22.3 nm, 20.18 nm, 18.7 nm and 21.55 nm respectively.

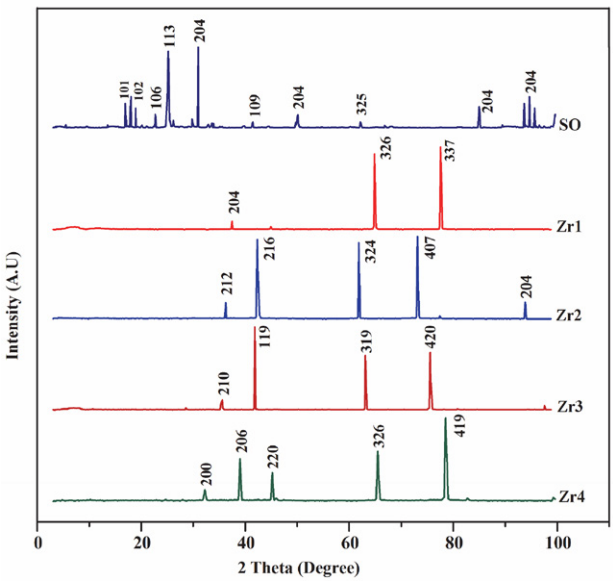

Figure 1. X- ray diffraction pattern of anodized aluminium coating comprising SO, Zr1, Zr2, Zr3 and Zr4.

3. 2. 2. Microstructure and Composition of the Coating

Microstructures related to SO, Zr1, Zr2, Zr3 and Zr4 coating are represented by Fig. S2 that depicts the differences in the morphological features. Fig. S2 of SO portrays distinctly dissimilar morphological characteristics from that of Fig S2 (b-d) which are associated with SO, Zr1, Zr2, Zr3 and Zr4 coating. SO microstructure exhibited the pores of different dimension that is formed as a result of hydrogen evolution during the process in addition to the many cracks that are visible which are formed due to the drying shrinkage. When zirconium silicate is introduced into the electrolyte, the coating becomes smoother and denser. The pores of different shapes are distributed all over the surface of the specimen after introducing the additive. Noticeably dissimilar surface morphologies prove that the addition of zirconium silicate into the electrolyte has a greater control over determining the surface morphology of the coatings. As the zirconium silicate concentration becomes higher (0.4 g/L), aluminium will be consumed at a higher rate near the bottom of the pore which is allowing continued growth of the porous layer.

The surface of Zr1, Zr2, Zr3 and Zr4 coating is smooth which is beneficial to resist the corrosion. Change in the morphology has been observed when the concentration of zirconium silicate was increased (0.3 g/L) even beyond the optimal level. Micro-sized fissures are detected with Zr4, which are created as a result of the local heating effect on the surface produced because of uneven electric field distribution and detained breakdown of the oxide layer. At lower zirconium silicate concentrations (0.1 g/L and 0.2 g/L) pores are formed along with the surfaces of micro-cracks. Only under the optimal concentration (0.3 g/L), the compact homogenous microstructure is developed. These results illustrate that the presence of zirconium silicate and its concentration are influential components that determine the morphology and properties of the coating.

3. 3. SEM Cross-sectional Studies

The cross-sectional SEM images of the SO and Zr3 are represented in Fig. 2. The thickness was measured from the cross-sectional images. The average thickness of the SO and Zr3 is 5.1 μm and 8.2 μm, respectively. It could be visibly inferred that the quality and thickness of the coating has been improved by adding zirconium silicate into the electrolyte bath. Closer examination of images reveals that a thin deposited layer of about 1 to 1.2 μm thickness comprising three distinct regions such as a dense barrier section at the Al /oxide interface, centre porous section followed by a columnar part of the outer surface. The outward growth of layer and retarded dissolution rate are the possible reasons for enhanced thickness value (82 μm) exhibited by Zr3.

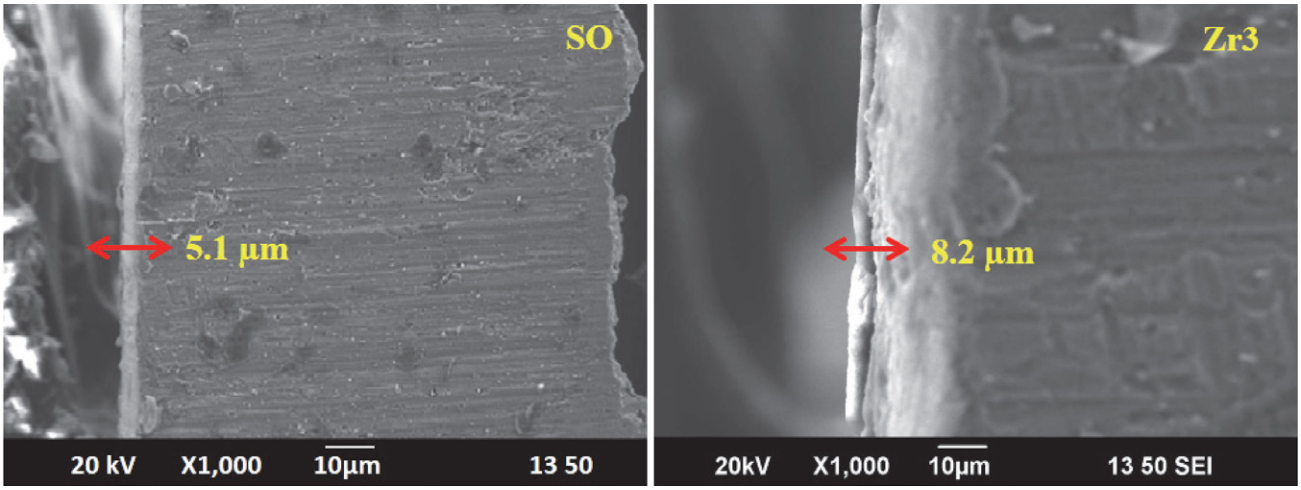

Figure 2. Cross-sectional SEM images of SO, and Zr3 coating

3. 4. EDS Analysis

The elements present in the various specimens are analysed by EDS spectra. Fig. S3 shows EDS spectrum of the SO and Zr3 in which both are fabricated in sodium oxalate electrolyte with the absence of additive and with the presence of optimal content (0.3g/L) of zirconium silicate additive. Aluminium and oxygen are the main constituents that are present in SO and Zr3 at 1.486 Kev (71.4 wt. % for SO and 55.8 wt. % for Zr3) and 2.307 Kev (27.2 wt. % that for SO and 39 wt. % for Zr3). In contrast, the EDS spectrum of Zr3 shows well-defined peaks for Zr and Si at 4.508 Kev and 0.525 Kev respectively. This reveals the incorporation of the additive into the coating. Similarly, the weight percentage of aluminium and oxygen in sample SO are found to be 71.4% and 86.4% respectively. Whereas, in the case of Zr3 sample, the weight percentage of both elements decreases to 55.8% and 39%. The existence of Zr and Si (0.6 wt. % and 0.3 wt. %), which evidences the role of additive towards the facilitating formation of the compact and mechanically stable coating.

3. 5. Studies on Micro Hardness

Micro hardness associated with bare aluminium, SO, Zr1, Zr2, Zr3 and Zr4 samples are measured using Vickers micro hardness tester and are represented in the Fig S4. The average micro hardness values associated with Zr1 (0.1 g/L), Zr2 (0.2 g/L), Zr3 (0.3g/L) and Zr4 (0.4g/L) are 372 HV, 381 HV, 410 HV and 393 HV respectively. The micro hardness value increases with the concentration of zirconium silicate from 0.1g/L to 0.4g/L and then decreases. The maximum micro hardness value (410 HV) is obtained for 0.3 g/L concentration. This is related to the change in surface morphology of the coating when zirconium silicate is incorporated into the electrolyte. These silica particles are helpful in preventing the generation of dislocations, the spread of cracks and in restraining grain boundary slides, which eventually resulted in improved mechanical properties. In addition, the increased driving force experiences at the metal / oxide interface, which promotes the reactions and on this account, the defect is formed over the surface.

3. 6. Studies on Corrosion Resistance of Anodised Layers

Electrochemical corrosion characteristics of SO, Zr1, Zr2, Zr3, Zr4 samples under investigation are relatively assessed by Tafel polarisation and electrochemical impedance spectroscopy (EIS) techniques in 3.5% NaCl solution.

3. 6. 1. Tafel Polarisation Studies

In a 3.5% NaCl solution, the potentiodynamic polarisation behaviour of different coatings and bare aluminium is shown in Fig. 3. Table. S1 summarizes the parameters obtained by fitting the potentiodynamic curves. It can be deduced from the Fig.3 that the corrosion potential of in anodic region associated with SO, Zr1, Zr2, Zr3 and Zr4 coating display a drastic shift in the direction of the positive potential as compared to bare aluminium (–0.699V) illustrating the enhanced corrosion resistance of the coating. I_{corr} is associated with bare aluminium is highest. (27×10^{-4} µA cm^{-2}) but due to passivation of the anodised samples which exhibit low I_{corr} values as evident from Table. S1. I_{corr} is determined to be low for the Zr3 specimen demonstrating its better corrosion-resistance. The observed values are consistent with earlier literature reports.[31–33]

The corrosion resistance of the Zr3 (6.70×10^4 Ω cm^{-2}) is high compared to SO (1.51×10^4 Ω cm^{-2}), Zr1 (2.19×10^4 Ω cm^{-2}), Zr2 (2.35×10^4 Ω cm^{-2}) and Zr4 (6.44×10^4 KΩ cm^{-2}). The corrosion resistance of the coating

increases with the concentration of zirconium silicate up to 0.3 g/L and after that begins to decline. These results are compliant with the open circuit potential values. This shows that the incorporation of zirconium silicate into the electrolyte bath imparts mechanical strength to the coating rather porous with smaller thickness is resulted when sodium oxalate alone is used as an electrolyte that produces a detrimental effect on its corrosion resistance. The difference in the resistance and polarisation behaviour is mainly owing to the structure and morphology of the coating. Since the corrosion rate depends on the coating thickness, the coating with lower thickness and high porous nature will undergo the corrosion readily due to uncomplicated accessibility of destructive ions. However when zirconium silicate is incorporated with sodium oxalate electrolyte, both pores size and the number of pores decreased. By increasing the concentration of zirconium silicate additive, highly thick non-porous morphology has been formed that helps to acquire more corrosion-resistant property due to the restricted penetrations of corrosive ions into the coatings.

This type of coating is generated when the optimal zirconium silicate concentration (0.3 g/L) is maintained during anodisation at appropriate temperature and voltage. However, when zirconium silicate concentration is exceeded above 0.3 g/L, the thickness is reduced through modified rate of deposition and perceptibly and the corrosion potential decreases. As a result of their lower corrosion current densities, thicker coatings with less porous nature reflect higher corrosion resistance. On the other hand, shape and porosity, not just thickness, have a significant effect in determining the specimen's corrosion resistance.

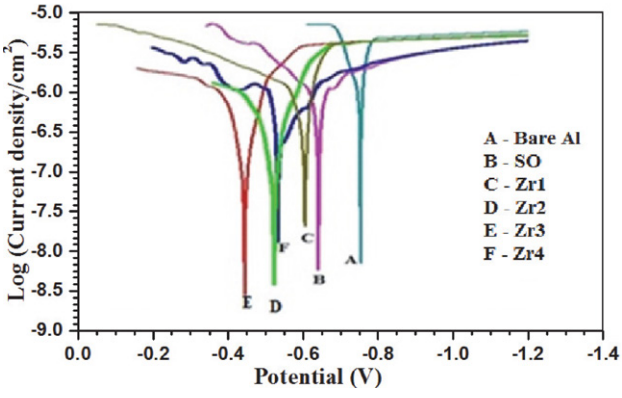

Figure 3. Tafel polarization plots for bare aluminium and various anodized coating immersed in 3.5% NaCl solution (a) bare Al, (b) SO, (c) Zr1, Zr2, Zr3 and Zr4.

3. 6. 2. Electrochemical Impedance Studies

EIS measurements were performed with bare aluminium, SO, Zr1, Zr2, Zr3 and Zr4 coating to distinguish the corrosion kinetics across the modified coating and substrate interface of aluminium specimens Fig. 4 and Fig. 5 show an electrical equivalent circuit model used in this study for the fitting analysis, which is a simplified electrochemical model that has been consistently reported for the comparative Nyquist of SO, Zr1, Zr2, Zr3 and Zr4 samples in 3.5% of NaCl obtained at open circuit potential after immersion of the samples for 500s. Based on the equivalent circuit model proposed, these EIS curves were best fitted and the resulting parameters are tabulated in Table. 1. R_p represents a measure of corrosion resistance that indicates the extent of protection against corrosion and is inversely proportional to $I_{corr.}$ Like the Tafel polarisation studies, EIS data also indicate that corrosion resistance improved, substantially after anodising as compared to the bare aluminium (R_f: 3011 Ω cm^{-2}; C_{dl}: 11.25μFcm^{-2}). Fascinatingly, the coating generated on the surface that plays a dual role in preventing corrosion both through decreasing rate of charge transfer process and diffusion across the surface layer. From Table.1 it is apparent that Zr4 (1607 Ω cm^{-2}) samples display high resistance compared to other samples under study, which demonstrates a role of silicate additive towards protecting surface corrosion. It is implied that water and electrolytic solution penetrate through the anodic layer which composed of larger pores to initiate the corrosive attack in case of the thin layered SO sample, but Zr1, Zr2, Zr3 and Zr4 samples comprising dense, close-packed network restricts the penetration of corrosive ions through them. R_p and C_{dl} are noted to be minimised for Zr3 layer, which is due to a diminution in local dielectric constant and/or to an increase in electrical double layer thickness.

On comparing passivation current densities, it is inferred that the anodic coating obtained using sodium oxalate-zirconium silicate electrolyte provides an excellent barrier for defending against corrosion. The features of the coating are reflected by the high-frequency section of the

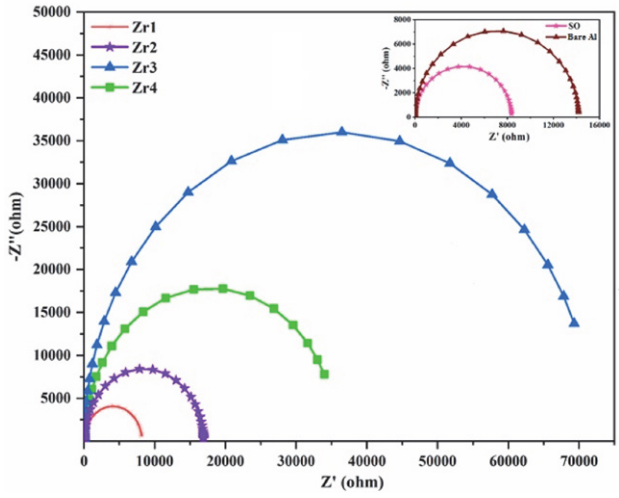

Figure 4. Nyquist plot curves associated with bare aluminium and various anodized aluminium coating immersed in 3.5% NaCl solution Zr1, Zr2, Zr3 and Zr4 anodic layers. Inset of figure shows that of bare Al and SO.

spectrum, while the lower portion of the spectrum is connected to the Faradic reaction occurring on the aluminium surface, according to the literature.[24–25] EIS of SO is different from that of all other samples which are consistent with the formation of a stable passive layer on these surfaces. Low capacitance that arises owing to strong interaction of small organic molecules on the surface that results in poor dissolution reaction. The surface homogeneity of coating also helps to develop good corrosion resistance, which higher resistance (R_f) compared to bare aluminium. By restricting the access of aggressive ions causing corrosion.[26–30]

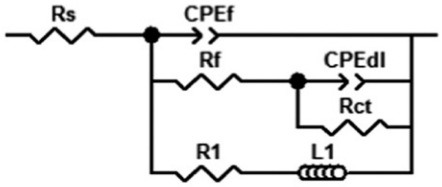

Figure 5. An electrochemical equivalent circuit model fitted for impedance data analysis of anodized aluminium layers in this study.

3. 6. 3. Wettability Studies

The aforementioned studies confirm that Zr3 exhibits suitable surface and further it is subjected to hydrophobic treatment. It can be seen from Fig. 6 that contact angle (CA) associated with the anodised aluminium surface. After Stearic acid 3 g/L immersion, the contact angle of Zr3 is increased to 122° ± 0.4° for 15 min (SA1) treatment. When the specimen is further subjected to KOH 10 g/L treatment the contact angle is increased to 152.76° ± 0.4° (SA2). Among SA1 and SA2, the SA2 sample shows a higher contact angle. The wettability of a solid surface is strongly affected by both surface structure and chemical composition.[34]

3. 6. 4. Studies on Corrosion Behaviour of Hydrophobic Surface SA1 and Superhydrophobic Surface SA2

To examine the corrosion resistance of the hydrophobic coating corrosion studies were carried out for Zr3, SA1 and SA2 samples for comparison. The results are shown in Fig. S5 and Fig. S6. Fig. S5 shows the Tafel polar-

Table 1. Corrosion parameters derived from EIS Nyquist plot analysis associated with bare aluminium, SO and various Zr3 anodic layers under applied voltage of 45 V for 65 min at room temperature.

Sample	CPE_f (μF cm^{-2})	R_F (Ohm cm^2)	CPE_{dl} (μF cm^{-2})	R_{ct} (Ohm cm^2)	R_1 (Ohm cm^2)
Bare Al	11.25	3011	198	1765	1298
SO	8.21	1023	209	1613	1267
Zr1	7.43	879	221	1658	1109
Zr2	6.02	674	227	1654	979
Zr3	5.45	476	238	1607	875
Zr4	5.77	489	241	1605	889

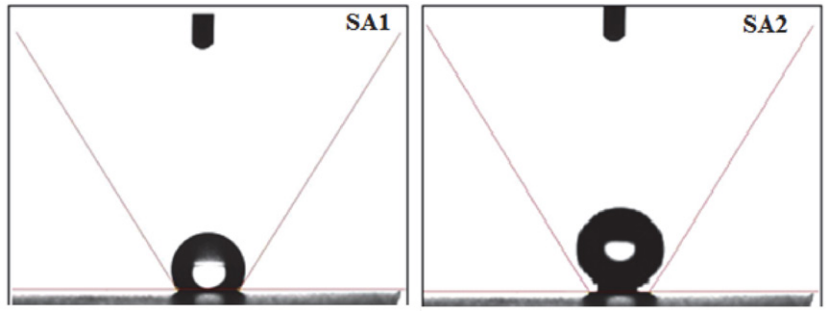

Figure 6. Effect of various treatment duration on contact angle of the coating.

Table 2. Corrosion parameters derived from EIS Nyquist plot analysis associated with SA1 and SA2.

Sample	CPE_f (μF cm^{-2})	R_F (Ohm cm^2)	CPE_d (μF cm^{-2})	R_{ct} (Ohm cm^2)	R_1 (Ohm cm^2)
SA1	8.5	438	217	1564	778
SA2	7.8	341	252	1245	651

isation curves for SA1 and SA2. Among all samples SA2 shows low I_{corr} (6.04×10^{-8} μA/cm^2) and high E_{corr} (–0.02 V) shifts towards a more positive direction compared to SA1 (I_{corr}: 7.01×10^{-7} μA/cm^2; E_{corr}: –0.321 V) and Zr3 (I_{corr}: 6.14×10^{-7} μA/cm^2; E_{corr}: –0.428V) as shown by Table S2. The obtained result shows that in the instance of SA2, chloride ion (Cl^-) transport may have been severely hindered. This demonstrates that a covering with a larger

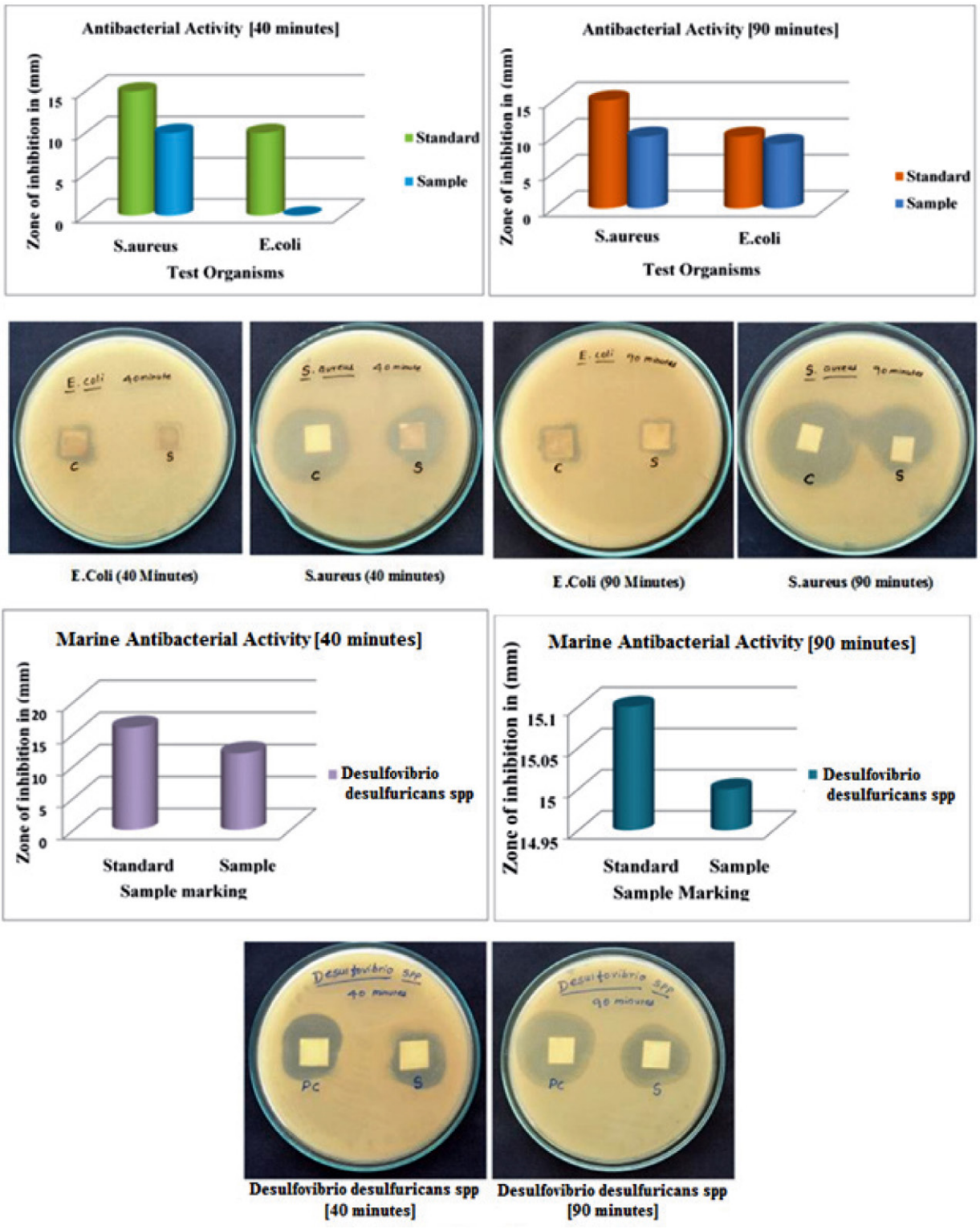

Figure 7. Marine antibacterial activities of Zr3 specimens tested with S.Aureus, E.Coli and D.desulfuricans.

contact angle inhibits corrosion better. Here SA2 has a higher contact angle than SA1 and Zr3. Two key elements might be responsible for the increased corrosion resistance mechanisms. For starters, the SA2 is made up of hierarchical micro-nanostructures that may readily trap significant volumes of air within the coating's micro-/nano-pores. The trapped air acts as a passivation layer, protecting the aluminium substrate from Cl attachment. Water transport against gravity is simple in a porous surface structure with a CA greater than 150°. Therefore, the NaCl solution can be pushed out from the pores of the SA1 by the pressure and the aluminium substrate could be effectively protected. Hence, the structure and properties are influence directly to its corrosion behaviour as exemplified by Tafel studies. Fig. S6 shows the impedance plots of Zr3, SA1, and SA2. Like Tafel studies, the SA2 sample shows higher corrosion resistance than other sample SA1 and Zr3. This model has been proposed for analysis of superhydrobhobic aluminium surface previously by recent researchers.[35–39]

3. 6. 5. Marine Bacterial Activity

The bacterial activity of Zr3 coating was tested against E.coli, S. aureus, and marine bacterial strain namely, D. desulfuricans for 24 h, which is shown in Fig. 7. From the results, it is shown that the zone of inhibition for Zr3 against S.aureus strains and D. desulfuricans is 10 mm (40 min), 12 mm (90 min). The zone of inhibition against D. desulfuricans is increased from 12 mm (40 min) to 15 mm (90 mm) respectively. The results show that the D. desulfuricans bacteria demonstrated higher activity than E.coli and S. aureus due to the minimal solid-liquid contact at the surface, weak surface interactions with bacteria, and low surface energy. The key to the antibacterial qualities is the self-cleaning concept, which allows for easy washing and eliminates the need for antibacterial chemicals. Due to the fact that this antibacterial design is simply structural, a product with permanent characteristics may be created for everyday use with minimum customer maintenance.

4. Conclusions

In conclusion, this work reports on the fabrication of the coatings by anodisation of aluminium in 0.1M sodium oxalate with and without the addition of zirconium silicate. The results revealed that experimental conditions such as additive concentration, applied voltage, process time and temperature play a crucial role in coating formation and tailoring of their surface properties which increases the thickness, growth rate, and micro hardness up to a certain concentration (0.3 g/L; Zr3) and then decreases. The maximum thickness (82 μm), growth rate (1.2 μm/min), and micro hardness (410HV) are obtained at the voltage of 55V in room temperature (35 ±1 °C) for 60 min. The SEM and EDX results demonstrate that the addition of zirconium silicate into the electrolyte has an impact on the morphology as it favours the formation of dense and uniform coating with fewer structure imperfections. The XRD studies confirmed the presence of δ alumina. Our studies further show that the coating formed with the addition of zirconium silicate has more corrosion resistance (6.70×10^4 Ω cm^{-2}) when compared to the sodium oxalate electrolyte (1.0 M) alone as an electrolyte. To extend its applications in the marine field, the surface of the Zr3 sample is modified to superhydrophobic (SA2). The superhydrophobic (SA2) sample shows higher corrosion resistance ($1.68\ x10^8$ Ω cm^{-1}), which is higher than the Zr3 sample (6.8×10^3 Ω cm^{-1}). The contact angle of the coating for the SA1 and SA2 sample is found to be 122° ± 0.4° and 152.76° ± 0.4°. This contact angle of super hydrophobic coating is improved owing to base (KOH) treatment. The marine applications and microbial activity were investigated against S. aureus (40 min: 10 mm; 90 min: 12 mm) and D.desulfuricans (40 min: 12 mm; 90 min: 15 mm). Thus the fabricated coating is compatible with industrial, biological, biomedical, optical, and aerospace applications with the specifically focused utility to mitigate the marine corrosion.

5. References

1. E. W. Lee, T. Oppenheim, K. Robinson, B. Aridkahari, N. Neylan, D. Gebreyesus, M. Richardson, M. Arzate, C. Bove, M. Iskandar, C. Sanchez, E. Toss, I. Martinez, D. Arenas, J. Ogren, J. Mclennan, R. Clark, W. E. Frazier, O. S. Es-Said, *Eng. Fail. Anal*., **2007**, *14*, 1538–1549. **DOI:**10.1016/j.engfailanal.2006.12.008
2. M. G. Mueller, M. Fornabaio, G. Zagar, A. Mortensen, *Acta Mater.,* **2016**, *105,* 165–175. **DOI:**10.1016/j.actamat.2009.11.043

Table 2. Zone of inhibition exhibited by Zr3 towards S.Aureus, E.Coli and D.desulfuricans for incubation period of 40 min and 90 min.

S.No.	Test Organisms	Zone of inhibition in (mm) on 40 min		Zone of inhibition in (mm) on 90 min	
		Control	Sample	Control	Sample
1	*S. aureus*	15mm	10mm	15mm	12mm
2	*E.coli*	10mm	HA	10mm	9mm
3	*D. desulfurican*	15mm	12mm	16mm	15mm

3. A. Ghahremaninezhad, A. Dolati, *J. Alloys Compd.,* **2009**, *480*, 275–278. **DOI:**10.1016/j.jallcom.2009.02.020
4. J. Bajat, I. Milosev, Z. Jovanovic, R. M. Jancic-Heinemann, M. Dimitrijevic, *Corros. Sci*., **2010**, *52(3)*, 1060–1069. **DOI:**10.1016/j.corsci.2009.11.035
5. E. Matykina, R. Arrabal, A. Mohamed, P. Skeldon, G. Thompson, *Corros. Sci*., **2009**, *51(12),* 2897–2905. **DOI:**10.1016/j.corsci.2009.08.004
6. V. Raj, M. Mubarak Ali, J. Mater, *Proc. Tech*., **2009**, *209(12-13),* 5341–5352. **DOI:**10.1016/j.jmatprotec.2009.04.004
7. K. Xhanaria, M. Finšgar, *RSC Adv*., **2016**, *6,* 62833. **DOI:**10.1039/C6RA11818F
8. I. Milošev, *Acta Chim. Slov.,* **2019,** *66,* 511. **DOI:**10.17344/acsi.2019.5162
9. B. Kuznetsov, M. Serdechnova, J. Tedim, M. Starykevich, S. Kallip, M. P. Oliveira, T. Hack, S. Nixon, M. G. S. Ferreira, M. L. Zheludkevich, *RSC Adv*., **2016**, *6(17),* 13942–13952. **DOI:**10.1016/j.jallcom.2014.12.176
10. S. Zhang, Q. Xu, Z. Wang, S. Hao, C. Sun, W. Ma, *Surf. Coat. Tec*hnol., **2018**, *346*, 48–52. **DOI:**10.1021/jp0560664
11. Z. Wang, Q. Li, Z. She, F. Chen, L. Li, *J. Mater. Chem*., **2012**, *22(9),* 4097–4105**. DOI:**10.1039/c2jm14475a
12. Y. Lai, X. Gao, H. Zhuang, J. Huang, C. Lin, *Adv. Mater*., **2009**, 21(37), 3799–3803. **DOI:**10.1002/adma.200900686
13. S. Jung, M. Dorrestijn, D. Raps, A. Das, C.M. Megaridis, D. Poulikakos, *Langmuir.,* **2011**, *27(6)*, 3059–3066. **DOI:**10.1021/la104762g
14. Z. She, Q. Li, Z. Wang, C. TaN, J. Zhou, L. Li, *Surf. Coat. Technol*., **2014**, *251*, 7–14. **DOI:**10.1016/j.surfcoat.2014.03.060
15. J. Y. Huang, S. H. Li, M. Z. Ge, L. N. Wang, T. L. Xing, G. Q. Chen, X. F. Liu, S. S. Al-Deyab, K. Q. Zhan, T. Chen, Y. K. Lai, *J. Mater. Chem., A*. **2015**, *3(6)*, 2825–2832. **DOI:**10.1039/C4TA05332J
16. H. Kim, K. Noh, C. Choi, J. Khamwanna, D. Villwock, S. Jin, *Langmuir*., **2011**, *27(16)*, 10191–10196. **DOI:**10.1021/la2014978
17. J. Yu, L. Qin, Y. Hao, S. Kuang, X. Bai, Y. M. Chong, W. Zhang, *ACS Nano.,* **2010**, *4(1)*, 414–422. **DOI:**10.1021/nn901204c
18. B. Qian, Z. Shen, *Langmuir.,* **2005**, *21(2)*, 9007–9009. **DOI:**10.1021/la051308c
19. A. V. Rao, S. S. Latthe, S. A. Mahadik, C. Kappenstein, *Appl. Surf. Sci*., **2011**, *257(13)*, 5772–5776. **DOI:**10.1016/j.apsusc.2011.01.099
20. A. Chaudhary, H. C. Barshilia, *J. Phys. Chem. C.,* **2011**, *115(37),* 18213–18220. **DOI:**10.1021/jp204439c
21. J. Li, Z. Jing, Y. Yang, Q. Wang, Z. Lei, *Surf. Coat. Technol*., **2014**, *258,*973–978. **DOI:**10.1016/j.surfcoat.2014.07.047
22. C. Dong, Y. Gu, M. Zhong, L. Li, K. Sezer, M. Ma, *J. Mater. Process. Technol*., **2011**, 211(7), 1234–1240. **DOI:**10.1016/j.jmatprotec.2011.02.007
23. T. Darmanin, E. T.de Givench, S. Amigoni, F. Guittard, *Adv. Mater*., **2013**, *25(10)*, 1378–1394. **DOI:**10.1002/adma.201204300
24. H. Wang, D. Dai, X. Wu, *Appl. Surf. Sci.,* **2008**, *254(17)*, 5599–5601. **DOI:**10.1016/j.apsusc.2008.03.004
25. W. Liu, Y. Luo, L. Sun, R. Wu, H. Jiang, Y. Liu, *Appl. Surf. Sci*., **2013**, *264*, 872–878. **DOI:**10.1016/j.apsusc.2012.10.167
26. R. Jafari, R. Menini, M. Farzaneh, *Appl. Surf. Sci*., **2010**, *257(3)*, 1540–1543. **DOI:**10.1016/j.apsusc.2010.08.092
27. S. Peng, W. Deng, *Colloids. Surf., A*. **2015**, *481,* 143–150. **DOI:**10.1016/j.colsurfa.2015.04.037
28. D. Ma, S. Li, C. Liang, *Corros. Sci*., **2009**, *517*, 713. **DOI:**10.1016/j.jmrt.2020.08.085
29. V. Raj, M. Mubarak Ali, *J.Mater. Proc. Tech.,* **2009**, *209(12-13),* 5341–5352. **DOI:**10.1016/j.jmatprotec.2009.04.004
30. V. Zinkevich, I. Bogdarina, H. Kang, M. A. W. Hill, R. Tapper, I. B. Beech, *Int. Biodeterior. Biodegrad*., **1996**, *37(3-4),* 163–172. **DOI:**10.1080/08927019909378396
31. M. Mubarak Ali, S. Sathiya, *Curr. Sci.,* **2020**, *118(2)*, 234. **DOI:**10.18520/cs/v118/i2/234-242
32. H. Ji, G. Chen,J. Yang, J. Hu, H. Song, Y Zhao, *Appl. Surf. Sci.,* **2013**, *266*,105. **DOI:**10.1016/j.apsusc.2012.11.103
33. V. Raj, M. Mumjitha, *Mater. Sci. Eng. B.,* **2014**, *(179)*, 25–35. **DOI:**10.1016/j.mseb.2013.10.001
34. S. Senbahavalli, S. Mohanapriya, V. Raj, *Materials Discovery.,* **2016,** *(3)*, 29–37. **DOI:**10.1016/j.md.2016.08.001
35. G. S. Hikku, K. Jeyasubramanian, A. Venugopal, R. Ghosh, *J. Alloys and Compounds.,* **2017,** *(716)*, 259–269. **DOI:**10.1016/j.jallcom.2017.04.324
36. D. Zang, R. Zhu, W. Zhang, J. Wu, X. Yu, Y. Zhang, *Corros. Sci.,* **2020,** *(83),* 86–93. **DOI:**10.1016/j.corsci.2014.02.003
37. Y. Huang, D. K. Sarkar, X. G. Chen, *Appl. Surf. Sci.,* **2015**, *356,* 1012–1024. **DOI:**10.3390/ma12010109
38. H. A. Sorkhabi, S. A. Nabavi, *Acta Chim. Slov.* **2000**, *47*, 507.
39. M. Lalić, S. Martinez, *Acta Chim. Slov.* **2019**, *66*, 513–522. **DOI:**10.17344/acsi.2019.5113

Povzetek

V tem delu smo preučili anodizacijo aluminija v 1.0 M raztopini natrijevega oksalata in metodološko ovrednotili vpliv cirkonijevega silikata kot aditiva. Podrobneje smo preučili vpliv aditiva na strukturo, morfologijo, mikrotrdoto in sestavo prevleke pod različnimi pogoji anodizacije. Površina prevleke je bila obdelana s stearinsko kislino, čas stika prevleke s kislino pa je bil optimiziran. Poleg že navedenega smo preučili tudi odvisnost morfologije površine, kinetskih parametrov in mikrostrukturnih lastnosti prevleke od elektrolita oziroma koncentracije aditiva, časa anodizacije in temperature. Analize z rentgensko praškovno difrakcijo (XRD) in vrstično elektronsko mikroskopijo (SEM), kombinirano z energijskodisperzijsko spektroskopijo (EDS), so pokazale ugoden vpliv aditiva na nastanek kristalinične prevleke z izboljšanimi protikorozijskimi lastnostmi. Prevleke z aditivom so superhidrofobne. Z namenom povečanja statičnega kontaktnega kota vode, ki je znašal 122° ± 0.4°, so bile prevleke z aditivom obdelane s KOH, kar je pod najugodnejšimi pogoji kot povečalo na 152.76° ± 0.4°. Pri tem kotu je korozijska upornost sistema znašala $1.68 \times 10\ \Omega\ cm^{-1}$, kar je skoraj osemkrat več kot pri čistem aluminiju ($8.36 \times 10^{1}\ \Omega\ cm^{-1}$). Prikazana je tudi učinkovitost tovrstnih površinsko modificiranih prevlek proti trem različnim vrstam bakterij; morski bakteriji *Desulfovibrio desulfuricans* in medicinsko relevantnima bakterijama *Staphylococcus aureus* ter *Escherichia coli.*

Except when otherwise noted, articles in this journal are published under the terms and conditions of the Creative Commons Attribution 4.0 International License

Scientific paper

Synthesis of Fused Quinoline Derivatives with Antiproliferative Activities and Tyrosine Kinases, Pim-1 Kinase Inhibitions

Rafat Milad Mohareb,[1,*] Rehab Ali Ibrahim,[2] Amira Mohamed Elmetwally,[3] and Marwa Soliman Gamaan[1]

[1] *Department of Chemistry, Faculty of Science, Cairo University, Giza, A. R. Egypt*

[2] *Higher Institute of Engineering and Technology, El-Tagammoe El-Khames, New Cairo, Egypt*

[3] *Egyptian Drug Authority (NODCAR), P.O. 29, Cairo AR Egypt*

** Corresponding author: E-mail: raafat_mohareb@yahoo.com*

Received: 02-05-2021

Abstract

Cyclohexan-1,3-dione (**1**) reacted with either 2-aminoprop-1-ene-1,1,3-tricarbonitrile (**2a**) or diethyl 3-amino-2-cyanopent-2-enedioate (**2b**) to give the 5,6,7,8-tetrahydronaphthalene derivatives **3a** and **3b**, respectively. The latter compounds underwent further heterocyclization reactions to give the thieno[2',3':5,6]benzo[1,2-*e*][1,3]oxazine derivatives. On the other hand, the reaction of compound **1** with trichloroacetonitrile afforded the (2,2,2-trichloroethylidene)cyclohexane derivative **14**. The latter underwent a series of reactions to produce 2,3,6,7-tetrahydroquinazoline, dihydrothieno[2,3-*h*]isoquinoline, octahydrobenzo[*h*]quinazoline and dihydrothieno[2,3-*h*]isoquinoline derivatives. The synthesized compounds were tested toward six cancer cell lines where most of them gave high inhibitions with c-Met enzymatic activity, with tyrosine kinases and Pim-1 inhibitions. The results obtained will encourage further work through such compounds to produce optimized anticancer agents.

Keywords: Cyclohexan-1,3-dione, trichloroacetonitrile, quinoline, isoquinoline, cytotoxicity

1. Introduction

With its origins rooted in organic synthesis and medicinal chemistry, heterocyclic compounds present themselves as a fundamental division of organic chemistry. Defined by IUPAC as "cyclic compounds having as ring members atoms of at least two different elements" (IUPAC Gold Book 2015),[1] heterocycles' ring structures are in essence composed by elements other than carbon, where the most frequent substituents are oxygen, nitrogen and sulfur.[2,3] According to the heteroatom(s) present in the ring structures, heterocycles can be classified as oxygen, nitrogen or sulfur based and, within each class, compounds are organized based on the size of the ring structure determined by the total number of atoms.[4] The type and size of ring structures, together with the substituent groups of the core scaffold, impact strongly on the physicochemical properties.[2,5] Among the various clinical applications, heterocyclic compounds have a considerable active role as anti-bacterial,[6,7] anti-viral,[8] anti-fungal,[9] anti-inflmmatory[10] and anti-tumor drugs.[11–13] The engineering and rationale behind drug design are closely related to the strategic incorporation of heterocyclic fragments with specific physicochemical properties. Potency and selectivity achieved through bioisosteric replacements, lipophilicity, polarity, and aqueous solubility can ultimately be fine-tuned to the point of altering and conditioning the possible mechanisms of action of pharmaceutical drugs in an attempt to obtain molecularly targeted agents.[14] Despite their versatility and potential, as for any other pharmaceutical, there are several issues hindering wider application and further development of such compounds into market drugs. Oncology is one of the areas where this is perhaps most noticeable, partially due to the intrinsic limitations regarding main therapeutic routes of chemotherapy, concomitant side effects and toxicity to healthy tissues. Such deleterious effects may be circumvented *via* selective targeting of delivery, passively or actively into cancerous cells.[15] It should be noted that

for some playmakers within the chemotherapy field, the success of "molecularly targeted agents", such as imatinib are merely fortunate exceptions and that the number of success in this area is considerably low.[16] Recent advances in interdisciplinary field of nanobiotechnology have led to the development of new inventive therapeutic strategies and drug delivery alternatives taking advantage of the architectural geniality of systems based on nanoscale devices particularly tailored to deliver drugs to a selected tissue.[17–19]

Recently our research group reported several reactions of cyclic β-diketones to produce thiazoles and thiophene derivatives. The produced compounds showed high anti-proliferative activities against cancer cell lines together with high inhibitions toward tyrosine kinases.[20–22] This encouraged us to continue this goal through the reaction of cyclohexan-1,3-dione with dimeric cyanomethylene and trichloroacetonitrile reagents together with using the produced molecule as a suitable starting material for subsequent heterocyclization to produce a variety of fused derivatives. The antiproliferative activities of the synthesized compounds and their inhibitions toward tyrosine kinases were determined.

2. Experimental

2. 1. General

All melting points are uncorrected and were recorded using an Electrothermal digital melting point apparatus. IR spectra (KBr discs) were measured using a FTIR plus 460 or PyeUnicam SP-1000 spectrophotometer. ^{1}H NMR spectra were measured using a Varian Gemini-300 (300 MHz) and Jeol AS 500 MHz instruments; spectra were recorded in DMSO-d_6 as the solvent using TMS as the internal standard and chemical shifts are expressed as δ ppm. MS (EI) spectra were measured using Hewlett Packard 5988 A GC/MS system and GCMS-QP 1000 Ex Shimadzu instruments. Analytical data were obtained from the Micro-analytical Data Unit at Cairo University and were performed on Vario EL III Elemental analyzer. The anti-tumor evaluation has been carried out through the National Cancer Research Centerat Cairo, Egypt where the IC_{50} values were calculated.

2. 1. 1. General Procedure for the Synthesis of the 5,6,7,8-Tetrahydronaphthalene 3a,b

Equimolar amounts of dry solids of compound **1** (1.12 g, 0.01 mol) and either of **2a** (1.32 g, 0.01 mol) or **2b** (2.14 g, 0.01 mol) and ammonium acetate (1.50 g) were heated in an oil bath at 120 °C for 1 h then were left to cool. The remaining product was triturated with diethyl ether and the formed solid product, in each case, was collected by filtration.

2,4-Diamino-5-oxo-5,6,7,8-tetrahydronaphthalene-1,3-dicarbonitrile (3a)

Yellow crystals from 1,4-dioxane, yield 1.58 g (70%). Mp 256–258 °C. IR (KBr) ν_{max} 3488–3352 (NH_2), 3055 (CH, aromatic), 2223, 2220 (2CN), 1703 (CO), 1632 cm^{-1} (C=C); ^{1}H NMR (DMSO-d_6, 300 MHz) δ 4.93, 4.53 (s, 4H, D_2O exchangeable, $2NH_2$), 2.93–2.80 (m, 4H, $2CH_2$), 1.98–1.28 (m, 2H, CH_2); ^{13}C NMR (DMSO-d_6, 75 MHz) δ 174.2 (C-5), 127.9, 125.6, 124.9, 123.5, 121.8, 120.4 (C-1, C-2, C-3, C-4, C-5, C-6), 116.8, 116.3 (2CN), 40.6, 38.9, 17.4 (C-6, C-7, C-8); MS *m/z* 226 (M^+, 36%). Anal. Calcd for $C_{12}H_{10}N_4O$: C, 63.71; H, 4.46; N, 24.76. Found: C, 63.92; H, 4.79; N, 24.80.

Ethyl 2-Amino-3-cyano-4-hydroxy-5-oxo-5,6,7,8-tetrahydronaphthalene-1-carboxylate (3b)

Orange crystals from ethanol, yield 1.89 g (69%). Mp 180–183 °C. IR (KBr) ν_{max} 3554–3338 (OH, NH_2), 3055 (CH, aromatic), 2220 (CN), 1708, 1689 (2CO), 1636 cm^{-1} (C=C); ^{1}H NMR (DMSO-d_6, 300 MHz) δ 10.26 (s, 1H, D_2O exchangeable, OH), 4.92 (s, 2H, D_2O exchangeable, NH_2), 4.22 (q, 2H, J = 7.31 Hz, $O\underline{CH_2}CH_3$), 2.80–2.96 (m, 4H, $2CH_2$), 1.98–1.28 (m, 2H, CH_2), 1.12 (t, 3H, J = 7.31 Hz, $OCH_2\underline{CH_3}$); ^{13}C NMR (DMSO-d_6, 75 MHz) δ 165.2, 164.3 (C-5, ester CO), 125.4, 123.0, 122.8, 122.5, 121.9, 120.5, 119.2 (C-1, C-2, C-3, C-4, C-5, C-6), 116.9 (CN), 50.3 ($O\underline{CH_2}CH_3$), 40.1, 38.5, 17.1 (C-6, C-7, C-8), 16.2 ($OCH_2\underline{CH_3}$); MS *m/z* 274 (M^+, 28%). Anal. Calcd for $C_{14}H_{14}N_2O_4$: C, 61.31; H, 5.14; N, 10.21. Found: C, 61.26; H, 5.39; N, 10.36.

2. 1. 2. General Procedure for the Synthesis of the 5,6,7,8-Tetrahydronaphthalene Derivatives 4a,b

A solution of either compound **3a** (2.26 g, 0.01 mol) or **3b** (2.74 g, 0.01 mol) in acetic acid (40 mL) and acetic anhydride (15 mL) was heated under reflux for 3 h then left to cool. The reaction mixture, in each case was evaporated under vacuum and the remaining product was triturated with ethanol and the formed solid product was collected by filtration.

***N*-(3-Amino-2,4-dicyano-8-oxo-5,6,7,8-tetrahydronaphthalen-1-yl)acetamide (4a)**

Pale yellow crystals from 1,4-dioxane, yield 1.82 g (68%). Mp 236–239 °C. IR (KBr) ν_{max} 3464–3342 (NH_2, NH), 3055 (CH, aromatic), 2223, 2220 (2CN), 1702, 1688 (2CO), 1630 cm^{-1} (C=C); ^{1}H NMR (DMSO-d_6, 300 MHz) δ 8.26 (s, 1H, D_2O exchangeable, NH), 4.56 (s, 2H, D_2O exchangeable, CH_2), 3.02 (s, 3H CH_3), 2.93–2.85 (m, 4H, $2CH_2$), 1.96–1.84 (m, 2H, CH_2); ^{13}C NMR (DMSO-d_6, 75 MHz) δ 174.3, 166.2 (C-8, CO amide), 125.9, 123.9, 123.7, 122.5, 122.0, 121.6, 119.8 (C-1, C-2, C-3, C-4, C-5, C-6), 116.5, 116.4 (2CN), 40.6, 38.5, 17.6 (C-6, C-7, C-8), 24.8 (CH_3); MS *m/z* 268 (M^+, 44%). Anal. Calcd for $C_{14}H_{12}N_4O_2$: C, 62.68; H, 4.51; N, 20.88. Found: C, 62.93; H, 4.63; N, 20.68.

Ethyl 4-Acetoxy-2-amino-3-cyano-5-oxo-5,6,7,8-tetrah ydronaphthalene-1-carboxylate (4b)

Pale brown crystals from ethanol, yield 2.17 g (60%). Mp 158–161 °C. IR (KBr) ν_{max} 3473–3328 (NH), 3055 (CH, aromatic), 2220 (CN), 1705, 1688 (2CO), 1630 cm^{-1} (C=C); ^{1}H NMR (DMSO-d_6, 300 MHz) δ 4.72 (s, 2H, D_2O exchangeable, NH_2), 4.23 (q, 2H, *J* = 6.56 Hz, O$\underline{CH_2}CH_3$), 3.01 (s, 3H CH_3), 2.96–2.82 (m, 4H, $2CH_2$), 1.96–1.81 (m, 2H, CH_2), 1.12 (t, 3H, *J* = 6.56 Hz, $OCH_2\underline{CH_3}$); ^{13}C NMR (DMSO-d_6, 75 MHz) δ 174.3, 166.1 (C-8, CO ester), 120.3, 121.8, 122.6, 123.2, 124.1, 125.1, 125.2 (C-1, C-2, C-3, C-4, C-5, C-6), 117.0 (CN), 50.2 (O$\underline{CH_2}CH_3$), 40.1, 38.5, 17.3 (C-6, C-7, C-8), 24.8 (CH_3), 16.6, 16.3 (two $OCH_2\underline{CH_3}$); MS *m/z* 316 (M^+, 30%). Anal. Calcd for $C_{16}H_{16}N_2O_5$: C, 60.75; H, 5.10; N, 8.86. Found: C, 60.43; H, 5.28; N, 8.90.

2. 1. 3. General Procedure for the Synthesis of the 3,4,7,8,9,10-Hexahydro-2*H*-naphtho[2,1-*e*][1,3] azine Derivatives 6a,b

To a solution of either of compound **4a** (2.68 g, 0.01 mol) or **4b** (3.16 g, 0.01 mol) in ethanol (40 mL) containing triethylamine (1.0 mL), phenyl isothiocyanate (1.30 g, 0.01 mol) was added and heated under reflux for 3 h then left to cool. The formed solid crystals, in each case, were collected by filtration.

5-Amino-4-imino-10-oxo-3-phenyl-2-thioxo-1,2,3,4,7, 8,9,10-octahydrobenzo[*h*]-quinazoline-6-carbonitrile (6a)

Yellowish white crystals from 1,4-dioxane, yield 2.64 g (73%). Mp 212–215 °C. IR (KBr) ν_{max} 3480–3329 (NH), 3055 (CH, aromatic), 2220 (CN), 1689 (CO), 1630 (C=C), 1209 cm^{-1} (C=S); ^{1}H NMR (DMSO-d_6, 300 MHz) δ 8.35, 8.28 (2s, 2H, D_2O exchangeable, 2NH), 7.42–7.26 (m, 5H, C_6H_5), 4.52 (s, 2H, D_2O exchangeable, NH_2), 2.96–2.83 (m, 4H, $2CH_2$), 1.96-1.82 (m, 2H, CH_2); ^{13}C NMR (DMSO-d_6, 75 MHz) δ 179.8 (C-2), 173.6 (C-10), 126.8, 126.1, 125.2, 125.1, 124.6, 124.1, 123.8, 123.2, 122.6, 121.8, 120.3 (C-1, C-2, C-3, C-4, C-5, C-6, C_6H_5), 117.0, 116.3, 116.1 (3CN), 46.8, 40.2, 38.5 (C-7, C-8, C-9); MS *m/z* 361 (M^+, 28%). Anal. Calcd for $C_{19}H_{15}N_5OS$: C, 63.14; H, 4.18; N, 19.38; S, 8.87. Found: C, 63.28; H, 4.25; N, 19.26; S, 8.69.

Diethyl 2-Cyano-4-(3-oxocyclohexylidene)-3-(3-phenylthioureido)pent-2-enedioate (6b)

Orange crystals from ethanol, yield 3.09 g (67%). Mp 211–214 °C. IR (KBr) ν_{max} 3468–3347 (NH), 3055 (CH, aromatic), 1689, 1687 (2CO), 1630 (C=C), 1209 cm^{-1} (C=S); ^{1}H NMR (DMSO-d_6, 200 MHz) δ 8.32 (s, 1H, D_2O exchangeable, NH), 7.40–7.23 (m, 5H, C_6H_5), 4.53 (s, 2H, D_2O exchangeable, NH_2), 4.22 (2q, 2H, *J* = 7.03 Hz, O$\underline{CH_2}CH_3$), 2.96–2.83 (m, 4H, $2CH_2$), 1.96–1.82 (m, 2H, CH_2), 1.12 (t, 3H, *J* = 7.03 Hz $OCH_2\underline{CH_3}$); ^{13}C NMR (DMSO-d_6, 75 MHz) δ 179.7 (C-2), 174.6, 166.1 (C-3, ester CO), 126.9, 126.5, 125.3, 125.0, 124.9, 124.6, 123.4, 123.1, 122.9, 122.3, 120.1 (C-1, C-2, C-3, C-4, C-5, C-6, C_6H_5), 50.1 (O$\underline{CH_2}CH_3$), 40.5, 38.5, 17.1 (C-7, C-8, C-9), 16.3 ($OCH_2\underline{CH_3}$); MS *m/z* 409 (M^+, 38%). Anal. Calcd for $C_{21}H_{19}N_3O_4S$: C, 61.60; H, 4.68; N, 10.26; S, 7.83. Found: C, 61.39; H, 4.78; N, 10.58; S, 7.57.

2. 1. 4. General Procedure for the Synthesis of the 3,4,7,8,9,10-Hexahydro-2*H*-naphtho[2,1-*e*] [1,3]azinone Derivatives 7a,b

A suspension of either compound **6a** (3.61 g, 0.01 mol) or **6b** (4.09 g, 0.01 mol) in sodium ethoxide [prepared through dissolving metallic sodium (0.46 g, 0.02 mol) in absolute ethanol (50 mL)] was heated in a boiling water bath for 6 h. The reaction mixture was poured onto ice/water then triturated with hydrochloric acid (till pH 7) and the formed solid product was collected by filtration.

5-Amino-4,10-dioxo-3-phenyl-2-thioxo-1,2,3,4,7,8,9, 10-octahydrobenzo[*h*]-quinazoline-6-carbonitrile (7a)

Yellow crystals from ethanol, yield 1.99 g (55%). Mp 210–212 °C. IR (KBr) ν_{max} 3472–3346 (NH_2), 3055 (CH, aromatic), 2220 (CN), 1688 (CO), 1630 cm^{-1} (C=C); ^{1}H NMR (DMSO-d_6, 200 MHz) δ 8.31 (s, 1H, D_2O exchangeable, NH), 7.24–7.48 (m, 5H, C_6H_5), 4.80 (s, 2H, D_2O exchangeable, NH_2), 2.98–2.81 (m, 4H, $2CH_2$), 1.94–1.80 (m, 2H, CH_2); ^{13}C NMR (DMSO-d_6, 75 MHz) δ 179.5 (C-2), 173.4, 168.2 (C-4, C-10), 126.9, 126.1, 125.7, 125.2, 124.4, 124.0, 123.8, 123.4, 122.3, 122.6, 120.0 (C-1, C-2, C-3, C-4, C-5, C-6, C_6H_5), 116.6 (CN), 40.6, 38.2, 17.3 (C-7, C-8, C-9); MS *m/z* 362 (M^+, 38%). Anal. Calcd for $C_{19}H_{14}N_4O_2S$: C, 62.97; H, 3.89; N, 15.46; S, 8.85. Found: C, 62.77; H, 4.19; N, 15.52; S, 8.59.

Ethyl 5-Amino-4,10-dioxo-3-phenyl-2-thioxo-3,4,7,8,9, 10-hexahydro-2*H*-naphtho-[2,1-*e*][1,3]oxazine-6-carboxylate (7b)

Pale brown crystals from ethanol, yield 2.70 g (66%). Mp 177–179 °C. IR (KBr) ν_{max} 3462, 3330 (NH_2), 3055 (CH, aromatic), 1689–1687 (3CO), 1630 (C=C), 1209 cm^{-1} (C=S); ^{1}H NMR (DMSO-d_6, 300 MHz) δ 7.25–7.42 (m, 5H, C_6H_5), 4.83 (s, 2H, D_2O exchangeable, NH_2), 4.23 (q, 2H, *J* = 7.43 Hz, O$\underline{CH_2}CH_3$), 2.98–2.83 (m, 4H, $2CH_2$), 1.93–1.80 (m, 2H, CH_2), 1.12 (t, 3H, *J* = 7.43 Hz, $OCH_2\underline{CH_3}$); ^{13}C NMR (DMSO-d_6, 75 MHz) δ 179.8 (C-2), 174.2, 166.5 (C-4, C-10), 127.1, 126.4, 125.9, 125.0, 124.6, 124.3, 123.5, 123.1, 122.5, 122.6, 120.3 (C-1, C-2, C-3, C-4, C-5, C-6, C_6H_5), 50.3 (O$\underline{CH_2}CH_3$), 40.8, 38.5, 17.0 (C-7, C-8, C-9), 16.1 ($OCH_2\underline{CH_3}$); MS *m/z* 410 (M^+, 18%). Anal. Calcd for $C_{21}H_{18}N_2O_5S$: C, 61.45; H, 4.42; N, 6.83; S, 7.81. Found: C, 61.50; H, 4.38; N, 4.40; S, 7.14.

2. 1. 5. 2-Phenyl-4-thioxo-7,8-dihydro-4*H*-benzo[*e*][1,3]oxazin-5(6*H*)-one (10)

To a solution of compound **1** (1.12 g, 0.01 mol) in 1,4-dioxane (40 mL) benzoyl isothiocyanate (1.63 g, 0.01

mol) [prepared by adding benzoyl chloride (1.40 g, 0.01 mol) to ammonium thiocyanate (0.76 g, 0.01 mol) in 1,4-dioxane (20 mL) with gentle heating for 5 min followed by filtration of the produced ammonium chloride] was heated under reflux for 3 h then left to cool. The formed solid crystals were collected by filtration.

White crystals from ethanol, yield 1.74 g (67%). Mp 188–191 °C. IR (KBr) ν_{max} 3055 (CH, aromatic), 1689 (CO), 1630 (C=C), 1208 cm^{-1} (C=S); ^{1}H NMR (DMSO-d_6, 300 MHz) δ 7.43–7.22 (m, 5H, C_6H_5), 2.78–2.68 (m, 2H, CH_2), 1.93–1.67 (m, 4H, $2CH_2$); ^{13}C NMR (DMSO-d_6, 75 MHz) δ 180.4 (C-4), 174.2 (C-2), 168.2 (C-5), 142.7, 133.3, 126.3, 125.2, 123.6, 121.1 (C_6H_5, C-2, C-4a, C-8a), 39.8, 36.8, 16.0 (C-6, C-7, C-8); MS *m/z* 259 (M^+ +2, 36%). Anal. Calcd for $C_{14}H_{11}NO_2S$: C, 65.35; H, 4.31; N, 5.44; S, 12.46. Found: C, 65.26; H, 5.28; N, 5.60; S, 12.46.

2. 1. 6. General Procedure for the Synthesis of the Thieno[2',3':5,6]benzo[1,2-*e*][1,3]oxazine Derivatives 12a,b

To a solution of compound **10** (2.57 g, 0.01 mol) in ethanol (40 mL), containing triethylamine (0.50 mL), either malononitrile (0.66 g, 0.01 mol) or ethyl cyanoacetate (1.07 g, 0.01 mol) was added. The reaction mixture was heated under reflux for 3 h then poured onto ice/water mixture containing a few drops of hydrochloric acid and the formed solid product was collected by filtration.

8-Amino-3-phenyl-1-thioxo-5,6-dihydro-1*H*-thieno[2',3':5,6]benzo[1,2-*e*][1,3]oxazine-9-carbonitrile (12a)

Orange crystals from ethanol, yield 2.35 g (70%). Mp 180–183 °C. IR (KBr) ν_{max} 3472–3353 (NH_2), 3055 (CH, aromatic), 2220 (CN), 1630 (C=C), 1208 cm^{-1} (C=S); ^{1}H NMR (DMSO-d_6, 300 MHz) δ 7.42–7.26 (m, 5H, C_6H_5), 4.78 (s, 2H, D_2O exchangeable, NH_2), 2.82–2.60 (2t, 4H, $2CH_2$); ^{13}C NMR (DMSO-d_6, 75 MHz) δ 179.6 (C-1), 176.3 (C-3), 142.6, 140.7, 134.2, 132.6, 132.7, 132.3, 127.2, 124.8, 122.4, 121.6 (C_6H_5, C-5, C-6, C-6a, C-9a, C-4a, C-9b), 116.8 (CN); MS *m/z* 339 (M^+ + 2, 28%). Anal. Calcd for $C_{17}H_{11}N_3OS_2$: C, 60.51; H, 3.29; N, 12.45; S, 19.01. Found: C, 60.37; H, 3.63; N, 12.52; S, 18.93.

Ethyl 8-Amino-3-phenyl-1-thioxo-5,6-dihydro-1*H*-thieno[2',3':5,6]benzo[1,2-*e*][1,3]oxazine-9-carboxylate (12b)

Grey crystals from acetic acid, yield 2.84 g (74%). Mp 177–180 °C. IR (KBr) ν_{max} 3459–3337 (NH_2), 3055 (CH, aromatic), 2930, 2970 (CH_2, CH_3), 1689 (CO), 1630 cm^{-1} (C=C); ^{1}H NMR (DMSO-d_6, 300 MHz) δ 1.12 (t, 3H, *J* = 6.59 Hz, CH_3), 2.78–2.65 (2t, 4H, $2CH_2$), 4.26 (q, 2H, *J* = 6.59 Hz, CH_2), 4.80 (s, 2H, D_2O exchangeable, NH_2), 7.45–7.21 (m, 5H, C_6H_6); ^{13}C NMR (DMSO-d_6, 75 MHz) δ 180.4 (C-1), 176.2 (C-3), 168.4 (ester CO), 142.3, 141.3, 134.1, 132.6, 132.9, 132.3, 128.3, 124.9, 123.3, 120.6, (C_6H_5, C-5, C-6, C-6a, C-9a, C-4a, C-9b), 16.1 ($OCH_2\underline{CH_3}$), 52.3 ($O\underline{CH_2}CH_3$); MS *m/z* 386 (M^+ +2, 28%). Anal. Calcd for $C_{19}H_{16}N_2O_3S_2$: C, 59.35; H, 4.19; N, 7.29; S, 16.68. Found: C, 59.28; H, 4.47; N, 7.37; S, 16.39.

2. 1. 7. 2-(1-Amino-2,2,2-trichloroethylidene) cyclohexane-1,3-dione (14)

Equimolar amounts of cyclohexan-1,3-dione (1.12 g, 0.01 mol) and trichloroacetonitrile (1.42 g, 0.01 mol) in absolute ethanol (40 mL) containing triethylamine (0.50 mL) was heated under reflux for 3 h. The solid product formed upon evaporation of the excess alcohol was collected by filtration.

Yellow crystals from ethanol, yield 1.99 g (78%). Mp 204–207 °C. IR (KBr) ν_{max} 3472–3346 (NH_2), 1702, 1688 (2CO), 1630 cm^{-1} (C=C); ^{1}H NMR (DMSO-d_6, 300 MHz) δ 4.85 (s, 2H, D_2O exchangeable, NH_2), 1.96–1.82 (m, 2H, CH_2), 2.95–2.80 (m, 4H, $2CH_2$); ^{13}C NMR (DMSO-d_6, 75 MHz) δ 173.4, 168.0 (C-1, C-3), 112.3, 90.8 (C-2, C-1 ethylidene), 94.8 (CCl_3), 40.8, 38.2, 17.1 (C-4, C-5, C-6); MS *m/z* 256 (M^+ + 2, 28%). Anal. Calcd for $C_8H_8Cl_3NO_2$: C, 37.46; H, 3.14; N, 5.46. Found: C, 37.80; H, 3.39; N, 5.52.

2. 1. 8. 1-Phenyl-2-thioxo-4-(trichloromethyl)-2,3,6,7-tetrahydroquinazolin-5(1*H*)-one (16)

Equimolar amounts of compound **14** (2.56 g, 0.01 mol) and phenyl isothiocyanate (1.30 g, 0.01 mol) in 1,4-dioxane (40 mL) containing triethylamine (0.50 mL) was heated under reflux for 2 h. The solid product formed upon pouring onto ice/water mxture was collected by filtration.

Yellow crystals from ethanol, yield 2.61 g (70%). Mp 168–170 °C. IR (KBr) ν_{max} 3470–3380 (NH), 3050 (CH aromatic), 1689 (CO), 1630 (C=C), 1208 cm^{-1} (C=S); ^{1}H NMR (DMSO-d_6, 300 MHz) δ 8.28 (s, 1H, D_2O exchangeable, NH), 7.42–7.29 (m, 5H, C_6H_5), 5.21 (t, 1H, CH), 2.95–2.80 (m, 4H, $2CH_2$); ^{13}C NMR (DMSO-d_6, 75 MHz) δ 178.8 (C-2), 168.2 (C-5), 135.2, 133.6, 130.3, 129.0, 123.9, 123.6, 121.5, 120.5 (C_6H_5, C-8, C-9, C-3, C-4), 94.4 (CCl_3), 40.8, 38.2 (C-6, C-7); MS *m/z* 373 (M^+, 42%). Anal. Calcd for $C_{15}H_{11}Cl_3N_2OS$: C, 48.21; H, 2.97; N, 7.50. Found: C, 48.45; H, 3.19; N, 7.28.

2. 1. 9. General Procedure for the Synthesis of the 3,5,6,7-Tetrahydroquinazoline Derivatives 18a,b

To a solution of compound **16** (3.73 g, 0.01 mol) in absoute ethanol (60 mL) either hydrazine hydrate (1.0 mL, 0.02 mol) or phenylhydrazine (2.16 g, 0.02 mol) was added. The reaction mixture, in each case, was heated under reflux for 2 h then poured onto ice/water containing a few drops of hydrochloric acid and the formed solid product was collected by filtration.

4-Hydrazinyl-5-hydrazono-1-phenyl-3,5,6,7-tetrahydroquinazoline-2(1*H*)-thione (18a)

Orange crystals from ethanol, yield 2.04 g (68%). Mp 210–212 °C. IR (KBr) ν_{max} 3489–3329 (NH_2), 3054 (CH, aromatic), 1630 (C=C), 1210 cm^{-1} (C=S); ^1H NMR (DMSO-d_6, 300 MHz) δ 8.41, 8.29 (2s, 2H, D_2O exchangeable, 2NH), 7.45–7.28 (m, 5H, C_6H_5), 5.62 (t, 1H, CH), 2.89–2.64 (m, 4H, $2CH_2$), 4.90, 4.78 (2s, 4H, D_2O exchangeable, $2NH_2$), ^{13}C NMR (DMSO-d_6, 75 MHz) δ 179.3 (C-2), 168.6 (C-5), 142.6, 140.7, 134.2, 132.6, 132.7, 132.3, 127.2, 124.8, 122.4, 121.6 (C_6H_5, C-4, C-4a, C-8, C-8), 39.8, 36.7 (C-6, C-7); MS *m/z* 300 (M^+, 40%). Anal. Calcd for $C_{14}H_{16}N_6S$: C, 55.98; H, 5.37; N, 27.98; S, 10.67. Found: C, 56.26; H, 5.49; N, 27.73; S, 10.88.

1-Phenyl-4-(2-phenylhydrazinyl)-5-(2-phenylhydrazono)-3,5,6,7-tetrahydroquinazoline-2(1*H*)-thione (18b)

Orange crystals from methanol, yield 2.71 g (60%). Mp 177–180 °C. IR (KBr) ν_{max} 3449–3352 (NH), 3055 (CH, aromatic), 1630 (C=C), 1208 cm^{-1} (C=S); ^1H NMR (DMSO- d_6, 300 MHz) δ 8.44–8.29 (4s, 4H, D_2O exchangeable, 4NH), 7.49–7.29 (m, 15H, $3C_6H_5$), 5.60 (t, 1H, CH), 2.93–2.64 (m, 4H, $2CH_2$); ^{13}C NMR (DMSO-d_6, 75 MHz) δ 179.6 (C-2), 168.4 (C-5), 141.8, 140.7, 133.0, 132.7, 132.1, 131.8, 127.2, 126.7, 126.5, 124.8, 123.8, 123.6, 123.3, 122.4, 120.9, 120.6, 120.3 ($3C_6H_5$, C-4, C-4a, C-8, C-8), 39.9, 36.5 (C-6, C-7); MS *m/z* 452 (M^+, 36%). Anal. Calcd for $C_{26}H_{24}N_6S$: C, 69.00; H, 5.35; N, 18.57; S, 7.09. Found: C, 69.21; H, 5.58; N, 18.80; S, 7.26.

2. 1. 10. General Procedure for the Synthesis of the 6,7-Dihydroisoquinoline Derivatives 20a,b

To a solution of compound **14** (2.65 g, 0.01 mol) in 1,4-dioxane containing ammonium acetate (2.00 g) either malononitrile (0.66 g, 0.01 mol) or ethyl cyanoacetate (1.13 g, 0.01 mol) was added. The whole reaction mixture was heated under reflux for 3 h and the solid product formed, in each case, upon pouring onto ice/water containing a few drops of hydrochloric acid, was collected by filtration.

3-Amino-8-oxo-1-(trichloromethyl)-5,6,7,8-tetrahydroisoquinoline-4-carbonitrile (20a)

Orange crystals from 1,4-dioxane, yield 1.97 g (65%). Mp 211–214 °C. IR (KBr) ν_{max} 3458, 3332 (NH_2), 3050 (CH aromatic), 2220 (CN), 1689 (CO), 1630 cm^{-1} (C=C); ^1H NMR (DMSO-d_6, 300 MHz) δ 4.80 (s, 2H, D_2O exchangeable, NH_2), 2.93–2.82 (m, 4H, $2CH_2$), 1.86–1.62 (m, 2H, CH_2); ^{13}C NMR (DMSO-d_6, 75 MHz) δ 168.2 (C-8), 164.2 (C-3), 124.2, 123.8, 121.5, 120.3, 119.6 (C-1, C-4, C-4a, C-8a), 117.2 (CN), 94.6 (CCl_3), 40.8, 38.2, 24.8 (C-5, C-6, C-7); MS *m/z* 304 (M^+, 28%). Anal. Calcd for $C_{11}H_8Cl_3N_3O$: C, 43.38; H, 2.65; N, 13.80. Found: C, 43.52; H, 2.80; N, 13.68.

Ethyl 3-Amino-8-oxo-1-(trichloromethyl)-5,6,7,8-tetrahydroisoquinoline-4-carboxylate (20b)

Pale brown crystals from 1,4-dioxane, yield 2.52 g (72%). Mp 180–180 °C. IR (KBr) ν_{max} 3468, 3329 (NH_2), 3045 (CH aromatic), 1702, 1689 (2CO), 1630 cm^{-1} (C=C); ^1H NMR (DMSO-d_6, 300 MHz) δ 4.85 (s, 2H, D_2O exchangeable, NH_2), 4.23 (q, 2H, J = 6.80 Hz, $O\underline{CH_2}CH_3$), 2.96–2.80 (m, 4H, $2CH_2$), 1.86–1.61 (m, 2H, CH_2), 1.12 (t, 3H, J = 6.80 Hz, $OCH_2\underline{CH_3}$); ^{13}C NMR (DMSO-d_6, 75 MHz) δ 168.2 (C-8), 164.8 (C=N), 124.9, 123.5, 122.8, 120.1, 119.8 (C-1, C-4, C-4a, C-8a), 94.5 (CCl_3), 50.3 ($O\underline{CH_2}CH_3$), 40.8, 38.7, 24.3 (C-5, C-6, C-7), 16.5 ($OCH_2\underline{CH_3}$); MS *m/z* 350 (M^+, 28%). Anal. Calcd for $C_{13}H_{13}Cl_3N_2O_3$: C, 44.41; H, 3.73; N, 7.97. Found: C, 44.60; H, 3.84; N, 18.26.

2. 1. 11. General Procedure for the Synthesis of the 5,6-Dihydrothieno[2,3-*h*]isoquinoline Derivatives 21a–d

To a solution of either compound **20a** (3.04 g, 0.01 mol) or **20b** (3.50 g, 0.01 mol) in 1,4-dioxane (40 mL) containing triethylamine (1.00 mL) either malononitrile (0.66 g, 0.01 mol) or ethyl cyanoacetate (1.07 g, 0.01 mol) was added. The reaction mixture, in each case, was heated under reflux for 1 h then poured onto ice/water containing a few drops of hydrochloric acid and the formed solid product was collected by filtration.

3,8-Diamino-1-(trichloromethyl)-5,6-dihydrothieno[2,3-*h*]isoquinoline-4,9-dicarbonitrile (21a)

Pale brown crystals from 1,4-dioxane, yield 2.95 g (77%). Mp > 300 °C. IR (KBr) ν_{max} 3493–3362 (NH_2), 3050 (CH aromatic), 2223, 2220 (2CN), 1630 cm^{-1} (C=C); ^1H NMR (DMSO-d_6, 300 MHz) δ 2.98–2.86 (m, 4H, $2CH_2$), 4.87, 4.84 (2s, 4H, D_2O exchangeable, $2NH_2$); ^{13}C NMR (DMSO-d_6, 75 MHz) δ 164.7 (C-3), 134.5, 132.4, 130.2, 129.8, 124.9, 122.6, 120.8, 120.6, 119.8 (C-1, C-4, C-4a, C-9, C-8, C-8a, C-6a, C-9a), 117.1, 116.8 (2CN), 94.8 (CCl_3), 40.9, 38.6 (C-5, C-6); MS *m/z* 384 (M^+, 62%). Anal. Calcd for $C_{14}H_8Cl_3N_5S$: C, 43.71; H, 2.10; N, 18.21; S, 8.34. Found: C, 43.52; H, 1.89; N, 17.82; S, 8.08.

Ethyl 3,8-Diamino-9-cyano-1-(trichloromethyl)-5,6-dihydrothieno[2,3-*h*]isoquinoline-4-carboxylate (21b)

Pale brown crystals from 1,4-dioxane, yield 3.17 g (73%). Mp 284–287 °C. IR (KBr) ν_{max} 3482–3339 (NH_2), 3050 (CH aromatic), 2220 (CN), 1688 (CO), 1630 cm^{-1} (C=C); ^1H NMR (DMSO-d_6, 300 MHz) δ 1.12 (t, 3H, J = 6.47 Hz, $OCH_2\underline{CH_3}$), 2.84–2.96 (m, 4H, $2CH_2$), 4.22 (q, 2H, J = 6.47 Hz, $O\underline{CH_2}CH_3$), 4.86, 4.86 (2s, 4H, D_2O exchangeable, $2NH_2$); ^{13}C NMR (DMSO-d_6, 75 MHz) δ 168.2 (CO ester), 164.8 (C-3), 133.6, 130.3, 128.0, 127.2, 124.7, 123.7, 122.7, 120.8, 119.6 (C-1, C-4, C-4a, C-9, C-8, C-8a, C-6a, C-9a), 116.9 (CN), 94.5 (CCl_3), 50.6 ($O\underline{CH_2}CH_3$), 40.6, 38.8 (C-5, C-6), 16.8 ($OCH_2\underline{CH_3}$); MS *m/z* 431 (M^+, 54%). Anal. Calcd for $C_{16}H_{13}Cl_3N_4O_2S$: C, 44.51; H, 3.04; N, 12.98; S, 7.43. Found: C, 44.72; H, 3.29; N, 13.18; S, 7.72.

Ethyl 3,8-Diamino-4-cyano-1-(trichloromethyl)-5,6-dihydrothieno[2,3-*h*]isoquinoline-9-carboxylate (21c)

Pale brown crystals from 1,4-dioxane, yield 2.58 g (60%). Mp 179–182 °C. IR (KBr) ν_{max} 3459–3321 (NH_2), 3050 (CH aromatic), 2220 (CN), 1689 (CO), 1630 cm^{-1} (C=C); ^{1}H NMR (DMSO-d_6, 300 MHz) δ 4.88, 4.84 (2s, 4H, D_2O exchangeable, $2NH_2$), 4.21 (q, 2H, J = 7.25 Hz, O$\underline{CH_2}CH_3$), 2.98–2.82 (m, 4H, $2CH_2$), 1.13 (t, 3H, J = 7.25 Hz, $OCH_2\underline{CH_3}$); ^{13}C NMR (DMSO-d_6, 75 MHz) δ 168.6 (CO ester), 164.5 (C-3), 116.8 (CN), 133.9, 131.2, 128.5, 127.6, 125.2, 123.9, 122.8, 120.6, 120.3 (C-1, C-4, C-4a, C-9, C-8, C-8a, C-6a, C-9a), 94.7 (CCl_3), 50.3 (O$\underline{CH_2}CH_3$), 40.8, 38.6 (C-5, C-6), 16.9 ($OCH_2\underline{CH_3}$); MS *m/z* 431 (M^+, 54%). Anal. Calcd for $C_{16}H_{13}Cl_3N_4O_2S$: C, 44.51; H, 3.04; N, 12.98; S, 7.43. Found: C, 44.72; H, 3.29; N, 13.18; S, 7.72.

Diethyl 3,8-Diamino-1-(trichloromethyl)-5,6-dihydrothieno[2,3-*h*]isoquinoline-4,9-dicarboxylate (21d)

Pale brown crystals from 1,4-dioxane, yield 2.58 g (60%). Mp 179–182 °C. IR (KBr) ν_{max} 3459–3321 (NH_2), 3050 (CH aromatic), 2220 (CN), 1689 (CO), 1630 cm^{-1} (C=C); ^{1}H NMR (DMSO-d_6, 300 MHz) δ 4.88, 4.84 (2s, 4H, D_2O exchangeable, $2NH_2$), 4.23, 4.21 (2q, 4H, J_1 = 5.80 Hz, J_2 = 7.25 Hz, two O$\underline{CH_2}CH_3$), 2.98–2.82 (m, 4H, $2CH_2$), 1.13, 1.12 (2t, 6H, J_1 = 5.80 Hz, J_2 = 7.25 Hz, two $OCH_2\underline{CH_3}$); ^{13}C NMR (DMSO-d_6, 75 MHz) δ 168.6, 167.2 (2CO ester), 164.5 (C-3), 133.9, 131.2, 128.5, 127.6, 125.2, 123.9, 122.8, 120.6, 120.3 (C-1, C-4, C-4a, C-9, C-8, C-8a, C-6a, C-9a), 116.8 (CN), 94.7 (CCl_3), 50.6, 50.3 (two O$\underline{CH_2}CH_3$), 40.8, 38.6 (C-5, C-6), 16.9, 16.7 (two $OCH_2\underline{CH_3}$); MS *m/z* 478 (M^+, 54%). Anal. Calcd for $C_{18}H_{18}Cl_3N_3O_4S$: C, 45.16; H, 3.79; N, 8.78; S, 6.70. Found: C, 44.92; H, 3.59; N, 8.92; S, 6.82.

2. 1. 12. General Procedure for the Synthesis of the 1-Hydroxy-5,6-dihydrothieno[2,3-*h*] isoquinoline derivatives 22a–d

A solution of either **21a** (3.86 g, 0.01 mol), **21b** (4.29 g, 0.01 mol), **21c** (4.31 g, 0.01 mol) or **21d** (4.31 g, 0.01 mol) in ethanol (60 mL) containing sodium hydroxide solution (10%, 5 mL) was heated under reflux for 4 h till ammonia gas evaluation cease. The solid product formed, in each case, upon pouring onto ice/water containing a few drops of hydrochloric acid (till pH 6) was collected by filtration.

3,8-Diamino-1-hydroxy-5,6-dihydrothieno[2,3-*h*]isoquinoline-4,9-dicarbonitrile (22a)

Pale yellow crystals from 1,4-dioxane, yield 1.98 g (66%). Mp 220–223 °C. IR (KBr) ν_{max} 3563–3362 (OH, NH_2), 3050 (CH aromatic), 2224, 2220 (2CN), 1630 cm^{-1} (C=C); ^{1}H NMR (DMSO-d_6, 300 MHz) δ 10.27 (s, 1H, D_2O exchangeable, OH), 4.89, 4.81 (2s, 4H, D_2O exchangeable, $2NH_2$), 2.96–2.83 (m, 4H, $2CH_2$); ^{13}C NMR (DMSO-d_6, 75 MHz) δ 164.8 (C-2), 133.8, 131.4, 130.6, 129.3, 125.3, 124.6, 123.8, 121.6, 120.7, 120.2 (C-1, C-4, C-4a, C-9, C-8, C-8a, C-6a, C-9a), 117.0, 116.5 (2CN), 40.7, 38.4 (C-5, C-6); MS *m/z* 283 (M^+, 55%). Anal. Calcd for $C_{13}H_9N_5OS$: C, 55.11; H, 3.20; N, 24.72; S, 11.32. Found: C, 54.85; H, 3.59; N, 24.83; S, 11.48.

Ethyl 3,8-Diamino-9-cyano-1-hydroxy-5,6-dihydrothieno[2,3-*h*]isoquinoline-4-carboxylate (22b)

Pale brown crystals from 1,4-dioxane, yield 2.17 g (66%). Mp 189–192 °C. IR (KBr) ν_{max} 3542–3359 (OH, NH_2), 3050 (CH aromatic), 2220 (CN), 1689 (CO), 1630 cm^{-1} (C=C); ^{1}H NMR (DMSO-d_6, 300 MHz) δ 10.22 (s, 1H, D_2O exchangeable, OH), 4.89, 4.84 (2s, 4H, D_2O exchangeable, $2NH_2$), 4.24 (q, 2H, J = 7.02 Hz, O$\underline{CH_2}CH_3$), 2.98–2.85 (m, 4H, $2CH_2$), 1.12 (t, 3H, J = 7.02 Hz, $OCH_2\underline{CH_3}$); ^{13}C NMR (DMSO-d_6, 75 MHz) δ 168.6 (CO ester), 164.3 (C-3), 133.8, 130.1, 128.2, 126.5, 124.1, 122.8, 122.2, 120.9, 120.6 (C-1, C-4, C-4a, C-9, C-8, C-8a, C-6a, C-9a), 116.7 (CN), 50.3 (O$\underline{CH_2}CH_3$), 40.8, 38.5 (C-5, C-6), 16.9 ($OCH_2\underline{CH_3}$); MS *m/z* 330 (M^+, 28%). Anal. Calcd for $C_{15}H_{14}N_4O_3S$: C, 54.53; H, 4.27; N, 16.96; S, 9.71. Found: C, 54.66; H, 4.30; N, 17.16; S, 9.89.

Ethyl 3,8-Diamino-4-cyano-1-hydroxy-5,6-dihydrothieno[2,3-*h*]isoquinoline-9-carboxylate (22c)

Pale brown crystals from 1,4-dioxane, yield 1.98 g (60%). Mp 201–204 °C. IR (KBr) ν_{max} 3539–3345 (OH, NH_2), 3050 (CH aromatic), 2220 (CN), 1689 (CO), 1630 cm^{-1} (C=C); ^{1}H NMR (DMSO-d_6, 300 MHz) δ 10.22 (s, 1H, D_2O exchangeable, OH), 5.01, 4.86 (2s, 4H, D_2O exchangeable, $2NH_2$), 4.23 (q, 2H, J = 6.85 Hz, O$\underline{CH_2}CH_3$), 2.96–2.80 (m, 4H, $2CH_2$), 1.12 (t, 3H, J = 6.85 Hz, $OCH_2\underline{CH_3}$); ^{13}C NMR (DMSO-d_6, 75 MHz) δ 168.4 (CO), 164.6 (C=N), 133.7, 132.5, 129.7, 127.9, 124.8, 123.3, 122.5, 120.4, 120.1 (C-1, C-4, C-4a, C-9, C-8, C-8a, C-6a, C-9a), 116.8 (CN), 50.5 (O$\underline{CH_2}CH_3$), 40.9, 38.2 (C-5, C-6), 16.7 ($OCH_2\underline{CH_3}$); MS *m/z* 330 (M^+, 36%). Anal. Calcd for $C_{15}H_{14}N_4O_3S$: C, 54.53; H, 4.27; N, 16.96; S, 9.71. Found: C, 54.82; H, 4.08; N, 17.26; S, 9.87.

Diethyl 3,8-Diamino-1-hydroxy-5,6-dihydrothieno[2,3-*h*]isoquinoline-4,9-dicarboxylate (22d)

Pale brown crystals from 1,4-dioxane, yield 2.58 g (60%). Mp 179–182 °C. IR (KBr) ν_{max} 3559–3321 (NH_2), 3050 (CH aromatic), 2220 (CN), 1689 (CO), 1630 cm^{-1} (C=C); ^{1}H NMR (DMSO-d_6, 300 MHz) δ 10.21 (s, 1H, D_2O exchangeable, OH), 4.84, 4.80 (2s, 4H, D_2O exchangeable, $2NH_2$), 4.24, 4.21 (q, 4H, J_1 = 6.39 Hz, J_2 = 7.25 Hz, two O$\underline{CH_2}CH_3$), 2.98–2.82 (m, 4H, $2CH_2$), 1.13, 1.12 (2t, 6H, J_1 = 6.39 Hz, J_2 = 7.25 Hz, two $OCH_2\underline{CH_3}$); ^{13}C NMR (DMSO-d_6, 75 MHz) δ 169.0, 168.6 (two CO ester), 164.5 (C-3), 133.9, 131.2, 128.5, 127.6, 125.2, 123.9, 122.8, 120.6, 120.3 (C-1, C-4, C-4a, C-9, C-8, C-8a, C-6a, C-9a), 116.8 (CN), 50.3, 50.1 (two O$\underline{CH_2}CH_3$), 40.8, 38.6 (C-5, C-6), 16.9, 16.6 (two $OCH_2\underline{CH_3}$); MS *m/z* 377 (M^+, 68%). Anal. Calcd for $C_{17}H_{19}N_3O_5S$: C, 54.10; H, 5.07; N, 11.13; S, 8.50. Found: C, 54.26; H, 4.85; N, 11.26; S, 8.79.

2. 1. 13. General Procedure for the Synthesis of the 5,6-Dihydrothieno[2,3-*h*]isoquinoline derivatives 24a–h

To a solution of either **21a** (3.86 g, 0.01 mol), **21b** (4.29 g, 0.01 mol), **21c** (4.31 g, 0.01 mol) or **21d** (4.31 g, 0.01 mol) in ethanol (60 mL) either potassium cyanide (1.28 g, 0.02 mol) or potassium thiocyanide (1.94 g, 0.01 mol) dissolved in water (10 mL) was added drop-wise. After complete addition, the whole mixture, in each case, was heated in a water bath at 60 °C for 2 h then was poured onto ice/water mixture containing a few drops of hydrochloric acid and the formed solid product was collected by filtration.

3,8-Diamino-5,6-dihydrothieno[2,3-*h*]isoquinoline-1,4,9-tricarbonitrile (24a)

Pale brown crystals from 1,4-dioxane, yield 1.69 g (58%). Mp 266–268 °C. IR (KBr) ν_{max} 3469–3341 (NH_2), 3045 (CH aromatic), 2223–2220 (3CN), 1630 cm^{-1} (C=C); ^{1}H NMR (DMSO-d_6, 300 MHz) δ 2.86–2.98 (m, 4H, $2CH_2$), 4.84, 4.87 (2s, 4H, D_2O exchangeable, $2NH_2$); ^{13}C NMR (DMSO-d_6, 75 MHz) δ 164.7 (C-3), 133.5, 132.6, 129.4, 127.8, 124.8, 122.7, 121.5, 120.9, 120.6 (C-1, C-4, C-4a, C-9, C-8, C-8a, C-6a, C-9a), 117.2, 117.1, 116.5 (3CN), 40.8, 38.4 (C-5, C-6); MS *m/z* 292 (M^+, 58%). Anal. Calcd for $C_{14}H_8N_6S$: C, 57.52; H, 2.76; N, 28.75; S, 10.97. Found: C, 57.69; H, 2.80; N, 28.66; S, 10.57.

Ethyl 3,8-Diamino-1,9-dicyano-5,6-dihydrothieno[2,3-*h*]isoquinoline-4-carboxylate (24b)

Pale yellow crystals from 1,4-dioxane, yield 2.10 g (62%). Mp 180–184 °C. IR (KBr) ν_{max} 3488–3331 (NH_2), 3050 (CH aromatic), 2224, 2220 (2CN), 1689 (CO), 1630 cm^{-1} (C=C); ^{1}H NMR (DMSO-d_6, 300 MHz) δ 4.97, 4.84 (2s, 4H, D_2O exchangeable, $2NH_2$), 4.22 (q, 2H, J = 6.41 Hz, $O\underline{CH_2}CH_3$), 2.98–2.83 (m, 4H, $2CH_2$), 1.14 (t, 3H, J = 6.41 Hz, $OCH_2\underline{CH_3}$); ^{13}C NMR (DMSO-d_6, 75 MHz) δ 168.8 (CO ester), 164.8 (C-3), 133.9, 132.1, 128.3, 126.8, 124.3, 123.6, 121.9, 120.8, 120.4 (C-1, C-4, C-4a, C-9, C-8, C-8a, C-6a, C-9a), 117.0, 116.3 (2CN), 50.3 ($O\underline{CH_2}CH_3$), 40.7, 38.4 (C-5, C-6), 16.8 ($OCH_2\underline{CH_3}$); MS *m/z* 339 (M^+, 63%). Anal. Calcd for $C_{16}H_{13}N_5O_2S$: C, 56.63; H, 3.86; N, 20.64; S, 9.45. Found: C, 56.80; H, 3.96; N, 20.80; S, 9.62.

Ethyl 3,8-diamino-1,4-dicyano-5,6-dihydrothieno[2,3-*h*]isoquinoline-9-carboxylate (24c)

Pale yellow crystals from 1,4-dioxane, yield 2.03 g (60%). Mp 222–225 °C. IR (KBr) ν_{max} 3488–3331 (NH_2), 3050 (CH aromatic), 2223, 2220 (2CN), 1689 (CO), 1630 cm^{-1} (C=C); ^{1}H NMR (DMSO-d_6, 300 MHz) δ 4.99, 4.86 (2s, 4H, D_2O exchangeable, $2NH_2$), 4.23 (q, 2H, J = 7.22 Hz, $O\underline{CH_2}CH_3$), 2.96–2.81 (m, 4H, $2CH_2$), 1.13 (t, 3H, J = 7.22 Hz, $OCH_2\underline{CH_3}$); ^{13}C NMR (DMSO-d_6, 75 MHz) δ 168.8 (CO ester), 164.9 (C-3), 133.9, 132.1, 128.1, 126.2, 124.1, 123.8, 121.9, 120.8, 120.1 (C-1, C-4, C-4a, C-9, C-8, C-8a, C-6a, C-9a), 117.0, 116.3 (2CN), 50.4 ($O\underline{CH_2}CH_3$), 40.8, 38.4 (C-5, C-6), 16.2 ($OCH_2\underline{CH_3}$); MS *m/z* 339 (M^+, 44%). Anal. Calcd for $C_{16}H_{13}N_5O_2S$: C, 56.63; H, 3.86; N, 20.64; S, 9.45. Found: C, 56.49; H, 3.77; N, 20.41; S, 9.53.

Diethyl 3,8-Diamino-1-cyano-5,6-dihydrothieno[2,3-*h*]isoquinoline-4,9-dicarboxylate (24d)

Yellow crystals from 1,4-dioxane, yield 2.70 g (70%). Mp 177–180 °C. IR (KBr) ν_{max} 3493–3352 (NH_2), 3050 (CH aromatic), 2220 (CN), 1689 (CO), 1630 cm^{-1} (C=C); ^{1}H NMR (DMSO-d_6, 300 MHz) δ 4.97, 4.84 (2s, 4H, D_2O exchangeable, $2NH_2$), 4.24, 4.22 (2q, 4H, J_1 = 6.80 Hz, J_2 = 7.51 Hz, two $O\underline{CH_2}CH_3$), 2.97–2.83 (m, 4H, $2CH_2$), 1.14, 1.12 (2t, 6H, J_1 = 6.80 Hz, J_2 = 7.51 Hz, two $OCH_2\underline{CH_3}$); ^{13}C NMR (DMSO-d_6, 75 MHz) δ 170.1, 168.9 (two CO ester), 164.7 (C-3), 134.2, 131.7, 128.5, 125.8, 124.2, 123.4, 121.6, 120.6, 120.3 (C-1, C-4, C-4a, C-9, C-8, C-8a, C-6a, C-9a), 117.1 (CN), 50.4, 50.1 (two $O\underline{CH_2}CH_3$), 40.9, 38.2 (C-5, C-6), 16.5, 16.2 (two $OCH_2\underline{CH_3}$); MS *m/z* 386 (M^+, 36%). Anal. Calcd for $C_{18}H_{18}N_4O_4S$: C, 55.95; H, 4.70; N, 14.50; S, 8.30. Found: C, 56.25; H, 4.59; N, 14.73; S, 8.62.

3,8-Diamino-1-thiocyanato-5,6-dihydrothieno[2,3-*h*]isoquinoline-4,9-dicarbonitrile (24e)

Pale brown crystals from 1,4-dioxane, yield 2.52 g (78%). Mp 243–247 °C. IR (KBr) ν_{max} 3482–3326 (NH_2), 3045 (CH aromatic), 2224–2220 (3CN), 1630 cm^{-1} (C=C); ^{1}H NMR (DMSO-d_6, 300 MHz) δ 4.86, 4.82 (2s, 4H, D_2O exchangeable, $2NH_2$), 2.96–2.84 (m, 4H, $2CH_2$); ^{13}C NMR (DMSO-d_6, 75 MHz) δ 164.8 (C-3), 133.9, 132.8, 129.6, 127.3, 123.2, 122.1, 121.8, 120.7, 120.4 (C-1, C-4, C-4a, C-9, C-8, C-8a, C-6a, C-9a), 40.6, 38.1 (C-5, C-6), 117.1, 116.4 110.8 (3CN); MS *m/z* 324 (M^+, 40%). Anal. Calcd for $C_{14}H_8N_6S_2$: C, 51.84; H, 2.49; N, 25.91; S, 19.77. Found: C, 51.69; H, 2.63; N, 26.25; S, 19.80.

Ethyl 3,8-Diamino-9-cyano-1-thiocyanato-5,6-dihydrothieno[2,3-*h*]isoquinoline-4-carboxylate (24f)

Yellow crystals from 1,4-dioxane, yield 2.74 g (74%). Mp 170–172 °C. IR (KBr) ν_{max} 3479–3343 (NH_2), 3050 (CH aromatic), 2221, 2220 (2CN), 1689 (CO), 1630 cm^{-1} (C=C); ^{1}H NMR (DMSO-d_6, 300 MHz) δ 4.97, 4.83 (2s, 4H, D_2O exchangeable, $2NH_2$), 4.22 (q, 2H, J = 6.84 Hz, $O\underline{CH_2}CH_3$), 2.98–2.81 (m, 4H, $2CH_2$), 1.13 (t, 3H, J = 6.84 Hz, $OCH_2\underline{CH_3}$); ^{13}C NMR (DMSO-d_6, 75 MHz) δ 168.6 (CO ester), 164.8 (C-3), 116.8, 112.6 (2CN), 133.5, 132.4, 128.8, 126.2, 124.4, 123.9, 122.3, 120.6, 120.0 (C-1, C-4, C-4a, C-9, C-8, C-8a, C-6a, C-9a), 50.2 ($O\underline{CH_2}CH_3$), 40.6, 38.1 (C-5, C-6), 16.5 ($OCH_2\underline{CH_3}$); MS *m/z* 371 (M^+, 32%). Anal. Calcd for $C_{16}H_{13}N_5O_2S_2$: C, 51.74; H, 3.53; N, 18.85; S, 17.27. Found: C, 52.01; H, 3.49; N, 18.63; S, 17.08.

Ethyl 3,8-Diamino-4-cyano-1-thiocyanato-5,6-dihydrothieno[2,3-*h*]isoquinoline-9-carboxylate (24g)

Yellow crystals from 1,4-dioxane, yield 2.04 g (55%). Mp 193–196 °C. IR (KBr) ν_{max} 3493–3329 (NH_2), 3050 (CH aromatic), 2224, 2220 (2CN), 1688 (CO), 1630 cm^{-1}

(C=C); ^{1}H NMR (DMSO-d_6, 300 MHz) δ 4.97, 4.82 (2s, 4H, D_2O exchangeable, $2NH_2$), 4.23 (q, 2H, J = 7.12 Hz, $O\underline{CH_2}CH_3$), 2.96–2.80 (m, 4H, $2CH_2$), 1.12 (t, 3H, J = 7.12 Hz, $OCH_2\underline{CH_3}$); ^{13}C NMR (DMSO-d_6, 75 MHz) δ 168.4 (CO ester), 164.7 (C-3), 132.8, 131.6, 120.3, 129.2, 126.2, 124.1, 123.9, 122.6, 121.8 (C-1, C-4, C-4a, C-9, C-8, C-8a, C-6a, C-9a), 116.6, 111.5 (2CN), 50.2 ($O\underline{CH_2}CH_3$), 40.6, 38.4 (C-5, C-6), 16.3 ($OCH_2\underline{CH_3}$); MS *m/z* 371 (M^+, 36%). Anal. Calcd for $C_{16}H_{13}N_5O_2S_2$: C, 51.74; H, 3.53; N, 18.85; S, 17.27. Found: C, 51.91; H, 3.42; N, 18.43; S, 17.33.

Diethyl 3,8-Diamino-1-thiocyanato-5,6-dihydrothieno[2,3-*h*]isoquinoline-4,9-dicarboxylate (24h)

Pale yellow crystals from 1,4-dioxane, yield 2.71 g (52%). Mp 166–169 °C. IR (KBr) ν_{max} 3470–3332 (NH_2), 3050 (CH aromatic), 2221, 2220 (CN), 1689 (CO), 1630 cm^{-1} (C=C); ^{1}H NMR (DMSO-d_6, 300 MHz) δ 4.97, 4.84 (2s, 4H, D_2O exchangeable, $2NH_2$), 4.23, 4.22 (2q, 4H, J_1 = 6.49 Hz, J_2 = 6.21 Hz, two $O\underline{CH_2}CH_3$), 2.98–2.81 (m, 4H, $2CH_2$), 1.13, 1.12 (2t, 6H, J_1 = 6.49 Hz, J_2 = 6.21 Hz, two $OCH_2\underline{CH_3}$); ^{13}C NMR (DMSO-d_6, 75 MHz) δ 168.8 (CO ester), 164.5 (C-3), 133.8, 131.3, 128.2, 124.9, 124.7, 122.6, 121.9, 120.8, 120.1, (C-1, C-4, C-4a, C-9, C-8, C-8a, C-6a, C-9a), 112.3, 117.0 (2CN), 50.3, 50.6 (two $O\underline{CH_2}CH_3$), 40.8, 38.3 (C-5, C-6), 16.1, 16.4 (two $OCH_2\underline{CH_3}$); MS *m/z* 418 (M^+, 24%). Anal. Calcd for $C_{18}H_{18}N_4O_4S_2$: C, 51.66; H, 4.34; N, 13.39; S, 15.32. Found: C, 51.49; H, 4.60; N, 13.26; S, 15.53.

2. 1. Biology Section

2. 2. 1. Cell Proliferation Assay

The anti-proliferative activities of the newly synthesized compounds (Table 1) were evaluated against the six cancer cell lines A549, HT-29, MKN-45, U87MG, SMMC-7721, and H460 using the standard MTT assay *in vitro*, with foretinib as the positive control.[23] The cancer cell lines were cultured in minimum essential medium (MEM) supplemented with 10% fetal bovine serum (FBS).

Table 1. *In vitro* growth inhibitory effects IC_{50} ± SEM (μM) of the newly synthesized compounds against cancer cell lines

Compound No	IC_{50} ± SEM (μM)					
	A549	H460	HT29	MKN-45	U87MG	SMMC-7721
3a	8.72 ± 2.62	6.25 ± 3.06	7.83 ± 2.54	8.01 ± 2.41	8.72 ± 2.63	8.08 ± 3.19
3b	3.46 ± 1.29	4.53 ± 1.44	3.65 ± 1.64	2.43 ± 0.86	3.82 ± 1.06	2.63 ± 1.16
4a	5.83 ± 1.43	6.73 ± 2.54	3.29 ± 1.13	2.62 ± 0.74	4.80 ± 2.43	3.78 ± 0.62
4b	7.72 ± 2.63	8.69 ± 2.36	6.73 ± 2.33	8.62 ± 1.43	7.25 ± 2.49	8.30 ± 3.59
6a	9.29 ± 2.59	8.17 ± 2.89	5.08 ± 1.69	4.32 ± 2.41	6.50 ± 1.52	6.30 ± 2.83
6b	0.32 ± 0.20	0.34 ± 0.13	0.52 ± 0.24	0.45 ± 0.12	0.53 ± 0.25	0.39 ± 0.14
7a	5.63 ± 1.28	3.49 ± 1.28	5.46 ± 2.36	6.05 ± 2.47	4.29 ± 1.59	6.07 ± 2.62
7b	1.26 ± 0.85	0.99 ± 0.63	0.86 ± 0.49	0.32 ± 0.19	0.68 ± 0.19	0.80 ± 0.38
10	8.24 ± 3.68	6.26 ± 2.34	5.29 ± 2.89	6.27 ± 1.29	3.83 ± 1.53	5.59 ± 2.32
12a	6.28 ± 1.78	4.83 ± 1.23	4.70 ± 1.20	6.73 ± 2.30	5.82 ± 2.69	6.49 ± 2.28
12b	0.34 ± 0.21	0.69 ± 0.30	0.53 ± 0.32	0.28 ± 2.39	0.42 ± 0.29	0.52 ± 0.26
14	0.52 ± 0.13	0.83 ± 0.20	0.71 ± 1.82	0.26 ± 0.12	0.60 ± 0.21	0.15 ± 0.02
16	0.31 ± 0.22	0.13 ± 0.07	0.22 ± 0.16	0.32 ± 0.17	0.42 ± 0.19	0.36 ± 0.15
18a	1.63 ± 0.23	1.63 ± 0.34	1.08 ± 0.81	0.92 ± 0.63	0.90 ± 0.71	1.31 ± 0.80
18b	0.62 ± 0.39	0.72 ± 0.53	0.39 ± 0.26	0.49 ± 0.26	0.58 ± 0.19	0.64 ± 0.28
20a	1.26 ± 0.69	1.38 ± 0.99	1.79 ± 0.82	0.96 ± 0.42	0.86 ± 0.26	0.57 ± 0.30
20b	0.30 ± 0.19	0.24 ± 0.10	0.43 ± 0.27	0.52 ± 0.18	0.23 ± 0.0.8	0.32 ± 0.17
21a	1.16 ± 0.75	1.80 ± 0.69	1.25 ± 0.48	2.04 ± 0.38	1.90 ± 0.58	1.49 ± 0.78
21b	0.31 ± 0.20	0.39 ± 0.12	0.23 ± 0.06	0.23 ± 0.06	0.28 ± 0.16	0.56 ± 0.23
21c	0.58 ± 0.17	0.52 ± 0.23	0.62 ± 0.22	0.42 ± 0.19	0.53 ± 0.25	0.72 ± 0.19
21d	0.49 ± 0.21	0.52 ± 0.15	0.46 ± 0.19	0.50 ± 0.27	0.70 ± 0.25	0.38 ± 0.18
22a	1.02 ± 0.72	1.26 ± 0.59	1.42 ± 0.69	1.26 ± 0.82	0.86 ± 0.31	1.63 ± 0.82
22b	1.12 ± 0.69	1.04 ± 0.80	1.36 ± 0.88	1.26 ± 0.73	2.13 ± 1.79	0.85 ± 0.41
22c	0.26 ± 0.19	0.35 ± 0.16	0.42 ± 0.27	0.19 ± 0.02	0.36 ± 0.18	0.28 ± 0.06
22d	0.32 ± 0.18	0.26 ± 0.13	0.51 ± 0.29	0.35 ± 0.29	0.28 ± 0.06	0.18 ± 0.07
24a	1.44 ± 0.86	1.22 ± 0.76	0.89 ± 0.54	0.95 ± 0.63	0.86 ± 0.39	1.39 ± 2.28
24b	1.05 ± 0.61	1.70 ± 0.72	0.96 ± 0.26	0.83 ± 0.39	1.46 ± 0.79	1.36 ± 0.87
24c	2.82 ± 0.93	1.69 ± 0.93	1.38 ± 0.62	0.79 ± 0.42	0.89 ± 0.32	1.67 ± 0.58
24d	0.27 ± 0.12	0.38 ± 0.09	0.52 ± 0.28	0.38 ± 0.19	0.46 ± 0.21	0.39 ± 0.18
24e	1.66 ± 0.26	1.42 ± 0.73	1.39 ± 0.86	0.72 ± 0.63	0.68 ± 0.31	1.41 ± 0.89
24f	0.87 ± 0.32	0.69 ± 0.28	0.39 ± 0.21	0.62 ± 0.28	0.72 ± 0.39	0.83 ± 0.36
24g	0.77 ± 0.26	0.82 ± 0.31	0.59 ± 0.82	0.32 ± 0.17	0.32 ± 0.18	0.21 ± 0.05
24h	0.53 ± 0.14	0.61 ± 0.28	0.42 ± 0.21	0.62 ± 0.18	0.60 ± 0.32	0.59 ± 0.15
Foretinib	0.08 ± 0.01	0.18 ± 0.03	0.15 ± 0.023	0.03 ± 0.0055	0.90 ± 0.13	0.44 ± 0.062

Approximate 4×10^3 cells, suspended in MEM medium, were plated onto each well of a 96-well plate and incubated in 5% CO_2 at 37 °C for 24 h. The compounds tested at the indicated final concentrations were added to the culture medium and the cell cultures were continued for 72 h. Fresh MTT was added to each well at a terminal concentration of 5 mg/mL, and incubated with cells at 37 °C for 4 h. The formazan crystals were dissolved in 100 µL of DMSO each well, and the absorbency at 492 nM (for absorbance of MTT formazan) and 630 nM (for the reference wavelength) was measured with an ELISA reader. All of the compounds were tested three times in each cell line. The results expressed as IC_{50} (inhibitory concentration 50%) were the averages of three determinations and calculated by using the Bacus Laboratories Incorporated Slide Scanner (Bliss) software.

The mean values of three independent experiments, expressed as IC_{50} values, are presented in Table 1. Most of the synthesized compounds exhibited potent anti-proliferative activity with IC_{50} values less than 30 µM. Generally, the variations of substituents within the aryl moiety together with the heterocycle ring being attached have a notable influence on the anti-proliferative activity.

2. 2. 3. Structure Activity Relationship

It is clear from Table 1 that most of the tested compounds have high inhibitions toward the six cancer cell lines. Considering the 5,6,7,8-tetrahydronaphthalene derivatives **3a** and **3b**, it is clear that compound **3b** (X = OH, R = COOEt) that is an oxygen-rich compound has higher inhibition than **3a** (X = NH_2, R = CN). Reaction of either compound **3a** or **3b** with acetic acid and acetic anhydride gave the acetylated derivatives **4a** and **4b**, respectively where both of two compounds showed moderate inhibition, surprisingly, compound **3a** exhibited higher inhibition than **4b**. For the 1,2,3,4,7,8,9,10-octahydrobenzo[*h*]quinazoline **6a** and the 3,4,7,8,9,10-hexahydro-2*H*-naphtho[2,1-*e*][1,3]oxazine **6b**, it is obvious that compound **6b** (Y = O, R = COOEt) showed higher inhibitions toward the six cancer cell lines than **6a** (Y = NH, R = CN). The same findings were noticed after hydrolysis of the exocyclic C=NH group present in **6a** and **6b** into C=O where compound **7b** exhibited stronger inhibitions than **7a**. The 7,8-dihydro-4*H*-benzo[*e*][1,3]oxazine derivative **10** exhibited low inhibitions. The reaction of compound **10** with either malononitrile or ethyl cynoacetate and elemental sulfur produces the thieno[2',3':5,6]benzo[1,2-*e*][1,3]oxazine derivatives **12a** and 1**2b**, respectively. It is obvious from Table 1 that compound **12b** (R = COOEt) displayed higher inhibitions than compound **12a** (R = CN). The reaction of cyclohexan-1,3-dione with trichloroacetonitrile gave the (2,2,2-trichloroethylidene)cyclohexane-1,3-dione derivative **14** which exhibited high inhibitions toward the six cancer cell lines. Its conversion into the 2,3,6,7-tetrahydroquinazoline derivative **16** through its reaction with phenyl isothiocyanate support the inhibition of the molecule where compound **16** showed high inhibitions. Increasing the nitrogen content of **16** through its reaction with either hydrazine hydrate or phenylhydrazine to give either **18a** or **18b**, respectively resulting in high cytotoxicities as well. Moreover, compound **18b** (R = Ph) was more cytotoxic than **18a** (R = H). The same argument appeared in the case of **20a** (R = CN) and **20b** (R = COOEt) where the latter showed higher cytotoxicities than the former. Considering the 5,6-dihydrothieno[2,3-*h*]isoquinoline derivatives **21a–d**, for which **21b** (R_1 = CN, R_2 = COOEt), **21c** (R_1 = COOEt, R_2 = CN) and **21d** (R_1 = R_2 = COOEt) were of high inhibitions toward the six cancer cell lines. However, in the case of the hydroxyl derivatives **22a–d** only compounds **22c** and **22d** were the most cytotoxic compounds. Finally, for the nucleophilic substituted compounds with the CN or the SCN moieties to give the eight compounds **24a–h**, all of them exihibited high inhibitions. However, compounds **24a**, **24b**, **24c** and **24e** showed from moderate to high inhibitions together with compounds **24d**, **24f**, **24g** and **24h** exhibiting high inhibitions. It is of great value to mention that compounds **6b**, **7b**, **12b**, **14**, **16**, **18b**, **20b**, **21b**, **21c**, **21d**, **22c**, **22d**, **24d**, **24f**, **24g** and **24h** were the most cytotoxic compounds among the tested compounds. On the other hand, compounds **3b**, **7a**, **18a**, **20a**, **21a**, **22a**, **22b**, **24a**, **24b**, **24c** and **24e** have moderate inhibitions. With special attention to compounds bearing the COOEt group within their structures there were some of them **6b**, **12b, 20b, 21b, 21c** and **21d** showing high inhibitions while other compounds with other subtituents have lower inhibitions. In most cases compounds with the electronegative COOEt and/or CN groups exhibited high inhibitions although in some cases the nature of heterocyclic ring was in some cases a controlling factor.[24] For example considering the inhibitions of compounds 5,6-dihydrothieno[2,3-*h*] isoquinoline derivatives **21a–d** we found that the presence of isoquinoline moiety enhanced the inhibitions[25] of compounds **21b**, **21c** and **21d.** While the presence of pyridine moiety, like in **24a–h**, enabled compounds **24d**, **24f**, **24g** and **24h** to exhibit high inhibitions. In fact the difference in anti-proliferative activities between fused heterocyclic compounds of the same substituents was reported before.[26]

2. 2. 4. HTRF Kinase Assay

c-Met (mesenchymal epithelial transition factor) is a multifunctional transmembrane tyrosine kinase and acts as a receptor for hepatocyte growth factor/scatter factor (HGF/SF).[27] It is expressed during embryogenesis in multiple epithelial tissues (liver, pancreas, prostate, kidney, muscle, bone-marrow) and was also discovered in numerous tumour cell communities on the cell surface.[28] Multiple oncogenetic characteristics of c-Met were outlined shortly after its discovery, including cell dissociation stimulation, migration, motility, and extracellular matrix invasion.[29,30] Moreover, the c-Met kinase activity has been revealed to be

correlated with prostate cancer where c-Met played a key role in the conversion of prostate cancer from the primary androgen-sensitive to androgen-insensitive status along with the increase in radio resistance. First, an inverse relationship between the expression of androgen receptor (AR) and c-Met has been observed in prostate epithelium and prostate cancer cells.[31] Second, AR signaling suppressed c-Met transcription while androgen removal improved the expression of c-Met.[32] Third, it is observed that c-Met expression is high in late stage bone metastatic prostate cancer.[33] Furthermore, the latest research has shown that c-Met expression is closely related to cellular radiosensitivity.[33]

Based on these reported observations, the c-Met kinase activity of all compounds was evaluated using homogeneous time-resolved fluorescence (HTRF) assay as previously reported.[34] Taking foretinib as the positive control, the results expressed as IC_{50} are summarized in Table 2. The anti-proliferative activity of all target compounds against the human prostatic cancer PC-3 cell line was measured by MTT assay using anibamine as the reference drug. The mean values of three independent experiments, expressed as IC_{50} values, are presented in Table 2. Generally, the variations of substituents within the aryl moiety together with the heterocyclic ring being attached have a notable influence on the anti-proliferative activity.

HTRF assay utilizes the signal generated by the fluorescence resonance energy transfer between donor and acceptor molecules in close proximity. Dual-wavelength de-

Table 2. c-Met enzymatic activity and PC-3 inhibition of the newly synthesized compounds.

Compound No	IC_{50} (nM) c-Met	IC_{50}(μM) PC-3	VERO[a] (μM)	SI PC-3[b]
3a	1.42 ± 0.80	1.73 ± 0.73	58.41 ± 6.32	33.76
3b	0.31 ± 0.16	0.25 ± 0.17	55.61 ± 6.24	> 100
4a	0.54 ± 0.16	2.31 ± 0.92	36.22 ± 6.27	15.68
4b	0.32 ± 0.21	0.28 ± 0.23	50.68 ± 6.14	> 100
6a	4.16 ± 1.83	0.26 ± 0.10	39.56 ± 6.31	> 100
6b	4.28 ± 1.80	0.30 ± 2.53	58.23 ± 5.16	> 100
7a	6.27 ± 2.19	8.46 ± 2.24	36.69 ± 8.12	4.37
7b	2.47 ± 0.88	4.05 ± 1.82	58.36 ± 6.27	14.41
10	4.72 ± 1.83	1.26 ± 0.97	32.28 ± 5.71	25.62
12a	8.41 ± 2.53	2.82 ± 1.03	58.27 ± 5.80	20.66
12b	1.33 ± 0.78	0.29 ± 0.06	60.81 ± 7.26	> 100
14	0.29 ± 0.09	0.26 ± 0.18	58.32 ± 6.93	> 100
16	0.63 ± 0.42	0.29 ± 0.13	60.35 ± 6.56	> 100
18a	4.51 ± 1.86	6.41 ± 2.20	63.40 ± 8.27	9.89
18b	0.82 ± 0.32	0.42 ± 0.23	60.22 ± 7.32	> 100
20a	2.46 ± 1.30	2.80 ± 1.01	56.32 ± 6.57	20.11
20b	0.49 ± 0.21	0.53 ± 0.12	65.43 ± 6.81	> 100
21a	3.65 ± 1.83	4.82 ± 1.26	40.41 ± 8.32	8.38
21b	4.82 ± 1.16	3.20 ± 1.68	30.23 ± 7.19	9.44
21c	0.22 ± 0.13	0.38 ± 0.16	42.53 ± 6.63	> 100
21d	1.18 ± 0.92	0.24 ± 0.07	40.53 ± 5.63	> 100
22a	5.28 ± 1.47	2.79 ± 1.01	60.29 ± 8.20	21.61
22b	0.36 ± 0.14	0.42 ± 0.09	42.49 ± 6.53	> 100
22c	1.81 ± 0.96	1.48 ± 0.79	56.27 ± 8.93	38.02
22d	0.36 ± 0.18	0.63 ± 0.17	36.58 ± 5.30	58.06
24a	6.36 ± 2.31	5.57 ± 1.29	60.47 ± 6.93	10.86
24b	1.42 ± 0.80	1.73 ± 0.73	58.41 ± 6.32	33.76
24c	0.21 ± 0.05	0.39 ± 0.15	58.37 ± 6.19	> 100
24d	2.58 ± 0.80	4.18 ± 1.48	48.26 ± 5.39	11.54
24e	2.68 ± 1.72	3.80 ± 1.49	58.01 ± 5.77	15.26
24f	1.18 ± 0.89	0.24 ± 0.11	54.52 ± 6.70	> 100
24g	2.37 ± 1.16	4.93 ± 1.77	38.73 ± 4.83	7.85
24h	1.32 ± 0.93	0.28 ± 0.17	60.72 ± 8.19	> 100
	Foretinib	**Anibamine**		
	1.16 ± 0.17	3.26 ± 0.35	–	–

[a] VERO, monkey kidney cell line (Cat No-11095–080).
[b] Selectivity index (SI) were calculated by IC_{50} values in normal cell line divided by IC_{50} values in PC-3 cancer cell line.

tection helps to eliminate media interference, and the final signal is proportional to the extent of product formation. Thus far, the reported applications of this technology for *in vitro* kinase assays have mainly focused on high-throughput screening. The MTT assay is a colorimetric assay for assessing cell metabolic activity. NAD(P)H-dependent cellular oxidoreductase enzymes may, under defined conditions, reflect the number of viable cells present. These enzymes are capable of reducing the tetrazolium dye MTT 3-(4,5-dimethylthiazol-2-yl)-2,5-diphenyltetrazolium bromide to its insoluble formazan, which has a purple colour. Other closely related tetrazolium dyes including XTT, MTS and the WSTs, are used in conjunction with the intermediate electron acceptor, 1-methoxyphenazine methosulfate (PMS). With WST-1, which is cell-impermeable, reduction occurs outside the cell *via* plasma membrane electron transport. However, this traditionally assumed explanation is currently contended as proof has also been found of MTT reduction to formazan in lipidic cellular structures without apparent involvement of oxido reductases. Tetrazolium dye assays can also be used to measure cytotoxicity (loss of viable cells) or cytostatic activity (shift from proliferation to quiescence) of potential medicinal agents and toxic materials. MTT assays are done in the dark since the MTT reagent is sensitive to light. Within this protocol, replacing the serum-containing media with serum-free media and MTT reagent in cell cultures incubated for 3 h at 37 °C adding MTT solvent and incubating for 15 min to be analyzed with microplate reader.

As shown in Table 2, all the tested compounds displayed potent c-Met enzymatic activity with IC_{50} values ranging from 0.21 to 8.41 nM and potent prostate PC-3 cell line inhibition with IC_{50} values ranging from 0.26 to 8.46 μM. Compared with foretinib (IC_{50} = 1.16 nM), the ten compounds (**3b**, **4a**, **4b**, **14**, **16**, **18b**, **20b**, **21c**, **22b**, **22d** and **24c**) exhibited higher potency with IC_{50} values less than 1.00 nM. Remarkably, among the synthesized compounds, **3a**, **3b**, **4a**, **4b**, **6a**, **6b**, **10**, **2a**, **12b**, **14**, **16**, **18b**, **20a**, **20b**, **21c**, **21d**, **22a**, **22b**, **22c**, **24c**, **24d**, **24f** and **24h** displayed much higher anti-proliferation activities against PC-3 cell line than the standard anibamine (IC_{50} = 3.26 μM).

All synthesized compounds were tested against the VERO, monkey kidney normal cell line, where they showed low activity against the normal cell line. Interestingly, from Table 2 compounds **3a**, **22c**, **22d** and **24b** showed SI > 30 while the fourteen compounds **3b**, **4b**, **6a**, **6b**, **12b**, **14**, **16**, **18b**, **20b**, **21d**, **22b**, **24c**, **24f** and **24h** exhibited SI > 100, while the rest of compounds showed SI < 30.

2. 2. 5. Inhibitory Effect of the Most Active Compounds Towards Tyrosine Kinases

The most active compounds that showed the highest inhibitions toward the six cancer cell lines were further evaluated against other five tyrosine kinases (c-Kit, Flt-3, VEGFR-2, EGFR, and PDGFR) using the same screening method (Table 3). These receptor tyrosine kinases (RTKs) have been implicated in vascular development by affecting the proliferation and migration of endothelial cells or pericytes. It is clear from Table 3 that compounds **7b**, **12b**, **16**, **20b**, **21b**, **22c**, **22d**, **24d**, **24f** and **24h** were the most potent towards the five tyrosine kinases. Compound **25g** showed high inhibitions towards the four kinases Flt-3 and VEGFR-2 with IC_{50} values of 0.32 and 0.29 nM, respectively while it showed moderate inhibition towards c-Kit and EGFR with IC_{50} 1.52 and 1.93 nM, respectively. Compound **24d** was the most active compound against Flt-3 kinase with IC_{50} 0.17 nM. Compounds **12b**, **16** and **24f** were the most active toward PDGFR with IC_{50} values og 0.28, 0.26 and 0.27 nM, respectively. Compounds **6b**, **18b** and **21c** showed the lowest potency among the tested compounds.

Table 3. Inhibition of tyrosine kinases [enzyme IC_{50} (nM)] by compounds **6b**, **7b**, **12b**, **14**, **16**, **18b**, **20b**, **21b**, **21c**, **21d**, **22c**, **22d**, **24d**, **24f**, **24g** and **24h**

Compound	c-Kit	Flt-3	VEGFR-2	EGFR	PDGFR
6b	1.80	2.43	1.72	2.93	1.05
7b	0.21	0.17	0.23	0.26	0.42
12b	0.30	0.51	0.29	0.33	0.28
14	1.08	2.62	1.17	2.39	1.52
16	0.28	0.16	0.52	0.74	0.26
18b	1.16	2.39	1.12	2.83	1.29
20b	0.31	0.46	0.35	0.29	0.33
21b	0.41	0.28	0.26	0.42	0.50
21c	1.22	2.96	1.53	2.72	1.38
22c	0.38	0.29	0.52	0.41	0.70
22d	0.27	0.25	0.41	0.66	0.37
24d	0.17	0.26	0.50	0.61	0.39
24f	0.25	0.36	0.42	0.36	0.27
24g	1.52	0.32	0.29	1.93	2.53
24h	0.22	0.26	0.36	0.28	0.37

2. 2. 6. Inhibition of Selected Compounds Towards Pim-1 Kinase

Compounds **7b**, **12b**, **16**, **20b**, **21b**, **22c**, **22d**, **24d**, **24f** and **24h** were selected to examine their Pim-1 kinase inhibition activity (Table 4) as these compounds showed high inhibition towards the tested cancer cell lines at a range of ten concentrations and the IC_{50} values were calculated. Compounds **7b**, **12b**, **16**, **22c** and **24f** were the most potent to inhibit Pim-1 kinase with IC_{50} value of 0.22, 0.28, 0.24, 0.30 and 0.26 μM, respectively. On the other hand, compounds **20b**, **21b**, **22d**, **24d** and **24h** were less effective (IC_{50} > 10 μM). These profiles in combination with cell growth inhibition data of compounds **7b**, **12b**, **16**, **20b**, **21b**, **22c**, **22d**, **24d**, **24f** and **24h** listed in Table 3 indicate that Pim-1 was a potential target of these compounds where SGI-1776 was used as the positive control with IC_{50} 0.048 μM in the assay.

Table 4. The inhibitor activity of compounds **7b**, **12b**, **16**, **20b**, **21b**, **22c**, **22d**, **24d**, **24f** and **24h** toward Pim-1 Kinase.

Compound	Inhibition ratio at 10 μM	IC_{50} (μM)
7b	96	0.22
12b	90	0.28
16	94	0.24
20b	22	> 10
21b	32	>10
22c	89	0.30
22d	24	> 10
24d	20	> 10
24f	92	0.26
24h	30	> 10
SGI-1776	–	0.048

3. Results and Discussion

Initially cyclohexan-1,3-dione was chosen as the model substrate for the synthesis of fused heterocyclic compounds through studying its reactivity toward some dimeric compounds and nitrile reagents to produce biologically active products. Thus, we studied the condensation of cyclohexane-1,3-dione (**1**) with some dimeric compounds. Thus, the reaction of cyclohexane-1,3-dione (**1**) with either of 2-aminoprop-1-ene-1,1,3-tricarbonitrile (**2a**) or diethyl 3-amino-2-cyanopent-2-enedioate (**2b**) in the presence of a catalytic amount of ammonium acetate in an oil bath at 120 °C gave the 5,6,7,8-tetrahydronaphthalene derivatives **3a** and **3b**, respectively. The structures of the latter products were confirmed through their respec-

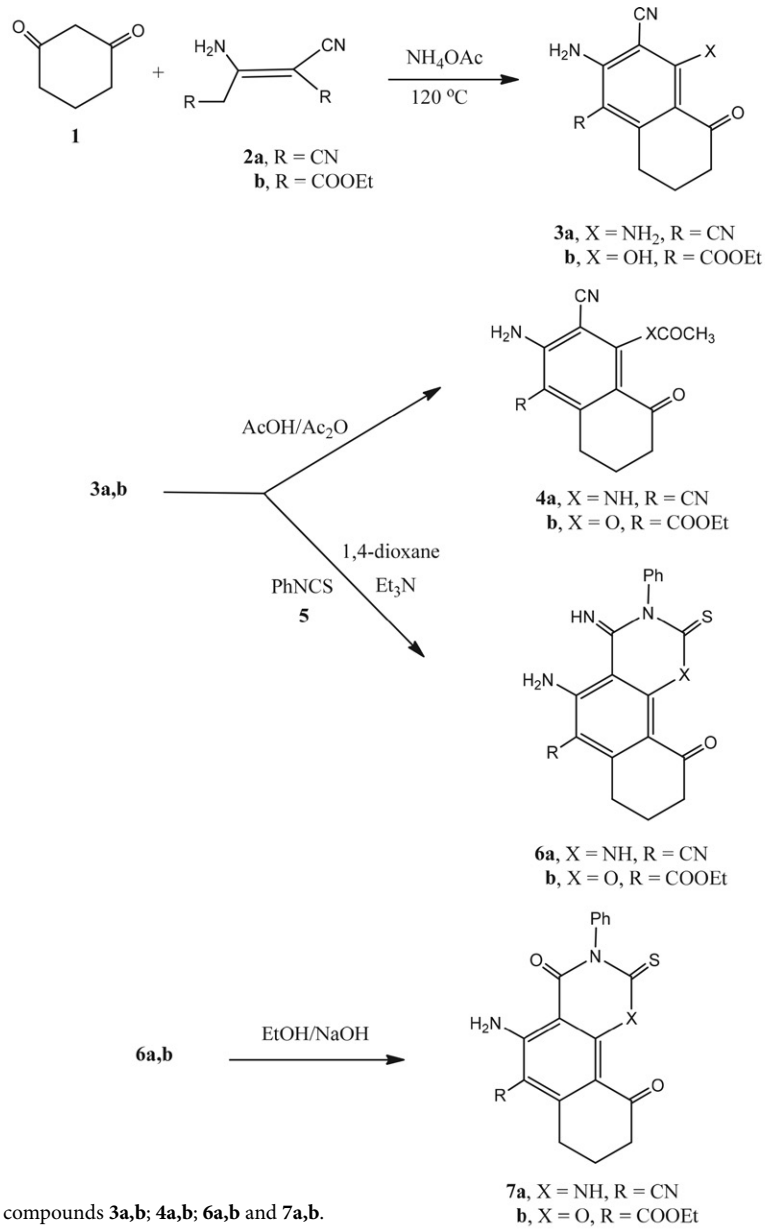

Schema 1. Synthesis of compounds **3a,b**; **4a,b**; **6a,b** and **7a,b**.

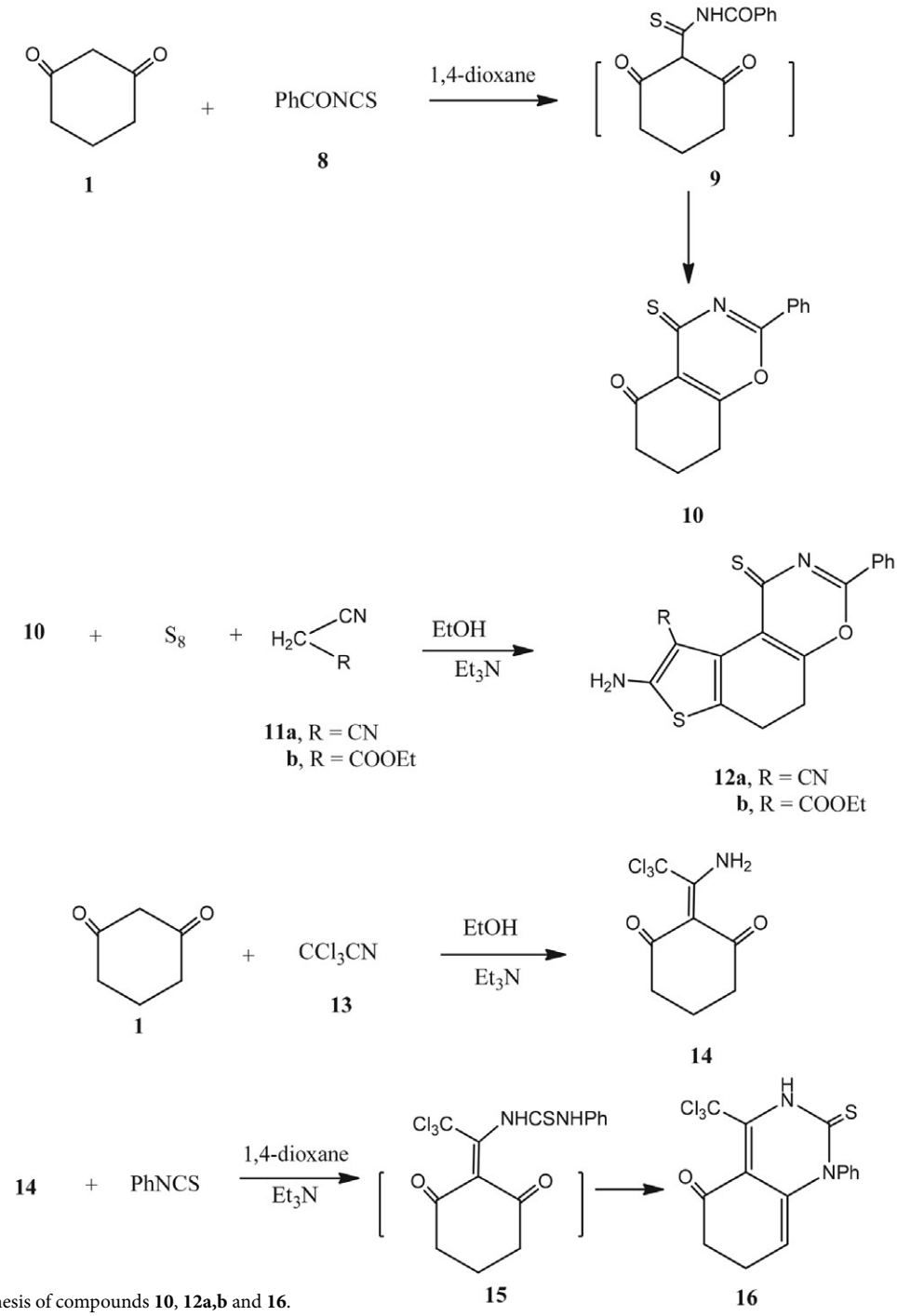

Schema 2. Synthesis of compounds **10**, **12a,b** and **16**.

tive analytical and spectral data. Thus, the ^{1}H NMR spectrum of compound **3a** revealed beside the expected signals, two singlets, D_2O exchangeable, indicating two NH_2 groups and the ^{13}C NMR spectrum showed the presence of a signal at δ 174.2 due to the C=N bonding, signals at δ 127.9, 125.6, 124.9, 123.5, 121.8, 120.4 indicating the aromatic carbons and two signals at d116.8, 116.3 confirming the presence of the two CN groups. The latter compounds when heated in acetic acid/acetic anhydride solution gave the *N*-acetamido derivative **4a** and the acetate ester derivative **4b**, respectively. On the other hand the reaction of either compound **4a** or **4b** with phenyl isothiocyanate (**5**) in 1,4-dioxane solution containing a catalytic amount of triethylamine gave the 1,2,3,4,7,8,9,10-octahydrobenzo[*h*] quinazoline **6a** and the 3,4,7,8,9,10-hexahydro-2*H*-naphtho[2,1-*e*][1,3]oxazine **6b**, respectively. Compounds **6a** and **6b** underwent ready hydrolysis of the exocyclic C=N when heated in ethanol containing hydrochloric acid to

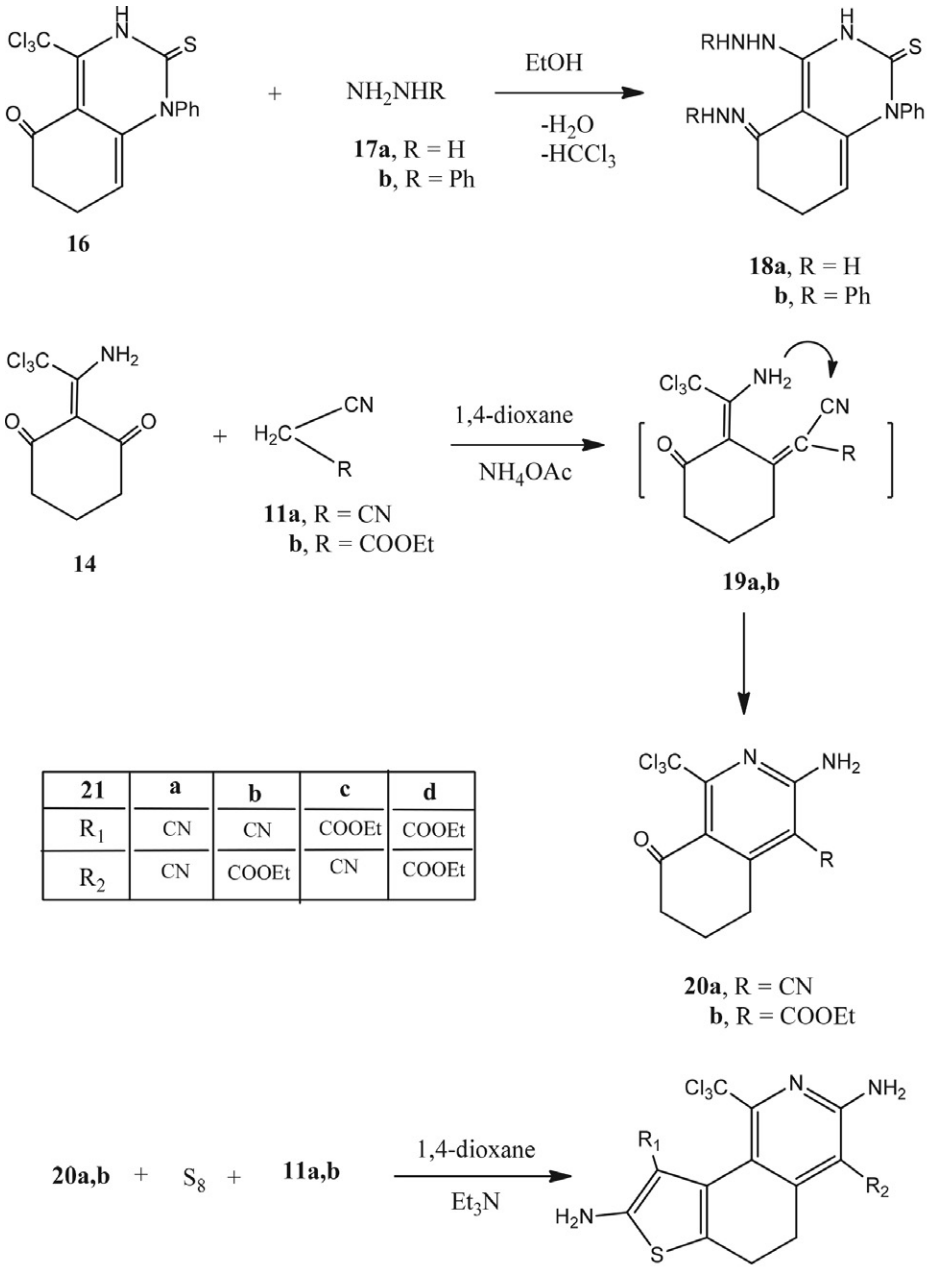

21	a	b	c	d
R_1	CN	CN	COOEt	COOEt
R_2	CN	COOEt	CN	COOEt

Schema 3. Synthesis of compounds **18a,b**; **20a,b** and **21a-d**.

afford the corresponding 4,10-dione derivatives **7a** and **7b**, respectively *via* ammonia liberation (Scheme 1). The chemical structures of new compounds were assured by spectral data (IR, ^{1}H and ^{13}C NMR, MS).

The reaction of cyclohexane-1,3-dione (**1**) with benzoyl isothiocyanate (**8**) in 1,4-dioxane gave the benzo[*e*][1,3]oxazin-5(6*H*)-one derivative **10**. Formation of the latter product was explained through the first addition of the methyleno group of compound **1** to the isothiocyanate moiety of **8** to give the intermediate **9** followed by the elimination of one molecule of water. The structure of compound **10** was based on the obtained analytical and spectral data. Thus, its mass spectrum revealed *m/z* 257 corresponding to its molecular mass. The ^{1}H NMR spectrum showed the presence of a multiplet at δ 7.43–7.22 due to the C_6H_5 group and the ^{13}C NMR spectrum showed three signals at δ 180.4, 174.2, 168.2 due to the presence of C-4, C-2 and C-5, respectively and signals at δ 142.7, 133.3, 126.3, 125.2, 123.6, 121.1 indicating the C_6H_5, C-2, C-4a and C-8a carbons.

Compound **10** is capable of forming fused thiophene derivatives through Gewald's thiophene reaction.[35,36] Thus, the reaction of compound **10** with elemental sulfur and either malononitrile (**11a**) or ethyl cyanoacetate (**11b**) in ethanol containing triethylamine gave the thieno[2',3':5,6]benzo[1,2-*e*][1,3]oxazine derivatives **12a**

and 1**2b**, respectively. Next we studied the reaction of cyclohexan-1,3-dione with trichloroacetonitrile followed by heterocyclization of the product in the aim of producing halogen-rich compounds that are characterized by high inhibitions toward cancer cell lines. Therefore, the reaction of cyclohexan-1,3-dione (**1**) with trichloroacetonitrile (**13**) in ethanol solution containing triethylamine gave the (2,2,2-trichloroethylidene)cyclohexane derivative **14**. The latter compound showed interesting reactivity toward a variety of chemical reagents. Thus, the reaction of compound **14** with phenyl isothiocyanate (**5**) in 1,4-dioxane solution containing a catalytic amount of triethylamine gave the 2,3,6,7-tetrahydroquinazoline derivatives **16** *via* the intermediate formation of Michael addition adduct **15** followed by the cyclization through water elimination (Scheme 2). The analytical and spectral data of compound **16** were in agreement with its proposed structure. Thus, the ^{1}H NMR spectrum showed the presence of a multiplet at δ 7.29–7.42 due to the presence of C_6H_5 group and a singlet at δ 8.28, D_2O exchangeable, due to the NH group and the ^{13}C NMR spectrum showed a signal at 94.4 indicating the CCl_3 group, signals at δ 120.5, 121.5, 123.6, 123.9, 19.0, 130.3, 133.6, 135.2 for the C_6H_5, C-8, C-9, C-3 and C-4 carbons and two signals at δ 168.2, 178.8 for the C-5 and C-2 carbons.

The reaction of compound **16** with two fold of either hydrazine hydrate (**17a**) or phenylhydrazine (**17b**) gave the 5-hydrazono-1-phenyl-3,5,6,7-tetrahydroquinazoline derivatives **18a** and **18b**, respectively. On the other hand, the reaction of compound **14** with either malononitrile (**11a**) or ethyl cyanoacetate (**11b**) in 1,4-dioxane solution containing a catalytic amount of triethylamine gave the 6,7-dihydroisoquinoline derivatives **20a** and **20b**, respectively. Formation of the latter products was assumed to took place *via* first Knoevenagel condensation of the cyanomethylene reagent to give the intermediates **19a**,**b** followed by Michael addition to produce **21a**,**b**. The Gewald's thiophene reactions of either **20a** or **20b** with elemental sulfur and either malononitrile (**11a**) or ethyl cyanoacetate (**11b**) gave the 5,6-dihydrothieno[2,3-*h*]isoquinoline derivatives **21a**–**d**, respectively (Scheme 3).

The trichloromethyl moiety present in compounds **21a**–**d** showed interesting reactivity toward nucleophilic displacement reactions. Thus, the heating of either **21a**, **21b**, **21c** or **21d** in ethanolic sodium hydroxide solution gave the 1-hydroxy-5,6-dihydrothieno[2,3-*h*]isoquinoline

21a-d

22	**a**	**b**	**c**	**d**
R_1	CN	CN	COOEt	COOEt
R_2	CN	COOEt	CN	COOEt

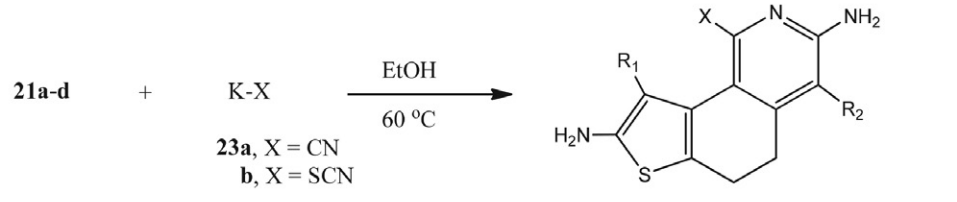

24a-h

24	**a**	**b**	**c**	**d**	**e**	**f**	**g**	**h**
R_1	CN	CN	COOEt	COOEt	CN	CN	COOEt	COOEt
R_2	CN	COOEt	CN	COOEt	CN	COOEt	CN	COOEt
X	CN	CN	CN	CN	SCN	SCN	SCN	SCN

Schema 4. Synthesis of compounds **22a-d** and **24a-h**.

derivatives **22a–d**, respectively. On the other hand, the reaction of either **21a**, **21b**, **21c** or **21d** with either potassium cyanide (**23a**) or potassium thiocyanate (**23b**) gave the corresponding nucleophlic displacement products **24a–h**, respectively (Scheme 4). All new compounds were confirmed by their correct spectral data and elemental analyses values (see the Experimental section).

4. Conclusion

The main findings of these studies is the synthesis of a series of novel heterocyclic derivatives synthesized from cyclohexan-1,3-dione followed by screening of the newly synthesized compounds towards six cancer cell lines. Sixteen compounds exhibited high inhibitions toward the cancer cell lines and the c-Met enzymatic activity revealed that eleven compounds were more active than the reference foretinib. In addition, twenty three compounds displayed much higher anti-proliferation activities against PC-3 cell line than the standard anibamine. Further tests toward the five tyrosine kinases c-Kit, Flt-3, VEGFR-2, EGFR, and PDGFR and Pim-1 kinase showed that compounds **7b**, **12b**, **16**, **20b**, **21b**, **22c**, **22d**, **24d**, **24f** and **24h** were the most potent of the tested compounds toward the five tyrosine kinases and compounds **7b**, **12b**, **16**, **22c** and **24f** were of the highest inhibitions toward Pim-1 kinase. The results obtained will encourage further work in the future in the field of the synthesis of target molecules as anticancer agents.

5. References

1. A. Gomtsyan, *Chem. Heterocycl. Compd.* **2012**, *48*, 7–10. **DOI:**10.1007/s10593-012-0960-z
2. R. Dua, S. Shrivastava, S. K. Sonwane, S. K. Srivastava, *Adv. Biol. Res. (Rennes)* **2011**, *5*, 120–144.
3. T. Eicher, S. Hauptmann, A.Speicher The Chemistry of Heterocycles: Structure, Reactions, Synthesis, and Applications, 3rd ed.; Wiley-VCH: Weinheim, Germany, **2012**, pp. 1–4.
4. H. B. Broughton, I. A.Watson, *J. Mol. Graph. Model.* **2004**, *23*, 51–58. **DOI:**10.1016/j.jmgm.2004.03.016
5. N. M. A. El-salam, M. S. Mostafa, G. A. Ahmed, O. Y. Alothman, *J. Chem.* **2013**, 1–8. **DOI:**10.1155/2013/890617
6. M. E. Azab, M. M. Youssef, E. A. El-Bordany, *Molecules* **2013**, *18*, 832–844. **DOI:**10.3390/molecules18010832
7. M. S. Salem, S. I. Sakr, W. M. El-Senousy, H. M. F. Madkour, *Arch. Pharm. (Weinheim)* **2013**, *346*, 766–773. **DOI:**10.1002/ardp.201300183
8. X. Cao, Z. Sun, Y. Cao, R. Wang, T. Cai, W. Chu, W. Hu, Y. Yang, *J. Med. Chem.***2014**, *57*, 3687–3706. **DOI:**10.1021/jm4016284
9. E. R. El-Sawy, M. S. Ebaid, H. M. Abo-Salem, A. G. Al-Sehemi, A. H. Mandour, *Arab. J. Chem.* **2013**, *7*, 914–923. **DOI:**10.1016/j.arabjc.2012.12.041
10. Y. Chen, K. Yu, N. Y. Tan, R. H. Qiu, W. Liu, N. L. Luo, L. Tong, C. T. Au, Z. Q. Luo, S. F. Yin, *Eur. J. Med. Chem.* **2014**, *79*, 391–398. **DOI:**10.1016/j.ejmech.2014.04.026
11. E. R. El-Sawy, A. H. Mandour, S. M. El-Hallouty, K. H. Shaker, H. M. Abo-Salem *Arab. J. Chem.* **2013**, *6*, 67–78. **DOI:**10.1016/j.arabjc.2012.04.003
12. Y. N. Mabkhot, A. Barakat, A. M. Al-Majid, S. Alshahrani, S. Yousuf, M. I. Choudhary, *Chem. Cent. J.* **2013**, *7*, 112–120. **DOI:**10.1186/1752-153X-7-112
13. F. Piedade, S. Bio, B. Nunes, *Environ. Toxicol. Pharmac.* **2020**, *73*, 103276. **DOI:**10.1016/j.etap.2019.103276
14. D. Peer, J. M. Karp, S. Hong, O. C. Farokhzad, R. Margalit, R. Langer, *Nat. Nanotechnol.* **2007**, *2*, 751–760. **DOI:**10.1038/nnano.2007.387
15. T. W. Hambley, W. N. Hait, *Cancer Res.* **2009**, *69*, 1259–1262. **DOI:**10.1158/0008-5472.CAN-08-3786
16. P. Martins, D. Rosa, A. R. Fernandes, P. V. Baptista, *Recent Pat. Nanomed.* **2014**, *3*, 1–14. **DOI:**10.2174/1877912304666140304000133
17. J. Conde, A. Ambrosone, V. Sanz, Y. Hernandez, V. Marchesano, F. Tian, H. Child, C. C. Berry, M. R. Ibarra, P. V. Baptista, C. Tortiglione, J. M. Fuente, *ACS Nano* **2012**, *6*, 8316–8324. **DOI:**10.1021/nn3030223
18. J. Conde, G. Doria, P. Baptista, *J. Drug Deliv.* **2011**, *2012*, 1–12. **DOI:**: 10.1155/2012/751075
19. R. M. Mohareb, N. Y. Abdo, K. A. EL-Sharkawy, *Anticancer Agent Med. Chem.* **2018**, *18*, 1736–1749. **DOI:**10.2174/1871520618666180604091358
20. R. M. Mohareb, E. M. Samir, P. A. Halim, *Bioorg. Chem.* **2019**, *83*, 402–413. **DOI:**10.1016/j.bioorg.2018.10.067
21. R. M. Mohareb, K. A. El-Sharkawy, F. O. El-Farouk, *Med. Chem. Res.* **2019**, *28*, 1885-1900. **DOI:**10.1007/s00044-019-02421-6
22. B. P. McKibben, C. H. Cartwright, A. L. Castelhano, *Tetrahedron Lett.* **1999**, *40*, 5471–5474. **DOI:**10.1016/S0040-4039(99)01108-9
23. J. S. Rubin, D. P. Bottaro, S. A. Aaronson, *Biochim. Biophys. Acta* **1993**, *1155* 357–371. **DOI:**10.1016/0304-419X(93)90015-5
24. R. M. Mohareb, R. A. Ibrahim, E. S. Alwan, *Acta Chim. Slov.* **2021**, *68*, 51–64. **DOI:**10.17344/acsi.2020.6090
25. R. M. Mohareb, Y. R. Milad, A. A. Masoud, *Acta Chim. Slov.* **2021**, *68*, 72–87 **DOI:**10.17344/acsi.2020.6182
26. R. M. Mohareb, F. M. Manhi, A. Abdelwahab, *Acta Chim. Slov.* **2020**, *67*, 83–95. **DOI:**10.17344/acsi.2019.5224
27. S. L. Organ, M. S. Tsao, *Ther. Adv. Med. Oncol.* **2011**, *3*, S7–S19. **DOI:**10.1177/1758834011422556
28. P. A. Humphrey, X. Zhu, R. Zarnegar, P. E. Swanson, T. L. Ratliff, R. T. Vollmer, M. L. Day, *Am. J. Pathol.* **1995**, *147*, 386–396.
29. M. Jeffers, S. Rong, G. F. Vande Woude, *J. Mol. Med.* **1996**, *74*, 505–513. **DOI:**10.1007/BF00204976
30. M. Verras, J. Lee, H. Xue, T. H. Li, Y. Wang, Z. Sun, *Progression Cancer Res.* **2007**, *67*, 967–975. **DOI:**10.1158/0008-5472.CAN-06-3552
31. F. De Bacco, P. Luraghi, E. Medico, G. Reato, F. Girolami, T.

Perera, P. Gabriele, P. M. Comoglio, C. Boccaccio, *J. Natl. Cancer Inst.* **2011**, *103*, 645–661. **DOI:**10.1093/jnci/djr093
32. S. Li, Y. Zhao, K. Wang, Y. Gao, J. Han, B. Cui, P. Gong, *Bioorg. Med. Chem.* **2013**, *21*, 2843–2855. **DOI:**10.1016/j.bmc.2013.04.013
33. W. Zhu, W. Wang, S. Xu, J. Wang, Q. Tang, C. Wu, Y. Zhao, P. Zheng, *Bioorg. Med. Chem.* **2016**, *24*, 1749–1756. **DOI:**10.1016/j.bmc.2016.02.046
34. W. Zhu, W. Wang, S. Xu, Q. Tang, C. Wu, Y. Zhao, P. Zheng, *Bioorg. Med. Chem.* **2016**, *24*, 1749–1756. **DOI:**10.1016/j.bmc.2016.02.046
35. R. Mishra, K. K. Jha, S. Kumar, I. Tomer, *Der Pharma. Chemica* **2011**, *3*, 38–54.
36. K. Wang, D. Kim, A. Dömling, *J. Comb. Chem.* **2010**, *12*, 111–118. **DOI:**10.1021/cc9001586

Povzetek

Cikloheksan-1,3-dion (**1**) reagira bodisi z 2-aminoprop-1-en-1,1,3-trikarbonitrilom (**2a**) ali z dietil 3-amino-2-cianopent-2-endioatom (**2b**) in daje 5,6,7,8-tetrahidronaftalenska derivata **3a** in **3b**. Ti dve spojini s heterociklizacijsko reakcijo dajeta tieno[2',3':5,6]benzo[1,2-*e*][1,3]oksazinska derivata. Po drugi strani reakcija spojine **1** s trikloroacetonitrilom daje (2,2,2-trikloroetiliden)cikloheksanski derivat **14**, ki je uporaben v seriji reakcij za sintezo 2,3,6,7-tetrahidrokinazolinskih, dihidrotieno[2,3-*h*]izokinolinskih, oktahidrobenzo[*h*]kinazolinskih in dihidrotieno[2,3-*h*]izokinolinskih derivatov. Vse sintetizirane spojine smo testirali na šestih rakavih celičnih linijah, kjer se jih je večina izkazala z visokimi inhibitornimi lastnostmi; raziskali smo tudi c-Met encimsko aktivnost ter inhibitorno aktivnost na tirozin kinaze in Pim-1. Dobljeni rezultati kažejo, da je nadaljevanje raziskovanja sintez na področju teh spojin z namenom optimizacije protirakavih učinkovin zelo obetavno.

Except when otherwise noted, articles in this journal are published under the terms and conditions of the Creative Commons Attribution 4.0 International License

DOI: 10.17344/acsi.2021.6819 *Acta Chim. Slov.* **2022,** *69,* 30–38
creative commons

Scientific paper

Glucose-Decorated Silica-Molybdate Complex: A Novel Catalyst for Facile Synthesis of Pyrano[2,3-d]-Pyrimidine Derivatives

Arezoo Pourkazemi, Negin Asaadi, Mahnaz Farahi,* Ali Zarnegaryan and Bahador Karami

Department of Chemistry, Yasouj University, P. O. Box 353, Yasouj 75918-74831, Iran

** Corresponding author: E-mail: farahimb@yu.ac.ir*

Received: 03-13-2021

Abstract

This article describes the preparation and identification of SiO_2@Glu/Si(OEt)$_2$(CH$_2$)$_3$N = Mo[Mo_5O_{18}] as a new bifunctional acid-base catalyst (both acidic and basic Lewis sites). Aminopropyltriethoxysilane was first reacted with hexamolybdate anions and then treated with glucose to prepare Glu/Si(OEt)$_2$(CH$_2$)$_3$N = Mo[Mo_5O_{18}]. Nano-silica was then modified by the prepared glucose/molybdate complex to obtain SiO_2@Glu/Si(OEt)$_2$(CH$_2$)$_3$N = Mo[Mo_5O_{18}]. The developed catalyst was characterized by FT-IR, EDX, XRD, FE-SEM and TGA analyzes. Its catalytic efficiency was investigated for the preparation of pyrano[2,3-*d*]pyrimidine derivatives by the reaction between various aldehydes, malononitrile and barbituric acid. The desired products were prepared in the presence of 0.004 g of the prepared catalyst in high to excellent yields.

Keywords: Silica nanoparticle; glucose; hexamolybdate anions; pyrano[2,3-*d*]pyrimidine; nanocatalyst

1. Introduction

Catalysis includes the variants of homogeneous, heterogeneous, and biological catalysis. Homogeneous catalysts offer many distinct advantages over their heterogeneous counterparts. For example, due to the high solubility of homogeneous catalysts, all catalytic sites are accessible. In addition, they often exhibit high chemoselectivity, regioselectivity, and/or enantioselectivity in organic transformations.[1] Despite these advantages, most homogeneous catalysts have not been used commercially because they have one major disadvantage compared to heterogeneous catalysts: They are difficult to separate from the reaction mixture and solvent. The usual separation method requires high temperatures, while most homogeneous catalysts are thermally sensitive and usually decompose below 150 °C.[2] Attempts have been made to solve the problem by immobilizing the catalysts on various supports such as carbon, silica, metal oxide, polymers, and nanocomposites.[1] Over the past century, the development of recoverable supported catalysts with high efficiency has been the subject of much research. Immobilized catalysts have significant advantages such as ease of handling, low solubility, possibility of recovery, and low toxicity.[3-8] In heterogeneous supported catalysis, the catalytic ability of materials usually depends on their microscopic structure, which directly affects the activity, selectivity, and thermal or chemical stability of the catalyst.[9] Nanomaterials are widely used as solid support materials for the preparation of many heterogeneous catalytic systems to solve various economic and environmental problems.[10] Nano-silica is widely used due to its unique properties, such as controllable particle size and non-toxicity. Nano-SiO_2 has a high surface-to-volume ratio and a porous structure that enables high chemical reactivity.[11] In addition, nano-silica has been used in various fields such as biomedicine, fillers, catalysis, and drug delivery systems. The size and uniformity of nano-silica particles have the greatest influence on their quality; therefore, SiO_2 nanoparticles with narrow and monodisperse size distribution are increasingly in demand.[12–14] Compared with the well-known methods for preparing nano-SiO_2, the Stöber method is considered to be the most effective method for preparing monodisperse silica spheres. This method provides a flexible chemical route to fabricate materials that are highly pure, chemically reactive, and well dispersed.[15]

The great attention given to nanoparticles is due to their exceptional properties: easy availability, chemical in-

ertness, high surface-to-volume ratio, high activity and selectivity, thermal stability, and low toxicity. Moreover, nanoscale systems significantly increase the contact between reactants and catalyst. They open new perspectives for mild catalysis of important reactions with lower environmental impact. Nanoparticles differ from their solid counterparts and exhibit special properties. Due to the above advantages, they have been developed as suitable replacements for conventional heterogeneous catalysts.[16]

Recently, inorganic-organic hybrid materials have been widely used as catalysts for organic reactions because they are well suited for various processes of environmentally friendly chemical transformations.[17] Several interesting new materials with novel properties are currently emerging in this rapidly growing field. They combine the typical advantages of organic components, such as flexibility, low density, toughness, and malleability, with the advantages of typical inorganic materials, such as hardness, chemical resistance, strength, and optical properties.[18] The properties of these materials are not just the sum of the individual contributions of the two phases, but the role of the internal interfaces could also be important. Organic-inorganic graft materials have emerged as surrogate materials for the development of unique products and have become a new area of academic research.

When the idea of a monomolecular bifunctional catalyst for helpful catalysis was first introduced in 2003, both homogeneous and heterogeneous catalysts with molecular design and their use in organic reactions became the focus of interest.[19] In this context, polyoxometalates (POMs) are an important class of nanoscale polynuclear clusters with significant physical and chemical properties based on transition metals in their highest oxidation states and oxygen bridges.[20] Polyoxometalate clusters, known for their enormous size and interesting properties for medicine and nonlinear optics, are a prominent class of linkers for the preparation of interpenetrating networks. The direct application of POM clusters as linkers promises an attractive route to the development of new entangled network structures. The main properties of polyoxometallates and the variation in their structures give them great potential for applications in various fields of chemical processing.[21] Despite the above advantages, the solubility and non-recoverability of POMs in various media limit their applications in some processes. Immobilization of these clusters on solid supports such as silica and magnetic nanoparticles could be an important way to overcome this problem. Hexamolybdates are a group of POMs used in various inorganic and organic reactions due to their thermal stability and radiation resistance. Lindqvist hexamolybdate cluster, $[Mo_6O_{19}]^{2-}$, as a unique class of metal oxide clusters, is an ideal building block for the construction of organic–inorganic hybrid assemblies.[22,23]

Carbon-based materials have attracted much attention from researchers because they are environmentally friendly, cheap, and nontoxic. Numerous studies have been conducted on these materials as catalyst supports, such as carbon nanotubes, carbon-polymer composites, mesoporous carbons, graphitized carbons, graphitized nitride carbons, carbides, and carbon aero-gels. In this context, cellulose has been used as a catalyst support due to its uniform shape, stability in aqueous solution, good mechanical strength, high specific surface area, biocompatibility and biodegradability. The development of cellulose-based composites with metal oxides such as silicon dioxide, titanium dioxide, zinc oxide, and iron oxides is of great interest for various high-technology applications.[24-26] Due to its polyhydroxy structure, glucose has been used as the main green monosaccharide catalyst and showed excellent catalytic activity in chemical reactions such as epoxidation and enantioselective Michael addition. It has also played the role of a green medium for carrying out reactions. Recently, Fe_3O_4 nanoparticles coated with glucose were prepared and used as a heterogeneous catalyst for the synthesis of pyrazole derivatives.[27]

Nowadays, several chemists have paid great attention to the development of new approaches to the production of nitrogen-containing heterocycles, which play an important role in our lives. They are components of many natural products, fine chemicals, and biologically active drugs that are of great importance in improving the quality of life.[28] Pyrano[2,3-*d*]pyrimidine derivatives represent a "privileged" structural motif that is widely used in naturally occurring compounds with a variety of important biological properties. Recently, a number of synthetic pyrano[2,3-*d*]pyrimidines have been investigated for their potent anticancer, antibacterial, antifungal, and antirheumatic properties.[29] They also exhibit anti-inflammatory,[30] anti-HIV,[31] cytotoxic,[32] antimicrobial,[33] antimalarial, and antihyperglycemic properties.[34] It is worth noting that many drug molecules bearing the pyrano-pyrimidine moiety are used in the treatment of various diseases such as bronchitis, as hepatoprotective agents, and as cardiotonic agents.[33]

With increasing public concern about environmental degradation and future resources, it is critical for chemists to develop new approaches that are less hazardous to human health and the environment. Therefore, in conjunction with our previous research on new heterogeneous catalysts,[35-41] we decided to introduce SiO_2@Glu/$Si(OEt)_2(CH_2)_3N = Mo[Mo_5O_{18}]$ nanocatalysts, whose catalytic activity was investigated in the one-pot synthesis of pyrano[2,3-*d*]pyrimidines.

2. Results and Discussion

The desired catalyst was synthesized in a simple manner as shown in Scheme 1. To prepare SiO_2@Glu/$Si(OEt)_2(CH_2)_3NH_2$ grafted $[Mo_6O_{19}]^{2-}$ composite (**3**), 3-aminopropyltriethoxysilane was reacted with tetrabutylammonium hexamolybdate followed by glucose to give

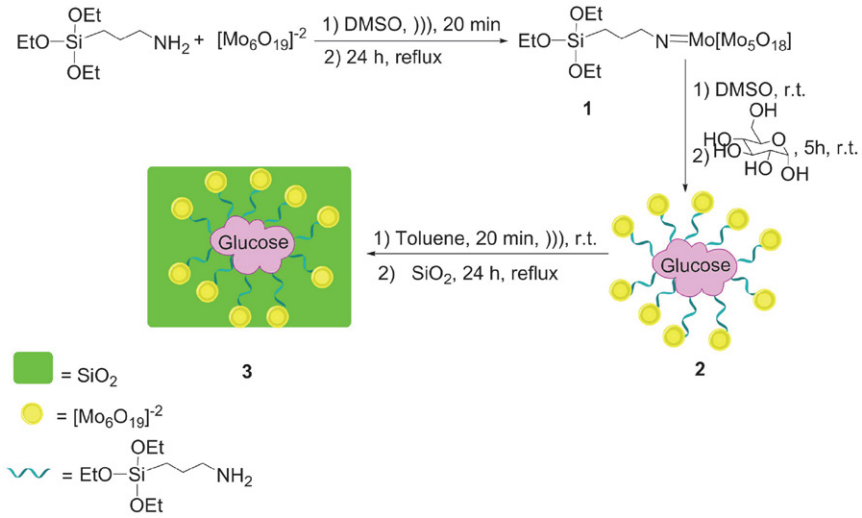

Scheme 1. Schematic representation of the synthesis of SiO_2@Glu/$Si(OEt)_2(CH_2)_3N$ = $Mo[Mo_5O_{18}]$ (**3**).

Glu/$Si(OEt)_2(CH_2)_3N$ = $Mo[Mo_5O_{18}]$ (**2**). SiO_2 nanoparticles were also synthesized by the Stöber method.[15] Finally, the OH groups on the silica surface can be grafted with Glu/$Si(OEt)_2(CH_2)_3N$ = $Mo[Mo_5O_{18}]$ to obtain the desired nanocatalyst **3**. The chemical and structural properties of the catalyst were investigated by FT-IR, EDX, XRD, FE-SEM and TGA analyzes.

The identification and determination of the organic functional groups were performed by FT-IR spectroscopy. Figure 1 shows the infrared spectra of glucose, SiO_2, SiO_2@Glu/$Si(OEt)_2(CH_2)_3N$ = $Mo[Mo_5O_{18}]$ and $[n\text{-}Bu_4N]_2[Mo_6O_{19}]$. In Figure 1a, the peaks at 3662 and 3385 cm^{-1} are assigned to the OH groups. Also, the peaks at 2939 and 1458 cm^{-1} are related to the stretching of CH and the symmetric bending stretching of CH_2, respectively. The bands at 1160 cm^{-1} (antisymmetric C-O-C stretching), 1116 cm^{-1}, and 1052 cm^{-1} (skeletal vibrations with C-O stretching) can be assigned.[18] Figure 1b shows the bands at 1080, 948, and 797 cm^{-1} that are due to Si-O stretching, Si-OH stretching, and symmetric Si-O-Si stretching, respectively.[15] In Figure 1c, the absorption peaks at 2934 and 2840 cm^{-1} correspond to the C-H vibrations of the alkyl chains.[35] Moreover, the bands at 953, 804, and 798 cm^{-1} are attributed to N = Mo, Mo-O, and Mo-O-Mo, respectively, confirming the presence of $[Mo_6O_{18}]^{-2}$ ions in the structure of the synthesized nanocatalyst.[22]

The XRD patterns of SiO_2@Glu/$Si(OEt)_2(CH_2)_3N$ = $Mo[Mo_5O_{18}]$ and SiO_2 are shown in Figure 2, which was used to study the crystallographic features of the prepared catalyst. It can be seen that the reflection peaks are in the 2θ range of 0–70°. In Figure 2a, the broad peak in the 2θ 20°–32° range is consistent with an amorphous silica phase.[36] The presence of sharp peaks proves the special status of the nanocatalyst structure. In Figure 2b, the XRD pattern shows that the amorphous structure of SiO_2 particles was preserved. The confirming peak indicating the

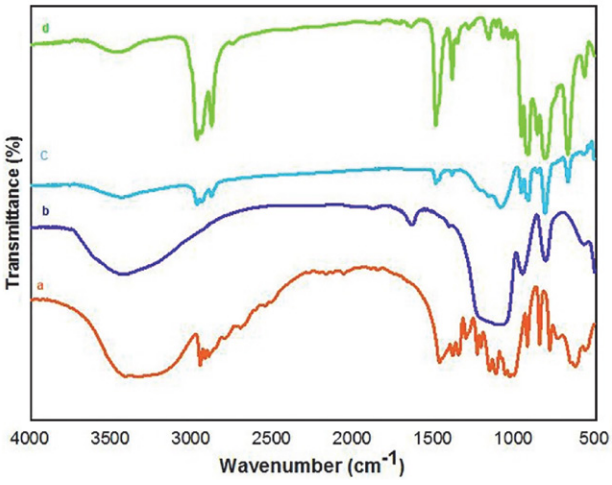

Figure 1. FT-IR Spectra of a) glucose, b) SiO_2, c) SiO_2@Glu/$Si(OEt)_2(CH_2)_3N$ = $Mo[Mo_5O_{18}]$ and d) $[n\text{-}Bu_4N]_2[Mo_6O_{19}]$.

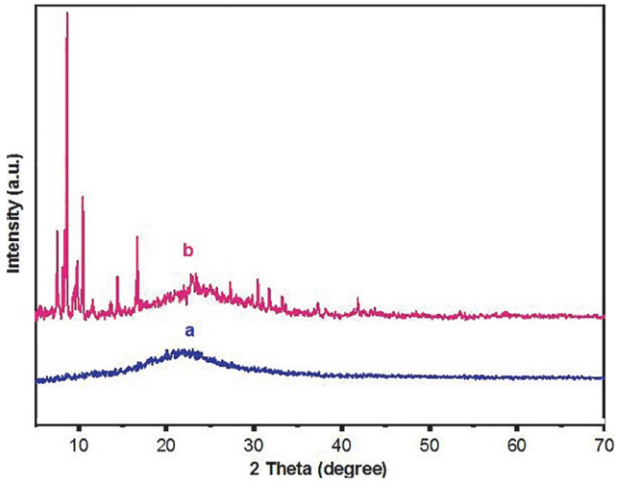

Figure 2. The XRD pattern of a) SiO_2 and b) SiO_2@Glu/$Si(OEt)_2(CH_2)_3N$ = $Mo[Mo_5O_{18}]$ nanocatalyst.

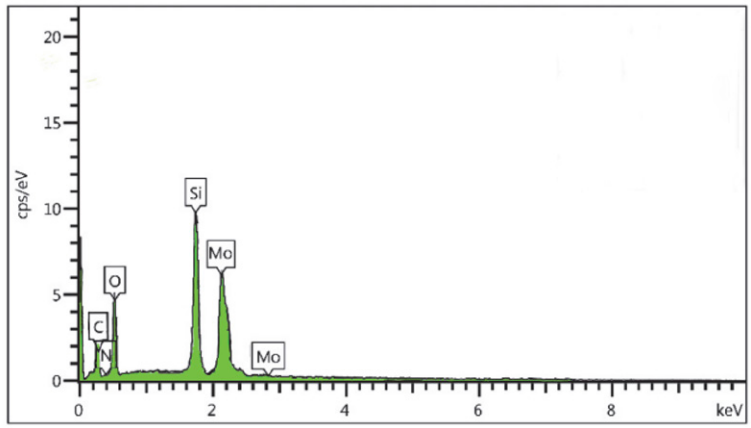

Figure 3. EDS analysis of SiO_2@Glu/Si(OEt)$_2$(CH$_2$)$_3$N = Mo[Mo_5O_{18}].

presence of the molybdate group appeared in the range of 2θ = 20°–30°, which can be attributed to the amorphous molybdate on the composite.[35,39]

Energy-dispersive X-ray spectroscopy (EDS) was selected to provide the necessary information on elemental structure of the catalyst. According to the Fig. 3, the EDS pattern clearly indicated the existence expected the elemental composition of C, N, O, Si, and Mo in the nanocatalyst structure.

The surface morphology and particle size distribution of the prepared nanocatalyst were observed using FE-SEM, and the corresponding image is shown in Figure 4. The results show that the particles are uniformly and regularly spherical with an average diameter of 22–42 nm.

The results of the thermal stability of nanocatalyst **3** by thermogravimetric analysis (TG) from 0 to 900 °C are shown in Figure 5. The results show that the first weight loss at a temperature of 120 °C (about 12%) is related to the removal of H_2O and other organic solvents left behind in the extraction process. The second weight loss at 220–320 °C (about 5%) is due to the removal of organic components located on the surface of the catalyst. The largest weight loss in a temperature range of 500–550 °C (about 12.5%) is related to the removal of propylamine groups attached to the catalyst framework.[22]

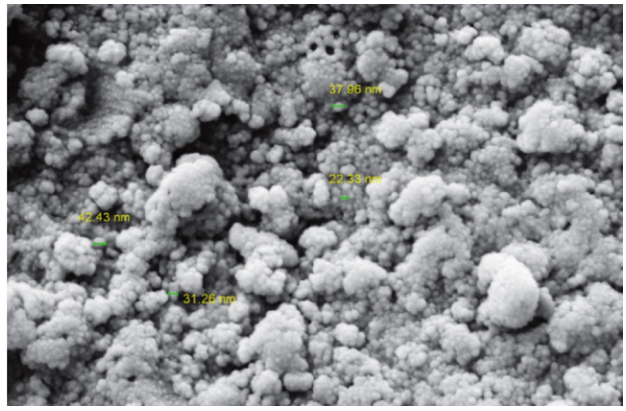

Figure 4. FE-SEM analysis of SiO_2@Glu/Si(OEt)$_2$(CH$_2$)$_3$N = Mo[Mo_5O_{18}].

After characterization to study the catalytic activity and efficiency of the newly developed catalyst, it was used as a catalyst for the synthesis of pyrano[2,3-*d*]pyrimidines **7** via the three-component reaction of arylaldehydes **4**,

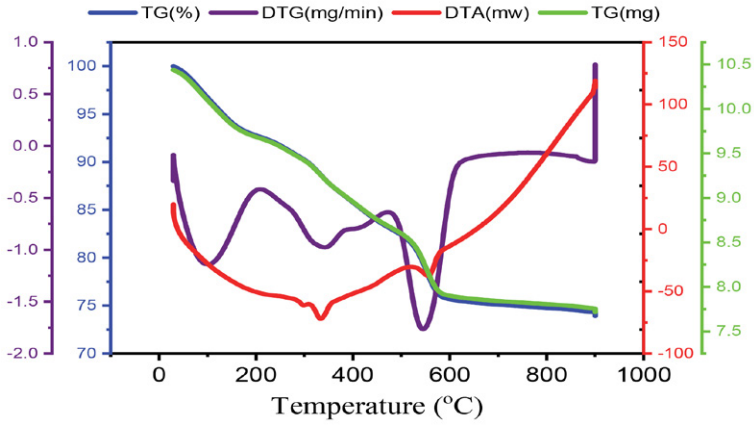

Figure 5. TG analysis of SiO_2@Glu/Si(OEt)$_2$(CH$_2$)$_3$N = Mo[Mo_5O_{18}].

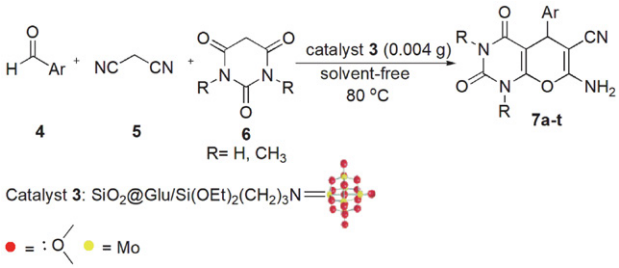

Scheme 1. Preparation of pyrano[2,3-*d*]pyrimidines **7** in the presence of SiO_2@Glu/Si$(OEt)_2(CH_2)_3N$ = Mo$[Mo_5O_{18}]$ nanocatalyst.

malononitrile **5**, and barbituric acid **6** under solvent-free conditions (Scheme 2).

To find the optimum reaction conditions, a three-component reaction between benzaldehyde, malononitrile, and 1,3-dimethylbarbituric acid was selected as a model reaction, and the effect of various parameters such as temperature, catalyst loading, and solvent was evaluated. The reaction did not proceed well in the absence of the catalyst after a long reaction time. The model reaction was carried out at 25, 60, 80 and 100 °C in the presence of 0.002 g catalyst **3**. The study showed that the reaction was affected by temperature, and the best result was observed at 80 °C. Next, the effect of the amount of catalyst was studied. It was found that the yield increased when the amount of catalyst was increased from 0.002 g to 0.004 g, and higher amount of catalyst did not have a good effect on the reaction process. Moreover, the model reaction was carried out with 0.004 g SiO_2@Glu/Si$(OEt)_2(CH_2)_3N$ = Mo$[Mo_5O_{18}]$

Table 1. Screening of various parameters in the synthesis of **7a** catalyzed by nanocatalyst **3**.[a]

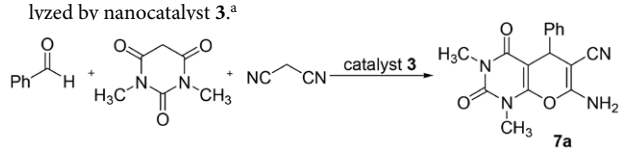

Entry	Catalyst loading (g)	Solvent	Temp. (°C)	Yieldb (%)
1	0.002	–	25	20
2	0.002	–	60	45
3	0.002	–	80	60
4	0.002	–	100	50
5	0.004	–	80	90
6	0.006	–	80	85
7	0.008	–	80	80
8	0.004	MeOH	Reflux	60
9	0.004	EtOH	Reflux	70
10	0.004	CH3CN	Reflux	75
11	0.004	Toluene	Reflux	65

[a] Reaction conditions: benzaldehyde (1 mmol), malononitrile (1 mmol), 1,3–dimethylbarbituric acid (1 mmol), time: 20 min. [b] Isolated yields.

Table 2. Preparation of various pyrano[2,3-*d*]-pyrimidines by nanocatalyst **3**.

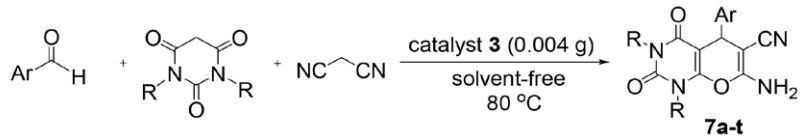

Entry	R	Aldehyde	Tim (min)	Yield[a] (%)	Mp (Lit) (°C)
7a	H	C6H5CHO	30	90	212–214 (212–213)[42]
7b	H	2,4-Cl C6H3CHO	15	93	242–244 (242–243)[42]
7c	H	3-NO2 C6H4CHO	20	95	260–262 (262–263)[43]
7d	H	4-NO2 C6H4CHO	20	93	237–239 (237–238)[43]
7e	H	3-Br C6H4CHO	25	95	280–282 (279–280)[43]
7f	H	4-Br C6H4CHO	20	90	228–230 (227–229)[43]
7g	H	4-OCH3 C6H4CHO	25	95	280–282 (281–282)[43]
7h	H	4-Cl C6H4 CHO	15	90	238–240 (239–240)[44]
7i	CH3	C6H5CHO	20	95	228–230 (228–229)[44]
7j	CH3	2-Cl C6H4 CHO	15	89	248–250 (250–251)[44]
7k	CH3	4-OCH3 C6H4CHO	30	95	224–225 (225–227)[44]
7l	CH3	4-Cl C6H4CHO	10	95	238–240 (239–241)[44]
7m	CH3	3-NO2 C6H4CHO	20	93	212–214 (212–213)[44]
7n	CH3	4-NO2 C6H4CHO	20	95	230–232 (231–232)[44]
7o	CH3	3-Br C6H4CHO	15	93	218–220 (218–219)[44]
7p	CH3	4-CH3 C6H4CHO	20	90	230–232 (229–230)[44]
7q	CH3	2,4-Cl2 C6H3CHO	10	95	211–213 (211–212)[30]
7r	CH3	1-Naphthaldehyde	40	93	360 (360–361)[44]
7s	CH3	Biphenyl-4-carboxaldehyde	30	95	275–277[b]
7t	CH3	Terephthalaldehyde	20	95	240–242[b]

[a] Isolated yields. [b] Novel product.

in some solvents such as methanol, ethanol, acetonitrile and toluene. As can be seen, considerable acceleration is observed especially for reactions carried out under solvent-free conditions. According to these results, the use of SiO_2@Glu/$Si(OEt)_2(CH_2)_3N$ = $Mo[Mo_5O_{18}]$ (0.004 g) as catalyst under solvent-free conditions at 80 °C would be the best choice (Table 1).

After optimization of the reaction conditions, the reaction of various aromatic aldehydes, malononitrile and barbituric acid derivatives was studied in the presence of nanocatalyst **3** under optimal conditions, which showed the successful formation of the corresponding pyrano[2,3-*d*]-pyrimidines (Table 2). Both aldehydes with electron-donating groups and aldehydes with electron-attracting groups were prepared in good to excellent yields.

The proposed mechanism for the formation of pyrano[2,3-*d*]pyrimidines **7** is shown in Scheme 3. According to the proposed mechanism, adduct **8** is first obtained by the condensation of aromatic aldehydes and malononitrile in the presence of the catalyst. Then, Michael addition of barbituric acid to this intermediate **9** is formed. The intramolecular cyclization of **9** gives the adduct **10**, which rearranges to give the pyrano[2,3-*d*]pyrimidinones **7**.

The main advantages of the presented protocol over existing methods become clear when our results are compared with those of some recent methods reported in articles (see Table 3).

To study the leaching of $[Mo_6O_{19}]^{2-}$ from SiO_2@Glu/$Si(OEt)_2(CH_2)_3N$ = $Mo[Mo_5O_{18}]$, we performed an in situ filtration technique. When the model reaction reached 50%, warm EtOAc (5 ml) was added, and catalyst isolation was performed by simple filtration. After removal of the solvent, the process was continued with the catalyst-free residue under the previously optimized conditions. As expected, the reaction stopped, confirming that no leaching of the supported catalytic centers occurred under the optimized conditions. The reusability of SiO_2@Glu/$Si(OEt)_2(CH_2)_3N$ = $Mo[Mo_5O_{18}]$ was also investigated in the model reaction. After completion of the reaction, EtOAc (5 mL) was added to the mixture, the catalyst was filtered, washed with EtOH (10 mL) and deionized water (10 mL), and then dried at 100 °C. The recovered catalyst was used ten times in the model reaction, and the yield was negligible (Figure 6). These experiments indicate high stability and durability of this nanocatalyst under the applied conditions. To test the stability of the catalyst structure, the recycled nanocatalyst was examined using FT-IR spectra. The FT-IR spectra of the freshly prepared catalyst and the recycled catalyst are shown in Figure 7 and confirm the chemical stability of catalyst **3**.

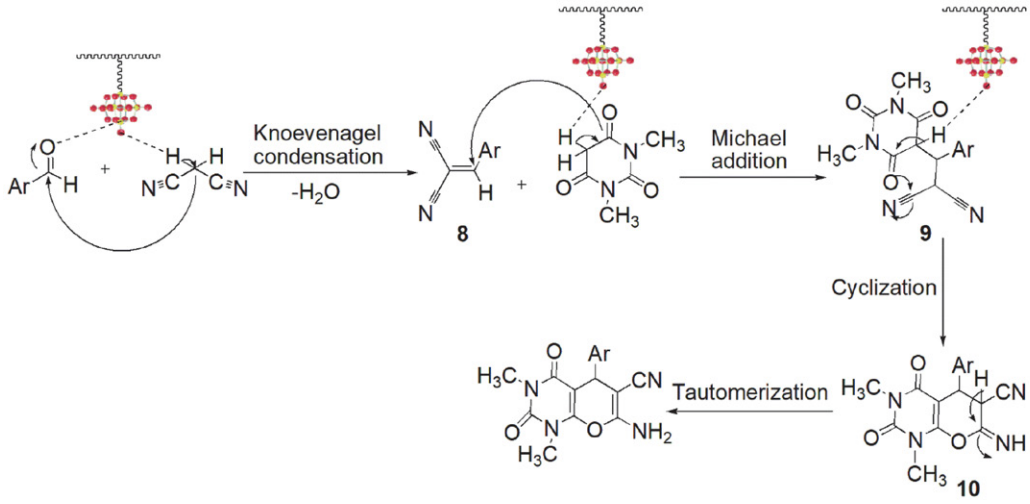

Scheme 3. The proposed mechanism for the synthesis of pyrano[2,3-*d*]pyrimidinones catalyzed by nanocatalyst **3**.

Table 3. Comparison of results for the synthesis of **7I** with other catalysts.

Entry	Catalyst	Catalyst loading	Condition	Time (min)	Yield[a] (%)[a]
1	Catalyst **3**	0.004 g	solvent-free, 80 °C	10	95[b]
2	Et_3N	20 mol %	EtOH, 50 °C	25	87[28]
3	Urea	10 mol %	EtOH:H_2O, r.t.	840	86[29]
4	Zn [(L) proline]$_2$	17 mol %	EtOH, Reflux	50	90[45]
5	{Fe_3O_4@SiO_2@$(CH_2)_3$-Urea-SO_3H/HCl} MNP	0.01 g	solvent-free, 60 °C	30	97[44]
6	Nano-basic silica	25 mol %	solvent-free	54	89[46]

[a] Isolated yields. [b] This study.

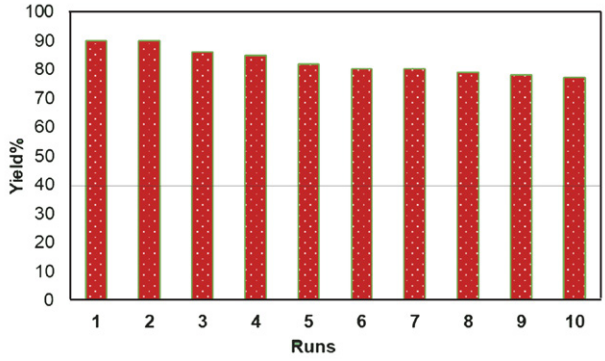

Figure 6. Reuse of SiO_2@Glu/Si(OEt)$_2$(CH$_2$)$_3$N = Mo[Mo_5O_{18}] nanocatalyst.

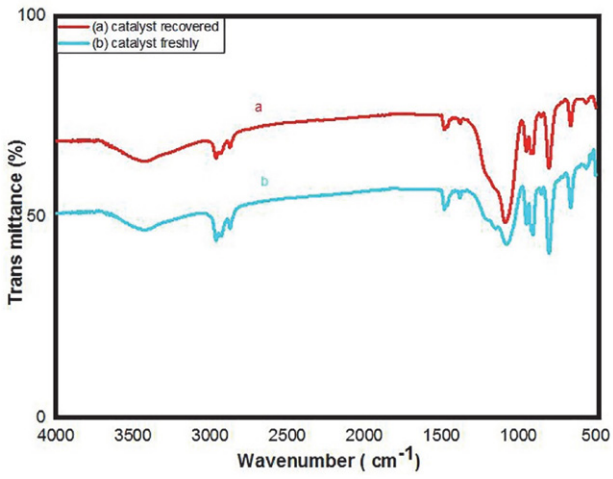

Figure 7. FT-IR spectra for comparison of fresh catalyst and recovered catalyst.

3. Experimental

All chemical materials were purchased from Merck and Aldrich. The reaction progress and purity of the compounds were monitored by TLC on silica gel SIL G/UV254 plates. Melting points were checked using a KSB1N electrothermal device and are correct. The IR spectra of all synthesized compounds were recorded in the KBr matrix using a spectrometer model JASCO FT-IR /680 plus. ^{1}H NMR spectra were recorded in DMSO-d_6 as solvent using a Bruker Avance Ultra Shield 400 MHz spectrometer, and ^{13}C NMR spectra were registered at 100 MHz. A scanning electron microscope (FE-SEM) was used to measure the size of the particles and the shape of the catalyst. X-ray diffraction (XRD) patterns were recorded with a Philips X Pert Pro X diffractometer using Ni filtered Cu-Ka radiation. Energy dispersion spectroscopy (EDS) was recorded using a TESCAN Vega instrument.

Preparation of the Glu/Si(OEt)$_2$(CH$_2$)$_3$N = Mo[Mo_5O_{18}]

First, the tetrabutylammonium hexamolybdate ([n-Bu4N]2 [Mo6O19]) was prepared according to the described procedure.[20] The tetrabutylammonium hexamolybdate (0.4 g) and DMSO (20 ml) were placed in a round bottom flask (50 ml) and dispersed for 20 minutes. Then 3-aminopropyltriethoxysilane (2.5 ml) was added dropwise to the mixture and stirred under reflux conditions for 24 hours under argon atmosphere. Dissolved glucose (0.26 g) in dry DMSO (5 mL) and H_2SO_4 (98%, 0.33 mL) were then added. The mixture was stirred at room temperature for 5 hours. Finally, the obtained product (compound **2**) was washed with ethanol, distilled and dried at 80 °C.

Protocol for the synthesis of nano-SiO_2

Tetraethyl orthosilicate (TEOS) (6.2 ml) was added to ethanol (100 ml) and ammonium hydroxide (6.5 ml), and the mixture was stirred at room temperature for 15 hours. The mixture was then filtered by centrifugation (4000 rpm, 30 min), and the resulting white powder was washed three times with ethanol and dried for 12 h at 60 °C.[15]

Preparation of the SiO_2@Glu/Si(OEt)$_2$(CH$_2$)$_3$N = Mo[Mo_5O_{18}]

To immobilize Glu/Si(OEt)$_2$(CH$_2$)$_3$N = Mo[Mo_5O_{18}] on the surface of SiO_2, the prepared SiO_2 nanoparticles (1.0 g) were dispersed in dry toluene (30 mL) by ultrasonication for 20 min. Compound **2** (0.5 g) was then added and the mixture was refluxed under argon atmosphere for 24 hours. Then the prepared SiO_2@Glu/Si(OEt)$_2$(CH$_2$)$_3$N = Mo[Mo_5O_{18}] was filtered and washed several times with ethanol and then with water. Finally, the brown powder was dried in vacuo at 80 °C for 24 hours.

General procedure for the synthesis of pyrano[2,3-*d*]-pyrimidines derivatives 7

SiO_2@Glu/Si(OEt)$_2$(CH$_2$)$_3$N = Mo[Mo_5O_{18}] (0.004 g) was added to the mixture of arylaldehyde (1 mmol), malononitrile (1 mmol), and barbituric acid (1 mmol) at 80 °C under solvent-free conditions. The progress of the reaction was monitored by TLC. After completion of the reaction, ethyl acetate was added and the catalyst was separated by filtration. For further purification of the product, the obtained powder was recrystallized from EtOH.

Spectral data

*7-Amino-5-(2,4-dichlorophenyl)-1,3-dimethyl-2,4-dioxo-1,3,4,5-tetrahydro-2H-pyrano[2,3-d]pyrimidine-6-carbonitrile (**7q**).* White solid; mp: 211–213 °C; IR (KBr) (ν_{max}, cm^{-1}) 3394, 3313, 3212, 3081, 2962, 2194, 1708, 1689, 1643, 1494, 1384, 1230, 1184, 1099, 1049, 844, 582, 755. ^{1}H NMR (400 MHz, DMSO-d_6) δ 3.09 (s, 3H), 3.39 (s, 3H), 4.88 (s, 1H), 6.93-7.55 (m, 5H) ppm. ^{13}C NMR (100 MHz, DMSO-d_6) δ 28.09, 29.63, 33.70, 57.19, 88.07, 118.86, 128.12, 129.01, 132.11, 132.44, 133.67, 140.85, 150.44, 151.05, 158.22, 160.78 ppm.

*5-([1,1'-Biphenyl]-4-yl)-7-amino-1,3-dimethyl-2,4-dioxo-1,3,4,5-tetrahydro-2H-pyrano[2,3-d]pyrimidine-6-carbonitrile (**7s**).* White solid; mp: 275–277 °C; IR (KBr) (ν_{max}, cm^{-1}) 3432, 3300, 3177, 3074, 2984, 2190, 1736, 1684, 1634, 1486, 1386, 1227, 1186, 1040, 1007, 850, 744, 751, 698, 571, 550. ^{1}H NMR (400 MHz, DMSO-d_6) δ 2.11 (s, 3H), 2.54 (s, 3H), 4.40 (s, 1H), 6.93-7.67 (m, 11H) ppm. ^{13}C NMR (100 MHz, DMSO-d_6) δ 28.17, 29.62, 36.70, 58.99, 81.25, 119.56, 127.39, 127.56, 127.56, 127.78, 128.02, 128.44, 129.37, 129.40, 129.59, 129.67, 138.72, 139.29, 140.47, 150.48, 158.20, 161.00, 161.27 ppm.

*7-Amino-5-(4-formylphenyl)-1,3-dimethyl-2,4-dioxo-1,3,4,5-tetrahydro-2H-pyrano[2,3-d]pyrimidine-6-carbonitrile (**7t**).* White solid; mp: 240–242 °C; IR (KBr) (ν_{max}, cm^{-1}) 3380, 3316, 3192, 3074, 2984, 2195, 1708, 1685, 1638, 1487, 1386, 1226, 1185, 1040, 1115, 847, 751, 698, 571. ^{1}H NMR (400 MHz, DMSO-d_6) δ 3.116 (s, 3H), 3.386 (s, 3H), 4.403 (s, 1H), 7.341-7.672 (m,6H), 9.146, (s, 1H) ppm. ^{13}C NMR (100 MHz, DMSO-d_6) δ 28.25, 29.63, 36.70, 58.99, 81.25, 128.03, 128.44, 129.37, 129.67, 130.79, 131.81, 140.47, 150.49, 158.20, 161.01, 161.28 ppm.

4. Conclusions

In this work, we have presented for the first time SiO_2@Glu/Si(OEt)$_2$(CH$_2$)$_3$N = Mo[Mo_5O_{18}] as a green and recyclable SiO_2-based nanocatalyst. The efficiency of this catalyst was evaluated in the synthesis of pyrano[2,3-*d*] pyrimidinone derivatives. This new catalytic system showed the advantages of environmentally friendly character, easy separation, non-toxicity, mild reaction conditions, short reaction times and good reusability.

Acknowledgements

The authors would like to thank the Research Council of Yasouj University for their generous support of this research work.

5. References

1. K. Zheng, C. Shen, J. Qiao, J. Tong, J. Jin, P. Zhang, *Catalysts* **2018**, *8*, 443–454. **DOI:**10.3390/catal8100443
2. D. J. Cole-Hamilton, *Science* **2003**, *299*, 1702–1706. **DOI:**10.1126/science.1081881
3. S. X. Fei, B. Han, L. Li, P. Mei, T. Zhu, M. Yang, H. Chen, *Int. J. Hydrogen Energy* **2017**, *42,* 25942–25950. **DOI:**10.1016/j.ijhydene.2017.08.204
4. C. Dai, Y. Li, C. Ning, W. Zhang, X. Wang, C. Zhang, *Appl. Catal. A Gen.* **2017**, *545*, 97–103. **DOI:**10.1016/j.apcata.2017.07.032
5. W. Shi, J. Yu, Z. Jiang, Q. Shao, W. Su, *Beilstein J. Org. Chem.* **2017**, *13*, 1661–1668. **DOI:**10.3762/bjoc.13.160
6. M. Celebi, M. Yurderi, A. Bulut, M. Kaya, M. Zahmakiran, *Appl. Catal. B Environ.* **2016**, *180*, 53–64. **DOI:**10.1016/j.apcatb.2015.06.020
7. T. Hattori, A. Tsubone, Y. Sawama, Y. Monguchi, H. Sajiki, *Catalysts* **2015**, *5*, 18–25. **DOI:**10.3390/catal5010018
8. S. Zhang, Y. R. Lee, H. J. Jeon, W. S. Ahn, Y. M. Chung, *Mater. Lett.* **2018**, *215*, 211–213. **DOI:**10.1016/j.matlet.2017.12.106
9. B. Karami, M. Kiani, S. J. Hosseini, M. Bahrami, *New J. Chem.* **2015**, *39*, 8576–8581. **DOI:**10.1039/C5NJ01302J
10. J. E. Gholtash, M. Farahi, B. Karami, M. Abdollahi, *Acta Chim. Slov.* **2020**, *67*, 866–875. **DOI:**10.17344/acsi.2020.5825
11. Y. Guo, J. Tang, Z. Wang, Y.-M. Kang, Y. Bando, Y. Yamauchi, *Nano Eng.* **2018**, *47*, 494–502. **DOI:**10.1016/j.nanoen.2018.03.012
12. P. R. Monich, F. V. Berti, L. M. Porto, B. Henriques, A. P. N. de Oliveira, M. C. Fredel, J. C. Souza, *Mater. Sci. Eng. C Mater. Biol. Appl.* **2017**, *79*, 354–362. **DOI:**10.1016/j.msec.2017.05.031
13. D. W. Lee, B. R. Yoo, *J. Ind. Eng. Chem.* **2016**, *38*, 1–12. **DOI:**10.1016/j.jiec.2016.04.016
14. R. S. Dubey, Y. Rajesh, M. A. More, *Mater. Today: Proc.* **2015**, *2*, 3575–3579. **DOI:**10.1016/j.matpr.2015.07.098
15. X. Jiang, X. Tang, L. Tang, B. Zhang, H. Mao, *Ceram. Int.* **2019**, *45*, 7673–7680. **DOI:**10.1016/j.ceramint.2019.01.067
16. L. Zare Fekri, A. R. Darya-Laal, *Polycycl. Arom. Comp.* **2020**, *40*, 1539–1556. **DOI:**10.1080/10406638.2018.1559207
17. C. Sanchez, B. Julián, P. Belleville, M. Popall, *J. Mater. Chem.* 2015, *15*, 3559–3592. **DOI:**10.1039/b509097k
18. H. S. Barud, R. M. N. Assunção, M. A. U. Martines, J. Dexpert-Ghys, R. F. C. Marques, Y. Messaddeq, S. J. L. Ribeiro, *J. Sol-Gel Sci. Technol.* **2008**, *46*, 363–367. **DOI:**10.1007/s10971-007-1669-9
19. F. Xue, Y. Dong, P. Hu, Y. Deng, Y. Wei, *RSC Adv.* **2015**, *5*, 73684–73691. **DOI:**10.1039/C5RA11798D
20. A. Zarnegaryan, M. Moghadam, S. Tangestaninejad, V. Mirkhani, I. Mohammadpoor-Baltork, *Polyhedron* **2016**, *115*, 61–66. **DOI:**10.1016/j.poly.2016.02.003
21. Z. Shi, X. Gu, J. Peng, X. Yu, E. Wang, *Eur. J. Inorg. Chem.* **2006**, *3*, 385–388. **DOI:**10.1002/ejic.200500662
22. S. Kargar, D. Elhamifar, A. Zarnegaryan, *J. Phys. Chem. Solids* **2020**, *146*, 109601–109612. **DOI:**10.1016/j.jpcs.2020.109601
23. M. Neysi, A. Zarnegaryan, D. Elhamifar, *New J. Chem.* **2019**, *43*, 12283–12291. **DOI:**10.1039/C9NJ01160A
24. N. Veronovski, M. Sfiligoj-Smole, J. L. Viota, *Text. Res. J.* **2010**, *80*, 55–62. **DOI:**10.1177/0040517509104012
25. U. M. Garusinghe, S. Varanasi, G. Garnier, W. Batchelor, *Cellulose* **2017**, *24*, 2511–2521. **DOI:**10.1007/s10570-017-1265-2
26. U. J. Kim, S. Kimura, M. Wada, *Carbohydr. Polym.* **2019**, *222*, 114975–114980. **DOI:**10.1016/j.carbpol.2019.114975
27. N. Esfandiary, A. Nakisa, K. Azizi, J. Azarnia, I. Radfar, A. Heydari, *Appl. Organomet. Chem.* **2017** *31*, 3641–3649. **DOI:**10.1002/aoc.3641
28. D. Azarifar, R. Nejat-Yami, F. Sameri, Z. Akrami, *Lett. Org. Chem.* **2012**, *9*, 435–439. **DOI:**10.2174/157017812801322435

29. a) G. Brahmachari, B. Banerjee, *ACS Sustain. Chem. Eng.* **2014**, *2*, 2802–2812. **DOI:**10.1021/sc400312n.
b) R. M. Mohareb, R. A. Ibrahim, E. S. Alwan, *Acta Chim. Slov*. **2021**, *68*, 51–64. **DOI:**10.17344/acsi.2020.6090
30. A. Khazaei, A. Ranjbaran, F. Abbasi, M. Khazaei, A. R. Moosavi-Zare, *RSC Adv.* **2015***, 5*, 13643–13647. **DOI:**10.1039/C4RA16664G
31. M. Nogueras, J. Cobo, M. L. Quijano, M. Melguizo, A. Sánchez, M. Melgarejo, *Nucleosides Nucleotides Nucleic Acids* **1994**, *13*, 447–457. **DOI:**10.1002/jlac.198919890241
32. E. M. Grivsky, S. Lee, C. W. Sigel, D. S. Duch, C. A. Nichol, *J. Med. Chem.* **1980**, *23*, 327–329. **DOI:**10.1021/jm00177a025
33. J. Davoll, J. Clarke, E. F. Elslager, *J. Med. Chem*. **1972**, *15*, 837–839. **DOI:**10.1021/jm00278a009
34. M. Bararjanian, S. Balalaie, B. Movassag, A. M. Amani, *J. Iran. Chem. Soc.* **2009**, *6*, 436–442. **DOI:**10.1007/BF03245854
35. F. Khosravian, B. Karami, M. Farahi, *New J. Chem.* **2017**, *41*, 11584–11590. **DOI:**10.1039/C7NJ02390A
36. M. Farahi, B. Karami, R. Keshavarz, F. Khosravian, *RSC Adv.* **2017**, *7*, 46644–46650. **DOI:**10.1039/C7RA08253C
37. S. Akrami, B. Karami, M. Farahi, *RSC Adv.* **2017**, *7,* 34315–34320. **DOI:**10.1039/C7RA06240K
38. B. Karami, M. Farahi, S. Akrami, D. Elhamifar, *New J. Chem. Chem*. **2018**, *42*, 12811–12816. **DOI:**10.1039/C8NJ02699H
39. H. M. Tanuraghaj, M. Farahi, *Monatsh. Chem.* **2019**, *150*, 1841–1847. **DOI:**10.1007/s00706-019-02471-x
40. H. M. Tanuraghaj, M. Farahi, *RSC Adv.* **2018**, *8*, 27818–27824. **DOI:**10.1039/C8RA05501G
41. a) J. E. Gholtash, M. Farahi, *RSC Adv.* **2018**, *8*, 40962–40967. **DOI:**10.1039/c8ra06886k
b) R. Keshavarz, M. Farahi, B. Karami, *Acta Chim. Slov.* **2021**, *68*, 332–340. **DOI:**10.17344/acsi.2020.6266
42. E. Mollashahi, M. Nikraftar, *J. Saudi Chem. Soc.* **2018**, *22*, 42–48. **DOI:**10.1016/j.jscs.2017.06.003
43. T. S. Jin, L. B. Liu, Y. Zhao, T. S. Li, *J. Chem. Res.* **2005**, *3*, 162–163. **DOI:**10.3184/0308234054213672
44. M. A. Zolfigol, R. Ayazi-Nasrabadi, S. Baghery, *Appl. Organomet. Chem.* **2016**, *30*, 273–281. **DOI:**10.1002/aoc.3428
45. M.M. Heravi, A. Ghods, K. Bakhtiari, F. Derikvand, *Synth. Commun.* **2010**, 40, 1927–1931. **DOI:**10.1080/00397910903174390
46. N. Sheikhan-Shamsabadi, M. Ghashang, (2017). *Main Group Met. Chem.* **2017**, 40, 19–25. **DOI:**10.1515/mgmc-2016-0034

Povzetek

Prispevek opisuje pripravo in identifikacijo SiO_2@Glu/Si$(OEt)_2(CH_2)_3N$ = Mo$[Mo_5O_{18}]$ kot novega bifunkcionalnega kislinsko-baznega katalizatorja (s kislimi in bazičimi Lewisovimi mesti). Najprej so aminopropiltrietoksisilan reagirali s heksamolibdatnimi anioni in nato obdelali z glukozo, ter tako pripravili Glu/Si$(OEt)_2(CH_2)_3N$ = Mo$[Mo_5O_{18}]$. Nano-siliko so nato modificirali s pripravljenim kompleksom glukoza/molibdat in dobili SiO_2@Glu/Si$(OEt)_2(CH_2)_3N$ = Mo$[Mo_5O_{18}]$. Razvit katalizator so okarakterizirali z FT-IR, EDX, XRD, FE-SEM in TGA analizo. Katalitsko učinkovitost novega katalizatorja so raziskali na primeru priprave derivatov pirano[2,3-*d*]pirimidina z reakcijo med različnimi aldehidi, malononitrilom in barbiturno kislino. Načrtovane produkte so pripravili v prisotnosti 0,004 g pripravljenega katalizatorja z visokim do odličnim izkoristkom.

Except when otherwise noted, articles in this journal are published under the terms and conditions of the Creative Commons Attribution 4.0 International License

Scientific paper

Synthesis of Glucose/Fructose Sensitive Poly(ethylene glycol) Methyl Ether Methacrylate Particles with Novel Boronate Ester Bridge Crosslinker and their Dye Release Applications

Şeküre Yildirim,[1] Hasan Akyildiz[1,2] and Zeynep Çetinkaya[1,3]

[1] *Department of Metallurgical and Materials Engineering, Konya Technical University, Konya, Turkey*

[2] *Nanotechnology and Advanced Materials Development, Application, and Research Center, Konya Technical University, Konya, Turkey*

[3] *Advanced Technology Research and Application Center, Selçuk University, Konya, Turkey*

* *Corresponding author: E-mail: zcetinkaya@ktun.edu.tr, + 90 332 205 1945*

Received: 03-18-2021

Abstract

In this study, it is aimed to develop glucose/fructose sensitive poly(ethylene glycol) methyl ether methacrylate (PEGMA) particles which can be employed in controlled drug delivery applications. For this purpose, a boric acid based crosslinker was synthesized using 4-vinylphenylboronic acid (VPBA) and its formation was confirmed by ^{1}H-NMR and FT-IR analyses. Sugar-sensitive polymeric particles were then achieved using this crosslinker and PEGMA monomer in single step and surfactant free emulsion polymerization technique. Polymeric particles were characterized by DLS, SEM, and TEM in terms of size and morphology. In order to determine the sensitivity of the particles to sugar molecules, first Rhodamine B dye (as a model drug) loading experiments were performed. Then, the particles were subjected to glucose/fructose rich media and dye release was monitored as a function of time using UV-Vis spectrophotometry. The results of the current study revealed that the PEGMA particles were more sensitive to fructose (~39% release) compared to glucose (~25% release) at pH 7.4 and 310 K.

Keywords: Controlled drug release, fructose sensitivity, phenylboronic acid, smart polymers, crosslinker

1. Introduction

Smart polymers are a group of materials which can modify some of their physical/chemical properties upon exposure to external stimuli such as temperature,[1] pH,[2] light[3], and magnetic/electric field.[4] They may also show response to variety of organic compounds. Examples of these compounds include carbohydrates, enzymes, acids, and sugar molecules.[5] Due to this unique behavior, these polymers are highly promising in various innovative applications such as biomedical and bioengineering studies.[6] Among these applications, non-invasive biosensors have attracted great attention as these sensors provide the opportunity to detect the level of glucose or fructose molecules in the metabolism without disturbing the patients.[7]

Glucose-sensitive biosensors can be classified into three types according to their chemical make-up and sensing mechanism.[8] These are known as glucose-oxidase, protein, and phenyl boronic acid (PBA) based systems. Glucose-oxidase sensors operate via the enzymatic oxidation of glucose molecules, whereas glucose-binding proteins are functioning through the binding of glucose molecules with glycol polymer-lectin complexes. These compounds are natural biological proteins which makes them intolerant to several environmental factors such as high temperature and pH. Further, the instability of these materials limits their widely use as glucose-sensitive systems. On the contrary, PBA is known to be the synthetic derivative of boronic acid with good stability and easy preparation.[7,9] Boronic acid can bind to diol and polyol species of saccharides with high affinity through reversible boronate ester

formation.[1a,7,10] For example, cis-1,2 and cis-1,3 diols of the sugar molecules are able to link reversibly with boronic acid. The details of this binding mechanism were well established in literature.[6]

PBA compounds exhibit an equilibrium between the charged and uncharged forms in aqueous media.[11] These two forms of PBA can react with the cis-1,2 diols of sugar molecules. While the uncharged PBA is hydrophobic in nature, the complex of this form with glucose is not stable in aqueous media due to hydrolysis. On the other hand, the complex of charged PBA-glucose can form hydrophilic phenyl borate which is highly stable. Moreover, the indicated reaction can shift the equilibrium towards the hydrophilic state[12] which in principle increase the swelling ratio of the polymer network. This provides an opportunity to use polymeric particles as sugar sensitive systems in glucose or fructose containing environments for controlled insulin release.[10] However, PBA-based glucose sensitive systems cannot function effectively at physiological pH due to the high pKa value (~9) of this compound.[13] This is due to low ionization of phenyl-boronic acid at pH = 7.4 which decrease the solubility of polymer in water and also its affinity to glucose. Among the proposed methods to reduce the pKa of PBA, using of alkaline solutions was suggested as a promising route which increase the binding between the boronic acid and sugar molecules.[6,14]

Up to now, many forms of PBA based system, such as hydrogels,[15] multi-layered films,[16] nanofibers,[17] and nanoparticles (NPs)[18] have been studied for insulin release applications. Chen et al., reported that a polymer network can be obtained by crosslinking the boronate ester of two separate polymers containing boronic acid functional PBA based system, such as hydrogels,[15] multi-layered films,[16] nanofibers,[17] and nanoparticles (NPs)[18] have been studied for insulin release applications. Chen et al., reported that a polymer network can be obtained by crosslinking the boronate ester of two separate polymers containing boronic acid functional groups and diols.[14a] With a similar approach, it has been shown that polymeric NPs can be synthesized using a polymer containing PEG (polyethylene glycol)-based boronic acid and another polymer containing diol groups.[14b] Further, the NPs synthesized with the surfactant free emulsion polymerization method were reported to exhibit smooth surface and high stability.[6,19] In addition, these samples were successfully employed in drug delivery and glucose/fructose sensing applications. However, only a few studies have been reported in literature which focused on the synthesis of a crosslinker with boronate ester bridge and using the surfactant free polymerization method in the production of stimuli responsive polymeric particles.[2a,14]

Here, we have synthesized PEGMA particles which are sensitive to glucose/fructose molecules similar to those mentioned above albeit using a novel crosslinker containing boronate ester bonds for the first time. The PEGMA particles were achieved using this novel crosslinker in one step and surfactant free emulsion polymerization method. These particles were loaded with a model drug (Rhodamine B dye) during the polymerization reaction and the amount of dye release was monitored carefully upon exposing the particles to glucose or fructose rich media and interpreted as the sensitivity level of the particles to sugar molecules.

2. Experimental

4-vinylphenyl boronic acid (VPBA, 97%, Sigma Aldrich), 4-allylatechol (%95, Sigma Aldrich), toluene (99.8%, Sigma Aldrich), and sodium hydroxide (NaOH, 97%, Sigma Aldrich) were used in the synthesis of the novel crosslinker. Poly(ethylene glycol) methyl ether methacrylate (PEGMA, Mn of 300 g/mol, 97%, Sigma Aldrich), acetone (99.8%, Sigma Aldrich) and 2,2'-azobis 2-methylpropinamide dihydrochloride (AMPDH, 97%, Sigma Aldrich) were employed in the production of PEGMA particles. Toluene and deionized water (18.2 MΩ.cm) were used as catalyst and for cleaning purposes where necessary.

2. 1. Synthesis of Boranate Ester Bridge Containing Crosslinker

The crosslinker was synthesized according to Scheme 1 given below.[20] The samples were obtained by mixing 1 mmol (0.150 g) of 4-allylcatechol and 1 mmol (0.147 g) of VPBA in 10 mL of toluene in a glass beaker equipped with a reflux system. The solution pH was adjusted to 8.2 using NaOH and continuously stirred at 450 rpm for 72 h at a temperature of 383 K. After the reaction completed, the system was cooled down to room temperature and brown colored precipitates were collected and washed with fresh toluene for 3 times and then dried in a vacuum oven for 24 h at 348 K. Hereafter, this novel boronate ester bridge containing crosslinker is referred as CRX-3.

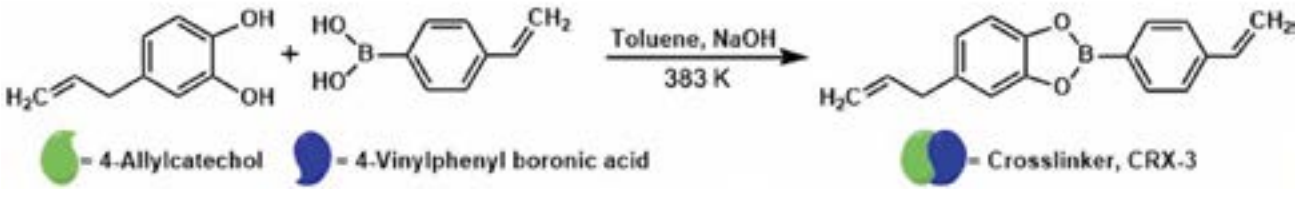

Scheme 1. Schematic representation of boronate ester bridge containing crosslinker (CRX-3) synthesis

2. 2. Synthesis of PEGMA Particles

PEGMA particles were obtained by mixing poly(ethylene glycol) methyl ether methacrylate monomer (Mn of 300 g/mol) with various amounts of CRX-3, as summarized in Table 1. Scheme 2 shows the emulsion polymerization reaction between the two precursors. For the synthesis of the particles; 300 μL of PEGMA monomer and proper amount of crosslinker were dissolved in 30 mL of acetone:water mixture (1/29, V/V). The amount of the crosslinker was calculated based on the mole % of the monomer. The reaction flask was first purged with ultra-high purity N_2 gas for 30 min to remove any dissolved oxygen. Polymerization process was carried out in this flask which was placed in a water bath on a magnetic stirrer at 343 K. 10 mg of AMPDH (free radical initiator) was added to the medium to initiate the polymerization reaction. The solution was stirred for 3 h at 400 rpm. After cooling to room temperature, pale orange color suspension was centrifuged at 7000 rpm for 10 min to collect the final PEGMA particles. Any unreacted monomer or reactant were then removed by rinsing the product for 3 times with distilled water. Finally, the particles were suspended in ultra-pure water for further use.

Table 1. Synthesis conditions for PEGMA particles.

Sample	PEGMA 300 (μL)	CRX-3 (%)[a]	AMPDH (mg)	Acetone (mL)	DI water (mL)
P-P-1	1				
P-P-2	3				
P-P-3	300	5	10	1	29
P-P-4	7.5				
P-P-5	10				

[a] According to the mole of the monomer.

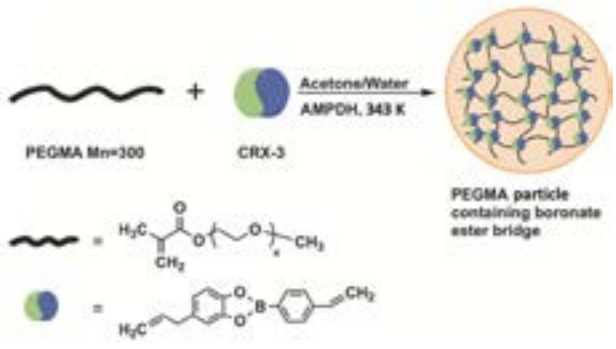

Scheme 2. Schematic representation of PEGMA particle synthesis using poly(ethylene glycol) methyl ether methacrylate monomer (Mn of 300 g/mol) and boronate ester bridge containing crosslinker

2. 3. Synthesis of Dye Loaded PEGMA Particles

In order to achieve dye loaded PEGMA particles, 1 mg of Rhodamine B (in powder form) was added to the reactants at the initial stage of polymerization reaction. Thereby, the dissolved dye molecules were forced to be trapped in the polymer network during polymerization. After the reactions completed, non-trapped dye molecules were removed by washing the particles in phosphate buffered saline (PBS) solution for 3 times. Then, certain amount of PEGMA particles were dispersed in 30 mL of PBS and poured into 3 separate vials with identical volumes i.e., 10 mL. 10 mg of fructose was added to the first vial, 10 mg of glucose was added to the second vial and the third vial left as it is, as the control sample. The vials were placed on a magnetic stirrer and heated to a constant temperature of 310 K. Finally, the absorbance data were recorded using a UV-Vis spectrophotometer after 0.5, 1, 2, 4, 6, 12, 24, and 48 h.

2. 4. Sample Characterization

Attenuated total reflectance/Fourier transform infrared (ATR/FT-IR) spectra of the samples were collected using a Bruker VERTEX-70 spectroscopy over the range of 4000 – 400 cm^{-1} at a resolution of 4 cm^{-1} and averaging 10 scans for each measurement. Solid-state ^{1}H-NMR spectrum was recorded on a Varian 400 MHz spectrometer with a 5 mm double-resonance probe, sample spinning rate of 8.0 kHz, contact time of 0.002 s, and a pulse delay of 5 s to verify the formation of the material. The following numbering scheme was used to determine the sample; 400 MHz, DMSO-d6, ppm, δ = 8.79–8.67 (Ar-OH), 8.07 (B-OH), 7.25–7.23 (d), 7.18–7.16 (c), 6.60 (b), 6.36–6.28 (f,e,g), 5.92 (a2), 5.88–5.85 (i), 5.04–5.00 (a1), 4.99–4.95 (j), 3.18–3.17 (h). The conversion efficiency for the crosslinker was estimated using an integration on the reduction of H peaks in ^{1}H-NMR spectra of CRX-3 compared to the one belonging to the precursors. The calculations were performed using MestraNova software.

The morphology of the PEGMA particles was investigated in as-centrifuged state using SM Zeiss LS-10 scanning electron microscope (SEM). The surfaces of the particles were coated with gold for 30 s prior to SEM analysis using a Cressington Sputter Coater system. For transmission electron microscope (TEM) examinations, the particles were first washed with DI-water for 3 times to remove any unreacted species and then mixed with 2 mL of fresh DI-water to obtain a dispersion in an ultrasonic bath. This dispersion was then dropped on a carbon-coated copper grid and dried for an overnight at room temperature. A JEOL 2100F model TEM was used to determine the size and morphology of the synthesized particles. The size of PEGMA particles were further verified using Malvern ZetaSizer Nano ZS dynamic light scattering (DLS) system. The polydispersity index (PDI) and average hydrodynamic diameters (dH) of the particles were measured after dispersing in 2 mL KCl solution (10 mM). The change in the absorbance of the samples during dye release was recorded via Biochrom Libra S22 UV-Vis spectrometer in the wavelength range of 450–650 nm.

3. Results and Discussion

3. 1. Structural and Morphological Evaluation of the Prepared Materials

^{1}H-NMR spectra of the synthesized crosslinker (Fig. 1a) and the precursors (4-allylcatechol (Fig. 1b) and VPBA (Fig. 1c)) are presented together for comparison. The spectra of VPBA and 4-allylcatechol exhibits (-OH) groups in Ar-OH, (δ= 8.79–8.67 ppm) and in B-OH, (δ= 8.07 ppm) peaks, respectively with high intensity. On the other hand, these peaks were almost disappeared in the spectrum of CRX-3. According to the integration calculations, the reduction of H peaks of Ar-OH groups in 4-allylcatechol molecule and B-OH groups in VPBA is more than 80% which also suggests that the product was obtained with a yield of more than 80%. A detailed ^{1}H-NMR spectrum for the crosslinker (Fig. S1) and the integration steps can be followed from the supplementary information.

The formation of the crosslinker was further verified by comparing the FT-IR spectra of CRX-3 and VPBA. The results are presented in Fig. 2. In the FT-IR spectrum of boronate esters, bands at 1220 and 1250 cm^{-1}, 1000 -1090 cm^{-1}, and 500–750 cm^{-1} are generally assigned to C–O stretching,[21] B–C stretching,[21b,21c,22] and out-of-plane vibrations,[21b,23] respectively. On the contrary, in some other studies, one can find that the assigned wavenumbers for C–O and B–C stretching were replaced; i.e., 1200 and 1270 cm^{-1} for B-C stretching[24] and 1100 and 1200 cm^{-1} for C-O stretching.[24a,25] In addition, bands around 1300 cm^{-1} are mostly attributed to B-O stretching in boronate esters.[26] The spectrum for our sample displayed 2 sharp peaks in this region at 1330 cm^{-1} and 1366 cm^{-1}. However, boronic acid have also been reported to exhibit stretching

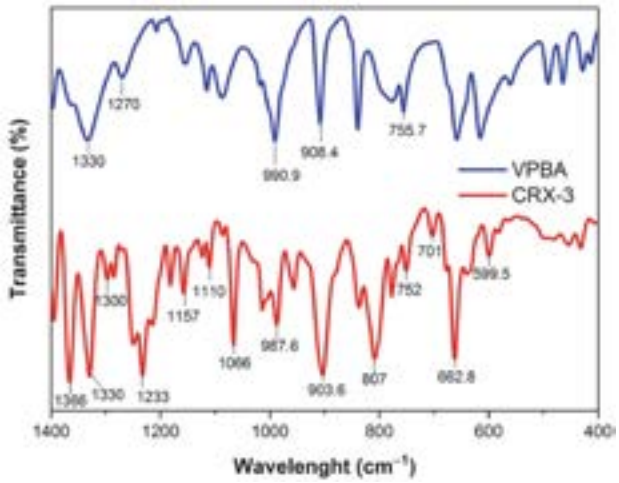

Figure 2. FT-IR spectrum of 4-vinylphenyl boronic acid (VPBA, top) and CRX-3 (bottom).

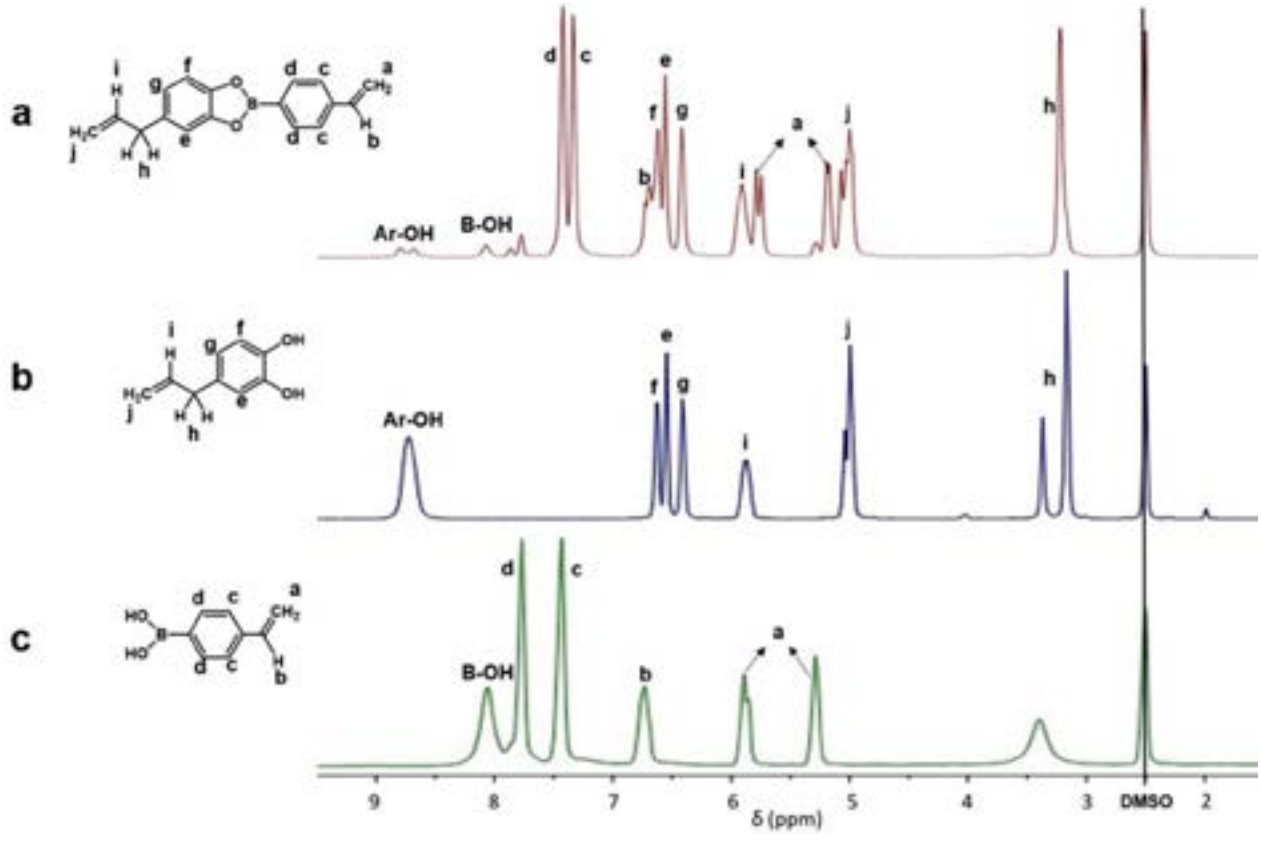

Figure 1. ^{1}H-NMR spectrum of a) CRX-3 b) 4-allylcatechol c) 4-vinylphenyl boronic acid.

here which makes the distinction between the boranate ester and boronic acid disputable.[27] As discussed above, peaks observed in the spectrum of the crosslinker at 1233 cm^{-1} and 1050 cm^{-1} are probably due to C–O and B-O stretching. The presence of these peaks was evaluated as the characteristic of boronate ester formation.[21a] Further, the vibrational mode at 662.8 cm^{-1} also designates that the boronic acid was consumed during the reaction in order to form the boronate ester bridge containing crosslinker.[27] These findings show that the 4-allylcatechol and 4-vinylphenyl boronic acid precursors almost reacted successfully to form the crosslinker under the experimental conditions applied in the current study.

As discussed in the experimental section, PEGMA particles were obtained by mixing constant amount of PEGMA 300 monomers and different amounts of CRX-3 (1, 3, 5, 7.5, and 10% mole of the monomer) in the presence of AMPDH. Further, the emulsion polymerization process yielded PEGMA including suspensions and the polymer content of these suspensions was collected by centrifugation. Morphological examination of these as-collected samples was carried out via SEM analysis. Fig. 3 (a and b) demonstrates SEM images of as-centrifuged P-P-3 sample. The product consists of uneven shaped and large sized (20–30 μm) individual agglomerates. Fig. 3a shows only a portion of the surface of a random agglomerate. As it is clear from this image, under the experimental conditions applied, the polymerization reaction ended-up with the formation of spherical shaped PEGMA (indicated by red arrows) embedded in an un-reacted matrix. Fig. 3b provides a closer view of the surface belonging to one of the PEGMA spheres. It is obvious that the large spheres are made-up of much smaller particles. As this image refer to unwashed state, it is not easy to determine the size and size distribution of the particles using the SEM micrograph. Yet, it can be stated that the particles exhibit a distinct spherical morphology, and the diameter of the largest particles can reach up to ~194 nm.

The size and morphology of cleaned PEGMA particles were investigated using DLS and TEM techniques. The average hydrodynamic diameter (dH) and polydispersity index (PDI) of the particles were extracted from DLS measurements. The results are demonstrated in Fig. 4. In addition, the numerical values can be followed from Table 2. No data are presented for P-P-1 and P-P-2 samples, since PEGMA formation could not be achieved when the amount of the crosslinker used was 1 or 3% mole of monomer probably due to insufficient linking. On the other hand, in case of CRX-3 additions at 5, 7.5, and 10% mole of monomer, PEGMA particles were successfully obtained. The values given in Table 2 states that the dH and PDI of the particles are directly proportional to the amount of the crosslinker used during synthesis. In consistent with the SEM examinations given above, the dH value of P-P-3

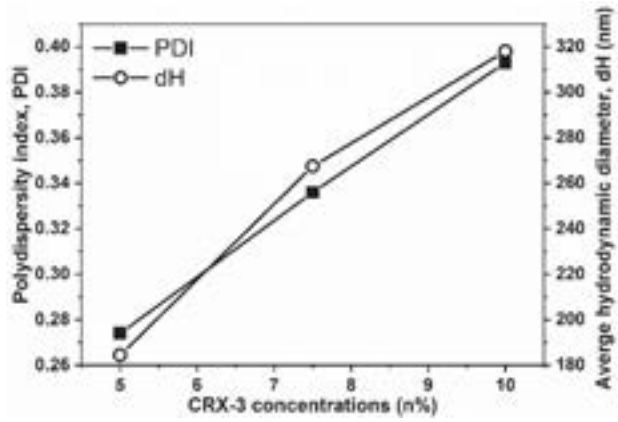

Figure 4. Polydispersity index and average hydrodynamic diameter values of the synthesized PEGMA particles as a function of the amount of CRX-3 used during synthesis

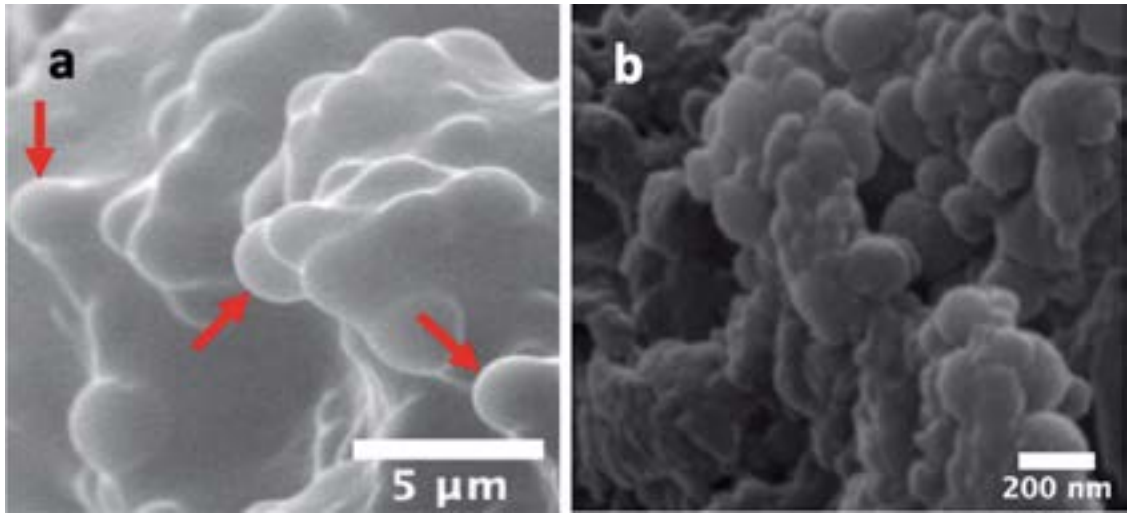

Figure 3. SEM images of P-P-3 sample in as-centrifuged state a) general view of the surface of a large sized agglomerate, 10k magnification, b) a closer view of the surface of a random sphere seen in (a), 100k magnification

sample was measured as 184.4 nm. In addition, dH values of 267.5 nm for 7.5% mole and 318 nm for 10% mole of monomer crosslinker additions were identified. Further, PDI values were obtained as 0.274, 0.336, and 0.393 for P-P-3, P-P-4, and P-P-5, respectively.

Above-mentioned findings show that the amount of CRX-3 used during synthesis is a significant parameter such that the formation of particles directly depends on the amount of crosslinker present in the reaction environment. Moreover, the amount of the crosslinker not only affects the size but also the size distribution of the PEGMA particles. In a similar study, the acetone/water ratio was reported as an another important parameter in terms of controlling the average hydrodynamic diameter of Poly methyl methacrylate (PMMA) particles.[6] It was stated that increasing the fraction of acetone in the solvent could be used as an effective way to reduce the size of the particles. On the other hand, for the current study, a constant value of acetone to water ratio (1/29 V/V) was used for all experiments. Increasing the amount of acetone in the solvent mixture led to the formation of strong agglomerates which are not dispersible by washing/ultrasonic treatments. Therefore, the observed difference in the diameter of the particles here can be ascribed to the change in the amount of CRX-3 used during the synthesis reactions.

As the size of the particles dictate a specific value for the surface area of the samples and further the reaction with sugar molecules was expected to proceed from boronate ester bridges exposed to the surface; the synthesis condition which provides the lowest hydrodynamic diameter for the particles was selected for further investigation. As seen from Fig. 4 and Table 2, the P-P-3 (synthesized by using CRX-3 at an amount of 5% mole of monomer) sample exhibited the lowest size with dH value of 184.4 nm. In addition, the PDI (0.274) of this sample is the lowest among others which indicate that the synthesized particles exhibit acceptable narrow size distribution.

Fig. 5 (a and b) shows low-resolution TEM images of P-P-3 sample. PEGMA particles are highly dispersed after the cleaning procedure and exhibit almost perfectly spherical morphology. Fig. 5a illustrates an array of PEGMA particles on holey carbon coated Cu grid with various sizes. In addition, two random spherical PEGMA particle with similar diameters can be seen in Fig. 5b. According to the measurements conducted using TEM images, the particles have sizes in the range of 90 to 186 nm. This result agrees well with SEM and DLS measurements given above. In addition, these observations reveal that the PEGMA particles were successfully formed by the surfactant free emulsion polymerization reaction using the boranate ester bridge containing crosslinker, exhibiting a particle size below 200 nm with a narrow size distribution.

Table 2. Average hydrodynamic diameters and polydipersity index of the synthesized PEGMA particles

Sample	dH (nm)	PDI[a]
P-P-1	–	–
P-P-2	–	–
P-P-3	184.4	0.274
P-P-4	267.5	0.336
P-P-5	318	0.393

[a] Multi-distribution indicator, unitless.

3. 2. Dye Loading and Sugar Sensitivity Experiments

Rhodamine B dye with specific absorbance in the visible region (λ_{max} = 554 nm) was used as a model drug in this study. Scheme 3a summarizes the dye loading process into the network of a PEGMA particle. In addition, the proposed dye release mechanism is presented in Scheme 3b. According to this mechanism, in case of the presence of sugar molecules in the environment, the trapped dye is expected to be released due to the high sensitivity of CRX-3 to these surrounding molecules. While the sugar molecules can bind to boronic acid, this simply breaks the bor-

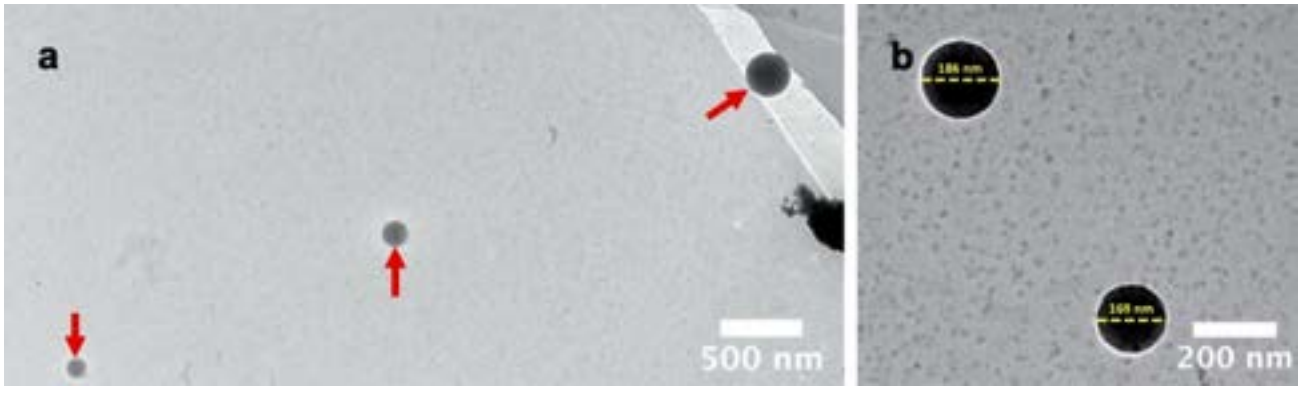

Figure 5. Low resolution TEM images of P-P-3 sample, a) an array of particles with different sizes b) two random PEGMA particles with similar diameters.

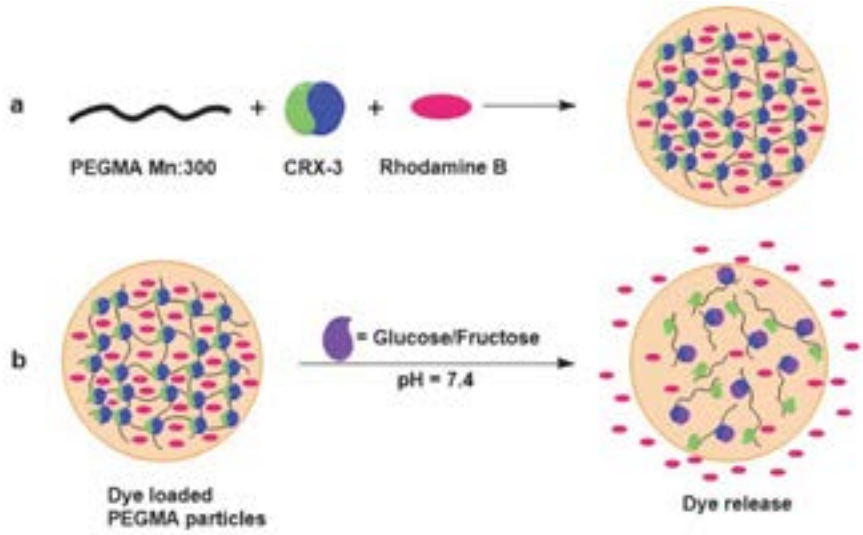

Scheme 3. Schematic representation of a) dye loading into PEGMA particles, b) dye release in the presence of glucose/fructose.

onate ester bridge between the monomers. Thus, the reaction will collapse the network of the polymer. Therefore, the amount of the liberated dye to the surrounding can be considered as a measure of drug released by the polymeric particles.

Fig. 6a shows the absorbance spectra of P-P-3 sample (1.25 10^{-2} g) dispersed in PBS, PBS + glucose, and PBS + fructose environments. These spectra were recorded after 2 h of the dispersion process. Absorbance behavior of the pure PEGMA particles (synthesized without dye loading) in the range of 450 to 650 nm was also presented for comparison. As seen, pure particles displayed no absorbance in this region. Therefore, any measured absorbance for other cases can be considered as due to the Rhodamine B dye molecules released from the network depending on the surrounding media. According to the measured values after 2 h, the lowest amount of dye was released in PBS environment, which also means that the particles are releasing a certain amount of dye (16.7 %) even in sugar free environment. In case of PBS with 10 mg/mL glucose, the released amount of dye (18.2 %) was only slightly increased compared to PBS environment, which suggests that the particles with boronate ester bridge containing crosslinker is only partially sensitive to glucose molecules. On the other hand, in case of PBS + 10 mg/mL fructose environment, the amount of the released dye increased substantially and reached to 24.5 % after 120 min.

Fig. 6b demonstrates time dependent increase of dye concentration in PBS+10 mg/mL fructose medium for a total holding duration of 48 h. The absorbance increases continuously as a function of time which means the quantity of the liberated dye is increasing in the environment

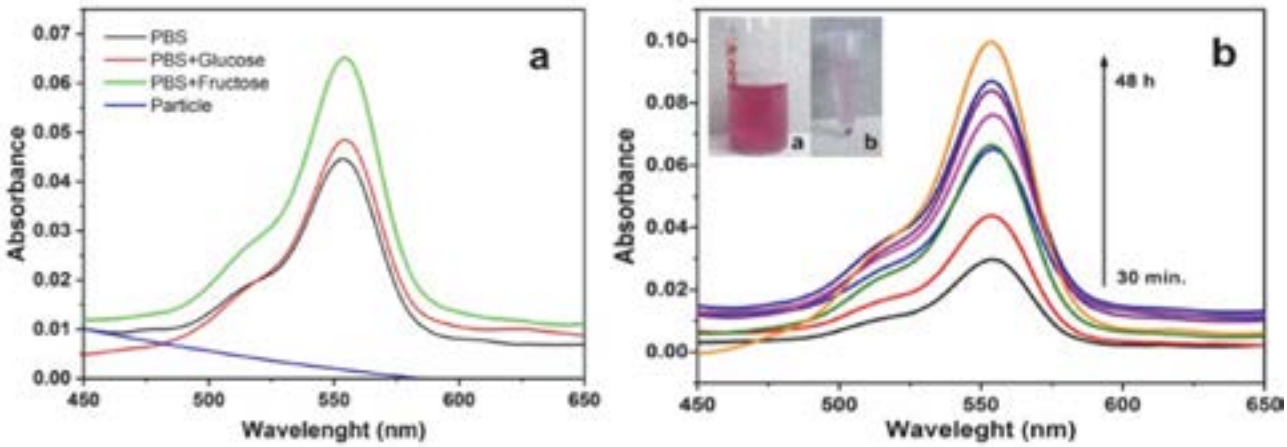

Figure 6. Absorbance spectra of P-P-3 sample after 2 h in a) PBS, PBS+10 mg/mL glucose, and PBS+10 mg/mL fructose environments, b) time dependent increase of dye release in PBS+10 mg/mL fructose environment (insets in (b) shows the digital images of the solution after releasing of Rhodamine B dye by the particles (left) and the collected particles with centrifuging (right)).

with time. After 48 h, a total of 39 % dye release was achieved. The inset (a) shows the deep pink color of the solution because of Rhodamine B dye that was released to the environment in the presence of fructose after 48 h by the P-P-3 sample. In addition, the inset (b) presents these PEGMA particles collected from the pink colored solution, which indicates that the particles can be separated from the solution via a simple centrifugation.

The cumulative release of the dye (after 48 h) by the P-P-3 sample dispersed in PBS, PBS + glucose, and PBS + fructose environments are presented in a comparative base in Fig. 7. This figure implies that the dye release by the particles reached a constant value of ~25 % in PBS or PBS + glucose environments within the first 6 h. After this period, the recorded amount of dye lost by the network was ascended only slightly. On the other hand, in PBS + fructose medium, dye release by the particles increased rapidly up to 28.52 % in 6 h. After this point, the concentration of Rhodamine B gradually continued to increase in the solution, but a decline in the slope of the curve is obvious. At the end of 48 h, total amount of the released dye was recorded as 39 %. As these dispersions were prepared by dividing a single and homogenous 30 mL PBS-PEGMA particles dispersion into three identical vials for dye release experiments (see section 2.3), the quantity of the particles in each vial and the amount of initially trapped dye by these particles can be assumed similar for each condition. As other parameters such as temperature, pH, time, etc. were all kept constant, the total amount of released dye for each case can be correlated to the presence of PBS, glucose, or fructose in these environments. The highest amount of dye was released in fructose environment. Therefore, it can be stated that the boranate ester bridge network is much more sensitive to external fructose molecules compared to glucose molecules.

In a recent study, Wu et. al., discussed on an amphiphilic boronic acid glucose sensor, where the hydrophobic group in glucose and hydrophilic boronic acid attached to each other with a dynamic covalent linkage, preferably an imine bond.[28] According to the proposed mechanism, the presence of glucose can induce aggregation of simple boronic acids due to its ability to crosslink the two boronic acid molecules.[29] On the other hand, experiments with fructose showed no sign of turbidity in the solutions which indicate little or no amphiphile aggregation.[28] Therefore, they stated that the binding of glucose may lead to formation of "*Gemini-type*" amphiphiles, which have a higher ability of aggregation compared to "*single-tail*" amphiphiles formed with boronic acid and fructose. Based on the dye release values for the current experiments, it is believed that the boranate ester bridge in the network has opened in the presence of glucose, but due to a similar mechanism discussed above or a competition between the network disintegration and amphiphile aggregation, the dye release by the particles was inhibited. On the contrary, fructose molecules probably have disintegrated the network to form a single tail amphiphiles, which allowed the liberation of the trapped dye in the network. As a result, higher number of dye molecules were released to the environment for fructose containing experiment. Of course, this speculation needs to be verified by further experiments, which will be considered in future studies. In addition, it is clear from the earlier studies that the affinity of samples to external molecules and the amount of the model drug released by the particles may scatter widely depending on various parameters, such as temperature,[1] time,[30] pH,[2] glucose/fructose concentration,[5,31] and etc. On the other hand, the current study aimed to propose a simple preparation route for the polymeric particles using a novel crosslinker. Therefore, the pH, polymeric particle dosage or sugar molecule concentration were kept constant in all experiments. And the amount of the dye liberated by the samples were measured as a function of time only. This also implies that the dye release performance of the particles can be improved by applying the optimized conditions.

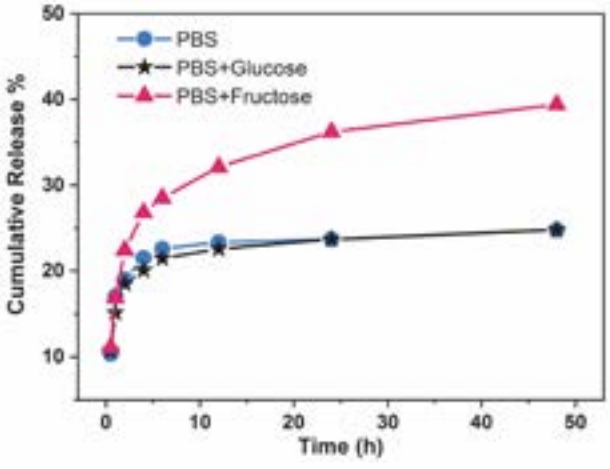

Figure 7. Time dependent Rhodamine B dye release % of P-P-3 sample dispersed in different environments

4. Conclusions

In this study, PEGMA particles were synthesized successfully in one step with surfactant free emulsion polymerization method using a novel boronate ester bridge containing crosslinker. The characterization studies have revealed perfectly spherical morphology for the particles. Further, the study has shown the tunability of the process in terms of achievable particle sizes. It was observed that PEGMA particles could be synthesized in various sizes depending on the amount of the crosslinker added to the polymerization reaction. The particles with the lowest average diameter and the narrower size distribution were then examined for controlled drug release application using their sensitivity against glucose or fructose molecules. The

total amount of dye release in glucose and fructose environments were recorded as 25% and 39%, respectively. Therefore, the experiments have revealed that the affinity of PEGMA particles with boronate ester bonds was 56% higher relative to fructose compared to glucose molecules. Finally, this study demonstrated that it is possible to synthesize a variety of polymeric particles with improved sensing ability by designing a suitable crosslinker.

Acknowledgement

Support for this work is provided by the Scientific Research Foundation (BAP) of Selçuk University (Project Number 191019020) which authors gratefully acknowledge.

5. References

1. a) A. S. Wadajkar, Z. Bhavsar, C. Y. Ko, B. Koppolu, W. Cui, L. Tang, K. T. Nguyen, *Acta Biomater.* **2012**, *8*, 2996–3004. **DOI:**10.1016/j.actbio.2012.04.042
   b) J. Zhang, H. Chen, L. Xu, Y. Gu, *J. Controlled Release* **2008**, *131*, 34–40. **DOI:**10.1016/j.jconrel.2008.07.019
2. a) A. S. Kamba, M. Ismail, T. A. T. Ibrahim, Zakaria, Z. A. B. , *Biomed Res. Int.* **2013,** *2013***,** 587451. **DOI:**10.1155/2013/587451
   b) B. H. Tan, K. C. Tam, Y. C. Lam, C. B. Tan, *Langmuir* **2004**, *20*, 11380–11386. **DOI:**10.1021/la0481290
3. a) M. F. Bedard, B. G. De Geest, A. G. Skirtach, H. Mohwald, G. B. Sukhorukov, *Adv. Colloid Interface Sci.* **2010**, *158*, 2–14. **DOI:**10.1016/j.cis.2009.07.007
   b) K. C. Hribar, M. H. Lee, D. Lee, J. A. Burdick, *ACS Nano* **2011**, *5*, 2948–2956. **DOI:**10.1021/nn103575a
4. a) A. Baeza, E. Guisasola, E. Ruiz-Hernández, M. Vallet-Regí, *Chem. Mater.* **2012**, *24*, 517–524. **DOI:**10.1021/cm203000u
   b) S. Kirchberg, M. Rudolph, G. Ziegmann, U. A. Peuker, *J. Nanomater.* **2012**; **DOI:**10.1155/2012/670531
   c) Zrínyi, *Colloid. Polym. Sci.* **2000**, *278*, 98–103. **DOI:**10.3390/ijms21228786
5. G. Springsteen, B. Wang, *Tetrahedron* **2002**, *58*, 5291–5300. **DOI:**10.1016/S0040-4020(02)00489-1
6. H. Sakalak, M. Ulasan, E. Yavuz, S. Camli, M. Yavuz, *J. Nanopart. Res.* **2014**, *16*, 1–10. **DOI:**10.1007/s11051-014-2767-6
7. a) T. Elshaarani, H. Yu, L. Wang, A. Zain ul, R. S. Ullah, M. Haroon, R. U. Khan, S. Fahad, A. Khan, A. Nazir, M. Usman, K.-u.-R. Naveed, *J. Mater. Chem. B* **2018**, *6*, 3831–3854. **DOI:**10.1039/C7TB03332J
   b) S. Cesur, M. E. Cam, O. Gunduz, *KONJES*, **2021**, *9*, 1, 17–24. **DOI:**10.36306/konjes.734840
8. a) L. Zhao, C. Xiao, L. Wang, G. Gai, J. Ding, *Chem. Commun.* **2016**, *52*, 7633–7652. **DOI:**10.1039/C6CC02202B
   b) Y. Tang, S. Malhotra, P. K. Varshney, *Acta Chim. Slov.*, **2018**, 65, 3, 687–697. **DOI:**10.17344/acsi.2018.4386
9. G. Springsteen, B. Wang, *Chem. Commun.* **2001**, 1608–1609. **DOI:**10.1039/b104895n
10. C. Cannizzo, S. Amigoni-Gerbier, C. Larpent, *Polymer* **2005**, *46*, 1269–1276. **DOI:**10.1016/j.polymer.2004.11.052
11. K. Kataoka, H. Miyazaki, M. Bunya, T. Okano, Y. Sakurai, *J. Am. Chem. Soc.* **1998**, *120*, 12694–12695. **DOI:**10.1021/ja982975d
12. A. P. Vogt, V. Trouillet, A. M. Greiner, M. Kaupp, U. Geckle, L. Barner, T. Hofe, C. Barner-Kowollik, *Macromol. Rapid Commun.* **2012**, *33*, 1108–1113. **DOI:**10.1002/marc.201200144
13. S. Kitano, I. Hisamitsu, Y. Koyama, K. Kataoka, T. Okano, Y. Sakurai, *Adv. Technol.* **1991**, *2*, 261–264. **DOI:**10.1023/A:1012033718302
14. a) W. Chen, Y. Cheng, B. Wang, *Angew. Chem. Int. Ed. Engl.* **2012**, *51*, 5293–5295. **DOI:**10.1002/anie.201201179
   b) Y. Li, W. Xiao, K. Xiao, L. Berti, J. Luo, H. P. Tseng, G. Fung, K. S. Lam, *Angew. Chem. Int. Ed. Engl.* **2012**, *51*, 2864–2869. **DOI:**10.1002/anie.201107144
15. A. Kikuchi, K. Suzuki, O. Okabayashi, H. Hoshino, K. Kataoka, Y. Sakurai, T. Okano, *Anal. Chem.* **1996**, *68*, 823–828. **DOI:**10.1021/ac950748d
16. M. Seno, K. Yoshida, K. Sato, J. Anzai, *Mater. Sci. Eng. C* **2016**, *62*, 474–479. **DOI:**10.1248/cpb.c17-00817
17. M. G. 3rd Lancina, R. K. Shankar, H. Yang, *J. Biomed. Mater. Res. A*, **2017,** *105*, 5, 1252–1259. **DOI:**10.1002/jbm.a.35984
18. A. Matuszewska, M. Uchman, A. Adamczyk-Wozniak, A. Sporzynski, S. Pispas, L. Kovacik, M. Stepanek, *Biomacromolecules* **2015**, *16*, 3731–3739. **DOI:**10.1021/acs.biomac.5b01325
19. Y. Guangzhi, L. Yang, J. Runping, X. Risheng, W. Xia, L. Licheng, Y. Junhe, *J. Appl. Polym. Sci.* **2009**, *112*, 410–415. **DOI:**10.1002/app.29429
20. S. Pasa, Synthesis and various applications of boron derivative compounds, PhD Thesis, Dicle University, Diyarbakır, **2014**, 1–250.
21. a) M. K. Smith, B. H. Northrop, *Chem. Mater.* **2014**, *26*, 3781-3795. **DOI:**10.1021/cm5013679
   b) A. P. Côte, A. I. Benin, N. W. Ockwig, M. O' 'Keeffe, A. J. Matzger, O. M. Yaghi, *Science* **2005**, *310*, 1166–1170. **DOI:**10.1126/science.1120411
   c) H. M. El-Kaderi, J. R. Hunt, J. L. Mendoza-Cortes, A. P. Côte, R. E. Taylor, M. O'Keeffe, O. M. Yaghi, *Science* **2007**, *316*, 268–272. **DOI:**10.1126/science.1139915
   d) X. Ding, J. Guo, X. Feng, Y. Honshihito, J. Guo, S. Seki, P. Maitarad, A. Saeki, S. Nagase, D. Jiang, *Angew. Chem. Int. Ed.* **2011**, *50*, 1289–1293. **DOI:**10.1002/anie.201005919
   e) X. Feng, L. L. Liu, Y. Honsho, A. Saeki, S. Seki, S. Irle, Y. P. Dong, A. Nagai, D. L. Jiang, *Angew. Chem., Int. Ed.* **2012**, *51*, 2618–2622. **DOI:**10.1002/anie.201106203
   f) M. Dogru, M. Handloser, F. Auras, T. Kunz, D. Medina, A. Hartschuh, P. Knochel, T. Bein, *Angew. Chem. Int. Ed.* **2013**, *52*, 2920–2924. **DOI:**10.1002/anie.201208514
22. a) X. Feng, L. Chen, Y. Honsho, O. Saengsawang, L. Liu, L. Wang, A. Saeki, S. Irle, S. Seki, Y. Dong, D. Jiang, *Adv. Mater.* **2012**, *24*, 3026–3031. **DOI:**10.1002/adma.201201185
   b) E. L. Spitler, W. R. Dichtel, *Nat. Chem.* **2010**, *2*, 672–677. **DOI:**10.1038/nchem.695

c) J.-T. Yu, Z. Chen, J. Sun, Z.-T. Huang, Q.-Y. Zheng, *J. Mater. Chem.* **2012**, *22*, 5369–5373. **DOI:**10.1039/c2jm15159f
23. R. W. Tilford, S. J. Mugavero, 3rd, P. J. Pellechia, J. J. Lavigne, *Adv. Mater.* **2008**, *20*, 2741–2746. **DOI:**10.1002/adma.200800030
24. a) Z. Kahveci, T. Islamoglu, G. A. Shar, R. Ding, H. M. El-Kaderi, *Cryst. Eng. Comm.* **2013**, *15*, 1524–1527. **DOI:**10.1039/C2CE26487K
b) S. Jin, K. Furukawa, M. Addicoat, L. Chen, S. Takashi, S. Irle, T. Nakamura, D. Jiang, *Chem. Sci.* **2013**, *4*, 4505–4511. **DOI:**10.1039/c3sc52034j
25. X. Feng, Y. Dong, D. Jiang, *Cryst. Eng. Comm.* **2013**, *15*, 1508–1511. **DOI:**10.1039/C2CE26371H
26. J. W. Colson, W. R. Dichtel, *Nat. Chem.* **2013**, *5*, 453–465. **DOI:**10.1038/nchem.1628
27. B. M. Rambo, J. J. Lavigne, *Chem. Mater.* **2007**, *19*, 3732–3739. **DOI:**10.1021/cm070757q
28. S. Camli, F. Buyukserin, O. Balci, G. Budak, *J. Colloid Interface Sci.* **2010**, *344,* 2, 528–532. **DOI:**10.1016/j.jcis.2010.01.041
29. Y. Tsuchido, Y. Sakai, K. Aimu, T. Hashimoto, K. Akiyoshi, T. Hayashita, *New J. Chem.* **2015**, *39*, 4, 2620–2626. **DOI:**10.1039/C4NJ01309C
30. X. Huang, S. Li, J. S. Schultz, Q. Wang, Q. Lin, *Sens. Actuators, B* **2009**, *140*, 603–609. **DOI:**10.1016/j.snb.2009.04.065
31. A. Ori, S. Shinkai, *J. Chem. Soc. D* **1995**, 1771–1772. **DOI:**10.1039/c39950001771

Povzetek

Namen študije je bil razvoj delcev metil eter poli(etilenglikol) metakrilata (PEGMA), občutljivih na glukozo/fruktozo, ki jih je mogoče uporabiti pri izdelavi kontroliranih dostavnih sistemov zdravil. V ta namen smo z uporabo 4-vinilfenilboronske kisline sintetizirali zamreževalec, osnovan na borovi kislini, ter njegovo tvorbo potrdili z ^{1}H-NMR in FT-IR analizama. Polimerne delce, občutljive na izbrana sladkorja, smo nato pripravili z uporabo tega zamreževalca in PEGMA monomera v enostopenjski emulzijski polimerizaciji brez uporabe površinsko aktivnih snovi. Morfologijo in velikost polimernih delcev smo določili z DLS, SEM in TEM. Za analizo občutljivosti delcev na molekule sladkorja smo najprej izvedli poskuse polnjenja z barvilom rodamin B (kot vzorčno zdravilo). Nato smo delce izpostavili medijem, bogatim z glukozo/fruktozo, sproščanje barvila pa smo spremljali z UV-VIS spektrofotometrijo v odvisnosti od časa. Rezultati študije so pokazali, da so delci PEGMA pri pH 7,4 in 310 K bolj občutljivi na fruktozo (~39 % sproščanje) kot na glukozo (~25 % sproščanje).

Except when otherwise noted, articles in this journal are published under the terms and conditions of the Creative Commons Attribution 4.0 International License

Scientific paper

Proposal of an HPLC/UV/FLD Screening Method for the Simultaneous Determination of Ten Antibiotics in Environmental Waters

Idalia Francisca Carmona-Alvarado,[1] María de la Luz Salazar-Cavazos,[1] Noemí Waksman de Torres,[1] Aurora de Jesús Garza-Juárez,[1,2] Lidia Naccha-Torres,[1] Jose Francisco Islas[2] and Norma Cavazos-Rocha[1,*]

Universidad Autónoma de Nuevo León[1]. Departamento de Química Analítica[2]. Departamento de Bioquímica y Medicina Molecular, Facultad de Medicina, Ave. Madero y Dr. Eduardo Aguirre Pequeño S/N Col. Mitras Centro. 64460 Monterrey, Nuevo León, México.

** Corresponding author: E-mail: norma.cavazosrc@uanl.edu.mx; nocavazos@yahoo.com*

Received: 04-05-2021

Abstract

An HPLC-UV/FLD method for simultaneous detection of ten antibiotics in surface waters was developed. Antibiotics were extracted from water using solid phase extraction. An Atlantis T_3 column was used with acetonitrile and 0.05% trifluoroacetic acid as a mobile phase for separation, with a total running time of 45 min. Signal detection was performed at 280 nm; fluoroquinolones were additionally quantified by fluorescence detection. Validation parameters such as linearity, recovery and precision were evaluated. The limits of detection (LOD) in river waters were in the range 0.1–1.3 μg/L for antibiotics detected by UV, and 0.039 and 0.073 μg/L for fluoroquinolones detected by FLD. LOD are sufficiently low to consider this method as a first alternative for HPLC-MS methods that will allow alerting for the presence of antibiotics in surface waters. This screening method is rapid, sensitive, reproducible and economical.

Keywords: Antibiotic analysis; emerging contaminants; simultaneous analysis by HPLC-UV/FLD; fluoroquinolones and sulfonamides; multiresidue analysis method; surface water analysis; antibiotic occurrence in environmental waters

1. Introduction

During recent years there has been an increase in the global interest for determining new and potentially dangerous compounds – contaminants, known as emerging contaminants.[1–3] These emerging contaminants include pharmaceuticals, pesticides, hormones, steroids, surfactants and surfactants' metabolites, endocrine disrupting compounds and perchlorate.[4] Particularly, antibiotics (as residues) are the pharmaceutical contaminants with the highest use worldwide; routinely used in both human and veterinary medicine. Administered antibiotics are partially metabolized in the body and the rest are excreted unchanged or as metabolite, into the ecosystems.[5,6] Later, these waste residues are further collected in the wastewaters and introduced to the wastewater treatment systems where antibiotics cannot be completely removed under current technology. Hence, they are continuously being discharged into the environment.[7,8] The presence of antibiotics in the aquatic environment can affect the evolution of the community structure; however, the most negative effect attributed to the occurrence of antibiotics is the development of antibiotic resistant bacteria and antibiotic resistant genes, which comprise health risks to humans and animals.[9,10] Current research has determined certain community-minded antibiotic hot-spots, which are deemed high risk, these include: hospital effluents, influents and effluents of municipal wastewater treatment plants, and to a lesser degree ground and seawater.[11–19] This overall global phenomenon has been of much interest, as such "Antimicrobial resistance and its global spread" was the theme of World Health Day 2011, given by the World Health Organization (WHO).[20] In addition, the WHO has further developed medically relevant guidelines for antimicrobials in animal food production.[21]

Antibiotics have been grouped in specific families according to their use and chemical structure. These families include: macrolides, fluoroquinolones, penicillins, sulfonamides, trimethoprim and cephalosporins. These emerg-

ing contaminants have been detected in environmental waters within the range of μg/L down to ng/L. To detect these concentration levels the analytical methods currently used for the analysis of antibiotics consist of a purification and concentration step followed by a separation step by means of high performance liquid chromatography (HPLC) or ultra-high performance liquid chromatography (UHPLC) coupled to tandem mass spectrometry or hybrid tandem spectrometers such as quadrupole time of flight and/or quadrupole-linear ion trap.[11,13,15-19,22-26] Also UV and fluorescence detection have been coupled to HPLC but only for determining one or two families or a few antibiotics.[14, 27–32] On the other hand, the most widely used technique for purification is by means of solid phase extraction (SPE), although some authors have used lyophilization[18] or dispersive liquid-liquid microextraction.[33] A variety of adsorbents have been used in SPE, but most authors agree that polymeric adsorbents have been more efficient in the extraction of antibiotics.[6,8,13,15] Detection limits for mass spectrometry are in a few ng/L to μg/L, while in the case of fluorescence (FLD) and UV absorption are in μg/L.

As mentioned above, the presence of antibiotics in the environment, especially in the aquifer, is a serious problem and has resulted in an increase in bacterial resistance, increasing health costs and mortality, causing a significant economic impact to private and governmental services. Thus, it is necessary to have rapid, simple, accessible, and reliable analytical methods for detecting and monitoring these emerging contaminants. Chromatographic methods with mass spectrometry are highly sensitive and specific, but high costs of acquisition and maintenance makes them inaccessible to routine laboratories. At a global scale there is an insufficient number of laboratories with this technology, to perform these monitoring tasks. A second burden is both the management of the equipment and interpretation of the results, which requires intense training and experience, further adding to the overall cost. Therefore, it is necessary to use analytical methods that are more cost-effective and accessible to analytical laboratories, especially in developing countries, that can allow carrying out studies; monitoring and quantifying the occurrence of these emerging contaminants in the environment. Considering aspects previously exposed, the aim of this work was to develop a sensitive and cost-effective multiresidue method for the simultaneous analysis of antibiotics commonly used in human and veterinary medicine using high performance liquid chromatography with ultraviolet and fluorescence detection (HPLC-UV/FLD) as an alternative to the HPLC-MS methods. To the best of our knowledge, it is the first method that includes nine antibiotics from 5 different families, and trimethoprim. The developed method would allow the continuous monitoring of environmental waters to detect the presence of these emerging pollutants.

2. Experimental

2. 1. Reagents

For the mobile phase, acetonitrile (ACN) and methanol were HPLC grade (J. T. Baker). Trifluoroacetic acid

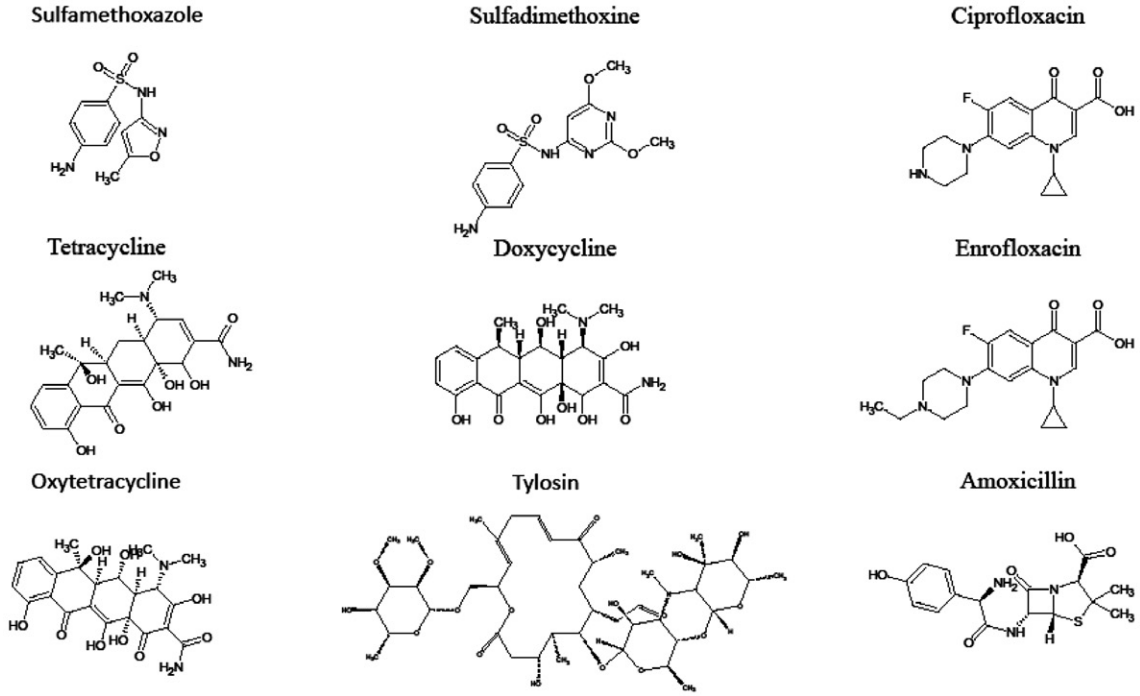

Figure 1. Assayed antibiotic molecules: sulfamethoxazole (SMX), sulfadimethoxine (SDX), ciprofloxacin (CIP), tetracycline (TETRA), doxycycline (DOX), enrofloxacin (ENRO), oxytetracycline (OXI), tylosin (TYL), and amoxicillin (AMOXI). Structures developed using ACD/Labs ChemSketch ®.

(TFA) 99.0% was from Sigma Aldrich (Sigma Aldrich Corp, St Louis, USA). HCl was J.T. Baker (Center Valley, PA, USA). Deionized water was purified by a Milli-Q System (Millipore Co., MA, USA). Sulfamethoxazole (SMX), sulfadimethoxine (SDX), ciprofloxacin (CIP), tetracycline (TETRA), doxycycline (DOXI), trimethoprim (TMP) were from Sigma Aldrich. Enrofloxacin (ENRO), oxytetracycline (OXI), tylosin (TYL) and amoxicillin (AMOXI) of MP Biomedicals (Irvine CA, U.S.A.) (Figure 1). All antibiotics were 98% purity or greater.

2. 2. Equipment and Chromatographic Conditions.

Chromatographic separation was achieved using an HP 1100 separation module (Agilent Technologies, Waldbronn Germany) equipped with a quaternary pump, autosampler and temperature control, coupled with a variable wavelength UV detector and FLD detector. Three different chromatographic columns were tested: Synergi C_{18} (150 mm × 2 mm, 4 μm) and Luna C_{18} (250 mm x 4.6 mm, 5 μm) of Phenomenex (Torrance CA, USA), and Atlantis T_3 (150 mm × 2.1 mm, 3 μm) of Waters (Waters Corporation, Milford, MA, USA). Samples were eluted in mobile phase (TFA 0.05%) and (ACN); gradient used is shown in supplementary Table S1. The flow rate was 0.2 mL/min and injection volume was 5 μL, column temperature was set at 35 °C. Detection by UV at λ 280 nm and fluorescence at λ_{ex} 278 nm and λ_{em} 450 nm. The mobile phases and standard solutions were filtered through a 0.45 μm Nylon filter (Waters Corporation, Milford, MA, USA) before use.

2. 3. Standard Solutions

Ten milliliters of stock solutions for each antibiotic were prepared at a concentration of 1000 μg/mL in methanol; only AMOXI was prepared in water. The solutions were stored in dark at –20 °C for up to 30 days. Stock solutions were further diluted for preparation of a standard mix, which contained the following concentrations: 4 μg/mL CIP and ENRO, 25 μg/mL TMP, OXI, TETRA, and SMX, and 50 μg/mL AMOXI, TYL, SDX, and DOX. From this standard mixture, and by appropriate dilutions, working aqueous standards were prepared and used to build calibration curves. The concentrations of these working aqueous standard solutions were for CIP and ENRO in the range 0.08–0.24 μg/mL; for TMP, OXI, TETRA, and SMX in the range of 0.5–1.75 μg/mL and for AMOXI, TYL, SDX, and DOX 1–3.5 μg/mL (supplementary Figure 2S). These solutions were prepared fresh daily, filtered and placed in amber glass vials prior to analysis by HPLC-UV/FLD.

2. 4. Antibiotic Extraction

SPE is the most employed technique for isolating and for the enrichment of antibiotics in the environmental waters, enabling concentrations of low concentrations.[2,7,8,34] However, the procedure is highly dependent on the correct selection of the stationary phase, also of pH of the sample, composition, and volume of solvent used for elution.[13] Due to the reasons stated above, the SPE was carried out considering three important steps: first, STRATA X and OASIS HLB cartridges were compared for the stationary phase selection. Deionized water samples were spiked with a standard mixture of antibiotics, and then extracted under appropriate conditions. Oasis HLB cartridges provided the best multiresidue retention with higher number of compounds and therefore were the one selected for further experiments. Once the most suitable adsorbent was selected, the effect of seven variables (pH of sample, flow rate of the sample load, composition, volume and flow rate of elution solvent, and washing solvent and drying time) for the extraction efficiency were evaluated through a series of experiments established with a Placket-Burman design. The results indicated the most favorable conditions for multiresidue extraction, therefore, the extraction procedure was: Oasis HLB cartridges (6 mL 500 mg, Waters Co., Milford MA, USA) were conditioned with 5 mL of methanol and 5 mL of H_2O pH 3. Next, 1000 mL of deionized water or sample was adjusted at pH 3 with HCl and passed through cartridge at a flow rate of 10 mL/min using a vacuum manifold system connected to a vacuum pump. The loaded cartridges were rinsed with 5 mL of water and were dried under vacuum for 1 min. The elution was performed with 3 mL of methanol at 1 mL/min. The sample extract was evaporated to dryness under nitrogen stream at 40 °C in a Glas-Col evaporator and reconstituted with 1 mL of water, filtered and transferred to a dark vial for analysis.

2. 5. System Validation

Calibration curves were constructed by triplicate at five concentration levels. The area values were plotted against the concentration. Deionized water was used as a blank. Limits of detection (LOD) and quantification (LOQ) were calculated from the calibration curve data according to equations LOD = 3.3 () and LOQ = 10 () where σ is the standard deviation of the calibration line intercept and s is the slope of the calibration line[35] (supplementary Table S2). The precision of system was evaluated and reported as % relative standard deviations (%RSD). Intra and intermediate precision of the system were calculated by means of injection of three working aqueous standards each in triplicate, at three concentration levels and in three different days (supplementary Table S3).

2. 6. Method Validation

River water (matrix) was collected and filtered through 0.45 μm pore size membranes. Accuracy was assessed as the (%) recovery as follows: Three samples of 1000 mL of matrix were spiked each with antibiotics at

three levels of concentration (low, medium and high) in order to obtain final concentrations of 1, 2 and 3 μg/L for AMOXI, TYL, SDX, DOXI; 0.08, 0.16 and 0.24 μg/L for ENRO, CIPRO, and 0.5, 1 and 1.5 μg/L for TMP, OXI, TETRA, and SMX. After one hour the sample was extracted with the SPE method previously described. Analyses were run in triplicate. Results were calculated from the calibration curves by means of external standard method.

Intraday precision was determined by assaying by triplicate three samples spiked at three levels. The intermediate precision was calculated by analyzing the samples fortified with the antibiotics at three levels of concentration in triplicate on three different days.

Selectivity was tested by examining different samples of river water free of antibiotics to confirm that the signals originating from the matrix did not interfere with the signals from the analytes. Identification of each compound in the spiked samples was made by the retention times.

2. 7. Matrix Effect

Calibration curves were constructed using river water, to take into consideration the matrix effect. Recoveries were compared with those of deionized water fortified with standard at the same concentration, using a paired *t*-test. Further, visual inspection of calibration curves was used to corroborate (supplementary Figure 3S). In addition, to discard contaminants (within study range), river water as internal control was analyzed.[35]

2. 8. Sample Analysis

Surface water samples from the city of Monterrey and metropolitan area were analyzed. The samples were collected on the following locations: Rio Pilon, Rio La Silla and the Rodrigo Gomez water dam. These samples were collected in plastic bottles, transported in cold and darkness, and stored at 4 °C until analysis. The samples were homogenized, filtered through a 0.45 μm Millipore filter and processed within 5 h after collection.

3. Results and Discussion

This work presents a simple and inexpensive HPLC method for the first screening of the analysis of antibiotics in water. The HPLC conditions established and described in the experimental section enabled efficient separation of all antibiotics from different families in a single run. First, the chromatographic separation was optimized using an aqueous standard mix solution of the antibiotics. To obtain chromatograms with a good resolution of the target compounds in a short time, various conditions (eluents, gradients) were tested. Three different chromatographic columns were used: Atlantis T_3 (150 mm x 2.1 mm, 3 μm), Synergi C_{18} (150 mm x 2 mm, 4 μm) and Luna C_{18} (250 mm x 4.6 mm, 5 mm). Individual chromatograms are shown in supplementary Figure 1S. Finally, after testing the three columns with a 0.05% TFA-acetonitrile mobile phase,[36] the best separation was achieved with the Atlantis T_3 column. In the Synergy C_{18}

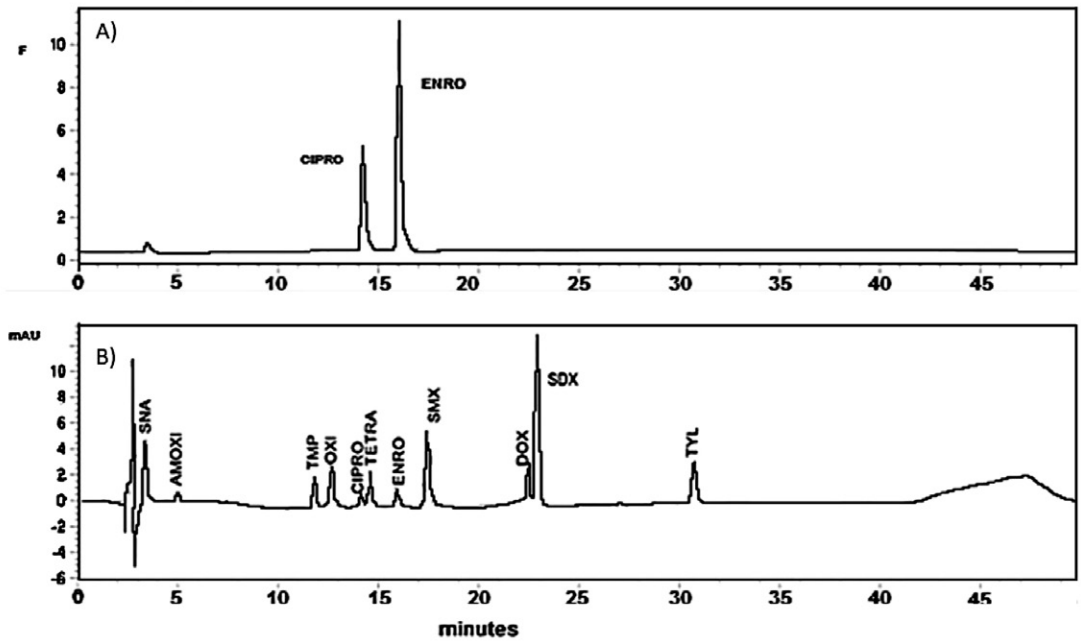

Figure 2. Chromatogram of the mixture of antibiotics. (A) fluorescence detection (λ_{ex} 278nm and λ_{em} 450 nm); (B) UV detection 280 nm. Elution order was amoxicillin (AMOXI), trimethoprim (TMP), oxitetracycline (OXI), ciprofloxacin (CIPRO), tetracycline (TETRA), enrofloxacin (ENRO), sulfamethoxazole (SMX), sulfadimethoxine (SDX), doxycycline (DOX) and tylosin (TYL). Separation conditions are described in text.

and Luna C_{18} columns, the pairs OXI-CIPRO, DOXI-SDX and TETRA-CIPRO, DOXI-SDX, respectively, did not present optimal resolution despite different tested elution gradients. Atlantis T_3 has a trifunctional C_{18} bonding phase along with a special endcapping procedure; these characteristics allowed for the best separation of antibiotics. Additionally, T_3 is a more stable column that is resistant to low pH and highly aqueous mobile phases.[37] Chromatographic parameters efficiency (plate number, N), resolution (R) and selectivity (α) are shown in supplemental material (supplementary Table S4). Performance of Atlantis T_3 column was better than Luna and Synergi, while resolution on Atlantis T_3 column was >1.4 and the separation of all antibiotics was complete, in the case of Synergi and Luna chromatographic columns, results showed selectivity values <1.2, the resolution values R for some antibiotics were below 1 and the compounds were not totally separated.

The developed method includes antibiotics from five different families and trimethoprim (Figure 1) using HPLC-UV/FLD. Chromatogram of a standard mixture of ten antibiotics is shown in Figure 2. For FLD detection (Figure 2A) quinolones showed maximum excitation and emission at λ = 278 nm and λ = 450 nm, respectively.[38] For UV detection (Figure 2B), the monitoring wavelength was at 280 nm. Complete elution of the antibiotics was obtained in the first 30 min. The established HPLC conditions allowed for efficient separation of all antibiotics from different families in a single run.

3. 1. Validation

System validation was performed for the range of concentrations established for each antibiotic, coefficients of determination for the calibration curves were over 0.99 with RSD of response factors (RFs) below 7%, and precision was 0.2 to 14%. Instrumental LOD and LOQ were assessed. The lowest LOD was 0.006 μg/mL for SMX and the highest was 0.225 μg/mL for DOX. Meanwhile, LOQ for SMX was 0.020 and for DOX it was 0.750 μg/mL

On the other hand, Table 1 shows the results for the validation of method. Evaluation of linearity was by means of the RFs and the coefficients of determination. The coefficients of variation of the response factors were between 6-15% and coefficients of determination were higher than 0.99 except for OXI, ENRO and TETRA. LOD and LOQ of the method were calculated from the matrix-matched calibration curves and taking into consideration 3.3 and 10 times the standard deviation of the calibration line intercept (matrix water free of antibiotics), and the calibration line slopes (Table 1). Hence, low amounts of antibiotics were detectable due to the solid-phase extraction. LOD were between 1.29 μg/L for DOXI to 0.039 μg/L for ENRO, while LOQ from 4.13 to 0.13 μg/L for DOXI and ENRO, respectively. Thus, the lowest LOD and LOQ were 0.039 and 0.130 μg/L, respectively, for ENRO.

Percentage recoveries were obtained from deionized water and matrix samples spiked with antibiotics at μg/L concentration. Table 2 shows the results of recoveries of the antibiotics in both deionized water and matrix (river water) in the experiments at low, medium, and high concentrations. Recoveries achieved for all antibiotics in deionized water ranged from 44% (SDX) to 130% (CIPRO) with %RSD between 1 and 16%. According to AOAC Guidelines for Standard Method Performance Requirements[39] taking into account analyte concentrations, precision and recovery results are acceptable. To determine the matrix effect, recovery experiments were carried out in river water spiked with antibiotics at the same concentrations (low, medium and high level) and the same extraction process was applied. Table 2 shows the recovery percentages, where it can be seen that the values obtained vary between 54% (DOX) to 121% (TETRA) with RSD of of 2–12%. Data on recoveries in deionized water were compared with those obtained in matrix through a *t*-test. As observed in Table 2, statistically significant differences were found for CIPRO, ENRO, TETRA, and SDX. Although recoveries for CIPRO and ENRO were within the acceptable limits when the tests were assayed in deionized water, matrix effect caused recoveries up to 190%, so, for a correct quantification, it would be necessary to apply

Table 1. Validation parameters of the method used for the analysis of the antibiotics in water.

Antibiotic	Linear equation $y = mx + b$	Determination coefficient (R^2)	%RSD of RF	LOD μg/L	LOQ μg/L
TMP	32069x –1.762	0.991	8	0.23	0.76
OXI	46188x – 8.811	0.989	15	0.56	1.88
TETRA	28873x + 8.06	0.970	10	0.10	0.35
SMX	61626x – 10.85	0.992	12	0.32	1.08
SDX	22898x – 2.847	0.990	6	0.45	1.52
DOX	56104x – 16.45	0.990	11	1.29	4.33
TYL	21441x – 1.001	0.993	6	0.45	1.49
CIPRO	15563x + 1.048	0.991	14	0.07	0.15
ENRO	42925x – 5.015	0.988	10	0.04	0.13

*Response factor

Table 2. Recovery from antibiotics in deionized water (DW) and river water (RW). Data shown as percentage of recovery$_{(\%RSD)}$.

Antibiotic	Low level		Medium level		High level		Matrix effect*
	DW	RW	DW	RW	DW	RW	
TMP	$80_{(9)}$	$91_{(9)}$	$84_{(14)}$	$104_{(3)}$	$106_{(1)}$	$90_{(5)}$	No
OXI	$83_{(6)}$	$82_{(2)}$	$90_{(12)}$	$90_{(7)}$	$85_{(15)}$	$92_{(10)}$	No
TETRA	$61_{(8)}$	$121_{(2)}$	$66_{(13)}$	$110_{(1)}$	$68_{(3)}$	$87_{(11)}$	Yes
SMX	$64_{(8)}$	$63_{(6)}$	$66_{(13)}$	$69_{(6)}$	$68_{(3)}$	$73_{(4)}$	No
SDX	$44_{(16)}$	$111_{(5)}$	$65_{(15)}$	$116_{(1)}$	$65_{(12)}$	$109_{(14)}$	Yes
DOX	$57_{(12)}$	$60_{(8)}$	$68_{(16)}$	$54_{(12)}$	$65_{(13)}$	$59_{(2)}$	No
TYL	$60_{(4)}$	$87_{(9)}$	$84_{(15)}$	$81_{(4)}$	$91_{(6)}$	$75_{(15)}$	No
CIPRO	$115_{(8)}$	$196_{(5)}$	$130_{(16)}$	$180_{(1)}$	$126_{(12)}$	$158_{(8)}$	Yes
ENRO	$70_{(15)}$	$139_{(12)}$	$69_{(12)}$	$143_{(1)}$	$71_{(4)}$	$123_{(12)}$	Yes

n = 3α = 0.05* = statistical difference due to matrix effect

methods such as standard addition or matrix-matched calibration curves.

3. 2. Solid Phase Extraction

Under normal circumstances, low concentrations of antibiotics in river waters are expected. Hence a preconcentration is necessary. Solid phase extraction has been shown over time to be the most widely used technique for this purpose. Antibiotics have different structure and charge depending on the pH. SPE extraction with different cartridges such as Oasis MX, Strata X, LiChrolut EN, C18 and OASIS HLB has been reported.[40] The results have shown that in multiresidue methods the cartridges with mixed phase have given the best results obtaining the highest number of compounds in a single step and with reproducible recoveries. With this idea in mind, the present work tested the performance of OASIS HLB and STRATA X cartridges obtaining the best results with OASIS HLB. These cartridges have a sorbent with balanced mixture of two monomers: *N*-vinylpyrrolidone (hydrophilic) and divinylbenzene (lipophilic). This combination allows the retention of nonpolar and polar (with acidic or basic nature) compounds, through hydrophobic and hydrophilic interactions.[15] The results obtained in our experiments showed that with OASIS HLB cartridges the recovery of all antibiotics was achieved, as shown in Figure 3. So the next step was the optimization of the extraction conditions. The sample volume was 1000 mL. Smaller volumes have been used in HPLC-mass spectrometry, where the detection capacity is ng/L. In this work it was considered to concentrate water samples for a factor of 1000, to enable detection and quantitation with UV and fluorescence detection. Cartridges with 500 mg of stationary phase were used. Since antibiotics in environmental waters can be detected at very low concentrations (ng/L), large volumes can be used, moreover, experiments were also carried out to confirm that the breakthrough volume was not exceeded. Several conditions that affect the performance of the SPE extraction were taken into account conducting a series of experiments in which factors involved during the process were combined in a Plackett Burman design. Seven factors at two levels of variation resulted in eight experiments. Table 3 shows the factors considered and the variation levels. The set of experiments to probe extraction efficiency are shown in supplementary Table S5. The results of the experiments indicated that the pH of the sample is very important in the extraction efficiency of antibiotics. It is in general adjusted between 2.5 to 4 to extract the majority of antibiotics. Herein, we probed the values of pH 3 and 5. For elution we used methanol and a combination of solvents used as a mobile phase (0.05%TFA/ACN 50:50) at a flow rate between 1 and 5 mL/min. Other factors considered are shown in Table 3.

The selection of conditions was based on obtained recoveries of all antibiotics. The results showed that at pH

Table 3. Factors considered in the extraction process and levels of variations carried out in the experiments

Factor	Levels	
	Low (-)	**High (+)**
pH	3	5
Flow rate of the sample load (mL/min)	3	10
Elution solvent	MeOH	TFA 0.05%: ACN (50:50)
Elution flow rate (mL/min)	1	5
Elution volume (mL)	1	3
Washing solvent	H_2O	H_2O:MeOH 90:10
Drying time (min)	0.5	1

3 and with an elution volume of 3 mL we were able to recover all antibiotics. Furthermore, it was observed that the variation of other factors (flow rate of sample loading, elution flow rate, solvent washing and drying time) did not affect the process, and the recovery was dependent mainly on the pH of the solution and the elution volume. Lastly, we must mention that in multiresidue analysis methods, the main objective is to extract the greatest number of compounds so, with the final conditions all antibiotics were obtained with acceptable values of recovery.[40]

3. 3. Sample Analysis

Figure 3 shows a chromatogram of river water fortified with antibiotics studied in this work. Next, Figure 4, shows chromatograms for the analyzed samples of the Rodrigo Gomez water dam (sample 1), La Silla and Pilon rivers (samples 2 and 3, respectively). No signals were observed at the retention times corresponding to the antibiotics. It is recommended to continue monitoring environmental waters, to confirm that there is no presence of the antibiotics studied considering the limits of detection established in this work for the target analytes.

3. 4. Applicability

Recently, studies done in surface waters have reported TMP, ENRO, AMOXI, SMX and CIP at concentrations from 0.03 to 0.25 μg/L in five samples of the river Ter[6] (North East of Spain). Meanwhile, in Taihu Lake, China,[41] SMX was reported at a concentration up to 0.600 μg/L,

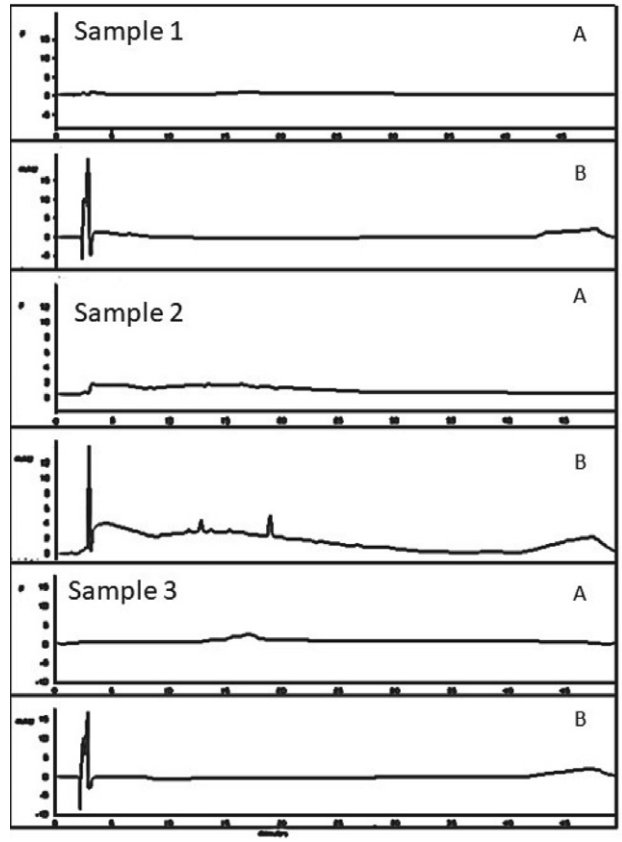

Figure 4. Chromatograms of river water samples 1, 2 and 3. Chromatograms A correspond to fluorescence detection λ_{ex} 278 nm and λ_{em} 450 nm. Chromatograms B correspond to UV detection at 280 nm. Conditions of analysis are described in the text.

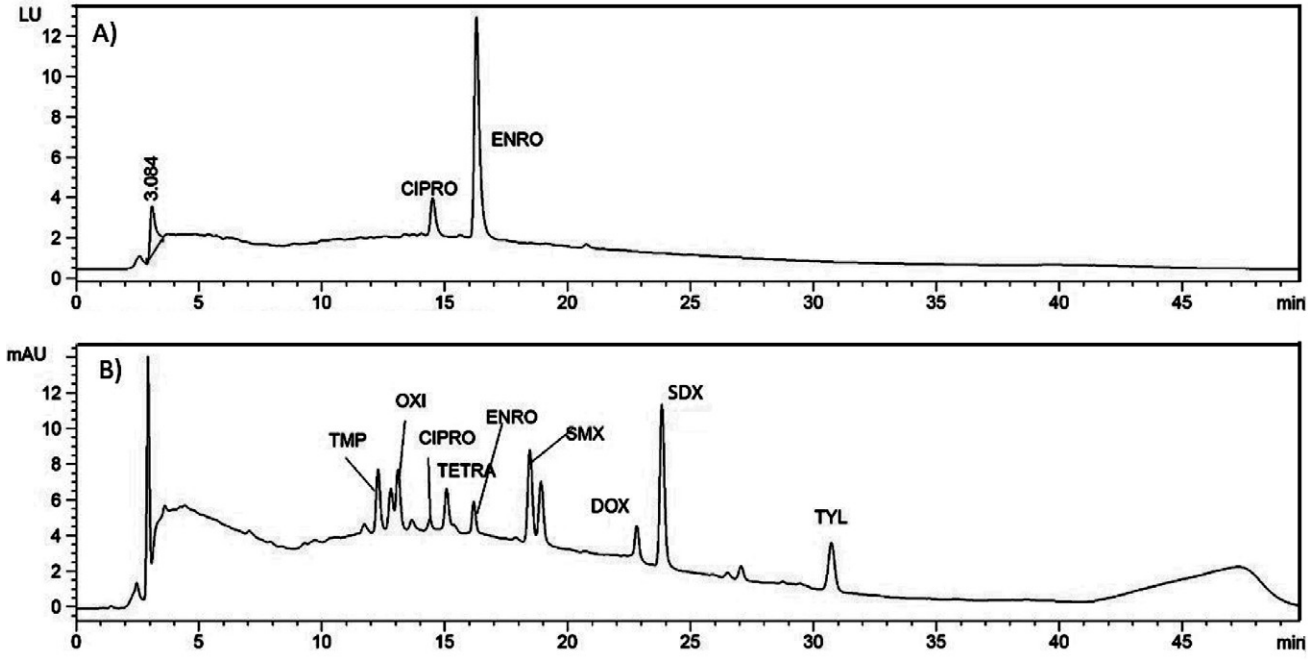

Figure 3. Chromatogram of the mixture of added antibiotics in river water. (A) fluorescence detection (λ_{ex} 278nm and λ_{em} 450 nm) (B) UV detection 280 nm. Conditions of analysis are described in the text.

while in Kenya and Spain studies have reported SMX in concentrations of 0.95 μg/L and over 13.7 μg/L, respectively. Concentrations of 1.6 up to 1670 μg/L of ENRO were reported in water samples from Poland.[42] Nonetheless, in Mexico, information about occurrence of antibiotics in environmental waters is lacking.[43,44] Thus, it is important to continue the analysis and monitoring of antibiotics in environmental waters in Monterrey and other major metropolitan areas, as the intense use of these antibiotics in urban centers poses high health risks. Considering the levels of concentration of antibiotics that have been reported around the world, the LODs reached by our method allows to continue with the monitoring and analysis of occurrence of these emerging contaminants in environmental waters.

HPLC-MS methods have been around for close to 20 years, during this time analysis of antibiotics has been well studied.[2,12,19,45] Through our work, previous HPLC-UV/FLD studies that included several pharmaceuticals and antibiotics were reviewed.[27–32] In that regard, in our research we included antibiotics of five different families. Moreover, our HPLC-UV/FLD method has detection limits comparable and, for some antibiotics, lower than other methods that also use UV and FLD detection.[14,31,46] Particularly, for FLD detection, the obtained detection limits are comparable with other methods using the LC-MS/MS technique.[19,35]

We should note that even though LOD and LOQ were optimized to a great extent, one drawback of our system was observed. In comparison with HPLC-MS our system is not capable of achieving sufficient specificity, as ultrafine resolution is still a technological limitation. Nonetheless, our proposed method continues to be an optimized, economical, and accessible system, which can be adopted by many laboratories worldwide, which may not have access to sufficient resources and highly trained personnel, to continue rapid monitoring of environmental or other residual waters, in search to detect emerging contaminants.

4. Conclusion

The presence of antibiotics in different environmental water matrices such as surface waters, groundwater, drinking water, hospital and urban wastewater, wastewater effluents and influents of treatment plants have been widely reported. Concentration and type of antibiotics may be influenced by several key factors, such as source of sample, season of the year, prevalence of diseases, as well as factories located in the vicinity or aquaculture activities. We believe, based on our results, that our method can be the first option for antibiotic and contaminant screening studies.

From our results, we demonstrate that our system is a simple and cost-efficient multiresidue analytical method for the determination of ten antibiotics of five different families. The method was validated and applied to samples of surface water. The method involved off-line solid phase extraction and quantification by HPLC in combination with UV and FLD detections. Complete separation was obtained in 30 min. This method is rapid, cost-efficient, reliable and reproducible, and for this reason represents an alternative for the analytical environmental laboratories that require investigation and monitoring of these emerging contaminants.

Acknowledgements

The authors wish to thank to ICRA (Catalan Institute for Research of Water) for their kind welcome and for sharing their knowledge during the stay.

Funding

This work was funding by the CONACYT (Grant project 130997) and PAICYT (Grant Project CS780-11).

Declaration of interest statement

Authors have declared no conflict of interest.

Authors' contributions

Research: I.F., C.-A., N. C-R, M.L., S.-C., N.W.-T., L.N.-T., A.J., G-J. Experiments and Analysis: I.F., C.-A., M.L., S.-C., N.C-R Writing: I.F., C.-A., M.L., S.-C., A.J.G.-J., J.F.I., N.C.C.-R. and Supervising: N.W.-T., A.J.,G-J, N.,C.-R.

5. References

1. B. González-Gaya, L. Cherta, L. Nozal and A. Rico. An optimized sample treatment method for the determination of antibiotics in seawater, marine sediments and biological samples using LC-TOF/MS, *Sci. Total Environ.* **2018**, *643,* 994–1004. **DOI:**10.1016/j.scitotenv.2018.06.079
2. C. Kim, H. D. Ryu, E. G. Chung, Y. Kim and J. kwan Lee. A review of analytical procedures for the simultaneous determination of medically important veterinary antibiotics in environmental water: Sample preparation, liquid chromatography, and mass spectrometry, *J. Environ. Managem.* **2018**, *217,* 629–645. **DOI:**10.1016/j.jenvman.2018.04.006
3. A. Gogoi, P. Mazumder, V. K. Tyagi, G. G. Tushara Chaminda, A. K. An and M. Kumar. Occurrence and fate of emerging contaminants in water environment: A review, *Groundw. Sustain. Dev.* **2018**, *6*, 169–180. **DOI:**10.1016/j.gsd.2017.12.009
4. A. I. Stefanakis., J. A. Becker, A review of emerging contaminants in water: Classification, sources, and potential risks. *Impact of Water Pollution on Human Health and Environmental Sustainability.* **2016**, 55–80. **DOI:**10.4018/978-1-4666-9559-7.ch003
5. L. Yao, Y. Wang, L. Tong, Y. Deng, Y. Li, Y. Gan, W. Guo, C.

Dong, Y. Duan and K. Zhao. Occurrence and risk assessment of antibiotics in surface water and groundwater from different depths of aquifers: A case study at Jianghan Plain, central China, *Ecotoxicol. Environ. Saf.* **2017,** *135*, 236–242. **DOI:**10.1016/j.ecoenv.2016.10.006

6. M. Gros, S. Rodriguez-Mozaz and D. Barcelo. Rapid analysis of multiclass antibiotic residues and some of their metabolites in hospital, urban wastewater and river water by ultra-high-performance liquid chromatography coupled to quadrupole-linear ion trap tandem mass spectrometry., *J Chromatogr A*. **2013,** *1292,* 173–188. **DOI:**10.1016/j.chroma.2012.12.072
7. J. Du, H. Zhao, S. Liu, H. Xie, Y. Wang and J. Chen. Antibiotics in the coastal water of the South Yellow Sea in China: Occurrence, distribution and ecological risks. *Sci. Total Environ.* **2017**, *595,* 521–527. **DOI:**10.1016/j.scitotenv.2017.03.281
8. J. Rossmann, S. Schubert, R. Gurke, R. Oertel and W. Kirch. Simultaneous determination of most prescribed antibiotics in multiple urban wastewater by SPE-LC-MS/MS, *J. Chromatogr. B Anal. Technol. Biomed. Life Sci.* **2014,** *969*, 162–170. **DOI:**10.1016/j.jchromb.2014.08.008
9. P. Grenni, V. Ancona and A. Barra Caracciolo. Ecological effects of antibiotics on natural ecosystems: A review, *Microchem. J.* **2018,** *136,* 25–39. **DOI:**10.1016/j.microc.2017.02.006
10. W. Calero-Cáceres and M. Muniesa. Persistence of naturally occurring antibiotic resistance genes in the bacteria and bacteriophage fractions of wastewater, *Water Res.* **2016**, *95,* 11–18. **DOI:**10.1016/j.watres.2016.03.006
11. S. Bayen, X. Yi, E. Segovia, Z. Zhou and B. C. Kelly. Analysis of selected antibiotics in surface freshwater and seawater using direct injection in liquid chromatography electrospray ionization tandem mass spectrometry, *J. Chromatogr. A* **2014,** *1338*, 38–43. **DOI:**10.1016/j.chroma.2014.02.034
12. C. Tong, X. Zhuo and Y. Guo. Occurrence and risk assessment of four typical fluoroquinolone antibiotics in raw and treated sewage and in receiving waters in Hangzhou, China, *J. Agric. Food Chem.* **2011,** *59,* 7303–7309. **DOI:**10.1021/jf2013937
13. J. L. Zhou, K. Maskaoui and A. Lufadeju. Optimization of antibiotic analysis in water by solid-phase extraction and high performance liquid chromatography-mass spectrometry/mass spectrometry, *Anal. Chim. Acta* **2012**, *731*, 32–39. **DOI:**10.1016/j.aca.2012.04.021
14. B. Chen, W. Wang and Y. Huang. Cigarette filters as adsorbents of solid-phase extraction for determination of fluoroquinolone antibiotics in environmental water samples coupled with high-performance liquid chromatography, *Talanta* **2012,** *88*, 237–243. **DOI:**10.1016/j.talanta.2011.09.066
15. E. Ngumba, P. Kosunen, A. Gachanja and T. Tuhkanen. A multiresidue analytical method for trace level determination of antibiotics and antiretroviral drugs in wastewater and surface water using SPE-LC-MS/MS and matrix-matched standards, *Anal. Methods* **2016**, *8*, 6720–6729. **DOI:**10.1039/C6AY01695B
16. K. Škrášková, L. H. M. L. M. Santos, D. Šatínský, A. Pena, M. C. B. S. M. Montenegro, P. Solich and L. Nováková. Fast and sensitive UHPLC methods with fluorescence and tandem mass spectrometry detection for the determination of tetracycline antibiotics in surface waters, *J. Chromatogr. B Anal. Technol. Biomed. Life Sci.* **2013,** *927*, 201–208. **DOI:**10.1016/j.jchromb.2012.12.032
17. S. Managaki, A. Murata, H. Takada, C. T. Bui and N. H. Chiem. Distribution of macrolides, sulfonamides, and trimethoprim in tropical waters: Ubiquitous occurrence of veterinary antibiotics in the Mekong Delta, *Environ. Sci. Technol.* **2007,** *41,* 8004–8010. **DOI:**10.1021/es0709021
18. F. Y. Hu, L. M. He, J. W. Yang, K. Bian, Z. N. Wang, H. C. Yang and Y. H. Liu. Determination of 26 veterinary antibiotics residues in water matrices by lyophilization in combination with LC-MS/MS, *J. Chromatogr. B Anal. Technol. Biomed. Life Sci.* **2014,** *949–950,* 79–86. **DOI:**10.1016/j.jchromb.2014.01.008
19. M. Ibáñez, C. Guerrero, J. V. Sancho and F. Hernández. Screening of antibiotics in surface and wastewater samples by ultra-high-pressure liquid chromatography coupled to hybrid quadrupole time-of-flight mass spectrometry, *J. Chromatogr. A* **2009,** *1216*, 2529–2539. **DOI:**10.1016/j.chroma.2009.01.073
20. L. Jiang, X. Hu, T. Xu, H. Zhang, D. Sheng and D. Yin. Prevalence of antibiotic resistance genes and their relationship with antibiotics in the Huangpu River and the drinking water sources, Shanghai, China, *Sci. Total Environ.* **2013,** *458–460*, 267–272. **DOI:**10.1016/j.scitotenv.2013.04.038
21. WHO guidelines on use of medically important antimicrobials in food-producing animals. GENEVA. https://apps.who.int/iris/bitstream/handle/10665/258970/9789241550130-eng.pdf;jsessionid=3A2F20A36FF4E80CC7E789DB31AADCD5?sequence=1; (assessed: March, 14, **2020**).
22. Z. Wang, X. Y. Wang, H. Tian, Q. H. Wei, B. S. Liu, G. M. Bao, M. L. Liao, J. L. Peng, X. Q. Huang and L. Q. Wang. High through-put determination of 28 veterinary antibiotic residues in swine wastewater by one-step dispersive solid phase extraction sample cleanup coupled with ultra-performance liquid chromatography-tandem mass spectrometry, *Chemosphere* **2019,** *230*, 337–346. **DOI:**10.1016/j.chemosphere.2019.05.047
23. J. Cha, S. Yang and K. H. Carlson. Occurrence of β-lactam and polyether ionophore antibiotics in surface water, urban wastewater, and sediment, *Geosystem Eng.* **2015,** *18,* 140–150. **DOI:**10.1080/12269328.2015.1010658
24. R. Mirzaei, M. Yunesian, S. Nasseri, M. Gholami, E. Jalilzadeh, S. Shoeibi and A. Mesdaghinia. Occurrence and fate of most prescribed antibiotics in different water environments of Tehran, Iran, *Sci. Total Environ.* **2018,** *619*, 446–459. **DOI:**10.1016/j.scitotenv.2017.07.272
25. M. S. Díaz-Cruz, M. J. García-Galán and D. Barceló. Highly sensitive simultaneous determination of sulfonamide antibiotics and one metabolite in environmental waters by liquid chromatography-quadrupole linear ion trap-mass spectrometry, *J. Chromatogr. A* **2008,** *1193,* 50–59. **DOI:**10.1016/j.chroma.2008.03.029

26. N. H. Tran, L. Hoang, L. D. Nghiem, N. M. H. Nguyen, H. H. Ngo, W. Guo, Q. T. Trinh, N. H. Mai, H. Chen, D. D. Nguyen, T. T. Ta and K. Y. H. Gin. Occurrence and risk assessment of multiple classes of antibiotics in urban canals and lakes in Hanoi, Vietnam, *Sci. Total Environ.* **2019,** *692*, 157–174. **DOI:**10.1016/j.scitotenv.2019.07.092
27. D. Ašperger, S. Babić, D. M. Pavlovic, D. Dolar, K. Košutić, A. J. M. Horvat and M. Kaštelan-Macan. SPE-HPLC/DAD determination of trimethoprim, oxytetracycline and enrofloxacin in water samples, *Int. J. Environ. Anal. Chem.* **2009,** *89*, 809–819. **DOI:**10.1080/03067310902822896
28. S. Cavenati, P. N. Carvalho, C. M. R. Almeida, M. Basto and M. T. S. D. Vasconcelos. Simultaneous determination of several veterinary pharmaceuticals in effluents from urban, livestock and slaughterhouse wastewater treatment plants using a simple chromatographic method, *Water Sci. Technol.* **2012,** *66,* 603–611. **DOI:**10.2166/wst.2012.218
29. Q. Yiruhan, J. Wang, C. H. Mo, Y. W. Li, P. Gao, Y. P. Tai, Y. Zhang, Z. L. Ruan and J. W. Xu. Determination of four fluoroquinolone antibiotics in tap water in Guangzhou and Macao, *Environ. Pollut.* **2010,** *158*, 2350–2358. **DOI:**10.1016/j.envpol.2010.03.019
30. D. M. Pavlović, S. Babić, D. Dolar, D. Ašperger, K. Košutić, A. J. M. Horvat and M. Kaštelan-Macan. Development and optimization of the SPE procedure for determination of pharmaceuticals in water samples by HPLC-diode array detection, *J. Sep. Sci.* **2010,** *33*, 258–267. **DOI:**10.1002/jssc.200900571
31. T. V. Madureira, M. J. Rocha, Q. B. Cass and M. E. Tiritan. Development and optimization of a HPLC-DAD method for the determination of diverse pharmaceuticals in estuarine surface waters, *J. Chromatogr. Sci.* **2010,** *48*, 176–182. **DOI:**10.1093/chromsci/48.3.176
32. D. M. Pavlović, D. Ašperger, D. Tolic and S. Babić. Development and optimization of the determination of pharmaceuticals in water samples by SPE and HPLC with diode-array detection, *J. Sep. Sci.* **2013,** *36,* 3042–3049 . **DOI:**10.1002/jssc.201300486
33. A. Herrera-Herrera, J. Hernández-Borges, T. Borges-Miquel, M.A, Rodríguez-Delgado. Dispersive liquid-liquid microextraction combined with ultra-high performance chromatography for the simultaneous determinatin of 25 sulfonamide and quijolone antibiotics in water samples, *J. Pharm. Biomed. Anal.* **2013,** *75,*130–137. **DOI:**10.1016/j.jpba.2012.11.026
34. S. Mokh, M. El Khatib, M. Koubar, Z. Daher and M. Al Iskandarani. Innovative SPE-LC-MS/MS technique for the assessment of 63 pharmaceuticals and the detection of antibiotic-resistant-bacteria: A case study natural water sources in Lebanon, *Sci. Total Environ.* **2017,** *609*, 830–841. **DOI:**10.1016/j.scitotenv.2017.07.230
35. ICH, Q2(R1); Validation of Analytical procedures: text and metohodology, International Conference on Harmonization. *Tech. Requir. Regist. Pharm. Hum. USE* (pp. 1–17).
36. N. Cavazos-Rocha, I. Carmona-Alvarado., L. Vera-Cabrera, N. Waksman-de-Torres., M. L. Salazar-Cavazos HPLC Method for the Simultaneous Analysis of Fluoroquinolones and Oxazolidinones in plasma. *J. Chromatogr. Sci*. **2014,** *52*, 1281–1287. **DOI:**10.1093/chromsci/bmu002
37. Waters, Atlantis T_3 and Acquity UPLC HSS T_3 Columns; Retrieved from https://www.waters.com/webassets/cms/library/docs/720001887en.pdf. (assessed: May 15 **2020)**
38. H. Zuyun, H. Houping, C. Ruxiu, Z. Yun'e-. Study on the fluorescence properties of some fluoroquinolones in various media. *Wuhan Univ. J. Nat. Sci.,* **1997***, 2*, 353–358. **DOI:**10.1007/BF02829921
39. AOAC, Appendix F: Guidelines for Standard Method Performance Requirements, *AOAC Off. Methods Anal.* (pp. 1–18).; Retrieved from http://www.eoma.aoac.org/app_f.pdf, (assessed: May 25 **2020)**
40. M. C. Moreno-Bondi, M. D. Marazuela, S. Herranz and E. Rodriguez. An overview of sample preparation procedures for LC-MS multiclass antibiotic determination in environmental and food samples, *Anal. Bioanal. Chem.* **2009,** *395*, 921–946. **DOI:**10.1007/s00216-009-2920-8
41. H. Ding, Y. Wu, W. Zhang, J. Zhong, Q. Lou, P. Yang and Y. Fang. Occurrence, distribution, and risk assessment of antibiotics in the surface water of Poyang Lake, the largest freshwater lake in China, *Chemosphere* **2017,** *184*, 137–147. **DOI:**10.1016/j.chemosphere.2017.05.148
42. M. Gbylik-Sikorska, A. Posyniak, T. Sniegocki and J. Zmudzki. Liquid chromatography-tandem mass spectrometry multiclass method for the determination of antibiotics residues in water samples from water supply systems in food-producing animal farms, *Chemosphere* **2015,** *119*, 8–15. **DOI:**10.1016/j.chemosphere.2014.04.105
43. J. A. Rivera-Jaimes, C. Postigo, R. M. Melgoza-Alemán, J. Aceña. D. Barceló and M. López de Alda. Study of pharmaceuticals in surface and wastewater from Cuernavaca, Morelos, Mexico: Occurrence and environmental risk assessment, *Sci. Total Environ.* **2018,** *613*, 1263–1274. **DOI:**10.1016/j.scitotenv.2017.09.134
44. J. Siemens, G. Huschek, C. Siebe and M. Kaupenjohann. Concentrations and mobility of human pharmaceuticals in the world's largest wastewater irrigation system, Mexico City-Mezquital Valley, *Water Res.* **2008,** *42*, 2124–2134. **DOI:**10.1016/j.watres.2007.11.019
45. H. B. Lee, T. E. Peart and M. L. Svoboda. Determination of ofloxacin, norfloxacin, and ciprofloxacin in sewage by selective solid-phase extraction, liquid chromatography with fluorescence detection, and liquid chromatography-tandem mass spectrometry, *J. Chromatogr. A* **2007,** *1139,* 45–52. **DOI:**10.1016/j.chroma.2006.11.068
46. H. Shaaban and T. Górecki. Fast ultrahigh performance liquid chromatographic method for the simultaneous determination of 25 emerging contaminants in surface water and wastewater samples using superficially porous sub-3 μm particles as an alternative to fully porous sub-2 μm partic, *Talanta* **2012,** *100,* 80–89. **DOI:**10.1016/j.talanta.2012.08.010

Povzetek

Razvili smo metodo HPLC-UV/FLD za hkratno detekcijo desetih antibiotikov v površinskih vodah. Antibiotike smo ekstrahirali iz vode z ekstrakcijo na trdno fazo. Za ločbo smo uporabljali kolono Atlantis T_3 z mobilno fazo iz acetonitrila in 0,05% trifluoroocetne kisline, celotni čas analize je bil 45 min. Signal smo detektirali pri 280 nm; fluorokinolone smo dodatno kvantificirali s fluorescenčno detekcijo. Ovrednotili smo nekatere validacijske parametre, kot so linearnost, izkoristek in natančnost. Meje zaznave (LOD) za rečno vodo so bile v območju 0,1–1,3 μg/L za antibiotike z UV detekcijo ter 0,039 oz. 0,073 μg/L za oba fluorokinolona, detektirana s FLD. LOD so dovolj nizke, da lahko to metodo označimo kot prvo alternativo metodam HPLC-MS. Omogočala bo opozarjanje na prisotnost antibiotikov v površinskih vodah. Ta presejalna metoda je hitra, občutljiva, ponovljiva in ekonomična.

Except when otherwise noted, articles in this journal are published under the terms and conditions of the Creative Commons Attribution 4.0 International License

DOI: 10.17344/acsi.2021.6899 *Acta Chim. Slov.* **2022,** *69,* 60–72
creative commons

Scientific paper

The Effect of Heuristics on the Reasoning of the Pre-Service Science Teachers on the Topic of Melting and Boiling Point

Gülen Önal Karakoyun[1,*] and Erol Asiltürk[2]

[1] *Van Yuzuncu Yil University, Muradiye Vocational High School, Chemistry and Chemical Business Technologies Department, Chemical Technology Program, Van, Turkey*

[2] *Firat University, Faculty of Education, Science Education Department, Elazig, Turkey*

* *Corresponding author: E-mail: gulenonal@yyu.edu.tr*
Tel.: +905442930447

Received: 04-19-2021

Abstract

The purpose of this study was to explore the effects of the heuristics on the reasoning processes of pre-service science teachers on the topic of melting and boiling point using the ten heuristic model proposed by Talanquer. In this phenomenographic study carried out in the spring semester of the 2018–2019 academic year, interviews were conducted with 30 teacher candidates enrolled in the Science Teaching Program of Firat University Faculty of Education. Participants were asked to answer three different questions during the interviews. These questions were about the ranking of some compounds according to their melting or boiling points. Six different answer patterns for each question were obtained from the answers. The findings of this study showed that students generally used shortcut strategies instead of analytical/scientific reasoning, as all ten heuristics affected participants' reasoning. This study also revealed that although not included in the model proposed by Talanquer, periodic trends heuristic also influenced participants' reasoning about the melting and boiling point.

Keywords: Chemistry education; cognitive constraints; heuristics; melting and boiling point; reasoning; science education.

1. Introduction

In order to make predictions about the melting and boiling points of compounds, it is necessary to know well the interactions between particles and the molecular structure-property relationships. The structure-property relationships and the effects of interactions between particles on melting and boiling points have an important place in chemistry curricula. Because of this importance, there are many studies in the literature on students' understanding of the structure-property relationships and the effects of interactions between particles on melting and boiling points.[1–6] In these studies, students' understanding of melting and boiling phenomena was examined from different dimensions. The findings of these studies showed that students often had difficulties in understanding interactions between particles and structure-property relationships, and could not make accurate predictions or rankings about the melting and boiling points of compounds due to these difficulties. It was also reported in the findings of these studies that students generally relied on shortcut strategies instead of analytical/scientific reasoning, students had various misconceptions regarding the mentioned subjects, and students' reasoning, judgment and decision-making processes about melting points and boiling points were generally flawed.

In order to understand the causes of students' learning difficulties, students' reasoning and cognitive constraints that constrain scientific reasoning should be explored in detail. Reasoning is the act of thinking about something logically. Cognitive constraints are cognitive factors/elements that restrict individuals' analytical/scientific reasoning.[7–11] The best known of cognitive elements include core knowledge,[12] intuitive rules,[13] implicit assumptions,[14] conceptual sources,[15] basic hypotheses and ontological beliefs,[16] inductive constraints,[17] primitive phenomenologies[18] and heuristics.[19]

Heuristics are related to the "dual process" theory, which was developed to explain the judgment and decision-making processes of individuals. According to the dual process theory, two different cognitive systems called System 1 and System 2 are used when individuals make judgments or decisions. System 1 includes cognitive processes that progress rapidly, automatically and unconsciously, while System 2 includes cognitive processes that progress slowly, prudently and consciously.[20–23] Using previous knowledge and beliefs, System 1 processes are contextual, relational, holistic, automatic, and working memory-independent processes. Slow and sequential System 2 processes are the processes that provide rule-based, analytical, abstract reasoning and use working memory.[23–26] No special effort is required to trigger System 1 processes.[23,27] System 1 processes are related to the intuitive reasoning of individuals. System 2 processes require special cognitive effort and conscious interventions.[27] The System 1 processes described in detail above are short-path reasoning strategies and are called heuristics.[20,23,28–30] In conditions where knowledge or motivation is lacking or when time is limited, heuristics play an extremely active role.[23,31,32] Heuristics enable decision-making in a short time without cognitive effort since they evaluate fewer factors and use fewer cues in the reasoning and judgment processes.[33] However, heuristics are responsible for various cognitive biases observed in the reasoning processes.[10,23]

There are many studies in the literature exploring the effects of heuristics on the judgment and decision-making processes of individuals' daily lives.[23,30,34] Research groups in different disciplines such as cognitive psychology, psychology, behavioral finance, and behavioral sciences generally carried out these studies. The heuristics identified in these studies were generally named with different names specific to the studied field. The heuristics identified in these studies and named with different names actually use similar cognitive processes.[23,30,31] For this reason, some scientists have started to study on collecting the heuristics that progress with the similar mechanism under a general heading. For example, Morewedge and Kahneman grouped the heuristics, which frequently affect the judgment and decision-making processes related to the daily lives of individuals, under three headings. These heuristics are representativeness, availability and recognition.[23,30,34] Today, many researchers have used this model by Morewedge and Kahneman to explore the effects of heuristics on judgment and decision-making processes related to the daily lives of individuals. Thus, confusion such as naming the heuristics that progress with similar cognitive processes with different names was prevented.[23,30]

Since the 2010s, science/chemistry educators have begun to explore in detail the roles of heuristics in students' reasoning processes related to chemistry subjects, and the working mechanisms of heuristics in the field of chemistry. The intuitive reasoning and heuristic uses of students in some chemistry subjects have been studied in detail in some research until today. Chemistry subjects explored in this context include chemical reactivity, bonding theories/molecular structures, addition reactions, IR and NMR spectra interpretation, chemical problem solving, elimination reactions, acidity/basicity strength of molecules, structure-property relations of molecules and classification of chemical substances.[2,11,23,26,29,35–37] The findings of these studies showed that due to the effects of intuitive judgments and heuristics, students generally answered the questions without using basic and significant chemistry knowledge. In addition to these studies mentioned above, in a theoretical study published in 2014, Talanquer explained ten heuristics that are likely to be used in chemistry subjects and the working mechanisms of these heuristics with examples specific to the field of chemistry.[10] The ten heuristics model of Talanquer has the quality to be used as a model in studies exploring the role of heuristics in the chemistry topics. For example, in three different studies recently conducted to examine the heuristic reasoning of students on "hydrogen bond" and "chemical structure – acidity/basicity relationship", the researchers carried out their research using the ten heuristic model.[38–40] Except for these three studies, there is no other study in the literature that explores the heuristics that are effective in chemistry topics based on the ten heuristic model proposed by Talanquer. These ten heuristics suggested by Talanquer are:[10]

Associative activation: Using mental structures present in memory to fill in the blanks.

Fluency: Using of easily accessible cues in the process of solving the problem.

Attribute substitution: evaluation of other easily accessible attributes instead of the target attribute / Substitution the original question with a simpler question.

One reason decision making: Simplifying reasoning by using a single clue or factor in the process of problem solving.

Surface similarity: The assumption that chemical compounds that are similar to each other in structural representation have similar properties and behavior.

Recognition: More value to recognized objects / less value to unrecognized.

Generalization: Generalization of learned models or rules

Rigidity: Reasoning in an inflexible or non-creative way.

Overconfidence: Exceeding true accuracy due to self-confidence in decision-making processes.

Affect: A positive or negative emotion towards an event, an object, or anything that affects learning.

The purpose of this study is to explore the effect of ten heuristics on the pre-service science teachers' reasoning processes about melting and boiling points. Therefore,

the research problem of this study can be expressed as follows: What is the role of the ten heuristics in the reasoning processes of the pre-service science teachers on the melting and boiling points? The research questions of this study are as follows:

- Which heuristics affect the reasoning of the students in the process of performing a task in which the compounds are ranked according to their melting and boiling points?
- How to explain the working mechanisms of these heuristics in a way specific to the field of chemistry?

2. Method

2. 1. Participants

This research was conducted at Firat University in the spring semester of the 2018–2019 academic year. The participants of the study were selected on a voluntary basis, considering their successes in General Chemistry I and General Chemistry II courses from the students enrolled in the Science Education Program. Of the 30 teacher candidates who voluntarily participated in the research, 16 were male and 14 were female. 1/3 of the participants were students who failed in the General Chemistry I and General Chemistry II courses, 1/3 of them were moderately successful and 1/3 of them are highly successful. Participants were students enrolled in the 2nd, 3rd and 4th grades. In the study, the real names of the participants were not used, instead the participants were named with a coding S1, S2, S3, S4 … S30. The grouping of the participants according to their success in General chemistry I/II courses is as follows: Failed students; S1, S5, S7, S13, S14, S16, S18, S20, S23, S24; Moderately successful students; S2, S3, S4, S8, S10, S17, S21, S25, S26, S30; Highly successful students; S6, S9, S11, S12, S15, S19, S22, S27, S28, S29.

2. 2. Data Collection and the Interview Protocol

In this qualitative study, the phenomenological research method was used. The interviews were conducted with the participants in order to properly examine the heuristic reasoning of the participants regarding "ranking chemical compounds according to their increasing melting/boiling points". The interviews were conducted according to the following eight-step interview protocol:

I. How do you feel when talking about the ranking of compounds according to their increasing melting/boiling points? Have you ever experienced any positive or negative effects on this chemistry topic during your education? If so, does it still have any effect on you?

II. If you are faced with questions about ranking compounds according to their increasing melting/boiling points, what level of confidence do you have that you can answer the questions correctly? How would you score your confidence level between 1 and 10 points (1 is the lowest, 10 is the highest)?

III. Do you have a constant judgment/bias about the ranking of compounds according to their increasing melting/boiling points? For example, do you have any approaches such as "I have judgments/reasoning regarding the order of compounds according to their increasing melting/boiling points, which I will not change regardless of the question, I always solve problems regarding the order of compounds according to their increasing melting/boiling points using my current judgments/reasoning"?

IV. During the interviews, the following three questions about melting/boiling points were asked/showed to the participants:

1) Rank the HI, HCl, NaI, NaCl compounds according to their increasing boiling points.
2) Rank the HCl, HBr, NaI, NaBr compounds according to increasing melting points.
3) Rank the H_2Se, H_2S, PH_3 compounds according to their increasing boiling points.

Note: At this stage, the participants were given 2 minutes to answer each question. These chemistry questions were taken from a different study previously done by Maeyer and Talanquer.[6]

V. You saw the questions, what do you feel? (This question was asked just before students started answering relevant chemistry questions)

VI. What level of confidence do you have that you can answer these questions correctly? (This question was asked just before students started answering relevant chemistry questions)

VII. What level of confidence do you have in yourself that you answered these questions correctly? (This question was asked after students answered relevant chemistry questions)

VIII. Explain in detail the reasons for your answers to each chemistry question. (There was no time limitation at this stage.)

Note: During the interviews, some additional questions were asked in order to obtain more explanatory in-depth information.

The third question in the interview protocol was prepared to explore the effects of rigidity heuristic. Participants' answers to this question were carefully examined. In addition, during the interviews, special attention was paid to whether the participants actually solved the questions using the strategies they were used to before, and whether they were flexible in solving the questions. The rigidity heuristic was coded when it was determined that the participants were not flexible. The second, sixth and seventh questions in the interview protocol were prepared to explore the effects of overconfidence heuristic. In cases where 8, 9 or 10 points were given as an answer to the sec-

ond, sixth and seventh questions, the overconfidence heuristic was coded. Students who gave such answers generally made the following statements: "I am confident; I definitely solved /will solve the questions correctly". The first and fifth questions in the interview protocol were prepared to explore the effects of affect heuristic. The affect heuristic was coded in cases where it was determined that the participant had negative or positive emotions due to experiences.

2. 3. Data Analysis

The interviews that were recorded with audio and visuals later were turned into written documents. Thus, interview transcripts were created for each student. With the analysis of the data obtained from the interview transcripts, heuristic reasoning was detected and coded. While coding, other similar studies on students' heuristic reasoning in chemistry were also used.[2,10,23,30,38] In order to ensure the inter-rater reliability, eight interview transcripts related to acidity strength and eight interview transcripts related to basicity strength (approximately 25% of total interview transcripts) were selected and the selected interviews were first evaluated and encoded separately by both the researcher and the consultant. The results of both evaluators were compared with each other. The encodings were revised so that there was over 90% agreement between the evaluators. After this compliance was achieved, all remaining interview transcripts were evaluated and coded by the researcher. Ten heuristics proposed by Talanquer[10] were used to create a coding scheme for heuristics. The heuristic encodings, except rigidity, overconfidence and affect, were carried out by associating the students' specific statements about the solution of the questions with heuristics. Specific student statements that are the basis of encodings were presented in the results and discussion section.

3. Results and Discussions

During the interviews, the following three questions about melting/boiling points were asked to the participants:

1. Rank the HI, HCl, NaI, NaCl compounds according to their increasing boiling points.
2. Rank the HCl, HBr, NaI, NaBr compounds according to increasing melting points.
3. Rank the H_2Se, H_2S, PH_3 compounds according to their increasing boiling points.

Table 1. Obtained Response Patterns

Response Pattern	Code name of students	n	%
	First question (Boiling point, HI, HCl, NaI and NaCl compounds)		
HI < HCl < NaI < NaCl	S1(F), S7(F), S11(HS), S21(MS), S23(F)	5	16.66
	HCl < HI < NaI < NaCl		
(Correct answer)	S9(HS), S12(HS), S20(F), S25(MS), S26(MS), S28(HS), S29(HS)	7	23.33
HCl < HI < NaCl < NaI	S2(MS), S17(MS), S19(HS)	3	10.00
NaCl < NaI < HCl < HI	S6(HS), S15(HS), S27(HS)	3	10.00
NaI < NaCl < HI < HCl	S4(MS), S14(F), S16(F)	3	10.00
HCl < NaCl < HI <NaI	S3(MS), S5(F), S8(MS), S10(MS), S13(F), S8(MS), S22(HS), S24(F), S30(MS)	9	30.00
	Second question (Melting Point, HCl, HBr, NaI and NaBr compounds)		
HCl < HBr < NaI < NaBr (Correct answer)	S6(HS), S9(HS), S12(HS), S20(F), S25(MS), S26(MS), S28(HS), S29(HS)	8	26.66
HCl < HBr < NaBr < NaI	S1(F), S2(MS), S3(MS), S5(F), S8(MS), S10(MS), S13(F), S17(MS), S18(F), S19(HS), S22(HS), S24(F)	12	40.00
NaBr < NaI < HCl < HBr	S15(HS), S27(HS)	2	6.66
HBr < HCl < NaI < NaBr	S7(F), S11(HS), S21(MS), S23(F), S30(MS)	5	16.66
NaBr < NaI < HBr < HCl	S14(F)	1	3.33
NaI < NaBr < HBr < HCl	S4(MS), S16(F)	2	6.66
	Third question (Boiling Point, H_2Se, H_2S and PH_3 compounds)		
$PH_3 < H_2S < H_2Se$ (Correct answer)	S1(F), S3(MS), S5(F), S6(HS), S8(MS), S9(HS), S10(MS), S12(HS), S13(F), S15(HS), S18(F), S19(HS), S22(HS), S24(F), S26(MS), S27(HS), S28(HS), S29(HS)	18	60.00
$H_2Se < PH_3 < H_2S$	S7(F)	1	3.33
$PH_3 < H_2Se < H_2S$	S4(MS), S16(F), S23(F)	3	10.00
$H_2S < H_2Se < PH_3$	S20(F), S21(MS), S30(MS)	3	10.00
$H_2S < PH_3 < H_2Se$	S2(MS), S17(MS), S25(MS)	3	10.00
$H_2Se < H_2S < PH_3$	S11(HS), S14(F)	2	6.66

Six different answer patterns were obtained for each question. Table 1 presents these different answer patterns, the code names of the students who gave these answers, the number and percentage of the students who gave these answers. The abbreviations in the form of F, MS and HS given in parentheses after the participant code names in Table 1 show the success of the mentioned student in General Chemistry I/II courses. F: Unsuccessful, MS: Intermediate successful, HS: High-level successful.

When the vapor pressure of a liquid is equal to the outside pressure (atmospheric pressure), evaporation begins to occur all over the liquid. This event is called boiling. The temperature at which the liquid begins to boil is called the boiling point. Boiling point is related to intermolecular forces. As inter-molecular forces grow, volatility and vapor pressure decrease. Therefore, boiling point increases. The interactions between particles in ionic bonded compounds are much greater than interactions in covalent bonded compounds. Therefore, the boiling points of ionic compounds are much higher than covalent bonded compounds. NaI and NaCl in the first question are ionic compounds. Their boiling points are much higher than those of covalent compounds HI and HCl. In order to compare the boiling points of ionic compounds among themselves, it is necessary to evaluate the charges and radii of the ions forming the compound. The greater the ion charge, the greater the interaction between the particles. The larger the ion radius, the weaker the interaction between the particles. On the differences between the relative values of physical properties, the effect of ion charge differences is more than the effect of ion radius differences. The charge values of the ions in both NaI and NaCl compounds are 1. The contribution of the charge values is the same. Therefore, radii are the factor enabling the comparison of inter-particle interactions for these two compounds. The cation part of these two compounds are the same. For this reason, the difference in the radii of the anion parts makes the interactions in NaI and NaCl compounds different. The radius of the iodine atom is greater than that of chlorine. Interactions in NaI compound containing iodine with greater radius will be less than interactions in NaCl compound. As a result, the boiling point of NaCl, which has a stronger interaction, is higher than NaI. Inter-particle interactions in covalent bonded compounds HI and HCl are dipole-dipole interactions and london forces (induced dipole-induced dipole interactions). The magnitude of the dipole – dipole interactions is related to the magnitude of the dipole moment values of the compounds. The dipole moment of a compound is related to the difference in electronegativity between atoms and the geometry of the compound. Dipole-dipole interactions of compounds with high dipole moment values are also higher. When considering for HI and HCl molecules with the same geometry; the electronegativity of the Cl atom is greater than the electronegativity of the I atom. Therefore, the electronegativity difference between hydrogen and chlorine atoms is greater than the electronegativity difference between hydrogen and iodine atoms. This ensures that the dipole moment of HCl is greater than the dipole moment of HI. Dipole-dipole interactions in HCl molecules with larger dipole moment are greater than dipole-dipole interactions in HI molecule. Another inter-particle interaction that is effective in HI and HCl compounds is london forces. London forces are related to the total number of electrons in the compound. The more electron-containing compounds, the greater the london forces. When considering for HI and HCl molecules; the london forces are higher in the HI molecule, whose total number of electrons is much more than HCl. When considering for these two compounds, the contribution of london forces to the interaction between particles is much greater than dipole-dipole interactions. In other words, the effect of london forces is more dominant in the comparison of the boiling points of these two molecules. As a result, the boiling point of HI, which has greater london forces, is higher than HCl. Because of all these explanations mentioned, the correct answer to the first question is HCl <HI <NaI <NaCl. Using the approaches explained in detail above, it will be seen that the correct answers for the second and third questions are HCl <HBr <NaI <NaBr and PH_3 <H_2S <H_2Se, respectively.

Participants are expected to answer the questions with the reasoning explained in detail above. However, in this study, it was found that the rates of students who gave correct answers to the first, second and third questions were 23.33%, 26.66% and 60.00%, respectively. Because scientific reasoning requires a great deal of cognitive effort, the majority of students may have answered the questions by relying on heuristic strategies that require less cognitive effort. Since the aim of this study was to explore the heuristic usage of the students, students' answers have been analyzed in terms of heuristics used. Codes were made by associating the specific statements in the participants' responses with ten heuristics. Summaries of student statements that provide a basis to encodings about these ten heuristics were presented in Table 2. The periodic trends heuristic in Table 2 is not included in the ten heuristics proposed by Talanquer.[10] However, since it was found in this study that the participants also used this heuristic, this heuristic was also taken into consideration and added to the Table 2.

Table 3 presents the numbers and percentages of the participants who used the relevant heuristics at least once in the process of solving the questions, together with the code names of the participants who used these heuristics. The percentages given in Table 3 express the ratio of the number of participants who have used the relevant heuristics at least once to the total number of participants (N = 30, total number of participants). Question 1, question 2 and question 3 were abbreviated as Q1, Q2, and Q3, respectively.

Table 2. Heuristic codes and summaries of student statements (for three questions)

Heuristic code	Summary of student statements
Associative activation	The higher the molecular weight of the compound, the higher its melting / boiling point. The melting / boiling point changes from left to right and from top to bottom on the periodic table. The higher the acidity strength, the higher the boiling point. The higher the total number of atoms in the molecule, the higher the boiling point. Metal-containing compounds have high melting / boiling points. Strong acids have higher melting / boiling points than salts. The more electronegative, the higher the melting / boiling point.
Fluency	Using the numbers in the formulas of the compounds as an easily obtainable clue.
Attribute Substitution	Replacing the original question with questions: How are the compounds sorted according to their molecular weight? What are the positions of Na, Cl, H, and I atoms relative to each other in the periodic table? How are the positions of S, Se and P atoms relative to each other on the periodic table? What are the positions of Na, Cl, H, Br and I atoms relative to each other in the periodic table? Which compounds are acids and which are salts? Which atoms are more electronegative? Which compound is more acidic? Which compound has more total atoms?
One-Reason Decision Making	Decision making by only evaluating the molecular weights of compounds. Decision making by only evaluating the electronegativities of atoms. Decision making by only evaluating the acidity of the compounds.
Surface similarity	NaI is like NaCl / NaI is like HI / H_2S is like H_2Se / NaI and NaBr are like NaCl / HBr is like NaBr.
Recognition	I know/recognize NaCl or I know/recognize HCl.
Generalization	Generally, all properties increase/decrease from top to bottom in the periodic table, so the melting/ boiling point also increases/decreases from top to bottom. Generally, all properties increase/decrease in the periodic table from left to right, so the melting/ boiling point also increases/decreases from left to right. Atoms with high electronegativity generally have high all other properties. Strong acids generally have high all other properties.
Rigidity	I will decide with the principle of "the greater the molecular weight of the compound, the higher its melting/boiling point".
Overconfidence	I solved / will solve the problem absolutely correctly My confidence level is 8–10.
Affect	I like / dislike the melting / boiling point subject, positive / negative emotion
Periodic Trends *	The melting/boiling point increases/decreases from left to right on the periodic table. The melting/boiling point increases/decreases from top to bottom on the periodic table.

*Periodic Trends heuristic is not included in the ten heuristics proposed by Talanquer. However, this heuristic was added to the list since it was determined that the participants in this study also used this heuristic.

Individuals' unconscious replacing the question asked to them by another simple question and focusing on this different simple question is a result of the effect of attribute substitution heuristic.[30] In this study, it was revealed that heuristics affect the interpretation of the students about the questions, and thus there are differences between the target attribute and the comments expressed by the students. In the process of solving the first, second and third questions, it was found that 27 (90.00%) of the participants evaluated other attributes instead of the intended target attribute or unconsciously evaluated the intended target attribute due to the effect of attribute substitution heuristic. Thus, these students replaced the original questions with other simple questions after reading the questions. The mentioned students focused on the answers to other simple questions. These different questions were provided in Table 2 collectively.

It is reported in the literature that more than one heuristics are effective in decision-making processes of individuals and that these heuristics support and trigger each other.[10] Similar to this situation stated in the literature, in this study, it was concluded that more than one

Table 3. The number and percentages of participants who have used relevant heuristics at least once

Heuristics	n			% (N=30)			Students
	Q1	Q2	Q3	Q1	Q2	Q3	
Associative activation	27	27	27	90.00	90.00	90.00	S1, S2, S3, S4, S5, S6, S7, S8, S10, S11, S13, S14, S15, S16, S17, S18, S19, S20, S21, S22, S23, S24, S25, S26, S27, S29, S30 (for questions 1,2 and 3)
Fluency	–	–	7	–	–	23.33	S2, S11, S14, S17, S21, S25, S30 (for question 3)
Attribute substitution	27	27	27	90.00	90.00	90.00	S1, S2, S3, S4, S5, S6, S7, S8, S10, S11, S13, S14, S15, S16, S17, S18, S19, S20, S21, S22, S23, S24, S25, S26, S27, S29, S30 (for questions 1,2 and 3)
One reason decision making	9	9	13	30.00	30.00	43.33	S1, S3, S5, S8, S10, S13, S18, S22, S24 (for questions 1 and 2); S3, S4, S5, S6, S7, S13, S16, S18, S20, S22, S23, S27, S29 (for question 3)
Surface similarity	4	9	7	13.33	30.00	23.33	S6, S11, S21, S30 (for question 1); S6, S11, S14, S20, S21, S25, S26, S29, S30 (for question 2); S1, S8, S10, S15, S19, S24, S26(for question 3)
Recognition	8	8	–	26.66	26.66	–	S11, S14, S20, S21, S25, S26, S29, S30 (for questions 1 and 2)
Generalization	9	13	11	30.00	43.33	36.66	S2, S4, S7, S11, S16, S17, S21, S23, S30 (for question 1); S2, S4, S7, S11, S16, S17, S20, S21, S23, S25, S26, S29, S30 (for question 2); S2, S4, S7, S11, S14, S16, S17, S21, S23, S25, S30 (for question 3)
Rigidity	3	3	3	10.00	10.00	10.00	S15, S19, S22 (for questions 1,2 and 3)
Overconfidence	4	4	4	13.33	13.33	13.33	S9, S19, S27, S29 (for questions 1,2 and 3)
Affect	4	4	4	13.33	13.33	13.33	S1, S8, S9, S23 S29 (for questions 1, 2 and 3)
Periodic trends	4	4	4	13.33	13.33	13.33	S2, S7, S17, S25 (for questions 1,2 and 3)

heuristics were effective at the same time. The reasoning of one of the students (S10) for the first question can be given as an exemplary.

Q10: *For me, the correct order is as follows: HCl <NaCl <HI <NaI*

Interviewer: *Could you explain the strategy you used to answer the question?*

S10: *Boiling points are related to the molecular weight of the compounds. Compounds with large molecular weights have high boiling points. Therefore, the ranking I made according to increasing molecular weights is also valid for boiling points.*

It is reported in the literature that individuals frequently use one of the flat or inverse proportion approaches that can be summarized as "the more A – the more B" or "the more A – the less B" in cases where associative activation heuristic is effective.[10] From the statements of the S10 coded student, it is understood that the heuristics of associative activation and attribute substitution triggered and support each other in the process of problem solving. S10 coded student used the straight-proportion approach in the form of "the greater the molecular weight, the higher the boiling point" to solve the problem. This approach, which can be summarized as "the more A – the more B", is the result of the influence of the associative activation heuristic. This student evaluated another attribute (molecular weights of compounds) instead of the target attribute. This student unconsciously replaced the original question with another, simpler question (which compound is heavier?). This situation is a result of the effect of attribute substitution heuristic. Table 2 collectively presents the mental structures used by the participants to solve the questions.

Individuals generally facilitate reasoning by using a single clue or factor to give a logical answer. In doing so, they use the first feature that comes to mind. Individuals' making decisions in this way is a consequence of the effect of one-reason decision-making heuristic.[10] The S10 coded student made a decision based on only one reason. S10 coded student only evaluated the molecular weight of the compounds in the decision-making process regarding the question. For this reason, the one-reason decision making heuristic was also effective in the decision-making process of the S10 coded student.

For a person who is new to any field, it is easier to examine obviously given properties than implicitly given properties. People tend to use easily accessible information when making judgments and decisions. The use of easily accessible cues by individuals to solve the problem is asso-

ciated with fluency heuristic.[10] The fluency heuristic is very often effective when there are explicit clues in the formulas or representations of molecules.[10] There are no parts in the compounds of HI, HCl, NaI, and NaCl that can be used by students as an easily accessible cue. For this reason, the heuristic of fluency did not affect the reasoning of the participants about this question. In the process of solving the second problem, no effect of fluency heuristic was found for the same reason. However, in the process of solving the third question (H_2Se, H_2S and PH_3 compounds), the effect of fluency heuristic was determined in the reasoning process of 7 (23.33%) of the participants. There are some parts in H_2Se, H_2S, and PH_3 compounds that can be used as easily accessible cues by students; while the number at the bottom of the hydrogen atom in the PH_3 molecule is 3, it is 2 in H_2Se and H_2S compounds. With the effect of fluency heuristic, some participants used this difference in numbers as a clue. The approaches of these participants were as follows: 1) "There are 3 hydrogens in the PH_3 molecule. The higher the hydrogen number in a molecule, the higher the acidity. Therefore, PH_3 is the strongest acid of these three compounds. The higher the acidity strength, the higher the boiling point. Therefore, PH_3 has the highest boiling point". 2) "PH_3 has 3 hydrogen atoms. The others are 2. The total number of atoms is higher in PH_3. Compounds with more total atoms have higher boiling points. Therefore, PH_3 has the highest boiling point. The reasoning of the S11 coded student in the process of solving the third question can be given as an exemplary reasoning process in which associative activation, attribute substitution and fluency heuristics are simultaneously effective;

Q11: *For me the correct order is: $H_2Se < H_2S < PH_3$*
Interviewer: Could you explain the strategy you used to answer the question?
S11: *As the acidity of a molecule increase, its boiling point also increases. Each of the H_2Se and H_2S molecules have two hydrogens, while the PH_3 molecule has three hydrogens. Because it has more hydrogen, PH_3 has more acidity than others. Therefore, PH_3 has the highest boiling point. Since the hydrogen numbers of H_2Se and H_2S are the same, the acidities of these two compounds are close to each other. That's why I thought I should evaluate another parameter. I evaluated the electronegativities of the S and Se atoms in the compounds to determine the boiling points of these two compounds. Generally, all properties of atoms with high electronegativity are also high. S atom is more electronegative than Se atom. Therefore, the boiling point of H_2S containing the S atom is higher than the boiling point of H_2Se containing the Se atom.*

From the statements of the S11 coded student, it is understood that the heuristics of associative activation, attribute substitution and fluency triggered and supported each other in the process of solving the question. S11 coded student used the straight-proportion approach, "The more acidity of the molecule, the higher its boiling point" to solve the problem. This approach, which can be summarized as "the more A – the more B", is the result of the influence of the associative activation heuristic. Similarly, the approach "The more electronegative the atom in the molecule and bound to hydrogen is, the higher its boiling point" is also related to the associative activation heuristic. Solving the question with this kind of reasoning, the student evaluated other attributes (the acidity of compounds and electronegativities of atoms) instead of the target attribute. This student also unconsciously replaced the original question with another, simpler questions such as "which compound is the more acidic?" and "which atom is more electronegative". This situation is a result of the effect of attribute substitution heuristic. The student coded S11 used the numbers at the bottom of the formulas of molecules as an easily accessible clue. Therefore, the fluency heuristic was also effective in the reasoning process of the S11 coded student.

The extra generalization of the patterns or rules that individuals have learned using the knowledge they have gained from a few events that they have previously experienced, without considering all the variables, is considered as an effect of the generalization heuristic.[10] S11 coded students' approaches such as "*Strong acids generally have high all other properties*" and " *Atoms with high electronegativity generally have high all other properties*" show that the generalization heuristic is also effective in the reasoning process of the student. Student expressions showing that generalization heuristic is effective are given in Table 2 collectively.

Recognized objects or events have a strong influence on the decisions people make. If one of more than one object is recognized and the others are not, the recognized object is given a higher value. The fact that individuals give more values to recognized objects or give less value to unrecognized objects is considered the effect of recognition heuristic.[10] NaCl and HCl compounds are compounds that students often hear and recognize know from lectures, from the laboratory or from daily life. In the process of solving the first and second questions involving these compounds, it was determined that some of the students (26.26%) valued NaCl or HCl more due to the effect of recognition heuristic. For example, this kind of effect of the recognition heuristic was observed on the reasoning of the participant with code S30 in the process of solving the first question.

Q30: *For me, the correct order is as follows: HI <HCl <NaI <NaCl*
Interviewer: *Could you explain the strategy you used to answer the question?*
Q30: *I know NaCl. It is table salt. I know it's solid. That's why I chose it as the one with the highest boiling point. NaI looks like NaCl. That's why NaI is probably also solid. I also know about HCl. The HCl is frequently mentioned in the lessons. It is also frequently used in chemistry laboratories. I know it is a liquid and a*

strong acid, as we use it many times in the lab. Strong acids generally have high all other properties. Therefore, its boiling point is also high. I have no information about HI. If it were strong acid, I would hear its name. It is probably a weaker acid than HCl. Therefore, its boiling point is lower than HCl.

The S30 student's statement that the NaCl compound, which s/he had previously known, is the compound with the highest boiling point among the compounds in the question is a result of the effect of recognition heuristic. The fact that S30 coded student gives less value to HI, which s/he did not know before, also shows that recognition heuristic is effective. The surface similarity heuristic was also effective in the reasoning process of the S30 student. The assumption that chemical compounds resembling each other in the structural representation are members of the same category and that such compounds have similar properties and behavior is a consequence of the effect of the surface similarity heuristic.[10] The student coded S30 thinks that the boiling point of the NaI compound is high because it resembles the NaCl compound. This situation is a result of the effect of surface similarity heuristic.

The reasoning of the S21 coded student in the process of solving the second problem can be given as another example in which the recognition and surface similarity heuristics are effective.

Q21: *For me, the correct order is: HBr <HCl <NaI <NaBr*

Interviewer: Could you explain the strategy you used to answer the question?

S21: *NaI and NaBr are ionic compounds. Their melting points are higher than others are. NaI and NaBr are similar to NaCl. I know NaCl. It is table salt and it is in solid form. It has a high melting point. Since they resemble NaCl, the melting points of NaI and NaBr compounds are also high. One of these two compounds has iodine and the other has bromine. In the periodic table, bromine is closer to chlorine. Therefore, when these two compounds are compared, the similarity of NaBr to NaCl is more. Since it is more similar to NaCl, the melting point of the NaBr is higher than that of NaI.*

Interviewer: *You said "the melting point of HCl is higher than HBr." Why is that?*

Q21: *I know HCl is a strong acid. I heard his name often in lectures. Strong acids generally have high all other properties. Therefore, the melting point of HCl is higher than the melting point of HBr.*

In this question about the melting point, the NaCl compound is not included. However, upon seeing the NaBr and NaI compounds in the question, the participant S21 came to mind the NaCl compound. This participant stated that he knew NaCl before and that its melting point is high. The participant mentioned also stated that NaBr and NaI compounds have high melting points due to their resemblance to NaCl. Participant with the code of S21 highly valued NaBr and NaI compounds because of the NaCl compound he knew before. Therefore, it can be said that recognition heuristic is effective in the reasoning process of the participant. In the reasoning process of the participant with the code of S21, the recognition heuristic and the surface similarity heuristic were dominantly effective. The student coded S21 thinks that NaBr and NaI compounds also have high melting points because they resemble NaCl. This situation is a result of the effect of surface similarity heuristic. H_2Se, H_2S and PH_3 in the third question are compounds that students do not know much. Therefore, the effect of recognition heuristic was not encountered in the process of solving the third question.

The affect heuristic was coded based on some important statements of the students with codes S1, S8 and S23. For S1, S8 and S23 coded students, the following are the expressions that form the basis for coding affect heuristic: "I hate verbal chemistry subjects", "I see myself closer to numerical logic", "I don't like dealing with abstract concepts and the relationships between them in chemistry lessons", "The issue of the relative ordering of compounds according to their melting/boiling points is the subject of verbal chemistry. Therefore, I do not like and are not interested in this topic". One of the participants (S9) stated that he liked the melting/boiling point topic and had a special interest in this subject. Based on this statement of the S9 coded student, the affect heuristic was coded for this student.

In this study, the procedure specified in the method section was followed to investigate the effects of rigidity heuristic. As a result of the operations performed according to the aforementioned procedure, it was concluded that the rigidity heuristic had an effect on the problem solving process of the students with codes S15, S19, and S22. The aforementioned students stated that no matter what the question was, they believed and trusted an approach to solving the question and that they would solve the question using this approach. The reasoning of the students in the process of solving the questions was examined carefully and it was determined that these students were not flexible in the process of solving the questions. The approaches that students have trusted are collectively given in Table 2.

In this study, the procedure described in the method section was followed to investigate the effects of overconfidence heuristic. As a result of the operations performed by following the mentioned procedure, it was concluded that the overconfidence heuristic was effective in solving the questions of the participants coded S9, S19, S27 and S29.

The heuristic of the periodic trends is not included in the ten heuristics proposed by Talanquer.[10] However, since it was determined in the study that the participants also used this heuristic, this heuristic was also taken into consideration. The heuristic of the periodic trends is also called arbitrary heuristic by some researchers. It is a result

of the effect of periodic trends heuristic to make evaluations such as only the feature increases or the feature decreases without knowing why the features change from left to right and from top to bottom in the periodic table. It has been determined that this heuristic is effective in the reasoning processes of all three problems of the students coded S2, S7, S17 and S25. The associative activation, generalization, and attribute substitution heuristics also played an active role in many of the reasoning in which periodic trends heuristic exhibited. These heuristics have triggered and supported each other.

Studies in the literature on melting and boiling points report that students have difficulties in explaining the factors affecting melting and boiling events, and students have various misconceptions about melting and boiling phenomena.[1–6] The misconceptions frequently identified in studies in the literature regarding melting and boiling points are as follows: "As the molecular weight of the compounds increases, their melting and boiling points increase", "As the branching of the molecule increases, the melting and boiling points increase", "The higher the number of bonds in the molecule, the higher the melting and boiling points", "The higher the melting and boiling points of the oxygen-containing molecules." [2,5] Similar to what is stated in the literature, in the present study, it was found that students often had difficulties in understanding structure-property relationships, could not make accurate predictions or rankings about the melting and boiling points of compounds due to these difficulties, and they generally rely on short-cut strategies instead of scientific reasoning. The fact that in-depth interviews were made with the participants in this study, whose main purpose was to examine the heuristic reasoning of the students, also enabled the detection of some misconceptions in the students. The misconception that "melting and boiling points increase as the molecular weight of the compounds increases" reported in the literature was also detected in this present study. In the present study, the following two misconceptions were also detected; "Compounds with high electronegativity have higher melting and boiling points", "Strong acids have higher melting and boiling points".

The fact that the participants used heuristics frequently caused the rate of students who gave correct answers to the questions to be low. Similar to the results of the present study, in many studies on students' reasoning in chemistry subjects, it was found that the accuracy rates of participant responses were generally low. For example, in two different studies on students' understanding of hydrogen bonding, the accuracy rates of participants' answers were found to be 27% and 16.66%. [38,39] The accuracy rate of the participants' answers was found to be 36% in a study on "chemical bond theories and molecular structures", and 31% in a study on addiction reactions topic. [23,35]

There is only one study in the literature investigating the effects of heuristics on the process of ranking compounds according to their melting and boiling points. [6] The questions asked to the participants in the study conducted by Maeyer and Talanquer [6] and the questions asked to the participants in the current study are the same. In the study conducted by Maeyer and Talanquer[6], it was determined that the heuristics of "recognition", "one-reason decision making", "periodic trends" and "representativeness" were effective in the reasoning processes of the participants. In the mentioned study, explanations and comments were made based on these four heuristics. In the present study, the reasoning of the participants was examined on the basis

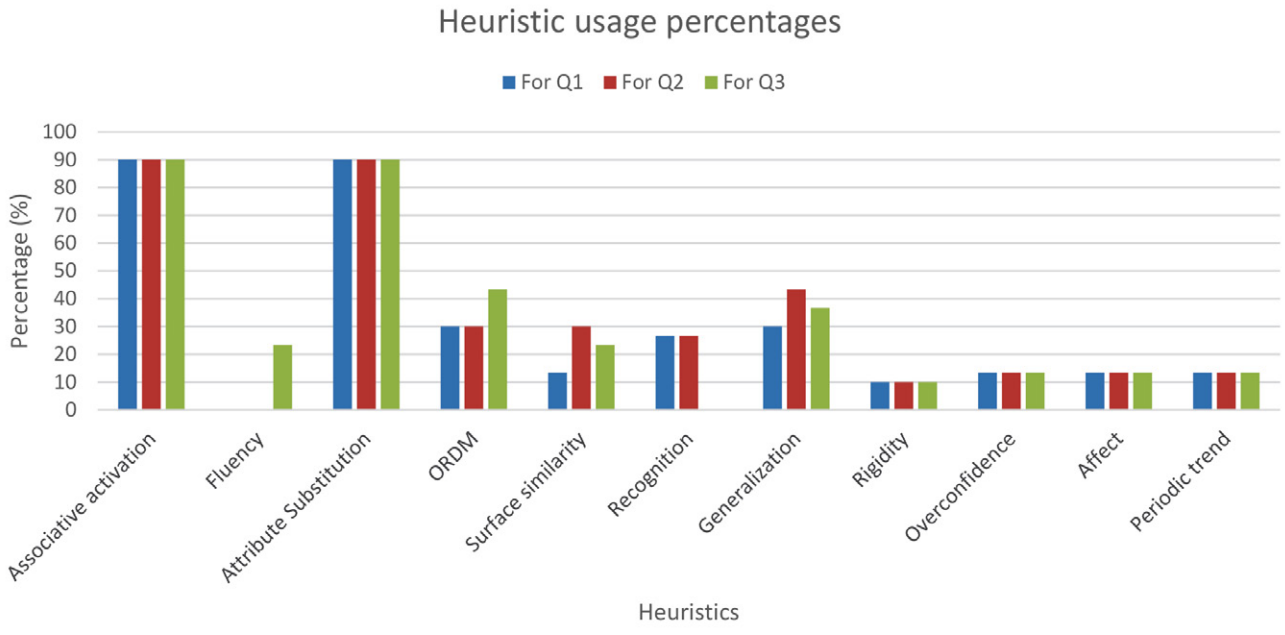

Figure 1. Graphical presentation of heuristic usage percentages.

of 10 heuristics. In order to present the results of the current research visually, the percentage of usage of the participants' heuristics is given as a graphical representation in Figure 1. Question 1, Question 2 and Question 3 are abbreviated as Q1, Q2 and Q3, respectively in Figure 1.

In the study conducted by Maeyer and Talanquer,[6] it was reported that the accuracy rates of student answers for the first, second and third questions were 5.90%, 8.80% and 20.60%, respectively. In this current study, in which students were asked to solve the same questions, the accuracy rates of student answers for the first, second and third questions were determined as 23.30%, 26.66% and 60.00%, respectively. Although the accuracy rates of student answers determined by the present study and the rates determined in the study conducted by Maeyer and Talanquer[6] were generally different, the accuracy rates of student answers were generally low in both studies. Only in the present study, the accuracy rate for the third question is partially high. However, the vast majority of students who answered the third question correctly in the present study answered the third question with an approach described as "the higher the molecular weight the higher the boiling point" rather than analytical reasoning. In the study conducted by Maeyer and Talanquer,[6] it was found that the percentages of participants who used one-reason decision-making, recognition and periodic trends heuristics in the process of solving the first problem were 70.60%, 52.90% and 14.70%, respectively. It was stated that these percentages were 82.40%, 26.50% and 11.80% respectively in the process of solving the second problem, and 73.50%, 14.70% and 44.10%, respectively, in the process of solving the third problem. In the present study, the percentages of participants using one-reason decision-making, recognition and periodic trends heuristics in the process of solving the first problem are 30.00%, 30.00% and 43.33%, respectively. During the solution of the second problem, these percentages were 26.66%, 26.66% and 0%, respectively, and in the process of solving the third problem, these percentages were determined to be 13.33%, 13.33% and 13.33%, respectively. The usage percentages of one-reason decision making, recognition and periodic trends heuristics determined in the study conducted by Maeyer and Talanquer[6] and the usage percentages determined in this present study are generally different. However, the explanations and determinations made in the present study regarding the action mechanisms of these three heuristics and the explanations and determinations made by Maeyer and Talanquer[6] are similar or the same.

This study revealed that pre-service science teachers rely on intuitive reasoning rather than analytical thinking when faced with questions about ranking compounds according to their melting and boiling points, and students frequently used heuristics. These heuristics reduced the cognitive effort in students and caused students to produce incorrect answers generally. Except for three studies on students' understanding of "hydrogen bonding" and "chemical structure – acidity/basicity relationship", the ten heuristic models proposed by Talanquer were not used in all other studies examining the effects of heuristics on chemistry subjects. With the current research carried out to fill this gap in the literature, the effects of all 10 heuristics proposed and defined by Talanquer on students' reasoning processes on the "melting and boiling points" were examined in detail.

4. Conclusions

The roles of all ten heuristics proposed by Talanquer in the process of ranking compounds according to their increasing melting and boiling points have been explored for the first time in this study. In this research, the melting and boiling point subject, which is a chemistry subject, has been evaluated and studied within the framework of a cognitive psychology theory. This study will make a significant contribution to the literature as it brings together different disciplines such as chemistry and cognitive psychology. The fact that heuristics have important roles in students' reasoning processes indicates that most students rely more on shortcut strategies rather than analytical reasoning. It is a known fact that cognitive constraints prevent scientific reasoning of individuals. The heuristics, whose working mechanisms are explained by this research, are typical examples of cognitive constraints that constrain students' scientific reasoning. The heuristics that the students had trusted, allowed them to make decisions without cognitive effort. However, due to these cognitive constraints, students' reasoning was often erroneous and students often gave incorrect answers. Knowing the students' thoughts and reasoning about melting and boiling points, as well as the role of heuristics in these processes, can help develop strategies that encourage meaningful learning about melting and boiling points. In order to develop measurement tools that will evaluate students' learning levels in chemistry subjects in a valid and reliable way, it is useful to examine students' reasoning strategies in detail. Therefore, this study may contribute to the development of measurement tools specific to the field of chemistry. For example, this study revealed that particular attention should be paid to the molecules or compounds involved in chemistry questions to be asked to students. In the first and second questions in this study, no effect of fluency heuristic was found, since there were no any explicit clue that the participants could easily obtain. However, an important effect of fluency heuristic was observed in the third question, as there was an explicit clue that the participants could easily obtain. In addition, the fact that the first and second questions included compounds such as NaCl or HCl that the students were recognized before caused the recognition heuristics to be used by some of the participants. Knowing these and similar situations and results will be useful for instructors who will prepare questions to evaluate students.

Forty percent of the students who had a high level of success in General Chemistry I/II courses answered the first question asked to them correctly in this study. For the second and third questions, these rates are 50% and 90%, respectively. 20% of the students who were intermediate level successful in the General Chemistry I/II courses correctly answered the first and second questions asked in this study. For the third question, this rate is 40%. Ten percent of the students who failed the General Chemistry I/II courses correctly answered the first and second questions asked in this study. For the third question, this ratio is 50%. These data show that students who are highly successful in general chemistry I/II courses have a higher rate of answering questions about melting and boiling points correctly than other students (who are unsuccessful or intermediate successful in general chemistry I/II courses). The percentage of students who answered the third question correctly is higher than the percentage of students who answered the first and second questions correctly. However, from the interview data analyzed in detail, it was determined that the majority of the students who answered the third question correctly answered the question without using scientific reasoning. It was determined that these students answered the third question using the approach of "the higher the molecular weight of a compound, the higher the boiling point", with the effect of associative activation heuristics. Regardless of their academic success in general chemistry courses, it is understood from a careful examination of Table 2 that heuristics are effective in the reasoning processes of the majority of students who answered the questions correctly or incorrectly.

As heuristic reasoning does not require cognitive effort and is fast and automatic, students often use it unconsciously. Developing effective and analytical reasoning skills instead of heuristic reasoning is a very time consuming and difficult process. Educating students in judgment and decision-making strategies can help students think effectively and analytically. Shortcut problem-solving strategies taught to students throughout their education life may have reduced students' tendency to use scientific reasoning skills. Thus, students may have acquired the habit of solving problems using shortcut strategies. Intuitive reasoning is one of the most commonly used types of reasoning. Therefore, it is important to investigate how intuitive judgment affects students' understanding and interpretation of chemistry topics. The data obtained from such research will be useful in creating successful reasoning and thinking methods specific to the field of chemistry. While teaching a chemistry subject to students, it can be very useful to explain to students the heuristic reasoning and the mechanisms of such reasoning that can make students mistake about that topic. It may be helpful to ask students to solve different types of chemistry problems in order to give students the habit of effective analytical and scientific reasoning instead of heuristic reasoning.

In this study, data were collected from a limited number of students enrolled in the Science Teaching Program of Firat University. As a necessity of the interview method, the fact that a small number of participants were interviewed is a limitation of this study. For this reason, we recommend that similar studies be carried out in different institutions. The participants who were interviewed within the scope of this study were determined on a voluntary basis and no reward was given to these participants for their time and effort. Another limitation of this study is the possibility that this situation negatively affects the students' motivation to spend time and their cognitive efforts to answer the questions. More studies are also needed on how System 2 processes can be activated more to correct biases caused by System 1 processes in different chemistry issues. In addition, it is beneficial to investigate the effects of various teaching strategies that will be planned to eliminate the negative effects of heuristics that affect chemistry subjects.

Conflicts of Interest

There are no conflicts of interest to declare.

Acknowledgements

The authors would like to thank the prospective teachers enrolled in the Science Education Program, Education Faculty throughout Firat University who participated in this research for being willing to share their experience. Gülen Önal Karakoyun and Erol Asiltürk contributed equally to this work. This study was prepared from the relevant parts of Gülen Önal Karakoyun's PhD thesis. ORCID numbers of authors: Gülen Önal Karakoyun; https://orcid.org/0000-0002-7675-0006; Erol Asiltürk; https://orcid.org/0000-0001-8126-7812.

5. References

1. M. M. Cooper, L. C. Williams, S. M. J. Underwood, *Chem. Educ.* **2015**, *92,* 1288. **DOI:**10.1021/acs.jchemed.5b00169
2. M. M. Cooper, L. M. Corley, S. M. Underwood, *J. Res. Sci. Teach.* **2013**, *50,* 699–721. **DOI:**10.1002/tea.21093
3. M. M. Cooper, S. M. Underwood, C. Z. Hilley, M.W. Klymkowsky, *J. Chem. Educ.* **2012,** *89*, 1351–1357. **DOI:**10.1021/ed300083a
4. V. Barker, R. Millar, *Int J. Sci. Educ.* **2000**, *22,* 1172–1200. **DOI:**10.1080/09500690050166742
5. H. J Schmidt, B. Kaufmann, D. F. Treagust, *Chem. Educ. Res. Pract.* **2009,** *10,* 265–272. **DOI:**10.1039/B920829C
6. J. Maeyer, V. Talanquer, *Sci. Educ*. **2010**, *94*, 963–984. **DOI:**10.1002/sce.20397
7. G. Hatano, K. Inagaki, *Int. J. Behav. Dev*. **2000**, *24*, 267–275. **DOI:**10.1080/01650250050118240
8. F. C. Keil, *Cogn. Sci*. **1990**, 14, 135–168. **DOI:**10.1207/s15516709cog1401_7
9. H. M. Wellman, S. Gelman, In: D. Kuhn, R. Siegler (Eds.):

Cognition, perception and language. Handbook of child psychology, Wiley, New York, **1998**, pp. 523–573.
10. V. Talanquer, *J. Chem. Educ.* **2014***, 91,* 1091–1097. **DOI:**10.1021/ed4008765
11. J. Maeyer, V. Talanquer, *J. Res. Sci. Teach.* **2013***, 50,* 748–767. **DOI:**10.1002/tea.21092
12. E. S. Spelke, K. D. Kinzler, *Dev. Sci.* **2007**, *10*, 89–96. **DOI:**10.1111/j.1467-7687.2007.00569.x
13. R. Stavy, D. Tirosh, How students (mis-)understand science and mathematics: Intuitive rules. Columbia University, Teachers College Press, New York, **2000.**
14. S. Vosniadou, *Learn. Instr.* **1994**, *4*, 45–69. **DOI:**10.1016/0959-4752(94)90018-3
15. E. F. Redish, In E. F. Redish, M. Vicentini, (Eds.): Proceedings of the international school of physics, "Enrico Fermi" course CLVI, IOS Press, Amsterdam, **2004.**
16. M. T. H. Chi, In S. Vosniadou (Ed.), International Handbook of Research on Conceptual Change, Routledge, New York, **2008**, pp. 61–82.
17. A. Perfors, J. B. Tenenbaum, T.L. Griffiths, F. Xu, *Cognition*, **2011**, *120*, 302–321. **DOI:**10.1016/j.cognition.2010.11.015
18. A. A. diSessa, *Cogn. Instr.* **1993**, *10*, 165–255. **DOI:**10.1207/s1532690xci1002&3_2
19. G. Gigerenzer, W. Gaissmaier, *Annu. Rev. Psychol.* **2011**, *62*, 451–482. **DOI:**10.1146/annurev-psych-120709-145346
20. S. A. Sloman, *Psychol. Bull.* **1996**, *119*, 3–22. **DOI:**10.1037/0033-2909.119.1.3
21. J. S. B. T. Evans, *Psychon. Bull. Rev.* **2006**, *13*, 378–395. **DOI:**10.3758/BF03193858
22. J. S. B. T. Evans, *Annu. Rev. Psychol.* **2008***, 59*, 255–278. **DOI:**10.1146/annurev.psych.59.103006.093629
23. M. Ugras, *J. Baltic Sci. Educ.* **2018***, 17*, 343–356. **DOI:**10.33225/jbse/18.17.356
24. K. E. Stanovich, *In The Robot's Rebellion: Finding Meaning in the Age of Darwin*, (Ed: K. E. Stanovich), Chicago: University of Chicago Press. **2004**, pp. 207–269. **DOI:**10.7208/chicago/9780226771199.001.0001
25. K. E. Stanovich, R. F. West, *Evolutionary versus instrumental goals: Hown evolutionary psychology misconceives human rationality Evolution and the psychology of thinking.* (Ed: D. Over.), Hove, England: Psychology Press. **2003**, pp. 171–230.
26. J. R. Maeyer, *Common-sense chemistry: the use of assumptions and heuristics in problem solving.* Ph. D. Thesis. Arizona: University of Arizona. **2013.**
27. K. E. Stanovich, R. F. West, *Behav. Brain Sci.* **2000***, 23*, 645–726. **DOI:**10.1017/S0140525X00003435
28. D. Kahneman, S. Frederick, Representativeness Revisited: Attribute Substitution in Intuitive Judgment. Cambridge University Press, Cambridge, **2002.** **DOI:**10.1017/CBO9780511808098.004
29. L. K. McClary, V. Talanquer, *Int. J. Sci. Educ.* **2011***, 33,* 1433–1454. **DOI:**10.1080/09500693.2010.528463
30. N. Graulich, *J. Chem. Educ.* **2014***, 92,* 205–211. **DOI:**10.1021/ed500641n
31. A. K. Shah, D. M. Oppenheimer, *Psychol. Bull.* **2008**, *134*, 207–222. **DOI:**10.1037/0033-2909.134.2.207
32. H. A. Simon, *Annu. Rev. Psychol.* **1990**, *41*, 1–19. **DOI:**10.1146/annurev.ps.41.020190.000245
33. P. M. Todd, G. Gigerenzer, *Behav. Brain Sci.* **2000***, 23*, 727–741. **DOI:**10.1017/S0140525X00003447
34. C. K. Morewedge, D. Kahneman, *Trends Cogn Sci.* **2010**, *14*, 435–440. **DOI:**10.1016/j.tics.2010.07.004
35. N. Graulich, H. Hopf, P. R. Schreiner, *Chem. Eur. J.* **2011***, 17,* 30–40. **DOI:**10.1002/chem.201002370
36. N. Graulich, H. Hopf, P. R. Schreiner, *Chem. Asian J.* **2011***, 6,* 3180–3188. **DOI:**10.1002/asia.201100110
37. M. C. Connor, S. A. Finkenstaedt-Quinn, G. V. Shultz, *Chem. Educ. Res. Pract.* **2019***, 20*, 522–541. **DOI:**10.1039/C9RP00033J
38. K. Miller, T. Kim, *Biochem. Mol. Biol. Educ.* **2017**, *45*, 411–416. **DOI:**10.1002/bmb.21061
39. G. O. Karakoyun, E. Asiltürk, *J. Sci Lear.* **2020**, *4*, 50–60. **DOI:**10.17509/jsl.v4i1.23737
40. G. O. Karakoyun, E. Asiltürk, *Acta Chim. Slov*. **2021**, *68*, (In Press). **DOI:**10.17344/acsi.2021.6666

Povzetek

Namen raziskave je bil proučiti učinke hevristike na procese sklepanja kandidatov za učitelje naravoslovja na temo tališča in vrelišča z uporabo desetih hevurističnih modelov, ki jih je predlagal Talanquer. V tej fenomenografski raziskavi, opravljeni v spomladanskem semestru študijskega leta 2018/19, so bili opravljeni razgovori s 30 bodočimi učitelji, ki so bili vpisani v program za izobraževanje na področju naravoslovja Fakultete za izobraževanje Univerze Firat. Udeleženci so morali med intervjuji odgovoriti na tri različna vprašanja. Vprašanja so se nanašala na razvrstitev nekaterih spojin glede na njihovo tališče ali vrelišče. Iz odgovorov smo dobili šest različnih vzorcev odgovorov za vsako vprašanje. Ugotovitve te študije so pokazale, da so študentje na splošno uporabljali strategije bližnjic namesto analitičnega/znanstvenega sklepanja, saj je vseh deset hevristik vplivalo na razmišljanje udeležencev. Ta študija je tudi pokazala, da čeprav hevristični periodični trendi niso vključeni v model, ki ga je predlagal Talanquer, so vplivali tudi na razmišljanje udeležencev o tališču in vrelišču.

Except when otherwise noted, articles in this journal are published under the terms and conditions of the Creative Commons Attribution 4.0 International License

Scientific paper

Synthesis of the New 1-(7-Methoxy-1-benzofuran-2-yl)-3-(4-methylphenyl)prop-2-en-1-one and Controlling of Spectroscopic, Optical and Conductivity Properties by Concentration

Demet Coskun,[1,*] Mehmet Fatih Coskun[1] and Bayram Gunduz[2]

[1] *Firat University, Department of Chemistry, 23200 Elâzığ, Turkey.*

[2] *Turgut Ozal University, Department of Engineering Basic Sciences, 44210 Malatya, Turkey.*

* *Corresponding author: E-mail: dcoskun@firat.edu.tr*

Received: 06-04-2021

Abstract

Chalcone derivatives have an important place in science due to their different applications ranging from their semiconductor properties to biological properties. In this work 1-(7-methoxy-1-benzofuran-2-yl)-3-(4-methylphenyl)prop-2-en-1-one (**2**) has been prepared by condensation of 1-(7-methoxy-1-benzofuran-2-yl)ethanone with 4-methylbenzaldehyde in basic medium. The chemical structure of **2** was confirmed by elemental analysis, FT-IR, ^{1}H NMR and ^{13}C NMR. UV spectroscopic characteristics, absorption band edges, optical band gaps, refractive indices, environmental behaviors and conductivity properties of **2** in solutions at different concentrations were investigated in detail. With the concentration, we examined how the spectroscopic, optical and conductivity properties of **2** have changed and can be controlled.

Keywords: Benzofuran; chalcone; absorption band edge; optical band gap; refractive index; environmental behavior; conductivity properties.

1. Introduction

Benzofurans and their derivatives are used in the science of materials due to their significant fluorescence, absorption and quantum values,[1] electrochemical behavior, thermal stability,[2] blue-light emitting,[3] layered organic light-emitting diodes (OLEDs)[4] and organic electroluminescence (OEL)[5] properties. Studies in recent years have indicated that benzofuran and its derivatives are good for electron transport and as perforated injection materials.[6] Benzofurans exhibit significant optical properties due to the possibility of $\pi \rightarrow \pi^*$ transitions.[7] They also belong in the semiconductor class. This is due to delocalization and intermolecular charge transfer.[8–10] Conjugated organic molecules are very important in the second harmonic production due to their many delocalized π-electrons and provide easy charge transfer to the first order polarization (β) nonlinear optical (NLO) applications.[11,12] Chalcones are a class of flavonoids with significant biological activity.[13–15] Chalcones are also important because of their optical applications such as second harmonic generating materials in nonlinear optics and their photophysical properties,[16–19] holographic recording materials,[20] fluorescent probes for sensing of metal ions,[21] photo refractive polymers,[22] and micro environment in micelles.[23] The simplest chalcone structure is formed by two benzene rings that are connected by α,α-conjugated enol-keto groups.[24] Conjugated double bonds between aromatic rings are responsible for nonlinear optical properties.[25] The spectroscopic and photophysical properties of chalcone compounds can be easily changed by conjugation. Many researchers have revealed different types of transmitter and receiver groups to increase nonlinear optical coefficients. In recent years, chalcone compounds containing phenyl groups have been reported to be important materials to create a donor-accepting regulation for high SHG.[26] Therefore, it is important to study the NLO properties and molecular structures of new chalcone derivatives. Previously, benzofuran-substituted chalcones in which the electron releasing groups are attached to the phenyl ring showed improved electro-optical properties. For this reason, in this study, we have selected benzofuran-substituted chalcone derivative **2** comprising of meth-

yl group. New chalcone derivative **2** was prepared using the reaction of 1-(7-methoxy-1-benzofuran-2-yl)ethanone with 4-methylbenzaldehyde in methanolic NaOH.

The aim of this study is to examine the effect of concentration on the spectroscopic, optical and conductivity properties and to investigate the important parameters for material science with device performance of compound **2**. These aims were accomplished with great success in this study.

2. Experimental

All chemicals for the synthesis of compound **2** were of analytical grade and were purchased from commercial sources. They were used without purification. Reactions were monitored by thin layer chromatography (TLC) using silica gel 60 plates. Büchi RE 11 rotary evaporator was used for solvent evaporation. A differential scanning calorimeter (Shimadzu DSC-50) was used for melting point measurement. A Leco CHNS-932 device was used for element analysis. NMR spectra were obtained by a Bruker AC 400 (400 MHz for ^{1}H NMR and 100 MHz for ^{13}C NMR) in deuterated dimethylsulfoxide (DMSO-d_6) at 25 °C. Chemical shift values were recorded in parts per million (ppm). FT-Infrared (FT-IR) spectrum was recorded as KBr pellet on a Perkin-Elmer Spectrum One FTIR spectrometer. 1-(7-methoxy-1-benzofuran-2-yl)ethanone (**1**) was synthesized as described before.[27]

General Procedure for Synthesis of Chalcone 2

4-Methylbenzaldehyde (1 mmol) and 1-(7-methoxy-1-benzofuran-2-yl)ethanone (1 mmol) in MeOH (5 mL) were cooled to 0–5 °C, added and mixed. Then 3 mL of aqueous NaOH (1 mol/L) was added and stirred for 3 hours at room temperature. The solution was poured onto the water-ice mixture and precipitated solid was filtered, washed with dilute HCl and water, dried and crystallized from ethanol.

1-(7-Methoxy-1-benzofuran-2-yl)-3-(4-methylphenyl) prop-2-en-1-one (2)

Yield: 80%, m.p. 103–104 °C. IR (KBr) ν_{max} 3140–3001 (arom. C-H), 2966–2842 (aliph. C–H), 1653 (C=O), 1593 (C=C) cm^{-1}. ^{1}H NMR (400 MHz, DMSO-d_6) δ 8.29 (s, 1H, 3-H), 7.81–7.79 (m, 4H, α,β-H, 12,14-H), 7.41 (d, J = 8.0 Hz, 1H, 4-H), 7.33–7.29 (m, 3H, 11,15-H, 5-H), 7.15 (d, J = 8.0 Hz, 1H, 6-H), 3.98 (s, 3H, OCH_3), 2.36 (s, 3H, R_2=CH_3). ^{13}C NMR (400 MHz, DMSO-d_6) δ 178.94, 153.77, 145.95, 145.27, 144.08, 141.66, 132.09, 131.07, 130.21, 129.52, 125.37, 121.19, 115.74, 115.58, 110.61, 56.36, 21.61. Anal. calcd. for $C_{19}H_{16}O_3$: C, 78.08; H, 5.48. Found: C, 78.10; H, 5.45.

Optical Measurements of Compound 2 Solutions

The solutions of the compound **2** in the chloroform solvent for 6.0, 4.0, 0.7 and 0.2 mM concentrations were precisely prepared. By using a digital vortex mixer (Four E's Scientific CO., Ltd.) the compound **2** was also better dissolved in chloroform. This process is very important in the solution technique for the most sensitive and accurate optical measurements. We recorded the optical measurements of the compound **2** solutions for selected concentrations with an UV-1800 Spectrophotometer (Shimadzu model) at room temperature.

3. Results and Discussion

3. 1. Synthesis and Characterization

First, 1-(7-methoxy-1-benzofuran-2-yl)ethanone was synthesized by the reaction of 1-chloroacetone and

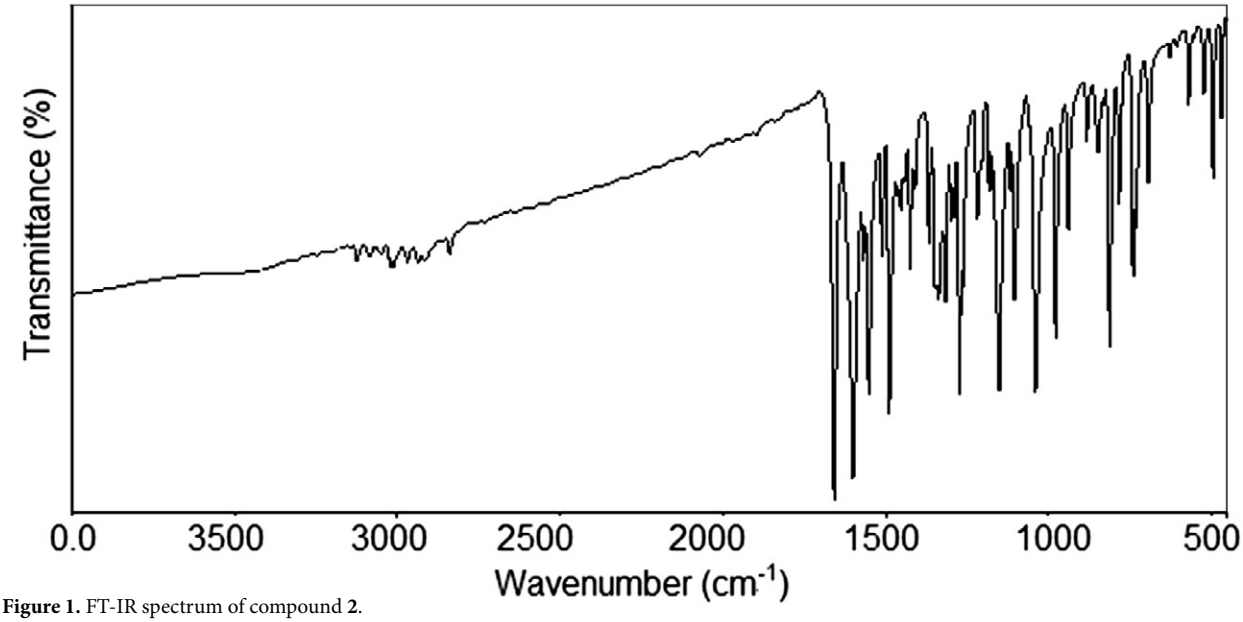

Figure 1. FT-IR spectrum of compound **2**.

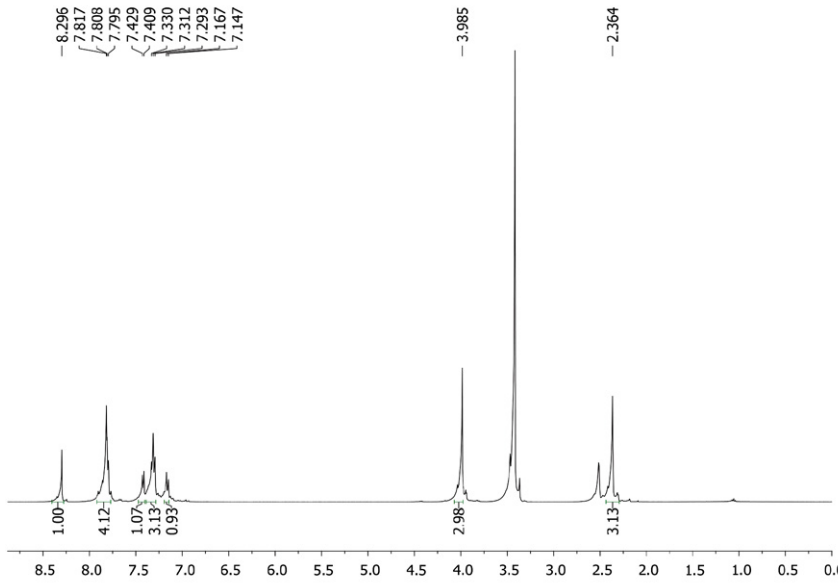

Figure 2. ^{1}H NMR (DMSO-d_6) spectrum of compound **2**.

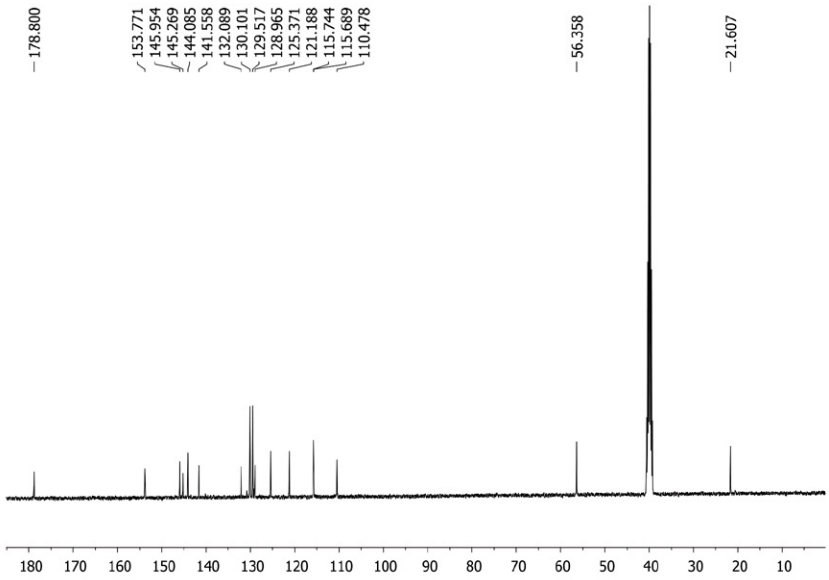

Figure 3. ^{13}C NMR (DMSO-d_6) spectrum of compound **2**.

3-methoxysalicylaldehyde.[27] Benzofuran-substituted chalcone derivative **2** was synthesized as shown in Figure 4. The most common method used for the synthesis of chalcones is the base-catalyzed Claisen–Schmidt reaction, which includes a condensation of a benzaldehyde derivative with an acetophenone derivative in ethanol or methanol with NaOH catalyst. For the characterization of **2**, FTIR, elemental analysis and NMR spectroscopy techniques were used.

In the FT-IR spectrum C=O stretching vibration of 1-(7-methoxy-1-benzofuran-2-yl)ethanol was observed at 1664 cm^{-1}. Also, C=O stretching vibration in chalcone structure was observed at 1653 cm^{-1}. The reason for the shifting of the C=O tensile vibration of chalcone to low wave numbers is the delocalization of π-electrons between the α and β carbons. This reduces the order of C=O bonds. After all, it increases the order of bonding between carbonyl carbon and a carbon atom. Another characteristic peak of the chalcone compound is the C=C stretching vibration at 1593 cm^{-1}. The most characteristic signals in ^{1}H NMR spectrum of the benzofuran-substituted chalcone was observed at 8.29 ppm (3-H belonging to the benzofuran ring) and at 7.81–7.79 ppm (α and β hydrogens of chalcone moiety) with a coupling constants about 15 Hz which characterizes the *trans* configuration. The β-H signal is in a lower area than α-H due to the resonance of π-electrons

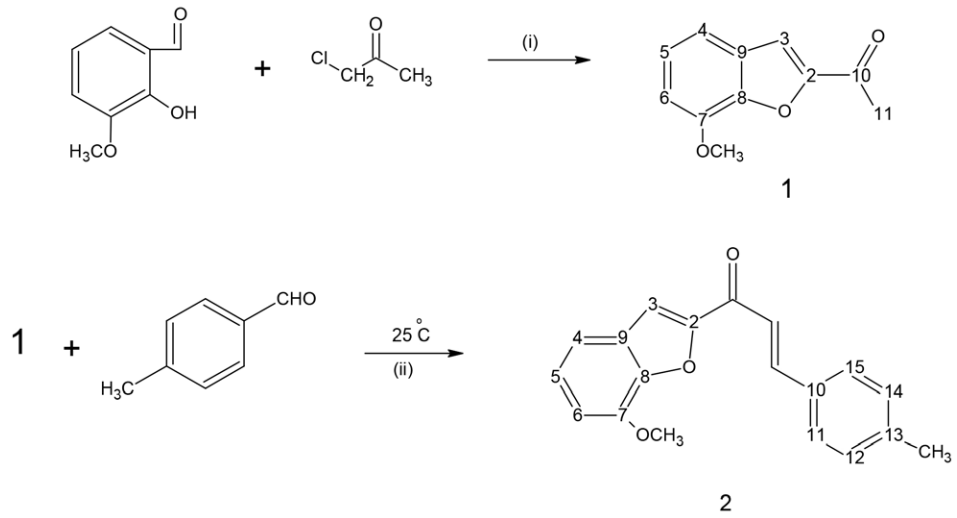

Figure 4. General synthesis of compounds **1** and **2**. Reagants and conditions: (i) K_2CO_3, acetone, reflux; (ii) NaOH, MeOH, r.t.

between α and β carbons with carbonyl group. In the ^{13}C NMR spectrum, carbonyl carbon was observed at about 178 ppm. The spectra FT-IR, ^1H NMR and ^{13}C NMR are given in Figures 1–3.

3. 2. UV Spectroscopic Characteristics and Absorption Band Edges of Compound 2 Solutions

Absorbance (A) is the amount of light absorbed by a solution (a sample). In other words, absorbance is a process of light that interacts with matter. Traditionally, absorbance measurements are carried out in a cuvette. We obtained UV spectra of the compound **2** solutions for 6.0, 4.0, 0.7 and 0.2 mM concentrations. Figure 5 shows the absorbance spectra of the compound **2** solutions at different concentrations. At higher molarities, it is normal that the absorbance curves do not appear completely. All absorbance curves of solutions below a certain concentration can be observed. As seen in Figure 5, all absorption curves are observed for 0.7 and 0.2 mM solutions. The maximum absorbance peak for 0.7 and 0.2 mM is observed at 347 and 345 nm, respectively. The compound **2** has a single peak and its absorbance decreases as the concentration is reduced.

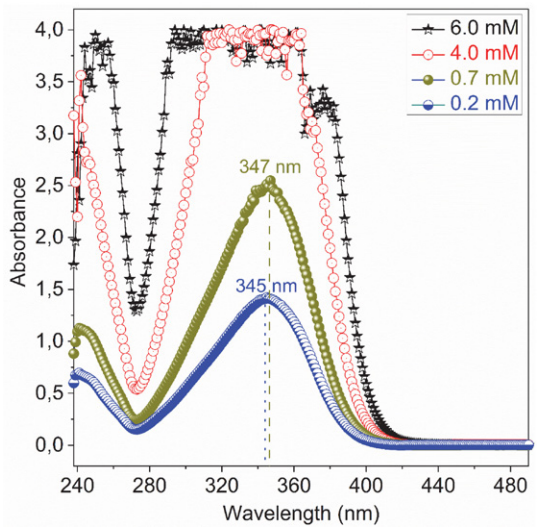

Figure 5. The absorbance spectra of the compound **2** solutions at 6.0, 4.0, 0.7 and 0.2 mM concentrations.

Transmittance (T) is defined as light passing through an object that is not reflected or absorbed. It is relatively easy to determine the permeability levels of an object. Transmittance is the transmitted part of the incoming light. The transmittance spectra of the compound **2** solutions at 6.0, 4.0, 0.7 and 0.2 mM are shown in Figure 6a. As can be seen in Figure 6a, all transmittance curves displays a peak at 273 nm and increase sharply in the range of about 350–420 nm. Transmittance increases with decreased concentration.

When examining the UV spectroscopic properties of a material, it is important to consider the absorbance band edge (E_{Abe}) of the material. Because this parameter is a specific parameter of any material, it gives very important information about the absorption and the behavior of the material in the environment. Therefore, we investigated the absorbance band edges of the compound **2** for different concentrations and we obtained the E_{Abe} values from the maximum peaks using the $dT/d\lambda$ curves vs. wavelength (λ) as seen in Figure 6b. While the concentration increased from 0.2 to 6.0 mM, the absorbance band edge of the compound **2** decreased from 3.002 to 2.877 eV. It is expected that the absorbance band edge decreases with increasing concentration as can be seen in the insert of Figure 6b. This result indicates that the absorbance band edge of the compound **2** can be controlled by concentration. Solutions with lower absorbance band edge are a desirable and preferred feature for metal-semiconductor based structures.

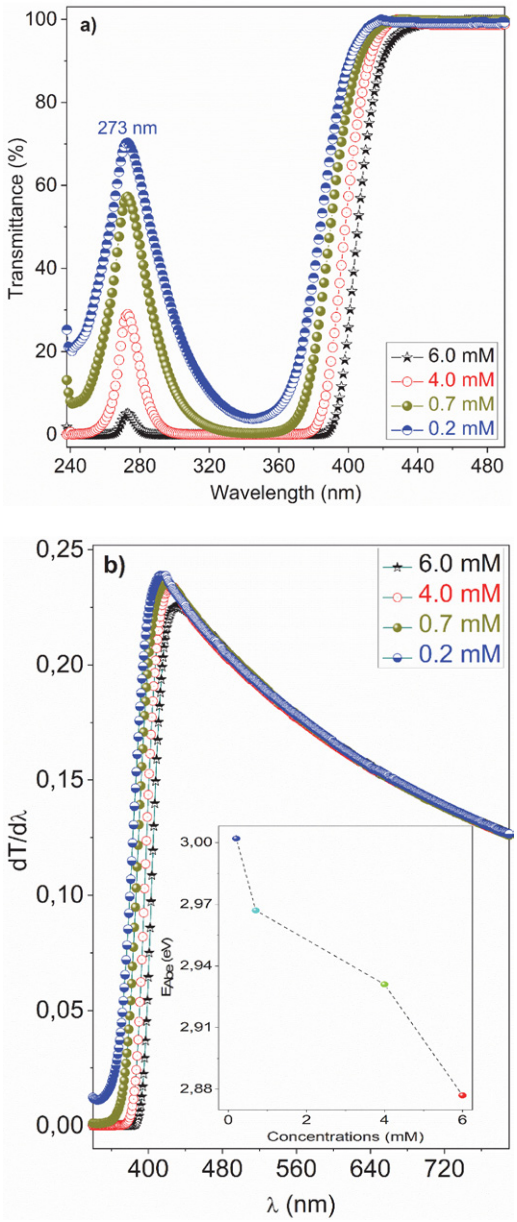

Figure 6. (a) Transmittance spectra and **(b)** d*T*/dλ curves vs. wavelength (λ) of the compound **2** solutions at 6.0, 4.0, 0.7 and 0.2 mM.

3. 3. Controlling of Optical Band Gap of Compound 2 Solutions

When it comes to optical properties, one of the first parameters that comes to mind is the optical band gap (E_g) parameter. This parameter is very important for the determination of material and device performance. The E_g can be estimated from the Tauc model[28] given by the following equation:

$$\alpha(h\vartheta) = A(E - E_g)^m \quad (1)$$

where α is absorption coefficient, $h\vartheta$ and E are the photon energy, A is a constant and m determines the type of the optical transitions. We found m as ½, which corresponds to allowed direct optical band gap (E_{gd}). Therefore, the $(\alpha h\vartheta)^2$ curves vs. E of the compound **2** solutions at 6.0, 4.0, 0.7 and 0.2 mM are plotted as seen in Figure 7a. By extrapolating the linear plot to $(\alpha h\vartheta)^2 = 0$, the E_{gd} values of the compound **2** at different concentrations were obtained. As seen in Figure 7b, the direct optical band gap of the compound **2** varies from 3.046 to 2.926 eV; that is, as the concentration increases, the optical band gap decreases. Materials with the lowest optical band gap are preferred for many electronic, optical and photonic devices, because the lowest band gaps weaken the mobility barrier of the carrier.

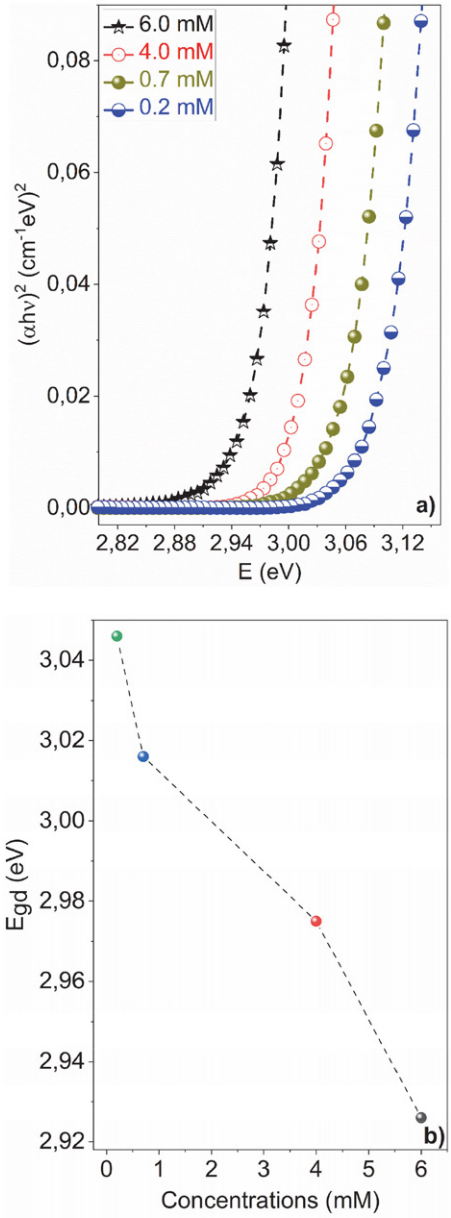

Figure 7. (a) $(\alpha h\vartheta)^2$ curves vs. E; **(b)** E_{gd} curves vs. concentrations of the compound **2** solutions.

3. 4. Controlling of Refractive Index of Compound 2 Solutions

Another parameter that comes to mind when talking about optical properties is the refractive index (n). The refractive index is a measure of the bending of a ray of light as it passes from one medium to another. The n can be explained with reflectance (R) and is calculated from following equation:[29,30]

$$n = \left\{ \sqrt{\frac{4R}{(R-1)^2} - k^2} - \frac{R+1}{R-1} \right\} \quad (2)$$

where $k = \alpha \lambda / 4\pi$. The refractive indices of the compound **2** solutions at 6.0, 4.0, 0.7 and 0.2 mM were calculated from Equation 2. The n curves of the compound **2** solutions for different concentrations are shown in Figure 8a. As seen in Figure 8a, the refractive index increases with increasing angular frequency (ω). This behavior is known as normal dispersion behavior. In addition, it is observed that the index of refraction increases with the increasing concentration. This indicates that the refractive index can vary and can be controlled with different concentrations.

There are many relations such as Herve–Vandamme, Kumar–Singh, Moss, Ravindra and Reddy[31,32] describing how to obtain the refractive indices based on optical band gaps. The refractive indices of the compound **2** solutions at 6.0, 4.0, 0.7 and 0.2 mM were obtained. The n curves vs. concentrations of the compound **2** for related relations are shown in Figure 8b. The refractive indices obtained from Reddy relation are the highest, while the refractive indices obtained from Ravindra relation are the lowest. Also, the index of refraction increases with increasing concentration for all correlations as seen in Figure 8b.

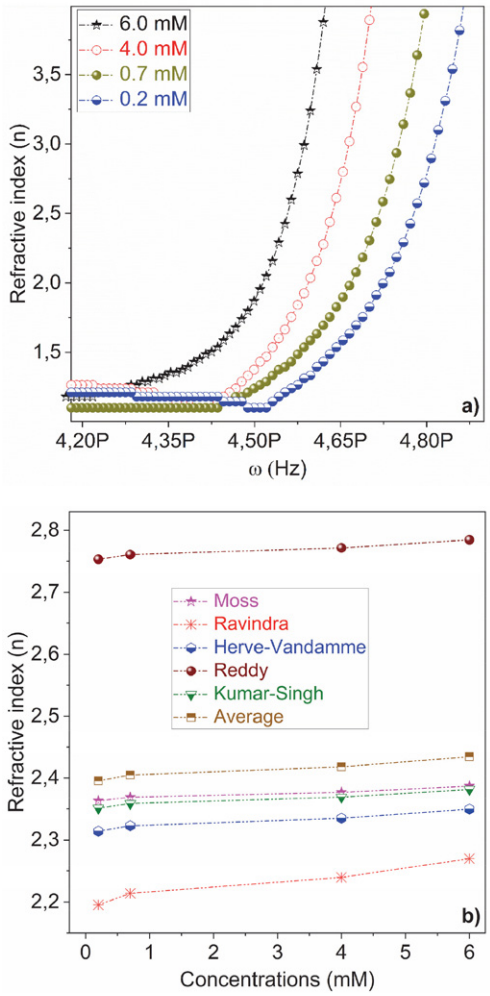

Figure 8. (a) n curves vs. angular frequency (ω); **(b)** n curves vs. concentrations of the compound **2** solutions.

3. 5. Environmental Behavior of Compound 2 Solutions

The behavior of a material in different environments, in other words, its interaction with light, is very important for the science of materials and devices. Incidence angle (Φ_1) and refraction angle (Φ_2) play an important role in investigating the behavior of the material in an environment. The Φ_1 is given by the following equation:[29,33]

$$\Phi_1 = tan^{-1}\left(\frac{n_2}{n_1}\right) \quad (3)$$

We calculated the incidence angle of the compound **2** solutions at 6.0, 4.0, 0.7 and 0.2 mM from Equation 3. The Φ_1 plots vs. E of the compound **2** for related concentrations are shown in Figure 9. These curves give the variation of the angle of incidence of the compound **2** according to the wavelength. In other words, it shows at which wavelengths the angles of incidence are decreasing and increasing. Also, as concentration increases, angles of incidence also increase. The Φ_2 is given by the equation:

$$\Phi_2 = sin^{-1}\left(\frac{n_1}{n_2}\sin\Phi_1\right) \quad (4)$$

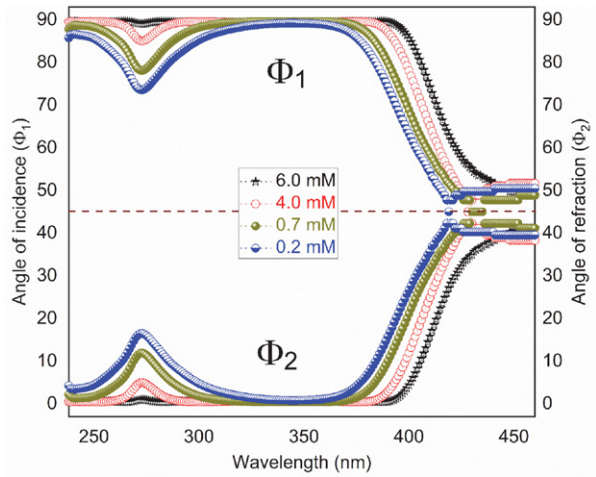

Figure 9. The incidence angle (Φ_1) and refraction angle (Φ_2) plots vs. E of the compound **2** at various concentrations.

The refraction angles of the compound **2** solutions at 6.0, 4.0, 0.7 and 0.2 mM were calculated from Equation 4. Figure 9 indicates the Φ_2 plots vs. *E* of the compound **2** for these concentrations. As expected, the angles of refraction are smaller than the angles of incidence. The angle of refraction varies with varying wavelengths. On the other hand, as the concentration increases, the angle of refraction decreases.

3. 6. Conductivity Properties of Compound 2 Solutions

Conductivity plays an important role in materials science and device performance. Optical and electrical components of conductivity make a great contribution to electronic and optical applications. The optical conductance (σ_{opt}) and electrical conductance (σ_{elec}) properties can be explained by the following equations,[34] respectively:

$$\sigma_{opt} = \frac{\alpha n c}{4\pi} \quad (5)$$

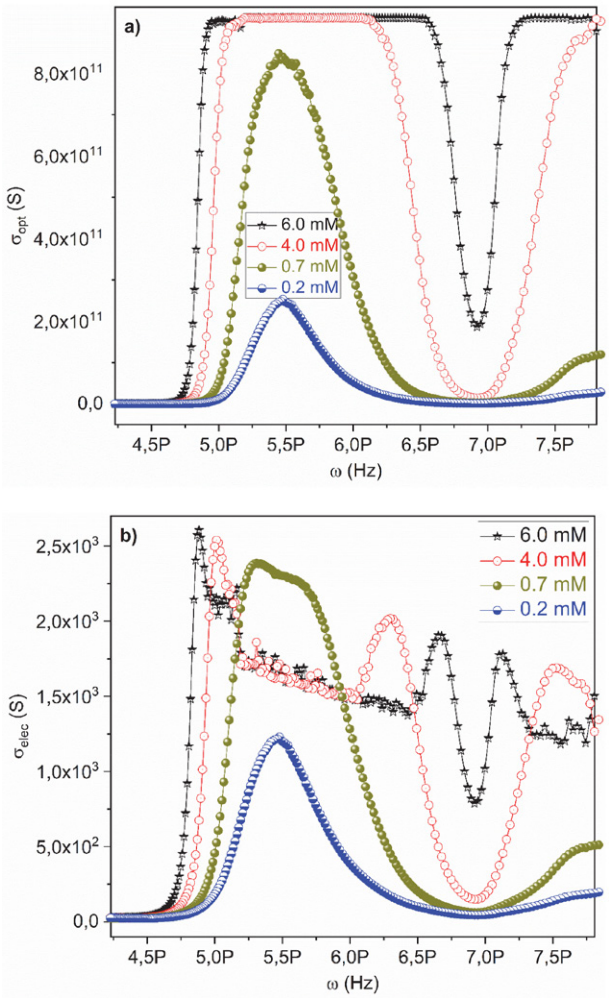

Figure 10. (a) σ_{opt} and **(b)** σ_{elec} curves vs. ω of the compound **2** solutions at 6.0, 4.0, 0.7 and 0.2 mM.

where *c* is the velocity of light. σ_{elec} is given as:

$$\sigma_{elec} = \frac{2\lambda\sigma_{opt}}{\alpha} \quad (6)$$

The σ_{opt} and σ_{elec} values of solutions of the compound **2** at 6.0, 4.0, 0.7 and 0.2 mM were calculated from Equations 5 and 6, respectively. The optical and electrical conductance curves vs. ω are shown in Figure 10a,b, respectively. As seen in Figure 10a, the compound **2** displays peaks at about 5.5 PHz at low concentrations, while the compound **2** displays pits at about 6.9 PHz at higher concentrations. The optical conductance values are of the order of 10^{11} S. On the other hand, the electrical conductance values are order of 10^3 S. As can be seen, both optical conductivity and electrical conductivity vary significantly with varying concentration and angular frequency.

4. Conclusions

We examined the effect of concentration on the spectroscopic, optical and conductivity properties and investigated the important parameters of the compound **2** for material science and device performance. The absorbance band edge of the compound **2** decreased from 3.002 to 2.877 eV, while the direct optical band gap of the compound **2** varies from 3.046 to 2.926 eV. The refractive index can vary and can be controlled by changing concentrations. Both, optical conductivity and electrical conductivity vary significantly with varying concentration and angular frequency. According to the data obtained, the compound **2** possesses promising properties for semiconductor and conjugated polymer technology and applications.

Acknowledgements

The authors thank Firat University for financial support of this work.

5. References

1. J.-X. Yang, X.-L. Wang, Tusong, L.-H. Xu, *Dyes Pigm.* **2005**, *67*, 27–33. **DOI:**10.1016/j.dyepig.2004.09.017
2. J. K. Xu, G. M. Nie, S. S. Zhang, X. J. Han, S. Z. Pu, L. Shen, Q. Xiao, *Eur. Polym. J.* **2005**, *41*, 1654–1661. **DOI:**10.1016/j.eurpolymj.2005.01.014
3. A. R. Hwu, K. S. Chuang, S. H. Chuang, S. C. Tsay, *Org. Lett.* **2005**, *7*, 1545–1548. **DOI:**10.1021/ol050196d
4. H. Tsuji, C. Mitsui, L. Ilies, Y. Sato, B. Nakamura, *J. Am. Chem. Soc.*, **2007**, *129*, 11902–11903. **DOI:**10.1021/ja074365w
5. S. Anderson, P. N. Taylor, G. L. B. Verschoor, *Chem. Eur. J.* **2004**, *10*, 518–527. **DOI:**10.1002/chem.200305284
6. S. Glenis, M. Benz, E. Legoff, J. L. Schindler, C. R. Kannewurf,

M. G. Kanatzidis, *J. Am. Chem. Soc*. **1993**, *115*, 12519–12525. **DOI:**10.1021/ja00079a035
7. Y. Y. Li, A. M. Ren, J. K. Feng, L. Yang, C. C. Sun, *Opt. Mater*. **2007**, *29*, 1571–1578. **DOI:**10.1016/j.optmat.2006.05.012
8. T. A. Fayed, *Chem. Phys*. **2006**, *324*, 631–638. **DOI:**10.1016/j.chemphys.2005.11.039
9. E. Sucre-Rosales, R. Fernández-Terán, N. Urdaneta, I. E. Hernández, L. Echevarria, *Chem. Phys*. **2020**, *537*, 110854. **DOI:**10.1016/j.chemphys.2020.110854
10. M. Koca, F. Dagdelen, Y. Aydogdu, *Mater. Lett*. **2004**, *58*, 2901–2905. **DOI:**10.1016/j.matlet.2004.05.016
11. M. Shkir, S. Muhammad, S. AlFaify, A. Irfan, P. S. Patil, M. Arora, H. Algarni, J. P. Zhang, *RSC Adv*. **2015**, *5*, 87320–87332. **DOI:**10.1039/C5RA13494C
12. C. Valverde, S. A. D. E. Castro, G. R. Vaz, J. L. D. Ferreira, B. Baseia, F. A. P. Osorio, *Acta Chim. Slov.* **2018**, *65*, 739–749. **DOI:**10.17344/acsi.2018.4462
13. K. Kiran, M. Sarasija, B. A. Rao, V. Namratha, D. Ashok, A. S. Rao, *Russ. J. Gen. Chem*. **2001**, *89*, 1859–1866. **DOI:**10.1134/S1070363219090214
14. N. Yaylı, O. Üçüncü, E. Aydın, Y. Gök, A. Yaşar, C. Baltacı, N. Yıldırım, M. Küçük, *J. Photochem. Photobiol. A: Chem*. **2005**, *169*, 229–234. **DOI:**10.1016/j.jphotochem.2004.06.015
15. D. Coskun, M. Erkisa, E. Ulukaya, M. F. Coskun, F. Ari, *Eur. J. Med. Chem*. **2007**, *136*, 212–222. **DOI:**10.1016/j.ejmech.2017.05.017
16. N. I. Rtishchev, G. I. Nosova, N. A. Solovskaya, V. A. Luk'yashina, E. F. Galaktionova, V. V. Kudryavtsev, *Russ. J. Gen. Chem*. **2001**, *71*, 1272–1281. **DOI:**10.1023/A:1013237415295
17. J. Zyss, I. Ledoux, M. Bertault, E. Toupet, *Chem. Phys*. **1991**, *150*, 125–135. **DOI:**10.1016/0301-0104(91)90062-X
18. S. R. Maidur, J. R. Jahagirdar, P. S. Patil, T. S. Chai, C. K. Quah, *Opt. Mater*. **2018**, *75*, 580–594. **DOI:**10.1016/j.optmat.2017.11.008
19. P. S. Patil, M. Shkir, S. R. Maidur, S. AlFaify, M. Arora, S. V. Rao, H. Abbas, V. Ganesh, *Opt. Mater*. **2017**, *72*, 427–435. **DOI:**10.1016/j.optmat.2017.06.038
20. W. C. Li, S. P. Deng, Y. G. Liu, L. S. Yao, X. H. Lu, L. Xuan, *Acta Polym. Sini*. **2011**, *7*, 758–765. **DOI:**10.3724/SP.J.1105.2011.10223
21. K. Rurack, J. L. Bricks, G. Reck, R. Radeglia, U. Resch-Genger, *J. Phys. Chem. A*. **2000**, *104*, 3087–3109. **DOI:**10.1021/jp994269k
22. S. J. Sun, G. Schwarz, R. H. Kricheldorf, T. C. Chang, *J. Polym. Sci. A: Polym. Chem*. **1999**, *37*, 1125–1133. **DOI:**10.1002/(SICI)1099-0518(19990415)37:8<1125::AID-POLA9>3.0.CO;2-J
23. M. Shannigrahi, S. Bagchi, *Spectrochim. Acta Part A Mol. Biomol. Spect*. **2005**, *61*, 2131–2138. **DOI:**10.1016/j.saa.2004.08.012
24. L. Kamath, K. B. Manjunatha, S. Shettigar, G. Umesh, B. Narayana, S. Samshuddin, B. K. Sarojini, *Opt. Laser Tech*. **2014**, *56*, 425–429. **DOI:**10.1016/j.optlastec.2013.09.025
25. P. Günter: *Nonlinear Optical Effects and Materials*, Springer, Berlin, **2000**. **DOI:**10.1007/978-3-540-49713-4
26. B. Ganapayya, A. Jayarama, R. Sankolli, V. R. Hathwar, S. M. Dharmaprakash, *J. Mol. Struct*. **2012**, *1007*, 175–178. **DOI:**10.1016/j.molstruc.2011.10.042
27. D. Coskun, B. Gunduz, M. F. Coskun, *J. Mol. Struct*. **2019**, *1178*, 261–267. **DOI:**10.1016/j.molstruc.2018.10.043
28. J. Tauc, A. Menth, *J. Non-Cry. Solids*. **1972**, *8*, 569–585. **DOI:**10.1016/0022-3093(72)90194-9
29. B. Gündüz, *Poly. Bull*. **2015**, *72*, 3241–3267. **DOI:**10.1007/s00289-015-1464-7
30. B. Gündüz, *Opt. Mater*. **2013**, *36*, 425–436. **DOI:**10.1016/j.optmat.2013.10.005
31. S. K. Tripathy, *Opt. Mater*. **2015**, *46*, 240–246. **DOI:**10.1016/j.optmat.2015.04.026
32. M. Cabuk, B. Gündüz, *App. Surf. Sci*. **2017**, *424*, 345–351. **DOI:**10.1016/j.apsusc.2017.03.010
33. F. Abeles: *Optical properties of solids*. North-Holland Publishing Company, Amsterdam, **1972**.
34. M. M. Abd El-Raheem, *J. Phys. Conden. Matt*. **2007**, *19*, 216209–216215. **DOI:**10.1088/0953-8984/19/21/216209

Povzetek

Halkonski derivati so pomembni v znanosti, saj njihove uporabe sežejo od polprevodniških lastnosti vse do bioloških učinkov. V tem delu smo s kondenzacijo 1-(7-metoksi-1-benzofuran-2-il)etanona s 4-metilbenzaldehidom v bazičnem mediju pripravili 1-(7-metoksi-1-benzofuran-2-il)-3-(4-metilfenil)prop-2-en-1-on (**2**). Kemijsko strukturo **2** smo potrdili z elementno analizo, FT-IR, ^{1}H NMR in ^{13}C NMR. Za različne koncentracije **2** v raztopinah smo podrobno določili UV spektroskopske lastnosti, robove absorpcijskih trakov, optične pasovne vrzeli, lomne količnike, obnašanje v odvisnosti od okolice in prevodnostne lastnosti. Preučili smo tudi, kako se spektroskopske, optične in prevodnostne lastnosti **2** spreminjajo v odvisnosti od koncentracije in kako lahko nanje vplivamo.

Except when otherwise noted, articles in this journal are published under the terms and conditions of the Creative Commons Attribution 4.0 International License

Scientific paper

Effects of Individual and Co-exposure of Copper Oxide Nanoparticles and Copper Sulphate on Nile Tilapia *Oreochromis niloticus*: Nanoparticles Enhance Pesticide Biochemical Toxicity

Özgür Fırat[1], Rabia Erol[1] and Özge Fırat[2,*]

[1] *Adiyaman University, Science and Letters Faculty, Biology Department, Adiyaman, TURKEY*

[2] *Adiyaman University, Kahta Vocational School, Veterinary Department, Adiyaman, TURKEY*

** Corresponding author: E-mail: ozfirat@adiyaman.edu.tr*
Phone: [+90] 4167258150

Received: 11-01-2021

Abstract

Copper, like iron and zinc, is one of the most essential trace elements for organisms. Different forms of copper have distinctive and specific uses. For example, copper oxide nanoparticles (CuO-NP) are widely used in the world as a nanomaterial. Copper sulphate ($CuSO_4$) is worldwide used as a fungicide in agriculture and as an algaecide in aquaculture. Nowadays, the increasing use of these chemicals raises concerns regarding their potential effects on the health of aquatic organisms and ecological risks. Therefore, in the present research, toxic effects of $CuSO_4$ and CuO-NP, alone and in combination, were evaluated using biochemical markers (plasma biochemical and gill and liver oxidative stress) in freshwater fish, *Oreochromis niloticus*. The fish were exposed to 0.05 mg/L $CuSO_4$, CuO-NP, and $CuSO_4$+CuO-NP for 4 and 21 days. Especially at 21 days, $CuSO_4$ and CuO-NP, alone and combined, generally increased plasma alkaline phosphatase, aspartate aminotransferase, alanine aminotransferase, lactate dehydrogenase, cortisol, glucose, creatinine, blood urea nitrogen, and tissue malondialdehyde while they decreased plasma total protein, and tissue superoxide dismutase, catalase, glutathione-S-transferase, glutathione reductase, and glutathione. Consequently, our results illustrate that $CuSO_4$ and CuO-NP have similar toxic effects in fish, however, co-exposure of CuO-NP and $CuSO_4$ is more toxic than effects of these chemicals alone.

Keywords: Fish; metal; nanoparticles; blood; biomarkers

1. Introduction

Most aquatic environments (e.g., seas and rivers) are contaminated by pollutants from natural and anthropogenic sources. These ecosystems are considered to be the ultimate receiving medium for pesticides, metals, and nanoparticles.[1] The entry of these dangerous substances into aquatic environments impairs the water quality to the extent that it is not suitable for aquatic organisms.

Copper (Cu) is one of the most essential trace elements for organisms like iron and zinc. The central role of copper in the cells is as a cofactor for many enzymes such as superoxide dismutase, monooxygenases, and cytochrome-c oxidase.[2] Different forms of copper have distinctive and specific uses. For example, copper oxide nanoparticles (CuO-NPs) are widely used in the world as a nanomaterial. Copper sulphate ($CuSO_4$), another form of copper, is worldwide used as an algaecide in aquaculture and as a fungicide in agriculture.[3] Nowadays, the increasing use of these chemicals raises concerns regarding their potential health problems on aquatic organisms and ecological risks.

Application, production, and use of nanoparticles (NPs) are increasing worldwide. While the global market for NPs reached $ 2.0 billion in 2017, it is estimated to reach approximately $ 7.0 billion by 2022.[4] CuO-NPs globally are one of the most widely used NPs and the fourth most commonly used metal oxide nanoparticle after titanium dioxide (TiO_2), silicon dioxide (SiO_2), and zinc oxide (ZnO). CuO-NPs are used in consumer products, medicine, and industrial applications. CuO-NPs are utilized in many different applications, including in gas sensors, cata-

lytic processes, solar cells, and lithium batteries, as well as in face masks, wound dressings, and socks.[5] These nanoparticles can also be toxic, which may be due to the particles themselves or the disintegration of ions from the particles.[6] In the aquatic environment, CuO-NPs are considered as a significant source of contamination due to their widespread applications in antifouling paints that used in boats and immersed structures, therefore, the potential toxicity CuO-NPs should not be ignored.[7]

$CuSO_4$ is used in aquaculture applications as a therapeutic agent for bacterial infections and various ectoparasitic and is reducing the incidence of fish parasites (trematodes, protozoa, and bacteria and external fungi, etc.).[8] Another application area of $CuSO_4$ is its usage as an effective fungicide in agriculture.

The blood indices, important biochemical indicators, provide valuable information to assess, monitor and quantify the health of the organisms e.g., fish. Therefore, they are used to explain and diagnose the toxicological effects of various stressors and chemicals. Plasma enzymes [alkaline phosphatase (ALP), aspartate aminotransferase (AST), alanine aminotransferase (ALT), lactate dehydrogenase (LDH)] activities and metabolite [cortisol, glucose, cholesterol, total protein, creatinine, blood urea nitrogen (BUN), etc.)] levels are often measured as sensitive indicators of the harmful effects of pesticides, metals, and nanoparticles on fish vital tissues (e.g., liver and kidney).[9,10]

The main disturbances occur in biological systems of organisms and are caused by pollutants released in aquatic ecosystems.[11] Various aquatic pollutants, such as pesticides and nanoparticles induce reactive oxygen species (ROS), which may lead to oxidative stress, showing role of ROS in pesticide and nanoparticle toxicities.[1,12] The oxidative stress induces as a result of unbalance between oxidating and antioxidating compounds, which may be triggered by the predominance of ROS production, incapacity of defence or changes in antioxidant systems of organisms.[13] Enzymatic [catalase (CAT), superoxide dismutase (SOD), glutathione-S-transferase (GST), glutathione peroxidase (GPX), glutathione reductase (GR)] and nonenzymatic [glutathione (GSH)] antioxidant defence systems play a vital role to neutralize the toxicity of oxidative stress on the biological functions/structures of the cells. Malondialdehyde (MDA) is widely used as a biomarker of toxic effects of pollutants on the cell membrane.

Fishes are consequential sources of proteins and lipids and the health of them is very paramount for human beings.[14] *Oreochromis niloticus* (Nile tilapia) is an important aquaculture species amongst cultivated freshwater fish in the world.[10] These fishes are being the most farmed tropical fish species globally depending on their strong immune systems, high growth rates, and vigorous tolerance to a wide range of environmental conditions including aquatic pollutants.[15]

Some studies have documented the toxic effects of co-exposure of nanomaterials with classical pollutants (pesticides or heavy metals) on aquatic organisms. For example, deleterious effects of carbon nanotubes as nanomaterial, carbofuran as pesticide, and the co-exposure of both on *Astyanax ribeirae* (fish),[16] *O. niloticus* (Nile tilapia)[17] and *Palaemon pandaliformis* (shrimp)[18] were identified in detail. In other studies, it was reported that co-exposure of graphene oxide (carbon-based nanomaterial) with trace elements (Cd, Zn) impaired the routine metabolism of the freshwater fish *Geophagus iporangensis*[19] and *P. pandaliformis*.[20]

In recent years, nanotoxicological researches show that nanoparticles are also dangerous for living organisms, just like pesticides and metals, which are more conventional pollutants.[1,21,22] The increasing use of CuO-NPs and $CuSO_4$ inevitably results in increased concentrations of their discharges into the aquatic environment, which in turn may then pose a potential risk to aquatic organisms. The effect of pesticides or heavy metals on fish has been the focus of extensive research for many years, however, the combined effect of these pollutants and nanomaterials is still a new subject that needs to be studied.[23] In addition, the effects of $CuSO_4$ and CuO-NPs on fish were individually investigated, but no study was found on the combined effects of these chemical. Considering the constant exposure of fish to these chemicals in the natural water medium, the present investigation aimed to determine the acute and subchronic effects of CuO-NPs as a nanoparticle and $CuSO_4$ as a pesticide, alone and in combination, on plasma biochemical indicators (ALP, ALT, AST, LDH, glucose, cortisol, cholesterol, total protein, creatinine, BUN) and tissue oxidative stress parameters (CAT, SOD, GR, GPX, GST, GSH, MDA) in freshwater fish, *Oreochromis niloticus*. The hypothesis of the present investigation was that $CuSO_4$ and CuO-NPs interact synergistically on the *O. niloticus*, thus provoking alterations in biochemical indicators in its blood, gill, and liver tissues.

2. Materials and Methods

Copper sulphate ($CuSO_4 \cdot 5H_2O$) and CuO-NPs (form: nanopowder particle size: <50 nm; surface area: 29 m^2/L) were purchased from Sigma–Aldrich Co. (USA). The morphology and size of CuO-NPs dispersed in distilled water were determined by transmission electron microscopy (TEM) (Hitachi High-Tech HT7700, Tokyo, Japan). TEM measurements demonstrated that CuO-NPs were 55 ± 10 nm of average particle size and showed spherical and oval shapes (Figure 1). For measurements of zeta potential and hydrodynamic diameter of CuO-NPs' suspension, Zetasizer instrument (Malvern Zetasizer Nano ZSP, UK) was used. The zeta size (328 nm), polydispersity index (0.236), potential (22.7 mV), conductivity (0.00792 mS/cm), and mobility (1.8631 μmcm/Vs) of these nanoparticles were found. The stock dispersion (10 g/L) of CuO-NPs was prepared immediately in redistilled

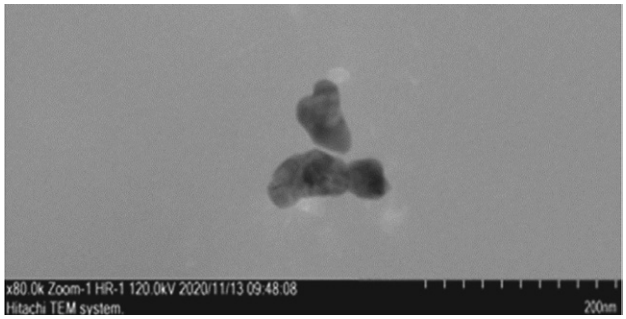

Figure 1. Transmission electron microscopy image of CuO-NPs.

water followed by sonication in an ultrasonic bath for 1 hour as previously described by Shahzad et al. (2018)[24]. 0.05 mg/L CuO-NPs (test concentration) was prepared daily by serial dilutions of this stock dispersion followed by sonication for 20 min to avoid aggregation before adding to the water of the experimental aquarium.

Male *O. niloticus* specimens, two years old, were used as research material in our study. *O. niloticus* (52.71 ± 0.63 g weight and 14.33 ± 0.28 cm total length, as mean ± SEM) were commercially obtained from the Aquaculture Unit of Fisheries Faculty of Cukurova University (CU), where they have been cultured for more than 30 years, and transferred to the Animal Ecophysiology Laboratory of the Science and Letters Faculty of the same university and kept in the glass aquariums containing clean tap water dechlorinated by intense aeration, static system for eight weeks to adapt to the ambient conditions (12-hour daylight /12-hour dark photoperiod, 25 ± 1 °C temperature, central ventilation system). The mean ± standard error of some physicochemical parameters of the waters was found as pH 7.98 ± 0.06, temperature 22.18 ± 0.42 °C, dissolved oxygen 7.65 ± 0.37 mg/L, and total hardness 318 ± 3.5 mg/L as $CaCO_3$. During the acclimatization and experimentation period, the fish were fed once daily at the same hour with commercial fish feed (Pinar Yem, Turkey), in an amount equivalent to 2% of their body weight.

All the experiments, including the controls, were set up in duplicate considering different exposure periods (4 and 21 days). In each repeat set the experiments were carried out in 4 glass aquariums sized 40 cm × 120 cm × 40 cm, each containing 120 L each of the experimental solutions and six fish. Solutions at the concentrations of 0.05 mg/L $CuSO_4$, CuO-NPs, and $CuSO_4$+CuO-NPs were added to the first three aquariums, respectively. The fourth aquarium contained only 120 L of free Cu-tap water and constituted the control. The range of 96-h LC_{50} for Nile tilapia was 5.03-14.27 mg Cu/L.[25] The 96 h LC_{50} value of CuO-NPs for *O. niloticus* was found as 100 mg/L.[26] The 0.05 mg/L concentration of CuO-NPs and $CuSO_4$ applied in the present investigation was therefore a sublethal concentration and eco-relevant considering the contamination levels of certain water resources.[5] The solutions of $CuSO_4$ and CuO-NPs in the treated groups were renewed every 24 hours.[27] The bottoms of aquaria were mixed very well with air at an interval of three times a day to minimize aggregation of NPs.[9] Test media were changed just after feeding, to prevent contamination of the environment with food remains. The control fish were maintained in the same manner. Fish were exposed to these chemicals for 4 and 21 days to determine their acute and subchronic exposures.

At the end of each duration six fish were removed from each aquarium and used as replicates for biochemical testing. After 4 and 21 days, the fish in the control and the treatment groups were individually caught and placed in the anaesthetic bath containing 75 mg/L tricaine methanesulfonate (MS222) for 1–2 min. Blood samples were taken from the caudal vein of each fish into tubes containing ethylene diamine tetra acetic acid (EDTA), anticlotting agent, and centrifuged at 3000 rpm over 10 min at 4 °C for the biochemical analyses of plasma. ALT, AST, ALP, LDH, cortisol, glucose, total protein, cholesterol, BUN and creatinine in the plasma samples were immediately determined using biochemical otoanalyzers (Beckman Coulter DXC 800 and Beckman Coulter DXI 800, USA). ALT, AST, and LDH activities were determined by UV test technique.[28,29] ALP activity was measured by use of the colorimetric assay.[30] Cortisol level was assayed using an electrochemiluminometric technique.[31] The enzymatic UV test was used for the determination of glucose level.[32] The levels of cholesterol,[33] total protein,[34] BUN,[35] and creatinine[36] were determined by colorimetric test. Following blood sampling, fish were dissected. The gill and liver tissues were homogenized in 0.05 M Na-P buffer (pH 7.4) containing 0.25 M sucrose with a ratio of 1/10 in using a steel homogenizer at 10000 rpm for 3 min. Thereafter, the homogenates were centrifuged at 10000 rpm for 30 min at +4 °C. The alteration in oxidative stress parameter in the gill and liver tissues determined using spectrophotometrically. The activity of CAT was evaluated following the method based on measuring the rate constant of hydrogen peroxide (H_2O_2) degradation by the enzyme.[37] The activity of SOD was determined by the inhibition of iodo-p-nitro tetrazolium violet reduction by superoxide anion radical generated by xanthine–xanthine oxidase.[38] The activity of GPX was measured according to Beutler (1984),[39] using t-Butyl hydroperoxide as the substrate. The activity was determined by calculating the difference in absorbance values during oxidation on nicotinamide adenine dinucleotide phosphate (NADPH) to $NADP^+$. The activity of GST was evaluated by the method of Habig et al. (1974)[40] who reported that activity of enzyme was calculated by monitoring the alterations in the absorbance at 340 nm. The GR activity was assayed by determination the oxidation of NADPH by oxidized glutathione at 340 nm.[41] MDA forms a pink complex with thiobarbutiric acid and this complex is measured at 535 nm in spectrophotometer.[42] Protein level was measured according to the method described by Lowry et al. (1951).[43] For statistical assessing, computer software pack-

age SPPS 22 was used. Before the statistical analysis, the data were analysed regarding normality distribution using Shapiro-Wilk's test, and Levene's test was used for homogeneity of variance (homoscedasticity). If the results were normal and homoscedastic, differences between means of experimental groups were evaluated using a variance analysis (one-way ANOVA) followed by Student-Newman-Keuls (SNK) multiple comparisons test. Significant differences were statistically considered at $p<0.05$. All procedures used in the animal experiment were carried out in accordance with the Animal Experiments Local Ethics Committee of the CU (Protocol 2/2018).

3. Results and Discussion

In the investigation, no death was observed in *O. niloticus* exposed to CuO-NPs and $CuSO_4$ and their combination. Similarly, CuO-NPs (0.02 mg/L) did not cause mortality in *O. niloticus*.[44] Aquatic ecosystems are the last ultimate receiving environment for almost all pollutants, and aquatic organisms are seriously threatened by toxic substances entering these environments. The ability of freshwater and marine fish to survive against both well-known pollutants such as metals and pesticides, and a new group of pollutants, nanoparticles, is primarily related to their adaptability and cellular defence mechanisms. It has been shown in many studies[1,10,45] that metals, pesticides and nanoparticles disrupt the internal balance in fish, cause serious toxic effects at the molecular, biochemical, and cellular levels, and even death. Similarly, in the present research significant biochemical and oxidative stress responses were observed in the *O. niloticus* following exposures of $CuSO_4$, CuO-NPs, and $CuSO_4$+CuO-NPs.

Table 1 shows the alterations in plasma enzyme activities of *O. niloticus* in response to the separate or combined effects of $CuSO_4$ and CuO-NPs. Changes in the plasma/serum biochemical parameters in response to environmental pollutants occur rapidly and therefore these parameters are attributed as biomarkers of the toxic effects of chemicals. Among these biochemical parameters, ALT, AST, ALP, and LDH are liver-originated enzymes. These enzymes are intracellular enzymes. Because ALT, AST, ALP, and LDH are sensitive to contaminants, they are recommended as key enzymes in the evaluation of hepatic cell damage and most liver diseases. These enzyme levels in blood plasma are low. However, due to the damage of hepatocyte cell membranes in the presence of toxicants that can cause cellular damage in the liver, their levels may increase by passing into the intercellular fluid and then into the blood. In the current work, all tested plasma enzyme activities of *O. niloticus* increased, especially at 21-d, under the effect of $CuSO_4$ and CuO-NPs and their combination compared that in the control, observing a statistically significant difference ($F = 60.289$, $p = 0.000$ for ALT; $F = 22{,}458$, $p = 0.000$ for AST; $F = 19.035$, $p = 0.001$ for ALP; $F = 13{,}233$, $p = 0.002$ for LDH). It is estimated that these increases in the plasma enzyme activities occur due to cellular damage caused by both copper forms in the fish liver. Similar elevation trends in the enzyme activities of fish blood serum were also found by Fırat et al. (2011)[46] for Nile tilapia *O. niloticus* after metals (copper and lead) and pesticide (cypermethrin) treatments. The researchers concluded that all tested pollutants induced significant increases in the serum ALT, AST, ALP, and LDH activities as a result of chemical toxicity on the liver. Also, it was reported that iron oxide nanoparticles and zinc nanoparticles increase serum ALT, AST, ALP, and LDH activities in *O. niloticus*.[21,47] In another investigation, it was observed that there was a significant elevation in serum ALT, AST, and ALP activities in CuONPs-exposed fish groups compared to the control group.[26]

Table 1. Effects of individual and co-exposure of $CuSO_4$ and CuO-NPs on plasma enzyme activity of *O. niloticus*

Group	4 days	21 days
	ALT activity (U/L)	
Control	18.21 ± 0.48 **a**	18.44 ± 0.77 **a**
0.05 mg/L CuSO4	20.49 ± 0.93 **a**	27.07 ± 0.68 **b**
0.05 mg/L CuO-NPs	31.15 ± 0.74 **b**	34.66 ± 0.56 **c**
0.05 mg/L Cu-Mix	34.28 ± 0.53 **b**	44.72 ± 0.39 **d**
	AST activity (U/L)	
Control	136 ± 4.5 **a**	128 ± 5.6 **a**
0.05 mg/L CuSO4	127 ± 6.1 **a**	169 ± 3.9 **b**
0.05 mg/L CuO-NPs	141 ± 5.4 **a**	197 ± 6.1 **c**
0.05 mg/L Cu-Mix	173 ± 3.3 **b**	213 ± 5.2 **c**
	ALP activity (U/L)	
Control	25.34 ± 0.51 **a**	24.79 ± 0.63 **a**
0.05 mg/L CuSO4	24.89 ± 0.47 **a**	33.21 ± 0.70 **b**
0.05 mg/L CuO-NPs	24.60 ± 0.39 **a**	34.59 ± 0.66 **b**
0.05 mg/L Cu-Mix	31.93 ± 0.41 **b**	36.05 ± 0.39 **b**
	LDH activity (U/L)	
Control	422 ± 12 **a**	429 ± 18 **a**
0.05 mg/L CuSO4	431 ± 22 **a**	558 ± 11 **b**
0.05 mg/L CuO-NPs	417 ± 27 **a**	573 ± 23 **b**
0.05 mg/L Cu-Mix	552 ± 19 **b**	581 ± 17 **b**

Data are expressed as mean ± standard error (n = 6). Small letters (a, b, c and d) are used to determine the differences between treatment groups at the same time. There is a statistical difference between data denoted by different letters ($p < 0.05$, Student-Newman-Keuls test). Cu-Mix: $CuSO_4$ + CuO-NPs

Energy may be urgently needed to cope with stressful situations that occur under the influence of toxic substances in the fish. Cortisol and glucose, important stress metabolites, play an active role in energy requirement processes in such cases. Under stress, the fish brain releases excessive amounts of catecholamines and corticosteroid hormones, which in turn increase the breakdown of liver glycogen, causing elevated blood glucose levels.[48] In our work, plasma cortisol and glucose levels of *O. niloticus* sig-

nificantly elevated in response to both alone- and co-exposure of $CuSO_4$ and CuO-NPs at 4 and 21 days (Table 2). Increases in the plasma metabolite levels of fish treated with 0.05 mg/L of $CuSO_4$, CuO-NPs, and $CuSO_4$+CuO-NPs at 4 days were found to be 47%, 51%, and 56% for cortisol (F = 26.100, p = 0.000), and 59%, 64%, and 86% for glucose (F = 20.916, p = 0.000), respectively. We concluded that the plasma cortisol and glucose levels increased depending on meet the increasing energy needs in stress situations caused by these chemicals. Similar to our study findings, it was observed that exposures to various toxicants such as metals (Zn, Cd, and Zn+Cd) and metal oxide nanoparticles (CuO-NPs) in *O. niloticus* caused significant elevations in serum glucose and cortisol levels.[47,49] The researchers emphasized in these studies that increases in glucose and cortisol levels might be important processes in dealing with stress caused by toxicants. In the study conducted by Soliman et al. (2021)[5] 15 mg/L $CuSO_4$ or CuO-NPs significantly increased blood glucose levels of *O. niloticus*.

The plasma/serum BUN and creatinine levels are measured frequently to assess the kidney dysfunction and damage caused by chemicals. In toxicological researches, these parameters have been used as biochemical indicators to provide valuable information about renal functions. In our investigation, the creatinine and BUN were significantly elevated by all tested chemicals at 21 days (Table 2). Significant increases in levels of the creatinine (F = 12.576, p = 0.002) and BUN (F = 19.109, p = 0.001) were found with the treatments of $CuSO_4$ (64% and 52%) and CuO-NPs (65% and 93%), while marginally significant elevations in these parameters were noted in fish exposed to $CuSO_4$+CuO-NPs (148% and 171%). The increased plasma creatinine and BUN levels may demonstrate the significant pathological alterations of fish kidneys associated with toxicity of all tested copper compounds. In agreement with our results, Canli et al. (2018)[9] reported that *O. niloticus* after exposure to 1, 5, 25 mg/L of metal oxide nanoparticles (Al_2O_3, CuO, and TiO_2) for 14-d showed striking elevations in the serum creatinine and BUN levels, as their levels elevated nearly 10 folds. The researchers noted increased creatinine and blood urea nitrogen may reflect kidney failure as a result of nanoparticle toxicities. Also, a significant dose-dependent increase in BUN and creatinine levels was reported in *O. niloticus* exposed to 10, 20 and 50 mg/L CuO-NPs for 25 days.[26]

The levels of plasma proteins are closely related to liver function as most of these proteins are synthesized in this tissue.[50] Various chemicals can cause significant changes in plasma total protein levels, which may indicate their effects on protein metabolism in the liver. Cholesterol, another biochemical parameter, is an important component of cell membranes. Compared with the control, the individual and combined effects of $CuSO_4$ and CuO-NPs declined total protein levels (F = 14.261, p = 0.000) after 21 days whereas they did not cause a significant change in cholesterol levels during both exposure periods (F = 0.426, p = 0.742) (Table 2). Declined total protein levels may be the result of increased protein degradation or reduced protein synthesis in the fish liver caused by these chemicals. These findings are in agreement with the results of Fırat et al. (2011)[46] who noted *O. niloticus* exposed to lead and cypermethrin for 21 days showed significant decreases in the serum total protein levels. The exposures of CuO-NPs and CuO-bulks declined serum total protein levels of *O. niloticus*.[47] Also, 21-d exposure of 0.5 and 1.0 mg/L silver-NP (Ag-NP) declined serum total protein levels of *Cyprinus carpio* (common carp).[51] In another study, significant changes in the serum cholesterol levels of *O. niloticus* were not observed following exposures of Al_2O_3-, CuO-, and TiO_2-NPs.[9]

Pollutants such as metals, pesticides, and metal-based nanoparticles that enter aquatic ecosystems from

Table 2. Effects of individual and co-exposure of $CuSO_4$ and CuO-NPs on plasma metabolite level of *O. niloticus*

Group	4 days	21 days
	Cortisol level (ng/dL)	
Control	4.67 ± 0.17 **a**	4.78 ± 0.11 **a**
0.05 mg/L $CuSO_4$	6.86 ± 0.13 **b**	6.16 ± 0.22 **b**
0.05 mg/L CuO-NPs	7.04 ± 0.21 **b**	6.20 ± 0.19 **b**
0.05 mg/L Cu-Mix	7.29 ± 0.16 **b**	6.77 ± 0.34 **b**
	Glucose level (mg/dL)	
Control	51.44 ± 0.63 **a**	53.61 ± 0.71 **a**
0.05 mg/L $CuSO_4$	81.88 ± 0.74 **b**	75.18 ± 0.46 **b**
0.05 mg/L CuO-NPs	84.25 ± 0.52 **b**	76.09 ± 0.84 **b**
0.05 mg/L Cu-Mix	95.73 ± 0.81 **b**	98.57 ± 0.84 **c**
	Cholesterol level (mg/dL)	
Control	211 ± 3.51 **a**	205 ± 4.63 **a**
0.05 mg/L $CuSO_4$	217 ± 2.12 **a**	221 ± 5.27 **a**
0.05 mg/L CuO-NPs	208 ± 3.05 **a**	214 ± 2.71 **a**
0.05 mg/L Cu-Mix	223 ± 2.42 **a**	230 ± 4.30 **a**
	Total Protein level (g/dL)	
Control	4.30 ± 0.11 **a**	4.33 ± 0.08 **a**
0.05 mg/L $CuSO_4$	4.28 ± 0.13 **a**	3.40 ± 0.06 **b**
0.05 mg/L CuO-NPs	4.31 ± 0.07 **a**	3.28 ± 0.15 **b**
0.05 mg/L Cu-Mix	4.34 ± 0.08 **a**	3.17 ± 0.10 **b**
	BUN level (mg/dL)	
Control	0.015 ± 0.002 **a**	0.014 ± 0.002 **a**
0.05 mg/L $CuSO_4$	0.015 ± 0.001 **a**	0.023 ± 0.003 **b**
0.05 mg/L CuO-NPs	0.016 ± 0.002 **a**	0.027 ± 0.003 **b**
0.05 mg/L Cu-Mix	0.017 ± 0.003 **a**	0.038 ± 0.004 **c**
	Creatinine level (mg/dL)	
Control	0.022 ± 0.003 **a**	0.023 ± 0.002 **a**
0.05 mg/L $CuSO_4$	0.022 ± 0.002 **a**	0.035 ± 0.002 **b**
0.05 mg/L CuO-NPs	0.024 ± 0.002 **a**	0.038 ± 0.003 **b**
0.05 mg/L Cu-Mix	0.025 ± 0.003 **a**	0.057 ± 0.002 **c**

Data are expressed as mean ± standard error (n = 6). Small letters (a, b and c) are used to determine the differences between treatment groups at the same time. There is a statistical difference between data denoted by different letters ($p < 0.05$, Student-Newman-Keuls test). Cu-Mix: $CuSO_4$ + CuO-NPs

natural or anthropogenic sources can cause oxidative stress in fish by producing ROS. It is well known ROS containing highly dangerous radicals such as hydroxyl and superoxide anion cause serious damage to cells. To cope with oxidative stress, there are mechanisms in cells that prevent ROS formation and/or repair cellular damage caused by them. One of the most important of these mechanisms is antioxidant defence systems. This system consists of enzymatic antioxidants such as CAT, SOD, GPX, GR and GST, or non-enzymatic antioxidants such as GSH. It has been emphasized by many researchers that cellular antioxidant defence systems can be used as biomarkers of oxidative damage caused by metal-based nanoparticles and metals.[1,44,52]

CAT and SOD constitute the cell's first line of defence against ROS and play important biological roles in protecting cells from oxidative stress.[53] In the current study, CAT and SOD activities indicated a significant decrease at the end of 21 days in both liver (F = 15.707, p = 0.001; F = 38.458, p = 0.000, respectively) and gill (F = 17.750, p = 0.001; F = 14.149, p = 0.001, respectively) of fish exposed to individually or in a mixture of $CuSO_4$ and CuO-NPs (Table 3). When compared to the control group, these declines in the fish liver in the treatment groups of $CuSO_4$, CuO-NPs, and $CuSO_4$+CuO-NPs were found to be 38%, 46%, and 48% for CAT, and 41%, 42%, and 51% for SOD, respectively. Considering the biological roles of these enzymes in antioxidant defence, the decreases in SOD and CAT activities under the effect of both copper forms may cause a decrease in the defence abilities of cells against the toxic effects of superoxide and hydroxyl radicals. Similar results to our study were also observed in the research conducted by Tunçsoy et al. (2017)[44]. They reported that the SOD and CAT activities reduced in the liver and gill tissues of *O. niloticus* exposed to 20 µg/L CuO-NPs. Also, it was found that the gill tissue SOD and CAT activities of *O. niloticus*, which was exposed to 1.0 and 5.0 mg / L TiO_2-NP for 4 and 14 days, decreased significantly at the end of the first exposure period.[1] These researchers noted that depending on reduced SOD and CAT activities the cells may remain vulnerable to the toxicity of radicals and suffer from oxidative stress. Ag NP and bulk Ag particle exposure caused consistent decreases in both SOD and CAT activities in estuarine ragworm (*Nereis diversicolor*).[54]

GPX protects the cell against damage induced by hydrogen peroxide. Therefore, this enzyme, like CAT, plays significant roles in cellular defence against ROS. Changes in GPX activity affect the defence abilities of cells against toxicants. In our study, liver GPX activity of *O. niloticus* decreased after 4 days in $CuSO_4$ (29%), CuO-NPs (39%), and $CuSO_4$+CuO-NPs (43%) (F = 10.937, p = 0.003) (Table 3). Declined GPX activity may cause the accumulation of H_2O_2 in the cell. Due to the decreasing activities of both CAT and GPX enzymes under the effect of both copper forms, the insufficient removal of H_2O_2 may induce this ROS to turn into hydroxyl radical and thus cause damage to cell components. Consistent with our results, in *C. carpio* exposed to different concentrations of ZnO-NPs for 14 days, 50 mg/L nanoparticle concentration declined the liver, gill, intestine and brain GPX activities.[55]

GR, like CAT and SOD, protects cells against oxidative stress as an antioxidant that forms the primary line of defence against oxidative damage. It also plays an important role in GSH metabolism. GST, another antioxidant enzyme, has very effective and important roles in detoxification processes in cells. This enzyme catalyses the GSH conjugation to xenobiotics, protecting cells and their components from the harmful effects of these chemicals. Our research showed that in response to the tested all copper forms, GR and GST activities increased in both tissues at 4 days and decreased in the liver at 21 days (F = 8.382, p = 0.008; F = 20.878, p = 0.000, respectively) (Table 3). The induction of GR and GST activities may be an adaptation response to the toxic effects of $CuSO_4$ and CuO-NPs. Similarly, it was reported that the gill GR and GST activities of *O. niloticus* increased after TiO_2-NPs exposure as a rapid adaptation response to neutralize the toxicity of this nanoparticle.[1] The inhibition of GST activity may be related to decreased intracellular GSH levels in the effect of these chemicals, as determined in our study. In parallel with the results in our study, a similar decrease in GST activity was found in the tissues of freshwater fish, *Labeo rohita* (Indian major carp), treated with Ag-NP for 28 days.[22]

GSH, a cysteine-rich and low molecular weight tripeptide, acts in the cell as a protective agent against many toxic compounds.[56] Therefore, maintaining intracellular levels of GSH is crucial in both normal cell function and neutralization of toxic stress. Under the single and combined effect of $CuSO_4$ and CuO-NPs, the liver and gill GSH levels of *O. niloticus* increased at 4 days whereas they decreased at 21 days (F = 31.336, p = 0.000; F = 12.103, p = 0.002, respectively) (Table 3). Increases in GSH levels are may be important in neutralizing the toxic effects of both copper forms on the cells. However, the decrease in its levels with increasing time of exposure may be the result of the toxic effect of the chemicals on the synthesis of GSH or the increased cellular utilization of this tripeptide under oxidative stress. Similar to our study results, it was noted that the GSH level of the gill and liver tissues of *C. carpio* significantly increased in the treatment group of 0.5 mg/L ZnO-NP at 14 days.[55] GSH levels increased in the initial periods of defence responses against aquatic pollutants.[57] In another investigation, the effect of ZnO and ZnO-NP caused a decrease in the liver GSH levels of *Danio rerio* (zebrafish).[58]

Lipid peroxidation disrupts the selective permeability of cell membranes and can initiate processes that cause serious damage to cells. Lipid peroxidation has been attributed as one of the most important markers of oxidative damage caused by toxicants such as metals, pesticides,

and nano-metals in aquatic organisms. MDA is one of the lipid peroxidation products and increases in its levels provide critical information about the oxidative stress of toxicants and the severity of this stress. In our research, $CuSO_4$ and CuO-NPs exposures, either separately or in combination, after 21 days caused significant increases in MDA levels of liver (F = 10.855, p = 0.003) and gill (F = 6.747, p = 0.014) (Table 3). The levels of MDA elevate as a result of lipid peroxidation that occurs due to copper-induced ROS. These increases in MDA levels most likely demonstrate that these chemicals induce oxidative stress in fish tissues. In agreement with the current investigation, it was reported a similar elevation in the levels of tissue MDA, clearly indicating the lipid peroxidation in 5 and 50 mg/L ZnO-NP treated the fish, *C. carpio*, for 10 and 14 days.[55] Also, $CuSO_4$ and Cu-NPs increased lipid peroxidation in the gill tissue of *Oncorhynchus mykiss* (rainbow trout).[59] In another study, an elevation in MDA levels was observed in rat liver following aluminium chloride administration.[60] In a study investigating the comparative toxicity of copper oxide bulk and nanoparticles on fish, it was found that CuO-NPs have a more toxic ef-

Table 3. Effects of individual and co-exposure of $CuSO_4$ and CuO-NPs on tissue oxidative stress parameters of *O. niloticus*

	Liver		Gill	
Group	**4 days**	**21 days**	**4 days**	**21 days**
		CAT activity (U/mg)		
Control	470 ± 13 **a**	461 ± 15 **a**	165 ± 6.8 **a**	172 ± 3.8 **a**
0.05 mg/L $CuSO_4$	481 ± 16 **a**	285 ± 20 **b**	171 ± 5.5 **a**	129 ± 4.4 **b**
0.05 mg/L CuO-NPs	493 ± 21 **a**	247 ± 16 **b**	166 ± 4.7 **a**	122 ± 2.9 **b**
0.05 mg/L Cu-Mix	497 ± 18 **a**	241 ± 21 **b**	164 ± 2.3 **a**	98 ± 1.7 **c**
		SOD activity (U/mg)		
Control	27.40 ± 0.62 **a**	27.98 ± 0.43 **a**	21.70 ± 0.51 **a**	21.95 ± 0.44 **a**
0.05 mg/L $CuSO_4$	27.89 ± 0.54 **a**	16.65 ± 0.34 **b**	20.97 ± 0.34 **a**	14.13 ± 0.26 **b**
0.05 mg/L CuO-NPs	26.71 ± 0.78 **a**	16.24 ± 0.59 **b**	22.06 ± 0.65 **a**	13.60 ± 0.51 **b**
0.05 mg/L Cu-Mix	28.22 ± 0.83 **a**	13.83 ± 0.27 **c**	21.14 ± 0.49 **a**	13.19 ± 0.74 **b**
		GPX activity (U/mg)		
Control	0.51 ± 0.02 **a**	0.52 ± 0.04 **a**	0.31 ± 0.03 **a**	0.30 ± 0.02 **a**
0.05 mg/L $CuSO_4$	0.36 ± 0.04 **b**	0.50 ± 0.04 **a**	0.30 ± 0.03 **a**	0.34 ± 0.04 **a**
0.05 mg/L CuO-NPs	0.31 ± 0.03 **b**	0.48 ± 0.05 **a**	0.33 ± 0.02 **a**	0.31 ± 0.02 **a**
0.05 mg/L Cu-Mix	0.29 ± 0.04 **b**	0.47 ± 0.03 **a**	0.31 ± 0.03 **a**	0.35 ± 0.04 **a**
		GR activity (U/mg)		
Control	0.081 ± 0.003 **a**	0.085 ± 0.004 **a**	0.035 ± 0.002 **a**	0.034 ± 0.003 **a**
0.05 mg/L $CuSO_4$	0.104 ± 0.004 **b**	0.064 ± 0.005 **b**	0.045 ± 0.003 **b**	0.033 ± 0.002 **a**
0.05 mg/L CuO-NPs	0.108 ± 0.003 **b**	0.063 ± 0.003 **b**	0.047 ± 0.002 **b**	0.030 ± 0.005 **a**
0.05 mg/L Cu-Mix	0.133 ± 0.002 **c**	0.058 ± 0.004 **b**	0.051 ± 0.004 **b**	0.029 ± 0.003 **a**
		GST activity (U/mg)		
Control	29.18 ± 0.84 **a**	31.41 ± 0.64 **a**	14.76 ± 0.57 **a**	15.28 ± 0.63 **a**
0.05 mg/L $CuSO_4$	37.14 ± 0.69 **b**	24.49 ± 0.33 **b**	18.61 ± 0.73 **b**	14.91 ± 0.49 **a**
0.05 mg/L CuO-NPs	44.85 ± 0.51 **c**	23.55 ± 0.48 **b**	18.89 ± 0.89 **b**	15.13 ± 0.54 **a**
0.05 mg/L Cu-Mix	47.29 ± 0.77 **c**	17.91 ± 0.21 **c**	23.04 ± 0.61 **c**	14.77 ± 0.42 **a**
		GSH level (μmol/mg)		
Control	2.61 ± 0.14 **a**	2.72 ± 0.18 **a**	1.49 ± 0.05 **a**	1.54 ± 0.04 **a**
0.05 mg/L $CuSO_4$	3.40 ± 0.23 **b**	2.08 ± 0.15 **b**	1.85 ± 0.04 **b**	1.23 ± 0.03 **b**
0.05 mg/L CuO-NPs	3.52 ± 0.19 **b**	1.65 ± 0.22 **c**	1.96 ± 0.05 **b**	1.22 ± 0.03 **b**
0.05 mg/L Cu-Mix	4.16 ± 0.17 **c**	1.51 ± 0.13 **c**	1.99 ± 0.06 **b**	1.17 ± 0.02 **c**
		MDA level (nmol/mg)		
Control	2.11 ± 0.03 **a**	2.04 ± 0.03 **a**	1.73 ± 0.02 **a**	1.74 ± 0.03 **a**
0.05 mg/L $CuSO_4$	2.06 ± 0.02 **a**	2.89 ± 0.04 **b**	1.75 ± 0.03 **a**	2.13 ± 0.02 **b**
0.05 mg/L CuO-NPs	2.07 ± 0.04 **a**	2.97 ± 0.03 **b**	1.72 ± 0.02 **a**	2.22 ± 0.04 **b**
0.05 mg/L Cu-Mix	2.05 ± 0.03 **a**	3.58 ± 0.02 **c**	1.71 ± 0.03 **a**	2.32 ± 0.03 **b**

Data are expressed as mean±standard error (n = 6). Small letters (a, b, c and d) are used to determine the differences between treatment groups at the same time. There is a statistical difference between data denoted by different letters ($p<0.05$, Student-Newman-Keuls test). Cu-Mix: $CuSO_4$ + CuO-NPs

fect than CuO-bulks in liver and gill tissues of *O. niloticus* in most oxidative stress parameters.[47]

Similar to our study results, it was determined in other studies that the combined effect of chemicals had more toxic effects. The combined toxic effects of silica nanoparticles (SiNPs) and methylmercury (MeHg) on zebrafish *D. rerio*, a good model organism for toxicological researches, had more severe toxicity than the single exposure alone.[61] Concomitant (iron oxide nanoparticles+mercury) exposure displayed a synergistic response to that of individual responses of either iron oxide nanoparticles or mercury which was evident by significant increases in GST and lipid peroxidation of the gills of *Anguilla Anguilla* (European eel).[62] In an investigation determining impact of co-exposure of aldrin, a pesticide, and titanium dioxide nanoparticles at biochemical and molecular levels in Zebrafish (*D. rerio*), it was observed that the combined effect of chemicals on oxidative stress parameters was generally higher than the effect alone.[63] Similarly, the combined effect of carbon nanotubes as nanomaterial and carbofuran as pesticide on *A. ribeirae* (fish) was found to be higher than the effect of these chemicals alone.[16]

4. Conclusions

The current investigation demonstrated that almost all biochemical and oxidative stress parameters examined were negatively affected by $CuSO_4$ and CuO-NPs, alone or in combination and that these chemicals caused cytotoxic and oxidative damage in *O. niloticus*. Also, our results illustrate that $CuSO_4$ and CuO-NPs have similar toxic effects in the fish; however, the combined effects of these two chemicals were higher than on the individual exposure regarding the biochemical changes and the oxidative stress observed in *O. niloticus*.

Acknowledgment

This study was partially funded by the Scientific Research Projects Unit of Adiyaman University (Grant of FEFYL/2018-0002).

Ethical approval

All applicable international, national, and/or institutional guidelines for the care and use of animals were followed. All procedures performed in studies involving animals were in accordance with the ethical standards of the institution or practice at which the studies were conducted.

Conflict of interest

The authors declare that they have no conflict of interest

5. References

1. Ö. Fırat, R. C. Bozat, *Hum. Ecol. Risk Assess.* **2019**, *25*, 1438–1447. **DOI:**10.1080/10807039.2018.1465338
2. S. C. Leary, D. R. Winge, P. A. Cobine, *Biochim. Biophys. Acta*. **2009**, *1793*, 146–153. **DOI:**10.1016/j.bbamcr.2008.05.002
3. K. C. de Andrade Waldemarin, F. T. Rantin, A. L. Kalinin, *Ecotoxicology*. **2012**, *21*, 783–794. **DOI:**10.1007/s10646-011-0838-3
4. BCC Research, Nanocomposites, nanoparticles, nanoclays and nanotubes: Global markets to 2022. https://www.bccresearch.com/market-research/nanotechnology/nanocomposites-nanoparticles-nanoclays-and-nanotubes-global-markets.html. **2018**, (assessed: May 22, 2021)
5. H. A. M. Soliman, M. Hamed, A. E. H. Sayed, *Environ. Sci. Pollut. Res*. **2021**, *28*, 30046–30057. **DOI:**10.1007/s11356-021-12859-0
6. M. Heinlaan, A. Kahru, K. Kasemets, B. Arbeille, G. Prensier, H. Dubourguier, *Water Res.* **2011**, 45:179–190. **DOI:**10.1016/j.watres.2010.08.026
7. A. A. Abdel-Khalek, S. R. Badran, M. S. Marie, *Fish Physiol. Biochem*. **2016**, *42*, 1225–1236. **DOI:**10.1007/s10695-016-0212-8
8. M. Kırıcı, C. Turk, C. Caglayan, M. Kırıcı, *Appl. Ecol. Environ. Sci.* **2017**, *15*, 1685–1696. **DOI:**10.15666/aeer/1503_16851696
9. E. G. Canli, A. Dogan, M. Canli, *Environ. Toxicol. Pharmacol.* **2018**, *62*, 181–187. **DOI:**10.1016/j.etap.2018.07.009
10. Ö. Fırat, R. Tutus, *Bull. Environ. Contam. Toxicol.* 2020, *105*, 582–587. **DOI:**10.1007/s00128-020-02990-y
11. M. J. A. Cortes-Diaz, J. Rodríguez-Flores, G. Castañeda-Peñalvo, M. Galar-Martínez, H. Islas-Flores, O. Dublán-García, L. M. Gómez-Oliván, *Sci. Total Environ.* **2017**, *606*, 811-823. **DOI:**10.1016/j.scitotenv.2017.06.208
12. M. R. Narra, *Chemosphere*. **2016**, *144*, 966–974. **DOI:**10.1016/j.chemosphere.2015.09.065
13. R. P. Bisognin, D. B. Wolff, E. Carissimi, O. D. Prestes, R. Zanella, T. R. Storck, B. Clasen, *Ecotoxicology*. **2020**, *29*, 1315–1326. **DOI:**10.1007/s10646-020-02264-7
14. S. Balami, A. Sharma, R. Karn, *Malaysian J. Halal Res.* **2020**, *2*, 32–34. **DOI:**10.2478/mjhr-2019-0012
15. C. E. Lind, S. K. Agyakwah, F. Y. Attipoe, C. Nugent, R. P. M. A. Crooijmans, A. Toguyeni, *Sci. Rep.* **2019,** *9*, 16767. **DOI:**10.1038/s41598-019-53295-y
16. E. Barbieri, A. M. T. Ferrarini, K. F. O. Rezende, D. S. T. Martinez, O. L. Alves, *Fish Physiol. Biochem.* **2019**, *45*, 417–426. **DOI:**10.1007/s10695-018-0573-2
17. J. Campos-Garcia, D. S. T. Martinez, O. L. Alves, A. F. G. Leonardo, E. Barbieri, *Ecotoxicol. Environ. Saf.* **2015**, *111*, 131–137. **DOI:**10.1016/j.ecoenv.2014.10.005
18. K. V. B. Alves, D. S. T. Martinez, O. L. Alves, E. Barbieri, *Chemosphere*. **2022**, *288*, 132359. **DOI:**10.1016/j.chemosphere.2021.132359
19. A. M. Z. Medeiros, F. Coa, O. L. Alves, D. S. T. Martinez, E. Barbieri, *Chemosphere*. **2020**, *243*, 125316. **DOI:**10.1016/j.chemosphere.2019.125316

20. C. B. Melo, F. Coa, O. L. Alves, D. S. T. Martinez, E. Barbieri, *Chemosphere*. **2019**, *223*, 157–164. **DOI:**10.1016/j.chemosphere.2019.02.017
21. M. Ates, V. Demir, Z. Arslan, H. Kayad, S. Yılmaz, M. Camas, *Aquat. Toxicol.* **2016**, *177*, 22–32. **DOI:**10.1016/j.aquatox.2016.05.005
22. M. S. Khan, N. A. Qureshi, and F. Jabeen, *Appl. Nanosci.* **2017**, *7*, 167–179. **DOI:**10.1007/s13204-017-0559-x
23. E. Barbieri, J. Campos-Garcia, D. S. T. Martinez, J. R M. C. Silva, O. L. Alves, K. F. O. Rezende, *Microsc. Microanal.* **2016**, *22*, 1162–1169. **DOI:**10.1017/S1431927616012009
24. K. Shahzad, M. N. Khan, F. Jabeen, N. Kosour, A. S. Chaudhry, M. Sohail, *Environ. Sci. Pollut. Res*. **2018**, *25*, 15943–15953. **DOI:**10.1007/s11356-018-1813-9
25. M. Abdel-Tawwab, M. A. A. Mousa, *Zagazig Vet. J.* **2005,** *33*, 80–87.
26. H. M. R. Abdel-Latif, M. A. O. Dawood, S. F. Mahmoud, M. Shukry, A. E. Noreldin, H. A. Ghetas, M. A, Khallaf, *Animals*. **2021**, *11*, 652–671. **DOI:**10.3390/ani11030652
27. H. M. Dutta, D. A. Arends, *Environ. Res.* **2003,** *91*, 157–162. **DOI:**10.1016/S0013-9351(02)00062-2
28. H. U. Bergmeyer, M. Horder, R. Rej, *J. Clin. Chem. Clin. Biochem.* **1986**, *24*, 481–495.
29. W. E. C. Wacker, D. D. Ulmer, B. L. Vallee, *New Eng. J. Med.* **1956**, *255*, 450–456. **DOI:**10.1056/NEJM195609062551001
30. D. Empfehlungen, *Z. Klin. Chem. Klin. Biochem.* **1972**, *10*, 182–192.
31. S. K. Chiu, C. P. Collier, A F. Clark, K. E. Wynn-Edwards, *Clin. Biochem.* **2003**, *36*, 211–214. **DOI:**10.1016/S0009-9120(02)00471-X
32. F. H. Schmidt, *Klin. Wochenschr.* **1961**, *39*, 1244–1250. **DOI:**10.1007/BF01506150
33. L. L. Abell, B. B. Levy, B. B. Brodie, F.E. Kendall, *J. Biol. Chem.* **1952**, *195*, 357–366. **DOI:**10.1016/S0021-9258(19)50907-3
34. T. E. Weichselbaum, *Am. J. Clin. Pathol.* **1946,** *16*, 40–48.
35. J. M. Orten, O. W. Neuhous, Biochemistry, 8th edition. Saint Louis, The CV Mosby Company, **1970**, pp. 49-54.
36. E. S. West, W. R. Todd, H. S. Mason, J. T. V. Brugger, Textbook of Biochemistry. 4th ed, New York, The Macmillan Comp, **1966**, pp. 71–75.
37. S. Lartillot, P. Kadziora, A. Athios. *Prep. Biochem.* **1988**, *18*, 241–246. **DOI:**10.1080/00327488808062526
38. Y. Sun, L. W. Oberley, Y. Li, 1988. *Clin. Chem.* **1988**, *34*, 497–500. **DOI:**10.1093/clinchem/34.3.497
39. E. Beutler, Red cell metabolism: A manual of biochemical methods. 2nd edition. Grune and Starton, New York **1984**, pp.101–105.
40. W. H. Habig, M. J. Pabst, W. B. Jakoby, *J. Biol. Chem.* **1974**, *249*, 7130–7139. **DOI:**10.1016/S0021-9258(19)42083-8
41. I. Carlberg, B. Mannervik, *J. Biol. Chem.* **1975**, *250*, 5475–5480. **DOI:**10.1016/S0021-9258(19)41206-4
42. I. M. Dubovskiy, V. V. Martemyanov, Y. L. Vorontsova, M. J. Rantala, E. V. Gryzanova, V. V. Glupov, *Comp. Biochem. Physiol.* **2008**, *148*, 1–5. **DOI:**10.1016/j.cbpc.2008.02.003
43. O. H. Lowry, N. J. Rosebrough, A. L. Farr, R. J. Randall, *J. Biol. Chem.* **1951**, *193*, 265–275. **DOI:**10.1016/S0021-9258(19)52451-6
44. M. Tunçsoy, S. Duran, Ö. Ay, B. Cicik, C. Erdem, *Bull. Environ. Contam. Toxicol.* **2017**, *99*, 360–364. **DOI:**10.1007/s00128-017-2129-z
45. N. Shah, A. Khan, N. B. Khan, M. Khisroon, *Biol. Trace Elem. Res.* **2021**, *199*, 305–314. **DOI:**10.1007/s12011-020-02122-x
46. Ö. Fırat, H. Y. Cogun, T. A. Yüzereroglu, G. Gök, Ö. Fırat, F. Kargin, Y. Kötemen, *Fish Physiol. Biochem.* **2011**, *37*, 657–666. **DOI:**10.1007/s10695-011-9466-3
47. A. A. Abdel-Khalek, M. Kadry, A. Hamed, M. A. Marie, *J. Basic Appl. Zool.* **2015**, *72*, 113–125. **DOI:**10.1016/j.jobaz.2015.08.003
48. K. K. Saxena, P. Gupta, *Pollut. Res.* **2005**, *24*, 669–670. **DOI:**10.1089/dna.2005.24.670
49. Ö. Fırat, F. Kargın, *Arch. Environ. Contam. Toxicol.* **2010**, *58*, 151–157. **DOI:**10.1007/s00244-009-9344-5
50. T. Garcia, D. Lafuente, J. Blanco, D. J. Sanchez, J. J. Sirvent, J. L. Domingo, M. Gomez, *Food Chem.l Toxicol.* **2016**, *92*, 177–187. **DOI:**10.1016/j.fct.2016.04.010
51. S. Vali, G. Mohammadi, K. R. Tavabe, F. Moghadas, S. H. Naseraba, *Ecotoxicol. Environ. Saf.* **2020**, *194*, 110353. **DOI:**10.1016/j.ecoenv.2020.110353
52. P. Akbary, S. S. Yarahmadi, A. Jahanbakhshi, *Environ.l Sci. Pollut. Res.* **2018**, *25*, 1800–1808. **DOI:**10.1007/s11356-017-0582-1
53. M. Karaca, L. Varışlı, K. Korkmaz, O. Özaydın, F. Perçin, H. Orhan, *Toxicol. Lett.* **2014**, *230*, 198–207. **DOI:**10.1016/j.toxlet.2014.02.013
54. M. Cozzari, A. C. Elia, N. Pacini, B. D. Smith, D. Boyle, P. S. Rainbow, F. R. Khan, *Environ. Pollut.* **2015**, *198*, 32–40. **DOI:**10.1016/j.envpol.2014.12.015
55. L. Hao, L. Chen, *Ecotoxicol. Environ. Saf.* **2012**, *80*, 103–110. **DOI:**10.1016/j.ecoenv.2012.02.017
56. V. D. G. Sinhorin, A. P. Sinhorin, J. M. dos Santos Teixeira, K. M. L. Miléski, P. C. Hansen, P. S. A. Moreira, N. H. Kawashita, A. M. Baviera, V. L. Loro, *Ecotoxicol. Environ. Saf.* **2014**, *106*, 181–187. **DOI:**10.1016/j.ecoenv.2014.04.040
57. S. A. Dar, A. R. Yousuf, M. H. Balkhi, F. A. Ganai, F. A. Bhat, *Chemosphere*. **2015**, *120*, 273–283. **DOI:**10.1016/j.chemosphere.2014.07.031
58. D. Xiong, T. Fang, L. Yu, X. Sima, W. Zhu, *Sci Total Environ.* **2011**, *409*, 1444–1452. **DOI:**10.1016/j.scitotenv.2011.01.015
59. B. J. Shaw, G. Al-Bairuty, R. D. Handy, *Aquat. Toxicol.* **2012**, *116*, 90–101. **DOI:**10.1016/j.aquatox.2012.02.032
60. A. Özkaya, K. Türkan, *Acta Chim. Slov.* **2021**, *68*, 222–228. **DOI:**10.17344/acsi.2020.6390
61. J. Duan, H. Hu, Q. Li, L. Jiang, Y. Zou, Y. Wang, Z. Sun, *Environ. Toxicol. Pharmacol.* **2016**, *44*, 120–127. **DOI:**10.1016/j.etap.2016.05.004
62. K. Srikanth, I. Ahmad, J. W. Rao, T. Trindade, A. C. Duarte, E. Pereira, *Comp. Biochem. Physiol.* **214**, *162*, 7–14. **DOI:**10.1016/j.cbpc.2014.02.007
63. R. C. Jhamtani, S. Shukla, P. Sivaperumal, M. S. Dahiya, R. Agarwal, *Environ. Toxicol. Pharmacol.* **2018**, *58*, 141–155. **DOI:**10.1016/j.etap.2017.12.021

Povzetek

Baker je, tako kot železo in cink, eden najpomembnejših elementov v sledovih za organizme. Različne oblike bakra imajo značilno in specifično uporabo. Nanodelci bakrovega oksida (CuO-NP) se npr. v svetu pogosto uporabljajo kot nanomaterial. Bakrov sulfat ($CuSO_4$) se po vsem svetu uporablja kot fungicid v kmetijstvu in kot algicid v ribogojništvu. Danes vse večja uporaba teh kemikalij vzbuja zaskrbljenost zaradi njihovih možnih učinkov na zdravje vodnih organizmov in ekoloških tveganj. Zato so bili v pričujoči raziskavi ovrednoteni toksični učinki $CuSO_4$ in CuO-NP, samostojno in v kombinaciji, z uporabo biokemijskih markerjev (plazemsko-biokemijski ter škržni in jetrni oksidativni stres) pri sladkovodnih ribah *Oreochromis niloticus*. Ribe so bile izpostavljene 0,05 mg/L $CuSO_4$, CuO-NP in $CuSO_4$ + CuO-NP 4 in 21 dni. Predvsem po 21 dneh sta $CuSO_4$ in CuO-NP, samostojno in v kombinaciji, na splošno povečala nivo plazemske alkalne fosfataze, aspartat aminotransferaze, alanin aminotransferaze, laktatne dehidrogenaze, kortizola, glukoze, kreatinina, dušika iz sečnine v krvi in tkivnih proteinov, medtem ko sta zmanjšala nivo skupnega malondialdehida v tkivih, tkivne superoksidne dismutaze, katalaze, glutation-S-transferaze, glutation reduktaze in glutationa. Posledično naši rezultati kažejo, da imata $CuSO_4$ in CuO-NP podobne toksične učinke pri ribah, vendar je sočasna izpostavljenost CuO-NP in $CuSO_4$ bolj strupena kot učinki posameznih kemikalij.

Except when otherwise noted, articles in this journal are published under the terms and conditions of the Creative Commons Attribution 4.0 International License

Scientific paper

A Facile Synthesis of Bioactive Five- and Six-membered *N*-heterocyclic Aromatic Compounds Using $AlCoFe_2O_4$ as a Green Catalyst

Fatemeh Mostaghni, Homa Shafiekhani and Nosrat Madadi Mahani

Department of Chemistry, Payame Noor University, P.O. Box 19395-4697 Tehran, Iran

** Corresponding author: E-mail: mostaghnif@yahoo.com*

Received: 06-19-2021

Abstract

Nitrogen-containing heterocycles have been extensively studied due to their broad biological and pharmaceutical applications. In this study, we synthesized five- and six-membered nitrogen-containing rings through one-pot multicomponent reaction using an aluminium-doped cobalt ferrite nano-catalyst. The nano-catalyst was prepared by the co-precipitation method from the corresponding metal salts. The obtained results show that the proposed catalyst has a high efficiency and has enabled the formation of the desired products with high efficiency and purity. In addition, simplicity of operation, facile purification of products, shorter reaction times, mild reaction conditions, easy separation and recyclability of the catalyst, are the main advantages of this catalyst.

Keywords: Green catalyst; magnetic nano-catalyst; *N*-heterocyclic aromatic compounds; one-pot multicomponents reactions

1. Introduction

Heterocyclic compounds have significant importance in medicinal chemistry.[1–3] Among them, nitrogen-containing heterocycles, are the most important heterocyclic moieties of choice for the many bio-active compounds.[4–6]

In recent years, imidazoles, benzimidazoles and pyridines are subject of intense investigations because of their wide biological and pharmaceutical applications. Numerous biological activities have been described for imidazole derivatives such as anti-viral, antimicrobial, antifungal, anti-tumor, anti-tubercular, and anti-inflammatory activities.[7–18] These compounds contain two nitrogen atoms placed at 1 and 3 position in their ring structure, which possesses both acidic and basic characteristics. Since both nitrogen atoms can carry hydrogen atom, these compounds appear in two tautomeric forms. In addition, imidazole moieties are very polar compounds, and possess affinity towards enzymes and protein receptors.[19]

Also, medicinal properties of pyridin ring, particularly 2,4,6-triarylpyridines known as Krohnke pyridines, include antimalarial, anaesthetic, antiparasitic, and antitumor activity, as well as agents that are used for photodynamic cell specific cancer therapy.[20–23]

In the past few decades, various methods included synthesis performed by various metal oxide catalysts in the presence or absence of a solvent as well as microwave-assisted synthesis, have been reported for the synthesis of imidazoles,[24–29] and Krohnke pyridines.[30–37]

In recent years, there has been increasing interest to develop a simple, efficient and eco-friendly, benign organic transformations catalyzed by cheap and recyclable metals or their salts, avoiding the harmful and pollutant conditions.

In this study, heterogeneous $AlCoFe_2O_4$ nanocatalyst was used as a suitable catalyst in one-pot multi-component reactions for preparation of bioactive five- and six-membered *N*-heterocyclic aromatic compounds. This catalyst was considered suitable for this purpose due to mild reaction conditions, short reaction times, easy separability and recyclability of the catalyst.

In addition, $AlCoFe_2O_4$ nano-particles have high saturation magnetization, strong anisotropy, high coercivity and excellent physiochemical stability.[38–41]

Many preparation methods for $AlCoFe_2O_4$ nano-particles have been reported, such as the ball milling, co-precipitation, hydrothermal synthesis, sol-gel, and reaction in a micro-emulsion.[42–46] Here, we synthesized the magnetic nano-catalyst ($AlCoFe_2O_4$) using co-precipitation method from metalic salts.

2. Experimental

2. 1. Material and Methods

All materials and reagents were purchased from Merck, and Aldrich and used without further purification. XRD patterns prepared using powder X-ray diffraction (Bruker diffractometer, Cu-Kα X-rays of wavelength λ = 1.5406 Å). Melting points of the synthesized compounds were determined on Electrothermal-9200 melting point apparatus. IR spectra was recorded on KBr Pellets by Shimadzu 8400S FT-IR spectrophotometer. ^{1}H and ^{13}C NMR spectra were recorded on a Bruker Advanced DPX spectrometer (400 MHz for ^{1}H NMR and 100 MHz for ^{13}C NMR). SEM image provided by the scanning electron microscope (FE-SEM, Mira3 Tescan). The absorption spectra was recorded on UV-VIS spectrophotometer (Perkin Elmer, Lambda 35).

2. 2. Synthesis of Nanocatalyst

$CoFe_{2-x}Al_xO_4$ nanocatalyst was prepared by the co-precipitation method from aqueous solutions of $CoCl_2$, $FeCl_3$ and aluminum nitrate. First, stoichiometric amounts of the three metallic salts were individually dissolved in 10 mL of deionized water. Then, the three metallic solutions were poured in the reaction vessel and stirred vigorous for 30 minutes at room temperature. Polyethylene glycol (average molecular weight: 4000, Qualigen) was then added to the above solution as a surfactant. Finally, the mixed solution was neutralized to pH 8 by drop-by-drop addition of 25% ammonia solution. The resulting solution was kept under stirring at 60 °C for 1 hour. The obtained particles were thoroughly washed several times with distilled water and filtered. Finally, the precipate was dried at 80 °C and calcined at 500 °C for 3 hours.

The synthesized nanocatalyst was characterized by powder X-ray diffraction (XRD), scanning electron microscopy (SEM-EDS), vibrating sample magnetometry (VSM), difuse reflectance and UV-vis spectroscopy.

2. 3. General Procedure for the Preparation of 2,4,6-Triphenylpyridines

Various amounts of nano-particle nanocatalyst were added to a stirred solution of acetophenones (2 mmol), aromatic aldehydes (1 mmol), and ammonium acetate (4 mmol). Then, the mixture was stirred at various temperatures under solvent-free condition. At the end of the reaction (monitored by TLC), the catalyst was separated using an external magnet and the reaction mixture was treated with ethanol to form crystals. The crude product was obtained by filtration and washed with ethanol. Purification of the crude product was performed by re-crystallization in ethanol.

Characterization data of selected compounds:

2,4,6-Triphenylpyridine (Table 3, entry 1)

IR (KBr): ν 3071, 1590, 1493, 1471, 1033, 871, 665 cm^{-1}; ^{1}H NMR (400 MHz, DMSO-d_6): δ 7.45–7.62 (m, 9H), 7.95 (d, J = 7.6 Hz, 2H), 8.19 (s, 2H), 8.24 (d, J = 7.5 Hz, 4H); ^{13}C NMR (100 MHz, DMSO-d_6): δ 117.17, 127.3, 127.5, 128.6, 128.9, 129.5, 130.1, 138.8, 139.4, 150.3, 157.4.

2,6-Bis(4-fluorophenyl)-4-phenylpyridine (Table 3, entry 2)

IR (KBr): ν 1601, 1595, 1506, 1421, 1330, 1223, 1160, 1116, 1075, 987, 825 cm^{-1}; ^{1}H NMR (400 MHz, DMSO-d_6): δ 7.37 (m, 5H), 7.51 (m, 2H), 8.13 (q, 2H), 8.23 (s, 2H), 8.32–8.41 (m, 4H); ^{13}C NMR (100 MHz, DMSO-d_6): δ 164.21, 161.67, 155.78, 155.53, 148.59, 148.52, 138.71, 134.96, 135.08, 134.12, 134.00, 129.68, 129.56, 129.27, 129.14, 128.86, 128.65, 126.87, 116.42, 116.26, 116.13, 115.89, 115.71, 115.56, 115.35.

2,6-Bis(4-fluorophenyl)-4-(4-chlorophenyl)pyridine (Table 3, entry 3)

IR (KBr): ν 1612, 1592, 1510, 1416, 1328, 1210, 1162, 1105, 1073, 994, 823 cm^{-1}; ^{1}H NMR (400 MHz, DMSO-d_6): δ 7.36 (m, 3H), 7.61 (m, 3H), 8.09 (m, 2H), 8.21 (s, 2H), 8.38 (m, 4H); ^{13}C NMR (100 MHz, DMSO-d_6): δ 164.21, 161.72, 155.49, 155.24, 154.98, 148.55, 137.43, 137.42, 135.12, 134.19, 133.94, 129.68, 129.50, 129.32, 129.13, 128.94, 128.59, 116.68, 116.45, 116.27, 116.12, 115.94, 115.72, 115.52, 115.31.

2,6-Bis(4-bromophenyl)-4-(4-fluorophenyl)pyridine (Table 3, entry 4)

IR (KBr): ν 1658, 1592, 1505, 1411, 1330, 1210, 1159, 1107, 1070, 997, 819 cm^{-1}; ^{1}H NMR (400 MHz, DMSO-d_6): δ 7.30 (t, J = 8.8 Hz, 2H), 7.72–7.82 (m, 5H), 7.88 (s, 1H), 7.92–8.02 (m, 4H), 8.10 (d, J = 8.4 Hz, 2H); ^{13}C NMR (100 MHz, DMSO-d_6): δ 116.3, 116.5, 122.0, 127.8, 131.0, 131.7, 131.72, 131.8, 131.9, 132.3, 136.9, 143.7, 162.7, 165.2, 188.6.

2,6-Bis(4-bromophenyl)-4-(4-methoxyphenyl)pyridine (Table 3, entry 5)

IR (KBr): ν 3008, 2937, 1665, 1596, 1511, 1463, 1329, 1309, 1261, 1219, 1175, 1037, 984, 819 cm^{-1}; ^{1}H NMR (400 MHz, DMSO-d_6): δ 3.81 (s, 3H), 7.05 (d, J = 8.2 Hz, 2H), 7.72–7.88 (m, 8H), 8.11 (d, J = 8.2 Hz, 4H); ^{13}C NMR (100 MHz, DMSO-d_6): δ 56.1, 115.2, 120.3, 128.1, 128.7, 131.3, 131.8, 132.4, 138.3, 145.5, 162.3, 189.1.

2. 4. General Procedure for the Preparation of 2,4,5-Triphenyl-1*H*-imidazoles

Various amounts of $AlCoFe_2O_4$ nanocatalyst were added to a stirred solution of aromatic aldehydes (1 mmol), benzoin (1 mmol), and ammonium acetate (4 mmol) in ethanol (10 mL). Then, the mixture was stirred at various temperature. At the end of the reaction (monitored by

TLC) the magnetic nanocatalyst was separated using an external magnet. Then, the reaction mixture was diluted with 50 mL of cold water. Finally, the crude product was collected by filtration and washed with EtOH. Purification of the crude product was performed by re-crystallization from acetone: water (9:1). Characterization data of selected compounds were as follow:

2,4,5-Triphenyl-1*H*-imidazole (Table 4, entry 1)

IR (KBr): ν 3445, 3082, 2853, 1641, 1504, 1462, 1398, 1128, 1070, 966, 766, 698 cm^{-1}; ^1H NMR (400 MHz, DMSO-d_6): δ 7.22 (dd, 1H, *J* = 7.2 Hz), 7.34 (dd, 2H, *J* = 7.2 Hz), 7.39 (dd, 2H, *J* = 7.2 Hz), 7.44–7.51 (m, 6H), 7.59 (d, 2H, *J* = 7.6 Hz), 8.10 (d, 2H, *J* = 7.2 Hz), 12.71 (br, 1H); ^{13}C NMR (100 MHz, DMSO-d_6): δ 125.2, 126.5, 127.0, 127.7, 128.1, 128.2, 128.3, 128.4, 130.3, 131. 0, 135.1, 137.1, 145.3.

2-(4–Chlorophenyl)-4,5–diphenyl–1*H*-imidazole (Table 4, entry 2)

IR (KBr): ν 3411, 3060, 2854, 1608, 1485, 1428, 1433, 1325, 1158, 833 cm^{-1}; ^1H NMR ($CDCl_3$): δ 12.76 (s, 1H), 7.84 (d, 2H, *J* = 8.6 Hz), 7.54 (d, *J* = 6.8 Hz 4H), 7.37–7.28 (m, 8H); ^{13}C NMR ($CDCl_3$): δ 144.82, 137.52, 135.19, 132.24, 130.83, 130.80, 129.24, 128.96, 128.54, 128.48, 128.49, 128.14, 127.15, 126.75, 126.34.

2-(4-Hydroxyphenyl)-4,5-diphenyl-1*H*-imidazole (Table 4, entry 3)

IR (KBr): ν 3438, 2964, 2828,1602, 1482, 1445, 1374, 1317, 1130, 1034, 968, 764, 692 cm^{-1}; ^1H NMR (400 MHz, $CDCl_3$): δ 12.51 (s, 1H), 7.20–7.52 (m, 10H), 6.99 (d, 2H, *J* = 7.8 Hz), 6.89 (d, 2H, *J* = 7.5 Hz); ^{13}C NMR ($CDCl_3$): δ 158.3, 156.55, 145.46, 129.18, 128.37, 127.93, 126.92, 124.74, 119.08, 116.54, 112.82.

2-(4-Methoxyphenyl)-4,5-diphenylimidazole (Table 4, entry 4)

IR (KBr): ν 1256, 1616, 2465, 2988, 3428 cm^{-1}; ^1H NMR (400 MHz, DMSO-d_6): δ 12.52 (s, br, 1H), 8.05 (d, *J* = 8.6 Hz, 2H), 7.50 (d, *J* = 6.3 Hz, 4H), 7.35 (m, 6H), 7.08 (d, *J* = 8.7 Hz, 2H), 3.83 (s, 3H); ^{13}C NMR (100 MHz, DMSO-d_6): δ 159.37, 145.81, 132.81, 127.84, 127.47, 126.56, 126.24, 123.13, 113.28, 54.45.

2-(4-Nitrophenyl)-4,5-diphenylimidazole (Table 4, entry 5)

IR (KBr): ν 3438, 3293, 2856, 1605, 1541, 1484, 1335, 1323, 1225, 1026, 838 cm^{-1}; ^1H NMR (400 MHz, DMSO-d_6) δ 7.45–7.52 (m, 2H), 7.74 (d, *J* = 4 Hz, 1H), 7.81–7.86 (m, 3H), 8.22–8.26 (m, 4H), 8.36–8.39 (m, 5H), 13.58 (s, 1H); ^{13}C NMR (100 MHz, DMSO-d_6) δ 159.2, 137.1, 133.2, 131.9, 131.2, 130.8, 129.2, 128.8, 128.6, 128.4, 128.1, 127.5, 127.1, 126.4, 126.1, 125.8, 124.3, 122.6.

3. Results and Discussion

3. 1. Characterization of the Nanocatalyst

Figure 1 shows the single-phase spinel nature of the synthesized nano catalyst was confirmed by the sharp peaks at 2θ (23.74, 29.89, 35.52, 43.14, 54.16, 57.10, 62.99), which are accredited to (111), (220), (311), (400), (422), (511) and (440). All the peaks were indexed within a single

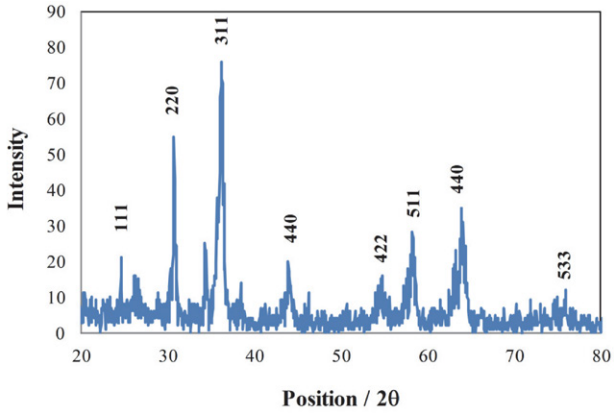

Figure 1. XRD patterns of $AlCoFe_2O_4$

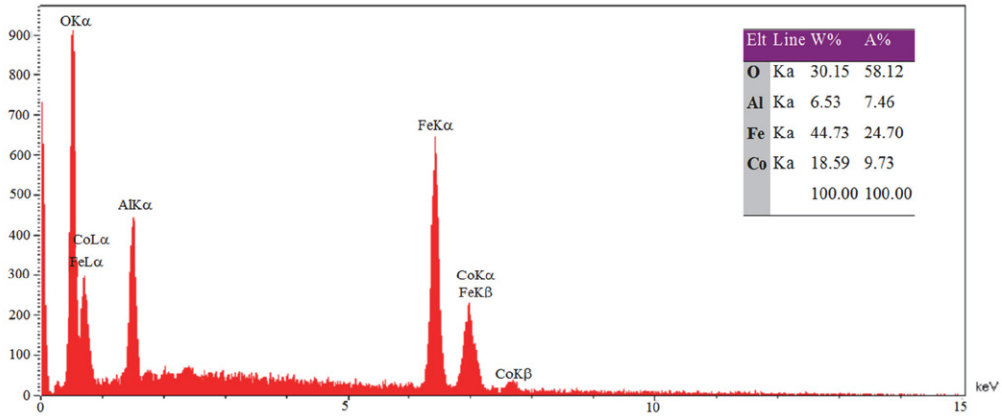

Figure 2. EDS of $AlCoFe_2O_4$

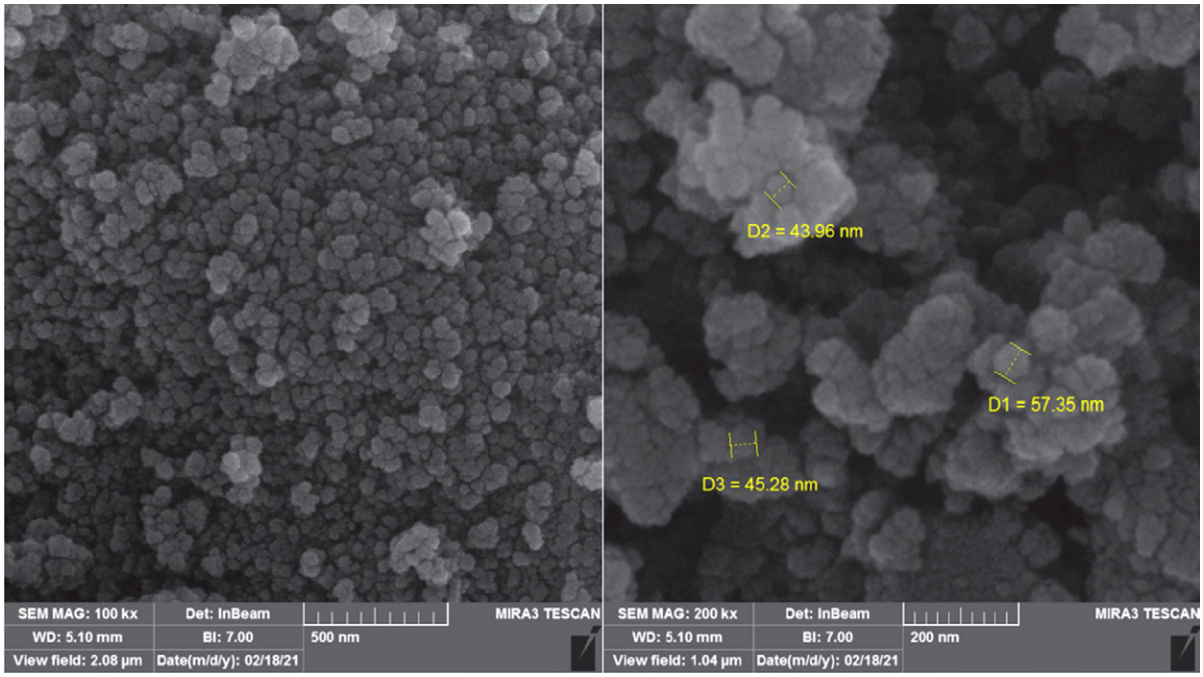

Figure 3. FESEM image of $AlCoFe_2O_4$ nanocrystals

phase cubic spinel structure with *Fd3m* space group (JCPDS Card No. 86-2267).

The crystallite size was calculated from intensity of the highly difracted peak (311) according to the Debye–Scherrer formula giving the crystal sizes of 6.63. To determine the elemental compositions of synthesized nanocatalyst, quantitative analysis was performed using EDS (Fig. 2). The obtained results approved the characteristic peaks of Al, Co, Fe, and O with 7.46, 9.73, 24.70 and 58.12 atomic percentage, respectively.

The above results indicated that the $AlCoFe_2O_4$ nanocatalyst has been successfully synthesized without any impurities. Figure 3 shows the microstructure of synthesized $AlCoFe_2O_4$ nanocrystals. As can be seen in this photograph, it was understood that the nanoparticles were cubic shape with an average diameter size less than 45 nm with some agglomeration. The cubic structure of spinel ferrites is mainly due to the lack of Co^{2+} ions at octagonal sites, which leads to the absence of co-operative active Jahn–Teller distortion.

Couplings at the atomic level, including the coupling between electron spins and between the electron spin and the angular momentum of the electron orbital are two factors that create magnetic properties in materials. Figure 4 showed the hysteresis loops of $AlCoFe_2O_4$ nanoparticles measured using a vibrating sample magnetometer (VSM).

As can be seen, the saturation magnetization (MS), the remanent magnetization (Mr) and coercivity (Hc) values obtained for the sample were 18.05 emu/gr, 394 Oe, and 4.44 emu/gr, respectively. The low values of remanent magnetization and coercivity of the nanoparticles are consistent with the properties of the soft magnetic material. Diffuse

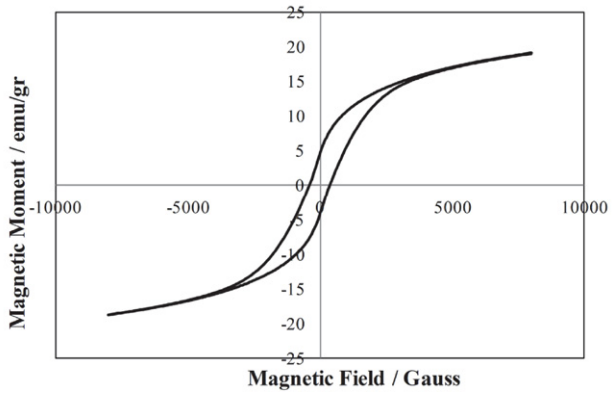

Figure 4. Hysteresis loop of $AlCoFe_2O_4$ nanoparticles

reflectance (DRS) and UV-vis spectra of the sample were obtained using a V-670, JASCO spectrophotometer. DRS spectra of synthesized nanocatalyst is shown in Figure 5.

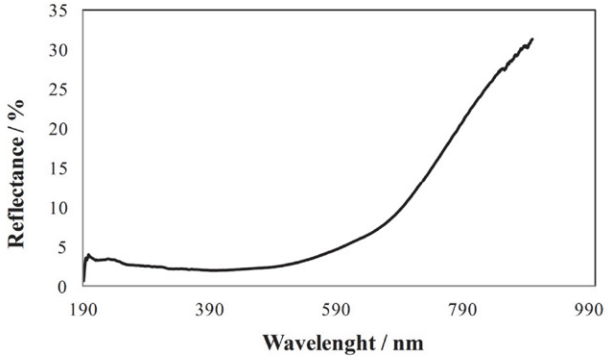

Figure 5. Diffuse reflectance spectra of $AlCoFe_2O_4$ nanocatalyst

As can be seen in the Figure 5, the synthesized nanocatalyst exhibited high value of diffuse reflectance percentage. The energy band gap of photocatalyst is determined using the absorption spectra according to the Tauc equation as follow:

$$(\alpha h\nu) = \beta\left(h\nu - E_g\right)^{\frac{n}{2}}. \quad (1)$$

Where α is the absorption coefficient, β is the absorption constant and E_g is the energy gap. The value of n for the direct optical gap is 1. According to Figure 6, the direct optical gap value is 1.43 ev.

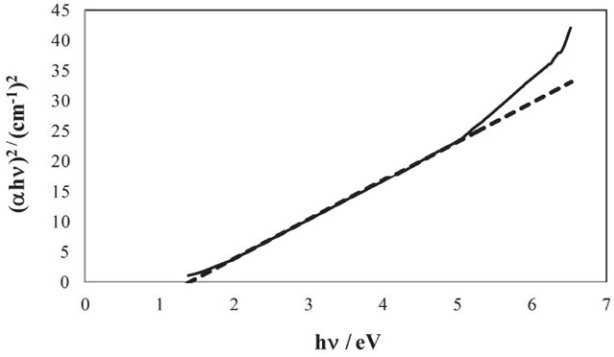

Figure 6. Plot $(\alpha h\nu)^2$ vs. photon energy (inset) of $AlCoFe_2O_4$ nanocatalyst

3. 2. Evaluation of Catalytic Properties

To evaluate the catalytic properties of the synthesized nanoparticles, the synthesis of pyridine and imidazole derivatives through one-pot three-component condensation was selected as the model reaction. Catalytic efficiency and optimal reaction conditions were evaluated by performing reactions at different temperatures and applying different amounts of nanocatalysts. The first derivative in each reaction was selected as the representative to optimize this reaction. The results are presented in Tables 1 and 2.

The results presented in Table 1 clearly show that at 120 °C and in the presence of 15 mol% of the catalyst, the reaction 1 led to the formation of triphenylpyridine at short reaction time and in high yield. It was also found that further increase in temperature led to a decrease in efficiency. This can be related to the possibility of side reactions. According to the results presented in Table 1, further increases in the amount of the catalyst did not have any significant effect on the reaction time and efficiency.

However, reaction 2 was also completed immediately and the pure product was obtained simply by recrystalliz-

Table 1. Optimization of reaction conditions for preparing 1,3,5-triphenylimidazole

Entry	Catalyst (mol%)	*T* (°C)	Time	Yield (%)
1	None	r.t	10 h	–
2	None	50	10 h	trace
3	None	80	10 h	19
4	2	r.t	5 h	35.5
5	2	50	10 min	53
6	2	80	10 min	49
7	5	r.t	5 h	83.5
8	5	50	10 min	98
9	5	80	10 min	78.5
10	7	r.t	5 h	84
11	7	50	10 min	99
12	7	80	10 min	73

Table 2. Optimization of reaction conditions for preparing 2,4,6-triphenylpyridine

Entry	Catalyst (mol%)	*T* (°C)	Time	Yield (%)
1	7	80	3 h	–
2	7	100	3 h	23
3	7	120	3 h	67
4	10	80	3 h	34
5	10	100	3 h	64
6	10	120	3 h	91
7	15	80	3 h	52
8	15	100	3 h	75
9	15	120	3 h	97
10	20	80	3 h	54
11	20	100	3 h	79
12	20	120	3 h	98

Table 3. Preparation of 2,4,6-triarylpyridine derivatives using $AlCoFe_2O_4$ nanocatalyst

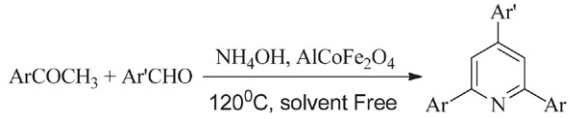

Entry	Ar	Ar‘	Time (min)	yield (%)	m.p. (°C)
1	Ph	Ph	60	97	135–137
2	4-F-C_6H_4-	Ph	60	95	174–176
3	4-F-C_6H_4-	4-Cl-C_6H_4-	90	94	224–226
4	4-Br-C_6H_4-	4-F-C_6H_4-	90	96	148–150
5	4-Br-C_6H_4-	4-OMe-C_6H_4-	60	98	177–189

Table 4. Preparation of 2,4,5-triarylimidazole derivatives using $AlCoFe_2O_4$ nanocatalyst

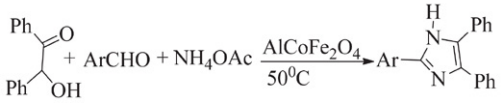

Entry	Ar	Time (min)	Yield (%)	m.p. (°C)
1	Ph	10	97	277–278
2	4-Cl-C_6H_4-	15	92	256–258
3	4-OH-C_6H_4-	10	98	268–270
4	4-OMe-C_6H_4-	10	98	230–232
5	4-NO_2-C_6H_4-	20	92	255–257

ing from ethanol without the need for any chromatographic technique. Table 2 shows that the optimal conditions were obtained with 5 mol% of catalyst at 50 °C. The reaction yield did not increase significantly with increasing the amount of catalyst. However, the reactions with the other benzaldehyde derivatives and aromatic ketones was investigated to develop the method. The results are presented in Tables 3 and 4.

The results indicate that the performance of the catalyst was efficient without the formation of by-products with the wide range of aromatic aldehydes containing electron acceptor and electron donor substituents. In general, this catalyst has produced pure products with high efficiency at short reaction times and low reaction temperatures which makes this catalyst economically and environmentally useful. Furthermore, the catalyst was also successfully recycled and used for at least 5 times without significant reduction in catalytic activity. We believe that the proposed catalyst is a green and efficient catalyst compared to the previously reported different catalysts.

4. Conclusion

In this research, we synthesized aluminum-doped cobalt ferrite nanocatalyst using co-precipitation method. The characterization results showed that the nanoparticles were cubic shape with an average diameter size less than 45 nm with some agglomeration. The low remanent magnetization and coercivity of the nanoparticles are consistent with the properties of the soft magnetic material. Furthermore, the prepared nanoparticles were used as an effective green catalyst for one-pot multicomponent reactions. The results showed that the synthesized nanoparticles were able to create the desired heterocycle products with high efficiency and purity. In both types of reactions, a wide range of acetophenones and aromatic aldehydes containing electron acceptor groups as well as electron donor groups on the aromatic ring provided the desired products at good isolated yields. In addition, simplicity of operation, facile purification of products, shorter reaction times, mild reaction conditions, easy separation and recyclability of the catalyst, were the main advantage of this catalyst.

Acknowledgments

We are grateful to Payam Noor University for encouragements.

5. References

1. E. El-Sayed, A. Fadda, A. El-Saadaney, *Acta Chim. Slov*. **2020**, *67*, 1024–1034. **DOI:**10.17344/acsi.2019.5007
2. G. H. Elgemeie, R. A. Mohamed, *Heterocycl. Commun*. **2014**, *20*, 257–269. **DOI:**10.1515/hc-2014-0156
3. J. R. Vishnu, A. Sethi, R. Pratap, *The Chemistry of Heterocycles*, 1st Ed. Elsevier, Amsterdam, **2019**
4. H. Beyzaei, S. Sargazi, G. Bagherzade, A. Moradi, E. Yarmohammadi, *Acta Chim. Slov*. **2021**, *68*, 109–117. **DOI:**10.17344/acsi.2020.6208
5. T. Chaban, J. Matiychuk, O. Shyyka, I. Chaban, V. Ogurtsov, I. Nektegayev, V. Matiychuk, *Acta Chim. Slov*. **2020**, *67*, 1035–1043. **DOI:**10.17344/acsi.2019.5439
6. F. Tok, B. Koçyiğit-Kaymakçıoğlu, Design, *Acta Chim. Slov*. **2020**, *67*, 1139–1147. **DOI:**10.17344/acsi.2020.6028
7. K. Bhandari, N. Srinivas, V. K. Marrapu, A. Verma, S. Srivastava, S. Gupta, *Bioorg. Med. Chem. lett.* **2010**, *20*, 291–293 **DOI:**10.1016/j.bmcl.2009.10.117
8. R. Thomas, M. Hossain, Y. S. Mary, K. S. Resmi, S. Armaković, S. J. Armaković, A. K. Nanda, V. K. Ranjan, G. Vijayakumar, C. Van Alsenoy, *J. Mol. Struct*. **2018**, *1158*, 156–175. **DOI:**10.1016/j.molstruc.2018.01.021
9. A. Gomtsyan, *Chem. Heterocycl. Comp*. **2012**, *48*, 7–10. **DOI:**10.1007/s10593-012-0960-z
10. X. Lu, X. Liu, B. Wan, S. G. Franzblau, L. Chen, C. Zhou, Q. You, *Euro. J. Med. Chem*. **2012**, *49*, 164–171. **DOI:**10.1016/j.ejmech.2012.01.007
11. N. Nagarajan, G. Vanitha, D. A. Ananth, A. Rameshkumar, T. Sivasudha, R. Renganathan, *J. Photochem. Photobiol. B.* **2013**, *127*, 212–222. **DOI:**10.1016/j.jphotobiol.2013.08.016
12. T. C. Chen, D. S. Yu, K. F. Huang, Y. C. Fu, C. C. Lee, C. L. Chen, F. C. Huang, H. H. Hsieh, J. J. Lin, H. S. Huang, *Euro. J. Med. Chem*. **2013**, *69*, 278–293. **DOI:**10.1016/j.ejmech.2013.06.058
13. X. D. Yang, W. C. Wan, X. Y. Deng, Y. Li, L. J. Yang, L. Li, H. B. Zhang, *Bioorg. Med. Chem. Lett*. **2012**, *22*, 2726–2729. **DOI:**10.1016/j.bmcl.2012.02.094

14. L. Xiaojing, J. Yanrong, J. Hao, G. Guanlei, X. Min, *Acta Chim. Sinica*, **2019**, *77*, 1194–1202.
15. M. Smitha, Y.S. Mary, M. Hossain, K. S. Resmi, S. Armaković, S. J. Armaković, R. Pavithran, A. K. Nanda, C. Van Alsenoy, *J. Mol. Struct*. **2018**, *1173*, 221–239. **DOI:**10.1016/j.molstruc.2018.06.110
16. E. Vessally, S. Soleimani-Amiri, A. Hosseinian, L. Edjlali, A. Bekhradnia, *Rsc Advances,* **2017**, *7*, 7079–7091. **DOI:**10.1039/C6RA25816F
17. Y. Bansal, R. Minhas, A. Singhal, R. K. Arora, G. Bansal, *Curr. Org. Chem*. **2021**, *25*, 669–694. **DOI:**10.2174/1385272825666210208141107
18. M. Gaba, C. Mohan, *Med. Chem. Res*. **2016**, *25*, 173–210. **DOI:**10.1007/s00044-015-1495-5
19. M. A. Chiacchio, D. Iannazzo, R. Romeo, S. V. Giofrè, L. Legnani, *Curr. Med. Chem*. **2019**, *26*, 7166–7195. **DOI:**10.2174/0929867325666180904125400
20. S. Prachayasittikul, R. Pingaew, A. Worachartcheewan, N. Sinthupoom, V. Prachayasittikul, S. Ruchirawat, V. Prachayasittikul, *Mini Rev. Med. Chem*. **2017**, *17*, 869–901. **DOI:**10.2174/1389557516666160923125801
21. D. Im, K. Jung, S. Yang, W. Aman, J. M. Hah, *Euro. J. Med. Chem*. **2015**, *102*, 600–610. **DOI:**10.1016/j.ejmech.2015.08.031
22. G. H. Elgemeie, R. A. Mohamed, *Heterocycl. Commun*. **2014**, *20*, 257–269. **DOI:**10.1515/hc-2014-0156
23. M. Hossain, A. K. Nanda, *Sci. J. Chem*. **2018**, *6*, 83–94.
24. A. A. Napoleon, F. R. Khan, E. D. Jeong, E. H. Chung, *Chin. Chem. Lett*. **2015**, *26*, 567–571. **DOI:**10.1016/j.cclet.2015.01.008
25. A. R. Moosavi-Zare, Z. Asgari, A. Zare, M. A. Zolfigol, M. Shekouhy, *RSC Advances,* **2014**, *4*, 60636–60639. **DOI:**10.1039/C4RA10589C
26. D. Tang, P. Wu, X. Liu, Y. X. Chen, S. B. Guo, W. L.Chen, J. G. Li, B. H. Chen, *J. Org. Chem*. **2013**, *78*, 2746–2750. **DOI:**10.1021/jo302555z
27. C. Y. Chen, W. P. Hu, P. C. Yan, G. C. Senadi, J. J. Wang, *Org. Lett.* **2013**, *15*, 6116–6119. **DOI:**10.1021/ol402892z
28. H. R. Shaterian, M. Ranjbar, *J. Mol. Liq*. **2011**, *160*, 40–49. **DOI:**10.1016/j.molliq.2011.02.012
29. Z. J. Cai, S. Y. Wang, S. J. Ji, *Org. Lett*. **2012**, *14*, 6068–6071. **DOI:**10.1021/ol302955u
30. H. Alinezhad, M. Tajbakhsh, N. Ghobadi, *Synth. Commun*. **2015**, *45*, 1964–1976. **DOI:**10.1080/00397911.2015.1041046
31. Z. Zarnegar, J. Safari, M. Borjian-borujeni, *Chem. Heterocycl. Compd*. **2015**, *50*, 1683–1691. **DOI:**10.1007/s10593-015-1638-0
32. Y. M. Ren, Z. Zhang, S. Jin, *Synth. Commun*. **2016**, *46*, 528–535. **DOI:**10.1080/00397911.2016.1152375
33. D. S. Rekunge, I. A. Kale, G. U. Chaturbhuj, *J. Iran. Chem. Soc*. **2018**, *15*, 2455–2462. **DOI:**10.1007/s13738-018-1434-8
34. M. Wang, Z. Yang, Z. Song, Q. Wang, *J. Heterocycl. Chem*. **2015**, *52*, 907–910. **DOI:**10.1002/jhet.2132
35. A. R. Moosavi-Zare, M. A. Zolfigol, S. Farahmand, A. Zare, A. R. Pourali, R. Ayazi-Nasrabadi, *Synlett*. **2014**, *25*, 193–196. **DOI:**10.1055/s-0033-1340088
36. M. Karim Koshteh, M. Bagheri, *J. Mex. Chem. Soc*. **2017**, *61*, 28–34. **DOI:**10.29356/jmcs.v61i1.118
37. X. Zhao, L. Zeng, N. Hosmane, Y. Gong, A. Wu, *Chin. Chem. Lett*. **2019**, *30*, 87–89. **DOI:**10.1016/j.cclet.2018.01.028
38. K. K. Gangu, S. N. Maddila, S. Maddila, S. B. Jonnalagadda, *J. Alloys Compd*. **2017**, *690*, 817–824. **DOI:**10.1016/j.jallcom.2016.08.201
39. H. Saeidian, F. Moradnia, *Quarterly J. Iran. Chem. Commun*. **2017**, *5*, 252–261.
40. J. Shen, X. Li, W. Huang, N. Li, X. Ye, *J. Mate. Res*. **2014**, *29*, 2211. **DOI:**10.1557/jmr.2014.250
41. J. Etemad Gholtash, M. Farahi, B. Karami, M. Abdollahi, *Acta Chim. Slov*. **2020**, *67*, 866–875. **DOI:**10.17344/acsi.2020.5825
42. S. H. Choi, Korean *J. Mater. Res*. **2018**, *28*, 371–375. **DOI:**10.3740/MRSK.2018.28.7.371
43. U. Kurtan, R. Topkaya, A. Baykal, M. S. Toprak, *Ceram. Int*. **2013**, *39*, 6551–6558. **DOI:**10.1016/j.ceramint.2013.01.088
44. M. Nasrollahzadeh, M. Bagherzadeh, H. Karimi, *J. Colloid Interface sci*. **2016**, *465*, 271–278. **DOI:**10.1016/j.jcis.2015.11.074
45. K. Sinkó, E. Manek, A. Meiszterics, K. Havancsák, U. Vainio, H. Peterlik, *J. Nanopart. Res.* **2012**, *6*, 1–4.
46. Y. Zhang, Z. Yang, B. P. Zhu, W. Yu, S. Chen, X. F. Yang, F. Jin, J. Ou-Yang, *Ceram. Int*. **2014**, *40*, 3439–3443. **DOI:**10.1016/j.ceramint.2013.09.087

Povzetek

Dušikove heterociklične spojine so predmet številnih raziskav, saj izkazujejo široko biološko in farmacevtsko uporabnost. V tej študiji smo sintetizirali pet- in šestčlenske dušikove obročne sisteme s pomočjo "one-pot" multikomponentne reakcije z uporabo kobaltovega feritnega nanokatalizatorja, dopiranega z aluminijem. Nanokatalizator smo pripravili z metodo so-obarjanja iz ustreznih kovinskih soli. Rezultati kažejo, da je katalizator visoko učinkovit in da omogoča tvorbo željenih produktov z visokimi izkoristki in čistotami. Enostavnost izvedbe ter preprostost čiščenja produktov, krajši reakcijski časi, milejši reakcijski pogoji, enostavnost ločbe in ponovna uporabnost katalizatorja so glavne odlike tega katalizatorja.

Except when otherwise noted, articles in this journal are published under the terms and conditions of the Creative Commons Attribution 4.0 International License

DOI: 10.17344/acsi.2021.7050 *Acta Chim. Slov.* **2022,** *69,* 98–107
creative commons

Scientific paper

Synthesis and Application of Silica Supported Calix[4]arene Derivative as a New Processing Aid Agent for Reducing Hysteresis of Tread Rubber Compounds Used in Low Rolling Resistance Tires

Seyedeh Nazanin Sadat-Mansouri,[1] Nasrin Hamrahjou,[1] Saeed Taghvaei-Ganjali[1,*] and Reza Zadmard[2]

[1] *Chemistry Department, IA-University, North Tehran Branch, Tehran 1651153311, Iran*

[2] *Chemistry and Chemical Engineering Research Center of Iran, Tehran, Iran*

* *Corresponding author: E-mail: s_taghvaei@iau-tnb.ac.ir*

Received: 07-13-2021

Abstract

Rolling resistance is one of the most important properties of a tire which is highly dependent on the viscoelastic properties of its rubber compounds. There are a lot of ways to reduce this parameter both in construction improvement of the tire and changing in rubber compound formulation especially in tire tread formulation. Rubber scientists have been trying to introduce new processing aid agents beyond the traditional tire components for reducing the rolling resistance. In this study, a unique structure of silica-supported calix[4]arene (SS-CSC[4]A) has been synthesized and applied as a processing aid agent in tire tread formulation. Fourier-transform infrared spectroscopy (FTIR), Nuclear Magnetic Resonance (^{1}HNMR and ^{13}CNMR), ^{29}Si CP/MAS spectroscopy, thermal gravimetric analysis (TGA), elemental analysis, and acid-base titration were used to characterize its structure. Scanning Electron Microscopy (SEM) use to investigate the effect of prepared material on qualification of filler dispersion in the rubber matrix. The viscoelastic properties of the prepared rubber compound were measured by Dynamic Mechanical Thermal Analysis (DMTA) which showed the great decrease in rolling resistance of rubber compound based on SS-CSC[4]A as a processing aid agent. The mechanical and rheological properties of obtained tread rubber compound measured by tensometer and MDR rheometer showed no sensible changes in these properties.

Keywords: Rolling resistance; tire tread compound; silica-supported calix[4]arene; dynamic mechanical thermal analysis; processing aid agent; wet grip.

1. Introduction

Styrene-butadiene rubbers (SBRs) are a group of synthetic elastomers which is a random copolymer of styrene and butadiene.[1] These rubbers have a huge contribution to the production of car tires[2] because of their unique properties especially excellent abrasion resistance and good aging stability.[3,4] It is notable that the ratio of styrene and butadiene has an important role in the properties of the final product in order to enhance the ecumenical properties of tread compound in a passenger car tire, SBR is normally blended with BR.

SBR and BR are used as elastomers because of their amorphous structures. The absence of crystalline structures in these polymers gives rise to the low mechanical properties which hinder their uses.[5] One of the most effective ways to improve the mechanical properties of these polymers is to prepare their compounds with the addition of fillers such as carbon black or silica.[6] Although, the addition of such a rigid additive to the SBR and BR blends can increase their mechanical strength, it can complicate the process ability, decrease the adhesion and rises the friction between the tires and the surface which results in the high rolling resistance, heat build-up and fuel consumption.[7,8]

As a best of our knowledge, high performance rubber tread is in high demand, for example, high wet skid resistance (WSR) and low rolling resistance, which is in line with the concept of "green tires".[9] Thus, it is necessary

to find alternative processing aid agents for using in rubber compounds to reduce heat build-up, hysteresis and rolling resistance. Generally, the processing aid agents used in rubber industry are polymers with low molecular weight, resins, fatty acids, and other hydrocarbon compounds.[10] The processing aid agent is a material that will be improved process ability and will be reduced plasticity. C5 (aliphatic hydrocarbon resin) and C9 (aromatic hydrocarbon resin) can do as processing and reinforcing agents. SP-1068 (phenolic resin) acts as a tackifying resin that makes strong hydrocarbon bonds with the rubber compound. G90 (coumarone indene resin) also acts as a tackifier and processing aid agent and belongs to the highly polar groups of processing aid agents.

Recently, Song[11] has reported a silica-based processing aid agent, utilizing terpene phenol resin (TPR) which enhanced the mechanical and fatigue properties, Kukreja et al.[12] found that the addition of palm oil in an NBR rubber matrix improved the aging resistance and plasticizing efficiency, Asharf et al.[13] reported that poly (methyl methacrylate) (PMMA) compounds with palm oil exhibited enhanced mechanical properties. Veiga et al.[14] investigated the replacement of carbon black by silica-organosilane coupling agent system and the number of processing steps on the mechanical properties, rolling resistance, and wet grip of truck tire treads. Hua et al.[15] studied the effect of vinyl and phenyl group content on the physical, dynamic and mechanical properties of HVBR and SSBR. Mensah et al.[16] explored the physico-mechanical properties of variable rubber blends including epoxide natural rubber (ENR), polybutadiene rubber (BR), and solution polymerized styrene-butadiene rubber (SSBR) filled by silanized silica and carbon black mixtures.

Calix[n]arenes are basket-shaped (vase-shaped) macrocyclic or cyclic oligomers composed of repeating *para*-alkyl phenolic monomers linked by methylene bridges to form a hydrophobic cavity and are simply functionalized both at the upper rim and lower rim. These compounds are based on the hydroxyl alkylation products of aldehydes and phenols with a defined upper rim, lower rim and a central annulus.[17]

Taghvaei-Ganjali and colleagues employed calix[4] arenes and their derivatives in sensors,[18] construction of polyurethane foams,[19] membrane electrode,[20] improvement of mechanical properties and thermal stability of polyurethane composite[21] and removal agents for ions.[22] As other researchers have reported, calix[n]arene derivatives can be used as heterogeneous catalytic system,[23] binders[24] and for detection of tryptophan.[25]

Our research group studied the use of calix[4]arene derivatives as sorbent,[26] filler,[27] tackifier resin,[28] anti-reversion agent[29] in rubber industry. Li et al. investigated the effect of phenolic antioxidants based on calixarene on the antioxidative properties of natural rubber.[30] Malekzadeh et al.[31] studied the influence of a silane coupling agent based on calix[4]arene on the properties of nano-silica filled rubber compound. As could be seen, the possible influence of calix[n]arenes as a processing aid agent on tire tread performance has not been examined in present literatures.

In the present study, a novel calixarene silica based 5, 11, 13, 17-tetrahydroxy 25, 26, 27, 28-tetrakis[chlorosulfonyl]calix[4]arene-bonded silica gel (SS-CSC[4]A), has been synthesized and applied as a processing aid agent in BR/SBR based rubber compounds in order to decrease of heat build-up and hysteresis which leads to reduction of rolling resistance.

2. Experimental

2. 1. Materials

Emulsion polymerized styrene butadiene rubber (E-SBR1502) was provided by Takhte Jamshid Petrochemical Company (Iran) and high-cis polybutadiene rubber 96% (BR) was purchased from Arak Petrochemical Company (Iran). N-330 carbon black was supplied by Pars Company (Iran). Aromatic oil (290, dark brown) was purchased from Iranol Company (Iran). The Hydrocarbon Resin (C5) was provided by Lesco Chemical (China). *p*-tert-Butylphenol was purchased from Merck (Germany) and applied without any purification and another three types of resins (C9, G90 and SP1068) were supplied by Taizhou Huangyan Donghai Chemical Company (China). N-cyclohexyl-2-benzothiazole sulfonamide (CBS), 1, 3-Diphenylguanidine (DPG) and 2, 2, 4-trimethyl-1, 2-dihydroquinoline (TMQ) and sulfur were supplied by Taizhou Huangyan Donghai Chemical Company (China). N-isopropyl-N'-phenyl-p-phenylene (IPPD) was provided by Nocil (India). The silica (Ultrasil VN3) was purchased from Evonik Company (Germany). Bis[3-(triethoxysilyl) propyl]tetrasulfide (TESPT) was purchased from Shin-Etsu company (Japan). Stearic acid (PALMAC 1600) was supplied by Acidchem Company (Malaysia) and Zinc oxide (ZnO) was manufactured by Sepid Oxide Shokuhie Company (Iran). Paraffin wax was supplied by Behran Company (Iran). N-(cyclohexylthio) phethalimide (PVI) was purchased from Changde Dingyuan (China). Silica-supported calix[4]arene derivative was synthesized in our research group.[32] All analytical grades of the reagents and solvents used in this study were provided by Merck Company (Germany) and were analytical pure grades.

2. 2. Synthesis

Synthetic strategy for preparation of silica-supported calix[4]arene derivative (SS-CSC[4]A) according to our published papar[32] has been illustrated in Figure 1.

2. 2. 1. Synthesis of *p*-tert-Butyl calix[4]arene (1)

p-tert-Butyl calix[4]arene was synthesized according to previously described method by Gutsche and Iqbal.[33]

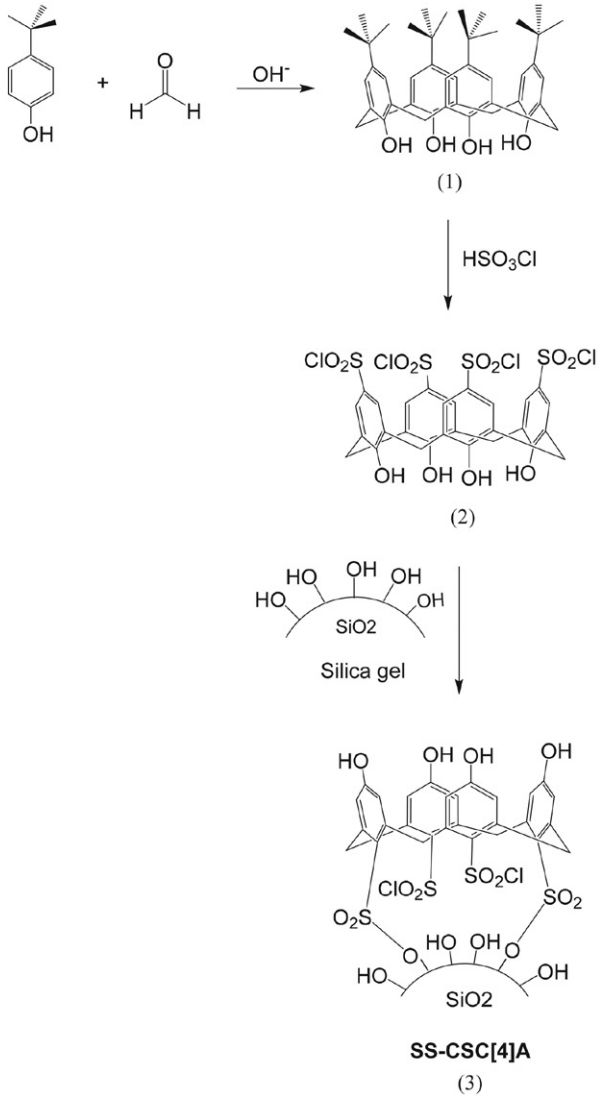

Figure 1. The synthetic strategy for silica-supported calix[4]arene.

Yield: 62%; mp: 342–344 °C; ATR-FTR: υ_{max} (cm^{-1}) = 3169, 2955, 1200, 1401; ^{1}H NMR (400 MHz, $CDCl_3$), δ(ppm): 1.21 (s, 36H, $CH(CH_3)_3$), 3.51 (d, 4H, $ArCH_2Ar$, *J* 12.8 Hz), 4.26 (d, 4H, $ArCH_2Ar$, *J* 12.8 Hz), 7.06 (s, 8H, Ar–H), 10.34 (s, 4H, OH); ^{13}C NMR: (100 MHz, $CDCl_3$), δ(ppm): 31.3, 32.4, 34.0, 126.2, 128.4, 144.5, 146.6.

2. 2. 2. Synthesis of Chlorosulfonyl-Calix[4]arene (2)

Chlorosulfonyl-Calix[4]arene (CSC[4]A) was prepared in accordance with a previous method described by Coquiere et al.[34] with some modification. A mixture of *p*-tert-butylcalix[4]arene (2 mmol) and dichloromethane (25 mL) was placed in a three necked 100 mL round-bottom flask equipped with a magnetic stirrer, reflux condenser and septum. The mixture was stirred for 15 min at room temperature in an inert atmosphere of nitrogen gas. Chlorosulfonic acid (5 mL) was slowly added by syringe at a rate to keep the temperature between 0 and 5 °C. When the addition of chlorosulfonic acid was finished, the solution mixture was refluxed for 2 h under vigorous stirring. After cooling, dry ether (30 mL) was added and the resulting oil after separating was triturated several times with methanol. CSC[4]A as a tan powder was given.

Yield 50%; mp > 230 °C; ATR-FTIR: υ_{max} (cm^{-1}) = 2881, 2829, 1455, 1936, 650, 455–1000. ^{1}H NMR: (500 MHz, DMSO-d_6, TMS), δ(ppm): 3.94 (8H, s, $ArCH_2Ar$), 7.39 (8H, s, Ar–H) and 11.39 (4H, s, 8OH); ^{13}C NMR: (125 MHz, DMSO-d_6), δ(ppm): 138.3 ($ArC–SO_2$), 30.4 ($ArCH_2Ar$); MS-FAB: m/z 817.0 (M^+, calcd 817.5)

2. 2. 3. Synthesis of Silica-Supported Calix[4] arene Derivative (SS-CSC[4]A) (3)

5 g of mesoporous silica gel was activated by refluxing with concentrated sulfuric acid and nitric acid [4:1] at 140 °C for 4 h to remove any adsorbed metal ions. The solution was filtered and obtained white powder was washed with distilled water until the neutral pH was gained. The residual solid was washed with acetone, methanol and dichloromethane, respectively and dried in an oven at 300 °C for 2 h to remove adsorbed surface water and maximize the number of silanol groups on the surface. Activated silica gel was put in a stream of dry nitrogen for 1 h and was used immediately.

100 mL round-bottom flask, equipped with a reflux condenser, a gas inlet tube for conducting of HCl gas over silver nitrate solution was used. It was charged with 50 mL anhydrous xylene, 1.5 g of activated silica gel and 1 g of CSC[4]A. The mixture was allowed to reflux under continuous stirring and a dry nitrogen atmosphere at 140 °C for 72 h. It was mentioned in order to prevent the crashing of silica gel particles and as a result changing the special surface area of silica particles during the reaction, the mechanical stirring was not used in this reaction. Instead, the stirring was done by bubbling of nitrogen gas over the reaction mixture. After carrying out the reaction, the suspension was vacuum filtered using a sintered glass funnel (porosity 3) and the residue was washed in sequence with dichloromethane (5 mL), diethyl ether (5 mL), methanol (5 mL) and hexane (5 mL). The unreacted CSC[4]A inside the pores of silica gel was extracted with acetone at reflux temperature for 12 h in a soxhlet system. The acetone solution was checked by thin layer chromatography and there was no evidence of unreacted CSC[4]A. The final product was dried in an oven at 150 °C for 12 h and kept in the desiccator.

SS-CSC[4]A was characterized by various physical techniques such as elemental analysis for C and Si, ATR-FTIR spectra for functional group confirmation, TGA for confirmation of covalently anchored organic groups and Solid-State ^{29}Si CP/MAS (cross-polarization/magic-angle spinning) NMR for the conformation of chemically bonding between silica gel and CSC[4]A.

Table 1. The results of elemental analysis and titration of SS-CSC[4]A.

Compound	Elemental analysis				Titration
	%C	%H	%S	Bonded amount (μmol/g)	Acid capacity (mmol H^+/g)
SS-CSC[4]A	3.11	0.45	1.15	92.82	0.17

The percentage of carbon, sulfur, hydrogen which was obtained from elemental analysis and resulting acidic properties of SS-CSC[4]A are given in Table 1. The carbon and sulfur contents were assigned to the loading of CSC[4]A over silica gel. The bonded amount was found to be 92.82 μmol/g (0.219 μmol/m^2) according to the carbon content shown in Table 1. Further, the sulfur content of SS-CSC[4]A was 0.36 mmol/g. The number of H^+ determined by acid-base titration was 0.17 mmol/g in the hydrolyzed sample. This value is half of the sulfur content, indicating that only two ester units took place onto SS-CSC[4]A and two acidic sites exist on the surface.

The TGA curve of SS-CSC[4]A shows two distinct stages of weight loss. The first weight loss is between 30 °C and 130 °C is attributed to the physically adsorbed water.[35] The second weight loss is observed between 160 °C and 900 °C which can be related to the decomposition of calixarene, corresponding to 92.82 μmol of CSC[4]A content per gram of silica.

FT-IR spectra were taken for a bare silica gel, CSC[4]A and SS-CSC[4]A. The major peaks of bare silica gel spectrum are: (a) a large broad band between 3200 and 3400 cm^{-1} attributed to the presence of the OH stretching frequency of the surface silanol group and adsorbed water (b) an intense peak at 1000–1250 cm^{-1} related to the antisymmetric Si–O–Si (siloxane) stretching in the amorphous silica (c) a band near 800 cm^{-1} is associated with the symmetric Si–O–Si stretching (d) a peak in the region 1600–1650 cm^{-1} is due to the bending mode of associated water molecules (e) the appearance of a peak at 900 cm^{-1} is related to Si–OH bending frequency. The infrared spectrum of the SS-CSC[4]A presented the same set of bands related to the silica gel, however some additional bands at 2883, 2827, 1457, 1936 and 650 which are assigned to the methylene asymmetric stretching, methylene symmetric stretching, C–H bending mode, benzene ring and C–S stretching mode respectively. Also, the appearance of the several peaks in the region between 1000 and 1500 cm^{-1} is a characteristic adsorption band of calixarenes. So, It is possible that the characteristic peaks of S=O group in compound SS-CSC[4]A which can be seen at 950–1040 cm^{-1}, overlapped with the strong broad band of siloxane in the compound SS-CSC[4]A. It is reasonable to mention here, because of the intense and broad band of siloxane in the region 1100 cm^{-1}, the intensities of the other bands in the spectrum are relatively small. To clarify the spectrum between 1200 and 4000 cm^{-1}, it was scaled up and magnified to show the differences more clearly. Considering the possible heterogeneity in the thickness of samples and the changes in the infrared beam positions, the band area of Si–OH bending frequency at 900 cm^{-1} after and before immobilization were calculated using the silica band at 1100 cm^{-1} as a reference band. The decrease of absorbance in the 900 cm^{-1} band region of SS-CSC[4]A in comparison with the spectrum of bare silica gel indicates that the Si–O–H vibration was affected due to the immobilization. These results which are obtained from IR spectrum are closely in agreement with published data.[36–38]

Direct evidence for chemical attachment of macrocyclic functionalized CSC[4]A to silica surface was done by ^{29}Si CP/MAS solid state NMR. Normally, the spectra of the bare silica gel shows three resonance peaks at −90, −100 and −110 ppm correspond to germinal silanol ($Si(OH)_2$, Q^2), free silanol (SiOH, Q^3) and siloxane (SiOSi, Q^4) respectively.[39] Because the resolution of the spectra is not sufficient to distinguish these signals, only one broad band was seen in the spectra. As a result of the introduction of functionalized calixarenes, the cross polarized ^{29}Si-MAS NMR spectra displayed unsymmetrical pattern when compared to the bare silica material.[40, 41] These results indicated the covalent-attachment of organic groups on the silica surface.

2. 3. Preparation of Rubber Compounds

In this study, seven tire tread compounds were prepared. The formulations of compounds are shown in Table 2. All compounds were mixed on a two-roll mill (Hiva Machinery Company, Iran) according to ASTM D3182 and vulcanization were done in 160 °C.

2. 4. Characterization

2. 4. 1. Cure Characteristics

Cure properties of tire tread compounds including scorch time (ts_2), cure time (tc_{90}), minimum torque (ML), maximum torque (MH) and cure rate index (CRI) were measured at 160 °C by a Moving Die Rheometer (MDR 2000) made by HIWA company according to ASTM D5289 standard. The curing characteristics of compounds have been shown in Table 3.

2. 4. 2. Mechanical Properties

The mechanical properties of prepared compounds including tensile strength, stress at 100% elongation

Table 2. Tire Tread Compound Formulations.

Ingredient	Component content (phr*)						
	A	B	C	D	E	F	G
BR	30	30	30	30	30	30	30
SBR	70	70	70	70	70	70	70
Carbon Black N330	45	45	45	45	45	45	45
Silica	20	20	20	20	20	20	20
Silane (TESPT)	1	1	1	1	1	1	1
ZnO	3	3	3	3	3	3	3
Stearic acid	2	2	2	2	2	2	2
Sulfur	1.6	1.6	1.6	1.6	1.6	1.6	1.6
P.Wax	2	2	2	2	2	2	2
IPPD	1.5	1.5	1.5	1.5	1.5	1.5	1.5
TMQ	1	1	1	1	1	1	1
Aromatic oil	37	37	37	37	37	37	37
CBS	1.4	1.4	1.4	1.4	1.4	1.4	1.4
DPG	2	2	2	2	2	2	2
PVI	0.3	0.3	0.3	0.3	0.3	0.3	0.3
Aliphatic hydrocarbon Resins (C5)	–	2	–	–	–	–	–
Aromatic hydrocarbon Resins (C9)	–	–	2	–	–	–	–
Coumarone Indene Resin (G90)	–	–	–	2	–	–	–
Phenolic Tackifying Resin (SP1068)	–	–	–	–	2	–	–
Para tert butyl phenol	–	–	–	–	–	2	–
SS-CSC[4]A	–	–	–	–	–	–	2

*phr represented the mass parts per 100 mass parts of BR/SBR blend.

Table 3. The results of curing behavior of rubber compounds.

Sample	ML (dN.m)	MH (dN.m)	MH-ML (dN.m)	Tc_{90} (Min)	T_{S2} (Min)	CRI (Min^{-1})
A	1.343 ± 0.213	7.570 ± 0.121	6.227 ± 0.234	13.672 ± 0.223	7.06 ± 0.211	15.125 ± 0.444
B	1.655 ± 0.111	8.277 ± 0.154	6.621 ± 0.054	14.721 ± 0.358	7.729 ± 0.276	14.301 ± 0.591
C	1.655 ± 0.132	8.139 ± 0.148	6.483 ± 0.229	13.823 ± 0.311	7.203 ± 0.257	15.106 ± 0.213
D	1.655 ± 0.112	8.691 ± 0.076	7.035 ± 0.211	14.125 ± 0.298	6.967 ± 0.122	13.972 ± 0.274
E	1.793 ± 0.163	8.415 ± 0.181	6.621 ± 0.017	13.832 ± 0.301	6.767 ± 0.130	14.156 ± 0.479
F	1.793 ± 0.224	8.691 ± 0.159	6.897 ± 0.326	15.46 ± 0.388	7.667 ± 0.199	12.832 ± 0.395
G	1.793 ± 0.194	8.691 ± 0.271	6.897 ± 0.077	14.682 ± 0.390	7.428 ± 0.295	13.784 ±0.565

(M100), 300% elongation (M300), and elongation at break were measured by a Universal Testing Machine (model; M350-5kN, Testometric Company, UK) according to the ASTM D412 C test method. Dumbbell-shaped specimens (2 mm thickness, 25 mm width and 100 mm length) were cut from molded sheets. The average values of the measured quantities and their standard errors were reported in Table 4.

Table 4. The results of mechanical properties of rubber compounds.

Sample	Processing aid agent	Tensile strength (MPa)	Elongation at break (%)	Modulus @ 100% (MPa)	Modulus @ 300% (MPa)
A	Blank	13.179 ± 0.876	647.693 ± 28.251	1.742 ± 0.027	5.042 ± 0.038
B	C5	13.227 ± 0.726	725.75 ± 24.344	1.493 ± 0.056	4.273 ± 0.096
C	C9	14.251 ± 0.44	746.179 ± 4.855	1.529 ± 0.085	4.436 ± 0.158
D	G90	14.958 ± 0.252	736.452 ± 4.583	1.729 ± 0.045	4.897 ± 0.105
E	SP-1068	14.549 ± 0.13	754.237 ± 6.797	1.820 ± 0.053	4.824 ± 0.086
F	*P*-tert	13.897 ± 0.319	745.163 ± 38.728	1.564 ± 0.131	4.443 ± 0.300
G	SS-CSC[4]A	14.175 ± 0.306	712.71 ± 23.45	1.762 ± 0.109	4-927 ± 0.230

2. 4. 3. Dynamic Mechanical Thermal Analysis (DMTA)

Dynamic mechanical thermal properties of tire tread compounds were examined by using a dynamic mechanical thermal analyzer (DMTA; Tritec-2000; England) at temperature range from –140 °C to 90 °C in tension mode deformation and a frequency of 1.0 Hz according to ASTM E1640. The results have been shown in Tables 5 and 6.

2. 4. 4. Scanning Electron Microscopy (SEM)

The degree of filler dispersion in compounds G and A (blank) was tested by scanning electron microscopy (SEM, Philips-XL 30, Netherlands) with an accelerating voltage of 25 kV. The samples were supper-coated with gold to increase their electric conductivity before the examination.

3. Results and Discussions

3. 1. Curing Characteristics

The cure properties that include scorch time (ts_2), optimum cure time (tc_{90}), maximum and minimum torque (MH and ML), the difference in torque (ΔM = MH-ML), and the cure rate index (CRI) of different tire tread compounds (A-G) are shown in Table 3.

These data show that there are no significant changes in cure properties of rubber compounds by changing in processing aid agents.

3. 2. Mechanical Properties

In order to investigate the mechanical properties, the results of tensile strength, elongation at break, modulus at 100% and modulus at 300% after optimum vulcanization can be seen in Table 4.

The results of mechanical properties of rubber compounds A-G show that SS-CSC[4]A acts as C9 resins according to aromatic behavior and there are slightly increasing in tensile strength and elongation at break in comparison with blank compound A without any significant changes in modulus %100 and %300.

3. 3. DMTA

Dynamic mechanical thermal analysis (DMTA) of tire tread compounds due to prediction tire tread performance, mainly heat build-up, hysteresis and rolling resistance as an indicator of fuel consumption efficiency, is important in tire industry. For this purpose, the dependence of the loss factor (tan *δ*) on temperature at a constant frequency could be characterized. Therefore, the tan δ values at about 90 °C, 60 °C, 25 °C, 0 °C and –10 °C are used to predict heat build-up, rolling resistance, dry grip, wet grip and ice grip, respectively.[15, 42–50] The loss factor that is the ratio between the loss modulus to storage modulus (tan δ = E''/E'), is related to the macromolecule's movements and phase transition in the polymers.[50–52] The lower value of tan δ at 60 °C, 90 °C causes lower hysteresis (lower rolling resistance) and lower heat build-up, and therefore lower fuel consumption efficiency (The main mechanism of en-

Table 5. The results of dynamic mechanical thermal properties of rubber compounds A-G.

Sample	Processing aid agent	Tg (°C)	Tan δ (max)	E'_G (MPa)	E'_R (MPa)	E' 30 °C (MPa)	CLD (mol/m^2)
A	Blank	–44.2	2.64E + 03	0.5328	3.134	10.31	0.3466
B	C5	–44.5	2.68E + 03	0.5369	4.622	10.53	0.5112
C	C9	–44.0	2.69E + 03	0.5505	5.841	10.71	0.6460
D	G90	–40.8	2.29E + 03	0.5116	4.876	11.27	0.5393
E	SP-1068	–43.9	2.61E + 03	0.4891	7.498	15.89	0.8293
F	*P*-tert	–44.0	2.44E + 03	0.5188	5.030	10.87	0.5563
G	SS-CSC[4]A	–44.3	2.73E + 03	0.5324	5.421	11.31	0.5990

Table 6. tan δ at various temperature for compounds A-G derived by DMTA.

Sample	Processing aid agent	90 °C	60 °C	tan δ @ 25 °C	0 °C	–10 °C
A	Blank	0.1627	0.1517	0.1668	0.1735	0.1773
B	C5	0.1378	0.1359	0.1564	0.1681	0.1746
C	C9	0.0922	0.1079	0.1413	0.1648	0.1739
D	G90	0.1321	0.1460	0.1615	0.1741	0.1797
E	SP-1068	0.1357	0.1512	0.1590	0.1672	0.1694
F	*P*-tert	0.1243	0.1326	0.1571	0.1717	0.1760
G	SS-CSC[4]A	0.1068	0.1176	0.1441	0.1549	0.1646

ergy loss in tread compound in a rolling tire is the Payne effect which has not been studied here).

On the other hand, the higher value of tan δ at low temperatures (–10 °C, 0 °C, 25 °C) indicates better grip properties of tire on the roads surface.[53,54] Figures 2–4 and Tables 5–6 represent the influence of different processing aid agents on tire tread performance and dynamic properties for tire tread compounds A-G.

As shown in Figure 3 and Table 5, C and E compounds had the highest and the lowest values of tan δ_{max} (peak of the tan δ). The almost same values of tan δ_{max} for the G and the blank compounds demonstrate that the amount of rubber chains participating in the glass transition for both compounds is in the same order.[55] Regarding this fact the value of E' at 30 °C directly relates to the dry handling property of a tire[56], the highest value of E' at 30 °C for the E compound indicates that the compound possessed the best dry handling property. The E' value at 30 °C for the G compound increased about 9.7% compared to the obtained parameter for the blank compound. The value of cross-linking density (CLD) parameter in Equation (1) was obtained by the following equation[55]:

$$CLD = E'/3RT \quad (1)$$

where E', R, and T are corresponded to the minimum storage modules, the universal gas constant, and the absolute temperature at the rubbery plateau zone, respectively.

Based on Equation (1), the higher value of E' at the rubbery region results in a higher degree of cross linking density. Therefore, from Table 5 it can be clearly seen that the E compound possessed the highest modulus at rubbery and so the highest degree of cross linking density. The higher E' value at the rubbery zone for the G compound compared to the blank compound led to the increment of the cross linking density (about 72.8%) for the SS-CSC[4]A containing compound. The value of E' at the glassy region for the G compound is the highest in comparison with other compounds and was about 3.4% more than the blank compound indicating the stronger structural interactions of SS-CSC[4]A in G compound with the matrix.

T_g is another parameter that can be obtained from the DMTA analysis. As can be seen, the lowest and highest values of T_g respectively belong to the B and E compounds. The T_g of tire tread compound decreases from –44.2 °C to –44.3 °C when there is SS-CSC[4]A. To understand the reason, the SS-CSC[4]A structure and its effect on silica particle dispersion have been studied. SS-CSC[4]A is a calixarene, that its cavity can relieve the force on itself by moving its flexible bonds, then it is accepted that when SS-CSC[4]A is added as mobile macromolecule to compound with cured chain, T_g must be decreased. On other hand, the addition of SS-CSC[4]A to compound provides better silica dispersion and more interaction between rubber chain and silica particle, which means we have to provide more energy for chain movement and this energy must be provided by higher temperature. According to the results, there is a trade-off between increasing and decreasing T_g when SS-CSC[4]A is added to compound, DMTA results show just 0.1 °C decrease in T_g, so the SS-CSC[4]A flexible bonds is the T_g controller.

In general, it is expected that with a gradual decrease in T_g, the values of tan δ will be increased. But as can be seen in results, tan δ values are lower than the blank compound at all temperatures in the presence of SS-CSC[4]A. At high temperature when it is well above T_g, the movement of the chains is very fast and long range. Regardless of the flexible structure, with the presence of SS-CSC[4]A as an external factor makes it difficult to move the polymer chain, so tan δ values were decreased.

According to Figure 4 and Table 6, the values of tan δ at 60 °C and 90 °C of compound G are decreased compared to blank compound (A), where the rolling resistance and heat build-up decreased by 22.5% and 34.4%, respectively. Which means the fuel consumption efficiency and heat build-up performance of compound G containing SS-CSC[4]A are improved. The fuel consumption of a passenger car will be reduced by 1–2% if the rolling resistance of tire is reduced by 10%, according to the literatures.[57–59]

But at lower temperature due to better dispersion of the silica particle and more interaction between matrix and filler, increasing of tan delta for silica filled in comparison to CB based compounds are mainly due to the higher polymer volume fraction in them. In fact, at a lower temperature, due to increase in stiffness of filler agglomerate and cluster, the release of occluded rubber is more difficult than the higher temperature. As in the case of silica compound, we have lower values of occluded rubber and thus polymer volume fraction is higher than CB compounds. As a result, tan δ values and grip decrease in G compound compared to blank compound.

Consequently, the use of SS-CSC[4]A as a processing aid agent in tire tread compounds, is beneficial for reduc-

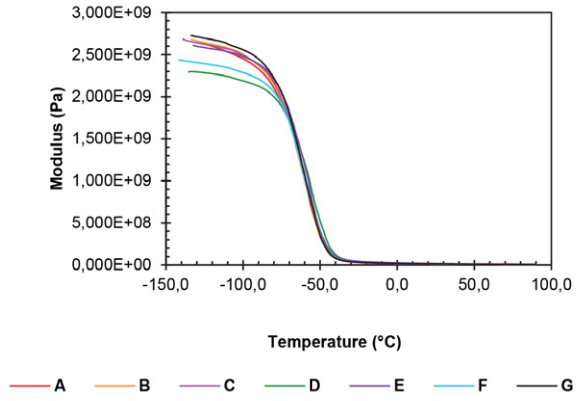

Figure 2. Storage modulus (E') versus temperature curves of rubber samples containing various processing aid agent.

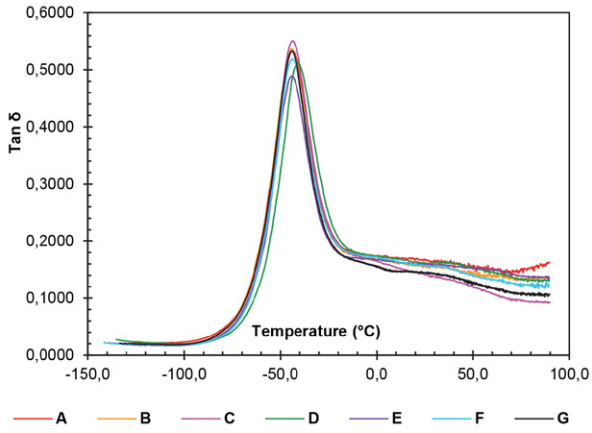

Figure 3. Loss factor (tan δ) versus temperature curves of rubber samples containing various processing aid agent.

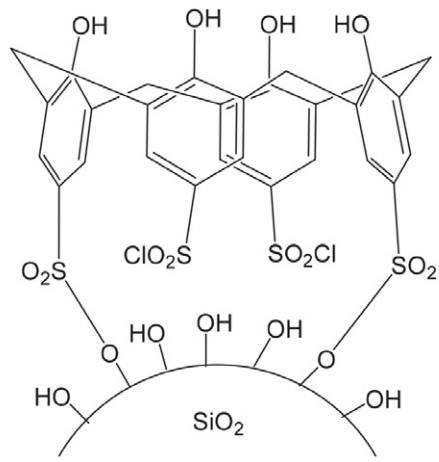

Figure 5. SS-CSC[4]A molecular structure.

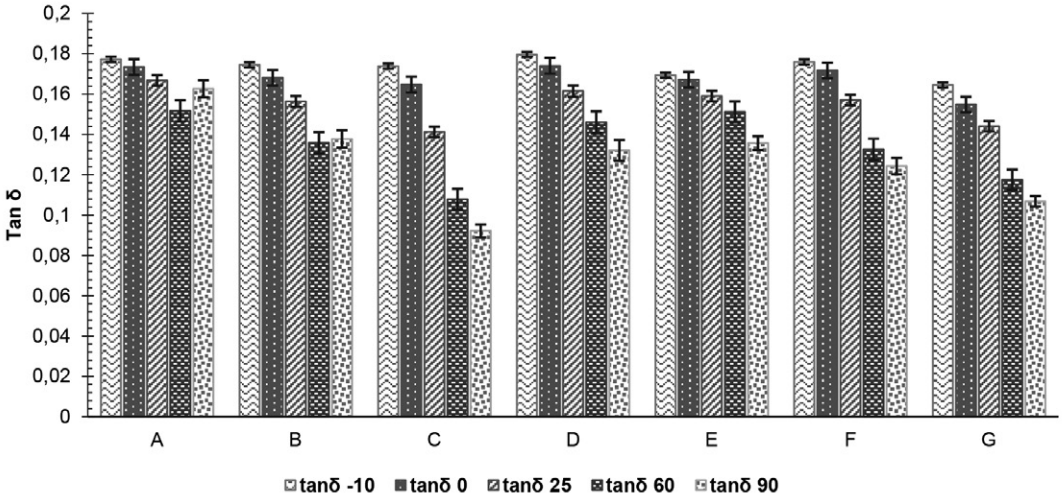

Figure 4. Loss factor (tan δ) values at different temperature of rubber samples containing various processing aid agent.

ing heat build-up, hysteresis and rolling resistance. This is because of better filler dispersion, stronger rubber-filler interaction, higher crosslink density and lower filler-filler interaction.

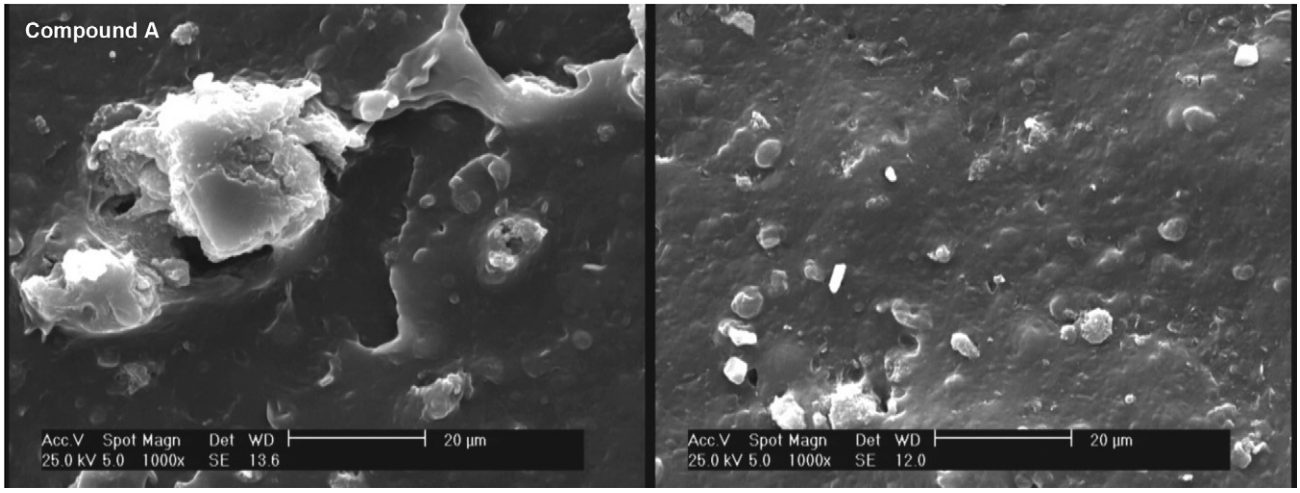

Figure 6. SEM images of compounds A and G.

3. 4. SEM Analysis

For investigating of the SS-CSC[4]A effect on silica dispersion in the rubber compound, the SEM analysis was done in compounds A (Blank) and G (SS-CSC[4]A) as a processing aid agent, are shown in Figure 6. As can be seen the presence of SS-CSC[4]A lead to better dispersion of silica particle in the rubber matrix.

According to the structure of SS-CSC[4]A, there is dual structural behavior. A fair dispersity to the silica as filler via lower rim silica-supported moiety and good physical connection to rubber matrix via upper rim moiety of aromatic based calixarene. As a result, better silica disperses is observed in the rubber matrix in the presence of SS-CSC[4]A as dispersing agents.

4. Conclusion

In this study in order for improvement of rolling resistance and heat build-up of tire tread compound a unique processing aid agent, SS-CSC[4]A was synthesized. FTIR and NMR proved the structure of SS-CSC[4]A. DMTA results showed a reduction in rolling resistance (22.5%) and heat build-up (34.4%), due to the effect of SS-CSC[4]A on silica dispersion and interaction between matrix and filler. SEM results showed a great silica dispersion when there is SS-CSC[4]A in the compound, and the tensile test did not illustrate any tangible changes for the compound containing SS-CSC[4]A. On the other hand, cure properties showed a slight increase in cure parameters because of the interaction enhancement between uncured polymeric chain, filler and macromolecule SS-CSC[4]A.

5. References

1. J. G. Speight, (Ed.): Handbook of industrial hydrocarbon processes, Gulf Professional Publishing, **2019**.
2. D. De, D. De, *Mater. Sci. Appl.* **2011**, *2*, 05, 486–496. **DOI:**10.4236/msa.2011.25066
3. R. Chawla, S. Sharma, *J. Mol. Model.* **2018**, *24*, 4, 1–9. **DOI:**10.1007/s00894-018-3636-5
4. Y. Li, P. Cheng, E. A. Siddig, C. Han, *Road Mater. Pavement Des.* **2020**, *21*, 7, 1902–1917. **DOI:**10.1080/14680629.2019.1574234
5. R. Sengupta, S. Chakraborty, S. A. Bandyopadhyay, S. Dasgupta, R. Mukhopadhyay, K. Auddy, A. S. Deuri, *Polym. Eng. Sci.* **2007**, *47*, 11, 1956–1974. **DOI:**10.1002/pen.20921
6. S. S. Choi, B. H. Park, H. Song, *Polym. Adv. Technol.* **2004**, *15*, 3, 122–127. **DOI:**10.1002/pat.421
7. S. K. Peddini, C. P. Bosnyak, N. M. Henderson, C. J. Ellison, D. R. Paul, *Polymer* **2014**, *55*, 1, 258–270. **DOI:**10.1016/j.polymer.2013.11.003
8. R. P. Kumar, K. M. Nair, S. Thomas, S. C. Schit, K. Ramamurthy, *Compos. Sci. Technol.* **2000**, *60*, 9, 1737–1751. **DOI:**10.1016/S0266-3538(00)00057-9
9. R. Huang, Q. Pan, Z. Chen, K. Feng, *Appl. Sci.* **2020**, *10*, 13, 4478. **DOI:**10.3390/app10134478
10. N. C. Kim, S. H. Song, *Int. J. Polym. Sci.* **2019**, *2019,* 1–9. **DOI:**10.1155/2019/9123635
11. S. H. Song, *Appl. Sci*. **2020**, *10*, 20, 7244. **DOI:**10.3390/app10207244
12. T. R. Kukreja, R. C. Chauhan, S. Choe, P. P. Kundu, *J. Appl. Polym. Sci.* **2003**, *87*, 10, 1574–1578. **DOI:**10.1002/app.11490
13. S. M. Ashraf, S. Ahmad, U. Riaz, M. Alam, H. O. Sharma, J. Macromol. *Sci., Part A: Pure Appl. Chem.* **2005**, *42*, 10, 1409–1421. **DOI:**10.1080/10601320500206903
14. V. D. A. Veiga, T. M. Rossignol, J. D. S. Crespo, L. N. Carli, *J. Appl. Polym. Sci.* **2017**, *134*, 39, 45334. **DOI:**10.1002/app.45334
15. J. Hua, K. Liu, Z. Wang, J. Geng, X. Wang, *J. Appl. Polym. Sci.* **2018**, *135*, 12, 45975. **DOI:**10.1002/app.45975
16. B. Mensah, B. Agyei-Tuffour, E. Nyankson, Y. D. Bensah, D. Dodoo-Arhin, J. K. Bediako, B. Onwona-Agyeman, A. Yaya, *Int. J. Polym. Sci.* **2018**, *2018,* 1–12. **DOI:**10.1155/2018/2473286
17. W. Sliwa, C. Kozlowski, (Ed.): Calixarenes and resorcinarenes: synthesis, properties and applications, John Wiley & Sons, **2009**. **DOI:**10.1002/anie.200903182
18. M. Hosseini, M. Rahimi, H. B. Sadeghi, S. Taghvaei-Ganjali, S. D. Abkenar, M. R. Ganjali, *Int. J. Environ. Anal. Chem.* **2009**, *89*, 6, 407–422. **DOI:**10.1080/03067310802713195
19. M. S. Mirmoeini, M. M. A. Nikje, M. Rasouli-Saniabadi, S. Taghvaei-Ganjali, *Macromol. Symp.* **2017**, 373, 1600101. **DOI:**10.1002/masy.201600101
20. S. Taghvaei-Ganjali, R. Zadmard, M. Zeyaei, K. Rahnama, F. Faridbod, M. R. Ganjali, *Res. Lett. Org. Chem.* **2009**, *2009, 1–5*. **DOI:**10.1155/2009/601089
21. S. Taghvaei-Ganjali, M. Rasouli-Saniabadi, M. S. Mirmoeini, *J. Inclusion Phenom. Macrocyclic Chem.* **2015**, *83*, 1, 45–52. **DOI:**10.1007/s10847-015-0539-2
22. M. Nouri, S. Mozafari, S. Taghvaei-Ganjali, *Iran. JOC*. 2011, *3*, 4, 807–809.
23. A. B. Chenari, M. Saber-Tehrani, M. Mamaghani, M. Nikpassand, *J. Inclusion Phenom. Macrocyclic Chem*. **2019**, *94*, 1, 45–53. **DOI:**10.1007/s10847-019-00894-x
24. K. D. Daze, C. E. Jones, B. J. Lilgert, C. S. Beshara, F. Hof, *Can. J. Chem.* **2013**, *91*, 11, 1072–1076. **DOI:**10.1139/cjc-2013-0186
25. T. T. Pang, L. M. Du, H. L. Liu, Y. L. Fu, *Can. J. Chem*. **2014**, *92*, 1139–1144. **DOI:**10.1139/cjc-2014-0150
26. Z. Servati, M. Saber-Tehrani, S. Taghvaei-Ganjali, R. Zadmard, *J. Porous Mater*. **2018**, *25*, 5, 1463–1474. **DOI:**10.1007/s10934-018-0559-6
27. H. Mohamadi, F. Motiee, M. Saber-Tehrani, S. Taghvaei-Ganjali, *Russ. J. Appl. Chem*. **2019**, *92*, 6, 809–816. **DOI:**10.1134/S1070427219060107
28. H. M. Pekachaki, S. Taghvaei-Ganjali, F. Motiee, M. Saber-Tehrani, *Rubber Chem. Technol*. **2019**, *92*, 3, 467–480. **DOI:**10.5254/rct.19.81510
29. H. Mohamadi, F. Motiee, S. Taghvaei-Ganjali, M. Saber-Tehrani, *Acta Chim. Slov*. **2021**, *68*, 1, 128–136. **DOI:**10.17344/acsi.2020.6225

30. H. Li, Y. Zhong, W. Wu, L. Zhang, X. Lai, X. Zeng, *J. Appl. Polym. Sci*. **2017**, *134*, 31, 45144. **DOI:**10.1002/app.45144
31. M. Malekzadeh, H. Nouri, M. Farahani, *JACR*. **2010**, *3*, 41–45.
32. S. Taghvaei-Ganjali, R. Zadmard, M. Saber-Tehrani, *Appl. Surf. Sci*. **2012**, *258*, 16, 5925-5932. **DOI:**10.1016/j.apsusc.2011.09.019
33. C. D. Gutsche, M. Iqbal, *Org. Synth*. **2003**, *68*, 234–234. **DOI:**10.1002/0471264180.os068.29
34. D. Coquière, H. Cadeau, Y. Rondelez, M. Giorgi, O. Reinaud, *J. Org. Chem*. **2006**, *71*, 11, 4059–4065. **DOI:**10.1021/jo052605p
35. S. Radi, A. Attayibat, A. Ramdani, M. Bacquet, *Eur. Polym. J*. **2008**, *44*, 10, 3163–3168. **DOI:**10.1016/j.eurpolymj.2008.07.021
36. M. Tabakci, *J. Inclusion Phenom. Macrocyclic Chem*. **2008**, *61*, 1, 53–60. **DOI:**10.1007/s10847-007-9392-2
37. H. Huang, C. Zhao, Y. Ji, R. Nie, P. Zhou, H. Zhang, *J. Hazard. Mater*. **2010**, *178*, 1–3, 680–685. **DOI:**10.1016/j.jhazmat.2010.01.140
38. R. Tian, J. Sun, H. Zhang, M. Ye, C. Xie, J. Dong, J. Hu, D. Ma, X. Bao, H. Zou, *Electrophoresis* **2006**, *27*, 4, 742–748. **DOI:**10.1002/elps.200500630
39. T. M. Suzuki, T. Nakamura, E. Sudo, Y. Akimoto, K. Yano, *Microporous Mesoporous Mater*. **2008**, *111*, 1–3, 350–358. **DOI:**10.1016/j.micromeso.2007.08.008
40. D. W. Sindorf, G. E. Maciel, *J. Am. Chem. Soc*. **1983**, *105*, 12, 3767–3776. **DOI:**10.1021/ja00350a003
41. E. F. Vansant, P. Van Der Voort, K. C. Vrancken, (Ed.): Characterization and chemical modification of the silica surface, Elsevier, Amsterdam, **1995**. **DOI:**10.1016/S0167-2991(06)81508-9
42. X. Zhao, K. Niu, Y. Xu, Z. Peng, L. Jia, D. Hui, L. Zhang, *Composites, Part B*. **2016**, *107*, 106–112. **DOI:**10.1016/j.compositesb.2016.09.073
43. X. Liu, S. Zhao, X. Zhang, X. Li, Y. Bai, *Polymer* **2014**, *55*, 8, 1964–1976. **DOI:**10.1016/j.polymer.2014.02.067
44. M. H. R. Ghoreishy, S. Taghvaei, R. Z. Mehrabian, *Iran. J. Sci. Technol*. **2011**, *24*, 4, 329–337.
45. C. Sirisinha, P. Sae-oui, K. Suchiva, P. Thaptong, *J. Appl. Polym. Sci*. **2020**, *137*, 20, 48696. **DOI:**10.1002/app.48696
46. U. Thepsuwan, P. Sae-oui, C. Sirisinha, P. Thaptong, *J. Appl. Polym. Sci*. **2019**, *136*, 4, 46987. **DOI:**10.1002/app.46987
47. P. Sae-Oui, K. Suchiva, C. Sirisinha, W. Intiya, P. Yodjun, U. Thepsuwan, *Adv. Mater. Sci. Eng*. **2017**, *2017,* 1–8. **DOI:**10.1155/2017/2476101
48. P. J. Martin, P. Brown, A. V. Chapman, S. Cook, *Rubber Chem. Technol*. **2015**, *88*, 3, 390–411. **DOI:**10.5254/rct.15.85940
49. Y. Gui, J. Zheng, X. Ye, D. Han, M. Xi, L. Zhang, *Composites, Part B*. **2016**, *85*, 130–139. **DOI:**10.1016/j.compositesb.2015.07.001
50. H. Roshanaei, F. Khodkar, M. Alimardani, *Iran. Polym. J*. **2020**, *29*, 10, 901–909. **DOI:**10.1007/s13726-020-00850-4
51. S. Ahmadi Shooli, M. Tavakoli, *J. Macromol. Sci., Part B: Phys*. **2016**, *55*, 10, 969–983. **DOI:**10.1080/00222348.2016.1230464
52. S. Ahmadi-Shooli, M. Tavakoli, *J. Macromol. Sci., Part B: Phys*. **2019**, *58*, 7, 619–633. **DOI:**10.1080/00222348.2019.1574428
53. M. Harper, J. Tardiff, D. Haakenson, M. Joandrea, M. Knych, *SAE Int. J. Veh. Dyn. Stab. and NVH* **2017**, *1*, 2, 179–189. **DOI:**10.4271/2017-01-1502
54. S. Ezzoddin, A. Abbasian, M. Aman-Alikhani, S. Taghvaei-Ganjali, *Iran. Polym. J*. **2013**, *22*, 9, 697–707. **DOI:**10.1007/s13726-013-0168-9
55. P. Thaptong, P. Sae-Oui, C. Sirisinha, *J. Appl. Polym. Sci*. **2016**, *133*, 17, 43342. **DOI:**10.1002/app.43342
56. T. Mondal, A. K. Bhowmick, R. Ghosal, R. Mukhopadhyay, *Polymer* **2018**, *146*, 31–41. **DOI:**10.1016/j.polymer.2018.05.031
57. J. Barrand, J. Bokar, *SAE Int. J. Passeng. Cars - Mech. Syst.* **2008**, *1*, 1, 9–17. **DOI:**10.4271/2008-01-0154
58. C. F. S. Gabriel, A. D. A. P. Gabino, A. M. F. de Sousa, C. R. G. Furtado, R. C. R. Nunes, *J. Elastomers Plast.* **2019**, *51*, 7–8, 712–726. **DOI:**10.1177/0095244318819196
59. P. Sae-oui, K. Suchiva, U. Thepsuwan, W. Intiya, P. Yodjun, C. Sirisinha, *Rubber Chem. Technol.* **2016**, *89*, 2, 240–250. **DOI:**10.5254/rct.15.84859

Povzetek

Kotalni upor (ang. rolling resistance) je ena najpomembnejših lastnosti pnevmatik, ki je zelo odvisna od viskoelastičnih lastnosti njenih komponent. Obstaja več načinov za zmanjšanje tega parametra, tako s samo konstrukcijo pnevmatike kot tudi s spreminjanjem njene sestave, še posebej pri načrtovanju profilnega dela. Raziskovalci na tem področju zato poskušajo z uvajanjem novih aditivov, ki bi zmanjšali kotalni upor. V tej študiji smo na silikatno osnovo sintetizirali derivat kaliks[4]arena (SS-CSC[4]A) edinstvene strukture in ga uporabili kot polnilo profilnega dela pnevmatik. FTIR, magnetno resonanco (^{1}HNMR and ^{13}CNMR), ^{29}Si CP/MAS spektroskopijo, termično gravimetrično analizo (TGA), elementno analizo in titracijo smo uporabili za karakterizacijo. Učinkovitosti dispergiranja polnila v gumi smo določili z vrstično elektronsko mikroskopijo (SEM). Viskoelastične lastnosti tako pripravljene gume smo izmerili z dinamično mehanično termično analizo (DMTA), ki je pokazala znatno zmanjšanje kotalnega upora v primerjave z gumo brez SS-CSC[4]A polnila. Meritve opravljene s tenzometrom in MDR reometrom pa niso pokazale drugih bistvenih razlik mehanskih in reoloških lastnosti.

Except when otherwise noted, articles in this journal are published under the terms and conditions of the Creative Commons Attribution 4.0 International License

DOI: 10.17344/acsi.2021.7053 *Acta Chim. Slov.* **2022,** *69,* 108–115
creative commons

Scientific paper

A Novel Solid-State PVC-Membrane Potentiometric Dopamine-Selective Sensor Based on Molecular Imprinted Polymer

Nurşen Dere,[1] Zuhal Yolcu[2] and Murat Yolcu[2,*]

[1] *Giresun University, Center Research Laboratory Application and Research Center, Giresun /Turkey*

[2] *Giresun University, Science and Arts Faculty, Chemistry Department, Giresun /Turkey*

* *Corresponding author: E-mail: murat.yolcu@giresun.edu.tr*

Received: 09-21-2021

Abstract

A novel solid-state polyvinylchloride (PVC) membrane potentiometric dopamine-selective microsensor was constructed based upon dopamine-imprinted polymer (DOP-IP) used as the ionophore in the membrane structure. The optimum membrane composition was determined as 4% (w/w) DOP-IP, 69% (w/w) bis(2-ethylhexyl) sebacate (DOS), 26% (w/w) PVC, and 1% (w/w) potassiumtetrakis(4-chlorophenyl) borate (KTpClPB). The detection limit of the microsensor was determined to be 3.71×10^{-7} mol L^{-1}. The microsensor exhibited a super-Nernstian response for dopamine over the concentration range of 10^{-6}–10^{-1} mol L^{-1}, with a short response time (<15 s) and a slope of 60.3 ± 1.3 mV per decade (R^2: 0.9998) over seven weeks. The microsensor was effectively performed in a pH range of 4.0–8.0 and a temperature range of 5–30 °C. The microsensor has been successfully demonstrated for the rapid, accurate, selective and reproducible determination of dopamine in pharmaceutical formulations with the recovery of 104.3–104.8%. The obtained results were in good harmony with the UV-Vis results at a confidence level of 95%.

Keywords: Dopamine; solid-state microsensor; molecular imprinted polymer; potentiometry

1. Introduction

Dopamine is one of the most important neurotransmitters that play specific roles in various physiological and pathological processes in the central nervous, cardiovascular, hormonal and renal systems of the human body, modulated by their levels in various brain tissues.[1–3] Determination of dopamine is important in the diagnosis, monitoring and prevention of certain diseases, such as Parkinson's, schizophrenia, HIV infections, hyperuricemia, and a type of arthritis.[4] There are many instrumental methods for dopamine determination, such as chromatography,[5] fluorimetry,[6] colorimetry,[7] spectrophotometry,[8] and electrochemistry.[9] These methods require both expensive equipment and complex sample preparation, and time. Electrochemical methods have several advantages compared to expensive instrumental methods. Especially, when evaluated in terms of ion-selective electrodes; electrochemical methods provide superiority such as short response time, low detection limit, simple design, low cost, wide operating range, high selectivity, minimum sample pretreatment, accuracy and precision, easy measurement process.[10]

The molecular imprinting method involves the polymerization of a functional monomer and crosslinker around a template which is removed using different solvents after the synthesis process.[11] This technique is a very suitable method for polymeric material formation with molecular recognition cavities created by the addition of template molecules during the process.[12] As a result, molecular imprinted polymers (MIPs) provide a wide range of binding sites with various affinities and selectivity that are interrelated to the template molecule in size, functionality, and shape.[13] The imprinted polymers have several advantages such as good physical and chemical stability, high selectivity and low cost.[14–16] MIPs are widely used in drug release,[17] solid-phase extraction,[18] enzyme mimics,[19] chromatographic separation,[20] cancer biomarkers,[21] and sensors.[22] Different potentiometric sensors based on MIP have been reported.[23–25] Several electrochemical sensors have also been reported for dopamine determination.[26–30]

In this work, a novel potentiometric dopamine-selective microsensor, that is solid-state PVC-membrane type, was designed using dopamine-imprinted polymer (DOP-IP) as an ionophore. The performance characteristics (limit of detection, linearity, slope with standard deviation, response time, selectivity, repeatability, reproducibility, pH, and temperature ranges, etc.) of the microsensor were investigated in detail. The microsensor was successfully used for dopamine determination in the content of the pharmaceutical formulations. The potentiometric results were compared with the UV-Vis spectroscopic results.

2. Experimental

2. 1. Reagents

Dopamine (DOP), methacrylic acid (MA), azobisisobutyronitrile (AIBN), ethylene glycol dimethacrylate (EGDMA), ethanol (EtOH), methanol, acetic acid, tetrahydrofuran (THF), high molecular weight polyvinylchloride (PVC), o-nitrophenyl octyl ether (NPOE), bis(2-ethylhexyl) sebacate (DOS), dibutyl sebacate (DBS), potassium tetrakis (4-chlorophenyl) borate (KTpClPB), graphite, solvents, and all other salts were purchased from Sigma-Aldrich. Epoxy resin (Ultrapure SU 2227) and hardener (Desmodur RFE) were supplied from Victor and Bayer AG, respectively.

2. 2. Apparatus

A multi-channel potentiometer supported by a computer program device and designed in our laboratory was used for the potentiometric measurements. Ag/AgCl electrode (Basi-MF-2079-RE-5B) was operated as a reference electrode. A Jenway 3040 model ion analyser was used for pH measurements. A Shimadzu AUX220 model analytical balance was used for measuring weight. A Kubota 4200 model centrifuge was used for centrifugation. Deionized water was supplied from a Sartorius Stedim Ariium 611UV model ultra-deionized water device. A Memmer (GmbH & Co. KG D.91126 Typ: WNB 14) shaker was used for the removal of dopamine molecules from the polymer. The solutions were homogenized using an Ultrasonic LC30 (Germany) stirrer. A Jeol JSM-6610 model instrument was used for scanning electron microscopy (SEM) analysis. A Thermo Scientific Evaluation Array UV-Vis spectrophotometer was used for the spectroscopic determination of dopamine.

2. 3. Synthesis of Dopamine-Imprinted Polymer

The dopamine-imprinted polymer (DOP-IP) was synthesized according to the method described in the literature.[31] The preparation process of the DOP-IP is sche-

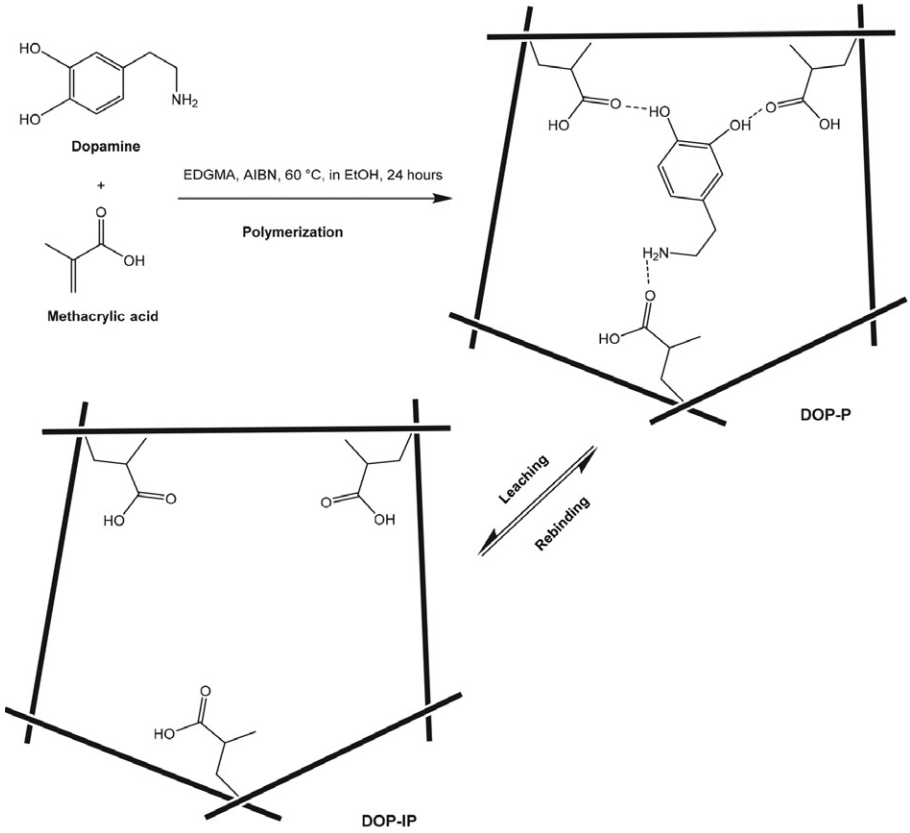

Figure 1. Schematic representation of the DOP-IP preparation process

matized in Figure 1. A 59 mg dopamine, 0.4 mL MA and 1.24 mL EGDMA were dissolved in 6.2 mL EtOH in a glass bottle. The mixture, pure nitrogen gas passed through for 20 min, was sonicated in a water bath for 30 min. Then 0.02 mg AIBN was added to the mixture. The mixture was heated to 60 °C in a thermostatically adjusted oil bath on a magnetic stirrer for 21 hours. A colorless translucent bulk of solid polymer was obtained. Polymer particles containing dopamine molecules (DOP-P) were washed with EtOH and filtered. Methanol/acetic acid (90/10; v/v) solution was repeatedly used for removal of the dopamine molecules until not detecting any dopamine in the filtered solution by UV-Vis method. Final polymer particles (DOP-IP) were then vacuum dried at 50 °C. The non-imprinted polymer (NIP) was synthesized by following the same procedure without dopamine.

2. 4. Fabrication of Solid-State Dopamine-Selective Microsensor

The solid-state dopamine selective microsensor used was manufactured according to the method described in our previous study.[32] The first stage, named as the solid contact production, of sensor fabrication, which occurs in two steps; involves the preparation of an amount of 300 mg of graphite, 210 mg of epoxy, and 90 mg of hardener in 3 mL of THF. A copper wire of about 10 mm length and 2 mm radius is dipped into this mixture several times until a thickness of about 0.5 mm is obtained, and left to dry for a day under laboratory conditions. The second stage contains the preparation of a selective membrane mixture. An amount of 10–15 mg of DOP-IP, 167.5–172.5 mg of NPOE, DOS or DBS, 65–67.5 mg of PVC, and 2.5 mg of KTpClPB were thoroughly mixed in 2.5 mL THF. Finally, the solid contact formed in the first stage is dipped 4–5 times in the membrane mixture and the prepared sensor is left to dry under laboratory conditions for 1 day. After these procedures, the performances of the microsensor are investigated in detail.

2. 5. Analysis Procedure of the Pharmaceutical Samples

The dopamine contents of the pharmaceutical samples were determined using both DOP-selective microsensor and UV-Vis spectrophotometric method in commercially available drug: Dopasel® (200 mg/5 mL). The drug sample was diluted with deionized water before the potentiometric and UV-Vis (at 280 nm) measurements.

3. Results And Discussion

3. 1. SEM Analysis

Scanning Electron Microscopy (SEM) was used for the investigation of surface morphologies of the polymers (NIP, DOP-P and DOP-IP). Figure 2a–f shows the relevant SEM images with the structural differences of the particles. When the general surface morphology is examined; it is seen that the polymers have different particle sizes, however, have spherical shapes as similarities. The NIP particles (Figure 2e–f) are substantially larger in size than the MIP particles (Figure 2a–d). Moreover, it is seen that an enhanced surface area and pores were observed on the DOP-IP surface (Figure 2c–d) than the DOP-P surface (Figure 2a–b). This situation can be considered as a result of the imprinting process. Consequently, the relatively porous surfaces of DOP-IP possess the specific cavities and suitableinteraction sites for the sorption of dopamine molecules.

3. 2. Optimum Membrane Composition

It is known that PVC-membrane sensors are significantly dependent not only on the structure of the ionophores but also on the ratio of membrane components, polymers, plasticizers and other additives. These effects on sensors; in addition to lowering the detection limit of the sensors, also increases the sensitivity and selectivity. The effects of PVC membrane components on the potentiometric response of the DOP-selective microsensor were

Table 1. Potentiometric performance characteristics of DOP–selective microsensors

No	Membrane Composition (mg/250 mg)						Potentiometric Behavior		
	PVC	NPOE	DOS	DBS	KTpClPB	MIP	Slope, mV/decade*	Linear range, mol L^{-1}	Detection limit, mol L^{-1}
I	65	172.5	–	–	2.5	10	49.6 ± 2.6	10^{-5}–10^{-1}	5.30×10^{-7}
II	65	–	172.5	–	2.5	10	60.3 ± 1.3	10^{-6}–10^{-1}	3.71×10^{-7}
III	65	–	–	172.5	2.5	10	45.3 ± 2.5	10^{-5}–10^{-1}	5.72×10^{-6}
VI	65	167.5	–	–	2.5	15	40.7 ± 2.8	10^{-4}–10^{-1}	2.84×10^{-5}
V	65	–	167.5	–	2.5	15	50.6 ± 2.2	10^{-4}–10^{-1}	6.22×10^{-5}
VI	65	–	–	167.5	2.5	15	42.1 ± 3.0	10^{-4}–10^{-1}	4.87×10^{-5}
VII	67.5	172.5	–	–	–	10	45.1 ± 1.8	10^{-5}–10^{-1}	2.62×10^{-6}
VIII	67.5	–	172.5	–	–	10	53.8 ± 1.6	10^{-6}–10^{-1}	4.95×10^{-7}
IX	67.5	–	–	172.5	–	10	44.3 ± 2.1	10^{-5}–10^{-1}	1.36×10^{-6}

*The average value of three determinations ± standard deviation

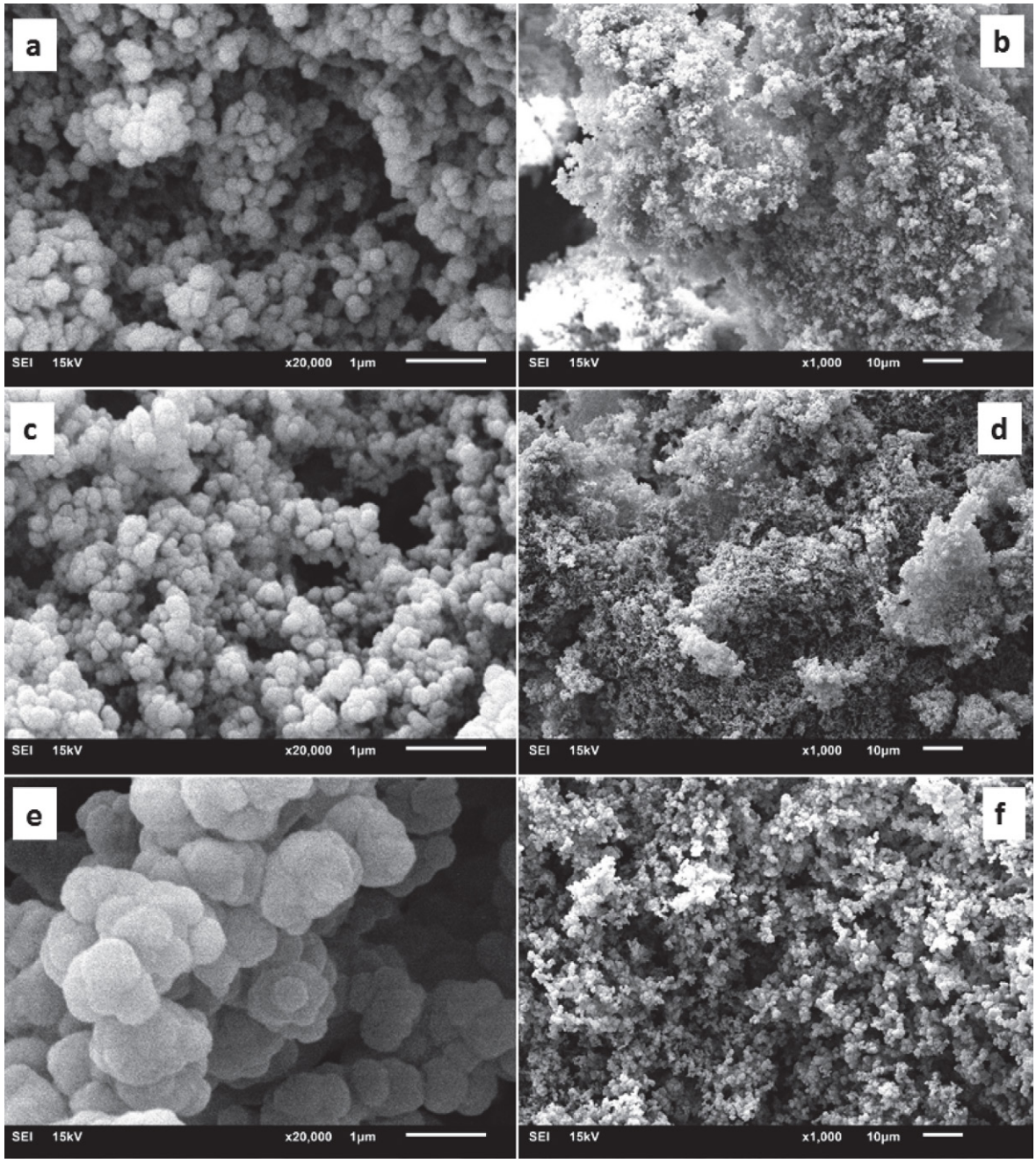

Figure 2. SEM images of the DOP-P (a, b), DOP-IP (c, d), and NIP (e, f)

investigated using different plasticizers (NPOE, DOS and DBS) and the results are summarized in Table 1. It can be seen that the best potentiometric performances (slope, detection limit, linear range) are for sensor number-II compared to the others. The potentiometric performance of the DOP-selective microsensor, which was prepared according to the optimum membrane composition, was investigated in more detail.

The potentiometric response of the DOP-selective microsensor was investigated in the standard dopamine solutions prepared in the concentration range of 10^{-8}–10^{-1} mol L^{-1} (Figure 3). It was determined that the sensor exhibited a linear response to dopamine as a super Nernst behaviour (60.3 ± 1.3 mV) in the concentration range of 10^{-6}–10^{-1} mol L^{-1} with a lower detection limit of 3.71 × 10^{-7} mol L^{-1} and a short response time (t_{95}) of <15 s according to the IUPAC recommendations.[33] The calibration graphs of microsensors prepared with DOP-IP and NIP are shown in Figure 4. The performance of the DOP-IP-based sensor is better than the NIP-based sensor, and it can be said that this situation in the NIP sensor is due to the non-specific interaction on the NIP surface.

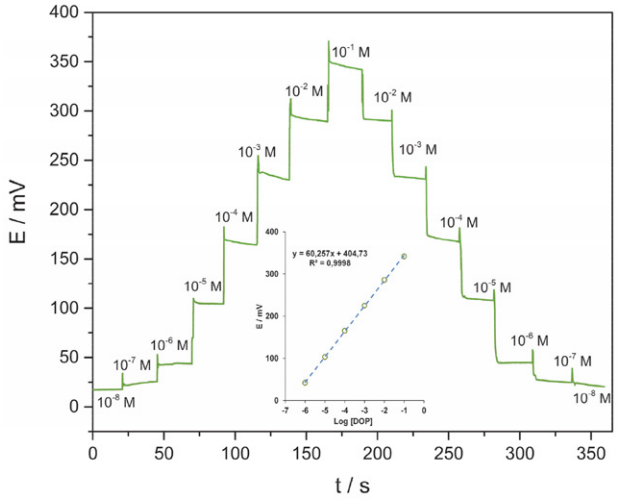

Figure 3. Potentiometric responses and calibration plot of the DOP-selective microsensor

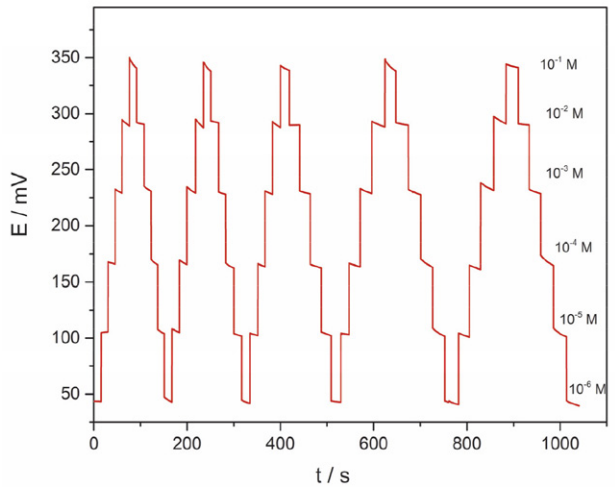

Figure 5. Repeatability measurements of the DOP-selective microsensor

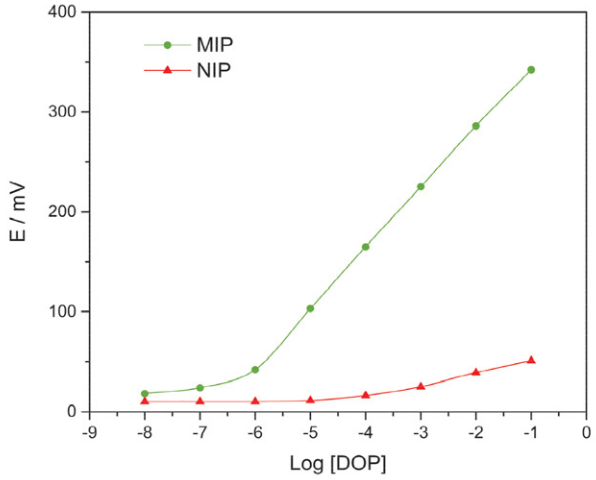

Figure 4. Calibration curves of the DOP-selective sensors based on MIP (•) and NIP (▲)

3. 3. Repeatability and Reproducibility

The repeatability (within-day) of the DOP-selective microsensor was investigated. For this purpose; the measurements were repeatedly taken in the concentration range of 10^{-6}–10^{-1} mol L^{-1} dopamine. The obtained potential-time graph is shown in Figure 5. It can be seen from Figure 5, the behaviour of the developed sensor is highly reproducible.

In order to determine the reproducibility (between-days) of the developed DOP-selective microsensor, the changes in the detection limit and slope values of the sensor have been monitored for two months. For this purpose, measurements were taken in standard dopamine solutions in the linear operating range of the DOP-selective microsensor on certain days and the obtained slope values against time are shown in Figure 6. As can be seen from Figure 6, especially after 42 days, a significant drift in the slopes indicates that the stability of the sensor has deteriorated (the initial slope value of 60.3 mV/decade decreased to 53.1 mV/decade). Therefore, the lifetime of the sensor was estimated to be about 6 weeks. Repeatability and reproducibility of the microsensor showed a difference in potential within 3–5 mV.

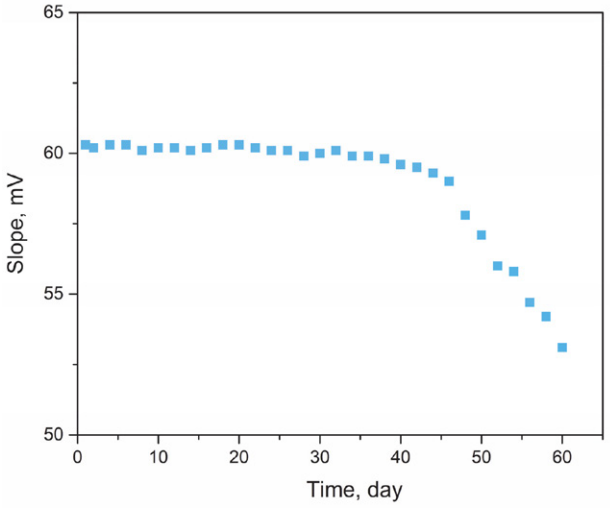

Figure 6. Reproducibility of the DOP-selective microsensor (slope values against time)

3. 4. Selectivity

The selectivity coefficients of the DOP-selective microsensor were calculated by using the separate solution method (SSM).[33] The obtained logarithmic selectivity coefficients (Log $K^{pot}_{DOP,\ X^{n+}}$) for dopamine molecules over other ions and molecules (X^{n+}) are summarized in Table 2. The prepared sensor exhibited high selectivity for dopamine over the commonly encountered and tested different species.

Table 2. Selectivity coefficients of the DOP–selective microsensor

Types	Log $K^{pot}_{DOP, X^{n+}}$	Types	Log $K^{pot}_{DOP, X^{n+}}$
K^+	–2.08	Zn^{2+}	–2.79
Li^+	–1.74	Ba^{2+}	–2.67
Na^+	–2.52	Ni^{2+}	–2.15
$NH4^+$	–2.11	Cd^{2+}	–3.03
Ca^{2+}	–2.93	Co^{2+}	–2.28
Mg^{2+}	–2.33	Cr^{3+}	–2.06
Cu^{2+}	–2.49	Fe^{3+}	–1.91
Ag^+	–3.02	Pb^{2+}	–3.05
Fructose	–3.25	Glucose	–3.18
Urea	–3.17	Lactose	–2.01
Triethanolamine	–2.05	Thiourea	–3.49
Ascorbic acid	–1.88	Thioacetamide	–3.18

3. 5. pH Effect

In order to examine the effect of pH on sensor responses, 1.0×10^{-3} mol L^{-1} dopamine solutions were examined in the pH range of 3.0–11.0 (Figure 7). It can be seen from Figure 7; the sensor potential remained significantly unchanged in the pH range of 4.0–8.0. However, the increase in potential values at low pH values (< 4.0) can be explained by the interaction of hydronium ions on the sensor membrane, as interference, and the decrease in potential values at high pH values (> 8) can be explained by the interference of hydroxyl ions. Therefore, the pH: 4.0–8.0 range can be considered the optimum operating range for the proposed sensor.

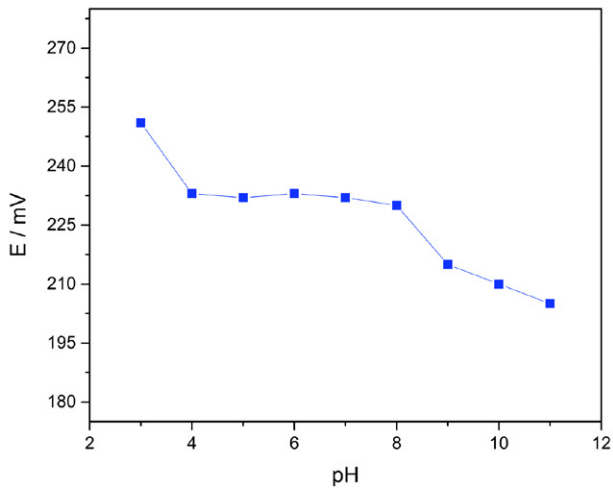

Figure 7. Effect of pH on the DOP-selective microsensor response

3. 6. Temperature Effect

Temperature is another important property for electrochemical sensors. To determine the optimum temperature range of the developed microsensor, the temperatures of the DOP solution were changed from 5 °C to 70 °C. The potential measurements for 10^{-2} mol L^{-1} DOP solution are shown in Figure 8. The DOP-selective microsensor can be able to operate in the temperature range of 5–30 °C (± 2 mV) approximately without significant changes on the performance of the microsensor. The performance of the sensor is affected above 30 °C by the temperatures. In addition, it was determined that the sensor was deformed above 30 °C.[34]

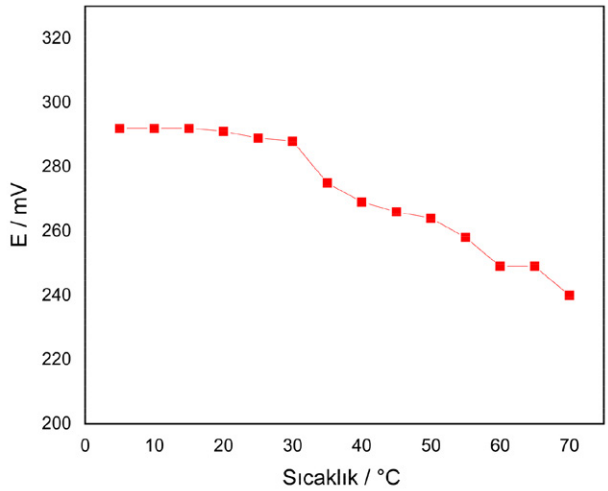

Figure 8. Effect of temperature on the DOP-selective microsensor performance

3. 7. Sample Analysis

The electroanalytical applicability of the prepared DOP-selective microsensor, the dopamine contents in the pharmaceutical samples were determined by the proposed microsensor. The obtained potentiometric results were compared with the results obtained with UV-Vis spectro-

Table 3. Determination of DOP in the drug sample

Pharmaceutical Product	Label value	Amounts of DOP (ppm) *		Recovery (%)	E_{ra} (%)	*t*-test	*f*-test
		Potentiometry	UV-Vis				
Dopasel®	400.0	417.2 ± 4.6	412.5 ± 2.5	104.3	4.25	1.55	3.39
	200.0	209.1 ± 5.5	205.3 ± 2.6	104.6	4.55	1.08	4.47
	100.0	104.8 ± 5.8	102.2 ± 2.8	104.8	4.80	0.70	4.29

* The average values (ppm) of three determinations ± standard deviation. E_{ra} is the relative error for the potentiometry versus label value. *t*-student's and *f*-test level (critical) values are 4.30 and 19.00 at 95% confidence, respectively.

photometric method. The recovery, relative error, t-test and f-test values were calculated and presented in Table 3. As can be seen from Table 3, the student's *t*-test and *f*-test values calculated at the 95% confidence level are lower than the $t_{critical}$ (4.3) and $f_{critical}$ (19.0) values, respectively. As a result, it can be concluded that there are no significant differences between the potentiometry and UV-Vis methods. It can be seen that the average values (with the recovery of 104.3–104.8% and the relative error of 4.25–4.80%) obtained by the proposed sensor were in satisfactory agreement with the labeled values.

3. 8. Comparison of the proposed sensor with the other DOP-selective sensors

The comparison of the developed sensor with both MIP-based and traditional ionophore-based dopamine-selective sensors available in the literature is summarized in Table 4. The developed sensor is considered to be comparable to the previously reported sensors in most cases as slope, linear range, response time, detection limit, and pH range. The developed microsensor is suitable for miniaturization due to its solid-state structure. The flow-cells with low dead volume can be easily prepared for this type of sensor. Therefore, they have the possibility to be used as detectors for the flow systems, which is another important advantage over conventional sensors.

4. Conclusions

In the current study, a novel solid-state type PVC membrane DOP-selective potentiometric microsensor was developed based on DOP-imprinted polymer. The DOP-selective microsensor was successfully applied for the rapid, accurate, selective, and reproducible determination of dopamine in pharmaceutical formulations. The obtained potentiometric results were found to be compatible with the results obtained by UV-Vis. The developed sensor has the advantages of fast response time, low detection limit, wide linear range, ease of preparation, and low cost. Therefore, the microsensor can be considered to be a notable addition to the list of dopamine selective sensors.

Acknowledgments

The authors acknowledge support by the Giresun University Scientific Research Projects Commission Presidency (project no: FEN-BAP-C-281119-81).

5. References

1. B. J. Venton and R. M. Wightman, *Anal. Chem.* **2003**, *75*, 414A-421A. **DOI:**10.1021/ac031421c
2. M. Jaber, S. W. Robinson, C. Missale and M. G. Caron, *Neuropharmacology* **1996**, *35*, 1503–1519. **DOI:**10.1016/S0028-3908(96)00100-1
3. J. M. Wilson, S. Sanyal and H. H. M. Van Tol, *Eur. J. Pharmacol.* **1998**, *351*, 273–286. **DOI:**10.1016/S0014-2999(98)00312-4
4. R. M. Wightman, L. J. May and A. C. Michael, *Anal. Chem.* **1988**, *60*, A769–&. **DOI:**10.1021/ac00164a001
5. C. Muzzi, E. Bertocci, L. Terzuoli, B. Porcelli, I. Ciari, R. Pagani and R. Guerranti, *Biomed. Pharmacother.* **2008**, *62*, 253–258. **DOI:**10.1016/j.biopha.2007.10.018
6. H. Y. Wang, Y. Sun and B. Tang, *Talanta* **2002**, *57*, 899–907. **DOI:**10.1016/S0039-9140(02)00123-6
7. L. Liang, Z. H. Zhao, F. G. Ye and S. L. Zhao, *New J. Chem.* **2021**, *45*, 6780–6786. **DOI:**10.1039/D1NJ00162K
8. M. Maminski, M. Olejniczak, M. Chudy, A. Dybko and Z. Brzozka, *Anal. Chim. Acta* **2005**, *540*, 153–157. **DOI:**10.1016/j.aca.2004.09.011
9. H. S. Wang, T. H. Li, W. L. Jia and H. Y. Xu, *Biosens. Bioelectron.* **2006**, *22*, 664–669. **DOI:**10.1016/j.bios.2006.02.007
10. L. Wu, L. Y. Feng, J. S. Ren and X. G. Qu, *Biosens. Bioelectron.* **2012**, *34*, 57–62. **DOI:**10.1016/j.bios.2012.01.007
11. L. M. Kindschy and E. C. Alocilja, *Transactions of the ASAE* **2004**, *47*, 1375–1382. **DOI:**10.13031/2013.16542
12. P. Y. Chen, P. C. Nien and K. C. Ho, in: J. Brugger and D. Briand (Eds.): Proceedings of the Eurosensors Xxiii Conference, Elsevier Science Bv, Amsterdam, **2009**, pp. 285–288.
13. A. Konishi, S. Takegami and T. Kitade, *Anal. Sci.* **2019**, *35*,

Table 4. Comparation of the DOP-selective microsensors in the literature

Ref	Slope, mV/decade	Linear range, mol/L	Response time, s	pH range	Detection limit, mol/L
[35]	53.85	1×10^{-5}–1×10^{-1}	NR	5.5–7.5	5.8×10^{-6}
[36]	NR	5×10^{-6}–8×10^{-5}	NR	6.5	2.1×10^{-6}
[37]	54.00	2×10^{-7}–1×10^{-5}	<10	7.0	1.5×10^{-7}
[38]	56.50	3×10^{-4}–1×10^{-2}	NR	4.5	8.0×10^{-5}
[39]	43.80	3×10^{-5}–1×10^{-3}	<10	4.0–8.5	1.3×10^{-5}
[40]	59.16	3×10^{-5}–3×10^{-3}	500	5.0–7.7	2.0×10^{-8}
[41]	53.30	7×10^{-5}–3×10^{-1}	10–15	2.0–10.0	4.5×10^{-5}
[42]	56.20	6×10^{-4}–1×10^{-1}	10	3.5–6.0	5.0×10^{-5}
This work	60.28	1×10^{-6}–1×10^{-1}	<15	4.0–8.0	8.4×10^{-7}

1111–1115. **DOI:**10.2116/analsci.19P166
14. T. Alizadeh and L. Allahyari, *Electrochim. Acta* **2013**, *111*, 663–673. **DOI:**10.1016/j.electacta.2013.08.075
15. D. Kumar and B. B. Prasad, *Sens. Actuator B-Chem.* **2012**, *171*, 1141–1150. **DOI:**10.1016/j.snb.2012.06.053
16. M. B. Gholivand, M. Torkashyand and G. Malekzadeh, *Anal. Chim. Acta* **2012**, *713*, 36–44. **DOI:**10.1016/j.aca.2011.11.001
17. J. Hu, H. Dai, Y. B. Zeng, Y. W. Yang, H. L. Wang, X. D. Zhu, L. Li, G. B. Zhou, R. Y. Chen and L. H. Guo, *Nanomaterials* **2019**, *9*, 11.
18. S. G. Ge, M. Yan, X. L. Cheng, C. C. Zhang, J. H. Yu, P. N. Zhao and W. G. Gao, *J. Pharm. Biomed. Anal.* **2010**, *52*, 615–619. **DOI:**10.1016/j.jpba.2010.01.030
19. M. Salgarello, G. Visconti and L. Barone-Adesi, *Aesthet. Plast. Surg.* **2013**, *37*, 1061–1062. **DOI:**10.1007/s00266-013-0186-1
20. S. M. Borisov, T. Mayr, G. Mistlberger, K. Waich, K. Koren, P. Chojnacki and I. Klimant, *Talanta* **2009**, *79*, 1322–1330. **DOI:**10.1016/j.talanta.2009.05.041
21. Y. T. Wang, Z. Q. Zhang, V. Jain, J. J. Yi, S. Mueller, J. Sokolov, Z. X. Liu, K. Levon, B. Rigas and M. H. Rafailovich, *Sens. Actuator B-Chem.* **2010**, *146*, 381–387. **DOI:**10.1016/j.snb.2010.02.032
22. M. Yolcu and N. Dere, *Can. J. Chem.* **2018**, *96*, 1027–1036. **DOI:**10.1139/cjc-2018-0178
23. H. Kamel, F. T. C. Moreira, S. A. A. Almeida and M. G. F. Sales, *Electroanalysis* **2008**, *20*, 194–202. **DOI:**10.1002/elan.200704039
24. M. Rizk, S. S. Toubar, H. E. E.-D. Sayour, D. Mohamed and R. M. Touny, *Eur. J. Chem.* **2014**, *5*, 18–23. **DOI:**10.5155/eurjchem.5.1.18-23.876
25. R. N. Liang, L. S. Chen and W. Qin, *Sci. Rep.* **2015**, *5*, 1–9. **DOI:**10.1038/srep12462
26. L. Kiss, V. David, I. G. David, P. Lazar, C. Mihailciuc, I. Stamatin, A. Ciobanu, C. D. Stefanescu, L. Nagy, G. Nagy and A. A. Ciucu, *Talanta* **2016**, *160*, 489–498. **DOI:**10.1016/j.talanta.2016.07.024
27. K. N. Mikhelson and I. S. Muratova, *Biosens. Bioelectron.* **2018**, *4*, 169–173.
28. S. A. Zaidi, *Sens. Actuator B-Chem.* **2018**, *265*, 488–497. **DOI:**10.1016/j.snb.2018.03.076
29. I. S. Muratova, L. A. Kartsova and K. N. Mikhelson, *Sens. Actuator B-Chem.* **2015**, *207*, 900–906. **DOI:**10.1016/j.snb.2014.07.034
30. I. Gualandi, D. Tonelli, F. Mariani, E. Scavetta, M. Marzocchi and B. Fraboni, *Sci. Rep.* **2016**, *6*, 35419. **DOI:**10.1038/srep35419
31. I. Royani, Widayani, M. Abdullah and Khairurrijal, *Int. J. Electrochem. Sci.* **2014**, *9*, 5651–5662.
32. I. Isildak, M. Yolcu, O. Isildak, N. Demirel, G. Topal and H. Hosgoren, *Microchim. Acta* **2004**, *144*, 177–181. **DOI:**10.1007/s00604-003-0072-7
33. R. P. Buck and E. Lindner, *Pure Appl. Chem.* **1994**, *66*, 2527–2536. **DOI:**10.1351/pac199466122527
34. A. Dybko, *Sensors* **2001**, *1*, 29–37. **DOI:**10.3390/s10100029
35. C. He, G. Li, Y. Wang and W. J. Zhou, *Meas. Sci. Technol.* **2021**, *32*, 7.
36. C. Wang, L. B. Qi and R. N. Liang, *Anal. Methods* **2021**, *13*, 620–625. **DOI:**10.1039/D0AY02100H
37. H. Kamel, A. G. E. Amr, N. H. Ashmawy, H. R. Galal, M. A. Al-Omar and A. Y. A. Sayed, *Polymers* **2020**, *12*, 13. **DOI:**10.3390/polym12061406
38. M. Durka, K. Durka, A. Adamczyk-Wozniak and W. Wroblewski, *Sensors* **2019**, *19*, 11. **DOI:**10.3390/s19020283
39. T. J. Yin and W. Qin, *Sens. Lett.* **2013**, *11*, 607–612. **DOI:**10.1166/sl.2013.2914
40. M. Pesavento, G. D'Agostino, R. Biesuz, G. Alberti and A. Profumo, *Electroanalysis* **2012**, *24*, 813–824. **DOI:**10.1002/elan.201100509
41. N. M. Kholoshenko, S. S. Ryasenskii and I. P. Gorelov, *Pharm. Chem. J.* **2006**, *40*, 334–336. **DOI:**10.1007/s11094-006-0122-7
42. M. Othman, N. M. H. Rizka and M. S. El-Shahawi, *Anal. Sci.* **2004**, *20*, 651–655. **DOI:**10.2116/analsci.20.651

Povzetek

Na osnovi polimera, vtisnjenega z dopaminom, ki se je uporabil kot ionofor v membranski strukturi, je bil izdelan nov polivinilkloridni (PVC) membranski potenciometrični mikrosenzor, selektiven za dopamin. Optimalna sestava membrane je bila določena kot 4 % (m/m) MIP, 69 % (m/m) bis(2-etilheksil) sebakata (DOS), 26 % (m/m) PVC in 1 % (m/m) kalijevega tetrakis(4-klorofenil) borata (KTpClPB). Meja zaznavanja mikrosenzorja je bila $3{,}71 \times 10^{-7}$ mol L^{-1}. Mikrosenzor je pokazal super-nernzijski odziv (angl. super-Nernstian response) na dopamin v razponu koncentracij 10^{-6}–10^{-1} mol L^{-1}, s kratkim odzivnim časom (<15 s) in naklonom 60,3 ± 1,3 mV na dekado (R^2 : 0,9998) znotraj sedmih tednov. Mikrosenzor je bil učinkovit v območju pH 4,0–8,0 in temperaturnem območju 5–30 °C. Uspešna demonstracija mikrosenzorja je pokazala hitro, natančno, selektivno in ponovljivo določanje dopamina v farmacevtskih formulacijah z izkoristkom 104,3–104,8 %. Dobljeni rezultati so dobro kolerilali z rezultati UV-Vis pri stopnji zaupanja 95 %.

Except when otherwise noted, articles in this journal are published under the terms and conditions of the Creative Commons Attribution 4.0 International License

DOI: 10.17344/acsi.2021.7055 *Acta Chim. Slov.* **2022,** *69,* 116–124
creative commons

Scientific paper

Combustion Synthesis of Nano Fe_2O_3 and its Utilization as a Catalyst for the Synthesis of N^{α}-Protected Acyl Thioureas and Study of Anti-bacterial Activities

Raghavendra Mahadevaiah,[1,3] Lalithamba Haraluru Shankraiah[1,*] and Latha Haraluru Kamalamma Eshwaraiah[2]

[1] *Department of Chemistry, Siddaganga Institute of Technology, B. H. Road, Tumakuru - 572 103, Karnataka, India*

[2] *Department of Electronics & Instrumentation Engineering, Siddaganga Institute of Technology, 10 B. H. Road, Tumakuru - 572 103, Karnataka, India*

[3] *Department of Chemistry, Channabasaveshwara Institute of Technology, B. H. Road, Gubbi, Tumkur - 572 216, Karnataka, India*

* *Corresponding author: E-mail: lalithambasit@yahoo.co.in; hslalithamba@gmail.com*

Received: 07-15-2021

Dedicated to Dr. Sree Sree Sree Shivakumara Mahaswamiji, Siddaganga Matt, Tumakuru, Karnataka, India

Abstract

A simple and eco-friendly nano Fe_2O_3 heterogeneous catalytic system is described for the synthesis of acyl thiourea derivatives from corresponding *in situ* generated acyl isothiocyanates and amino acid esters in acetone obtained in good yields. The structures of synthesized acyl thioureas were confimed by ^{1}H NMR, ^{13}C NMR, mass, and FTIR analysis. Fe_2O_3 NPs has been prepared *via* a solution combustion route using ascorbic acid as the reducing agent and ferric nitrate as the source of iron. The prepared nano material has been characterized by XRD, SEM, UV-Visible, and FTIR analysis. More prominently, the Fe_2O_3 and other impurities are removed though a simple work-up and the material prepared shows to be effective in catalyzing the conversion of reactants to products in good yields. Further, some of the synthesized acyl thioureas were evaluated for *in vitro* antibacterial activity against *Staphylococcus aureus* and *Escherichia coli.*

Keywords: *N*-protected acyl thioureas; *in vitro* antibacterial activity; Fe_2O_3 nanoparticles; solution combustion.

1. Introduction

Many acyl thiourea derivatives are well known to possess a diverse range of biological activities such as anticancer,[1] antiviral,[2] fungicidal,[3] anti-microbial,[4] antimycobacterial,[5] antitumor,[6] anti-inflammatory,[7] herbicidal,[8] anti-aggregating,[9] analgesic, and are often employed as local anesthetic, and antihyperlipidemic.[10] Therefore, the acyl thiourea linkage has received greater attention because of its potent biological as well as structural aspects. The ability to provide a hydrogen bond donor and acceptor point makes it an efficient anion receptor and enables it to play a key role in some epoxy resin curing agents containing amino functional groups and to act as chelating agents in catalysis.[11–13] Aroylthiourea ligands are an important class of compounds in the field of coordination chemistry and catalysis.[14–16] Thiourea and its derivatives have long been studied for their use against the corrosion of a wide range of metals in various corrosion environments.[17–18] Also the thiourea and its derivatives have found wide range of applications in agriculture, medicine, and analytical chemistry.[19–20]

In the past, Benjawan and his group synthesized and evaluated the acyl thiourea derivatives for the *in vitro* evaluation of activity against *Mycobacterium tuberculosis* showing promising results.[21] Substituted thioureas are an important

class of sulphur-containing organic compounds or intermediates in the synthesis of a variety of heterocyclic compounds such as 2-imino-1,3-thiazolines, imidazole-2-thiones, (benzothiazolyl)-4-quinazolinones. Pyrimidine-2-thiones *N*-(substituted phenyl)-*N*-phenylthioureas have been developed as calixarenes containing thioureas as neutral receptors towards α,α-dicarboxylate anions, anion-binding sites in a hydrogen-bonding receptor, and *N*-4-substituted-benzyl-*N*-*tert*-butylbenzyl thioureas as antagonists in rate DRG neurons and vanilloid receptor ligands.[22–28]

There are several works demonstrating the synthesis of acyl thiourea derivatives including: (a) reaction of functionalized diisothiocyanate with various benzenamines in the presence of PEG-400,[29] (b) difluoromethyl pyrazole acyl thiourea derivatives were successfully synthesized using PEG-600 as a phase transfer catalyst,[30] (c) The application of benzoyl / carbethoxy isothiocyanate towards the synthesis of substituted-3-benzoyl/carbethoxy thioureas in the presence of nucleophile such as amine and NH_4SCN was investigated,[31] (d) reaction of acid chloride with potassium thiocyanate to obtain acyl isothiocyanate intermediate, this is coupled with the amines employing TBAB as an organic catalyst to afford *N*-(*o*-fluorophenoxyacetyl) thioureas derivatives,[32] (e) Zhong *et al.* synthesized three different acyl thiourea derivatives of chitosan and their antimicrobial behavior against four species of bacteria were investigated.[33] Therefore, the application of nano Fe_2O_3 for the synthesis of N^{α}-protected acyl thioureas is, according to the literature survey, not established yet. Hence, herein we report a simple and efficient route for the synthesis of biologically active acyl thioureas employing nano Fe_2O_3. Furthermore, the synthesized compounds were screened for *in vitro* activity in anti-bacterial studies.

Nowadays, nano metaloxide semiconductors have attracted a lot of attention, as their properties can be controlled by changing the crystallite size, shape, surface-to-volume ratio, temperature and also by synthetic routes.[34–35] From the view point of the basic research purpose Fe_2O_3 is an important semiconductor for the study of magnetic properties, and polymorphism and structural phase transitions of nanoparticles.[36,37] In the last decades, nanostructured iron oxides such as α-Fe_2O_3, γ-Fe_2O_3, β-Fe_2O_3 and Fe_2O_3, have received remarkable interest from both theoretical and experimental viewpoints because of their potential applications in sensing devices and biomedical applications, such as magnetic resonance imaging, biosensors, hyperthermia, and drug delivery in cancer therapy, and detoxification and also in industrial applications.[38–41] At the same time there is an increased interest in using iron oxide NPs for the removal of various pollutants (As^{5+}, Cr^{6+}, dyes) from wastewaters.[42–45]

Several synthetic methods have been developed for the preparation of Fe_2O_3 nanoparticles due to its inherent biocompatible nature, magnetic properties as well its stability towards oxidation.[46–49] There are many methods available to prepare nano Fe_2O_3 including: co-precipitation, plasma chemical synthesis, micro emulsions, thermal decomposition, sol-gel, and flame spray pyrolysis etc.[50–57] Some of these are expensive and time consuming. Here, we have prepared Fe_2O_3 nanopowder by eco-friendly simple low-cost solution combustion method using ascorbic acid as the reducing agent.[58] Although the synthesis of Fe_2O_3 nanoparticles has seen substantial progress, the preparation of pure, large surface area nano Fe_2O_3 powders is still one of the top goals in the field.

2. Experimental Section

2. 1. General

All the chemicals were purchased from Sigma-Aldrich and Merck and used without purification. The pathogenic bacterial strains were purchased from National Chemical Laboratory Pune, India. IR spectra were recorded on Bruker Alpha-II FTIR spectrometer. ^{1}H NMR and ^{13}C NMR spectra were recorded using Bruker AMX 400 MHz spectrometer using TMS as the internal standard and DMSO as the solvent. Mass spectra were recorded on a Micromass Q-ToF Micro Mass Spectrometer. Powder XRD data were recorded on Shimadzu X-ray diffractometer (PXRD-7000) using Cu-Kα radiation of wavelength λ = 1.541 Å. IR spectra were recorded on Bruker Alpha-T FTIR spectrometer (KBr windows, 2 cm^{-1} resolution). The absorption spectrum and band gap were measured using Lambda-35 (Perkin Elmer) spectrophotometer in the wavelength range 200–800 nm diffused reflectance mode. Morphological features were studied by using Hitachi-7000 Scanning Electron Microscopy.

2. 2. Solution Combustion Synthesis of Nano Fe_2O_3

1 g of $Fe(NO_3)_3 \cdot 9H_2O$ (acting as oxidizing agent) and 0.6 g of ascorbic acid (acting as reducing agent) were mixed and stirred in 10 mL distilled H_2O to get homogeneous solution. This solution was poured into silica crucible and kept in a preheated muffle furnace at 500 °C. The homogeneous solution first undergoes dehydration, then decomposition and large amounts of gases were released during the process. Fe_2O_3 NPs were formed within 5 minutes. In continuation of our interest a facile protocol for the nano Fe_2O_3 catalyzed synthesis of acyl thioureidopeptides was developed in peptide chemistry.

2. 3. Reusability and Recyclability of Nano Fe_2O_3

Catalyst was reused and recycled without any loss of activity and product yield. The nano Fe_2O_3 can be recycled by a simple protocol after the completion of the reaction. The catalyst was removed by filtration, washed with methanol and dried. The recovered catalyst was reused for the

second, third and fourth consecutive cycles without any significant loss in catalytic activity.

2. 4. General Procedure for the Synthesis of N^{α}-Protected Acyl Thioureas

To the protected amino acid (1 mmol) dissolved in CH_2Cl_2 (5 mL), $SOCl_2$ (1.5 mmol) was added and the mixture was sonicated at rt for about 40–50 min and monitored through TLC. The excess of CH_2Cl_2 and $SOCl_2$ were carefully eliminated by rotary distillation and the residue was precipitated after the addition of hexane (5 mL) and then filtered and dried to get pure acid chlorides. To the formed acid chloride were added ammonium thiocyanate and acetone, this reaction mixture was refluxed for 1 h and the solvent was removed on a rotary evaporator to obtain a crude product of acyl isothiocyanates. This intermediate was dissolved in CH_2Cl_2 (30 mL), then subjected to H_2O and brine wash and dried over anhydrous Na_2SO_4. The organic phase containing acyl isothiocyanate intermediate was coupled with neutralized amino acid esters followed by the addition of nano Fe_2O_3 (0.5 mmol). The reaction mixture was stirred for 4–6 h at rt and monitored by TLC. After the completion of the reaction, Fe_2O_3 was removed by filtration and the organic phase was washed with 5% HCl (20 mL), 5% Na_2CO_3 (20 mL), H_2O, and brine and dried over anhydrous Na_2SO_4 to get crude product of acyl thioureas; then, it was purified by the trituration with hexane–diethyl ether system to afford analytically pure products.

3. Results and Discussion

3. 1. Characterization of Fe_2O_3 NPs

3. 1. 1. Powder X-Ray Diffraction Technique

Figure 1 shows the XRD pattern of Fe_2O_3 NPs calcined at 500 °C. The diffraction peaks observed at 24.18, 33.34, 35.68, 40.85, 49.63, 54.28, 62.55 and 64.22 could be indexed to the (012), (104), (022) (202), (103), and (123) planes respectively, consistent with the standard XRD data of Fe_2O_3 (JCPDS no. 72-1191). The average crystallite size of the prepared sample was calculated by Debye–Scherrer equation (Equation 1) and it was observed to be 30 nm.

$$D = \frac{0.9\,\lambda}{\beta cos\theta} \quad (1)$$

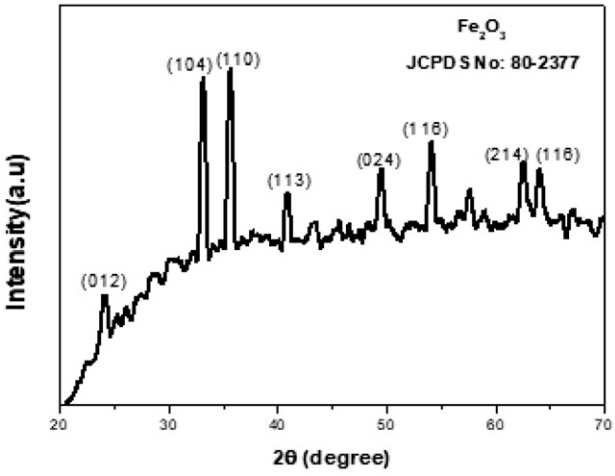

Figure 1. XRD patterns of the Fe_2O_3 NPs.

3. 1. 2. Fourier Transform Infrared Spectroscopy

From Figure 2 the two peaks at 442 and 530 cm^{-1} are observed in the FTIR spectrum of the Fe_2O_3 NPs. In comparison with the literature, we conclude that these peaks were assigned to the stretching and bending modes of the Fe–O bond. The absorption peaks around 1587 and 1383 cm^{-1} are due to the asymmetric and symmetric bending vibration of C=O.

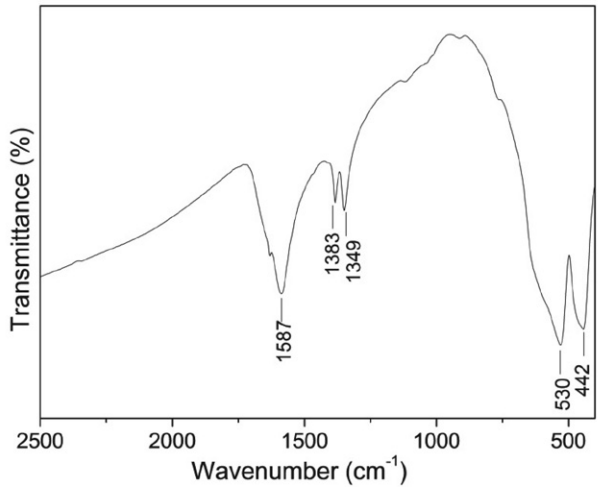

Figure 2. FTIR spectrum of Fe_2O_3 NPs.

3. 1. 3. Scanning Electron Microscopy Analysis

Figure 3 shows the SEM image of the prepared nano Fe_2O_3 which clearly shows that the particles have roughly irregular spongy cave like structure. The size and the shape of the Fe_2O_3 strongly depend on the preparation technique.

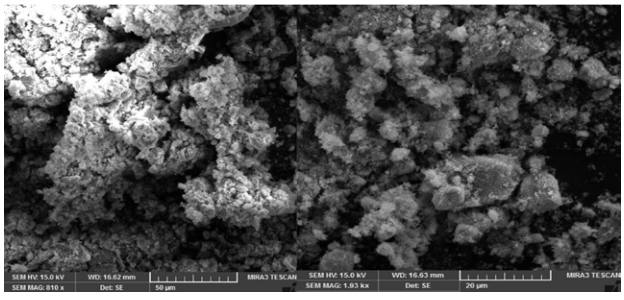

Figure 3. SEM images of Fe_2O_3 NPs.

3. 1. 4. UV-Visible Analysis

The optical properties of nano Fe_2O_3 were studied by UV-visible DRS spectroscopy. The spectrum was recorded in the wavelength region between 200 to 1200 nm at rt. The band gap energy of the samples can be evaluated from the E_g measurements using Kubelka–Munk model and the $F(R)$ was estimated using the equation 2

$$F(R) = \frac{(1-R)^2}{2R} \quad (2)$$

where $F(R)$ is the remission or Kubelka–Munk fuction, and R is the reflectance. A graph was plotted between $[F(R)h\nu]^2$ and hν, the intercept value is the band gap energy of the Fe_2O_3 NPs. From the Figure 4a it was observed that Fe_2O_3 NPs show strong reflectance peak at 510 nm wavelength. From Figure 4b the estimated band gap of nano Fe_2O_3 was found to be 2.5 eV which was higher when compared with the reported value for the bulk Fe_2O_3 (2.1 eV) owing to the quantum confinement effect exerted by the nanostructured materials. Thus there is a blue shift of the band edge of Fe_2O_3 NPs with respect to the bulk Fe_2O_3.

3. 1. 5. Application of Nano Fe_2O_3 as the Catalyst for the Synthesis of N^{α}-Protected Acyl Thioureas of *N*-Protected Amino Acids

To avoid the restrictions, such as cost of synthesis, prolonged reaction conditions, and low yields, the studies were made to develop a well-organized method with higher yields for the synthesis of acyl thioureas in the presence of nano Fe_2O_3. Therefore, we described the synthesis of acyl thiourea derivatives of protected amino acids bearing different side chains employing Fe_2O_3 nano powder under mild reaction conditions. The protocol is based on a three-step strategy, a direct chlorination of the carbonyl group of the protected amino acid with a thionyl chloride followed by the nucleophilic substitution reaction with ammonium thiocyanate in acetone under reflux condition to form acyl isothiocyanates as key intermediates, further being coupled with amino acid esters employing nano Fe_2O_3 as the catalyst leading to the desired acyl thioureas **5a**–**m** in good yields (Scheme 1, Table 1). Basically, acyl thiourea in its basic structure has one sulfur atom, which has six valence electrons. It is believed that the present protocol provides a greater flexibility of amino acids at our convenience and is

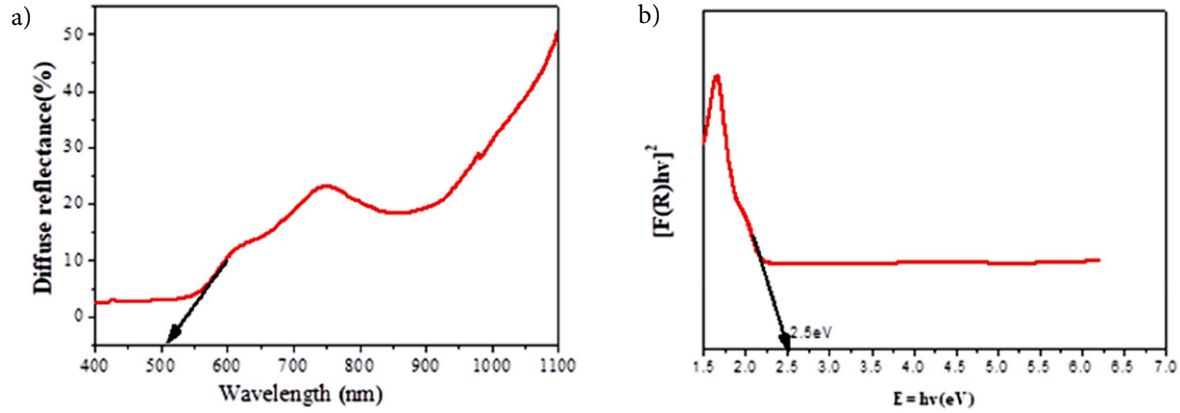

Figure 4. (a) DRS spectrum; **(b)** Energy band gap plot of Fe_2O_3 NPs.

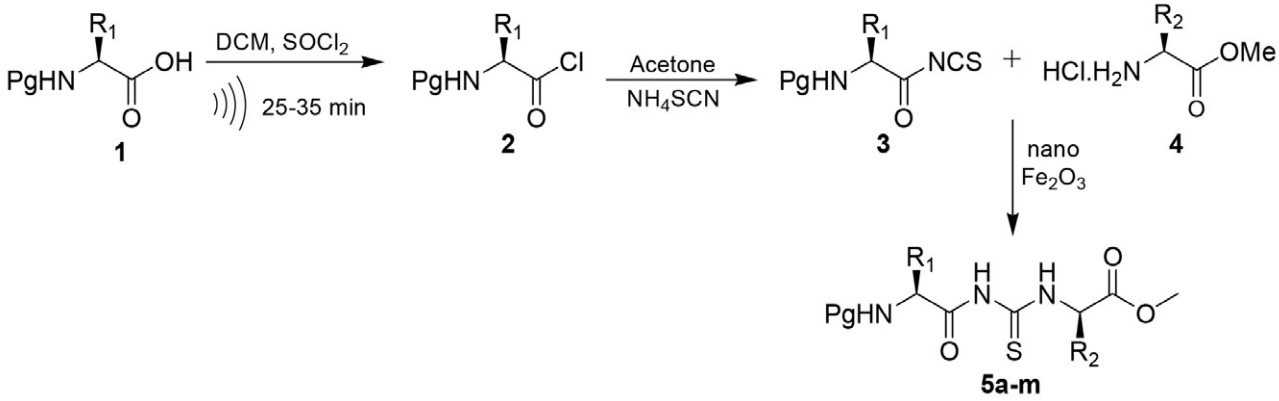

R_1, R_2: H, alkyl, aryl groups
Pg (Protecting group): Fmoc (fluorenylmethyloxycarbonyl), Cbz (benzyloxycarbonyl).

Scheme 1. Synthesis of acyl thioureas employing nano Fe_2O_3

Table 1. List of N^{α}-protected acyl thioureas synthesized *via* scheme 1

Entry	Acyl thioureas	Yield (%)	M.p. (°C)	$[\alpha]_D^{25}$ in degrees
5a	Fmoc-Val-ψ[CONHCSNH]-Ala-OMe	80	184	–55.45
5b	Fmoc-Phe-ψ[CONHCSNH]-Ser-OMe	81	170	–50.91
5c	Cbz-Val-ψ[CONHCSNH]-Gly-OMe	85	165	–9.09
5d	Cbz-Met-ψ[NHCONH]-Phe-OMe	86	180	–16.82
5e	Boc-Ala-ψ[CONHCSNH]-Ser-OMe	81	*Gum*	–22.39
5f	Boc-Leu-ψ[CONHCSNH]-Ala-OMe	79	*Gum*	–18.43
5g	Fmoc-Phe-ψ[CONHCSNH]-Ala-OMe	83	185	–24.56
5h	Fmoc-Leu-ψ[CONHCSNH]-Ile-OMe	84	91	–20.62
5i	Fmoc-Ala-ψ[CONHCSNH]-Val-OMe:	90	180	–17.27
5j	Fmoc-Try-ψ[CONHCSNH]-Ala-OMe	87	205	–12.73
5k	Boc-Val-ψ[CONHCSNH]-Ala-OMe	75	*Gum*	–23.18
5l	Fmoc-Ile-ψ[CONHCSNH]-Val-OMe	86	159	–9.09
5m	Cbz-Thr-ψ[CONHCSNH]-Val-OMe	90	165	–11.10

superior to the other methods. N^{α}-Protected amino acid was dissolved in CH_2Cl_2 (dichloromethane), thionyl chloride was added and the mixture was sonicated at rt for about 40–50 minutes yielding acyl chlorides **2**. Then, the carbonyl group in **2** (in the form of acyl chloride) was modified by the nucleophilic substitution reaction. To the acyl chlorides **2** ammonium isothiocyanate was added, yielding acyl isothiocyanates **3** under reflux condition. The formed acyl isothiocyanate intermediates **3** were trapped with amino acid esters **4** employing nano Fe_2O_3 as an efficient, eco-friendly catalyst to form the final product acyl thioureas **5a–m** as monitored by TLC. The reaction was complete in about 6 h and all the compounds were isolated, after a simple work-up, and purified by hexane-diethyl ether system and their structures were confirmed by mass, ^{1}H NMR, ^{13}C NMR, and FTIR spectroscopy techniques.

3. 1. 6. Spectral Data of the Synthesized Compounds 5a–m

(*S*)-Methyl 2-(3-((*S*)-2-(((9*H*-Fluoren-9-yl)methoxy) carbonyl)-3-methylbutanoyl)thioureido)propanoate (*Fmoc-Val-ψ[CONHCSNH]-Ala-OMe*) (5a). Yield 80%, m.p. 184 °C. ^{1}H NMR (400 MHz, DMSO-d_6): δ 1.01 (d, J = 12.0 Hz, 6H), 1.30 (d, J = 8.0 Hz, 3H), 2.0 (br, 1H), 2.70 (m, 1H), 3.60 (m, 1H), 3.70 (s, 3H), 4.45–4.70 (m, 4H), 6.0 (br, 2H), 7.20–7.90 (m, 8H). ^{13}C NMR (100 MHz, DMSO-d_6): δ 17.0, 17.80, 32.0, 47.0, 52.30, 54.0, 61.0, 68.0, 126.0, 128.0, 128.40, 129.0, 140.0, 143.80, 156.0, 170.0, 175.0, 187.0. MS: Calcd. for $C_{25}H_{29}N_3O_5S$: *m/z* 506.1726 (M + Na^+), found: 506.1060.

(*S*)-Methyl 2-(3-((*S*)-2-(((9*H*-Fluoren-9-yl)methoxy) carbonyl)-3-phenylpropanoyl)thioureido)-3-hydroxypropanoate (*Fmoc-Phe-ψ[CONHCSNH]-Ser-OMe*) (5b). Yield 81%, m.p. 170 °C. ^{1}H NMR (400 MHz, DMSO-d_6): δ 2.10 (s, 1H), 2.90 (*d*, J = 6.0 Hz, 2H), 3.50 (t, J = 10.0 Hz, 1H), 3.70 (s, 3H), 4.40–4.90 (m, 6H), 6.0 (br, 2H), 7.10–7.90 (m, 13H), 8.0 (br, 1H). ^{13}C NMR (100 MHz, DMSO-d_6): δ 38.0, 46.50, 51.20, 53.0, 62.0, 68.70, 126.0, 127.0, 127.80, 128.0, 128.40, 128.70, 129.0, 140.0, 141.0, 143.0, 156.0, 176.0, 187.10. MS: Calcd. for $C_{29}H_{29}N_3O_6S$: *m/z* 570.1675 (M + Na^+), found: 570.2275.

(*S*)-Methyl 2-(3-(2-(Benzyloxycarbonyl)-3-methylbutanoyl)thioureido)acetate (*Cbz-Val-ψ[CONHCSNH]-Gly-OMe*) (5c). Yield 85%, m.p. 165 °C. ^{1}H NMR (400 MHz, DMSO-d_6): δ 1.0 (d, J = 8.0 Hz, 6H), 2.70 (m, 1H), 3.70 (s, 3H), 4.40–4.50 (m, 3H), 5.30 (s, 2H), 6.10 (br, 2H), 7.10–7.30 (m, 5H), 8.0 (br, 1H). ^{13}C NMR (100 MHz, DMSO-d_6): δ 20.89, 21.67, 46.67, 56.18, 64.93, 65.26, 126.98, 127.51, 127.54, 129.08, 129.14, 129.28, 129.38, 129.44. MS: Calcd. for $C_{17}H_{23}N_3O_5S$: *m/z* 404.1256 (M + Na^+), found: 404.2250.

(*S*)-Methyl 2-(3-((*S*)-2-(Benzyloxycarbonyl)-4-(methylthio)butanoyl)thioureido)-3-phenylpropanoate (*Cbz-Met-ψ[NHCONH]-Phe-OMe*)(5d). Yield 86%, m.p. 180 °C. ^{1}H NMR (400 MHz, DMSO-d_6): δ 2.0 (s, 3H), 2.30–2.50 (m, 4H), 3.30–3.50 (m, 4H), 3.70 (s, 3H), 5.30 (s, 2H), 6.10 (br, 2H), 7.10–7.30 (m, 10H), 8.01 (br, 1H). ^{13}C NMR (100 MHz, DMSO-d_6): δ 17.10, 29.0, 32.0, 38.0, 52.0, 54.50, 60.0, 66.0, 126.0, 127.40, 127.60, 127.90, 128.50, 129.0, 139.0, 141.0, 156.0, 171.0, 175.50, 187.0. MS: Calcd. for $C_{24}H_{29}N_3O_5S_2$: *m/z* 526.1446 (M + Na^+), found: 526.2130.

(*S*)-Methyl 2-(3-((*S*)-2-(*tert*-Butoxycarbonyl)propanoyl) thioureido)-3-hydroxypropanoate (*Boc-Ala-ψ[CONHCSNH]-Ser-OMe*) (5e). Yield 81%, Gum. ^{1}H NMR (400 MHz, DMSO-d_6): δ 1.29 (s, 9H), 1.50–1.59 (d, J = 6.0 Hz, 3H), 2.0 (br, 1H), 3.40–3.55 (m, 1H), 3.78 (s, 3H), 4.10–4.25 (t, J = 10.0 Hz, 2H), 4.60–4.75 (m, 1H), 6.45 (br, 1H), 8.01 (br, 2H). ^{13}C NMR (100 MHz, DMSO-d_6): δ 19.0, 28.0, 50.0, 51.80, 61.0, 80.0, 155.0, 172.0, 176.20, 188.0. MS: Calcd. for $C_{13}H_{23}N_3O_6S$: *m/z* 372.1205 (M + Na^+), found: 372.3041.

(*S*)-Methyl 2-(3-((*S*)-2-(*tert*-Butoxycarbonyl)-4-methylpentanoyl)thioureido)propanoate (*Boc-Leu-ψ[CONHCSNH]-Ala-OMe*) (5f). Yield 79%, Gum. ^{1}H NMR (400 MHz, DMSO-d_6): δ 1.0 (d, *J* = 10.0 Hz, 6H), 1.25 (d, *J* = 8.0 Hz, 3H), 1.50 (s, 9H), 1.70–1.85 (m, 3H), 3.60 (m, 1H), 3.70 (s, 3H), 4.50 (t, *J* = 4.0 Hz, 1H), 6.20 (br, 2H), 8.0 br, 1H). ^{13}C NMR (100 MHz, DMSO-d_6): δ 17.0, 22.0, 22.7, 28.40, 41.20, 51.0, 52.10, 55.20, 80.0, 155.0, 171.40, 175.50, 188.0. MS: Calcd. for $C_{16}H_{29}N3O_5S$: *m/z* 398.1726 (M + Na^+), found: 398.2230.

(*S*)-Methyl 2-(3-((*S*)-2-(((9*H*-Fluoren-9-yl)methoxy)carbonyl)-3-phenylpropanoyl)thioureido)propanoate (*Fmoc-Phe-ψ[CONHCSNH]-Ala-OMe*) (5g). Yield 83%, m.p. 185 °C. ^{1}H NMR (400 MHz, DMSO-d_6): δ 1.30 (d, *J* = 8.0 Hz, 3H), 2.90 (d, *J* = 10.0 Hz, 2H), 3.60 (s, 3H), 3.70 (m, 1H), 4.40–4.90 (m, 4H), 6.02 (br, 2H), 7.10–7.90 (m, 13H), 8.0 (br, 1H). ^{13}C NMR (100 MHz, DMSO-d_6): δ 18.0, 37.60, 47.10, 52.0, 54.60, 55.0, 67.0, 126.0, 126.60, 128.0, 128.40, 128.70, 129.0, 140.0, 141.0, 143.0, 156.20, 176.60, 171.0, 187.0. MS: Calcd. for $C_{29}H_{29}N_3O_5S$: *m/z* 554.1726 (M + Na^+), found: 554.5204.

(2*S*,3*S*)-Methyl 2-(3-((*S*)-2-(((9*H*-Fluoren-9-yl)methoxy)carbonyl)-4-methylpentanoyl)thioureido)-3-methylpentanoate (*Fmoc-Leu-ψ[CONHCSNH]-Ile-OMe*) (5h). Yield 84%, m.p. 91 °C. ^{1}H NMR (400 MHz, DMSO-d_6): δ 1.0–1.30 (m, 14H), 1.70–1.85 (m, 3H), 2.50 (m, 1H), 3.40 (d, *J* = 6.0 Hz, 1H), 3.68 (s, 3H), 4.40–4.70 (m, 4H), 6.20 (br, 2H), 7.22–7.84 (m, 8H), 8.0 (br, 1H). ^{13}C NMR (100 MHz, DMSO-d_6): δ 14.69. 22.30, 22.92, 28.17, 28.25, 37.69, 38.68, 47.85, 50.02, 55.81, 59.63, 78.09, 126.45, 126.61, 128.06, 128.18, 128.25, 138.05, 144.30, 145.25, 155.59, 170.79. MS: Calcd. for $C_{29}H_{37}N_3O_5S$: *m/z* 562.2352 $[M+Na]^+$, found: 562.3050.

(*S*)-Methyl 2-(3-((*S*)-2-(((9*H*-Fluoren-9-yl)methoxy)carbonyl)propanoyl)thioureido)-3-methylbutanoate (*Fmoc-Ala-ψ[CONHCSNH]-Val-OMe*) (5i). Yield 90%, m.p. 180 °C. IR (KBr): 3455, 2062, 1640, 1434, 1275, 706 cm^{-1}. ^{1}H NMR (400 MHz, DMSO-d_6): δ 1.10–1.20 (d, *J* = 10.0 Hz, 6H), 1.50–1.57 (d, *J* = 8.0 Hz, 3H), 2.70–2.94 (m, 1H), 3.40–3.50 (t, *J* = 6.0 Hz, 1H), 3.75 (s, 3H), 4.48–4.75 (m, 4H), 6.38–6.47 (br, 2H), 7.16–7.50 (m, 8H), 7.98 (br, 1H). ^{13}C NMR (100 MHz, DMSO-d_6): δ 20.92, 21.32, 21.69, 46.67, 54.81, 56.16, 64.93, 65.29, 126.03, 126.98, 127.51, 127.55, 128.47, 129.08, 140.66, 143.76, 156.57, 157.26. MS: Calcd. for $C_{25}H_{29}N_3O_5S$: *m/z* 506.1726 $[M+Na]^+$, found: 506.2440.

(*S*)-Methyl 2-(3-((*S*)-2-(((9*H*-Fluoren-9-yl)methoxy)carbonyl)-3-(1*H*-indol-3-yl)propanoyl)thioureido)propanoate (*Fmoc-Try-ψ[CONHCSNH]-Ala-OMe*) (5j). Yield 87%, m.p. 205 °C. ^{1}H NMR (400 MHz, DMSO-d_6): δ 1.27–1.34 (d, *J* = 8.0 Hz, 3H), 2.0 (br, 1H), 3.05–3.12 (d, *J* = 6.0 Hz, 2H), 3.30–3.59 (m, 1H), 3.80 (s, 3H), 4.40–4.80 (m, 4H), 6.0 (br, 1H), 6.30 (s, 1H), 7.12–7.98 (m, 12H), 8.12 (br, 1H), 8.85 (br, 1H). ^{13}C NMR (100 MHz, DMSO-d_6): δ 14.62, 37.61, 47.75, 49.93, 55.73, 59.53, 77.97, 125.97, 126.15, 126.36, 126.53, 127.97, 128.10, 128.17, 128.53, 129.25, 137.94, 138.01, 144.25, 144.46, 145.19, 155.17, 155.48, 156.23, 170.69. MS: Calcd. for $C_{31}H_{30}N4O_5S$: *m/z* 593.1835 $[M+Na]^+$, found: 593.3030.

(*S*)-Methyl 2-(3-((*S*)-2-(*tert*-Butoxycarbonyl)-3-methylbutanoyl)thioureido)propanoate (*Boc-Val-ψ[CONHCSNH]-Ala-OMe*) (5k). Yield 75%, Gum. ^{1}H NMR (400 MHz, DMSO-d_6): δ 1.0–1.28 (m, 9H), 1.50 (s, 9H), 2.60 (m, 1H), 3.60 (m, 1H), 3.70 (s, 3H), 6.0 (br, 2H), 8.0 (br, 1H). ^{13}C NMR (100 MHz, DMSO-d_6): δ 17.0, 17.40, 28.40, 32.0, 52.0, 55.0, 60.0, 80.0, 156.0, 172.0, 177.0, 187.0. MS: Calcd. for $C_{15}H_{27}N_3O_5S$: *m/z* 384.1569 $[M+Na]^+$, found: 384.2060.

(*S*)-Methyl 2-(3-((2*S*,3*S*)-2-(((9*H*-Fluoren-9-yl)methoxy)carbonyl)-3-methylpentanoyl)thioureido)-3-methylbutanoate (*Fmoc-Ile-ψ[CONHCSNH]-Val-OMe*) (5l). Yield 86%, m.p. 159 °C. ^{1}H NMR (400 MHz, DMSO-d_6): δ (ppm) 1.20–1.46 (m, 12H), 1.65–1.90 (m, 2H), 2.70–2.92 (m, 2H), 3.33–3.46 (d, *J* = 6.0 Hz, 1H), 3.60 (s, 3H), 4.60–4.79 (m, 4H), 6.10–6.21 (br, 2H), 7.17–7.65 (m, 8H), 8.06–8.18 (br, 1H). ^{13}C NMR (100 MHz, DMSO-d_6): δ 10.0, 15.0, 18.20, 24.80, 30.0, 37.10, 47.0, 52.0, 57.80, 62.70, 67.0, 126.60, 128.40, 128.60, 129.0, 141.0, 143.40, 156.0, 171.40, 175.50, 187.0. MS: Calcd. for $C_{28}H_{35}N_3O_5S$: *m/z* 548.2195 $[M+Na]^+$, found: 548.3090.

(*S*)-Methyl 2-(3-((2*S*,3*S*)-2-(Benzyloxycarbonyl)-3-hydroxybutanoyl)thioureido)-3-methylbutanoate (*Cbz-Thr-ψ[CONHCSNH]-Val-OMe*) (5m). Yield 74%, Gum. ^{1}H NMR (400 MHz, DMSO-d_6): δ 1.0 (d, *J* = 6.0 Hz, 6H), 1.20 (d, *J* = 8.0 Hz, 3H), 2.0 (s, 2H), 2.75 (m, 1H), 3.40 (d, *J* = 4.0 Hz, 1H), 3.70 (s, 3H), 4.20–4.60 (m, 2H), 5.40 (s, 2H), 6.0 (br, 2H), 7.20–7.40 (m, 5H). ^{13}C NMR (100 MHz, DMSO-d_6): δ 18.0, 19.0, 30.0, 51.4, 60.0, 62.40, 65.0, 67.60, 127.2, 127.9, 129.0, 140.0, 156.10, 172.0, 175.7, 188.0. MS: Calcd. for $C_{19}H_{27}N_3O_6S$: *m/z* 448.1518 $[M+Na]^+$, found: 448.2024.

3. 2. *In vitro* Anti-bacterial Activity

3. 2. 1. Determination of Zone of Inhibition by Agar Well Diffusion Method

Finally, the synthesized acyl thioureas were tested for the antibacterial activity by agar well diffusion method. For this, the synthesized acyl thiourea samples **5a–j** were subjected for the antibacterial activities against two Gram positive bacteria: *Escherichia coli* (MTCC1692) and *Staphylococcus aureus* (MTCC 3160) employing agar well diffusion method.[59,60] The bacterial pathogens were cultured on Mueller–Hinton broth agar for 24 h at 37 °C.[61] The inoculums were prepared by allowing bacteria

to grow on media containing nutrient broth at 37 °C with permanent stirring at 250 rpm for overnight. After obtaining 24 h fresh culture, Mueller–Hinton agar plates were prepared, strains of *S. aureus*, and *E. coli* were swabbed uniformly on individual plates using sterile cotton swabs. Wells of approximately 6 mm diameter were made on MH agar plates using gel puncture. Synthesized samples, approximately 200 mg were dissolved in 2 mL of DMSO. With a concentration of 500 µg/µL were used to measure the activity of the synthesized molecules and streptomycin sulphate (50 mg/2 mL) was used as the standard antibiotic. To each well, a volume of 50 µL of streptomycin sulphate standard (**S**) and 100 µL respective samples were added to individual plates. The plates were incubated at 37 °C for 24 h and inhibition zones obtained were measured. Antibacterial activity was evaluated in terms of the diameters of growth inhibition zones (mm). If the growth inhibition zones were less than 10 mm in diameter, confluent growth over the plates were scored as the absence of antibacterial activity, zones of 10–15 mm as weak activity, zones of 15–20 mm as moderate-marked activity, and greater than 20 mm as marked activity. Results are summarized and analyzed in Table 2 and Figures 5 and 6.

Table 2. Antibacterial activity of acyl thioureas **5a–j** against *E. coli* and *S. aureus*

Compound	Treatment (concentration in µg/µL)	*E. coli*	*S. aureus*
S	50	14.55 ± 0.88	12.67 ± 0.33
5a	100	14.67 ± 0.67	13.67 ± 0.88
5b	100	16.00 ± 0.58	10.33 ± 0.67
5c	100	15.67 ± 0.88	10.00 ± 1.0
5d	100	16.67 ± 0.88	12.67 ± 0.33
5e	100	12.67 ± 0.33	13.67 ± 0.88
5f	100	13.66 ± 0.88	11.33 ± 0.88
5g	100	10.67 ± 0.88	10.67 ± 1.2
5h	100	14.67 ± 0.67	12.33 ± 0.33
5i	100	13.67 ± 0.88	13.33 ± 1.2
5j	100	17.33 ± 0.33	31.00 ± 1.2

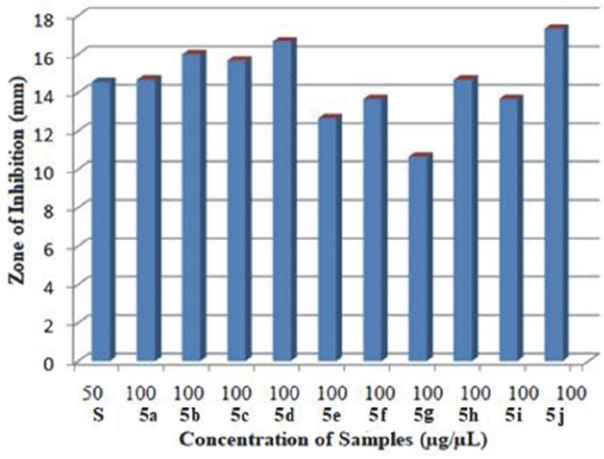

Figure 5. Antibacterial activity of acyl thioureas against *E. coli*

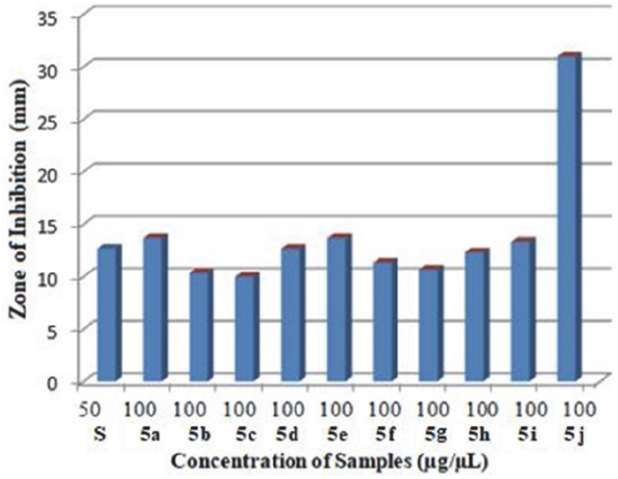

Figure 6. Antibacterial activity of acyl thioureas against *S. aureus.*

4. Conclusions

We have developed a highly convenient and effective protocol for the synthesis of substituted acyl thiourea derivatives from the carboxyl group of N^{α}-amino acids and organic acids by nano Fe_2O_3-catalysed coupling of acyl isothiocyanates and amino acid esters at room temperature in very good yields. Some of the synthesized acyl thiourea derivatives showed promising anti-bacterial activity against two bacterial pathogens, possibly due to the presence of pharmacologically active keto-thiourea group. The presented protocol underlines the potential applicability of nano Fe_2O_3 as inexpensive, user friendly and efficient catalyst prepared *via* solution combustion method using ascorbic acid as a novel reducing agent. This work can be considered as a very good step towards the emerging trend of heterogeneous and environmentally friendly synthesis of acyl thiourea derivatives from N^{α}-amino acids.

Acknowledgements

We thank the Principal, Director, CEO of Siddaganga Institute of Technology, Tumakuru, Karnataka, for the research facilities. One of the authors (HSL) is thankful to the Vision Group of Science and Technology, Dept. of Information Technology, Biotechnology and Science & Technology, Government of Karnataka for providing funds under CISEE programme (VGST-GRD No. 472) to carry out the present research work by means of a sponsored project. And also thankful to the Dept. of Science and Technology, Govt. of India for the Instrumental facilities under Nano mission project.

Conflict of interest

The authors declare that they have no conflict of interest.

5. References

1. I. Koca, A. Ozgür, E. Muhammet, M. Gümüs, K. A. Cos, B. Kun, Y. Tutar, *Eur. J. Med. Chem*. **2016**, *122*, 280–290. **DOI:**10.1016/j.ejmech.2016.06.032
2. Z. M. Zhong, R. Xing, S. Liu, L. Wang, S. B. Cai, P. C. Li, *Carbohydr. Res.* **2008**, *343*, 566–570. **DOI:**10.1016/j.carres.2007.11.024
3. L. P. Duan, J. Xue, L.L. Xu, H. B. Zhang, *Molecules* **2010**, *15*, 6941–6947. **DOI:**10.3390/molecules15106941
4. Z. Zhong, R. Xing, S. Liu, L. Wang, S. Caia, P. Lia, *Carbohydrate Res*. **2008**, *343*, 566–570. **DOI:**10.1016/j.carres.2007.11.024
5. G. M. Dobrikov, V. Valcheva, Y. Nikolova, I. Ugrinova, E. Pasheva, V. Dimitrov, *Eur. J. Med. Chem.* **2013**, *63*, 468–473. **DOI:**10.1016/j.ejmech.2013.02.034
6. H. J. Ochel, K. Eichhorn, G. Gademann, *Cell Stress Chaperones* **2001**, *6*, 105–112. **DOI:**10.1379/1466-1268(2001)006<0105:GTPOAC>2.0.CO;2
7. A. P. Keche, G. D. Hatnapure, R. H. Tale, A. H. Rodge, S. S. Birajdar, V. M. Kamble, *Chin. J. Org. Chem*. **2006**, *26*, 1584–1586.
9. A. Ranise, F. Bondavalli, O. Bruno, S. Schenone, D. Donnoli, C. Parrillo, M. L. Cenicola, F. Rossi, *Farmaco* **1991**, *46*, 1203–1216.
10. A. Ranise, A. Spallarossa, O. Bruno, S. Schenone, P. Fossa, G. Menozzi, F. Bondavalli, L. Mosti, A. Capuano, F. Mazzeo, G. Falcone, W. Filippelli, *Farmaco* **2003**, *58*, 765–780. **DOI:**10.1016/S0014-827X(03)00132-0
11. C. Radu, *Chem. Commun.* **2008**, *3*, 295–307.
12. H. Arslan, N. Duran, G. Borekci, C. K. Ozer, C. Akbay, *Molecules* **2009**, *14*, 519–527. **DOI:**10.3390/molecules14010519
13. G. Chun-ling, L. Liu, J. L. Zhao, D. Wang, Y. J. Chen, *Tetrahedron* **2007**, *18*, 455–463. **DOI:**10.1016/j.tetasy.2007.02.016
14. G. Kemp, A. Roodt, W. Purcell, K. R. Koch, *J. Chem. Soc. Dalton Trans.* **1997**, *23*, 4481–4483. **DOI:**10.1039/a705887j
15. K. R. Koch, C. Sacht, T. Grimmbacher, S. Bourne, *S. Afr. J. Chem.* **1995**, *48*, 71–77.
16. S. Saeed, R. Hussain, *Eur. Chem. Bull.* **2013**, *2*, 465–467. **DOI:**10.1007/s00238-011-0670-2
17. M. A. Quraishi, F. A. Ansari, D. Jamal, *Mat. Chem. Phys.* **2003**, *77*, 687–690. **DOI:**10.1016/S0254-0584(02)00130-X
18. A. Gupta, M. M. Singh, *Portugaliae Electrochim. Acta.* **1999**, *17*, 21–43. **DOI:**10.4152/pea.199901021
19. S. Saeed, N. Rashid, M. H. Bhatti, P. G. Jones, *Turk. J. Chem.* **2010**, *34*, 761–770.
20. G. Binzet, G. Kavak, N. Külcü, S. Özbey, U. Flörke, H. Arslan, *J. Chem.* **2013**, 1–9. **DOI:**10.1155/2013/536562
21. B. Phetsuksiri, A. R. Baulard, A. M. Cooper, D. E. Minnikin, J. D. Douglas, G. S. Besra, P. J. Brennan, *Antimicrob. Agents Chemother.* **1999**, *43*, 1042–1051. **DOI:**10.1128/AAC.43.5.1042
22. E. Maquoi, N. E. Sounni, L. Devy, F. Olivier, F. Frankenne, H. W. Krell, F. Grams, J. M. Foidart, A. Noel, *Clin. Cancer Res.* **2004**, *10*, 4038–4047. **DOI:**10.1158/1078-0432.CCR-04-0125
23. R.-S. Zeng, J.-P. Zou, S.-J. Zhi, J. Chen, Q. Shen, *Org. Lett*. **2003**, *5*, 1657–1659. **DOI:**10.1021/ol030024l
24. M. Dhooghe, A. Waterinckx, N. De Kimpe, *J. Org. Chem.* **2005**, *70*, 227–232. **DOI:**10.1021/jo048486f
25. R. Lakhan, B. J. Ral, *J. Chem. Eng. Data.* **1986**, *31*, 501–502. **DOI:**10.1021/je00046a035
26. J. Lee, J. Lee, M. Kang, M. Shin, K. Ji-Min, K. Sang-Uk, L. Ju-Ok, C. Hyun-Kyung, S. Young-Ger, P. Hyeung-Geun, O. Uhtaek, K. Hee-Doo, P. Young-Ho, H. Hee-Jin, K. Young-Ho, A. Toth, Y. Wang, R. Tran, L. V. Pearce, D. J. Lundberg, P. M. Blumberg, *J. Med. Chem.* **2003**, *46*, 3116–3126.
27. L. Nie, L. Zhao, J. Han, Z. Xuan, R. Yang, L. Wen-Xia, W. Fang-Ying, X. Jian-Wei, Z. Yu-Fen, J. Yun-Bao, *J. Org. Chem.* **2004**, *69*, 6449–6454.
28. H.-g. Park, J.-y. Choi, S.-h. Choi, M.-k. Park, J. Lee, Y.-g. Suh, H. Cho, U. Oh, J. Lee, S.-U. Kang, J. Lee, H.-D. Kim, Y.-H. Park, Y. S. Jeong, J. K. Choi, S.-s. Jew, *Bioorg. Med. Chem. Lett.* **2004**, *14*, 787–791. **DOI:**10.1016/j.bmcl.2003.11.019
29. H. Peng, Y. Liang, L. Chen, F. Liwu, W. Haiqin, H. *Bioorg. Med. Chem. Lett.* **2011**, *21*, 1102–1104. **DOI:**10.1016/j.bmcl.2010.12.130
30. X. H. Liu, C. X. Tan, J. Q. Weng, *Phosphorus Sulfur Silicon Relat. Elem.* **2011**, *186*, 558–564.
31. L. Zhonghua, Y. Zhang, W. Yangang, *Phosphorus Sulfur Silicon Relat. Elem.* **2003**, *178*, 293–297. **DOI:**10.1080/10426500307952
32. K. Shao-Yong, X. Si-Jia, *Arkivoc* **2006**, (*x*), 63–68. **DOI:**10.3998/ark.5550190.0007.a08
33. Z. Zhong, R. Xing, S. Liu, L. Wang, S. Cai, L. Pengcheng, *Carbohyd. Res*. **2008**, *343*, 566–570. **DOI:**10.1016/j.carres.2007.11.024
34. R. Srivastava, B. C. Yadav, Adv. Mat. Lett. **2012**, *3*, 197–203. **DOI:**10.5185/amlett.2012.4330
35. L. Chen, X. Pang, G. Yu, J. Zhang, Adv. Mat. Lett. **2010**, *1*, 75–78. **DOI:**10.5185/amlett.2010.4117
36. C. Yoon, K. L. Sung, C. K. Kima, K. Young-Ho, C. S. Yoona, *J. Magn. Magn. Mater*. **2004**, *272–276*, 1167–1168.
37. E. Rafiee, N. Rahpeima, S. Eavani, *Acta Chim. Slov.* **2014**, *61*, 177–184.
38. M. Chirita, I. Grozescu, *Chem. Bull. "POLITEHNICA" University (Timişoara).* **2009**, *54*, 1–8.
39. K. Rudzka, J. L. Viotab, J. A. M. Gamez, A. Carazo, A. Ruiz-Extremera, A. V. Delgado, *Colloids Surf.* **2013**, *111*, 88–96. **DOI:**10.1016/j.colsurfb.2013.05.010
40. K. Kluchova, R. Zboril, J. Tucek, M. Pecova, L. Zajoncova, I. Safarik, M. Mashlan, I. Markova, D. Jancik, M. Sebela, H. Bartonkova, V. Bellesi, P. Novak, D. Petridis, *Biomaterials* **2009**, *30*, 2855–2863. **DOI:**10.1016/j.biomaterials.2009.02.023
41. P. Moroz, H. Pardoe, S. K. Jones, T. G. S. Pierre, S. Song, B. N. Gray, *Phys. Med. Biol.* **2002**, *47*, 1591–1602. **DOI:**10.1088/0031-9155/47/9/312
42. S. C. N. Tang, I. M. C. Lo, *Water Res.* **2013**, *47*, 2613–2632. **DOI:**10.1016/j.watres.2013.02.039

43. S. Lin, D. Lu, Z. Liu, *Chem. Eng. J.* **2012**, *211-212*, 46–52. **DOI:**10./j.cej.2012.09.018
44. T. A. Aragaw, F. M. Bogale, B. A. Aragaw, *J. Saudi Chem. Soc.* **2021**, *25*, 101280. **DOI:**10.1016/j.jscs.2021.101280
45. P. N. Dave, L. V. Chopda, *J. Nanotechnol.* **2014**, *2014*, article ID 398569.
46. U. Jeong, X. Teng, Y. Wang, H. Yang, Y. Xia, *Adv. Mater*. **2007**, *19*, 33–60. **DOI:**10.1002/adma.200600674
47. M. T. A. El-oi, R. B. Azevedo, E. C. D. Lima, A. C. M. Pimenta, P. C. Morais, *J. Magn. Magn. Mater.* **2005**, *289*, 168–170. **DOI:**10.1016/j.jmmm.2004.11.049
48. S. He, Y. Feng, N. Gu, Y. Zhang, X. Lin, *Environ. Pollut.* **2011**, *159*, 3468–3473. **DOI:**10.1016/j.envpol.2011.08.024
49. Y. H. Chen, *J. Alloys Compounds* **2013**, *553*, 194–198. **DOI:**10.1016/j.jallcom.2012.11.102
50. W. Jiang, M. Pelaez, D. D. Dionysiou, M. H. Entezari, D. Tsoutsou, K. O'Shea, *Chem. Eng. J*. **2013**, *222*, 527–533. **DOI:**10.1016/j.cej.2013.02.049
51. A. Afkhami, M. Saber-Tehrani, H. Bagheri, *Desalination* **2010**, *263*, 240–248. **DOI:**10.1016/j.desal.2010.06.065
52. S. K. Sahoo, K. Agarwal, A. K. Singh, B. G. Polke, K. C. Raha, *Int. J. Eng. Sci. Technol.* **2010**, *2*, 118–126.
53. Y. Leconte, S. Veintemillas-Verdaguer, M. P. Morales, R. Costo, I. Rodriguez, P. Bonville, B. Bouchet-Fabre, N. Herlin-Boime, *J. Colloid Interface Sci*. **2007**, *313*, 511–518. **DOI:**10.1016/j.jcis.2007.05.010
54. R. Strobel, S. E. Pratsinis, *Adv. Powder Technol*. **2009**, *20*, 190–194. **DOI:**10.1016/j.apt.2008.08.002
55. A. D. Abid, M. Kanematsu, T. M. Young, I. M. Kennedy, *Aerosol Sci. Technol.* **2013**, *47*, 169–176. **DOI:**10.1080/02786826.2012.735380
56. M. F. Silva, A. A. W. Hechenleitner, D. M. F. De Oliveira, M. Agüeros, R. Peñalva, J. M. Irache, E. A. G. Pineda, *Eur. J. Pharmaceutical Sci*. **2013**, *49*, 343–351. **DOI:**10.1016/j.ejps.2013.04.006
57. K. Uma, H. S. Lalithamba, M. Raghavendra, V. Chandramohan, C. Anupama, *Arkivoc* **2016**, (*iv*), 339–351. **DOI:**10.3998/ark.5550190.p009.605
58. B. L. Shinde, L. A. Dhale, V. S. Suryavanshi, K. S. Lohar, *Acta Chim. Slov.* **2017**, *64*, 931–937.
59. B. Secerov, Z. Andri, N. Abazovi, R. Krsmanovi, M. Mitri, A. Montonea, M. D. Dramianin, *Acta Chim. Slov.* **2008**, *55*, 486–491.
60. H. S. Lalithamba, M. Raghavendra, K. Uma, K. V. Yatish, D. Mousumi, G. Nagendra, *Acta Chim. Slov.* **2018**, *65*, 354–364. **DOI:**10.17344/acsi.2017.4034
61. N. T. M. Tho, T. N. M. An, M. D. Tri, T. V. M. Sreekanth, J. S. Lee, P. C. Nagajyothi, K. D. Lee, *Acta Chim. Slov.* **2013**, *60*, 673–678.

Povzetek

Opisujemo enostaven in okolju prijazen heterogeni katalitski sistem, temelječ na Fe_2O_3 nanodelcih, uporaben za sintezo acil tiosečninskih derivatov iz ustreznih *in situ* pripravljenih acil izotiocianatov in estrov aminokislin. Sinteza poteka v acetonu in daje produkte z dobrimi izkoristki. Strukture pripravljenih acil tiosečnin smo potrdili z ^{1}H NMR, ^{13}C NMR, masno in FTIR analizo. Nanodelce Fe_2O_3 smo pripravili s pomočjo sežiga raztopine, z uporabo askorbinske kisline kot reducenta ter **železovega**(III) nitrata kot vira **železovih** ionov. Pripravljen nanomaterial smo okarakterizirali z XRD, SEM, UV-vidno in FTIR analizami. Pomembno je, da lahko Fe_2O_3 in ostale nečistoče po sintezi enostavno odstranimo. Katalitski sistem je učinkovit in katalizira pretvorbe reaktantov v produkte z dobrimi izkoristki. Za nekatere izmed pripravljenih acil tiosečnin smo določili *in vitro* antibakterijske aktivnosti proti *Staphylococcus aureus* in *Escherichia coli.*

Except when otherwise noted, articles in this journal are published under the terms and conditions of the Creative Commons Attribution 4.0 International License

Scientific paper

Acetyl Cellulose Film with 18-crown-6 Ether for Colorimetric Phosgene Detection

Martin Lobotka,[1,*] Vladimír Pitschmann[2,3] and Zbyněk Kobliha[1]

[1] *University of Defence, NBC defence institute, Víta Nejedlého 691, 682 01 Vyškov*

[2] *Oritest spol. s r.o., Čerčanská 640/30, 150 00 Prague, Czech Republic*

[3] *Czech Technical University in Prague, Faculty of Biomedical Engineering, nám. Sítná 3105, 272 01 Kladno, Czech Republic*

** Corresponding author: E-mail: lobotka@oritest.cz*

Received: 12-08-2021

Abstract

The use of a cellulose detection film as a carrier for a colorimetric sensor to detect phosgene and allied compounds to be evaluated primarily visually is studied. For the case study, a benzimidazole-rhodamine dye and an acetyl cellulose film were selected. The detection complex was modified using cyclic ether 18-crown-6 to achieve more desirable analytic properties. The chromatic properties of detection film was verified using reflectance colorimetry in the visible light spectrum. The employed detection agent demonstrated high sensibility to phosgene vapours, but acid gases, acyl chlorides, base organic solvents, and in higher concentrations, even some organophosphorus substances interfered. The detection film application was adjusted to the in-situ preparation of simple detection devices (a spray or a marker) as well as to manufacture detection strips with beforehand excluded polymer film.

Keywords: Crown ether, phosgene, polymer film, acetyl cellulose, chromogenic chemosensor

1. Introduction

The highly toxic colourless gas phosgene, mostly in mixtures with other toxic gases, was firstly utilised for military purposes during World War I. From the chemical point of view, it is a derivate of carbonic acid with two allied compounds: diphosgene (trichloromethyl carbonochloridate) and triphosgene (bis(trichloromethyl) carbonate). This highly reactive gas demonstrates distinct toxic properties due to a significant hydrolytic reaction on tissues and is classified as a pulmonary agent. The allied compound diphosgene has risen to military significance. Concerning diphosgene, it is a colourless liquid ensuring easier manipulation.[1] The toxic properties of diphosgene correspond with phosgene, the LC_{50} dose represents 2,000–3,200 mg m^{-3} (500–800 ppm) at 1 min exposure.[1,2] The permissible value of work exposure due to the NIOSH regulations is 0.4 mg m^{-3} (0,1 ppm) at 8 h shift.[1,3] Phosgene is currently utilised when producing agrochemicals, polycarbonates, and pharmaceutical substances; in 2015, the world production amounted to 8.526 million tonnes.[4]

The colorimetric detection of phosgene/diphosgene is currently conducted using the well-known reaction with benzylpyridine derivates, for example 4-(4-Nitrobenzyl) pyridine: distinct red colouring. The method has been predominantly applied in the form of detection tubes or paper strips also known as continuous detectors in the form of cards.[5–10] Furthermore, the reaction of phosgene with Harrison's reagent (4-(dimethylamine) benzaldehyde/diphenylamine) produces a yellow condensation product.[11–13] Newer detection methods use more complex chromogenic agents with organic chemosensor structures, or other heterocyclic compounds, which, after the reaction with an analyte, change colours distinctly. To illustrate the case, the reaction between phosgene and substituted BODIPY oxime forming orange colouring or with phenylenediamine/BODIPY unit as fluorophore can be utilised.[14,15] Out of other detection agents, the compounds with coumarin, benzothiazole, imidazole, benzimidazole-rhodamine, o-phenylenediamine/pyronine, o-hydroxyaniline, carboxyimide, and quinazolinone skeletons were employed for colorimetric and fluorometric detection.[16–30]

The authors, purposefully and on a long-term basis, concentrate on the issues of phosgene and its allied compounds detection. The aim of the work was to propose a different carrier of detection agents in the form of a thin polymer film. It is going to be carry several advantages of the solution, such as the abilities to prepare a detector in the place of detection (in situ), to minimise the usage of chemicals and supporting materials, and to allow the continuous monitoring of the environment to check the presence of toxic substances.

2. Experimental

2. 1. Chemicals and Materials

To prepare polymer films, acetyl cellulose (Carl Roth GmBH, Germany), cyclic ether 18-crown-6 (Sigma-Aldrich, USA), and acetone as a dissolving agent (Merck, Darmstadt, Germany) were employed. Benzimidazole/rhodamine B dye was employed as a detection agent (The University of Chemistry and Technology, Prague, CZE; the spectral data correspond with the literature). To verify the method, trichloromethyl chloroformate (diphosgene), ammonia, benzoyl chloride, diethyl ether, hydrochloric acid, nitromethane, pyridine, carbon disulphide, (all Sigma-Aldrich, USA), isopropyl methylphosphonofluoridate (sarin, The University of Defence, CZE), and petrol (Cepro, CZE) were employed.

To apply polymer films, a refillable marker with a dosing valve and 4 mm tip 211EM (Molotow, Lahr, Germany) was utilised. The objective colorimetric measurements were conducted using the reflectance spectrophotometer Ultrascan XE (HunterLab, Reston, USA) with 9.5 mm entrance slit. The micrographs were taken using a scanning electron microscope (SEM).

2. 2. Preparation of Polymer Solution with Detection Agent

The base solution supply of the polymer was prepared by dissolving 4 g of acetyl cellulose in 100 ml of anhydrous acetone in a heated ultrasonic bath. 8 mg of rhodamine-benzimidazole dye was dissolved in 5 ml of the base solution to form a pink solution. The transition of the colouring dye to the colourless form was conducted by adding 750 mg of ether 18-crown-6. The solution turned light pink, colourless after the application on the carrier.

2. 3. Phosgene Detection

The concentration of diphosgene in the range from 0.1 to 5 mg/m^3 in a toluene solution was prepared in the test chamber with the volume of 0.712 m^3 using the forced air circulation. The colouring of the detection film depending on the diphosgene vapour concentration and the exposure time ranging from 1 to 10 min were observed. Apart from the intended, primary visual evaluation, the instrumental reflectance measurement was conducted to objectively evaluate the changes in film colouring. After each exposure in the test chamber, the new concentration of the analyte was prepared for the following measurement.

The chemosensors were prepared by excluding the thin detection film from 50 µl detection polymer solution. The film was subsequently distributed on a PE pad with the diameter of 16 mm. After the distribution, the film was left for drying at the laboratory temperature for the period of 3 min. To evaluate the changes in the colouring of the detection film, the method of reflectance colorimetry in the colour space CIELAB 10°/D65 was employed. The records were interpreted as the dependence of the reflectance on the wavelength of the visible spectrum in the interval of λ = 380–750 nm.

3. Results and Discussion

3. 1. Method Characteristics

To detect phosgene and its allied compounds, the benzimidazole-rhodamine dye was selected. Historically, the phosgene detection was based on its reaction with the nitrogen of the benzimidazole unit releasing the pink form of the dye (Figure 1) that can be evaluated in the UV spectrum of electromagnetic radiation.[19]

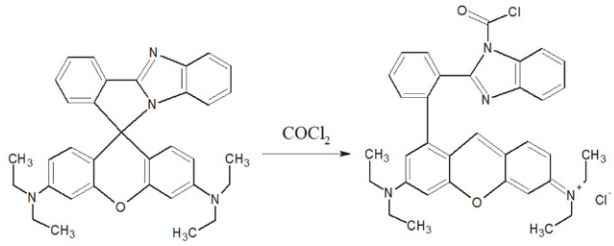

Figure 1: Benzimidazole-rhodamine dye and the end product after the reaction with phosgene are presented.[19]

The previous research already applied the agent into the polymer matrix formed by polyethylene oxide, formed using the technology of electrostatic fibre formation, whose fibrous structure was the functional base for the chemosensor to detect phosgene using colorimetric and fluorescent evaluation.[19] The simple release of the polymer film from the solution by evaporating the dissolving agent was employed. This simple method can be easily utilised for the in-situ preparation of simple detection means to monitor toxic substances in the atmosphere, to simplify the whole testing procedure, and at the same time, to minimise financing costs.

Three ways were utilised to employ the detection film. Firstly, it was utilised in the form of the solution applicated by the refillable marker. Secondly, the preparation of simple detection strips made from supporting materials

(PE strip) and the released detection film on its surface was utilised. Thirdly, the application of the polymer solution using a mechanical spray for larger areas was utilised.

3. 2. Detection Film Characteristics

The naturally released films from acetone were unstable and mostly unable to preserve the transparent

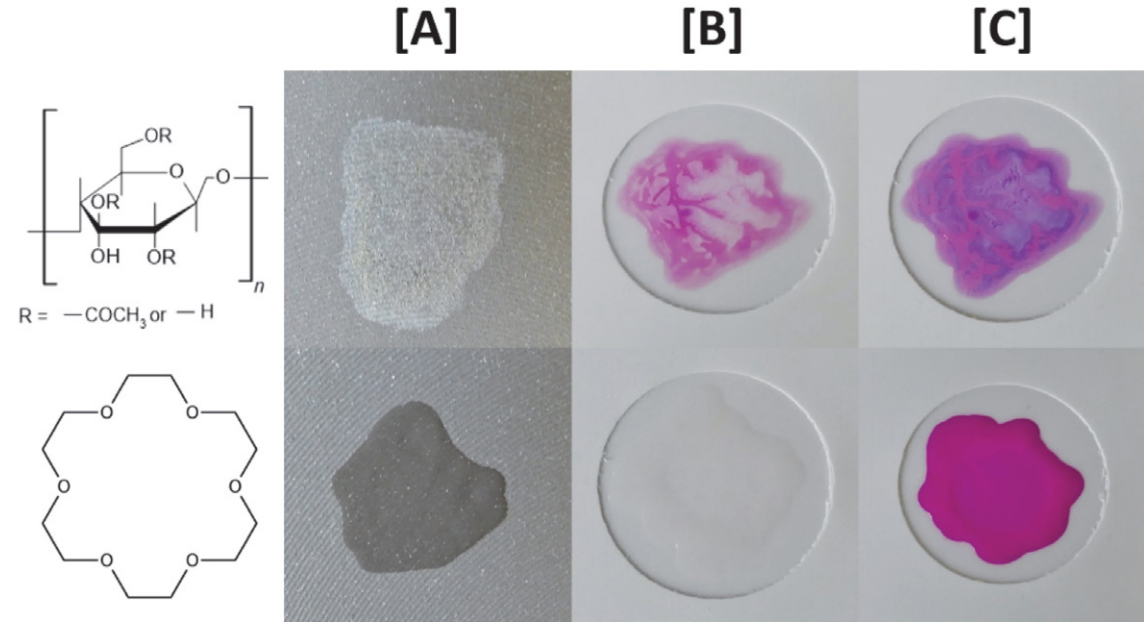

Figure 2: The non-modified (the upper row) and the modified 15% ether 18-crown-6 acetyl cellulose film (the lower row) are compared. The natural appearance of the polymer film after the evaporation of the dissolving agent [A], the excluded polymer film with the benzimidazole-rhodamine agent [B], and after being exposed to diphosgene vapours [C] are presented.

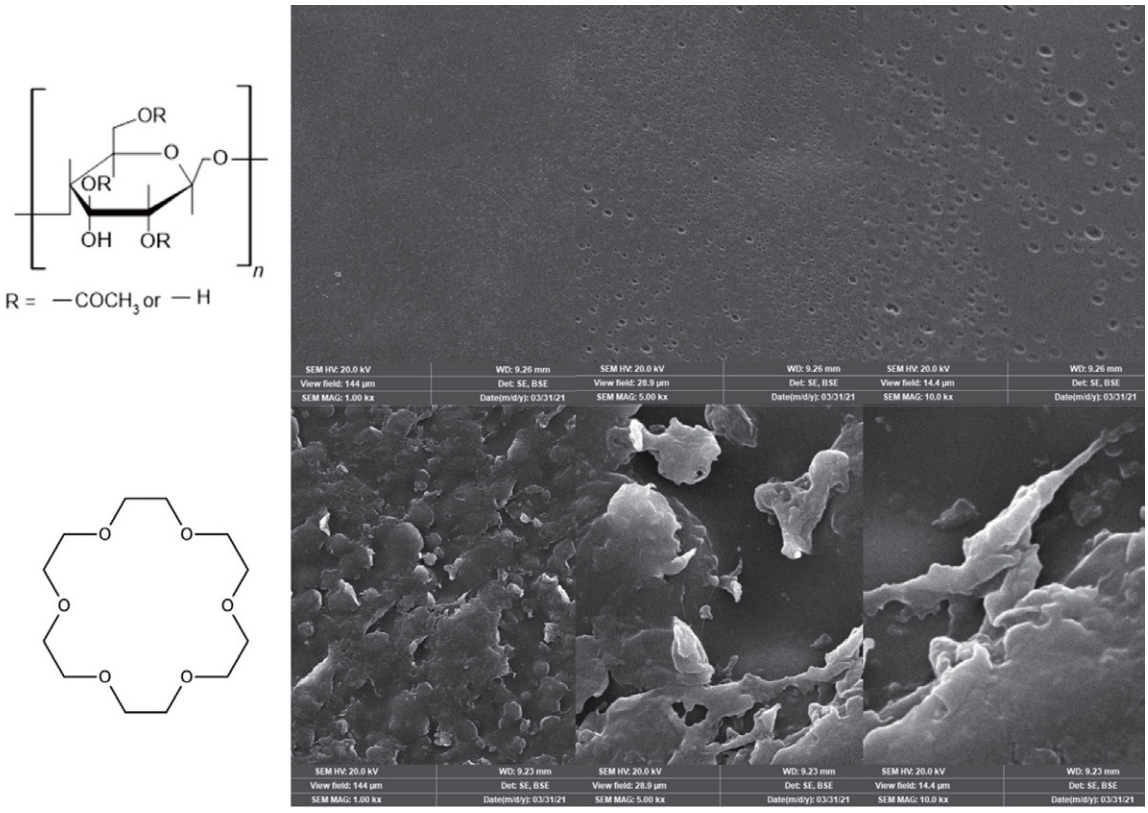

Figure 3: The micrographs of the acetyl cellulose film (the upper row) and the film with the addition of 15% ether 18-crown-6 (the lower row) are compared at various magnifications.

appearance. Besides, the colouring agent was also unable to preserve the transparent appearance and after the evaporation of the dissolving agent, it coloured heavily (Figure 2).

The further study of the issue aimed at removing these drawbacks by modifying the film using ether 18-crown-6. The cyclic ether improved the structure of the released film and preserved the detection agent in the transparent form (Figure 2). The homogeneity of the distribution of the detection agent inside the polymer film was significantly improved. The growing percentage of ether 18-crown-6 in the polymer decreases its rigidity; with over 20% percentage of ether 18-crown-6, it formed a gel-like mixture. The 15% value of ether 18-crown-6 mass in the acetone solution of the polymer was selected to reach the compromise between the sufficient film rigidity and the positive impact on the detection.

The stabilisation of the colouring agent can be probably assigned to the ability of the cyclic ether to bind a hydrogen cation inside the cyclic molecule in the form of hydronium cation.[31–33]

After evaluating the impact of the addition of ether 18-crown-6 to the structure of the released acetyl cellulose films, the scanning electron microscopy of the samples without the detection agent was conducted. The micrographs demonstrated much higher heterogeneity of the modified films (Figure 3) in comparison with the naturally released ones and this probably contributed to the better accessibility of the analytic agent on their surfaces.

3. 3. Verifying Methods of Using Detection Films

Detection marker

Filling the cartridge of the refillable marker by the solution of the detection film allows to produce simple detection devices in the place of detection (in situ) (Figure 4). The advantage of the solution is the sufficient capacity of the cartridge that ensures conducting the tens of tests using a single cartridge; this means an extremely low cost per use. The application is possible on all materials with the good potential of the easy evaluation of the colour change, for example white cotton fibre, paper, plastic material, or ceramics. The 5 ml filling of the detection polymer solution suffices for approximately 500 tests.

Strip detector

The PE strips with the 12 × 80 mm dimensions were marked with the glued label with 5 mm circular openings. 10 µl of the solution of the detection film was applied to the openings using a micropipette. After the evaporation of the dissolving agent, the simple detection device with 5 mm active surface that can be packed into the hermetic packaging (Figure 4) was produced.

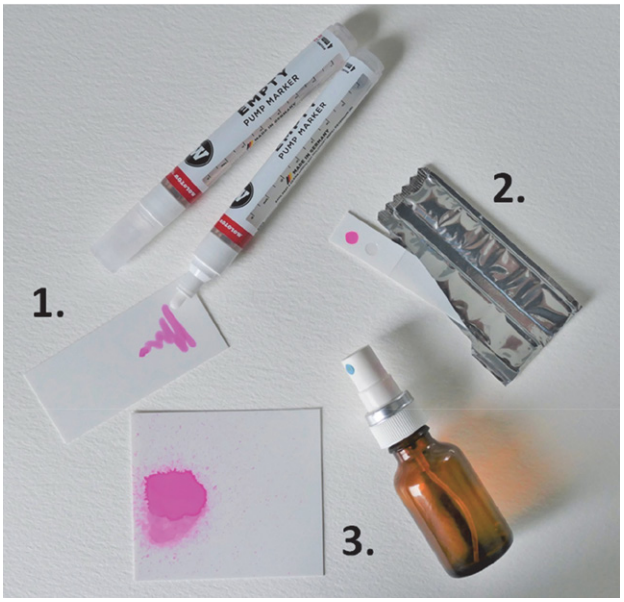

Figure 4: The proposed application utilises either the polymer solution for the in-situ release of the detection films (1 – the detection marker, 3 – the detection spray) or the beforehand released film on the suitable carrier (2 – the test strip). The pink colouring was reached by the exposure of the detection devices to diphosgene vapours.

Detection spray

The simple hand spray was the last laboratory-verified application of the detection film. The volatile dissolving agent helps to the quick drying of the film on the base which lasted only a few tens of seconds. The commercially easily accessible hand spray suitable for the application on larger surfaces was utilised (Figure 4).

3. 4. Sensibility, Stability, and Interference

Measuring the dependence of diphosgene concentration on the colouring intensity of the detection film is depicted in the Figure 5. The absorption maximum of the detection film is in 570 nm wavelength range. The detection limit when visually evaluated is in the case of 10 min exposure on the border of 0.125 mg/m^3. LOD was determined on the set of 5 samples tested at the given concentration and the exposure time which produced colour perception in an observer. The sensibility of the solution when exposed to phosgene satisfies the requirements of workplace hygiene according to NIOSH.

The work verified the stability of the detection films during long-term diphosgene measurement in the atmosphere. The long-term measurements manifested themselves in the measurable decrease of the film colouring; nevertheless, the effect was infinitesimal when evaluated visually (Figure 6). The solution is feasible when considering the visual evaluation and/or continuous atmosphere monitoring.

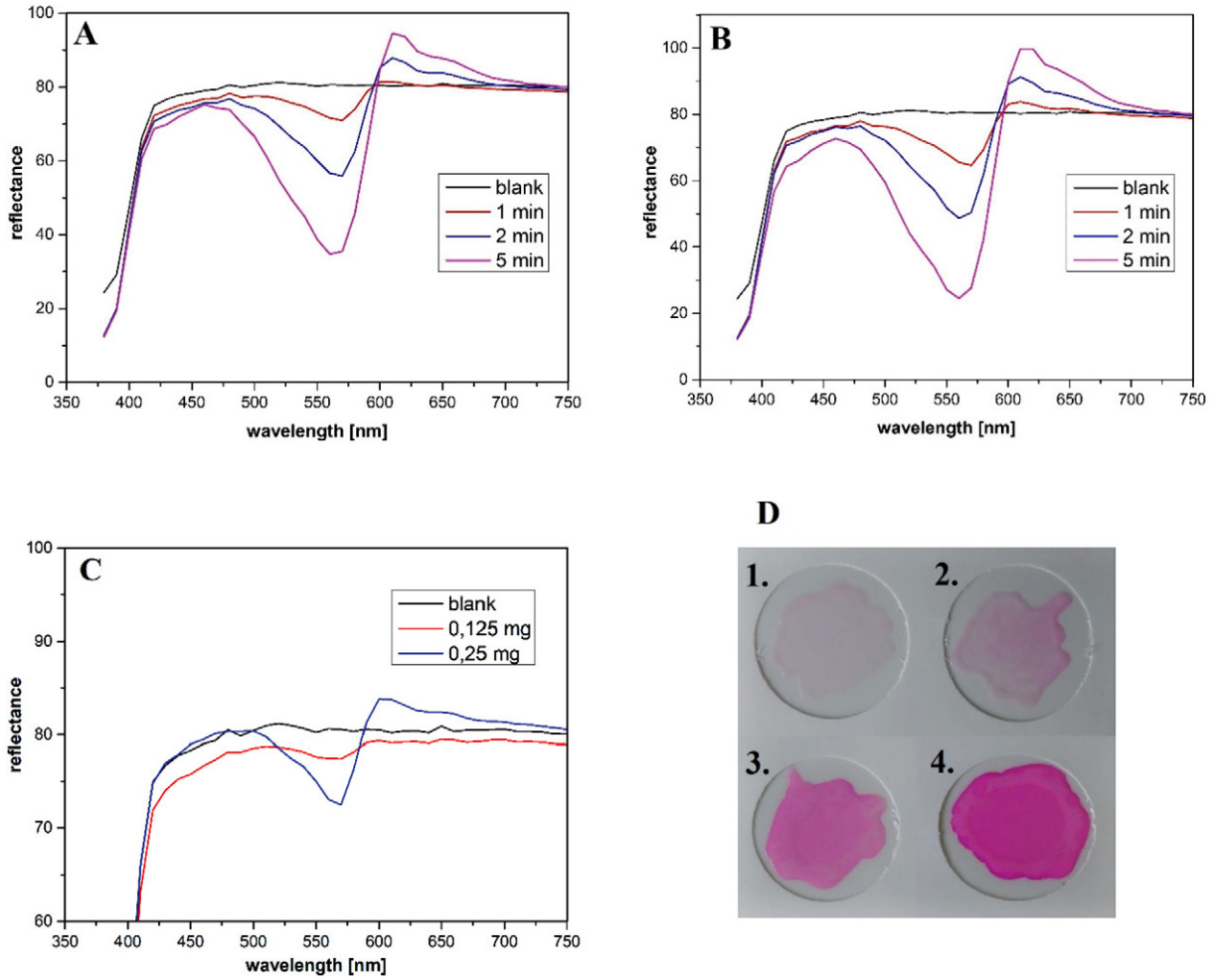

Figure 5: The colouring of the detection film at the diphosgene concentration of 2.2 mg/m^3 (A) and 4.4 mg/m^3 (B) depending on the exposure time is measured. The low concentrations (C) were measured at 10 min exposure time. The colouring examples of the detection film (D) (diphosgene concentration/exposure time) were given at 1) 0.25 mg/m^3/5 min; 2) 0.5 mg/m^3/5 min; 3) 2.2 mg/m^3/2 min; 4) 4.4 mg/m^3/2 min.

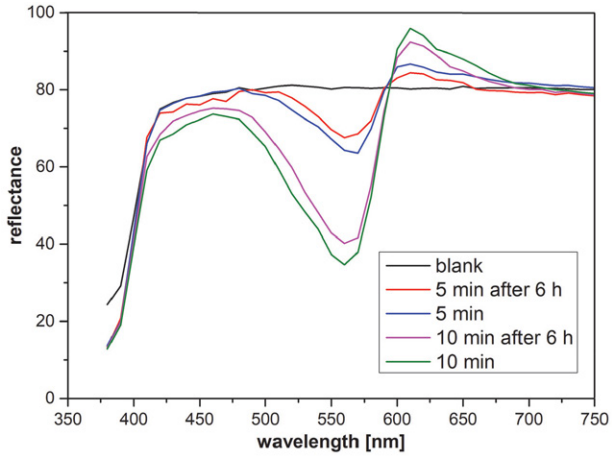

Figure 6: The colouring of the detection film after the diphosgene vapour exposure at the concentration of 1 mg/m^3 and 5, 10 min exposure is presented. The sample set was placed in uncontaminated environment for 6 h and subsequently exposed to the corresponding analyte concentration.

3.4 Interference Substance Influence on Detection Film

The detection agent is sensitive to acidic gases, or the substances which produce acidic products when in the presence of atmospheric humidity; the acidic products protonate the imidazole nitrogen in the molecule.[34] The reaction of colouring films on the selected most significant interfering substances was instrumentally measured (Figure 7). Based on the measured data, it is evident that the most significant interfering substance is hydrogen chloride which leads to the highly sensitive reaction with the detection film, as in the case of diphosgene. Benzoyl chloride is a less significant interferent; in the concentration of 2.8 mg/m^3 and 2 min exposure time, it does not produce any colour change of the film.

Due to the possible need of toxic substance analysis in the military, the nerve agent sarin (GB) was tested as an analyte; however, at the selected 0.5 mg/m^3 sarin concentration and 10 min exposure time, no colouring of the detection film was observed. The colour reaction was ob-

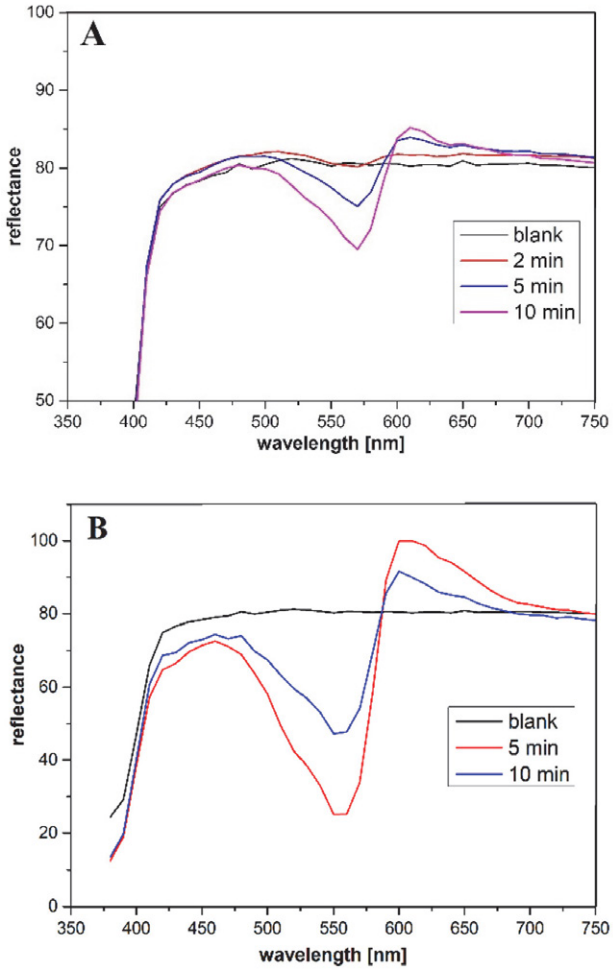

Figure 7: The colour reaction of the detection film depending on the exposure time concerning the most significant interfering substances, for example (A) benzoyl chloride at the concentration of 2.8 mg/m^3 and (B) hydrogen chloride at the concentration of 5.8 mg/m^3, were measured.

servable at the high concentrations of sarin, over 10 mg/m^3. Contrarily, the colour reaction of the detection system was not observed in aliphatic and aromatic hydrocarbons, chlorinated dissolving agents, base substances, and other dissolving agents (the Table 1). The colour reaction of the diphosgene after the exposure to common dissolving agents and chemicals was examined. The detection film demonstrated high affinity to pyridine when its vapours significantly inhibited the colour reaction even after longer period after the interrupting the exposure. Nitromethane achieved the same, even though a bit weaker result. Ammonia, on the other hand, inhibited the reaction only slightly as it was quickly released from the film.

4. Conclusions

The tested solution provides a cheap and simple carrier of the detection chemicals which represents a possible alternative to the currently commonly used carriers (paper or silica gel) The proposed cellulose carrier, modified with ether 18-crown-6, represents the possibility to prepare simple detection devices in the place of detection (in situ) owing to the thin polymer film with evenly distributed detection chemicals on its surface. To verify the abilities of the carrier, the rhodamine-imidazole dye integrated into the polymer matrix was utilised. This simple detection device in the form of a PE card with the applied detection film was exposed to diphosgene vapours. The ascertained LOD when evaluated visually and 10 min exposure time amounted to 0.125 mg/m^3 (0.03 ppm). All the considered detection solutions (a marker, a strip sensor, and/or a spray) were functional.

The proposed polymer carrier is suitable also for the integration of analytical agents sensitive to other toxic va-

Table 1: The overview of the interferences of the proposed detection film, the substances were tested in the form of concentrated gases.

Chemicals	The reaction of the film to chemicals	The reaction of the film to diphosgene after the exposure to chemicals
ammonia	No reaction	Slight decrease in sensibility
benzoyl chloride	Pink-purple colouring, weaker than gaseous hydrogen chloride	–
diethyl ether	No reaction	Detection potential preserved
hydrogen chloride	Pink-purple colouring, significant interference	–
car petrol	No reaction	Detection potential preserved
nitromethane	No reaction	Decrease in sensibility
pyridine	No reaction	Significant decrease in sensibility
sarin (GB)	0.5 mg/m^3, 10-min exposure – no reaction, the reaction noticed over concentrated vapours	Detection potential preserved
carbon disulphide	No reaction	Detection potential preserved

pours and gases which will be the topic of the subsequent development of the research.

5. References

1. E. Halámek, Z. Kobliha, V. Pitschmann, Analysis of Chemical Warfare Agents; University of Defence: Brno, Czech republic, **2009**. ISBN: 978-80-7231-658-8.
2. J. Borak J, W. F. Diller**,** *J. Occup. Environ. Med.* **2001**, *43* (2), 110–119. **DOI:**10.1097/00043764-200102000-00008
3. Centers for desease control and prevention, The National Institute for Occupational Safety and Health (online), NIOSH Pocket Guide to Chemical Hazards – Phosgene, https://www.cdc.gov/niosh/npg/npgd0504.html (10.3.2021).
4. Gen Consulting Company, Global Phosgene Outlook 2016-2021**, 2016**.
5. A. M. Agree, R. L. *Talanta* **1966**, *13 (8)*, 1151-1160. **DOI:**10.1016/0039-9140(66)80163-7
6. B. Witten, A. Prostak, *Anal. Chem.* **1957**, *29*, 885–887. **DOI:**10.1021/ac60126a008
7. Morphix Technologies (online), SafeAir® Chemical Detection Badges, Phosgene, Virginia, USA, https://www.morphtec.com/safeair/ (10.3.2021).
8. V. Pitschmann, Z. Kobliha, E. Halámek, I. Tušarová, *J. Serb. Chem. Soc.*, **2007**, *72(10)*, 1031-1037. **DOI:**10.2298/JSC0710031P
9. V. Pitschmann, Z. Kobliha, E. Halámek, I. Tušarová, *Chem. Anal.*, **2008**, *53(2)*, 47–57.
10. V. Pitschmann, I. Tušarová, Z. Kobliha, D. Vetchý, *Hem. Ind.*, **2012**, *66(1)*, 79–84. **DOI:**10.2298/HEMIND110530057P
11. A. P. Vargas, F. Gámez, J. Roales, T. Lopes-Costa, J. M. Pedrosa, *ACS Sensors* **2018**, *3*, 1627–1631. **DOI:**10.1021/acssensors.8b00507
12. A. L. Linch, S. S. Lord, K. A. Kubitz, M. R. De Brunner, *Am. Ind. Hyg. Assoc. J.* **1965**, *26 (5)*, 465–474. **DOI:**10.1080/00028896509342759
13. A. P. Vargas, T. Lopes-Costa, M. G. Guillén, M. B. S. Jiménez, J. M. Pedrosa, Detection of phosgene by using TiO_2/indicator nanocrystalline thin films, 10th International Conference on Composite Science and Technology, Lisboa, Portugal, **2015**.
14. T. I. Kim, B. Hwang, J. Bouffard, Y. Kim, *Anal. Chem.*, **2017**, *89*, 12837–12842. **DOI:**10.1021/acs.analchem.7b03316
15. X. Hong-Cheng, X. Xiang-Hong, S. Qin-Hua, *Anal. Chem.*, **2017**, *89 (7)*, 4192–4197. **DOI:**10.1021/acs.analchem.7b00203
16. F. Weiyong, G. Shengyi, Z. Enbo, Y. Xinyu, F. Guoqiang, *Anal. Chim. Acta*. **2018**, *1029*, 97–103.
17. X. Hong-Cheng, X. Xiang-Hong, S. Qin-Hua, *ACS Sensors*, **2017**, *2 (1)*, 178–182.
18. B. Luoyi, F. Weiyong, F. Guoqiang, *Dyes and Pigments*, **2019**, *163*, 483–488. **DOI:**10.1016/j.dyepig.2018.12.013
19. H. Ying, Z. Xin, J. Hyeseung, N. Sang-Jip, H. K. Myung, Y. Juyoung, *Anal. Chem.* **2018**, *90 (5)*, 3382–3386. **DOI:**10.1021/acs.analchem.7b05011
20. W. Cuiyan, X. Hai, L. Yaqian, X. Ruihua, L. Peijuan, P. Xiao, Z. Zile, G. Biao, L. Haitao, Z. Youyu, *Talanta* **2019**, *200*, 78–83. **DOI:**10.1016/j.talanta.2019.03.003
21. X. Zhou, Y. Zeng, C. Lilyan, X. Wu, J. Yoon, *Angew. Chem. Int. Ed.* **2016**, *55*, 4729–4733. **DOI:**10.1002/anie.201601346
22. V. Pitschmann, L. Matějovský, J. Zeman, D. Vetchý, M. Dymák, M. Lobotka, S. Pavloková, Z. Moravec, *Chemosensors*, **2020**, *8(4)*, 107 (8040107). **DOI:**10.3390/chemosensors8040107
23. Q. Hu, T. Gong, Y. Mao, Y. Yin, Y. Wang, H. Wang, *Acta A Mol. Biomol. Spectrosc.* **2021**, *253*, 119589. **DOI:**10.1016/j.saa.2021.119589
24. Z. J. Li, W. J. Zhang, W. Z. Bi, Q. J. Ma, S. X. Feng, X. L. Chen, L. B. Qu, *RSC Advances*, **2021**, *11*, 10836. **DOI:**10.1039/D1RA00811K
25. L. Yang, F. Wang, J. Zhao, X. Kong, K. Lu, M. Yang, J. Zhang, Z. Sun, J. You, *Talanta*, **2021**, *221*, 121477. **DOI:**10.1016/j.talanta.2020.121477
26. Z. Lintao, Z. Hongyan, W. Shuangfei, W. Shan, H. Ji-Ting, Y. Juyoung, *Commun. Chem.*, **2019**, *55*, 13753–13756. **DOI:**10.1039/C9CC07437F
27. H. Qiao, D. Chong, W. Juanjuan, S. Dongdong, Z. Lintao, S. Ruilong, *Anal. Chem.*, **2018**, *90*, *14*, 8686–8691. **DOI:**10.1021/acs.analchem.8b02119
28. Z. Lintao, Z. Hongyan, J. Lirong, W. Shan, H. Ji-Ting, Y. Juyoung, *Anal. Chem.*, **2019**, *91*, *18,* 12070–12076. **DOI:**10.1021/acs.analchem.9b03230
29. Ch. Tianhong, J. Lirong, H. Ji-Ting, W. Wei, Z. Lintao, B. Guang-Ming, *J. Mater. Chem.*, **2020**, *8*, 24695–24702. **DOI:**10.1039/D0TA08333J
30. F. Zeng, G. Bao, B. Zhou, Y. Han, *New J. Chem.* **2021**, 45(*12),* 5631–5636. **DOI:**10.1039/D1NJ00037C
31. J. W. *Steed, J. L. Atwood, Supramolecular Chemistry (2nd ed.), Wiley,* **2009**. ISBN: 978-0-470-51234-0.
32. J. L. Atwood, S. G. Bott, A. W. Coleman, K. D. Robinson, S. B. Whetstone, C. M. Means, J. *Am. Chem. Soc.* **1987***, 109 (26), 8100–8101.* **DOI:**10.1021/ja00260a033
33. J. L. Atwood, S. G. Bott, C. M. Means, A. W. Coleman, H. Zhang, M. T. *May, Inorganic Chemistry,* **1990***, 29 (3), 467–470.* **DOI:**10.1021/ic00328a025
34. X. Zhongwei, Ch. Mingliang, Ch. Jianming, H. Jiahuai, H. Shoufa, *RSC Advances*, **2014**, *4*, 374–378.

Povzetek

Proučevali smo uporabo celuloznega detekcijskega filma kot nosilca za kolorimetrični senzor za detekcijo fosgena in sorodnih spojin na podlagi vizualne evalvacije. Za demonstracijo koncepta smo izbrali benzimidazol-rodaminsko barvilo in acetilcelulozni film. Detekcijski kompleks smo modificirali z uporabo cikličnega etra 18-krona-6, da smo dosegli bolj ugodne analitične lastnosti. Kromatske lastnosti detekcijskega filma smo preverili z odbojno kolorimetrijo v spektru vidne svetlobe. Uporabljen detekcijski agent je pokazal visoko občutljivost na hlape fosgena, vendar pa so interferirali plini kislin, acil kloridi, bazična organska topila in v višjih koncentracijah celo nekatere organofosforne snovi. Aplikacija detekcijskega filma je bila prilagojena in situ pripravi enostavnih detekcijskih naprav (razpršilo ali marker) ter izdelavi detekcijskih trakov s predhodno izločeno polimerno folijo.

Except when otherwise noted, articles in this journal are published under the terms and conditions of the Creative Commons Attribution 4.0 International License

Scientific paper

Modulation of Cerium Carbonate Crystal Growth by Polyvinylpyrrolidone using Density Functional Theory

Deyun Sun,[1,2,3] Yanhong Hu,[1,2,3,*] Mao Tang,[1,2,3] Ze Hu,[1,2,3] Peng Liu [1,2,3] Zhaogang Liu[1,2,3] and Jinxiu Wu[1,2,3]

[1] *College of Materials and Metallurgy, Inner Mongolia University of Science and Technology, Baotou 014010, China;*

[2] *Key Laboratory of Rare Earth Hydrometallurgy and Light Rare Earth Application in Inner Mongolia Autonomous Region, Baotou 014010, China;*

[3] *Key Laboratory of Green Extraction and Efficient Utilization of Light Rare Earth Resources, Ministry of Education, Baotou 014010, China*

* *Corresponding author: E-mail: Bthyh@163.com*

Received: 08-12-2021

Abstract

Cerium carbonate crystal morphology is predicted using density functional theory (DFT) simulations in this paper. In the nucleation phase, the ketone group in polyvinylpyrrolidone (PVP) will preferentially bind to Ce3+ to form complexes and provide heterogeneous nucleation sites for the system, prompting the nucleation of cerium carbonate crystals. In the growth stage, due to the adsorption of PVP, the probability of (120) crystal plane appearing in the equilibrium state is the greatest, resulting in the formation of hexagonal flake cerium carbonate crystals with (120) crystal plane as the oblique edge. Experimentally, hexagonal sheet cerium carbonate crystals were successfully prepared using PVP as a template agent. Therefore, DFT can be used to predict the morphology of cerium carbonate crystals, which not only elucidates the growth mechanism of cerium carbonate crystals, but also greatly reduces the experimental cost.

Keywords: Cerium carbonate hydrate; Polyvinylpyrrolidone (PVP); Self-assembly template method; Density functional theory; Morphology control

1. Introduction

Rare earth ore resources in Bayan Obo, Baotou rank first in the world, with light rare earths accounting for more than 98%, while 50% of them are cerium resources. Due to its special electronic structure, cerium oxide has superior oxygen storage and redox ability. It is widely used in many fields such as electronic ceramics, polishing powder, catalyst, sensors, fuel cells, UV absorption, etc.[1–11] It has become an indispensable material for high-tech industries and cutting-edge innovations. The cerium oxide with different morphologies has obvious functional differences, which will have a huge impact on the performance of products. Therefore, the development of industrial preparation technology of rare earth compounds with special morphology is very important. So far, cerium oxide with special morphology has been prepared by physical, chemical and many other ways at home and abroad.[12–14] Using polymers as self-assembly templates to regulate material properties provides a new idea for the artificial synthesis of crystal materials and bio-intelligent materials with special functions.[15–18] The self-assembly-template method is favored by more and more experts and scholars because of its simplicity, low cost and strong controllability. Sodium polystyrene sulfonate (PSS), nonylphenol polyoxyethylene ether (NPEO), polyallylammonium chloride (PAH), polyvinylpyrrolidone (PVP) and ethylenediaminetetraacetic acid disodium (EDTA-2Na) were used as templates in our research group. Spherical cerium oxide for catalytic materials, shuttle-shaped cerium oxide for improving glass properties, hexagonal flake cerium oxide for solid oxide fuel cells, and flower-like cerium oxide for UV absorption were prepared by self-assembly template method.[19–22] Lin Wang et al. synthesized polyaniline (PANI) with nanoscale spherical or string-like morphology using PS-b-P2VP as a templating agent for modulation by template-self-assembly method, and the average diameter of each sample was found to be less than 200 nm and showed a tendency to decrease with increasing pH.[23] Using chitosan as a new carbon and nitrogen source precursor and triblock amphiphilic copolymer (F127) as a soft template, nitrogen-doped mesoporous carbon nanoparticles (NMCs) with pore size distribution between 3.05 and 6.09 nm were

successfully prepared by Xianshu Wang et al. The analysis revealed that the nitrogen-doped mesoporous carbon materials have well-developed pores, and the nanoparticles have a spherical shape with an average diameter of about 300–400 nm and a worm-like mesoporous structure.[24]

With the rapid progress of science and technology and the development of interdisciplinary, the method of computer theoretical calculation to synthesize new materials has attracted more and more attention of scientists. Ab initio quantum chemistry method can be used to study the nucleation mechanism and growth mode of materials from the atomic or molecular scale, and disclose the mechanism that cannot be explained in experiments. The morphology control mechanism of cerium carbonate crystals, the precursor of cerium oxide, was studied in our previous research, by molecular dynamics method, and the interaction between the template agent and the crystal surface was simulated. The relationship between the template agent and the crystalline surface of cerium carbonate crystals was revealed from the energy perspective, and the growth mechanism of cerium carbonate crystals was further disclosed.[25–26] Ning Liu et al. successfully predicted the crystal habit of FOX-7 to be spindle-shaped under vacuum conditions with the help of molecular dynamics method. The crystalline habit of FOX-7 in H_2O/DMF solution conditions varied significantly with temperature conditions, and the crystalline habit in different ratios of solvents was blocky when the temperature was 298 K.[27] Balbuena Cristian et al. studied the synthesis of silver nanoparticles with polyvinylpyrrolidone as capping agent, the nucleation of atomic clusters and the subsequent growth of nanoparticles by molecular dynamics, finding that the formation of crystals follows Ostwald ' s law of phase transition. As the process progresses, a series of ordered structures appear inside the particle: icosahedral, body-centered cubic and face-centered cubic, and finally a block-silver equilibrium configuration.[28]

This paper uses a combination method of computational simulation and experimental research. The interaction mechanism of PVP with Ce^{3+} and H_2O in aqueous solution before precipitation and the adsorption of PVP on the main crystal plane after precipitation were calculated and simulated. The process of morphological change of cerium carbonate crystals under the regulation of PVP is explained from the atomic point of view by analyzing the electronic structure and energy change in different cases.[29–33] And the morphology of cerium carbonate crystals was predicted. Then, the cerium carbonate crystals were successfully prepared by the self-assembly-template method using $CeCl_3$ as raw material, NH_4HCO_3 as precipitant and PVP as template agent. The phase structure, morphology and dimensions of cerium carbonate crystals were characterized by Scanning electron microscope (SEM), Transmission electron microscope (TEM) and Diffraction of X-rays (XRD). The experimental results are compared and analyzed with the simulated prediction results to verify the correctness of the prediction results.

2. Material and Methods

2. 1. Experimental Materials

The cerium chloride ($CeCl_3$) used in this experiment was prepared by dissolving and de-hybridizing industrial cerium carbonate provided by Baogang Rare Earth High-Tech Company, Inner Mongolia, China, and hydrochloric acid (analytically pure) provided by Tianjin Damao Chemical Reagent Factory, Tianjin, China. NH_4HCO_3 and anhydrous ethanol were produced by Tianjin Beilian Fine Chemicals Development Co. Ltd., Tianjin, China, and polyvinylpyrrolidone was produced by Shanghai Maclean Biochemical Technology Co. The selected chemicals were analytically pure, which could be used without further purification. The water used in all experiments was deionized water.

2. 2. Preparation Method of $Ce_2(CO_3)_3$ Crystals

At room temperature, deionized water was added to a certain concentration of $CeCl_3$ solution to dilute to 0.05 mol/L, and then PVP was added to prepare the mixed solution of PVP and $CeCl_3$. After stirring at a constant speed for 15 min, 0.05 mol/L NH_4HCO_3 solution was dropped into the mixed solution of $CeCl_3$ and PVP at a certain speed by a peristaltic pump for 1 h. After dripping, the solution was stirred with a stirring paddle at constant speed for 15 minutes before aging. The precipitate obtained by aging at room temperature was filtered, washed and dried to obtain $Ce_2(CO_3)_3$ crystals. The prepared $Ce_2(CO_3)_3$ crystals were characterized by SEM, TEM and XRD.

2. 3. Characterization

XRD was performed using Bruker D8 Advance X-ray diffractometer with CuKa radiation(graphite monochromator). The crystal structure was determined using CuKa radiation(40kV, 40mA), 4° step and the geometric scanning Bragg–Brentano(θ–θ) and the angle range from 5–60°(2θ)were performed. SEM images were taken with Quanta 400 produced by Holland JEI Company, fitted with a field emission source, and working at 15 kV. All samples were mounted on copper stubs and sputter-coated with gold prior to examination. TEM images were taken with a JEM-2100 transmission electron microscope produced by JEI Company, Netherlands, with electron diffraction selected to characterize the samples, observe the morphology and analyze the crystal structure.

2. 4. Computing Method

In this paper, the Vienna Ab Initio simulation software package[34–37] was adopted to perform DFT calculation using GGA (Generalized Gradient Approximation) method.[38–41] The nucleation and growth of cerium carbonate crystals before and after precipitation were studied using

the LOBSTER software package involving chemical bonding analysis.[42–43] Since Ce is in the +3 valence ionic state in cerium carbonate crystals, making only one electron in the 4f orbital. And the 4f orbitals are usually significantly lower in energy than the 5d orbitals and are accompanied by an extremely contracted radial distribution of the orbitals, exhibiting a hemi-nucleation-like property and therefore not involved in bonding.[44] For the sake of brevity, the density of states (DOS) of the PBEsol+U pseudopotential considering the f-orbital electrons, DOS that treats the f-orbiting electrons as a simplified pseudopotential of the inner layer electrons, and fractional density of states (PDOS) of each element were calculated using the PBEsol function, as shown in Figure 1. Without considering the peak intensity, it is found that in the electronic structures calculated by these two methods, there is not much deviation in the positions of the peaks produced by the total and partial density of states of C, H and O, except Ce. The PBEsol+U pseudopotential is compared with the simplified pseudopotential and it is found that the spin-up α and spin-down β orbitals are not equal in energy in the 6s and 5p orbitals of Ce. The spin-up α orbitals near the Fermi energy level have DOS for f and d orbitals but not on the β orbitals and exhibit 100% spin polarization for the f orbitals. This is because Ce is not pure +3 valence, and the electrons in its 4f orbitals are partially out of domain, so there is a mixed 4f and 5d feature on the PDOS, and the f orbitals have a corresponding effect on the 6s and 5p orbitals making their α and β orbitals unequal in energy. In this way, although the mixed f-d orbitals are near the Fermi energy level, they do not interact with other elements in the cell because the f orbitals are occupied by only one electron and have low energy. Therefore, the density of states with little difference is reflected in the total DOS diagram. In view of the above situation, considering the calculation efficiency, the f-orbit electrons of Ce are selected as the simplified pseudopotential of the inner electrons in the calculation method, while PBEsol functional is selected as the functional file.[44–45] Other relevant calculation parameters are as follows: the plane wave truncation energy ENCUT is 350 eV, and the point K in Brillouin zone is divided by Gamma point with grid size of 4 × 3 × 2. The pseudopotential file Ce selects the simplified pseudopotential of + 3 valence, and the pseudopotential of other elements such as H, O, Cl, N, C, selects the PAW pseudopotential of + 1, –2, –1, + 5, + 4 valence. Until the energy difference between the two iteration steps is stabilized below 10–7 eV and the force is stabilized less than –0.05 eV/Å. Considering the spin polarization of the whole system, the Ce outer electron in the simplified pseudopotential is $6s^2 5p^6$, and there is no solitary electron. Therefore, the system can be represented by a single molecular orbital Ψi, which can be regarded as a closed-shell system. The whole calculation process is optimized with interatomic static force at 0 K. The optimized structure is a relatively stable ground state structure with high similarity to the experimental value.

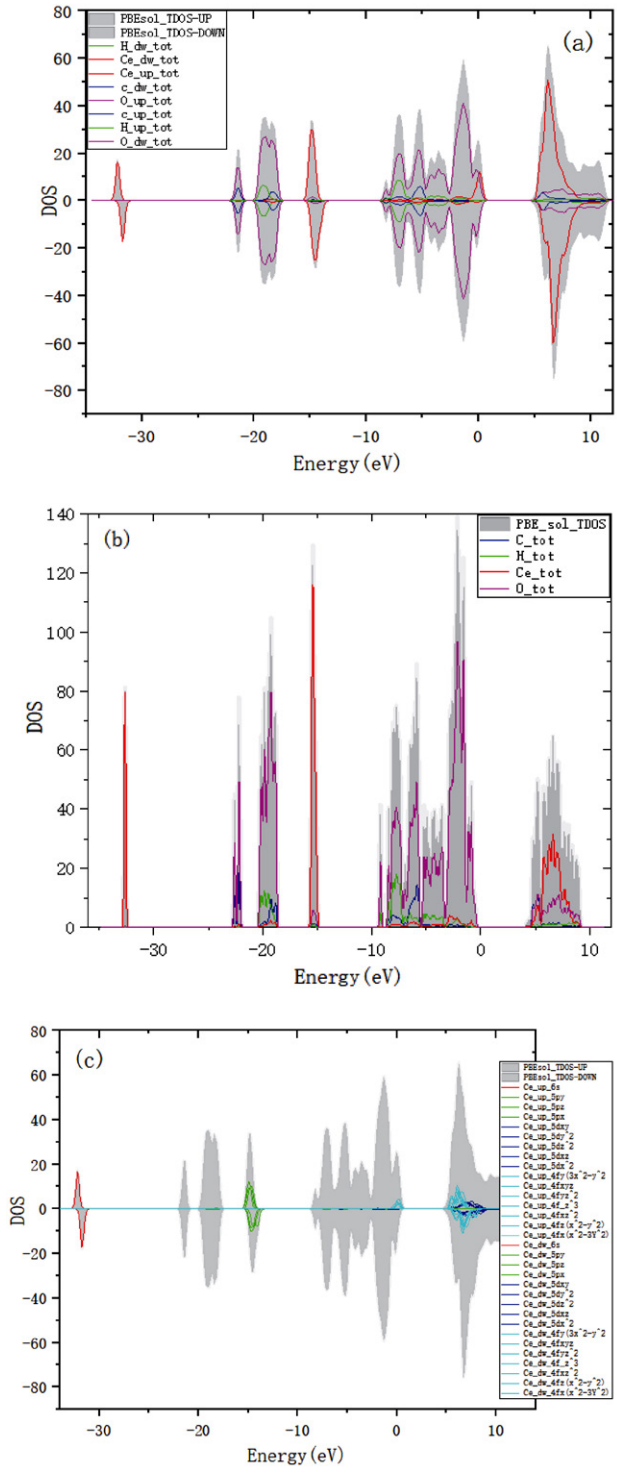

Figure 1. DOS and PDOS plots calculated by PBEsol functional (a) DOS and PDOS plots calculated by PBEsol+U pseudopotential (b) DOS and PDOS plots calculated by PBEsol simplified pseudopotential (c) PDOS plots calculated by PBEsol+U for Ce

For the analysis of chemical bonds, we used the LOBSTER package to calculate the COHP (Crystal Orbital Hamiltonian) as well as the ICOHP (Integral of COHP)

method. COHP can obtain bonding information from the calculation results of energy band structure; the bonding, non-bonding and anti-bonding interactions between paired atoms in the material can be determined. COHP, which is the Hamiltonian matrix multiplied by the corresponding density of states matrix, is calculated as shown in equation (1),

$$\begin{aligned}\sum_j f_j\varepsilon_j\delta(\varepsilon_j-\varepsilon) &= \sum_j f_j \sum_{RL}\sum_{R'L'} u^*_{RL,j}H_{RL,R'L'}u_{R'L',j}\delta(\varepsilon_j-\varepsilon)\\ &= \sum_{RL}\sum_{R'L'} H_{RL,R'L'}\sum_j f_j\, u^*_{RL,j}u_{R'L',j}\delta(\varepsilon_j-\varepsilon)\\ &= \sum_{RL}\sum_{R'L'} H_{RL,R'L'}N_{RL,R'L'}(\varepsilon)\\ &= \sum_{RL}\sum_{R'L'}\mathrm{COHP}_{RL,R'L'}(\varepsilon)\end{aligned} \quad (1)$$

where f_j represents the occupation number, ε_j represents the energy band energy, R represents the atom, L represents the atomic orbital, j represents the energy band (molecular orbital), $H_{RL,R'L'}$ represents the Hamiltonian matrix element, and $N_{RL,R'L'}$ (ε) represents the DOS (density of states) matrix. Bonding contribution reduces the energy of the system, and COHP is negative; the inverse bond contribution increases the system energy, and COHP is positive; the non-key contribution is represented by the zero value of COHP. In practical applications, positive, negative and zero values of-COHP are commonly used to represent bond, anti-bond and non-bond interactions. The integral over the entire occupied orbital COHP is usually denoted as ICOHP, which allows a quantitative analysis of the bonding strength between pairs of atoms. It is defined by equation (2):

$$\mathrm{ICOHP} = E_{band} = \int_{-\infty}^{\varepsilon_F}\sum_{RL}\sum_{R'L'}\mathrm{COHP}_{RL,R'L'}(\varepsilon)\,d\varepsilon \quad (2)$$

Analysis of the absolute value of ICOHP alone has no meaning, only comparative analysis of its relative value can reflect the significance of ICOHP. In comparison, the smaller the value of ICOHP, the stronger the stability of bonding and vice versa.[43,46–47]

2. 5. Modeling

During the static calculation, the system before precipitation was an aqueous solution system of $CeCl_3$ and polymer PVP. Scaling to a scale based on actual experimental density with "Calculation" in "Material Studio" software,[48] the slab model of the aqueous solution system mixed with $CeCl_3$ and polymer PVP was constructed; according to the density of 1 g/cm^3, 2 Ce, 6 Cl, 20 H_2O, and 3 PVP molecular monomers were added to make them randomly distributed in the slab model. Following the above convergence criteria, we optimized the whole slab model, calculated its COHP, ICOHP, and studied the interaction mechanism of polymer PVP monomer with other elements in the system. The mechanism of PVP modulation of cerium carbonate crystals after the addition of precipitant was simulated, and the cerium carbonate crystal structure was derived from the ICSD (Inorganic Crystal Database) crystal library as shown in Figure 2. Three crystal planes (010), (001) and (120), which are easy to be exposed were selected. According to the atomic ratios of the cerium carbonate crystal, the crystal plane layers with thickness of 9.3546 Å, 9.037 Å and 7.989 Å were cut respectively. These atomic layers were put at the bottom to construct a slab configuration with a top vacuum layer thickness of 13 Å. According to different thickness, the atoms at the bottom of each crystal plane are fixed at a ratio of 60%, and the rest are released. (001) crystal plane is fixed from the bottom with 0–9.4 Å thickness atoms; (010) crystal plane is fixed from the bottom with 0–5.4 Å thickness atoms; (120) crystal plane is fixed from the bottom with 0–4.8 Å thickness atoms. The entire slab configuration is optimized according to the above convergence criteria and meets the relevant convergence requirements.

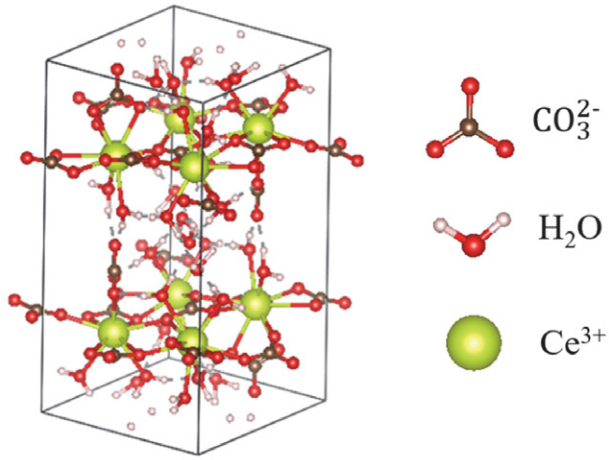

Figure 2. $Ce_2(CO_3)_3$ crystal structure diagram, in which the green ball represents the Ce element, and each Ce element is surrounded by 4 carbonate ions and 4 water molecules

In the AIMD (Ab Initio Molecular Dynamics) simulation,[49–51] using "Calculation" function in "Material Studio" software, scaling based on actual experimental density in a certain proportion, the slab model of mixed aqueous solution system of Ce^{3+}, Ce_3^{2-} nd polymer PVP monomer was constructed. According to the density of 1 g/cm^3, 8 Ce^{3+}, 12 Ce_3^{2-}, 20 H_2O and 2 PVP polymer monomers were added to make them randomly distributed in the slab model. The nucleation and growth of $Ce2(CO_3)_3$ crystals in solution were analyzed by molecular dynamics simulations, and the set of uniformly distributed Ce^{3+} Ce_3^{2-} and H_20 in the slab model was used as the initial configuration. The NVT ensemble at 300 K is selected, and these values

represent the synthesis conditions in the experiment. The total simulation time for the equilibrium motion was 1500 ps with a time step of 1 fs, during which data were collected every 500 ps for subsequent analysis.

In the optimization of PVP molecules, considering that the use of DFT calculations for macromolecular polymers will occupy too many resources, while the electronic structure analysis of the crystal surface only needs to consider the interaction between a small part of the crystal and the polymer monomer atoms, and the PVP polymer monomer has similar properties to the PVP polymer, only the PVP polymer monomer (Figure 3) was taken for structural optimization, and then its adsorption relationship with the crystal surface and subsequent electronic structure analysis were investigated.

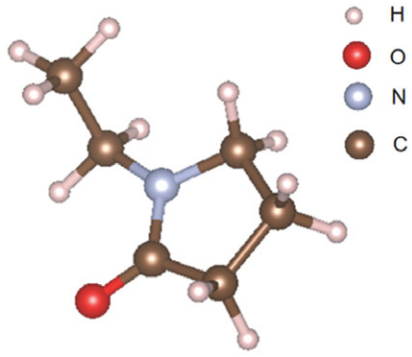

Figure 3. Schematic diagram of PVP monomer molecule

3. Results and Discussion

3. 1. Mechanism Study

3. 1. 1. The Interaction Mechanism of PVP in the System Before Precipitation

In the constructed slab model, the results before and after optimization are shown in Figure 4. The two Ce^{3+} in the constructed slab model are #7_Ce and #8_Ce, respectively, and it is found that the PVP, H_2O and Cl^- in the system are gradually aggregated around Ce^{3+}, in which C=O in PVP, O in H_2O, and Cl^- will interact around the center Ce^{3+} with a tendency to form bonds, while H atoms in H_2O will form hydrogen bonds with C=O in PVP. As the atoms move to the position where the force is the least, the atoms in the entire system will aggregate toward the Ce^{3+} position to form the corresponding complex. The ICOHP and bond lengths between the major bond-forming atoms in the system are shown in Table 1. The analysis revealed that although the bond length of the chemical bond formed between PVP-$Ce^{3+}$was the longest, its ICOHP value was the smallest. It is because of the large atomic radius and atomic mass of Ce^{3+}, and its unique electronic structure as well as chemical properties. Thus, although the bond length between PVP-Ce^{3+} is the longest, the stability is stronger than that between PVP-H_2O and H_2O-H_2O to form chemical bonds. This shows that the bonding effect between Ce^{3+} and PVP is the greatest, so when no precipitation agent is added, the PVP molecules in the system will preferentially complex with Ce^{3+} to form a more stable complex.

Table 1. The bond length and ICOHP value between each atom after the optimization before precipitation is completed

atomNU	atomNU	bond length (Å)	-ICOHP(eV)
O in PVP	Ce^{3+}	2.38	–3.57
O in PVP	H_2O	1.65	–1.17
H_2O	H_2O	1.86	–0.90

3. 1. 2. Analysis of Crystal Planes Easily Exposed Without Polymer PVP

According to the research results of Li Erxiao and others,[26] crystal planes easy to display in PVP adsorption cerium carbonate crystal were selected, and the (001), (010), (120) crystal planes before and after the

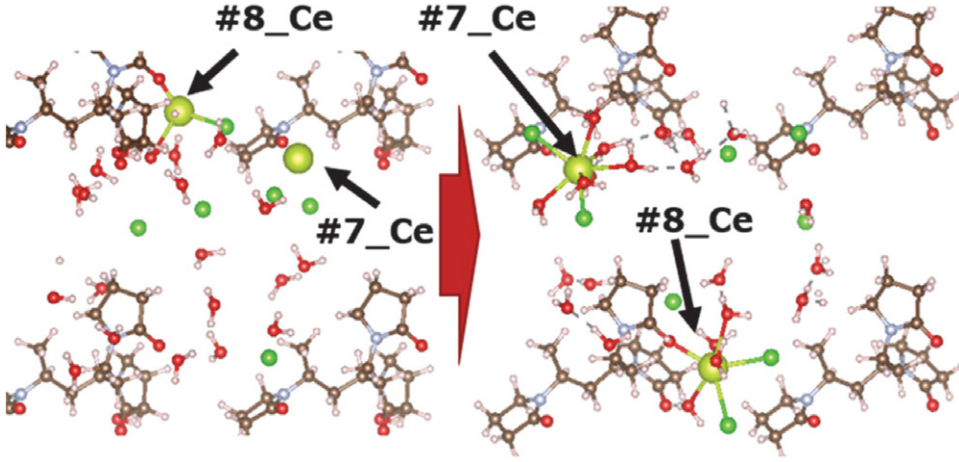

Figure 4. Optimization diagram of each atom in the system before precipitation

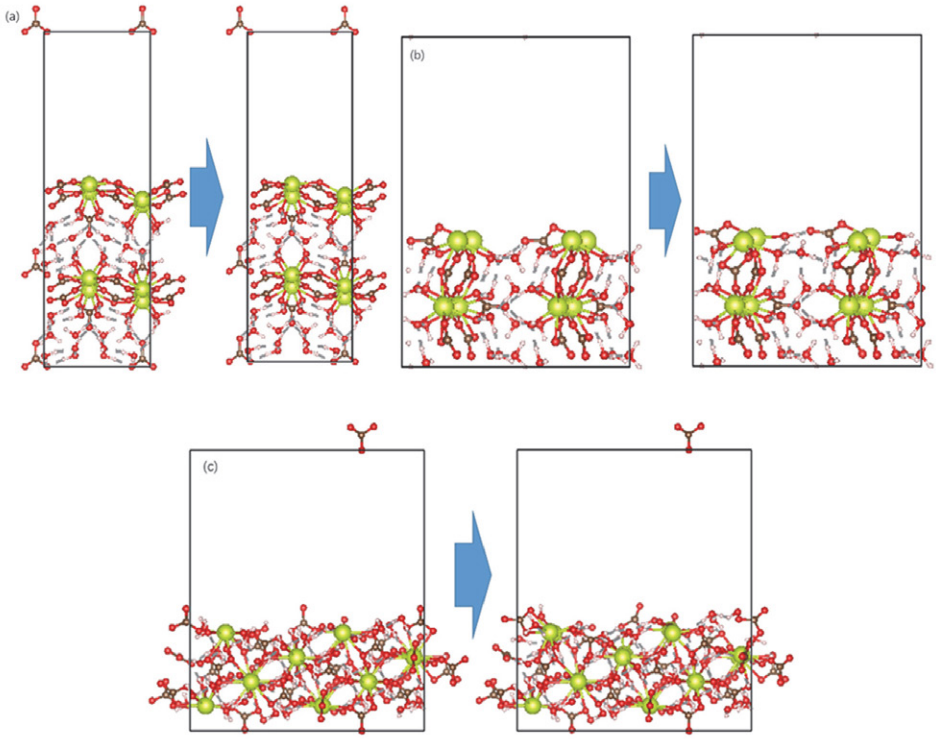

Figure 5. (a) cerium carbonate crystal (001) crystal plane before and after optimization, (b) cerium carbonate crystal (010) crystal plane before and after optimization, (c) cerium carbonate crystal (120) crystal plane before and after optimization

optimization of each crystal plane cut out are shown in Figure 5. It is found that after the optimization of these three crystal planes, the reconstruction of the crystal planes has occurred, and the bonding distance between the surface layer atoms and the bottom layer atoms has slightly increased. This is because the top of the constructed surface is in a vacuum layer. The surface atoms are only subject to the interaction between themselves and the bottom atoms, resulting in different forces from the internal atoms.

The formula for calculating the surface energy of crystal plane is shown in Formula 1,[52] where σ is the surface energy of the crystal; E^{rel} is the relaxation energy, indicates the energy released when the crystal plane is optimized to a stable state; E_{surf} is the energy of the slab configuration after optimization; N_{atoms} is the number of atoms in the slab configuration; E_{bulk} is the energy of a single atom in the bluck structure and represents the ratio of the energy of the unit cell to the number of atoms in the unit cell after optimization. The calculated results of (001), (010) and (120) crystal planes are shown in Table 2, indicating that the surface energy of the (120) crystal plane was the lowest, 9.48 J/m^2, and its growth rate was the slowest; the (001) crystal plane had the highest energy, 17.1 J/m^2, and its growth rate was the fastest. The order of growth speed between crystal planes is (001) > (010) > (120).

$$\sigma = \left(1/2\left(E_{surf} - N_{atoms} * E_{bulk}\right) + E^{rel}\right)/A \quad (3)$$

Table 2. Relative crystal plane parameters of crystal planes easily exposed when PVP is not added

planes	E^{rel} (meV)	N_{atoms}	E_{surf} (eV)	E_{bulk} (eV)	A (Å^2)	σ (J/m^2)
001	2.19	152	–766.41	–6.11	77.23	17.1
010	3.94	152	–748.27	–6.11	133.29	11.1
120	1.36	304	–1514.18	–6.11	301.35	9.48

3. 1. 3. Analysis of Crystal Planes Easily Exposed after Adding Polymer PVP

Figure 6 shows the adsorption structure diagram of the PVP monomer on the (001), (010), (120) crystal planes of cerium carbonate crystals after calculation by DFT. The length of the Ce-O bond formed by the O contained in the ketone group in the PVP monomer and the Ce^{3+} of the (010) crystal plane is the smallest, 2.37 Å, while the Ce-O bond length formed by O and Ce^{3+} of (120) crystal plane is the longest, 2.42Å. The Ce-O bonds after adsorption is shorter than the Ce-O bonds in the cerium carbonate crystal. From the analysis of the C-O bonds length inside the PVP monomer, it is found that, except for the (001) crystal plane adsorption which causes the C-O bonds bond length to remain unchanged, the (010) and (120) crystal plane adsorption will cause the C-O bonds bond length to be elongated. From the analysis of the Ce-O-C bonds angle

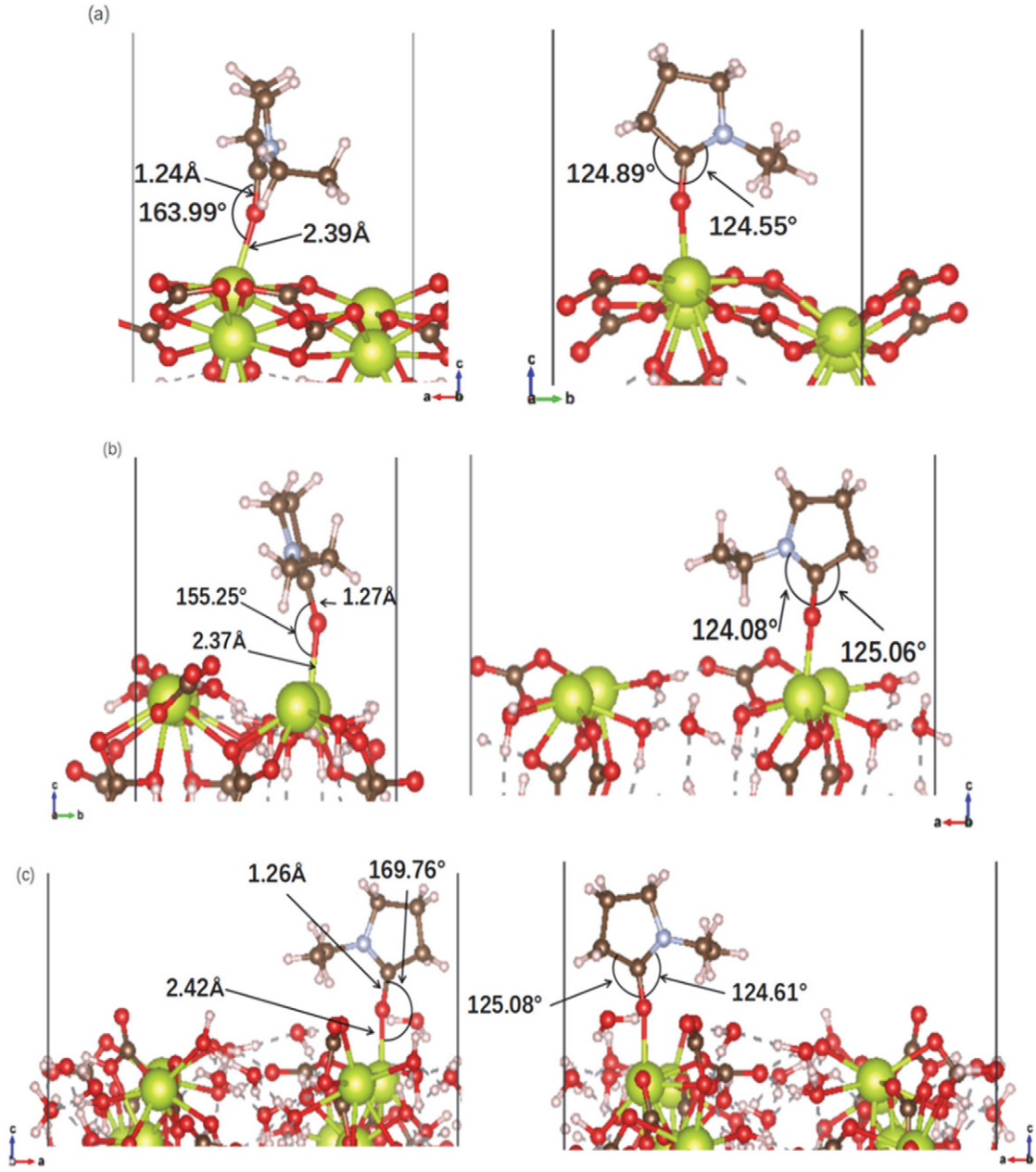

Figure 6. (a) The best adsorption structure of PVP monomer on the surface of stoichiometric cerium carbonate (001), showing two side views in the plane model, (b) the best PVP monomer on the surface of stoichiometric cerium carbonate (010) Adsorption structure, showing two side views in the plane model, (c) the best adsorption structure of PVP monomer on the surface of stoichiometric cerium carbonate (120), showing two side views in the plane model

formed by the adsorption of Ce^{3+} from the PVP monomer ketone group, it is found that the bond angle formed by the adsorption of the (010) crystal plane is the smallest, 155.25°, and the bond angle formed by the adsorption of the (120) crystal plane is the largest, 169.76°. From the analysis of the bond angles of O-C-N and O-C-C bonds formed inside PVP monomer after adsorption, it is found that the bond angles of O-C-N bonds and O-C-C bonds after adsorption are smaller than the bond angles before adsorption. It is because the Ce-O bond formed by the ketone group and Ce^{3+} in PVP monomer after adsorption has a certain interaction with C and N attached to O inside PVP monomer, which makes the bond angle smaller in general.

The adsorption energy of the molecules adsorbed on the crystal surface calculation is shown in formula 2,[52] where E_{bind} is the adsorption energy of PVP adsorbs the cerium carbonate crystal face, E_{tot} is the total energy of the system after PVP adsorbs the cerium carbonate crystal face, and E_{solv} is the single point energy of the PVP monomer. E_{surf} is the total energy of the cerium carbonate crystal face system without adsorption of

PVP monomer. The crystal planes calculated according to Formula 2 are shown in Table 3. The adsorption energy of each crystal plane is analyzed. When the adsorption energy is positive, additional absorption energy is required for the occurrence of adsorption, and when the adsorption energy is negative, the energy is released. The definition of adsorption indicates that the adsorption energy of whichever crystal plane and PVP monomer is negative. It shows that the PVP monomer needs to release energy after adsorbing (001), (010), (120) crystal planes. Comparing the size of adsorption energy, it is found that the adsorption energy of (120) crystal plane is the largest. The adsorption energy difference between (001) and (010) crystal planes is only about 2eV, indicating that PVP molecules are more likely to adsorb (120) crystal planes during the growth of cerium carbonate crystal, and inhibit the growth of crystal planes, so that they can finally be exposed.

$$E_{bind} = E_{tot} - (E_{solv} + E_{surf}) \quad (4)$$

Table 3. After adding PVP, PVP monomer and easy to show surface adsorption related energy parameter table

planes	E_{tot}(eV)	E_{solv}(eV)	E_{surf}(eV)	E_{bind}(eV)
001	−1023.43	−110.31	−768.60	−144.51
010	−1008.87	−110.31	−752.21	−146.34
120	−1930.42	−110.31	−1527.74	−292.37

3. 1. 4. Electronic Structure Analysis of the Growth Mechanism of Cerium Carbonate Crystals Regulated by PVP

In order to further study the interaction mechanism between PVP and cerium carbonate crystal surface, the COHP value of PVP monomer adsorption on different crystal faces was calculated, and its electronic structure was analyzed. When cerium ions are exposed on the crystal surface, the central cerium ion loses two water molecular ligands along the +b axis, which reduces the original 10-ligand structure (Figure 7a) to an 8-ligand structure (Figure 7b), and coordination unsaturation occurs, therefore the cerium ions have a greater tendency to be adsorbed by the polar element O in the system.

The COHP of each crystal plane adsorbed by PVP is shown in Figure 8, and the COHP value of each crystal plane adsorbed by PVP monomer is analyzed. It is found that the three crystal planes (001), (010), and (120) have basically the same bonding conditions after adsorption of the PVP monomer, only when the (100) crystal surface is adsorbed, a negative peak of -COHP value appears near the fermi level, which indicates that there is an unstable component at this position. Because the peak is small, it almost has no effect on the bonding stability. Comparing the ICOHP value after PVP adsorption on each crystal plane, the ICOHP value of (120) crystal plane is the smallest, which is −3.49eV, indicating that the stability of PVP monomer and (120) crystal plane adsorption is the strongest.

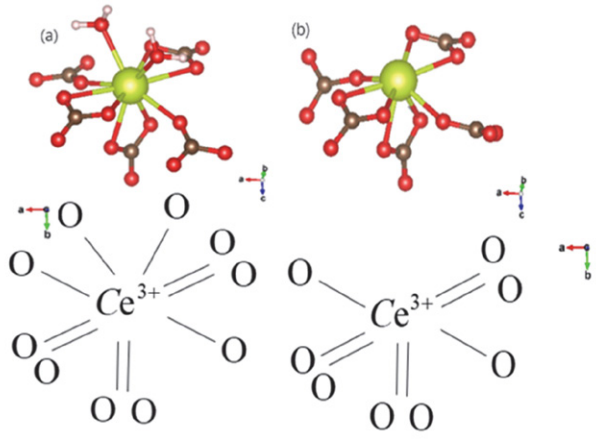

Figure 7. (a) 10 ligand structure diagram; (b) 8 ligand structure diagram

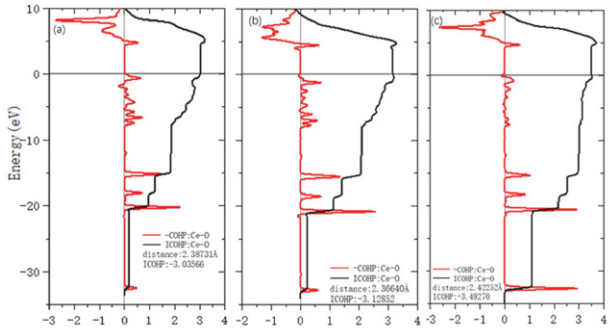

Figure 8. (a) PVP monomer adsorption (001) crystal plane COHP map, (b) PVP monomer adsorption (010) crystal plane COHP map, (c) PVP monomer adsorption (120) crystal plane COHP map

3. 1. 5. AIMD Simulation of Growth Process of Cerium Carbonate Crystals Regulated by PVP

In this section, an ab initio molecular dynamics (AIMD) method is used to simulate the process of PVP regulating the growth of cerium carbonate crystals at the atomic scale. Figure 9 shows sequential snapshots of the complex formed by Ce_3^{2-} and PVP and Ce^{3+} from the initial state to 1500ps. In the initial state, the atoms are uniformly distributed in the system. With the passage of simulation time, Ce_3^{2-} gradually shifts to the heterogeneous nucleation site formed between PVP and Ce^{3+}. When the simulation time reaches 1500ps, it can be seen that growth of cerium carbonate crystals along the PVP adsorption direction is inhibited, leading to the growth of cerium carbonate crystals in other directions.

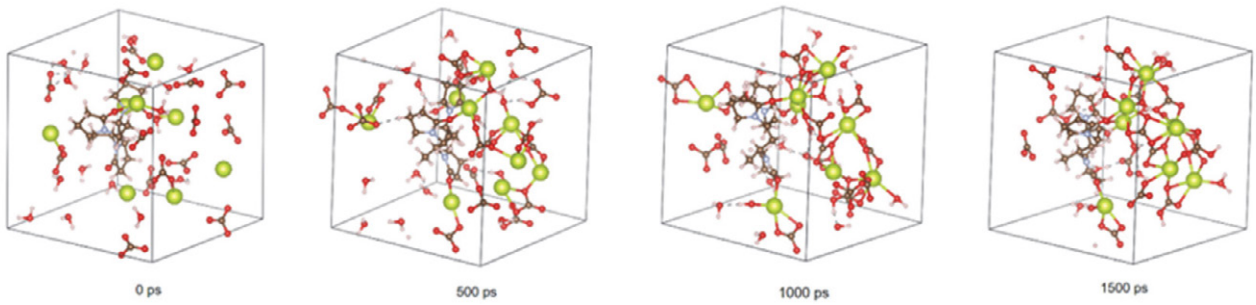

Figure 9. Snapshot of AIMD simulation of PVP-controlled cerium carbonate crystal growth process at 300K

3. 2. Simulation of PVP Controlling Cerium Carbonate Crystal Growth Process

Figure 10 is a simulation process diagram of using polymer PVP liquid phase precipitation method to control the morphology of cerium carbonate crystals, which is mainly divided into the following three stages:

1. In the first stage, $CeCl_3$, PVP and H_2O are added to the slab configuration and optimized to a stable state. The ketone groups in the system and PVP will preferentially form complexes, providing heterogeneous nucleation sites for subsequent crystal crystallization.

2. In the second stage, with the addition of precipitant, the complex formed by PVP and Ce^{3+} is combined to produce heterogeneous nucleation. With the continuous addition of the precipitating agent, Ce_3^{2-} combines at the heterogeneous nucleation point where PVP molecules

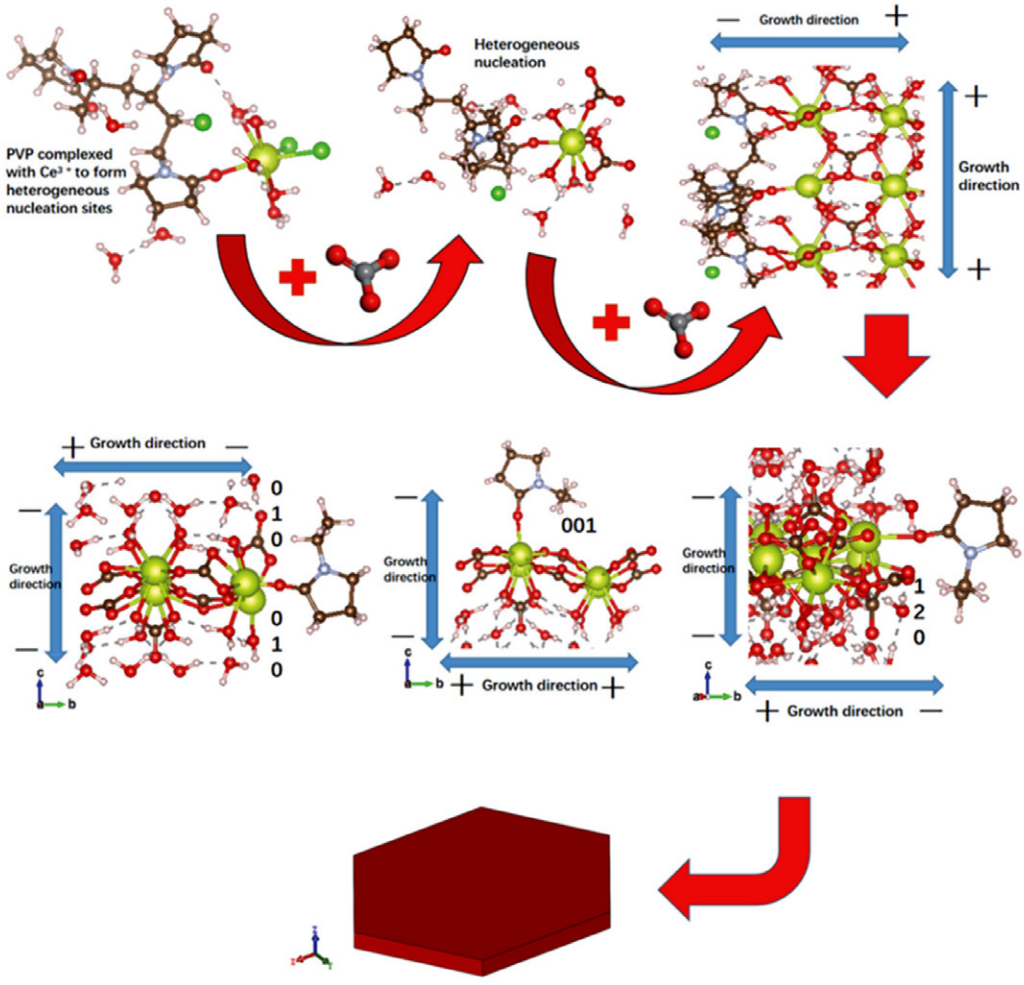

Figure 10. Process diagram of PVP regulating cerium carbonate crystal growth

are adsorbed and gradually grows into cerium carbonate crystals. In the process of crystal growth, according to the symmetry of cerium carbonate crystal PBNB, the growth of (010) crystal plane along the C axis and + B axis is inhibited, (001) crystal plane along the C axis is inhibited, (120) crystal plane along the axis (210) and C axis is inhibited. Moreover, the (120) crystal plane has the strongest PVP adsorption ability and the slowest growth rate, making the (120) crystal plane most likely to appear in the system.

3. In the third stage, after crystal gradually fills the whole solution system, each crystal face fragment will combine with each other. According to the classical crystal growth theory,[53] the crystal face with a faster growth rate will disappear, while the crystal face with a slower growth rate will eventually remain. For the PVP molecules are adsorbed on the (120) crystal plane and hinder the (120) crystal plane, the growth rate of (120) crystal plane is the slowest compared with other crystal planes such as (001) and (010) crystal planes, so the (120) crystal plane has a greater probability of being retained, and each crystal face finally grows around the (120) crystal face into a hexagonal plate-shaped cerium carbonate crystal.

3. 3. Experimental Verification Analysis

3. 3. 1. SEM Analysis of Products in Different Growth Stages of Cerium Carbonate Crystals

Figure 11 shows the SEM images of the cerium carbonate crystal morphology prepared using the liquid phase precipitation method, with $CeCl_3$ as the Ce source, PVP as the template, NH_4HCO_3 as the precipitant, when the Ce^{3+} concentration is 0.03M, the pH value of the initial solution is 2, and the R value (The ratio of Ce_3^{2-} to Ce^{3+}) is about 2:1. Figure 11 (a) is the SEM image obtained when the precipitating agent (NH_4HCO_3) is added dropwise for 10 minutes. At this time, the cerium carbonate crystals are slightly rounded at both ends, slender and fusiform, without obvious edges and corners. This is because at early reaction stage cerium carbonate crystal grows into an amorphous state, and the crystal lattice is not perfect yet. Figure 11 (b) is the SEM image obtained when the precipitating agent (NH_4HCO_3) is dropped for 30 minutes. The cerium carbonate crystals have been transformed from the original fusiform shape to the angular, narrow and long hexagonal flake. With the extension of the precipitant dropping time, the morphology of the cerium carbonate crystals remained in the shape of hexagonal flake, and the length of each side changed significantly. The length of the sides on both sides of the tip part gradually became longer, and the length of the length direction gradually became shorter. It indicates that the growth process of cerium carbonate crystals is regulated by PVP. At the beginning of the reaction, because the reaction speed is too fast, PVP has not yet played a regulatory role. Cerium carbonate crystals rapidly nucleate and grow into a long and narrow spindle shape. As the reaction progresses, PVP is selectively adsorbed on the crystal surface of cerium carbonate, which makes Cerium carbonate crystals eventually grow into hexagonal flake.

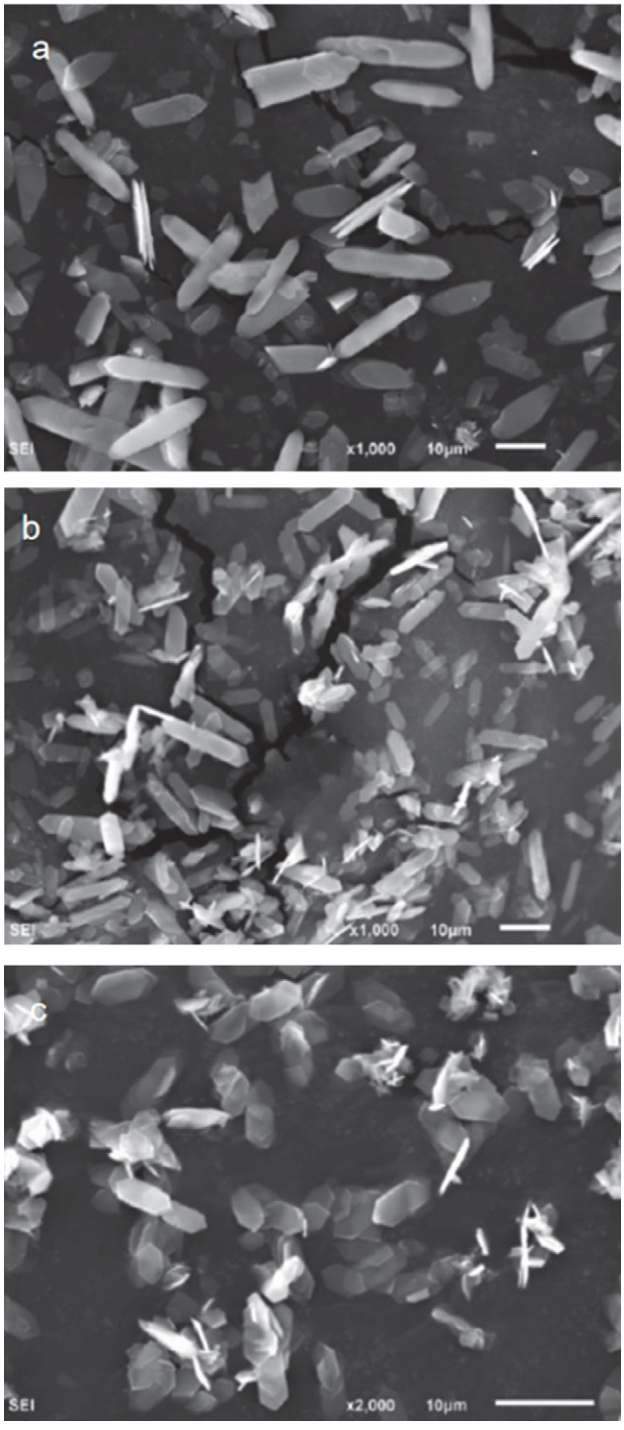

Figure 11. SEM images of different reaction stages of cerium carbonate crystals: (a) 10 min, (b) 30 min, (c) 50 min

3. 3. 2. Analysis of Crystal Morphology

Figure 12 shows the transmission electron microscopy (TEM) of the hexagonal flake cerium carbonate crystal.

From the figure, it can be measured that the angles formed by each plane of the hexagonal flake cerium carbonate crystal are about 90° and 135°. Since the cerium carbonate crystal belongs to the orthorhombic system, formula 3 can be used to calculate the angle of each crystal plane, where cos φ is the cosine of the angle between the two crystal planes, $(h_1\ k_1\ l_1)$, $(h_2\ k_2\ l_2)$, is the crystal plane index of two crystal planes. The unit cell parameters obtained from PDF card (#38-0377) are: a = 9.482 Å, b = 16.938 Å, c = 8.965 Å. The cosine values of the angles between the crystal planes are listed in Table 4 (Supplementary materials).

$$cos\varphi = \frac{\frac{h_1h_2}{a^2}+\frac{k_1k_2}{b^2}+\frac{l_1l_2}{c^2}}{\sqrt{\left(\frac{h_1^2}{a^2}+\frac{k_1^2}{b^2}+\frac{l_1^2}{c^2}\right)\times\left(\frac{h_2^2}{a^2}+\frac{k_2^2}{b^2}+\frac{l_2^2}{c^2}\right)}} \quad (5)$$

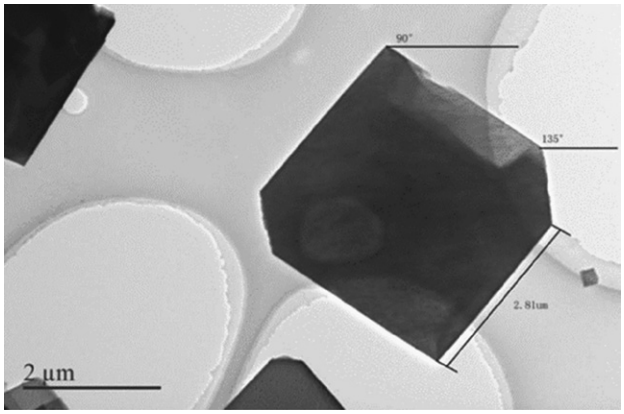

Figure 12. Transmission electron microscope image of hexagonal flake cerium carbonate crystal

The diffraction pattern of hexagonal flake cerium carbonate crystal is shown in Figure 13. According to the measurement of the ruler in the diffraction pattern from near to far, the distance R between the surrounding spots and the central spot is calculated. According to d=1/R, the crystal plane spacing d of each spot around the center diffraction spot is calculated, and the PDF card (#38-0377) of the cerium carbonate crystal is found to preliminarily determine the crystal plane represented by each spot. According to the angles of crystal planes measured in Figure 12, it is determined that the sides of the hexagonal flake cerium carbonate crystal are (002), (040), and (240) respectively by looking up Table 4 (Supplementary materials).

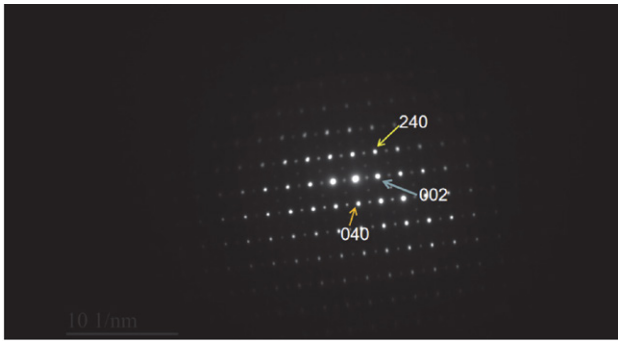

Figure 13. Diffraction pattern of hexagonal flake cerium carbonate crystal

Figure 14 shows XRD images of cerium carbonate crystals regulated by PVP. The four strongest peaks are (020), (040), (060), and (200) crystal planes. These four crystal planes belong to the {100} crystal plane family. Because (240) crystal plane is inclined plane of hexagonal flake crystal, the intensity of (240) crystal plane peak is relatively weak in XRD. Therefore, the hexagonal flake cerium carbonate crystal with (240) crystal plane as inclined plane and {100} crystal plane group as top and side can be seen in the SEM.

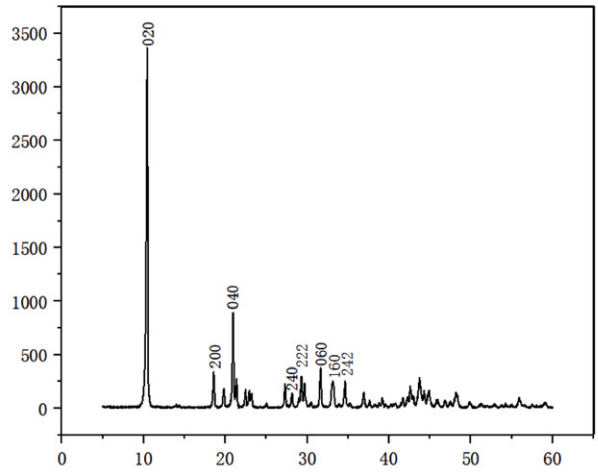

Figure 14. XRD pattern of hexagonal flake cerium carbonate crystal

4. Conclusions

The morphology of cerium carbonate crystal controlled by PVP was simulated by computer. When adding PVP without precipitating agent, the ketone group in PVP would preferentially complex with Ce^{3+}. After adding precipitant, heterogeneous nucleation points of cerium carbonate crystal would be formed around the complex, and the cerium carbonate crystal would grow gradually around the nucleation points. By calculating the interaction relationship between exposed Ce^{3+} and polymer PVP on three crystal faces of cerium carbonate (120), (010) and (001), it is found that the absolute value of adsorption energy of (120) crystal surface is the largest, and the gap of adsorption energy of (010) and (001) is only about 2eV, which indicates that due to the adsorption of PVP in the growth process of cerium carbonate crystal, the growth resistance of the (120) plane is much greater than that of the (010) and (001) plane. In the equilibrium state, the probability of forming (120) crystal plane is the greatest, thus the hexagonal plate-like cerium carbonate crystal structure

that grows around the (120) crystal plane will eventually appear. The experimentally prepared cerium carbonate crystals were analyzed by SEM, TEM, and XRD. The morphology of the prepared cerium carbonate crystals is a hexagonal sheet-like cerium carbonate crystal with (240) crystallographic planes as bevels and {100} crystallographic families as top and sides. It is found that the morphology of cerium carbonate crystal prepared in the experiment was similar to that of cerium carbonate crystal simulated by computer. Therefore, density functional theory can be used to predict the morphology of cerium carbonate crystals, which not only elucidates the growth mechanism of cerium carbonate crystals, but also greatly reduces the experimental cost.

Acknowledgments

The financial support from National Science Foundation of China (21666029); Ministry of education innovation team project (IRT1065); Inner Mongolia Natural Science Foundation (2016MS0223); grassland talents individual training project; Inner Mongolia Autonomous Region Science and Technology Major Project (2019ZD023) is gratefully acknowledged.

5. References

1. T Z Gao, X L Yu, Y X Zhang, S Q Zhang, F Zhou, L Nie. *Preparation and UV-Shielding Properties of Ceria with Different Morphologies.* Wet Metallurgy, 2018,37(06):497–500. **DOI:**10.13355/j.cnki.sfyj.2018.06.014.
2. Z M Wang, X L Zhu, Y M Li, Z Y Shen, J L Zuo. *Controllable preparation of flake and spherical CeO_2 nanoparticles and their photocatalytic properties.* Journal of Artificial Crystals, 2017,46(08):1559–1563+1586. **DOI**:10.1088/1475-7516/2017/08/022
3. YN Feng, JZ Gan, XH Chen, J Zhang, HJ Duan, ZX Cui, YQ Xue. *Study of morphology and particle size on the photocatalytic degradation of salt-based magenta by cerium dioxide nanoparticles.* Applied Chemical Industry, **2019**,48(01):14–17. **DOI**:10.16581/j.cnki.issn1671-3206.2019.01.002
4. SD Huang, GS Yang, CR Zhang, W Zhou, Y Zhao, LT Liu, L Cheng, Y Du, Z Wang, YJ Men. *Rare earth polishing powder and its preparation method.* CN112080207A. 2020–12–15.
5. EW Liang, B Wang, SS Zhang, Z Feng, MY Liu. *Research on the preparation process and color development mechanism of rare earth polishing powder.* Rare Earths, **2020**,41(04):102–110. **DOI**: 10.16533/J.CNKI.15-1099/TF.202004013
6. GF Gu, XT Cao, MH Liu, XL Wang, HQ Wan, SR Zheng, ZY Xu. *Study on the catalytic performance of Pd-M/CeO_2 catalyst for toluene.* Environmental Science and Technology, **2020**,43(11):110–115. **DOI**:10.19672/j.cnki.1003-6504.2020.11
7. HH Ding. *Liquid-phase preparation of CeO_2 and its composites and their catalytic applications*. Shanghai University of Engineering and Technology, Shanghai, **2018**.
8. HJ Li. *Hydrothermal synthesis of micro/nano cerium dioxide with different morphology and its properties.* Anhui University, Hefei, **2018**.
9. D Zhao. *Design and catalytic performance study of cerium-based nanomaterials.* Liaoning University of Petroleum and Chemical Technology, Fushun, **2020**.
10. J Feng, HL Chen, XM Zhang. *Controlled morphology synthesis of cerium dioxide nanoparticles and their catalytic properties.* Chemical Environmental Protection, **2018**,38(05):559–564.
11. Q Hu. *Preparation and performance study of one-dimensional semiconductor oxide-based methanol gas sensors.* Lanzhou University, Lanzhou, **2020**.
12. T Li. Study on the reaction crystallization process and crystal morphology control of cerium carbonate. South China University of Technology, Guangzhou, 2020.
13. W Xu, ZH Lin, PF Hu, ZW Jin, Y Chen, CJ Qiu. *Controlled synthesis of cerium oxide nanoparticles and their polishing properties.* Shandong Chemical, **2020**,49(02):30–32. **DOI**:10.19319/j.cnki.issn.1008-021x.2020.02.010
14. CS Li, YX Chen, WX Li, QG Ren, FQ Fan, F Ye, M Sun. *Ultrasound-assisted synthesis of cerium oxide nanoparticles and their tribological properties.* New Chemical Materials, **2019**,47(S1):154–157. **DOI**: CNKI:SUN:HGXC.0.2019-S1-034.
15. MM Du. *Superstructure self-assembly based on RhuA protein programmable.* University of Science and Technology of China, Hefei,**2021**.
16. Y Zhang. *Self-assembly, property regulation and template effect of nanocellulose*. Qilu University of Technology, Jinan, **2020**.
17. J L Xie. *Self-assembly of colloidal particles into large-size colloidal fibers by controlled crack growth.* University of Electronic Science and Technology, Chengdu, **2020**.
18. J L Qin, QY Li, R Yang, ZY Qiao, Y Liu, DR Gao, TY Chang, XP Jia, XF Zhao, YZ Zhang, XF Cheng. *Design and synthesis of amphiphilic polyurethanes and study of their assembly behavior.* Shandong Chemical, **2020**,49(02):1–4+9. **DOI**: 10.19319/j.cnki.issn.1008-021x.2020.02.001
19. X Zhang. *Molecular dynamics study of NPEO-regulated cerium carbonate crystal growth*. Inner Mongolia University of Science and Technology, Baotou, **2020**.
20. L Xu, YH Hu, M Li, ZG Liu, MT Wang, XW Zhang, T Tian. *Study on the morphology of cerium carbonate particles regulated by ethylenediaminetetraacetic acid disodium template*. Rare Earths, **2019**,40(05):84–90. **DOI**: 10.16533/J.CNKI.15-1099/TF.201905011
21. EX Li, YH H, M Li, ZG Liu, MT Wang, XW Zhang, WJ Zuo, X Zhang. *Synthesis of Cerium Carbonate with Special Morphology Controlled by Polyvinyl Pyrrolidone.* Chemical Progress, **2019**,38(09):4212–4217. **DOI**: 10.16085/j.issn.1000-6613.2018-2390
22. Y Zhang. *Study on the Mechanism of PAH Regulating Rare Earth Carbonates with Special Morphologies.* Inner Mongolia University of Science and Technology, Baotou, **2015**.
23. L Wang, YH Zhang, MESLM Aziguli, HD Lan. *Induced modulation of polyaniline morphology, size and electrochemical*

properties using PS-b-P2VP as a template agent. Journal of Higher School Chemistry, **2019**,40(08):1748–1756. **DOI**: CNKI:SUN:GDXH.0.2019-08-024

24. XS Wang, H Wu, RQ Xie, HY Pan, Q Lin. *Preparation of nitrogen-doped mesoporous carbon spheres with tunable pore structure by chitosan-F127 soft template method.* Journal of Artificial Crystals, **2019**,48(04):737–744. **DOI**: 10.16553/j.cnki.issn1000-985x.2019.04.029.
25. X Zhang, YH Hu, M Li, ZG Liu, M Tang, Z Hu. *Molecular dynamics simulation of the crystal growth mechanism of cerium carbonate regulated by nonylphenol polyoxyethylene ether.* Rare Earths, **2021**,42(05):68–74.
26. EX Li. *MS simulation study on the mechanism of PVP-regulated cerium carbonate growth.* Inner Mongolia University of Science and Technology, Baotou, **2019**.
27. N Liu, C Zhou, ZK Wu, YJ Shu, BZ Wang, QL Zhao, WL Wang. Prediction of the crystalline morphology of FOX-7 in H2O/DMF solvent. Energetic materials, 2018, 26(06): 471–476.
28. Balbuena Cristian, Gianetti Melisa Mariel, Soulé Ezequiel Rodolfo. *Molecular dynamics simulations of the formation of Ag nanoparticles assisted by PVP.* Physical chemistry chemical physics: PCCP 23.11(2021). **DOI:**10.1039/D1CP00211B
29. YF Yu. *Theoretical study on the kinetics of graphene epitaxial growth on Ni(111) surface.* Shandong University, Jinan,**2020**.
30. SL Yuan, H Zhang, DJ Zhang. *Molecular simulation: theory and experiment.* Beijing: Chemical Industry Press, **2016**: 162.
31. JT Cai, DX Li, BL Liu, BS Guo, DQ Wei, H Wang. *Molecular dynamics simulation of controlled crystallization of urea (520) crystal plane.* CIESC Journal, **2019**, 70(1): 128–135.
32. XQ Tang, XM Liu, Y Chen, JH Chen. *Density functional theory study on lead activation and xanthate adsorption on sphalerite surface.* Nonferrous Metal Engineering, **2021**,11(03):90–95. **DOI**: CNKI:SUN:YOUS.0.2021-03-014.
33. Q Ren, Y Liu, T Gao, ZX Zhou, CS Zhao, HF Chai. *Study on the crystal structure and density functional theory of diethyl 2,2-bis (4-chloro-2-fluorobenzyl) malonate.* Journal of Synthetic Crystals, **2021**,50(02):338–344. **DOI**: 10.16553/j.cnki.issn1000-985x.2021.02.01.
34. Kresse, G.; Hafner, J. *Ab initio molecular dynamics for liquid metals.* Phys. Rev. B: Condens. Matter Mater. Phys. **1993**, 47(1): 558–561. **DOI:**10.1103/PhysRevB.47.558
35. Kresse, G.; Furthmüller, J. *Efficiency of ab-initio total energy calculations for metals and semiconductors using a plane-wave basis set.* Comput. Mater. Sci. **1996**, 6(1): 15–50. **DOI:**10.1016/0927-0256(96)00008-0
36. Kresse, G.; Joubert, D. *From ultrasoft pseudopotentials to the projector augmented-wave method.* Phys. Rev. B: Condens. Matter Mater. Phys. **1999**, 59, 1758–1775. **DOI:**10.1103/PhysRevB.59.1758
37. Blöchl, P. E. *Projector augmented-wave method.* Physical review. B, Condensed matter,**1994**,50(24). **DOI:**10.1103/PhysRevB.50.17953
38. J. P. Perdew, K. Burke, M. Ernzerhof. *Generalized Gradient Approximation Made Simple.* Physical review letters,**1996**,77(18). **DOI:**10.1103/PhysRevLett.77.3865
39. Z Chen. *Study of multilayer graphene and its adsorption to hydrogen atoms.* Guangxi Normal University, Guilin, **2021**.
40. SY Liu. *Study on Stability, Kinetic Energy Density and Strong Interaction of Fullerene Isomers by Density Functional Theory.* Hunan Normal University, Changsha, **2020**.
41. H Jiang, WY Zhang. *Density Functional Theory Method for Electronic Band Structure Calculation of Materials.* China Science: Chemistry, **2020**,50(10):1344–1362. **DOI:**10.1360/SSC-2020-0142
42. S Maintz, VL Deringer, AL Tchougréeff, R Dronskowski. *Analytic projection from plane-wave and PAW wavefunctions and application to chemical-bonding analysis in solids.* J. Comput. Chem. **2013**, 34, 2557–2567. **DOI:**10.1002/jcc.23424
43. S Maintz, VL Deringer, AL Tchougréeff, R Dronskowski. LOBSTER: *A tool to extract chemical bonding from plane-wave based DFT.* J. Comput. Chem. **2016**, 37, 1030–1035. **DOI:**10.1002/jcc.24300
44. G Wang, M Zhou, Goettel, J. T, Schrobilgen, G. J, J Su, J Li, Schlöder, T, Riedel, S. *Identification of an iridium-containing compound with a formal oxidation state of IX*. Nature: International weekly journal of science, **2014**, 514(7523). **DOI**: 10.1038/nature13795.
45. XZ Shi, JL Wang, Z Cao. *Electronic structure of monazite and adsorption mechanism of octylhydroxamic acid on its (100) surface.* Chinese Journal of Nonferrous Metals. **2021**,31(08):2238–2246. **DOI**: CNKI:SUN:ZYXZ.0.2021-08-023.
46. R Dronskowski, PE Blöchl, *Crystal orbital Hamilton populations (COHP): energy-resolved visualization of chemical bonding in solids based on density-functional calculations.* J.Phys. Chem.**1993**, 97, 8617–8624. **DOI:**10.1021/j100135a014
47. VL Deringer, AL Tchougréeff, R Dronskowski. *Crystal orbital Hamilton population (COHP) analysis as projected from plane-wave basis sets.* J. Phys. Chem. A **2011**, 115,5461–5466. **DOI:**10.1021/jp202489s
48. YL Liao, M Li, ZX Zhong. *Stability analysis of silicon nitride based on 'Materials Studio'.* Equipment manufacturing technology. **2018**(06):90–92. **DOI:**10.1088/1475-7516/2018/06/026
49. BH Zhou, X Zuo. *Ab initio molecular dynamics of hydrogen diffusion in α-quartz.* Journal of Terahertz Science and Electronic Information, **2020**,18(02):325–329. **DOI**: CNKI:SUN:XXYD.0.2020-02-028.
50. WL Luo, QQ Wang, W Ruan, AD Xie, LJ Shi, XL Wang, T Gao. *Ab initio Molecular Dynamics of Pu-H_2 System.* Chemical Research and Applications, **2019**,31(04):593–597. **DOI**: CNKI:SUN:HXYJ.0.2019-04-001.
51. M Luo, SQ Liu, CY Ouyang. *Ab initio molecular dynamics simulation of irradiation particles behavior in tungsten.* The European Physical Journal B,**2018**,91(10). **DOI:**10.1140/epjb/e2018-90226-2.
52. DS Sholl, JA Steckel. *Density Functional Theory: A Practical Introduction.* John Wiley & Sons, Inc:**2009**-03-30. **DOI:**10.1002/9780470447710
53. T Zhou. Theoretical research on solvation growth and morphology control of TKX-50. North Central University, Taiyuan,**2020**.

Povzetek

V prispevku smo opisali napoved morfologije kristala cerijevega karbonata z uporabo simulacij na osnovi teorije gostotnega funkcionala (DFT). V fazi nukleacije se bo ketonska skupina v polivinilpirolidinu (PVP) preferenčno vezala na Ce3+ in tako tvorila kompleks, kar povzroči nastanek heterogenih nukleacijskih mest in s tem nukleacijo kristalov cerijevega karbonata. V fazi rasti je zaradi adsorpcije PVP največja verjetnost tvorbe (120) kristalnih ravnin v ravnotežju, kar povzroči nastanek heksagonalnih kristalov cerijevega karbonata. Eksperimentalno smo uspešno pripravili heksagonalne plasti kristalov cerijevega karbonata z uporabo PVP kot templata. Ugotovili smo, da metodo DFT lahko uporabimo za napoved morfologije kristalov cerijevega karbonata, s čemer pripomoremo k boljšemu razumevanju mehanizma rasti kristalov cerijevega karbonata in občutno zmanjšamo stroške eksperimenta.

Except when otherwise noted, articles in this journal are published under the terms and conditions of the Creative Commons Attribution 4.0 International License

Scientific paper

Synthesis, Structure, Thermal Decomposition and Computational Calculation of Heterodinuclear Ni^{II} – Zn^{II} Complexes

Yaprak Gürsoy Tuncer,[1] Hasan Nazır,[1] Kübra Gürpınar,[1] Ingrid Svoboda,[2] Nurdane Yılmaz,[3] Orhan Atakol[1] and Emine Kübra İnal[1,*]

[1] *Ankara University, Faculty of Science, Department of Chemistry, 06100, Ankara, Turkey*

[2] *TU-Darmstadt, Materialwissenschaft, Strukturforschung, Alarich-Weiss Strasse 2, 64287, Darmstadt, Germany*

[3] *Kastamonu University, Faculty of Education, Department of Mathematics and Science Education, 37200, Kastamonu, Turkey*

* *Corresponding author: E-mail: inal@science.ankara.edu.tr*

Received: 09-07-2021

Abstract

Mononuclear NiL complex was prepared by the use of bis-*N,N*'-salicylidene-1,3-propanediamine and Ni(II) salts. NiL was treated with $ZnBr_2$ and pyrazole and 3,5-lutidine coligands in a dioxane medium to prepare the following diheteronuclear complexes: $[NiL \cdot ZnBr_2 \cdot (pyrazole)_2]$ and $[NiL \cdot ZnBr_2 \cdot (3,5\text{-lutidine})_2]$. The complexes were characterized by elemental analysis, TG, IR and mass spectrometry. The effects of heterocyclic one- and two- nitrogen atoms containing co-ligands were also examined. Theoretical formation enthalpies, dipole moments and the relative levels of HOMO and LUMO energies were determined by the use of Gaussian09 program. The occupancy levels of the atomic orbitals were determined by the NBO analysis of Gaussian09. The effect of pyrazole and lutidine upon the complex formation was evaluated by the use of X-ray diffraction, TG and theoretical calculations. NiL complex with lutidine forms a square pyramidal conformation since lutidine is a much stronger coligand than pyrazole.

Keywords: Salpn type ligand; Ni(II)-Zn(II) dinuclear complex; square-pyramidal coordination; thermal decomposition; heterocyclic coligand

1. Introduction

Bis-*N,N*'-salicylidene-1,3-propanediamine (LH_2) has been known to give homo- and heteropolynuclear complexes with Fe(II), Co(II), Ni(II), Cu(II), Zn(II) and Cd(II) ions since 1990.[1–3] This compound that is classified as a Schiff base and a tetradentate ONNO type ligand gives heterodinuclear complexes with Lewis acids such as $ZnCl_2$ and $ZnBr_2$, and polynuclear complexes with a μ-bridge forming co-ligands such as acetate,[4–9] formate,[10,11] nitrate,[7,12,13] nitrite,[14] benzoate,[15,16] pseudohalogen or azides.[17–20] In complexes prepared with Lewis acids, it is very common that one or two solvent molecules enter the coordination sphere. The complex maintains its existence with the coordination of solvent molecules. If these solvent molecules are thermally removed from the structure, the dinuclear structure decomposes.[21–23]

In addition to LH_2 ligand giving mononuclear NiL and CuL complexes with Ni(II) and Cu(II), the resulting mononuclear complexes may be utilized to obtain polynuclear complexes. The molecular models of NiL and CuL mononuclear complexes were first reported in 1985.[24] In this study, it was determined that Cu(II) complex had a squashed tetrahedral and Ni(II) complex a square planar coordination sphere. If there are Lewis acids present in the medium, these Lewis acids are coordinated especially to NiL mononuclear complex through phenolic oxygens. As a result, Lewis acids withdraw electrons from NiL unit which decreases electron density upon Ni(II) and enables it to coordinate the solvent molecules or coligands present in the medium (Figure 1).

Mononuclear NiL complex can form a square pyramidal coordination sphere by coordinating H_2O molecule

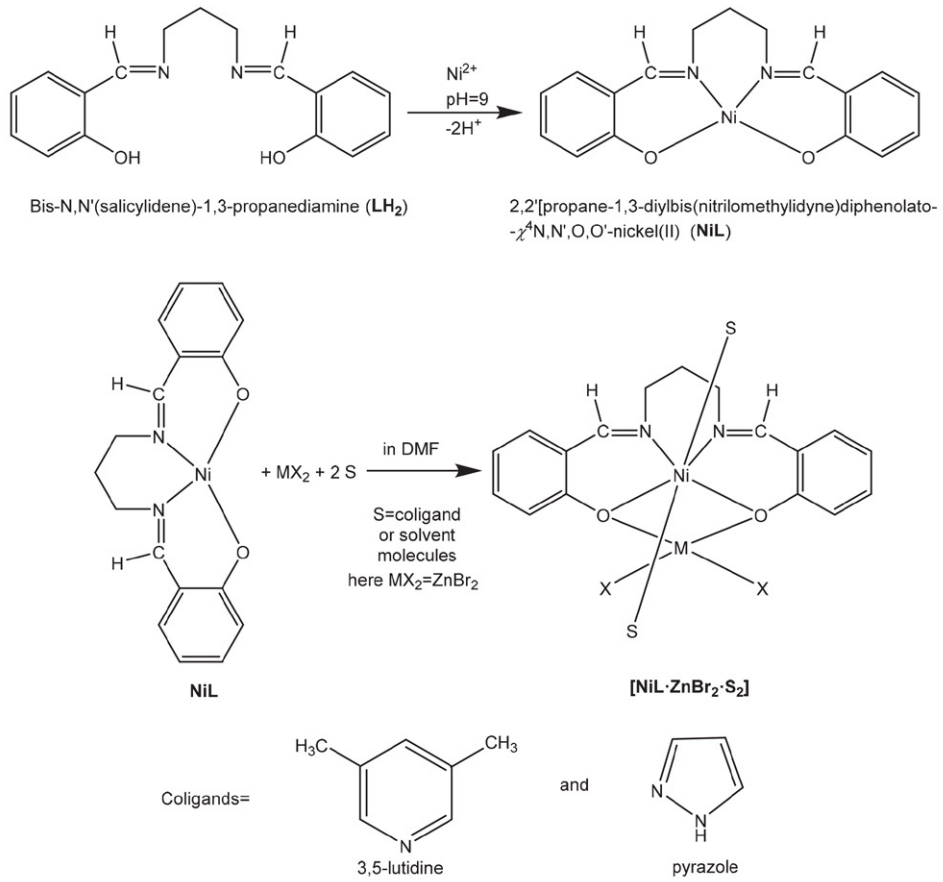

Figure 1. Dinuclear complex formation with the effect of Lewis acid in the medium.

if there is no Lewis acid in the medium.[25] Generally, trinuclear complexes are formed if there are coligands capable of establishing μ-bridges (Y) such as $HCOO^-$, $C_6H_5COO^-$, AcO^-, NO_2^-, NO_3^-.[4–16] In these trinuclear complexes, NiY_2 is located in the center. Terminal groups are the solvent molecules such as DMF or dioxane coordinated by NiL.[4–9,26] If coligands containing more than one nitrogen donor, such as pyrazole or dicyandiamide, are added to the medium, polynuclear complexes are formed.[27]

This study is devoted to determine the type of coordination sphere formed by NiL and $ZnBr_2$ together with one or two nitrogen-containing coligands. In a previous study, it was reported that NiL mononuclear complex forms a square pyramidal or octahedral coordination sphere with $ZnCl_2$, $ZnBr_2$, and 4-methylpyridine (4-picoline).[28] Based upon the picoline concentration there formed a square pyramidal complex with a [NiL·$ZnCl_2$ · (4-picoline)] or an octahedral coordination sphere with [NiL·$ZnBr_2$·(4-picoline)$_2$] stoichiometries. The major target of this study is to investigate the complexes formed if the reaction medium contains more than one heteroatom such as pyrazole and triazole. In this context, the coligands chosen were multi heteroatom containing pyrazole and a single heteroatom containing 3,5-lutidine, complexes were prepared in DMF and dioxane media.

The complexes obtained were characterized by IR spectroscopy, elemental analysis, mass spectrometry and thermogravimetric analysis. The goal of the study was to prepare two complexes and elucidate the differences between their thermal behavior. Two complexes designed for the study were obtained as single crystals, their molecular models and unit cell structures were determined by X-ray diffraction methods. The determination of the number of pyrazoles coordinated by NiL unit and their locations was one of the major targets of the study since pyrazole coordination has various isomerization possibilities. The main purpose of the study is to investigate the difference between pyrazole complexes containing multiple nitrogen donors and lutidine complexes containing a single nitrogen donor. In previous studies, it has been reported that NiL and pyrazole give a polynuclear complex. As a result, both ligands give mononuclear complexes, the interesting thing is that the difference between them is obtained by thermogravimetric analysis, not by XRD study. The removal temperatures of the coligands from the structure enabled us to evaluate the strengths of the ligands upon the molecular structure.

The variation in the thermal behavior of complexes [NiL · $ZnBr_2$ · (pyrazole)$_2$] (**1**) and [NiL · $ZnBr_2$ · (3,5-lutidine)$_2$] (**2**) was elucidated by thermal analysis and theoret-

ical calculations were carried out upon the molecular structures, by using Gaussian 09 software.[29] With natural bond analysis (NBO) in Gaussian 09 program, the occupancy levels of d orbitals of the central atoms, the molecular dipole moment of the complexes, the electron distributions, the relative energy levels of the highest occupied molecular orbital (HOMO) and the lowest unoccupied molecular orbital (LUMO), the energy difference between HOMO and LUMO were calculated. The values of the theoretical and experimental bond lengths and bond angles were compared. All the theoretical results were interpreted according to the strength of the ligands.

2. Experimental

All the reagents used in the study were supplied from Sigma-Aldrich and used without further purification. In this study, Shimadzu IRAffinity-1 FTIR spectrometer equipped with three reflectional ATR units was used for IR spectra with 4 cm^{-1} accuracy. C, H, and N analyses were performed on Eurovector 3018 CHNS analyzer. Metal analyses were carried out on GBC Avanta PM Model atomic absorption spectrometer using FAAS mode. Complex (2–3 mg) was dissolved in 1 mL HNO_3 (63%) with heating, diluted to 100 mL and given to nebulizer of atomic absorption spectrometer for metal analysis. The mass spectra of the ligands were obtained by Shimadzu QP2010 Plus GCMS apparatus equipped with a direct inlet (DI) unit with an electron impact ionizer (EI). DI temperature was varied between 40–300 °C and ionization was carried out with electrons with 70 eV energy. The NMR spectra were recorded on the Bruker Ultrashield 300 MHz NMR spectrometer using d_6-DMSO solution as a solvent. The thermogravimetric analyses were carried out by Shimadzu DTG 60H. In thermogravimetric analyses, the temperature was varied between 30–600°C. These analyses were performed at 5, 10, 15, 20 and 25 °C min^{-1} heating rates and under N_2 atmosphere in Pt pans. The calibration of the instrument was done with metallic In and Zn.

2. 1. Preparation of bis-*N,N'*-salicylidene-1,3-propanediamine (LH_2)

The Schiff base was prepared *via* condensation reaction in EtOH using 2-hydroxybenzaldehyde and 1,3-diaminopropane. 2-hydroxybenzaldehyde (0.1 mol, 12.20 g) was dissolved in 120.0 mL of warm EtOH, then 0.05 mol (3.70 g) of 1,3-diaminopropane was added to and heated up to the boiling point. The mixture was left aside for 4–5 h and yellow crystals were precipitated, then the crystals were filtered and dried in air (25.90 g), yield: 91%, mp: 58 °C (determined by TG). Anal. Calcd for $C_{17}H_{18}N_2O_2$: C, 72.32; H, 6.43; N, 9.92. Found: C, 71.95; H, 6.33; N, 10.09. IR ν, cm^{-1}: 2627 (OH), 3021–3019 (CH), 2929-2862 (CH), 1629 (C=N), 1608 (C=C), 1274-1151 (C–O), 762 (CH). λ_{max}: 243nm, ε: 7045 $dm^3\,mol^{-1}\,cm^{-1}$ in DMSO, λ_{max}: 242 nm, ε: 7865 $dm^3\,mol^{-1}\,cm^{-1}$ in MeOH. ^{1}H NMR (CH_3COCH_3-d_6) δ 13.51 (s, 1H) (O–H), 8.60 (s, 1H) (–CH=), 7.43 (d, J = 1.8 Hz) (H_{Ar}), 7.32 (t, J = 1.8 Hz) (H_{Ar}), 6.88 (t, 1.8 Hz) (H_{Ar}), 3.68 (t, J = 7.2 Hz) (N–CH_2–), 2.01 (p, J = 7.2 Hz) (–CH_2–). ^{13}C NMR (CH_3COCH_3-d_6) δ 166.6, 161.1, 132.7, 132.1, 119.1, 118.9 (C_{Ar}), 116.9 (–C=N), 58.5 (N–CH_2–), 31.9 (–CH_2–). MS *m/z*: 282 $[M]^+$, 161 $[HO–C_6H_4–CH=N–CH_2–CH_2–CH_2]^+$, 148 $[HO–C_6H_4–CH=N–CH_2–CH_2]^+$ (base peak), 134 $[HO–C_6H_4–CH=N–CH_2]^+$, 120 $[HO–C_6H_4–CH=N]^+$, 107 $[HO–C_6H_4–CH_2]^+$, 77 $[C_6H_5]^+$.

2. 2. Preparation of the Complexes

The complexes were prepared in two steps. The mononuclear NiL complex synthesized in the first step was converted into the dinuclear complex in DMF or dioxane medium in the second step.

2. 2. 1. Preparation of Mononuclear Complex (NiL)

NiL was prepared by ammonia in an ethanol solution of LH_2 and $NiCl_2 \cdot 6H_2O$ outlined in the literature.[33] 0.01 mol of LH_2 (2.82 g) was dissolved in 100.0 mL of hot EtOH under stirring. 10.0 mL of concentrated ammonia (20%) solution was added and the mixture was heated up to boiling temperature. A solution of 0.01 mol $NiCl_2 \cdot 6H_2O$ (2.36 g) in 30.0 mL hot water was added to this mixture. After the mixture was left on the bench for an hour, the light green precipitate of $NiL{\cdot}NH_3$ was filtered and dried at 150 °C for 4–5 h (3.45 g), yield: 95%, mp: 311 °C. The light green crystals are coordinatively ammonia bonded and leaves ammonia at 150 °C, the color of the complex changes to brown (NiL). The brown complex was recrystallized in EtOH:dioxane mixture (1:1, v/v). Anal. Calcd for $C_{17}H_{16}N_2O_2Ni$: C, 60.28; H, 4.76; N, 8.27; Ni, 17.33. Found: C, 60.55; H, 3.17; N, 7.93; Ni, 17.19. IR ν, cm^{-1}: 3061–3030 (CH), 2922–2866 (CH), 1607 (C=N), 1589-1541 (C=C), 1475 (CH), 1228–1124 (C–O), 725–744 (CH). MS *m/z*: 340 (isotope peak, because of ^{60}Ni isotope), 338 $[M]^+$ (base peak), 219 $[Ni–O–C_6H_4–CH=NH–CH_2–CH_2–CH_2]^+$, 205 $[Ni–O–C_6H_4–CH=NH–CH_2–CH_2]^+$, 179 $[Ni–O–C_6H_4–CH=NH]^+$, 134 $[O–C_6H_4–CH=NH–CH_2]^+$, 107 $[HO–C_6H_4–CH_2]^+$, 58 $[Ni]^+$.

2. 2. 2. Preparation of Complex 1, [NiL · $ZnBr_2$ · (pyrazole)$_2$]

0.001 mol of NiL (0.340 g) was dissolved in 50.0 mL hot DMF under stirring and heated up to 100–110 °C. A solution of 0.001 mol $ZnBr_2$ (0.226 g) and 0.002 mol pyrazole (0.140 g) in 30.0 mL hot MeOH was added to this solution. The mixture was left on the bench for 2–4 days at room temperature. The light purple crystals were filtered

and dried in air (0.41 g), yield: 58%. mp: 190 °C (decomposition). Anal. Calcd for $C_{23}H_{24}Br_2N_6NiO_2Zn$: C, 39.56; H, 3.18; N, 12.03; Ni, 8.40; Zn, 9.36; Br, 22.88. Found: C, 40.17; H, 3.27; N, 11.93; Ni, 8.01; Zn, 9.47; Br; 21.83. IR ν, cm^{-1}: 3335 (NH), 3120 (CH), 3034–3017 (CH), 2929–2861 (CH), 1631–1618 (C=N), 1593-1552 (C=C), 1475 (CH), 1298–1118 (C–O), 759 (CH). MS *m/z*: 338 (molecular peak of NiL and base peak), 179, 132, 107, 77, 58, 44.

2. 2. 3. Preparation of Complex 2, [NiL · $ZnBr_2$ · (3,5-lutidine)$_2$]

This complex was prepared as given above using 0.001 mol of NiL (0.340 g), 0.001 mol of $ZnBr_2$ (0.226 g) and 0.002 mol of 3,5-lutidine (0.220 g). The mixture was left on the bench for 2–4 days at room temperature. The light purple crystals were filtered and dried in air (0.59 g), yield: 76%. mp: 157 °C (decomposition). Anal. Calcd for $C_{31}H_{34}Br_2N_4NiO_2Zn$: C, 44.52; H, 4.42; N, 7.68; Ni, 8.06; Zn, 8.97; Br, 21.93. Found: C, 40.08; H, 3.93; N, 7.35; Ni, 7.73; Zn, 8.59; Br, 21.81. IR ν, cm^{-1}: 3031–3009 (CH), 2921–2865 (CH), 1618 (C=N), 1595-1550 (C=C), 1475 (CH), 1301–1107 (C–O), 752 (CH). MS *m/z*: 338 (molecular peak of NiL), 107 (coligand and base peak), 92, 79, 71, 58, 43.

2. 3. X-Ray Crystallography

A single crystals of [NiL · $ZnBr_2$ · (pyrazole)$_2$] (**1**) and [NiL · $ZnBr_2$ · (3,5-lutidine)$_2$] (**2**) were analyzed on Oxford Diffraction Xcalibur Single Crystal X-ray Diffractometer with a sapphire CCD detector using Mo*K*α radiation (λ = 0.71073 Å) operating in ω/2θ scan mode. The unit-cell dimensions were determined and refined by using the angular settings of 25 automatically centered reflections in 2.588° ≤ θ ≤ 26.369° for **1** and 2.556°–27.894° for **2**. The data was collected at 293(2) K. The empirical absorption corrections were applied by the semi-empirical method via the CrysAlis CCD software.[30] The model was obtained from the results of the cell refinement and the data reductions were carried out using the solution software SHELXL 2014-6.[31] The structure of the complexes was solved by direct methods using in WinGX package.[32] The treatment of hydrogen atoms was made geometrically. Supplementary material for structure has been deposited to the Cambridge Crystallographic Data Center as CCDC no: 1949380, 1949381 (deposit@ccdc.cam.ac.uk or http://www.ccdc.cam.ac.uk).

3. Results

3. 1. X-Ray Studies

The Ortep drawing obtained from X-ray diffraction studies of complexes **1** and **2** were depicted in Figures 2 and 3. The crystal data and data collection conditions of

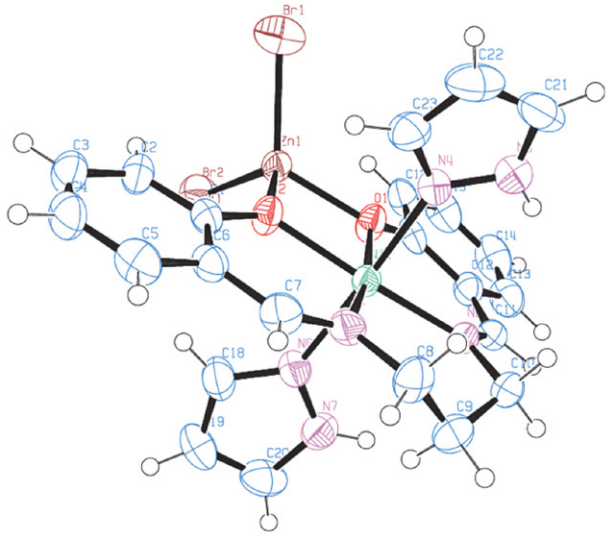

Figure 2. The Ortep drawing of **1**.

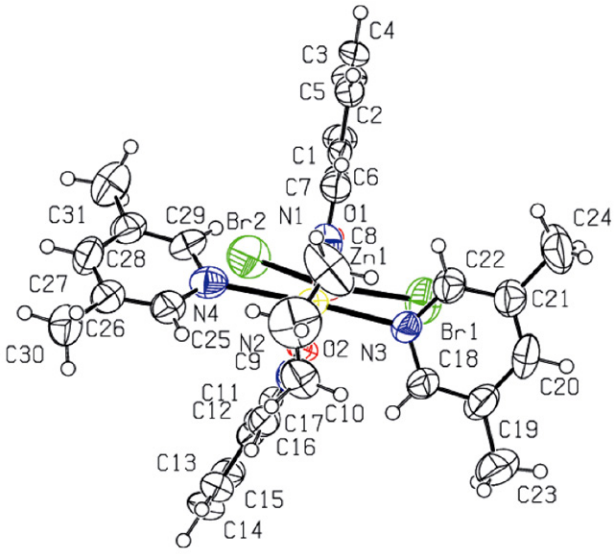

Figure 3. The Ortep drawing of **2**.

these complexes were tabulated in Table 1, the bond lengths and the bond angles are shown in Table 2.

As seen in Figures 2 and 3, Ni(II) ion in both complexes is in an octahedral coordination sphere between the O_2N_2 donors of the Schiff base, pyrazole and the two nitrogens of lutidine. On the other hand, Zn(II) ions are located in a distorted tetrahedral coordination sphere between two phenolic oxygen and two bromine atoms. However, based on the angle values given in Table 2, it can be concluded that the distortion value of the coordination sphere is highly extensive. The bond lengths in the equatorial plane of the octahedral coordination sphere of **1**, Ni(II) and donor atoms, are around 2 Å while the axial bond lengths change between 2.138 and 2.178 Å. The corresponding values are 2.154–2.338 Å for **2**. The equatorial bond lengths of Ni(II) donor atom are approximately 2 Å while axial bond lengths

Table 1. Crystal data and data collection conditions.

	1	**2**
Molecular Formula	$C_{23}H_{24}Br_2N_6NiO_2Zn$	$C_{31}H_{34}Br_2N_4NiO_2Zn$
Molar mass/ g mol^{-1}	700.38	778.52
T/ K	293(2)	293(2)
Crystal System	Monoclinic	Monoclinic
Space Group	$P2_1/n$	$P2_1/c$
a /Å	9.0086(3)	9.1210(5)
b /Å	15.7423(6)	18.9500(10)
c /Å	18.2777(7)	18.9770(10)
Alpha	90	90
Beta	98.856(4)	101.916(6)
Gamma	90	90
V /Å^3	2561.17(16)	3209.4(3)
Z	4	4
Calc. Density/ g cm^{-3}	1.816	1.611
μ /mm^{-1}	4.825	3.858
F (000)	1392	1568
Reflections Collected	11155	24685
Reflections Unique	5229	7144
*R*1, w*R*2 (2σ)	0.0591, 0.1678	0.0773, 0.1992
*R*1, w*R*2 (all)	0.0835, 0.1868	0.1699, 0.2489
Data / Parameters	5229/ 320	7144/ 370
GOOF of F^2	1.058	1.022
Largest Difference Peak Hole /e Å^{-3}	1.031, –1.866	1.072, –1.514
CCDC No	1949380	1949381

Table 2. The selected bond lengths and angles around the coordination sphere of the complexes.

Bond Lengths / Å	**Bond Angles / °**
1	
N1–Ni1 2.027(5)	N7–N6–Ni1 125.8(5)
N2–Ni1 2.019(5)	Zn1–O1–Ni1 98.9(19)
N3–N4 1.336(8)	Zn1–O2–Ni1 99.0(19)
N4–Ni1 2.138(6)	N2–Ni1–N1 99.2(2)
N6–N7 1.324(8)	N2–Ni1–O2 170.0(2)
N4–Ni1 2.138(6)	N1–Ni1–O2 90.8(2)
N6–Ni1 2.178(6)	N2–Ni1–O1 90.6(2)
O1–Zn1 1.971(5)	N1–Ni1–O1 169.7(2)
O1–Ni1 2.042(5)	O2–Ni1–O1 79.5(18)
O2–Zn1 1.978(4)	N2–Ni1–N4 91.1(2)
O2–Ni1 2.031(4)	N1–Ni1–N4 87.4(2)
Ni1–Zn1 3.049(10)	O2–Ni1–N4 90.6(2)
Zn1–Br1 2.325(12)	O1–Ni1–N4 89.3(2)
Zn1–Br2 2.328(11)	N2–Ni1–N6 92.1(2)
	N1–Ni1–N6 90.6(2)
	O2–Ni1–N6 86.4(2)
	O1–Ni1–N6 92.1(2)
	N4–Ni1–N6 176.4(2)
	O1–Zn1–O2 82.5(18)
	O1–Zn1–Br1 119.6(15)
	O2–Zn1–Br1 109.2(15)
	O1–Zn1–Br2 113.1(15)
	O2–Zn1–Br2 121.4(15)
	Br1–Zn1–Br2 109.4(4)
2	
N1–Ni1 2.024(7)	N2–Ni1–O1 170.6(3)
N2–Ni1 2.004(8)	N2–Ni1–N1 98.9(3)
N3–Ni1 2.154(7)	O1–Ni1–N1 90.1(3)
N4–Ni1 2.338(8)	N2–Ni1–O2 92.0(3)
O1–Zn1 2.017(5)	O1–Ni1–O2 79.1(2)
O1–Ni1 2.020(5)	N1–Ni1–O2 169.1(3)
O2–Zn1 1.967(5)	N2–Ni1–N3 92.8(3)
O2–Ni1 2.030(5)	O1–Ni1–N3 89.6(2)
Ni1–Zn1 3.072(14)	N1–Ni1–N3 92.7(3)
Zn1–Br2 2.326(16)	O2–Ni1–N3 87.1(2)
Zn1–Br1 2.332(15)	N2–Ni1–N4 86.0(3)
	O1–Ni1–N4 90.9(3)
	N1–Ni1–N4 91.8(3)
	O2–Ni1–N4 88.4(2)
	N3–Ni1–N4 175.4(3)
	N2–Ni1–Zn1 130.9(2)
	O1–Ni1–Zn1 40.4(14)
	N1–Ni1–Zn1 130.2(2)
	O2–Ni1–Zn1 39.0(15)
	N3–Ni1–Zn1 83.5(19)
	N4–Ni1–Zn1 93.9(2)
	O2–Zn1–O1 80.6(2)
	O2–Zn1–Br2 112.2(16)
	O1–Zn1–Br2 110.7(16)

differ from each other. The lengths of the bond between pyrazole and lutidine nitrogen atoms indicate that the coligands are located axially in the octahedral coordination sphere. In fact, the largest angle among these three atoms is formed between these two atoms.

The angle of N4NiN6 in **1** was measured as 176.4° and the angle of N3NiN4 in **2** was measured as 175.4°. In addition, in the coordination of Zn(II) the bond angles for **1** were found to be between 121.44°–82.52° and 79.07°–117.95° for **2**, respectively, showing a high tetrahedron distortion for these compounds.

Pyrazole coligand participates in the coordination through a double bond nitrogen atom. The N-H nitrogen of the pyrazole ring does not participate in the coordination. Since the electron pair present on this atom is donated to the π system of the ring, there is no electron pair left to donate to Ni(II) ion.

3. 2. Thermal Analysis

The TG and DTA curves of **1** and **2** are given in Figure 4. The thermoanalytical data of these complexes are tabulated in Table 3.

As can be seen from Figure 4 and Table 3, pyrazole coligands are separated from the structure in a single step. On the other hand, the removal of lutidine from the structure is a two-step process. In this process which is described as the first thermal reaction in Table 3, the coligands are removed from the structure leaving a NiL mononuclear complex and $ZnBr_2$ behind. The thermogravimetric curve of **1** depicted in Figure 4 displays a sin-

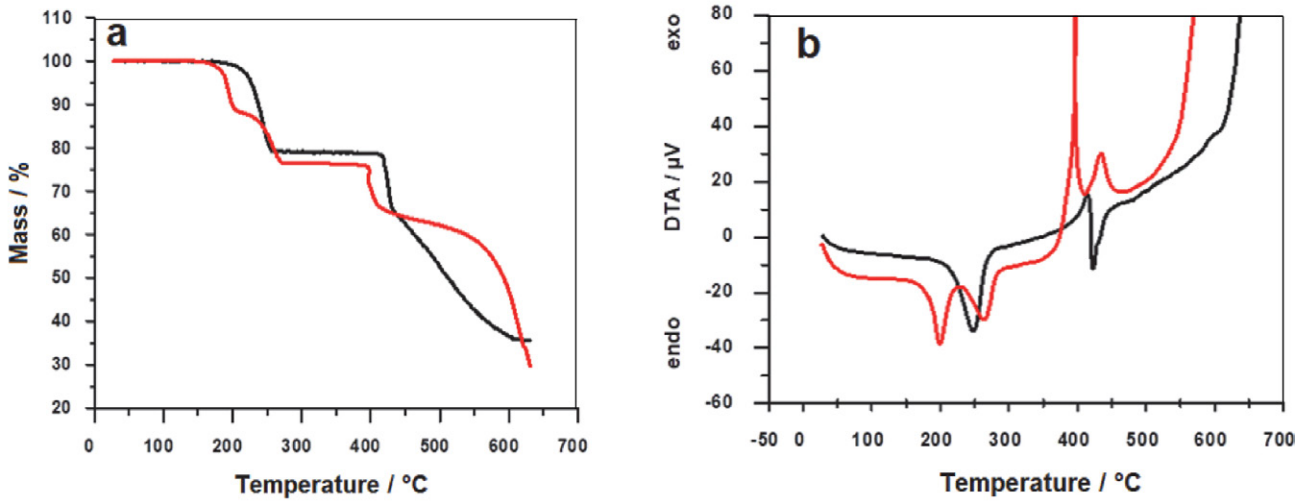

Figure 4. a. TG curves, b. DTA curves of **1** and **2** (black: **1**, [NiL·$ZnBr_2$·(pyrazole)$_2$], red: **2**, [NiL·$ZnBr_2$·(3,5-lutidine)$_2$].

Table 3. Thermoanalytical data of the complexes prepared.

Complex	1st Thermal Reaction Removal of coligands			2nd Thermal Reaction Decomposition of NiL residue	
	Temperature range / °C	Calcd mass loss / %	Final mass loss/ %	Temperature range / °C	Final mass loss/ %
1	197–232	1st pyrazole loss: 9.71 Total loss: 19.42	Total loss: 20.10 ± 0.58	380–420	11.42 ± 1.27
2	157–202–264	1st lutidine loss: 13.76 Total loss: 27.52	1st mass loss: 13.49 ± 0.35 2nd mass loss: 12.98 ± 0.77 Total loss: 26.47 ± 0.52	380–402	10.11 ± 2.17

gle step endothermic mass loss between 197–232 °C corresponding to two pyrazole molecules (Table 3). The theoretically calculated mass of two pyrazole molecules in **1** was 19.42% while the experimentally determined value was 20.10%. Subsequently, a mass loss of about 10% was observed at around 380 °C which is the dissociation temperature of NiL mononuclear complex.[23]

The situation in **2** is entirely different. Two lutidine coligands in a complex molecule detach from the structure in two identical stages with two equal mass losses. The first mass loss of approximately 13.49% occurs in a temperature range of 157–202 °C. Subsequently, a second mass loss of 12.98% was observed between 202–264 ° C. Since the mass of lutidine is 13.76% of the mass of the complex, lutidines leave the structure one by one by two consecutive endothermic reactions. The residual NiL and $ZnBr_2$ mixture gives a mass loss of 10% at 380 °C corresponding to the dissociation of NiL complex.

3. 3. Computational Results

The relative energy levels of HOMO and LUMO, dipole moments and formation energies obtained by using the sets in the Gaussian 09 program are given in Table 4. The orbital occupation values of the donor atoms are tabulated in Table S1 and the types of orbitals are given in Table S2. Figure 5 shows ESP maps and HOMO-LUMO images of the complexes.

Table 4. The relative energy levels of HOMO and LUMO, dipole moments and formation energies of the complexes prepared in the study, calculated with Gaussian 09.

Complex	E_{HOMO} / eV	E_{LUMO} / eV	ΔE / eV	μ / D	IP / eV	E_A / eV	$\Delta H°_f$ / kJ mol^{-1}
1	−6.167	−2.569	3.598	12.947	6.167	2.569	2173.76
2	−6.070	−2.497	3.573	12.501	6.070	2.497	2113.91

Optimization – b3lyp/6-31G(d), NImag: 0, IP: ionization potential, E_A: electron affinity

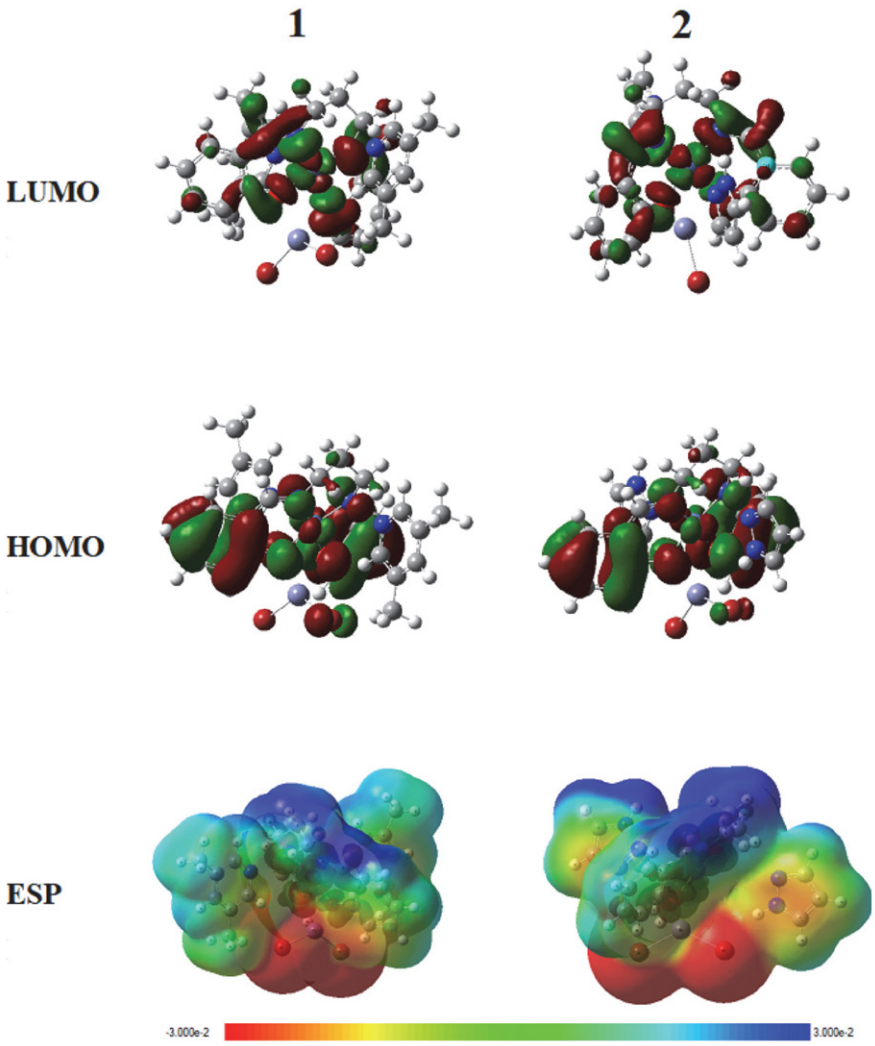

Figure 5. HOMO-LUMO images and ESP maps of the complexes.

The dipole moments, formation enthalpies and relative energy levels of HOMO and LUMO of the complexes came out to be highly similar. This is a highly expected outcome since the two complexes are very similar to each other. In both complex Ni(II)ion is in O_2N_4 octahedral coordination sphere while Zn(II) is located in a neighboring tetrahedral O_2Br_2 coordination sphere. Pyrazole and lutidine donate electrons to Ni(II) ion while Zn(II) ion attracts the electrons towards bromine atoms via phenolic oxygens. That is why chelate rings assume partially positive and bromine atoms partially negative charges as clearly seen in ESP maps given in Figure 5.

Since the diameter of the molecule is large, it is quite normal for the dipole moment to be high. Among the data obtained from NBO studies, the electron occupation values indicate that Ni(II) ion is in octahedral coordination. When focusing on Ni(II) ions, it can easily be seen that three d orbitals are occupied and the remaining two contain empty sites. This is expected for the octahedral crystal field splitting theory. On the other hand, Zn(II) possesses 10 d electrons, all d orbitals were found to be filled. There are two nitrogen atoms in the pyrazole ring. One of the nitrogen atoms has a hydrogen atom and an electron pair, the other one attached to the ring with a double bond. However, both nitrogens donate electrons to the π system of the aromatic ring and there are unfilled p orbitals in nitrogen atoms in the ring. This distribution is more homogeneous in iminic nitrogens.

4. Discussion

The difference between the two complexes is not clear from IR data. The most important result from IR data is the difference between the C=N vibrations of the ligand and the complexes. While C=N vibration was observed at 1608 cm^{-1} in ligand, it was observed at 1598 and 1595 cm^{-1} in complexes. This data proves that iminic nitrogen is co-

ordinated to the structure. It is already known that when the imine nitrogen is coordinated to a metal, the stretch vibration shifts to a low energy by 10–30 cm^{-1}. Apart from this, O–H stretches observed around 2600 cm^{-1} due to the strong hydrogen bonds are not observed in the complex spectra. In complexes, vibrations between nitrogen and metal ion in coligands cannot be determined from the spectra because IR spectra were recorded with ATR equipment and it is not possible to observe vibrations less than 600 cm^{-1} with ATR. However, in the theoretical calculations, the Ni–N(pyrazole) stretches can be observed at 334 cm^{-1} for **1**, at 450 cm^{-1} for **2**; the Ni–N(imine) stretches can be observed at 423 cm^{-1} for **1**, at 472 cm^{-1} for **2**; the Ni–O(phenol) stretches can be observed at 623 cm^{-1} for **1**, at 602 cm^{-1} for **2** (Figure S1).

The most important difference between the complexes is the variation of coordinative bond lengths observed in X-ray diffraction patterns. In **1**, the pyrazole molecule is attached to Ni(II) with electron pair of the non-hydrogen bonded nitrogen atom of the pyrazole ring. The distance between two pyrazoles with Ni(II) ion is very close to each other, as seen in Table 2, these distances are 2.138 and 2.178 Å. However, the situation is different in **2**. The two lutidines have different distances to Ni(II) ion. These distances are found to be 2.154 Å and 2.338 Å. This is also seen in the TG and DTA curves. As can be seen in Figure 4, both pyrazole coligands in **1** leave the structure in a single-stage process. The same situation is not valid for **2**, the removal of lutidine from the complex structure takes place in two distinctive stages. This shows that the coordinative effects of pyrazole and lutidine are different, lutidine is a stronger ligand than pyrazole. This is an expected result because the pyrazole ring is a more acidic and electron-withdrawing group,[34] lutidine is a better electron-donating ligand. If the phenolic oxygens of NiL unit coordinate a Lewis acid, the electrons of phenolic oxygen are attracted by Lewis acid resulting in the decrease of the electron density around the Ni(II) ion provided by the phenolic oxygens of the ligand to Ni(II) ion. Under this condition, Ni(II) ion compensates for the decreasing electron density by the coordination of solvent molecules or coligands present in the medium. If the electrons provided by a single coligand are sufficient, a square pyramidal coordination sphere is formed. If the electrons provided are not sufficient, then an octahedral coordination sphere occurs by the coordination of two coligands. In fact, in similar studies carried out by picoline, there were square-pyramidal or octahedral coordination spheres formed depending upon the picoline concentration.[28] If the coligand concentration in the medium is sufficiently high then an octahedral coordination sphere is formed by the addition of a new coligand to the square pyramidal structure of Ni(II) ion (Scheme 1).

This situation is clearly illustrated in Figure 4. While the pyrazole molecules are thermally discarded from the structure with a single-stage process, this takes in two distinctive processes in the case of lutidine. Therefore, the distance of the lutidine molecules to Ni(II) ion is different. DTA curves verify the fact that lutidine molecules are removed from the structure by two distinctive endothermic reactions. The total mass loss observed in these endothermic reactions is approximately equal to the mass of two lutidine molecules. Similarly, in the case of using pyrazole as a coligand, the mass loss in a single endothermic reaction is equal to the mass of two pyrazole molecules.

The visual observation of the chelate rings that occurred in both complexes showed that they have semi-chair conformation. Both complexes give a six-membered chelate ring with two nitrogen molecules of the Schiff base, a trimethylene bridge connecting to these two nitrogen atoms, and a central Ni(II) ion. The interplanar angles were calculated by the use of Parst program.[35] For **1**, the angle between the atomic planes of C8–C9–C10 and C8–N1–N2–C10 was 62.85°, the angle between C8–N1–N2–C10 and N1–Ni1–N2 was 7.35°. The ideal value of these angles in chair conformation is 62°. Under these conditions, one side of the chelate ring is in a stressed position and it appears to be a semi-chair structure.

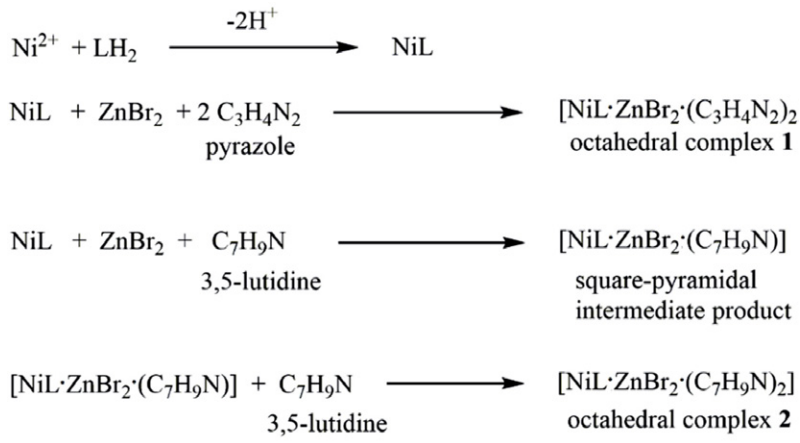

Scheme 1. Schematic preparation reactions of the complexes.

On the other hand, for **2** these angles are 50.74 and 10.77°. In both complexes, the aromatic rings of the coligands are not in the same plane. The angle between the two pyrazole planes in **1** is 20.74° and the angle between two lutidine planes in **2** is 57.39° (Figure 1). These values are similar to the data in the literature, the angles between the N1-Ni-N2 plane and C8-N1-N2-C9 plane have been reported between 5.0 and 8.9°.[23,24,36]

The theoretical study results, unfortunately, do not clearly show the difference between the complexes. Almost all the values of the two complexes are quite close to each other. The energy differences of HOMO-LUMO orbitals and dipole moments are approximately the same in these two complexes. The electron occupation values in the d orbitals of Ni(II) ion obtained from NBO analysis are close. In these two complexes, the occupation values of the d_{xy}, d_z^2, d_x^2-$_y^2$ orbitals are the same, only there is a slight difference in the d_{yz} and d_{zx} orbitals. As can be seen from Table 5, the occupancy value of the d_{yz} orbital for **1** is 1.14 electrons, the d_{zx} orbital is 1.60 electrons, the same orbitals have occupancy levels of 1.02 and 1.71 electrons in **2**. This result shows that the energy of the d_{yz} orbital in **2** is higher and according to the crystal field theory, the lutidine coligand offers more electrons to Ni(II) central ion. However, the difference is not significant and the second-order perturbation results in the NBO analysis reveal that there is no difference between the numerical values obtained from the two complexes and it is not possible to determine the electron donation effects of the coligands from the theoretical calculations, but at this point, thermal analysis brings an advantage. It is possible to interpret the difference between the strengths of the two coligands using thermogravimetric results. The stronger electron-donating coligand lutidine can form an intermediate stable compound of [NiL·$ZnBr_2$·(3,5-lutidine)] in the dinuclear complex, although a pyrazole molecule cannot offer enough electrons, [NiL·$ZnBr_2$·(pyrazole)] molecule does not form, instead [NiL·$ZnBr_2$·$(pyrazole)_2$] complex is formed with two pyrazole molecules. In this study, the complex was prepared at different 3,5-lutidine concentrations, but all the complex stoichiometries obtained were [NiL·$ZnBr_2$·$(3,5\text{-lutidine})_2$] and [NiL·$ZnBr_2$·(3,5-lutidine)] could not be prepared. However, thermogravimetry shows that this complex can be prepared. This work also proves the importance of thermogravimetry in the study of complexes.

5. Conclusion

Lewis acids can attract electrons from the oxygens of the coordination sphere of bis-*N,N*'-salicylidene-1,3-propanediamine-Ni(II) complex forming polynuclear μ-complexes. This results in a decrease of the electron density upon Ni(II) ion. Therefore, Ni(II) ion coordinates the solvent molecules or the coligands present in the medium by withdrawing electrons. If the coligand possesses a sufficiently high electron density, it forms a square pyramidal coordination sphere. If the electron density of the coligand is not sufficiently high, then Ni(II) ion attaches two coligands forming an octahedral coordination sphere.

Acknowledgments

This research did not receive any specific grant from funding agencies. The authors (Y. Gürsoy Tuncer and K. Gürpınar) thank to The Scientific and Technological Research Council of Turkey (TUBITAK) for financial support (Project number: 118F128). The authors declare that there is no conflict of interest.

6. References

1. C. Fukuhara, K. Tsuneyoshi, N. Matsumoto, S. Kida, M. Mikuriya, M. Mori, *Dalton Trans.* **1990**, *11*, 3473–3479; **DOI:**10.1039/DT9900003473
2. A. Gerli, K. S. Hagen, L. G. Marzilli, *Inorg. Chem.* **1991**, *30*, 4673–4676; **DOI:**10.1021/ic00024a043
3. S. Mirdya, M.G.B. Drew, A.K. Chandra, A. Banerjee, A. Frontera, S. Chattopadhyay, *Polyhedron* **2020**, *179*, 114374; **DOI:**10.1016/j.poly.2020.114374
4. S. Uhlenbrock, R. Wegner, B. Krebs, *Dalton Trans.* **1996**, *18*, 3731–3736; **DOI:**10.1039/dt9960003731
5. F. Ercan, O. Atakol, C. Arıcı, I. Svoboda, H. Fuess, *Acta Crystallogr. C* **2002**, *58*, 193–196; **DOI:**10.1107/S0108270102001609
6. T. G. Dastidar, S. Chattopadhyay, *Polyhedron* **2022**, *211*, 115511; **DOI:**10.1016/j.poly.2021.115511
7. Y. Li, L. Xu, M. Duan, B. Zhang, Y. Wang, Y. Guan, J. Wu, C. Ling, Z. You, *Polyhedron* **2019**, *166*, 146–152; **DOI:**10.1016/j.poly.2019.03.051
8. S. Ghosh, G. Aromi, P. Gamez, A. Ghosh, *Eur. J. Inorg. Chem.* **2015**, *18*, 3028–3037; **DOI:**10.1002/ejic.201500273
9. S. Öz, Ü. Ergun, M. Yakut, I. Svoboda, A. Atakol, E. K. İnal, N. Yılmaz, O. Atakol, *Russ. J. Coord. Chem.* **2014**, *40*, 571–582; **DOI:**10.1134/S1070328414080089
10. Y. N. Chen, Y. Y. Ge, W. Zhou, L. F. Ye, Z. G. Gu, G. Z. Ma, W. S. Li, H. Li, Y. P. Cai, *Inorg. Chem. Commun.* **2011**, *14*, 1228–1232; **DOI:**10.1016/j.inoche.2011.04.028
11. C. Arıcı, D. Ülkü, O. Atakol, *Anal. Sci.* **2002**, *18*, 959–960; **DOI:**10.2116/analsci.18.959
12. A. Finelli, N. Herault, A. Crochet, K. M. Fromm, *Cryst. Growth Des.* **2018**, *18*, 1215–1226; **DOI:**10.1021/acs.cgd.7b01769
13 S. Ghosh, A. Ghosh, *Inorg. Chim. Acta*. **2016**, *442*, 64–69; **DOI:**10.1016/j.ica.2015.11.029
14. O. Atakol, L. Tatar, M. A. Akay, D. Ülkü, *Anal. Sci.* **1999**, *15*, 101–102; **DOI:**10.2116/analsci.15.101
15. P. Seth, A. Figuerola, J. Jover, E. Ruiz, A. Ghosh, *Polyhedron* **2016**, *117*, 57–63; **DOI:**10.1016/j.poly.2016.05.021
16. A. Hazari, A. Das, P. Mahapatra, A. Ghosh, *Polyhedron* **2017**, *134*, 99–106; **DOI:**10.1016/j.poly.2017.06.007

17. A. Hazari, K. J. Gomez-Garcia, M. G. B. Drew, A. Ghosh, *Polyhedron* **2017**, *138*, 145–153; **DOI:**10.1016/j.poly.2017.09.012
18. R. Kurtaran, L. T. Yıldırım, A. D. Azaz, H. Namli, O. Atakol, *J. Inorg. Biochem*. **2005**, *99*, 1937–1944; **DOI:**10.1016/j.jinorgbio.2005.05.016
19. A. Hazari, L. K. Das, A. Bauza, A. Frontera, A. Ghosh, *Dalton Trans.* **2016**, *45*, 5730–5740; **DOI:**10.1039/C5DT04941E
20. A. Hazari, S. Giri, C. Diaz, A. Ghosh, *Polyhedron* **2016**, *118*, 70–80; **DOI:**10.1016/j.poly.2016.07.035
21. M. Aksu, S. Durmuş, M. Sarı, K. C. Emregül, I. Svoboda, H. Fuess, O. Atakol, *J. Therm. Anal. Calorim*. **2007**, *90*, 541–547; **DOI:**10.1007/s10973-006-7729-5
22. M. Sönmez, H. Nazır, E. Emir, I. Svoboda, L. Aksu, O. Atakol, *J. Therm. Anal. Calorim*. 2018, *131*, 3077–3091; **DOI:**10.1007/s10973-017-6720-7
23. A. Atakol, H. Nazır, I. Svoboda, M. L. Aksu, O. Atakol, *J. Therm. Anal. Calorim*. **2020**, *139*, 1863–1882; **DOI:**10.1007/s10973-019-08630-w
24. M. G. B. Drew, R. N. Prasad, R. P. Sharma, *Acta Crystallogr. C* **1985**, *41*, 1755–58; **DOI:**10.1107/S0108270185009337
25. Y. Elerman, M. Kabak, O. Atakol, *Acta Crystallogr. C* **1993**, *49*, 1905–1906; **DOI:**10.1107/S0108270193004615
26. O. Atakol, C. Arıcı, F. Ercan, D. Ülkü, *Acta Crystallogr. C* **1999**, *55*, 511–513; **DOI:**10.1107/S0108270198014334
27. S. Biswas, C. Diaz, A. Ghosh, *Polyhedron* **2013**, *51*, 96–101; **DOI:**10.1016/j.poly.2012.12.019
28. O. Atakol, H. Nazır, C. Arıcı, S. Durmuş, I. Svoboda, H. Fuess, *Inorg. Chim. Acta* **2003**, *342*, 295–300; **DOI:**10.1016/S0020-1693(02)01163-5
29. M. J. Frisch, G. W. Trucks, H. B. Schlegel, G. E. Scuseria, M. A. Robb, J. R. Cheeseman, G. Scalmani, V. Barone, B. Mennucci, G. Petersson, H. Nakatsuji: Gaussian 09, Revision D. 01, Gaussian. Inc., Wallingford CT, **2009**.
30. CrysAlis C. CrysAlis RED, Version 1.171. Oxford Diffraction Ltd., Abdingdon, UK, **2002**.
31. G. M. Sheldrick, *Acta Cryst. C* **2015**, *71*, 3–8; **DOI:**10.1107/S2053229614024218
32. L. J. Farrugia, *J. Appl. Crystallogr.* **1999**, *32*, 837–838; **DOI:**10.1107/S0021889899006020
33. N. Acar, O. Atakol, Ş. B. Sopacı, D. C. Duman, I. Svoboda, S. Öz, *J. Therm. Anal. Calorim*. **2017**, *127*, 1319–1327; **DOI:**10.1007/s10973-016-6004-7
34. J. A. Joule, K. Mills: Heterocyclic Chemistry, Wiley-VCH, Weinheim, Germany, **2010**, pp. 485–488.
35. A. L. Spek, *Acta Crystallogr. D* **2009**, *65*, 148–155; **DOI:**10.1107/S090744490804362X
36. F. Akhtar, M. G. B. Drew, *Acta Crystallogr. B* **1982**, *38*, 1149–1152; **DOI:**10.1107/S0567740882005184

Povzetek

Enojedrni kompleks NiL smo pripravili z uporabo bis-*N*,*N*'-saliciliden-1,3-propandiamina in Ni(II) soli. NiL smo reagirali s $ZnBr_2$, pirazolom in 3,5-lutidinom kot soligandoma v dioksanu in izolirali diheterojedrna kompleksa: [NiL · $ZnBr_2$ · $(pyrazole)_2$] in [NiL · $ZnBr_2$ · $(3,5\text{-lutidine})_2$]. Kompleksa smo okarakterizirali z elementno analizo, TG, IR in masno spektrometrijo. Proučili smo učinek heterocikličnih ligandov. Z uporabo programa Gaussian09 smo izračunali tvorbene entalpije, dipolne momente ter energije HOMO in LUMO orbital. Zasedenost atomskih orbital smo določili z NBO analizo. Vpliv pirazola in lutidina na tvorbo kompleksa smo ovrednotili z uporabo rentgenske difrakcije, TG in teoretičnih izračunov. Kompleks NiL z lutidinom tvori kvadratno piramidalno konformacijo, saj je lutidin veliko močnejši koligand kot pirazol.

Except when otherwise noted, articles in this journal are published under the terms and conditions of the Creative Commons Attribution 4.0 International License

Scientific paper

Synthesis, Characterization, X-Ray Crystal Structures and Antibacterial Activity of Zinc(II) and Vanadium(V) Complexes Derived from 5-Bromo-2-((2-(methylamino) ethylimino)methyl)phenol

Cheng Liu

School of Medicine, Huaqiao University, Quanzhou 362021, P. R. China

** Corresponding author: E-mail: liucheng_hqu@163.com*

Received: 09-24-2021

Abstract

Three new zinc(II) and one vanadium(V) complexes, $[Zn_2Cl_2L_2]$ (**1**), $[Zn_2I_2L_2]$ (**2**), $[ZnCl_2(HL)]$ (**3**), and $[V_2O_2(\mu\text{-}O)_2L_2]$ (**4**), where L is 5-bromo-2-((2-(methylamino)ethylimino)methyl)phenolate, have been synthesized and characterized by elemental analyses, IR and UV-Vis spectra, as well as molar conductivity. Structures of the complexes were confirmed by single crystal X-ray diffraction. Complexes **1** and **2** are isostructural dinuclear zinc compounds, with the Zn atoms in square pyramidal coordination. The Zn atoms in the mononuclear complex **3** are in tetrahedral coordination. Complex **4** is a dinuclear vanadium(V) compound, with the V atoms in octahedral coordination. The complexes were assayed for antibacterial activities by MTT method.

Keywords: Schiff base; Zinc complex; Vanadium complex; X-ray diffraction; Antibacterial activity

1. Introduction

Schiff bases are important compounds due to their easy preparation, good coordination, and excellent biological activities.[1] For the past few decades, the coordination chemistry of Schiff base ligands has been the subject of great interest. Schiff bases are capable of forming coordinate bonds with various inorganic metal salts through azomethine group.[2] Recently, metal complexes with biologically active ligands have received considerable attention. The biological activities of the organic ligands can be enhanced during coordination with metal salts.[3] It has been reported that chelation is a good way to cure many diseases like cancer.[4] Zinc is the second most abundant metal in the human body, and zinc homeostasis alterations have been linked to many diseases like neuropsychiatric disorders, bone diseases, and skin disorders.[5] Zinc homeostasis causes a variety of health problems that include growth retardation, immunodeficiency, hypogonadism, and neuronal and sensory dysfunctions.[6] Recently, zinc complexes have attracted much attention in the field of cancer therapy based on the facts that zinc is significantly non-toxic even at higher doses compared with other metals, which is beneficial to biocompatibility.[7] Zinc complexes also show biological activities like anticancer, DNA binding, antioxidant, antibacterial, and antitumor.[8] Moreover, vanadium chemistry has attracted great attention due to its interesting structural features and biological relevance.[9] Many vanadium complexes were synthesized and found to show medicinal properties like insulin mimetic activity.[10] They also show anticancer, antitumor, antifungal and antibacterial activities.[11] Some complexes with tridentate Schiff base ligands have been reported.[12] Herein, we report the synthesis, characterization, and single crystal structures of three new zinc(II) and one vanadium(V) complexes, $[Zn_2Cl_2L_2]$ (**1**), $[Zn_2I_2L_2]$ (**2**), $[ZnCl_2(HL)]$ (**3**), and $[V_2O_2(\mu\text{-}O)_2L_2]$ (**4**), where L is 5-bromo-2-((2-(methylamino)ethylimino)methyl)phenolate. The antibacterial activity of the compounds against Gram-positive bacterial strains (*B. subtilis*, *S. aureus* and *St. faecalis*) and Gram-negative bacterial strains (*E. coli*, *P. aeruginosa* and *E. cloacae*) by MTT method was studied.

2. Experimental

2. 1. Materials and Physical Methods

4-Bromosalicylaldehyde, *N*-methylethane-1,2-diamine, zinc chloride, zinc iodide, vanadium(IV)oxy acetylacetonate and sodium azide were purchased from

Aldrich. The solvents used in the synthesis and biological assay were obtained from Xiya Chemical Co. Ltd. and used as received. Elemental analyses for C, H and N were performed on a Perkin-Elmer 2400 II analyzer. FT-IR spectra were recorded as KBr pellets on Bruker Tensor-27. UV-Vis spectra were recorded on Lambda 35 spectrophotometer. Single crystal X-ray diffraction was carried out with a Bruker Apex II CCD diffractometer. Molar conductivity was measured in methanol with a DDS-11A molar conductivity meter.

2. 2. Synthesis of 5-Bromo-2-((2-(methylamino)ethylimino)methyl) phenol (HL)

4-Bromosalicylaldehyde (2.0 g, 0.010 mol) and *N*-methylethane-1,2-diamine (0.74 g, 0.010 mol) were stirred at reflux for 30 min in methanol (50 mL). The solvent was removed by distillation under reduced pressure to give yellow product. The solid was re-crystallized from ethanol to give the Schiff base. The yield was 0.22 g (85%). Anal. Calc. (%) for $C_{10}H_{13}BrN_2O$: C, 46.71; H, 5.10; N, 10.89. Found (%): C, 46.55; H, 5.21; N, 10.72. IR data (KBr, cm^{-1}): 3412, 3277, 1638. UV–Vis data [methanol, λ/nm (ε/L mol^{-1} cm^{-1})]: 230, 265, 310, 405. ^{1}H NMR (500 MHz, DMSO-d_6) δ 10.53 (s, 1H, OH), 10.16 (s, 1H, NH), 8.51 (s, 1H, CH=N), 7.53 (d, 1H, ArH), 7.45 (s, 1H, ArH), 7.11 (d, 1H, ArH), 3.71 (t, 2H, CH_2), 3.23 (d, 3H, CH_3), 2.88 (m, 2H, CH_2).

2. 3. Synthesis of $[Zn_2Cl_2L_2]$ (1)

4-Bromosalicylaldehyde (0.20 g, 1.0 mmol) and *N*-methylethane-1,2-diamine (0.074 g, 1.0 mmol) were stirred at reflux for 30 min in methanol (30 mL). Then, zinc chloride (0.14 g, 1.0 mmol) and sodium azide (0.065 g, 1.0 mmol) dissolved in 20 mL methanol were added. The final mixture was further stirred at reflux for 1 h. Diffraction quality single crystals were obtained after a few days by slow evaporation of colorless solution of the complex in open atmosphere. The yield was 0.19 g (53%). Anal. Calc. (%) for $C_{20}H_{24}Br_2Cl_2N_4O_2Zn_2$: C, 33.65; H, 3.39; N, 7.85. Found (%): C, 33.46; H, 3.51; N, 7.73. IR data (KBr, cm^{-1}): 3310, 1649. UV–Vis data [methanol, λ/nm (ε/L mol^{-1} cm^{-1})]: 226 (17,530), 268 (15,540), 333 (5,780). Λ_M (10^{-3} mol L^{-1} in methanol): 35 Ω^{-1} cm^2 mol^{-1}.

2. 4. Synthesis of $[Zn_2I_2L_2]$ (2)

This complex was synthesized by the similar method as described for complex **1**, with zinc chloride replaced by zinc iodide (0.32 g, 1.0 mmol). The diffraction quality block like colorless single crystals that deposited over a period of 5 days were collected by filtration and washed

Table 1. Crystallographic data and refinement details for the complexes

	1	**2**	**3**	**4**
Chemical Formula	$C_{20}H_{24}Br_2Cl_2N_4O_2Zn_2$	$C_{20}H_{24}Br_2I_2N_4O_2Zn_2$	$C_{10}H_{13}BrCl_2N_2OZn$	$C_{22}H_{32}Br_2N_4O_8V_2$
Molecular weight	713.89	896.79	393.40	742.22
Crystal color, habit	Colorless, block	Colorless, block	Colorless, block	brown, block
Crystal size, mm	0.25×0.23×0.23	0.22×0.20×0.17	0.20×0.20×0.15	0.19×0.18×0.16
Crystal system	Orthorhombic	Orthorhombic	Triclinic	Monoclinic
Space group	*Aba*2	*Aba*2	*P*-1	*C*2/*c*
Unit cell dimensions:				
a, Å	14.6638(18)	15.064(2)	7.3196(18)	25.308(2)
b, Å	21.2929(19)	21.180(2)	14.086(2)	6.8247(17)
c, Å	8.2244(17)	8.739(2)	14.539(2)	16.7172(16)
α, °	90	90	81.282(1)	90
β, °	90	90	76.416(1)	105.867(2)
γ, °	90	90	75.596(1)	90
V, Å^3	2567.9(7)	2788.3(8)	1404.4(5)	2777.4(8)
Z	4	4	4	4
ρ_{calcd}, g cm^{-3}	1.847	2.136	1.861	1.775
μ, mm^{-1}	5.213	6.824	4.959	3.602
θ Range collected, deg	2.36–25.50	2.35–25.50	1.45–25.50	1.67–25.49
T_{min} and T_{max}	0.3557 and 0.3802	0.3152 and 0.3900	0.4371 and 0.5233	0.5477 and 0.5964
Reflections collected/unique	7270/2356	7321/2399	7483/5172	7107/2573
Observed reflections ($I \geq 2s(I)$)	2134	1834	3957	2049
Data/restraints/parameters	2356/1/146	2399/1/146	5172/0/309	2573/0/175
GOOF on F^2	1.056	1.087	1.051	1.073
R_1, wR_2 ($I \geq 2s(I)$)	0.0375, 0.0980	0.0551, 0.1357	0.0406, 0.0954	0.0348, 0.0866
R_1, wR_2 (all data)	0.0443, 0.1065	0.0791, 0.1497	0.0599, 0.1088	0.0494, 0.0928

with methanol. The yield was 0.18 g (40%). Anal. Calc. (%) for $C_{20}H_{24}Br_2I_2N_4O_2Zn_2$: C, 26.78; H, 2.70; N, 6.25. Found (%): C, 26.59; H, 2.63; N, 6.34. IR data (KBr, cm^{-1}): 3310, 1646. UV–Vis data [methanol, λ/nm (ε/L·mol^{-1}·cm^{-1})]: 212 (18,360), 241 (17,460), 268 (15,655), 336 (5,460). Λ_M (10^{-3} mol L^{-1} in methanol): 31 Ω^{-1} cm^2 mol^{-1}.

2. 5. Synthesis of [$ZnCl_2$(HL)] (3)

This complex was synthesized by the similar method as described for complex **1**, but without sodium azide. The diffraction quality block like colorless single crystals that deposited over a period of 5 days were collected by filtration and washed with methanol. The yield was 0.20 g (51%). Anal. Calc. (%) for $C_{10}H_{13}BrCl_2N_2OZn$: C, 30.53; H, 3.33; N, 7.12. Found (%): C, 30.40; H, 3.41; N, 7.27. IR data (KBr, cm^{-1}): 3122, 1632. UV–Vis data [methanol, λ/nm (ε/L·mol^{-1}·cm^{-1})]: 225 (19,210), 245 (17,830), 268 (13,380), 365 (5,110). Λ_M (10^{-3} mol L^{-1} in methanol): 40 Ω^{-1} cm^2 mol^{-1}.

Table 2. Selected bond distances (Å) and angles (°) for the complexes

1			
Zn1-O1	2.030(4)	Zn1-N1A	2.080(5)
Zn1-O1A	2.103(4)	Zn1-N2A	2.215(6)
Zn1-Cl1	2.268(2)		
O1-Zn1-N1A	140.3(2)	O1-Zn1-O1A	75.84(16)
O1-Zn1-N2A	96.1(2)	O1-Zn1-Cl1	108.37(17)
N1-Zn1-Cl1A	110.86(18)	O1-Zn1-Cl1A	113.16(17)
N2-Zn1-Cl1A	103.84(17)		
2			
Zn1-O1	2.000(7)	Zn1-N1A	2.037(12)
Zn1-O1A	2.117(7)	Zn1-N2A	2.193(10)
Zn1-I1	2.5873(19)		
O1-Zn1-N1A	135.6(5)	O1-Zn1-O1A	76.1(3)
O1-Zn1-N2A	94.8(4)	O1-Zn1-I1	108.8(3)
N1-Zn1-I1A	114.9(4)	O1-Zn1-I1A	109.9(3)
N2-Zn1-I1A	105.1(3)		
3			
Zn1-O1	1.950(3)	Zn1-N1	2.007(4)
Zn1-Cl1	2.2447(16)	Zn1-Cl2	2.2158(15)
Zn2-O2	1.940(4)	Zn2-N3	2.009(4)
Zn2-Cl3	2.2377(17)	Zn2-Cl4	2.2095(17)
O1-Zn1-N1	96.33(15)	O1-Zn1-Cl2	111.63(12)
N1-Zn1-Cl2	113.18(13)	O1-Zn1-Cl1	108.65(13)
N1-Zn1-Cl1	111.15(13)	Cl2-Zn1-Cl1	114.42(6)
O2-Zn2-N3	96.77(17)	O2-Zn2-Cl4	109.71(13)
N3-Zn2-Cl4	113.77(14)	O2-Zn2-Cl3	110.72(13)
N3-Zn2-Cl3	109.38(13)	Cl4-Zn2-Cl3	115.02(7)
4			
V1-O1	1.875(2)	V1-O2	1.6529(19)
V1-O3	1.574(2)	V1-N1	2.140(3)
V1-N2	2.113(2)	V1-O2A	2.2764(19)
O3-V1-O2	106.43(11)	O3-V1-O1	101.21(11)
O2-V1-O1	99.09(9)	O3-V1-N2	92.27(11)
O2-V1-N2	94.48(10)	O1-V1-N2	157.25(10)
O3-V1-N1	96.48(11)	O2-V1-N1	155.66(9)
O1-V1-N1	84.11(10)	N2-V1-N1	76.15(10)
O3-V1-O2A	171.10(10)	O2-V1-O2A	79.35(9)
O1-V1-O2A	84.26(8)	N2-V1-O2A	80.39(8)
N1-V1-O2A	76.96(8)		

2. 6. Synthesis of [$V_2O_2(\mu$-O)$_2L_2$] (4)

4-Bromosalicylaldehyde (0.20 g, 1.0 mmol) and *N*-methylethane-1,2-diamine (0.074 g, 1.0 mmol) were stirred at reflux for 30 min in methanol (30 mL). Then, vanadium(IV)oxy acetylacetonate (0.26 g, 1.0 mmol) dissolved in 20 mL methanol was added. The final mixture was further stirred at reflux for 1 h. Diffraction quality single crystals were obtained after a few days by slow evaporation of brown solution of the complex in open atmosphere. The yield was 0.26 g (70%). Anal. Calc. (%) for $C_{22}H_{32}Br_2N_4O_8V_2$: C, 35.60; H, 4.35; N, 7.55. Found (%): C, 35.75; H, 4.23; N, 7.46. IR data (KBr, cm^{-1}): 3251, 1650, 934, 848. UV–Vis data [methanol, λ/nm (ε/L·mol^{-1} cm^{-1})]: 223 (16,630), 252 (15,120), 363 (4,330). Λ_M (10^{-3} mol L^{-1} in methanol): 27 Ω^{-1} cm^2 mol^{-1}.

2. 7. X-Ray Structure Determination

Intensity data of the complexes were collected at 298(2) K on a Bruker Apex II CCD diffractometer using graphite-monochromated MoK_a radiation (λ = 0.71073 Å). For data processing and absorption correction the packages SAINT and SADABS were used.[13] Structures of the complexes were solved by direct and Fourier methods and refined by full-matrix least-squares based on F^2 using SHELXL.[14] The non-hydrogen atoms were refined anisotropically. The hydrogen atoms have been placed at geometrical positions with fixed thermal parameters. Crystallographic data of the complexes are summarized in Table 1. Selected bond lengths and angles are listed in Table 2.

2. 8. Antibacterial Activity

Antibacterial activity of the complexes was tested against *B. subtilis*, *S. aureus*, *S. faecalis*, *P. aeruginosa*, *E. coli*, and *E. cloacae* using MTT medium. The minimum inhibitory concentrations (MICs) of the compounds were determined by a colorimetric method using MTT dye.[15] Penicillin and Kanamycin were tested as reference drugs. A stock solution of the Schiff base ligand and the complexes (50 μg mL^{-1}) in DMSO was prepared and quantities of the compounds were incorporated in specified quantity of sterilized liquid medium. A specified quantity of the medium containing the compounds was poured into micro-titration plates. Suspension of the microorganism was prepared to contain approximately 10^5 cfu mL^{-1} and applied to micro-titration plates with serially diluted compounds in DMSO to be tested, and incubated at 37 °C for 24 h for bacteria. After the MICs were visually determined on each micro-titration plate, 50 μL of phosphate buffered

saline (PBS 0.01 mol L^{-1}, pH 7.4: $Na_2HPO_4{\cdot}12H_2O$ 2.9 g, KH_2PO_4 0.2 g, NaCl 8.0 g, KCl 0.2 g, distilled water 1000 mL) containing 2 mg mL^{-1} of MTT was added to each well. Incubation was continued at room temperature for 4–5 h. The content of each well was removed, and 100 μL of isopropanol containing 5% 1 mol L^{-1} HCl was added to extract the dye. After 12 h of incubation at room temperature, the optical density (OD) was measured with a microplate reader at 570 nm.

3. Results and Discussion

3. 1. Chemistry

The Schiff base HL was facile synthesized by the reaction of 4-bromosalicylaldehyde with *N*-methylethane-1,2-diamine in methanol (Scheme 1). The complexes were prepared in a similar method, by the reaction of HL with various inorganic salts (Scheme 2). The dinuclear zinc complexes **1** and **2** were prepared in the presence of sodium azide, even though it is not a component of the compounds. Interestingly, the mononuclear complex **3** was obtained with no sodium azide presented during the synthesis. The solubility values of complexes **1**, **2**, **3** and **4** in methanol are 63, 54, 47 and 61 mg/mL, respectively. The conductivity values of the complexes (27–40 Ω^{-1} cm^2 mol^{-1}) indicated that they are non-electrolytes in methanol solution.[16]

3. 2. IR and UV-Vis Spectra Study

The weak absorptions at 3310-3122 cm^{-1} for complexes **1**-**3**, and 3251 cm^{-1} for complex **4** are assigned to $\nu_{N\text{-}H}$. The characteristic imine stretching for the complexes **1**-**4** is observed at 1632-1650 cm^{-1}.[17] The Schiff base ligand coordination through the phenolate oxygen is indicated by the absorption bands of the Ar–O bonds at 1178-1205 cm^{-1} in the complexes **1**-**4**.[18] In general, the infrared spectra of complexes **1** and **2** are similar to each other, due to the isostructural nature. The V=O bonds of complex **4** are indicated by the absorption at 848 and 934 cm^{-1}, which may be assigned to symmetric and asymmetric ν(O=V=O) vibration.[19]

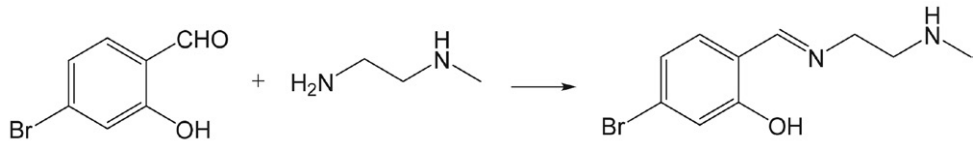

Scheme 1. The synthetic procedure for HL.

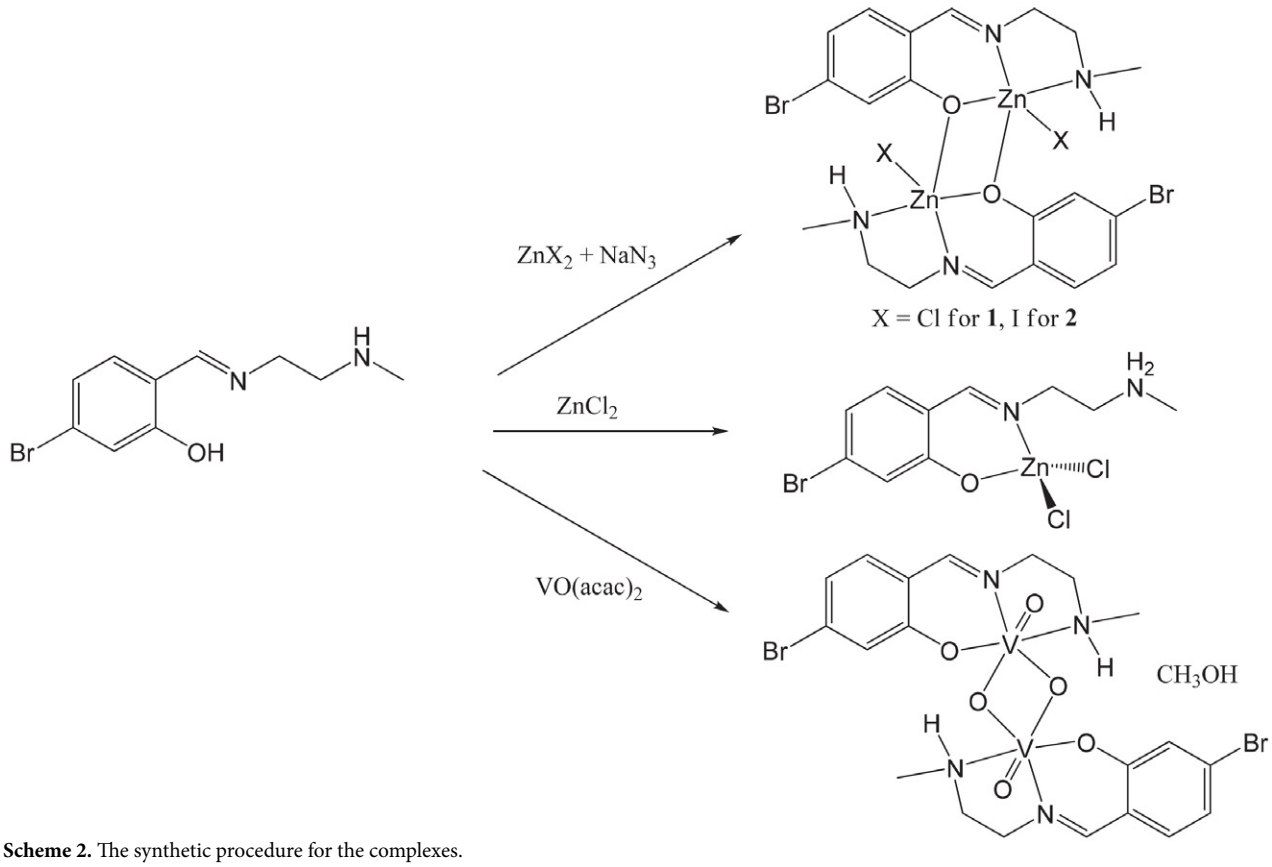

Scheme 2. The synthetic procedure for the complexes.

The absorption spectral data of the complexes were measured in methanol. In the complexes, peaks between 212–245 nm, 252–268 nm and 333–363 nm are assigned to $\pi \rightarrow \pi^*$, $n \rightarrow \pi^*$ and ligand to metal charge transfer transitions, respectively.[20]

3. 3. Structure Description of Complexes 1 and 2

Molecular structures of complexes **1** and **2** are shown in Figs. 1 and 2, respectively. The complexes are phenolate O bridged dinuclear zinc compounds. The molecules of the complexes possess crystallographic two fold rotation symmetry. The Zn atom is in square pyramidal coordination, with the basal plane defined by the phenolate O, imino N and amino N atoms of one Schiff base ligand, and one phenolate O atom of the other Schiff base ligand, and with the apical position occupied by one chloride ligand, *viz.* Cl for **1** and I for **2**. In general, the coordination geometry around the Zn atoms in both complexes displays distortion, as evidenced by the coordinate bond lengths and angles. The Zn–O and Zn–N bonds in both complexes are similar and range from 2.030(4) to 2.215(6) Å for complex **1**, and range from 2.000(7) to 2.193(10) Å for complex

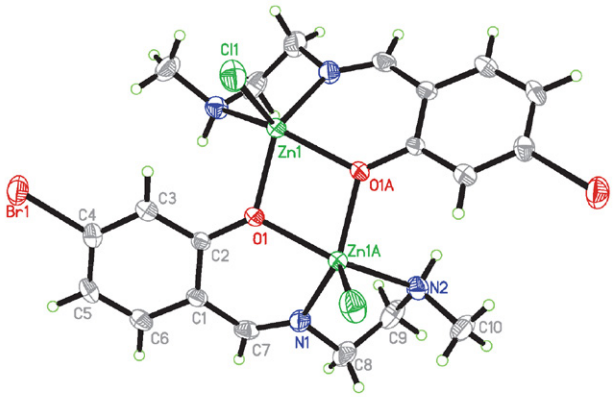

Fig. 1. Molecular structure of complex **1**. Atoms labeled with the suffix A are related to the symmetry operation 1 – *x*, 1 – *y*, *z*.

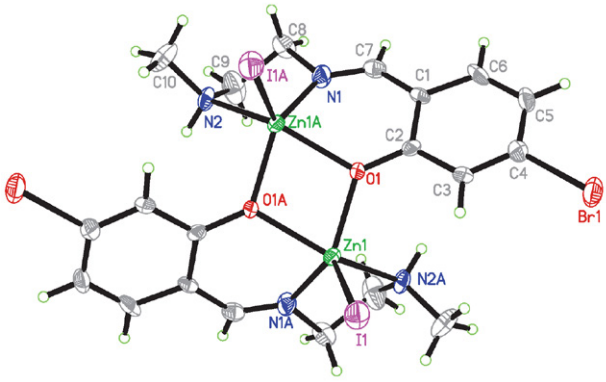

Fig. 2. Molecular structure of complex **2**. Atoms labeled with the suffix A are related to the symmetry operation 1 – *x*, 1 – *y*, *z*.

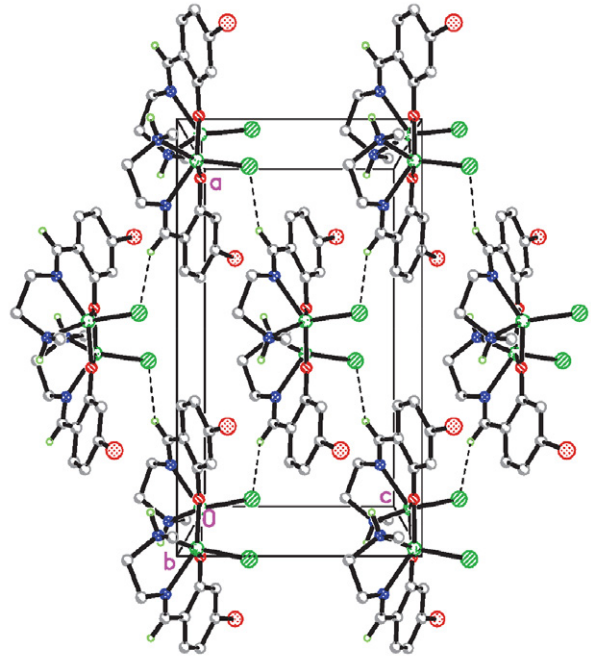

Fig. 3. Molecular packing diagram of complex **1**, viewed along the *b* axis. Hydrogen bonds are drawn as dashed lines.

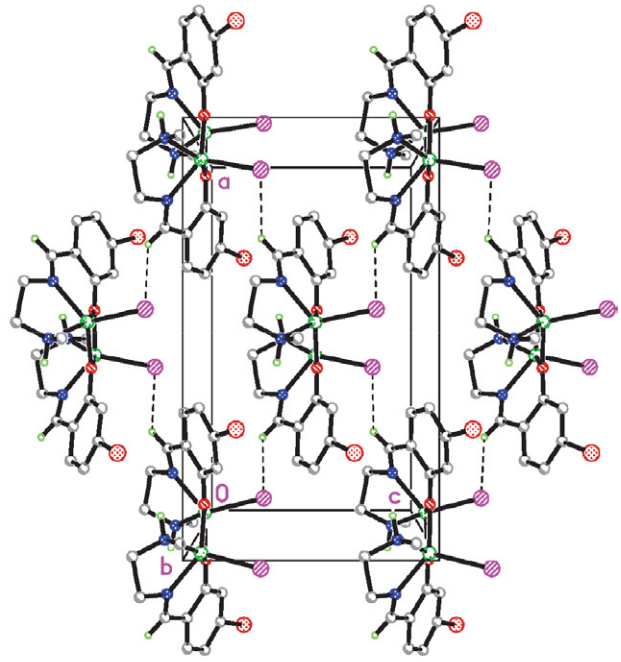

Fig. 4. Molecular packing diagram of complex **2**, viewed along the *b* axis. Hydrogen bonds are drawn as dashed lines.

2. The *cis* and *trans* bond angles in the basal planes are 75.84(16)-96.1(2)° and 140.3(2)-142.8(2)° for complex **1**, and 76.1(3)-94.8(4)° and 135.6(5)-144.9(4)° for complex **2**. The bond angles among the apical and basal donor atoms are 103.84(17)-113.16(17)° for complex **1**, and 105.1(3)-114.9(4)° for complex **2**. All the bond angles indicate that the square pyramidal coordination is distorted from ideal

model. Even though, the coordinate bond values are comparable to those observed in similar Schiff base zinc complexes with square pyramidal coordination.[21] The average deviation (0.001(5) Å for complex **1**, 0.051(5) Å for complex **2**) of the four basal donor atoms and the displacement (0.681(3) Å for complex **1** and 0.695(3) Å for complex **2**) of the Zn atoms from the least-squares planes defined by the four donor atoms indicate that the O_2N_2 cavities afford almost perfect planes to the Zn centers. The two benzene rings of the Schiff base ligands form a dihedral angle of 56.4(5)° for complex **1**, and 65.2(5)° for complex **2**.

In the crystal structures of complexes **1** and **2** (Figs. 3 and 4), the complex molecules are linked through C–H···Cl and C–H···I hydrogen bonds (Table 3), respectively, to form two dimensional network.

3. 4. Structure Description of Complex 3

Molecular structure of complex **3** is shown in Fig. 5. The complex is a mononuclear zinc compound. The asymmetric unit of the compound contains two independent molecules. The Schiff base ligand adopts zwitterionic form, with the H atom of the phenol group transfer to the amino group. The Zn atom is coordinated by the phenolate O and imino N atoms of the Schiff base ligand, and two Cl ligands, forming tetrahedral geometry. The coordination geometry around the Zn atoms displays distortion, as evidenced by the coordinate bond lengths and angles. The Zn–O and Zn–N bonds in the molecules are similar and range from 1.940(4) to 2.009(4) Å. The bond angles are 96.33(15)-114.42(6)° for Zn1, and 96.77(17)-115.02(7)° for Zn2. The coordinate bond values are comparable to those observed in similar Schiff base zinc complexes with tetrahedral coordination.[22]

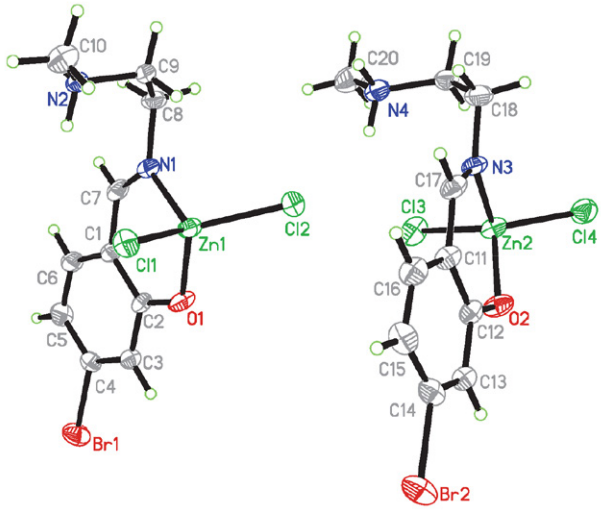

Fig. 5. Molecular structure of complex **3**. Atoms labeled with the suffix A are related to the symmetry operation 1 – *x*, 1 – *y*, *z*.

In the crystal structure of the complex (Fig. 6), the complex molecules are linked through C–H···Cl, N–H···Cl and N–H···O hydrogen bonds (Table 3), to form two dimensional network.

3. 5. Structure Description of Complex 4

Molecular structure of complex **4** is shown in Fig. 7. The complex is an oxo O bridged dinuclear vanadium compound, with V···V separation of 3.050(1) Å. There are two methanol molecules of crystallization, which connect to the complex molecule through O–H···O hydrogen bonds (Table 3). The molecule of the complex possesses crystallographic inversion center symmetry. The V atom is in octahedral coordination, with the equatorial plane defined by the phenolate O, imino N and amino N atoms of one Schiff base ligand, and one bridging O atom (O2), and with the axial positions occupied by terminal O atom (O3) and the other bridging O atom (O2A). The coordination geometry around the V atoms displays distortion, as evidenced by the coordinate bond lengths and angles. The V–O and V–N bonds in the equatorial plane are range from 1.653(2) to 2.140(3) Å, and the axial bonds are 1.574(2) and 2.276(2) Å. The obvious difference of the axial bonds from the equatorial bonds is caused by the Jahn-Teller effects. The *cis* and *trans* bond angles in the equatorial plane are 76.15(10)-99.09(9)° and 155.66(9)-157.25(10)°. The

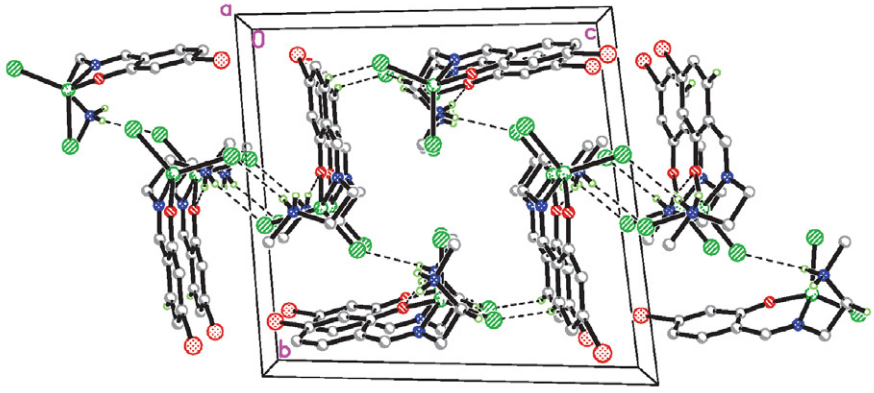

Fig. 6. Molecular packing diagram of complex **3**, viewed along the *a* axis. Hydrogen bonds are drawn as dashed lines.

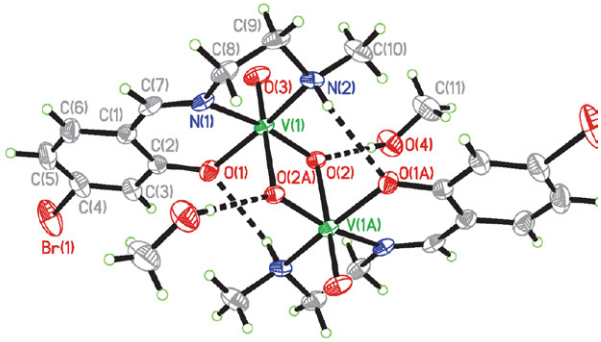

Fig. 7. Molecular structure of complex **4**. Atoms labeled with the suffix A are related to the symmetry operation 1/2 – *x*, 1/2 – *y*, 1 – *z*.

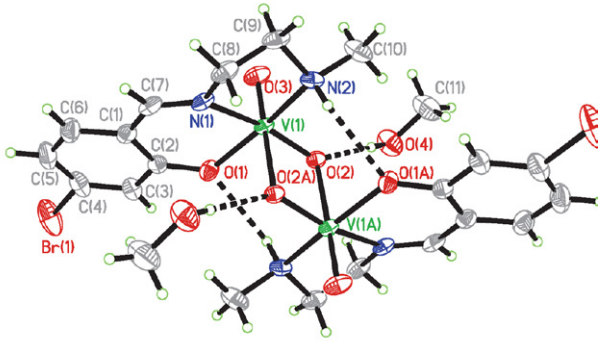

Fig. 8. Molecular packing diagram of complex **4**, viewed along the *b* axis. Hydrogen bonds are drawn as dashed lines.

bond angles among the axial and equatorial donor atoms are 79.96(8)-106.43(11)°. All the bond angles indicate that the octahedral coordination is distorted from ideal model. Even though, the coordinate bond values are comparable to those observed in similar Schiff base vanadium complexes.[23] The average deviation (0.063(5) Å) of the four equatorial donor atoms and the displacement (0.315(2) Å) of the V atom from the least-squares plane defined by the four donor atoms indicate that the O_2N_2 cavity afford somewhat distortion to the V center.

In the crystal structure of the complex (Fig. 8), the complex molecules are linked through C-H···O and N-H···O hydrogen bonds (Table 3), to form two dimensional network.

Table 3. Hydrogen bond distances (Å) and bond angles (°) for the complexes

D–H···*A*	*d*(*D*–H)	*d*(H···*A*)	*d*(*D*···*A*)	Angle (*D*–H···*A*)
1				
C7–H7···Cl1^{i}	0.93	2.74	3.583(6)	151
2				
C7–H7···I1^{ii}	0.93	3.00	3.719(13)	136
3				
N2–H2A···Cl1^{iii}	0.90	2.53	3.274(4)	140(6)
N2–H2A···Cl1	0.90	2.92	3.551(4)	128(6)
N2–H2B···O1^{iv}	0.90	1.91	2.793(5)	166(6)
N4–H4A···Cl2	0.90	2.51	3.277(5)	144(6)
N4–H4A···Cl3	0.90	2.87	3.444(5)	123(6)
N4–H4B···O2^{iv}	0.90	1.97	2.856(6)	168(6)
C6–H6···Cl4^{v}	0.93	2.83	3.647(6)	148(6)
C19–H19B···Cl4^{iv}	0.97	2.73	3.628(6)	154(6)
4				
O4–H4···O2	0.82	1.93	2.738(3)	170(5)
N2–H2···O4^{vi}	0.91	2.60	3.169(4)	121(5)
N2–H2···O1^{vii}	0.91	2.34	3.007(3)	130(5)
C3–H3···O4^{viii}	0.93	2.52	3.400(5)	157(5)
C7–H7···O3^{ix}	0.93	2.58	3.020(4)	109(5)
C8–H8B···O3^{ix}	0.97	2.57	3.240(4)	126(5)
C9–H9B···O4^{vi}	0.97	2.54	3.217(5)	127(5)

Symmetry codes for i): 1/2 + *x*, 1 – *y*, –1/2 + *z*; ii): –1/2 + *x*, 1 – *y*, –1/2 + *z*; iii): 2 – *x*, 1 – *y*, – *z*; iv): 1 + *x*, *y*, *z*; v): 1 – *x*, 1 – *y*, 1 – *z*; vi): *x*, –1 + *y*, *z*; vii) 1/2 – *x*, 1/2 – *y*, 1 – *z*; viii) 1/2 – *x*, 3/2 – *y*, 1 – *z*; ix) 1/2 – *x*, –1/2 + *y*, 1/2 – *z*.

3. 6. Antibacterial Activity of the Compounds

The Schiff base ligand and the complexes were screened for antibacterial activities against three Gram-positive bacterial strains (*B. subtilis*, *S. aureus*, and *St. faecalis*) and three Gram-negative bacterial strains (*E. coli*, *P. aeruginosa*, and *E. cloacae*) by MTT method. The MICs of the compounds against the bacteria are presented in Table 4. The Schiff base ligand has weak activity against *B. subtilis*, *S. aureus* and *E. coli*, while no activity against the remaining bacteria. In general, the complexes have higher activity than the Schiff base ligand. The zinc complexes **1** and **2** have equal activities against all the bacterial strains. Both complexes showed strong activity against *B. subtilis*, *S. aureus* and *E. coli* (MICs

Table 4. MICs (μg mL^{-1}) of the compounds and related materials

Tested material	Gram positive			Gram negative		
	B. subtilis	*S. aureus*	*St. faecalis*	*P. aeruginosa*	*E. coli*	*E. cloacae*
HL	25	12.5	> 50	> 50	12.5	> 50
1	3.12	1.56	25	> 50	6.25	> 50
2	3.12	1.56	25	> 50	6.25	> 50
3	1.56	0.39	6.25	> 50	12.5	> 50
4	12.5	6.25	12.5	> 50	12.5	> 50
Penicillin	1.56	1.56	1.56	6.25	6.25	3.12
Kanamycin	0.39	1.56	3.12	3.12	3.12	1.56

= 1.56-6.25 μg mL^{-1}), weak activity against *St. faecalis* (MIC = 25 μg mL^{-1}), and no activity against *P. aeruginosa* and *E. cloacae*. Complexes **1** and **2** have similar activity against *S. aureus* and *E. coli* when compared with the reference drugs Penicillin and Kanamycin. In general, complex **3** has better activity against the Gram positive bacteria than complexes **1** and **2**. However, complex **3** has worse activity against the Gram negative bacteria than **1** and **2**. Complex **3** has higher activity against *S. aureus* and similar activity against *B. subtilis* when compared with the reference drugs. Complex **4** has effective activity against *S. aureus*, but weak or no activity against the remaining bacteria.

As a comparison with the zinc complexes derived from 4-fluoro-2-((pyridin-2-ylmethylimino)methyl)phenol and 4-fluoro-2-((2-(hydroxymethyl)phenylimino) methyl)phenol, the current zinc complexes have weaker activity against *B. subtilis*, *St. faecalis*, *P. aeruginosa* and *E. coli*, but higher activity against *S. aureus*.[24] The complexes have similar activities against *S. aureus* and *E. coli* when compared with the zinc complexes derived from 5-bromo-2-((2-(diethylammonio)ethylimino)methyl)phenol.[12f]

4. Conclusion

Two new dinuclear zinc(II) complexes, one new mononuclear zinc complex, and one new dinuclear vanadium(V) complex have been synthesized and characterized. Crystal structures of the complexes are determined and described. The Zn atoms in the dinuclear zinc complexes are in square pyramidal coordination. The Zn atom in the mononuclear zinc complex is in tetrahedral coordination. The V atom in the dinuclear vanadium complex is in octahedral coordination. The three zinc complexes have effective antibacterial activities against *B. subtilis* and *S. aureus*, which deserve further study.

5. Supplementary Materials

The crystal data for the complexes have been deposited with the Cambridge Crystallographic Data Centre (CCDC nos. 2111648 (**1**), 2111649 (**2**), 2111650 (**3**) and 2111651 (**4**); deposit@ccdc.cam.ac.uk or http://www.ccdc.cam.ac.uk).

Acknowledgment

The author acknowledges Huaqiao University for supporting this work.

7. References

1. (a) M. Pervaiz, S. Sadiq, A. Sadiq, U. Younas, A. Ashraf, Z. Saeed, M. Zuber, A. Adnan, *Coord. Chem. Rev.* **2021**, *447*, 214128; **DOI:**10.1016/j.ccr.2021.214128
(b) A. R. E. Mahdy, M. Y. Alfaifi, M. S. El-Gareb, N. Farouk, R. F. M. Elshaarawy, *Inorg. Chim. Acta* **2021**, *526*, 120504; **DOI:**10.1016/j.ica.2021.120504
(c) H. Keypour, F. Forouzandeh, S. Hajari, M. Jamshidi, S. H. M. Farida, R. W. Gable, *Polyhedron* **2021**, *207*, 115380; **DOI:**10.1016/j.poly.2021.115380
(d) S. Menati, R. Azadbakht, H. A. Rudbari, G. Bruno, *Polyhedron* **2021**, *205*, 115296. **DOI:**10.1016/j.poly.2021.115296
2. (a) E. A. Bowman, B. L. England, M. A. Patterson, N. S. Price, K. E. Stepler, H. A. Curnutte, R. E. Lease, C. A. Bradley, P. R. Craig, *Inorg. Chim. Acta* **2021**, *524*, 120415; **DOI:**10.1016/j.ica.2021.120415
(b) A. N. Zheng, Q. Q. Zhou, B. J. Ding, D. F. Li, T. Zhang, Z. S. Hou, *Eur. J. Inorg. Chem.* **2021**, *2021*, 3385–3395; **DOI:**10.1002/ejic.202100356
(c) M. Bialek, J. Fryga, G. Spaleniak, M. A. Matsko, N. Hajdasz, *J. Catal.* **2021**, *400*, 184–194; **DOI:**10.1016/j.jcat.2021.05.036
(d) P. Ghanghas, A. Choudhary, D. Kumar, K. Poonia, *Inorg. Chem. Commun.* **2021**, *130*, 108710; **DOI:**10.1016/j.inoche.2021.108710
(e) M. Barwiolek, D. Jankowska, M. Chorobinski, A. Kaczmarek-Kedziera, I. Lakomska, S. Wojtulewski, T. M. Muziol, *RSC Advances* **2021**, *11*, 24515–24525. **DOI:**10.1039/D1RA03096E
3. (a) B. K. Mallandur, G. Rangaiah, N. V. Harohally, *Synth. Commun.* **2017**, *47*, 1065–1070; **DOI:**10.1080/00397911.2017.1309668
(b) L. Shi, H.-M. Ge, S.-H. Tan, H.-Q. Li, Y.-C. Song, H.-L. Zhu, R.-X. Tan, *Eur. J. Med. Chem.* **2007**, *42*, 558–564. **DOI:**10.1016/j.ejmech.2006.11.010
4. (a) C. A. R. Yu, M. H. Majd, F. Shiri, S. Shahraki, P. Karimi, *Mol. Divers.* **2021. DOI:**10.1007/s11030-021-10293-5;
(b) M. Pellei, F. Del Bello, M. Porchia, C. Santini, *Coord. Chem. Rev.* **2021**, *445*, 214088. **DOI:**10.1016/j.ccr.2021.214088
5. (a) D. C. P. Rossi, J. A. L. Figueroa, W. R. Buesing, K. Candor, L. T. Blancett, H. M. Evans, R. Lenchitz, B.L. Crowther, W. Elsegeiny, P. R. Williamson, J. Rupp, G. S. Deepe, *J. Clin. Invest.* **2021**, *131*, e147268;
(b) V. M. M. Gimenez, I. Bergam, R. J. Reiter, W. Manucha, *Life Sci.* **2021**, *281*, 119770. **DOI:**10.1016/j.lfs.2021.119770
6. (a) Q. Cao, J. Yang, H. Zhang, L. Hao, G.-G. Yang, L.-N. Ji, Z.-W. Mao, *Chem. Commun.* **2019**, *55*, 7852–7855; **DOI:**10.1039/C9CC03480C
(b) S. Hojyo, B.-H. Bin, T. Kukada, *Exp. Opt. Orphan Drugs* **2017**, *5*, 865–873; **DOI:**10.1080/21678707.2017.1394184
(c) T. L. Huang, G. Y. Yan, M. Guan, *Inter. J. Mol. Sci.* **2020**, *21*, 1236; **DOI:**10.3390/ijms21041236
(d) B. Szewczyk, *Front. Aging Neurosci.* **2000**, *5*, 33;
7. T. Hara, T. Takeda, T. Takagishi, K. Fukue, T. Kambe, T. Fukada, *J. Physiol. Sci.* **2017**, *67*, 283–301. **DOI:**10.1007/s12576-017-0521-4
8. (a) M. Pellei, F. del Bello, M. Porchia, C. Santini, *Coord.*

Chem. Rev. **2021**, *445*, 214088;
DOI:10.1016/j.ccr.2021.214088
(b) M. Lavanya, J. Haribabu, K. Ramaiah, C. S. Yadav, R.K. Chitumalla, J. Jang, R. Karvembu, A. V. Reddy, M. Jagadeesh, *Inorg. Chim. Acta* **2021**, *524*, 120440;
DOI:10.1016/j.ica.2021.120440
(c) E. Halevas, B. Mavroidi, M. Pelecanou, A.G. Hatzidimitriou, *Inorg. Chim. Acta* **2021**, *523*, 120407;
DOI:10.1016/j.ica.2021.120407
(d) Q. Poladian, O. Sahin, T. Karakurt, B. Ilhan-Ceylan, Y. Kurt, *Polyhedron* **2021**, *201*, 115164;
DOI:10.1016/j.poly.2021.115164
(e) F. Ramilo-Gomes, Y. Addis, I. Tekamo, I. Cavaco, D. L. Campos, F. R. Pavan, C. S. B. Gomes, V. Brito, A. O. Santos, F. Domingues, A. Luis, M. M. Marques, J. C. Pessoa, S. Ferreira, S. Silvestre, I. Correia, *J. Inorg. Biochem.* **2021**, *216*, 111331.
DOI:10.1016/j.jinorgbio.2020.111331

9. (a) H. Kargar, P. Forootan, M. Fallah-Mehrjardi, R. Behjatmanesh-Ardakani, H. A. Rudbari, K. S. Munawar, M. Ashfaq, M. N. Tahir, *Inorg. Chim. Acta* **2021**, *523*, 120414;
DOI:10.1016/j.ica.2021.120414
(b) V. P. McCaffrey, O. Q. Conover, M. A. Bernard, J. T. Yarranton, N. R. Lessnau, J. P. Hempfling, *Polyhedron* **2021**, *205*, 115268. **DOI:**10.1016/j.poly.2021.115268
10. (a) J. Szklarzewicz, A. Jurowska, M. Jurowska, G. Kazek, M. Gluch-Lutwin, J. Sapa, *Inorg. Chim. Acta* **2021**, *516*, 120135;
DOI:10.1016/j.ica.2020.120135
(b) S. Trevino, A. Diaz, *J. Inorg. Biochem.* **2020**, *208*, 111094;
DOI:10.1016/j.jinorgbio.2020.111094
(c) T. Kolesa-Dobravc, K. Maejima, Y. Yoshikawa, A. Meden, H. Yasui, F. Perdih, *New J. Chem.* **2018**, *42*, 3619–3632.
DOI:10.1039/C7NJ04189F
11. (a) I. Kostova, *Anti-Cancer Agents Med. Chem.* **2009**, *9*, 827–842; **DOI:**10.2174/187152009789124646
(b) L. Reytman, J. Hochman, E. Y. Tshuva, *J. Coord. Chem.* **2018**, *71*, 11–13; **DOI:**10.1080/00958972.2018.1461848
(c) S.K. Mal, T. Chattopadhyay, A. Fathima, C. S. Purohit, M. S. Kiran, B. U. Nair, R. Ghosh, *Polyhedron* **2017**, *126*, 23–27;
DOI:10.1016/j.poly.2017.01.008
(d) X.-L. Hong, M.-H. Zeng, L.-J. Liu, X.-L. Ye, D.-S. Yi, *J. Coord. Chem.* **2017**, *70*, 1438–1450;
DOI:10.1080/00958972.2017.1290800
(e) M. Khosravan, L. Abdolahi, S. Y. Ebrahimipour, *Inorg. Chem. Commun.* **2021**, *128*, 108561;
DOI:10.1016/j.inoche.2021.108561
(f) V. Mirdarvatan, B. Bahramian, A. D. Khalaji, M. Poupon, M. Dusek, R. Mazandarani, *Polyhedron* **2021**, *194*, 114939.
DOI:10.1016/j.poly.2020.114939
12. (a) P. Chakraborty, J. Adhikary, S. Samanta, D. Escudero, A. C. Castro, M. Swart, S. Ghosh, A. Bauza, A. Frontera, E. Zangrando, D. Das, *Cryst. Growth Des.* **2014**, *14*, 4111–4123;
DOI:10.1021/cg500717n
(b) G. Marinescu, A. M. Madalan, M. Andruh, *J. Coord. Chem.* **2015**, *68*, 479–490;
DOI:10.1080/00958972.2014.997721
(c) C. Maxim, T. D. Pasatoiu, V. Ch. Kravtsov, S. Shova, C. A. Muryn, R. E. P. Winpenny, F. Tuna, M. Andruh, *Inorg. Chim. Acta* **2008**, *361*, 3903–3911; **DOI:**10.1016/j.ica.2008.03.013
(d) L. M. Mokry, C. J. Carrano, *Inorg. Chem.* **1993**, *32*, 6119–6121; **DOI:**10.1021/ic00078a036
(e) H.-Y. Qian, *Acta Chim. Slov.* **2021**, *68*, 700–708;
DOI:10.17344/acsi.2021.6721
(f) H.-Y. Liu, X. Gan, J.-Y. Ding, Z.-T. Li, Q. Chen, *Acta Chim. Slov.* **2021**, *68*, 693–699. **DOI:**10.17344/acsi.2021.6716
13. G. M. Sheldrick, SAINT (version 6.02), SADABS (version 2.03), Madison (WI, USA): Bruker AXS Inc, **2002**.
14. G. M. Sheldrick, *Acta Crystallogr.* **2008**, *A64*, 112–122.
DOI:10.1107/S0108767307043930
15. J. Meletiadis, J. Meis, J. W. Mouton, J. P. Donnelly, P. E. Verweij, *J. Clin. Microbiol.* **2000**, *38*, 2949–2956.
16. W. J. Geary, *Coord. Chem. Rev.* **1971**, *7*, 81–122.
DOI:10.1016/S0010-8545(00)80009-0
17. (a) R. Biswas, C. Diaz, A. Bauza, A. Frontera, A. Ghosh, *Dalton Trans.* **2013**, *42*, 12274–12283; **DOI:**10.1039/c3dt51153g
(b) G. Marinescu, A. M. Madalan, S. Shova, M. Andruh, *J. Coord. Chem.* **2012**, *65*, 1539–1547.
DOI:10.1080/00958972.2012.675435
18. A. Majumder, G. M. Rosair, A. Mallick, N. Chattopadhyay, S. Mitra, *Polyhedron* **2006**, *25*, 1753–1762.
DOI:10.1016/j.poly.2005.11.029
19. E. Kwiatkowski, G. Romanowski, W. Nowicki, M. Kwiatkowski, K. Suwinska, *Polyhedron* **2003**, *22*, 1009–1018.
DOI:10.1016/S0277-5387(03)00041-X
20. A. Ray, D. Sadhukhan, G. M. Rosair, C. J. Gomez-Garcia, S. Mitra, *Polyhedron* **2009**, *28*, 3542–3550.
DOI:10.1016/j.poly.2009.07.017
21. (a) H. Kargar, A. A. Ardakani, M. N. Tahir, M. Ashfaq, K. S. Munawar, *J. Mol. Struct.* **2021**, *1233*, 130112;
DOI:10.1016/j.molstruc.2021.130112
(b) D. M. Gonzalez, J. Cisterna, I. Brito, T. Roisnel, J.-R. Hamon, C. Manzur, *Polyhedron* **2019**, *162*, 91–99.
DOI:10.1016/j.poly.2019.01.043
22. (a) N. Farahani, M. Khalaj, *J. Mol. Struct.* **2021**, *1228*, 129747;
DOI:10.1016/j.molstruc.2020.129747
(b) H. Kargar, R. Behjatmanesh-Ardakani, V. Torabi, A. Sarvian, Z. Kazemi, Z. Chavoshpour-Natanzi, V. Mirkhani, A. Sahraei, M. N. Tahir, M. Ashfaq, *Inorg. Chim. Acta* **2021**, *514*, 120004. **DOI:**10.1016/j.ica.2020.120004
23. (a) S. Y. Ebrahimipour, I. Sheikhshoaie, A. C. Kautz, M. Ameri, H. Pasban-Aliabadi, H. A. Rudbari, G. Bruno, C. Janiak, *Polyhedron* **2015**, *93*, 99–105;
DOI:10.1016/j.poly.2015.03.037
(b) I. Sheikhshoaie, S.Y. Ebrahimipour, N. Lotfi, J. T. Mague, M. Khaleghi, *Inorg. Chim. Acta* **2016**, *442*, 151–157;
DOI:10.1016/j.ica.2015.11.026
(c) S. K. Mal, M. Mitra, H. R. Yadav, C. S. Purohit, A.R. Choudhury, R. Ghosh, *Polyhedron* **2016**, *111*, 118–122.
DOI:10.1016/j.poly.2016.03.033
24. H.-Y. Qian, *Acta Chim. Slov.* **2021**, *68*, 638–644.
DOI:10.17344/acsi.2021.6656

Povzetek

Sintetizirali smo tri nove koordinacijske spojine cinka(II) in eno vanadija(V), $[Zn_2Cl_2L_2]$ (**1**), $[Zn_2I_2L_2]$ (**2**), $[ZnCl_2(HL)]$ (**3**), and $[V_2O_2(\mu\text{-}O)_2L_2]$ (**4**), kjer je L = 5-bromo-2-((2-(metilamino)etilimino)metil)fenolat, ter produkte karakterizirali z elementno analizo, IR in UV-Vis spektroskopijo ter meritvami molarne prevodnosti. Strukture produktov smo določili z monokristalno rentgensko analizo. Produkta **1** in **2** sta izostrukturni dvojedrni cinkovi spojini s cinkovimi atomi v kvadratno piramidalni koordinaciji. Cinkovi atomi v enojedrni spojini **3** so tetraedrično koordinirani. Spojina **4** je dvojedrna z vanadijevimi atomi v oktaedrični koordinaciji. Antibakterijsko učinkovitost produktov smo preverili z metodo MTT.

Except when otherwise noted, articles in this journal are published under the terms and conditions of the Creative Commons Attribution 4.0 International License

Scientific paper

The Students' Perceptions Using *3DChemMol* Molecular Editor for Construction and Editing of Molecular Models

Danica Dolničar,[1,*] Bojana Boh Podgornik[1] and Vesna Ferk Savec[2]

[1] *Faculty of Natural Sciences and Engineering, University of Ljubljana, Snežniška 5, 1000 Ljubljana, Slovenia*

[2] *Faculty of Education, University of Ljubljana, Kardeljeva ploščad 16, 1000 Ljubljana, Slovenia*

* *Corresponding author: E-mail: danica.dolnicar@ntf.uni-lj.si*

Received: 09-30-2021

Abstract

The paper presents a study in which 54 university students were introduced to a newly developed, free, web-based *3DChemMol* molecular editor with a toolbar, which they then evaluated. The tool aims to increase representational competence related to submicroscopic representations. Students who used the software for the first time, were instructed to create molecular models using the model building/editing tools in three activities with varying levels of difficulty: 1) building a simple model (butanoic acid), 2) converting one model (hexane) into two models, 3) converting from a non-cyclic to a cyclic structure (glucose). It took students from two up to 15 minutes to accomplish each of the activities. Several types of help were available in the *3DChemMol* molecular editor toolbar to assist students during their activities, including a video tutorial, button hovering, action status display, and a help menu. Undo/redo and restart options were also available. Students' completion level, difficulties, and use of the help features were investigated using student self-evaluation questionnaires. The *3DChemMol* molecular editor proved to be a useful support for students in completing simple chemistry activities. Students were successful in model building, although they encountered some specific difficulties, especially in steps that involved spatial operations, such as rotating the selected part of molecule around the bond. In students' perception, the video tutorials were the preferred and most frequently used type of help, and the undo function was considered essential. The results suggest that the *3DChemMol* molecular editor can be used effectively in introductory chemistry courses at the tertiary level, whether for direct instruction, self-study, or other forms of support in the pedagogical process. The results and new findings of this study will be used to further optimize the interface in future versions of the evaluated tool.

Keywords: Representational competence; submicroscopic representations; learning chemistry; 3D model building; model editing tool

1. Introduction

1. 1. Visualization and Molecular Models in Chemistry Education

The concept of visualization can be understood in three ways:[1] visualization of objects (physical or graphic representations, static or dynamic, analog or digital, can be accompanied by sensory data), introspective visualization (mental models), and interpretive visualization (making meaning from the previous two forms). Vekiri[2] states that graphical representations allow for more efficient processing of information compared to verbal representations, which reduces working memory load. The adoption of visualization is not automatic but a function of prior knowledge.[3]

Understanding the core ideas introduced in chemistry education involves engagement with their representations and the associated phenomena.[4] Johnstone[5,6] was the first to propose three levels of representation of scientific concepts and processes: (1) macroscopic (e.g., chemistry experiments), (2) submicroscopic (e.g., molecular models) and (3) symbolic (e.g., chemical formulae). The three types of representations relate to phenomena perceived through our senses and support explanations at qualitative and quantitative levels.[4] Students often struggle with understanding and using the triplet concept. 3D models of molecules represent the submicroscopic representation,

the use of which is important to bridge the gap between the macroscopic and symbolic levels.[7]

Kozma and Russell[8] defined representational competence in science education as a set of five distinct abilities of students: to analyze the features of representations, transform between representations, create new representations, explain the usefulness of representations, and explain the advantages of representations. Activities aimed at improving representational competence support spatial thinking[9] which is critical for understanding 3D spatial concepts in STEM (science, technology, engineering and mathematics) disciplines.[10]

The use of physical and virtual molecular models promotes representational competence[11–13] and fosters spatial understanding,[14] although the impact of spatial ability on success is influenced by learning strategy and task demands.[15] Students who used models were more likely to implement new concepts, transform from 2D to 3D representations, and answer visual-spatial tasks. In the past, physical modeling kits with balls and sticks or magnets were used to construct 3D analog models of chemical compounds.[16–18] Later, molecular modeling software brought chemical visualizations into the digital virtual realm.[19–21] Since then, numerous stand-alone and web-based applications for viewing and manipulating chemical structures have become available, such as, ArgusLab, Avogadro, BALLView, Biovia discovery studio visualizer, Chime, Chimera, JME molecular editor, Jmol/JSmol, Oscail X, Pymol, RasMol, Spartan, SwissPDB Viewer, Tinker, Chemis 3D Molecular Viewer Applet, VMD, Yasara, and others.[20,22–26]

Some reported course activities and research involved the construction or use of physical models by students.[27–32] Thayban et al.[33] found that virtual models were more effective than physical model in learning symmetry. On the other hand, the use of physical or virtual molecular models was found to assist students in solving chemistry problems that require spatial thinking.[34]

Studies at all levels of chemistry education indicate that in order to construct correct mental models of chemical compounds, students should be engaged in constructing and manipulating three-dimensional (3D) visualizations.[35,36] The construction of submicroscopic models is part of representational competencies.

Kelly and Akaygun[37] suggested that visualizations are too often used only as a method of direct instruction. Instead of being passive observers students should become interactive participants and critical thinkers. In a survey[38] that was part of the workshop for molecular visualization in science education researchers, educators, and software developers discussed the role of molecular modeling in college chemistry and were asked about the features of molecular representation and the types of interactions with molecular visualization that most help students. The responses suggested that students should be able to create their own visualizations and interact with existing ones.

In some reported course activities, students were using molecular modeling software. Some of the advantages over physical modeling are flexibility in model building, switching between different representations, and accuracy of structural representations.[39] According to Kozma,[8] the construction, calculations and manipulation of molecular models support the laboratory practice of synthesis by looking at reaction sites and speculating on reaction mechanisms. Clauss and Nelsen[40] used WebMo and Gaussian to teach students the fundamentals of computational chemistry by performing *ab initio* and DFT (density functional theory) calculations in an undergraduate laboratory course with the goal of gaining a deeper understanding of their experimental work. Linenberger et al.[41] conducted a guided experiment using the student version of Spartan to discover the relationship between structure and molecular properties, e.g., through measurements, calculating dipole moments, and studying electron density potential maps and molecular shapes. Raiyn and Rayan[42] reported on the impact of a workshop using ChemDraw in a college chemistry course that significantly improved students' understanding of 3D structure and polarity, boiling point, and isomerism. Rothe & Zygmunt[43] used Gauss View 5 and Gaussian in an undergraduate chemical reaction engineering course to promote understanding of the relationship between molecular properties and macroscopic concepts such as internal energy, enthalpy, rate constants, and activation energies. In a web-based chemistry course, Dori et al.[44] gave first-year students the task of using Weblab and IsisDraw to create molecular models, calculate molecular weight, and construct the hybridization and electric charge distribution of carbon atoms. On the posttest, which required higher-order thinking skills, the experimental students showed better reasoning skills and a better ability to transfer between levels of representation than the control group. Ealy[45] introduced molecular modeling using Spartan Pro to a general chemistry laboratory. Students performed measurements and investigated properties such as symmetry, electrostatic potential, and dipole. The experimental group performed significantly better than the control group, and the test results at the end of the semester also showed that a transfer of knowledge had occurred. In an ethnographic study by Kozma,[46] students who first conducted experiments in the laboratory and then constructed molecular models using Spartan. When using the computer modeling software, students referred to chemical concepts (e.g., atoms, bonds, electronegativity, dipole moment) more frequently than in the laboratory session. Yet, they did not relate the models to the materials they synthesized. Molecular modeling was used by pre-service teachers in combination with classroom materials and mind map tools to learn hydrogen bond.[47] Kolar et al.[48] suggested the didactic use of computational chemistry to create models of amides to illustrate acid-base properties. Winfield et al.[49] have developed activities that incorporate model building in the iSpartan

tool to teach conformations of alkanes. Similarly, Johnson et al.[50] reported integrating of iSpartan into the classical organic chemistry laboratory experiment to help students learn about the stability of alkenes. Conformational analysis of small molecules using Vega ZZ software was used by Soulère[51] in an undergraduate chemistry course.

User-friendliness of graphical interfaces to optimize small and medium sized molecules has enabled the possibility to introduce computational chemistry tools to the undergraduate level.[52] Rodriguez-Becerra et al.[53] described the use of educational computational tools on pre-service chemistry teachers, with Avogadro used for model building.

Due to the identified deficiency in educational use of molecular modeling in chemistry classes by teachers and/or students,[54] molecular modeling was introduced into chemistry education by Aksela et al.,[55] developing pedagogical solutions, training mentors, creating teaching materials and investigating their effectiveness. The modeling approach was adopted by schools and the experiences were shared in a book.[56] The Edumol.fi web application was used.[57]

1. 2. Tools for Building Molecular Models in Teaching Organic Chemistry

At the beginning of this study, we analyzed existing molecular modeling tools for teaching organic chemistry at the university undergraduate level in order to select the most appropriate tool to serve as the basis for the development of a new tool, *3DChemMol* molecular editor.[58] Its editing functionality and help tools are described and evaluated in this article.

Some of the external factors influencing the potential for wider adoption of molecular visualization tools for teaching and active learning could be their suitability for a particular level of education (primary/secondary and college), their focus (small molecules, macromolecules, crystal structures), the presence of editing feature (molecular modeling), functionalities (display of properties), and their cost and convenience. The degree of complexity and the usability of the user interface could also play a role. With the advent of web-based technologies (HTML5, CSS, WebGL, canvases, and the use of JavaScript), there has been a shift from standalone applications and web applications requiring plug-ins to readily available web-based tools.[59] In terms of availability, molecular modeling tools have been developed that are open source.[60] In this study we focus on the software that is suitable for education, focuses on small molecules, allows molecular modeling and is freely available. Some of the tools are compared in Table 1. Due to immediate availability, we limited our choice to web-based applications that do not require installation. These criteria exclude tools such as *Spartan*[20] (proprietary, standalone), *Web Doodle Web Components*[61] (proprietary, web-based), *Avogadro*[62] and *Jmol*[63] (free, standalone), leaving us with mainly web-based tools. We also excluded web tools that are viewers only (e.g. *3dmol.js*[64]) or those that involve creating a 3D model by drawing a 2D structure (e.g. *MolView*[65]). The remaining web-based interfaces were based on *JSmol*,[66] a web version of *Jmol*. They included interfaces for the creation of 3D models: *CheMagic*,[67] *MolCalc*[68] and *3DChemMol*.[58] The latter was developed by the first author of this study. The original *JSmol* editing module is menu-based, cumbersome to use, and lacks a functional undo and help function. *CheMagic* has implemented both, but the functionalities of the tool (as in *JSmol*) are all visible at once, which can be distracting if you are only focused on editing. *MolCalc's* editing feature creates the input for the computational software. It is simple and efficient but uses only basic editing functions. *3DChemMol* was designed to structure the *JSmol* functionalities into multiple toolbars accessible from the main menu, including editing, with additional interactive functions with toolbars for model exploration (e.g., electronegativity, measurement, symmetry, creating conformations and isomers, model comparison, and exercises). It was chosen for our study because the new editing interface is intended to resemble that of familiar 2D editing tools.

1. 3. Motivation and Aims of the Study

The aim of this study was to evaluate the newly developed *3DChemMol* molecular editor tool and to investigate university students' first encounter with a 3D structure editing tool while performing three specific activities

Table 1: Characteristics of selected freely available user interfaces for 3D model building

Tool name	Type	Technology	GUI elements	Characteristics
Avogadro	S	C++, Qt	Menus, toolbars, dialogs	Editing dialog, mode switching for rotation
Jmol	S	Java	Menus, toolbar, dialogs	Editing menu on right click
JSmol (original)	W	JavaScript, JQuery	Menus (right click)	Editing menu on right click
CheMagic (JSmol)	W	JavaScript, JQuery	Dashboard buttons	All tool functionalities at once, editing buttons, undo, help
MolCalc (JSmol)	W	JavaScript, JQuery	Buttons	Basic editing (adding, deleting), input for computational software
3DChemMol (JSmol)	W	JavaScript, JQuery	Menus, toolbars	Editing toolbar, undo, help

Types: S = standalone, W = web-based

for creating and editing molecular models. The research questions were as follows:

- RQ1: How successful were students in performing simple chemistry activities using the *3DChemMol* molecular editor, and how was their success related to the time required and the perceived difficulty of the activity?
- RQ2: What types of difficulties did students encounter when performing activities with *3DChemMol* molecular editor? What was the cause and a possible remedy?
- RQ3: How did students use the different types of help available in *3DChemMol* molecular editor and additional support when they encountered problems?

2. Methods

2. 1. Participants

A total of 54 students of the University of Ljubljana participated in the study. They were enrolled in the second year of study (aged 20 to 21) at the Faculty of Education (17 students, 31.5%) or the Faculty of Health (37 students, 68.5%) in the study year 2020/21. They had already taken basic chemistry courses in general and inorganic chemistry; therefore, basic knowledge and understanding of chemistry principles and basic ICT skills were assumed. Introduction to building 3D models of chemical compounds was designed as a foundation for organic chemistry and other higher level chemistry courses that follow in their program of study. Apart from the field of study, there were no additional differences between the groups, important for the purpose of this research.

2. 2. Materials

2. 2. 1. Model Building Tool

The editing module of the web-based tool *3DChemMol* molecular editor (http://www2.arnes.si/~supddoln/3dchemmol), previously created by the author of this study,[58] was used to construct the molecular models. The tool is based on *JSmol* software for visualization and editing of 3D molecular models. Model creation is performed in 3D using a graphical user interface consisting of the model window and toolbar (Figure 1). The tool contains basic model building functionalities, but also some advanced features that allow the creation of different conformations and isomers.

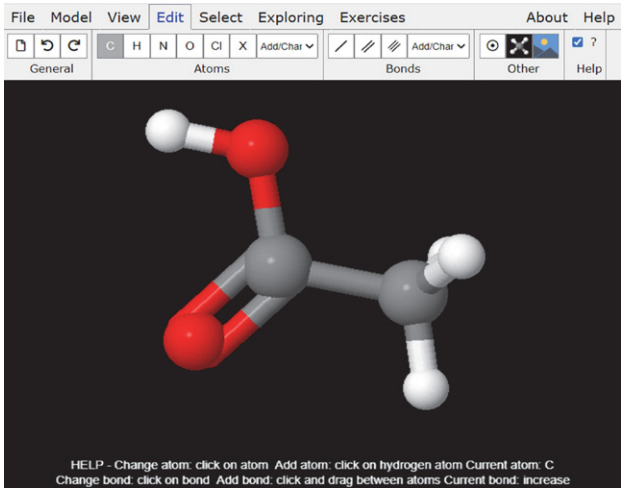

Figure 1: User interface of the *3DChemMol* molecular editor

The available model interactions (e.g., clicking or dragging on atoms/bonds) depend on the current action mode. There are four atom action modes (add/edit, delete, move, invert-substitute switch) and three bond action modes (add/edit, delete, rotate around bond). Switching between action modes is done by selecting a mode from the list.

One of the additional elements implemented in the tool is the Undo/Redo function, which did not work in the original *JSmol* application.

Four types of help are integrated and available at all times: a) status indicator of the currently available action mode, displayed at the bottom of the model window (optional), b) explanations of button actions when hovering the mouse over them, c) help menu with image and text explanations of the toolbar, d) video tutorial with examples of structure building, also available from the help menu.

One of the standard functions of model building is geometry optimization. The tool also allows to quickly create an image from the model window.

2. 2. 2. Problem Set

Three simple activities were designed to guide students in building and editing models using our tool. Each activity required students to create or edit a specific molecule with a limited number of actions.

- Activity 1: Build a simple model of the molecule – butanoic acid (new model, add/change atoms, change bond type). This activity did not require any change in action mode – all the functions needed to build a model were already present.
- Activity 2: Convert from one to two models of the molecules – hexane to ethene and butane (delete bonds, delete atoms, manually add hydrogen atoms, change bond type).
- Activity 3: Convert from a non-cyclic to a cyclic model of the molecule – glucose (add bonds, rotate branches around a bond, change bond type).

The full list of steps for each activity can be found in Table 2. All activities included common features such as changing the bond type (with some differences) and automatic geometry optimization. At the end of each activity, students had to create an image of the final model of the molecule. Time for each activity was not limited.

Some steps required a simple click on a toolbar button, while others required direct interaction with the model or a combination of both (Table 2). The model interactions available depended on the current action modes.

Table 2: Steps for each activity with the required interaction with the toolbar and the 3D model

		Interaction with the toolbar			Interaction with the 3D model		
Step #	**Step content**	**Button click**	**Type change**	**Mode change**	**Atom click**	**Atom drag**	**Bond click**
Activity 1: Building a simple model of the molecule							
1	New model	x					
2	Adding C atoms				x		
3	Adding heteroatoms		x		x		
4	Changing the bond type						x
5	Model centering	x					
6	Geometry optimization	x					
7	Creating an image	x					
Activity 2: Converting one model into two models of the molecules							
1	Deleting bonds			x			x
2	Changing the bond type		x				x
3	Deleting atoms			x	x		
4	Adding hydrogen (manually)		x	x		x	
5	Geometry optimization	x					
6	Creating an image	x					
Activity 3: Converting from a non-cyclic to a cyclic form of the molecule							
1	Adding a bond					x	
2	Changing the bond type						x
3	Geometry optimization	x					
4	Rotating a branch around the bond			x			x
5	Geometry optimization	x					
6	Creating an image	x					

For each activity, students were provided with the editing tool interface, which contained the initial model on the left half of the screen and activity instructions in Google Forms on the right half (Figure 2). The activity instructions consisted of a) general information about the availability of free model rotation, undo/redo functions, and various types of help; b) an image of the 3D output model (which was also displayed in the interface); c) a

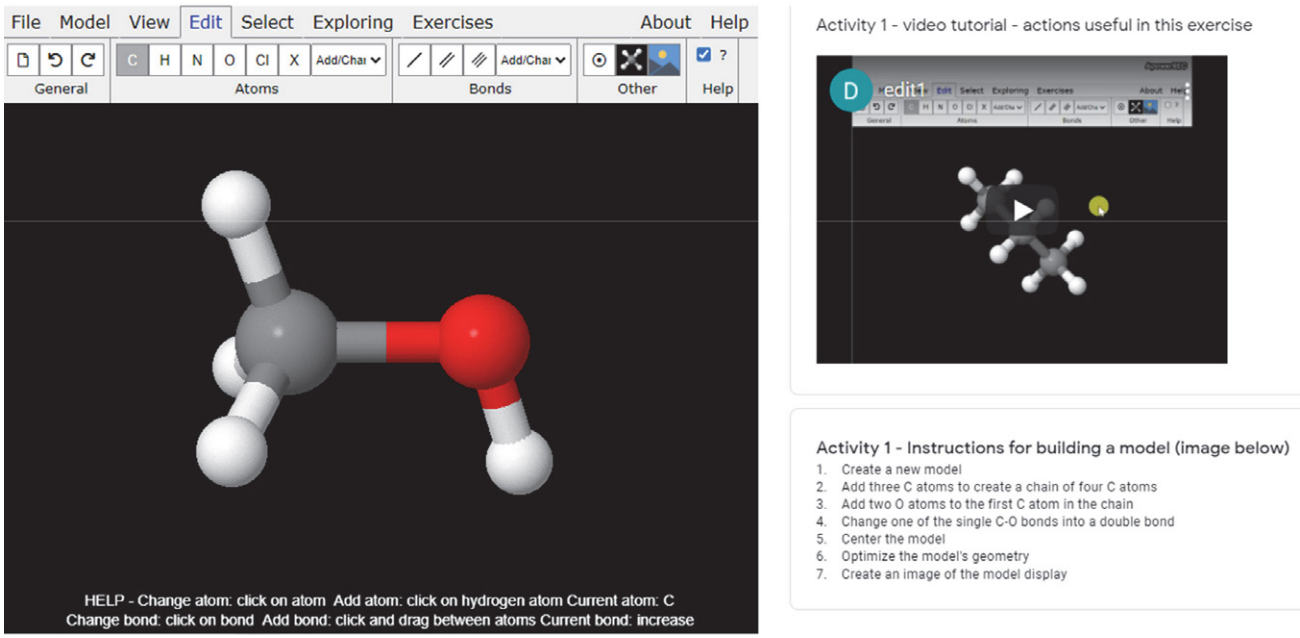

Figure 2: Activity display for the first activity (left: interface for model building, right: activity instructions)

short, annotated video tutorial explaining relevant actions on another example model; d) step-by-step instructions on how to build the target model, which referred to individual actions rather than elements of the interface; e) an image of the 3D target model. Students could scroll up and down through the instructions.

2. 2. 3. Students' Self-evaluation Questionnaires

For each activity, a self-evaluation questionnaire was included at the end of the activity instructions (Google Forms) with the following items/questions:

- degree of activity completion – completion level (Likert scale 1–5: 1 = started, 5 = fully completed);
- time spent on the activity (in minutes, as reported by students);
- perception of activity difficulty – perceived difficulty level (Likert scale 1–5: 1 = easy, 5 = difficult);
- type(s) of help used (multiple choice: a) video tutorial (single view), b) video tutorial (multiple views), c) hover on toolbar, d) current action status, e) help menu);
- other actions used (multiple choice: a) free view rotation, b) undo, c) redo, d) restart activity);
- severity of difficulties encountered for each step of the activity – step difficulty level (Likert scale 1–5: 1 = no difficulties, 5 = severe difficulties);
- difficulty description (text).

Prior to the study, two researchers (the co-authors of the study) optimized the instrument by performing a face validity[69] check. They completed the suggested activities and reviewed the questionnaires and then suggested changes and adjustments.

2. 3. Data Collection

The testing was conducted in May 2021 and was supervised by the authors in an online format. The Zoom videoconferencing tool and a web browser were used to display the tool and instructions with the questionnaires. Students consented to data analysis.

Prior to testing, a standardized introductory protocol was used that included clarification of purpose, instructions, voluntary participation, and acknowledgement of participation. The research was approved by the competent authorities of University of Ljubljana. None of the students had any prior experience with the tool. The teacher first gave a general introduction/demonstration of the entire *3DChemMol* molecular editor. Students had access to the interface. Students were then given links to the activities. After completing each activity, they completed the questionnaire and moved on to the next activity.

2. 4. Data Analysis

Data from the students' self-evaluation questionnaires were collected in Google Spreadsheets and transferred to Excel and Statistical Package for the Social Sciences (SPSS), version 26 for analysis, which was performed for each of the three activities.

- Mean scores were calculated for continuous and ordinal questionnaire items, including completion level, time spent, perceived activity difficulty level, and step difficulty levels. Step difficulty mean was also calculated for each activity. The two multiple-choice questions (type of help used, other items used) were transformed into multiple dichotomous variables, one for each response (1 if the response was selected and 0 if it was not). Means were calculated for each response.
- The distributions of the variables were examined using the frequency of the results expressed as a percentage of students. This was done for ordinal items and multiple-choice responses, and also for time spent on activity, where scores were first divided into five groups.
- Correlations between parameters were calculated using Spearman correlation coefficient (r_s).
- The open-ended questions from the student self-evaluation questionnaires were also recorded in Google Spreadsheets and transferred to Excel. The students' responses were coded using a coding table. The coding table was derived from a qualitative analysis of 20% of the questionnaires (n = 11 participants); the reliability of the coding was ensured by independent coding by two researchers (the authors of this article). Finally, both evaluations were contrasted at the points where differences occurred and, after consideration, the more appropriate one was selected. Altogether, 99% reliability was achieved.

3. Results and Discussion

3. 1. Completion Level of the Activities

Completion level of the activities was measured by the self-evaluation questionnaire. For each activity, the time spent on the activity and the perceived level of difficulty were also reported.

3. 1. 1. Means and Distributions

Students were relatively successful in completing the simple chemistry activities, as measured on a Likert scale of 1 to 5. The average score was above 4 for all 3 activities (Figure 3). For the first two activities, the completion level was very high with 91 and 96% of students reporting that they completed the activity, compared to only 53% for the third activity (Figure 4).

The completion time, measured in minutes, showed that the majority of students took between 3 and 5 minutes for each of the first two activities, while most students took 6–10 minutes for the last activity (Figure 5), with a significantly higher mean (Figure 3).

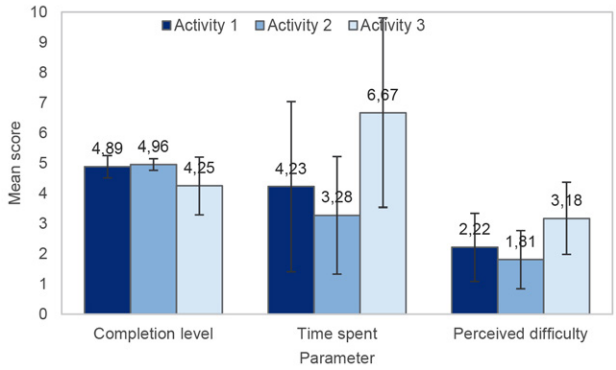

Figure 3: Mean scores with SD (whiskers) by activity for activity completion level (1–5), time spent on activity (min), and perceived activity difficulty (1–5)

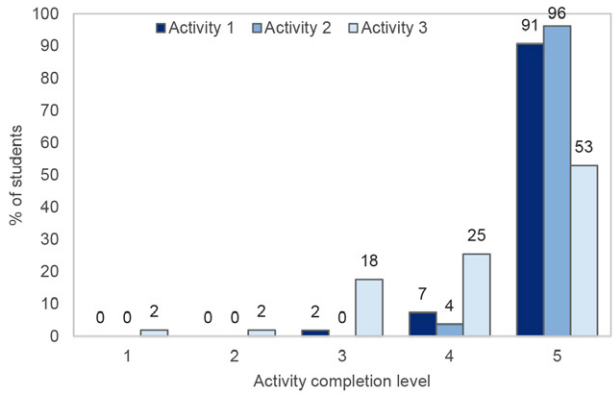

Figure 4: Distribution of activity completion levels by activity (5 = fully completed)

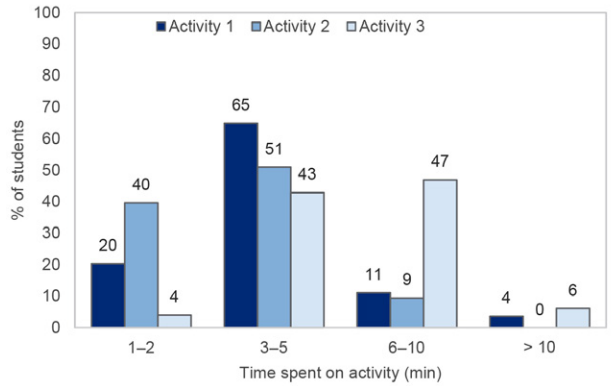

Figure 5: Distribution of time spent on activity by activity

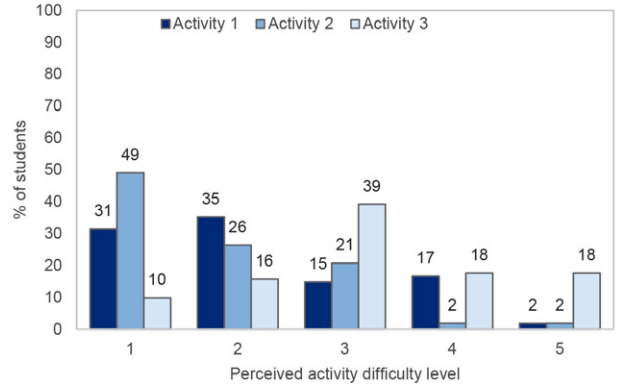

Figure 6: Distribution of perceived activity difficulty by activity (5 = difficult)

Perceived difficulty, expressed on a Likert scale of 1–5 (5 being difficult), showed that the second activity was considered the easiest with a mean of 1.81, and the third activity was considered the most difficult, with a mean of 3.18 (Figure 3). The most common response for activity 1 was difficulty level 2, for activity 2 was difficulty level 1, and for activity 3 was difficulty level 3 (Figure 6).

3. 1. 2. Correlations

No significant correlation was found between time spent and activity completion (Table 3). Some students took more time, but still completed the activity. An example is a comment on activity 1: "I had trouble adding atoms at first but figured it out after a few minutes." As expected, time spent correlated positively with perceived difficulty (most strongly for the second – overall easiest activity). Students who spent more time on the activity perceived it to be more difficult. The negative correlation between completion and perceived difficulty was significant for the third – the hardest overall activity – suggesting that students who did not complete the activity perceived it to be more difficult. For example, a student's comment was: "It is difficult to have spatial orientation." The lower correlation between perceived difficulty and completion level for the first two activities was due to the high completion levels for these activities. Similar correlations between perceived difficulty as a determinant of Web search performance and time have been found in a study by Kim.[70]

Table 3: Spearman correlations between completion level (Compl.), time spent (Time) and perceived difficulty of activities (Perc. diff.)

Param.	Compl.	Time	Perc. diff.
Activity 1: Building a simple model of the molecule			
Compl.	1.000		
Time	–0.069	1.000	
Perc. diff.	–0.239	0.404[b]	1.000
Activity 2: Converting one model into two models of the molecules			
Compl.	1.000		
Time	–0.081	1.000	
Perc. diff.	–0.266	0.584[b]	1.000
Activity 3: Converting from a non-cyclic to a cyclic form of the molecule			
Compl.	1.000		
Time	–0.158	1.000	
Perc. diff.	–0.469[b]	0.435[b]	1.000

[b] $p < 0.01$

3. 2. Difficulties During the Activities

3. 2. 1. Mean Scores by Activity

The step difficulty mean for each activity reflects the average amount of difficulties students encountered during steps of an activity. The scores (Figure 7) show the same trend as the time spent and perceived difficulty of the activities (Figure 3). Students reported the greatest step difficulty mean on the third activity and the smallest on the second activity. Means ranged from 1.62 to 1.91, which is relatively low given the Likert scale of 1 and 5. For all activities, some students specifically stated: "No problems," and several others made no comment. Mean scores are low due to the proportion of steps that are not problematic and those that are less problematic. Examples of repeated comments in all activities related to some technical difficulties were: "I can't save the image."

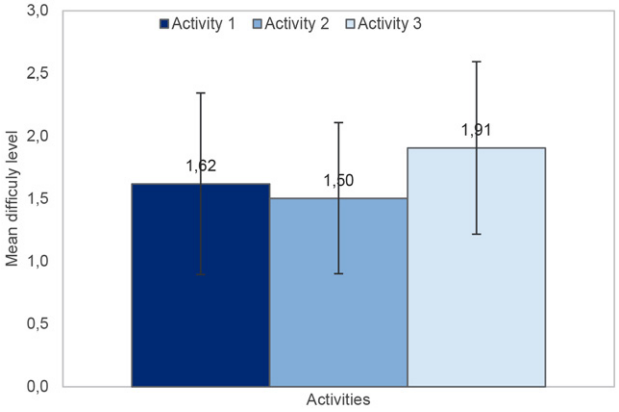

Figure 7: Step difficulty mean with SD (whiskers) by activity (1 = no difficulties, 5 = severe difficulties)

3. 2. 2. Mean Scores by Interaction Type

In the previous section the steps were grouped by activities. Here we grouped steps in multiple ways and calculated step difficulty mean for each group. The grouping in Table 4 by type of interaction shows that bond interactions caused more difficulties than atom interactions. Toolbar interactions with button click were the least problematic.

Table 4: Step difficulty mean by interaction type

Interaction type	Step diff. mean
Toolbar button click	1.48
Atom interaction	1.76
Bond interaction	1.86

Steps with atom and bond interactions were also classified into four groups (Table 5). Actions that required selection of the atom or bond type on a toolbar button prior to direct interaction with the model caused fewer difficulties than those that did not require a preceding action on the toolbar. On average, the most difficult actions were those that required a change of action mode (selection on the toolbar from a list of modes, e.g., add/change, delete). The action requiring a combination of type and mode change was also deemed more difficult.

Table 5: Step difficulty means for direct interaction with the model, depending on the preceding action

Preceding action	Step diff. mean
Button type change	1.54
No action	1.80
Button mode change	1.95
Button type + mode change	1.98

Another classification of steps was applied to direct interactions with atoms and bonds: clicking, dragging and repeated actions (Table 6). Repeated mouse clicking caused the most difficulties, followed by mouse dragging. A single mouse click on a bond or on atom was the least problematic. Repeated clicking was related to geometry changes in our case.

Table 6: Step difficulty means in direct interaction with the model, depending on the type of mouse interaction and repetition

Direct interaction type	Step diff. mean
Mouse click	1.58
Mouse drag	2.07
Mouse click + repetition	2.90

The last grouping of atom and bond interactions concerned geometry change (Table 7). The fewest difficulties arose from automatic geometry optimization. No direct interaction with the model was required. Actions where no significant geometry change occurred (nothing added, no automatic hydrogen adjustment) were considered less problematic. The most difficulties occurred when the geometry was changed, highlighting the importance of spatial abilities.

Table 7: Step difficulty means when interacting directly with the model, depending on the type of geometry change

Type of geometry change	Step diff. mean
Geometry optimization	1.35
Small geometry change	1.59
Significant geometry change	1.96

3. 2. 3. Scores by Step

Step difficulty levels for each step of the three activities, presented in Table 8, were ranked from 1 (easiest) to 18 (most problematic). Scores for individual steps ranged between 1.21 and 2.90. Total step difficulty mean was 1.66.

Activity 1: Building a model of butanoic acid. The easiest steps involved two actions available through a simple button click: creating a new structure (ranked 4 out of 18) and geometry optimization (ranked 5). Moderate difficulties were encountered in adding C atoms (rank 9) to build the main skeleton of the structure. This step is crucial. Some of the students reported difficulties, such as: "When clicking with the mouse, an atom was deleted instead of added." This was because the mouse was moved when clicking on a hydrogen atom. Instead, the "drag" event was registered, which in *Jmol* is associated with deleting an atom when applied to a hydrogen atom. Comments also related to adding heteroatoms (rank 13): "I can't position the chain as it is shown in the result." and "Sometimes atoms are added in strange ways." Another comment: "In the beginning, I had a lot of problems with adding atoms unevenly." Students were paying attention to structure but not configuration. Adding and replacing atoms only required clicking on existing atoms. There was not much chance for error, so "strange ways" and "unevenly" likely refers to configurations that result in isomers of the target structure. In this first activity, students have not yet learned how to make configuration changes. Adding atoms correctly required good spatial orientation. There were some difficulties with centering the model (ranked 12). Comment: "I had trouble centering the model until I found the centering button. It would be beneficial if centering was automatic because centering has to be applied repeatedly when building larger structures." This difficulty could have to do with familiarity with the center button, but students also forgot that they could not only rotate the model during model construction but also zoom it out. The zoom button was not part of the editing toolbar, but was an available mouse shortcut (mouse wheel). Surprisingly, most of the difficulties with this activity occurred when it came to changing the bond type (ranked 15), which should be quite simple by just clicking on a bond to increase its order. Increasing the bond order was not included as a toolbar button but was part of the default add/delete action mode. There was no need to change the action mode. The comment "The number of hydrogens doesn't automatically adjust." suggests that students tried to use a different method where they selected the bond type and clicked on a bond. This process does not currently adjust the hydrogens. Students did not know the shortcut even though it was shown in the introductory video. The two methods should be made compatible. Creating an image (ranked 14) also caused difficulties for some students, as expressed in a comment: "I can't convert to an image. Numbers appear instead." The reason here was that some system configurations automatically generated a text file with the structure in mol format

Table 8: Steps for each activity with interaction types, step difficulty levels and ranks

Step #	Step content	Button, atom, bond	Type, mode chg .	Mouse click, drag, rep.	Geom. chg.	Inter. type*	Step diff. level	Step diff. rank
Activity 1: Building a simple model of the molecule								
1	New model	c				c	1.44	4
2	Adding C atoms	a	–	k	y	a	1.52	9
3	Adding heteroatoms	a	t	k	y	t+a	1.67	13
4	Changing the bond type	b	–	k	y	b	1.93	15
5	Model centering	c				c	1.63	12
6	Geometry optimization	c			g	c	1.46	5
7	Creating an image	c				c	1.69	14
Activity 2: Converting one model into two models of the molecules								
1	Deleting bonds	b	m	k	n	m+b	1.49	8
2	Changing the bond type	b	t	k	n	t+b	1.40	3
3	Deleting atoms	a	m	k	n	m+a	1.47	6
4	Adding hydrogen	a	tm	d	n	tm+ad	1.98	16
5	Geometry optimization	c			g	c	1.21	1
6	Creating an image	c				c	1.47	7
Activity 3: Converting from a non-cyclic to a cyclic form of the molecule								
1	Adding a bond	a	–	d	y	ad	2.16	17
2	Changing the bond type	b	–	k	y	b	1.57	11
4	Rotating a branch	b	m	kr	y	m+br	2.90	18
3&5	Geometry optimization	c			g	c	1.37	2
6	Creating an image	c				c	1.53	10

* Key to interaction types: c – toolbar button click, a – atom interaction, b – bond interaction, t – button type change, m – button mode change, k – mouse click, d – mouse drag, r – repetition, g – geometry optimization, n – small geometry change, y – significant geometry change

instead of the image file. This technical issue needs to be addressed and fixed in the future. The issue mentioned in a comment: "I had no particular problems constructing the model, but the angles between atoms aren't the same." was either related to configuration or the student did not optimize the model geometry correctly. A comment from a student who reported no individual difficulties was: "The correct tool is not visible." In this case, the comment could refer to shortcuts built into the editor that are not explicitly visible in the toolbar (e.g., changing the bond type in general mode). This activity did not require any action mode changes but some students had expected them.

Activity 2: Splitting the model of hexane into models of butane and ethene (cracking). In this assignment, several students reported, "I had no problems." Geometry optimization and bond change were considered the easiest steps by students (ranked 1 and 3, respectively). Here, bond change was performed by first selecting the bond type from the toolbar (no shortcut used). This method did not automatically adjust the number of hydrogen atoms, but unlike the first activity, the subsequent steps were designed to solve this problem. Deleting atoms and bonds did not cause too many difficulties (rank 6 and 8), however, a student commented: "Problems switching between adding and deleting atoms." The reason is that the delete function is not immediately visible but is in a list of action modes in the toolbar. The most problematic part of the activity was the manual hydrogen addition (ranked 16). It consists of selecting the hydrogen atom type in the toolbar and then dragging out an existing atom with the mouse. A typical comment was: "Problems with adding the single H atom due to the fact that addition and modification appear together." As with the first activity, more than one action is available in Add/Change mode, depending on the type of interaction (click, drag), the object of interaction (atom, bond), and sometimes the type of atom (hydrogen, non-hydrogen). There is no separate button or selection on the toolbar for this action. As with the first activity, students may have been looking for a separate mode and could not find the button. Adding the H atoms by dragging was otherwise covered in the tutorial video and also shown in the action mode text help at the bottom of the screen. Interestingly, some of the difficulties were related to a functionality not being available. A student commented: "The button to move one of the models did not work, so I could only rotate the left model." The reason is that moving and rotating individual models is not possible in edit mode. Only the entire view can be rotated. This functionality could be incorporated in the future, as it is already present in other toolbars of this software. Image creation difficulties were not rated as severe (rank 7) for this activity, although the same technical obstacles were encountered. Comment: "I could not save the image, so I took a screenshot instead." Perhaps the severity changed or there were other novice difficulties saving the file in the first activity.

Activity 3: Converting the noncyclic form to a cyclic form of glucose. The only unproblematic action in this activity was geometry optimization (rank 2). Changing the bond type from double to single bond was perceived moderately difficult (rank 11). Some students remembered the shortcut from the first activity, others did not. A typical comment was: "I had a problem changing the bond." Creating an image was also still an issue (ranked

Table 9: Summary of the most frequent difficulties with example student comments

Act. #	Step #	Theme / Step	Category*	Possible issue	Step diff. rank**	Example student comment
1	2	Ading C atoms	a	Interface	9	"When clicking with the mouse, an atom was deleted instead of added."
	3	Adding heteroatoms	a	Spatial ability	13	"I can't position the chain as it is shown in the result."
	4	Changing the bond	b	Interface	15	"The number of hydrogens doesn't automatically adjust."
	5	Model centering	c	Interface	12	"I had trouble centering the model until I found the centering button."
	7	Creating an image	c	Technical	14	"I can't convert to an image. Numbers appear instead."
2	4	Adding hydrogen	a	Interface	16	„Problems with adding the single H atom due to the fact that addition and modification appear together."
3	1	Adding a bond	b	Interface	17	„I didn't know how to connect the O atom to the other side..."
	4	Rotating a branch	b	Spatial ability	18	"One of the groups was always oriented in the wrong direction." „It is difficult to have spatial orientation."

* Key to categories – interaction types: a – atom interaction, b – bond interaction, c – toolbar interaction

** Key to step difficulty rank: 1 = easiest, 18 = most difficult among all steps

10) to some, with a comment: "I couldn't save the image." Adding a bond between two existing atoms and especially rotating a branch around a bond were the two most problematic steps overall (ranked 17 and 18). The latter step had a difficulty of 2.9, which is one grade above the former step at 2.16. Some students did not know how to connect two atoms, as evident in a comment: "I didn't know how to connect the O atom to the other side and what the correct rotation was." or a comment: "Having trouble connecting the structure properly." Dragging was required in Add/Modify mode, so no mode change was required in this step and no toolbar button was available. The appropriate action was demonstrated in the tutorial video and shown in the action status help at the bottom of the screen. Perhaps the model itself was part of the problem. It needed to be properly oriented so that the atoms could be reached with the mouse. Good spatial orientation could be related to this action. This was even more evident when the branch was rotated, as a student wrote in a comment: "I couldn't get the model aligned the way it was in the picture. One of the groups was always oriented in the wrong direction." or another student "I couldn't place the atoms in the position shown in the resulting image." The branch rotations around the bond were done in 60-degree increments. Students had to determine the correct degree of rotation by applying (repeating) the action the appropriate number of times. Another comment "It is difficult to have spatial orientation." suggested that this activity required more spatial orientation than the first two activities. Comment, "It was difficult to begin the activity. Watching the tutorial video was crucial. Still, I had trouble rotating the bonds." The first sentence (beginning of the activity) refers to the bond addition. Although this activity proved to be the most difficult overall, four students indicated, "No problems." This is consistent with the research of Harle and Towns who noted that rotational transformations were among the tasks that students had particular difficulty with.[71]

The most typical themes and categories of students' difficulties that emerged from the above analysis are listed in Table 9. Of the eight themes, three each related to atom and bond manipulations and the remaining two to toolbar interaction. Two of the issues are probably related to the students' lack of spatial orientation, which could be improved through training. Another requires solving a technical issue. The rest could be possibly avoided/fixed by redesigning parts of the user interface (e.g. even more visible action status, separation of actions that are too similar, separate buttons instead of mode selection).

3. 2. 4. Correlations

There are significant correlations between most steps within an activity in terms of difficulties (Tables 10–12). Mean of step difficulties is included as step mean. In the

Table 10: Spearman correlations between step difficulty levels within Activity 1

Step	Description	Step 1	2	3	4	5	6	7	Step mean
1	New model	1.000							
2	Adding C atoms	0.620[b]	1.000						
3	Adding heteroatoms	0.479[b]	0.646[b]	1.000					
4	Changing the bond type	0.441[b]	0.508[b]	0.482[b]	1.000				
5	Model centering	0.408[b]	0.473[b]	0.414[b]	0.505[b]	1.000			
6	Geometry optimization	0.426[b]	0.587[b]	0.392[b]	0.343[a]	0.718[b]	1.000		
7	Creating an image	0.272[a]	0.408[b]	0.255	0.238	0.281[a]	0.506[b]	1.000	
	Step mean	0.629[b]	0.690[b]	0.625[b]	0.752[b]	0.690[b]	0.631[b]	0.568[b]	1.000

[a] $p < 0.05$, [b] $p < 0.01$

Table 11: Spearman correlations between step difficulty levels within Activity 2

Step	Description	Step 1	2	3	4	5	6	Step mean
1	Deleting bonds	1.000						
2	Changing the bond type	0.562[b]	1.000					
3	Deleting atoms	0.687[b]	0.740[b]	1.000				
4	Adding hydrogen	0.401[b]	0.283[a]	0.332[a]	1.000			
5	Geometry optimization	0.423[b]	0.672[b]	0.439[b]	0.351[a]	1.000		
6	Creating an image	0.185	0.313[a]	0.254	0.119	0.357[b]	1.000	
	Step mean	0.675[b]	0.657[b]	0.698[b]	0.765[b]	0.537[b]	0.474[b]	1.000

[a] $p < 0.05$, [b] $p < 0.01$

Table 12: Spearman correlations between step difficulty levels within Activity 3

Step	Description	Step 1	2	4	3 and 5	6	Step mean
1	Adding a bond	1.000					
2	Changing the bond type	0.350[a]	1.000				
4	Rotating a branch	0.276[a]	0.270	1.000			
3 and 5	Geometry optimization	0.285[a]	0.326[a]	0.086	1.000		
6	Creating an image	0.365[b]	0.169	0.037	0.331[a]	1.000	
Step mean		0.777[b]	0.579[b]	0.630[b]	0.501[b]	0.516[b]	1.000

[a]$p < 0.05$, [b]$p < 0.01$

final step – saving the image of the result – the correlations are not as strong, as the difficulties with image creation were largely a technical issue. Difficulties with rotating a branch around a bound (third activity) also do not correlate with all other steps of the activity, as many students had difficulties in this step.

3. 2. 5. Correlations with Completion Level of the Activities

The step difficulty mean for each activity correlated positively with time spent and perceived activity difficulty and negatively with activity completion (Table 13). The completion level for the second activity was very high, so the correlation with step difficulty mean was not significant.

3. 3. Help Tools Used During Activities

The forms of help available included the tutorial video, the help menu, the description of the toolbar button when the user hovers over it, and the description of the actions currently available on the structure (atom and bond actions). If students made mistakes, they could undo and

Table 13: Spearman correlations of step difficulty mean with completion level (Comp.), time spent (Time) and perceived activity difficulty (Perc. diff.)

Step	Description	Comp.	Time	Perc. diff.
Activity 1: Building a simple model of the molecule				
1	New model	–0.419[b]	0.421[b]	0.522[b]
2	Adding C atoms	–0.421[b]	0.422[b]	0.503[b]
3	Adding heteroatoms	–0.235	0.512[b]	0.553[b]
4	Changing the bond type	–0.135	0.503[b]	0.290[a]
5	Model centering	–0.231	0.585[b]	0.353[b]
6	Geometry optimization	–0.290[a]	0.458[b]	0.356[b]
7	Creating an image	–0.121	0.224	0.292[a]
Mean		–0.334[a]	0.620[b]	0.539[b]
Activity 2: Converting one model into two models of the molecules				
1	Deleting bonds	–0.305[a]	0.410[b]	0.307[a]
2	Changing the bond type	–0.341[a]	0.488[b]	0.518[b]
3	Deleting atoms	–0.296[a]	0.494[b]	0.492[b]
4	Adding hydrogen (manually)	–0.041	0.467[b]	0.496[b]
5	Geometry optimization	0.083	0.506[b]	0.428[b]
6	Creating an image	–0.152	0.205	0.276[a]
Mean		–0.215	0.558[b]	0.599[b]
Activity 3: Converting from a non-cyclic to a cyclic form of the molecule				
1	Adding a bond	–0.104	0.305[a]	0.280[a]
2	Changing the bond type	–0.333[a]	0.298[a]	0.344[a]
4	Rotating a branch	–0.445[b]	0.409[b]	0.468[b]
3 and 5	Geometry optimization	–0.115	0.203	0.236
6	Creating an image	–0.211	0.063	0.179
Mean		–0.424[b]	0.493[b]	0.508[b]

[a]$p < 0.05$, [b]$p < 0.01$

redo previous actions. They were free to rotate the models during the construction process. If none of the previous actions helped, they could restart the activity.

3. 3. 1. Distributions

Of the above actions with help tools, free rotation and the undo button were used by most students (70–94%) (Figure 8). The frequency of free rotation was lowest in the second activity because fewer configuration changes (deleting atoms and bonds as opposed to adding them) were made than in the other two activities. Nevertheless, 14% of students reported not rotating the model in the third activity, which involved a larger configuration change when adding a bond to form a ring, as well as rotating a branch around a bond. The number of students who used the undo feature increased by 20% in the third activity, as only 6% of students did without it. This indicates the importance of the undo function, which did not work in the original *JSmol* interface. Redo function was not used as frequently, although its use increased with each activity and one in four students used it by the third activity.

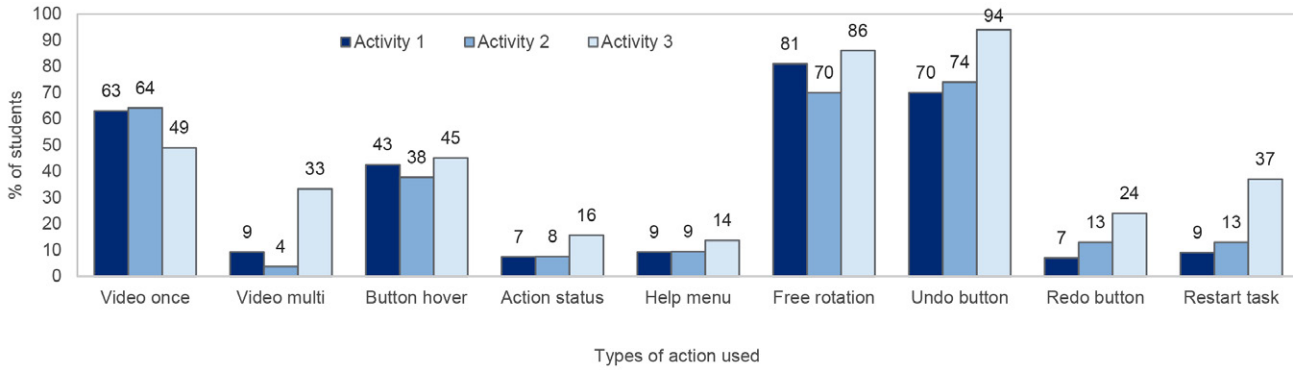

Figure 8: Distribution of actions with help tools by activity

The most commonly used type of help was watching the tutorial video once, followed by the mouse-over button action. About 30% of students reported not watching the video in the first two activities, but in the third activity, the number of multiple video viewings increased significantly: One in three students watched the video more than once, compared to 4–9% in the previous activities. An example of a student comment on this activity is: "Watching the tutorial video was crucial." The use of the mouse-over action was comparable in all three activities and was used by less than half of the students. The last two help options (action status and help menu) were used less frequently, increasing from less than 10% in the first two activities to about 15% in the last activity. This could mean that students were not confused about the current action status (work mode) or that they missed the textual status display at the bottom of the screen. Interestingly, they also made little use of the help menu, which could indicate that they found the video tutorials largely sufficient. This is consistent with the conclusion of a study by Van Der Meij,[72] in which video tutorials that previewed the training activities were the most effective for learning software. The help menu provided similar information to hovering over the buttons. Finally, the level of activity restarting was low (9%) for the first activity, indicating that building a new structure by adding atoms and changing bonds was not a problem, especially because the undo function was available. This value increased slightly in the second activity and significantly in the third activity. Nearly two out of five students estimated that they were too far off course compared to the target model or did not get close enough, so they started over. They were not discouraged and there was no time limit on the activity. In this activity, the importance of good spatial ability was probably most pronounced. Starting over was the chosen strategy.

3. 3. 2. Correlations

Interestingly, for all three activities, there was a significant negative correlation between using the video (once) and hovering buttons, suggesting that students who did not watch the video relied on hovering buttons in the toolbar (Table 14). No significant correlation with the four types of help was found for free rotation or the use of the undo button in any of the activities. This could mean that these two functionalities were used by all. In the first activity, the negative correlation with button hovering was also observed for multiple video views. There, the use of redo was positively associated with the help menu and negatively associated with watching the video once. In the second activity, use of the help menu was negatively correlated with viewing the video once, indicating that students for whom viewing the video once was sufficient did not use it. With the fewest geometry changes in this activity, students who used free rotation were less likely to use the undo button. In this way, the rotation helped. It is surprising that this was not the case in the third activity, where students could benefit from free rotation even more. There, use of the help menu correlated significantly with other types of help, aside from watching the video once. Students who

Table 14: Spearman correlations between actions with help tools

	Video once	Video multi	Button hover	Action status	Help menu	Free rotat.	Undo button	Redo button	Restart activity
Activity 1: Building a simple model of the molecule									
Video once	1.000								
Video multi	–0.416[b]	1.000							
Button hover	–0.270[a]	–0.275[a]	1.000						
Action status	0.071	–0.090	0.185	1.000					
Help menu	–0.152	–0.102	–0.017	–0.090	1.000				
Free rotat.	–0.168	0.152	0.218	0.135	–0.177	1.000			
Undo button	0.006	0.067	0.067	0.184	0.067	–0.205	1.000		
Redo button	–0.369[b]	–0.090	0.042	0.190	0.398[b]	0.135	0.029	1.000	
Restart activity	–0.020	0.118	0.242	0.154	0.118	0.152	0.207	–0.090	1.000
Activity 2: Transformation of one into two models of the molecules									
Video once	1.000								
Video multi	–0.058	1.000							
Button hover	–0.554[b]	–0.154	1.000						
Action status	–0.084	–0.057	0.072	1.000					
Help menu	–0.297[a]	–0.064	0.015	0.152	1.000				
Free rotat.	–0.149	0.130	0.258	0.188	–0.069	1.000			
Undo button	–0.002	–0.106	0.113	0.009	0.193	–0.301[a]	1.000		
Redo button	–0.057	–0.077	0.271[a]	0.100	0.255	0.135	0.234	1.000	
Restart activity	–0.057	–0.077	0.156	–0.111	0.065	0.014	0.107	0.012	1.000
Activity 3: Transformation from noncyclical to cyclical form of the molecule									
Video once	1.000								
Video multi	–0.610[b]	1.000							
Button hover	–0.337[a]	–0.139	1.000						
Action status	–0.099	0.038	0.259	1.000					
Help menu	–0.163	0.322[a]	0.326[a]	0.298[a]	1.000				
Free rotat.	–0.179	0.161	0.132	0.015	–0.006	1.000			
Undo button	0.078	0.177	–0.108	0.108	0.100	0.142	1.000		
Redo button	–0.174	0.098	0.333[a]	0.269	0.047	0.087	0.139	1.000	
Restart activity	–0.107	0.315[a]	0.198	0.002	0.282[a]	–0.164	0.020	0.146	1.000

[a]$p < 0.05$, [b]$p < 0.01$

needed help used all available types of help. Students who restarted the activity were also more likely to consult the help menu and watch the video multiple times.

3. 3. 3. Correlations with Completion Level of the Activities

For the first two activities, activity completion correlated negatively, and perceived difficulty correlated positively with help menu use (Table 15). Students who did not need to consult the help menu were more likely to complete the activity. Those who did consult the help menu perceived the activity to be more difficult. On the third activity, students who did not have to watch the instructional video multiple times were more likely to complete the activity. Multiple video viewings also correlated positively with perceived activity difficulty. It seems that consulting the static help menu did not help solve the easier activities and that the tutorial videos were not sufficient to solve the more difficult activities. One of the possible remedies would be to create help tutorials/videos for individual actions that students found particularly difficult, covering multiple examples. The use of undo correlated with time spent on the first two activities and redo did on the last two activities. Both also correlated positively with perceived difficulty – students who used them found the activities more difficult. With the third activity, the amount of time spent restarting was significantly higher, and these students were less likely to complete the activity they also perceived as more difficult. Starting over did not help enough.

3. 3. 4. Correlations with Difficulties by Activity

The difficulty level referenced is the average step difficulty for each activity (step difficulty mean). In the first activity, one video view seemed sufficient for students who reported fewer difficulties overall (Table 16). In the second

Table 15: Spearman correlations between actions with help tools and completion level (Comp.), time spent (Time) and perceived difficulty (Perc. diff.)

	Video once	Video multi	Button hover	Action status	Help menu	Free rotat.	Undo button	Redo button	Restart activity
Activity 1: Building a simple model of the molecule									
Comp.	0.286[a]	–0.114	0.022	0.090	–0.351[b]	0.024	–0.070	–0.149	–0.330[a]
Time	–0.114	0.079	0.062	–0.207	0.252	0.034	0.286[a]	0.078	0.033
Perc. diff.	–0.108	0.028	0.088	–0.161	0.293[a]	–0.008	0.205	0.033	0.101
Activity 2: Transformation of one into two models of the molecules									
Comp.	0.0584	0.039	–0.050	0.057	–0.275[a]	0.085	–0.119	–0.508[b]	–0.215
Time	–0.164	0.235	0.059	0.010	0.420[b]	–0.068	0.371[b]	0.336[a]	0.185
Perc. diff.	–0.106	0.266	0.122	0.129	0.351[b]	0.090	0.353[b]	0.502[b]	0.219
Activity 3: Transformation from noncyclical to cyclical form of the molecule									
Comp.	0.138	–0.419[b]	0.050	–0.084	–0.187	–0.187	–0.224	–0.228	–0.315[a]
Time	–0.185	0.165	0.308[a]	–0.006	0.371[b]	0.130	0.147	0.435[b]	0.349[a]
Perc. diff.	–0.195	0.391[b]	0.106	0.086	0.177	0.181	0.330[a]	0.379[b]	0.297[a]

[a]$p < 0.05$, [b]$p < 0.01$

activity, more difficulties likely resulted in multiple video views. On the third activity, no correlation was found between difficulty and video views. Difficulty level correlated positively with help menu use on the first two activities. This means that students who had difficulties were more likely to consult the help menu. In both activities where the action mode was changed (activities two and three), the difficulty level correlated with the use of the action status help. Students who had difficulties consulted this help. Hovering over buttons, free rotation, and restarting the activity did not significantly correlate with difficulty levels. For all activities, using the undo button, as well as the redo button, were positively correlated with problems.

was visible in the action mode description. Those who had difficulties changing the bond type also used the undo and redo buttons. Difficulties with centering the model correlated with the use of button hover, indicating difficulty in visually identifying the correct button. Students who used free rotation were less likely to have difficulties with geometry optimization.

Activity 2. The use of the help menu, as well as the use of the redo button, correlated with difficulty levels in this activity. The exception was manually adding hydrogen, the step that was perceived as the most difficult and, like the shortcut for changing the bond, was not explicitly shown in the toolbar. Undo was used most frequently with the

Table 16: Spearman correlations between actions with help tools and step difficulty mean

Activity no.	Video once	Video multi	Button hover	Action status	Help menu	Free rotat.	Undo button	Redo button	Restart activity
1	–0.278[a]	–0.012	0.238	0.117	0.313[a]	–0.068	0.336[a]	0.243	0.187
2	–0.186	0.287[a]	0.110	0.305[a]	0.357[b]	–0.191	0.331[a]	0.325[a]	0.151
3	–0.0724	0.169	0.026	0.299[a]	0.169	0.021	0.296[a]	0.313[a]	0.176

[a]$p < 0.05$, [b]$p < 0.01$

3. 3. 5. Correlations with Difficulties by Step

Activity 1. Consultation of the help menu correlated with step difficulty levels in almost all individual steps (Table 17). In general, students who had difficulties consulted the help menu. The exception was changing the bond type, where difficulties were inversely correlated with watching the video multiple times. Students who watched the video multiple times had fewer difficulties with this step. The shortcut for this step was not available in the toolbar but

manual hydrogen addition. In this activity, multiple video views correlated with difficulties changing bond type and deleting atoms. Students used multiple videos when they encountered these difficulties.

Activity 3. In contrast to the previous two activities, correlations between difficulty and help menu use were absent or low (not significant). For the two most difficult steps, bond addition and branch rotation, there was a low correlation with the use of action status and undo. Two problems were possibly associated with these steps:

Table 17: Spearman correlations between use of help tools and step difficulty level

Step	Video once	Video multi	Button hover	Action status	Help menu	Free rotat.	Undo button	Redo button	Restart activity
Activity 1: Building a simple model of the molecule									
1 New model	–0.005	–0.178	0.125	0.015	0.416[b]	0.014	0.090	0.294[a]	0.290[a]
2 Adding C atoms	–0.219	–0.047	0.040	–0.043	0.440[b]	–0.149	0.215	0.308[a]	0.122
3 Adding heteroat.	–0.298[a]	0.176	0.119	–0.065	0.303[a]	0.088	0.269	0.145	0.090
4 Chg. bond type	–0.196	–0.272[a]	0.237	0.158	0.247	–0.014	0.314[a]	0.334[a]	0.050
5 Model centering	–0.385[b]	–0.023	0.300[a]	–0.173	0.351[b]	–0.017	0.129	0.227	0.135
6 Geometry optim.	–0.192	–0.022	0.117	–0.158	0.520[b]	–0.292[a]	0.280[a]	0.158	0.129
7 Creating image	–0.048	–0.075	0.170	0.168	0.080	–0.310[a]	0.139	–0.018	0.115
Mean	–0.278[a]	–0.012	0.238	0.117	0.313[a]	–0.068	0.336[a]	0.243	0.187
Activity 2: Converting one model into two models of the molecules									
1 Deleting bonds	–0.132	0.120	0.181	0.140	0.272[a]	–0.203	0.158	0.433[b]	0.119
2 Chg. bond type	–0.151	0.390[b]	0.124	0.204	0.442[b]	–0.039	0.214	0.453[b]	0.127
3 Deleting atoms	–0.078	0.408[b]	0.120	0.121	0.381[b]	–0.203	0.192	0.329[a]	0.162
4 Adding hydrogen	–0.238	0.137	0.096	0.218	0.2548	–0.097	0.450[b]	0.118	0.046
5 Geometry optim.	–0.356[b]	0.218	0.098	0.098	0.427[b]	0.043	0.121	0.299[a]	0.129
6 Creating image	–0.2206	0.185	–0.104	0.243	0.328[a]	–0.122	–0.144	0.214	–0.187
Mean	–0.186	0.287[a]	0.110	0.305[a]	0.357[b]	–0.191	0.331[a]	0.325[a]	0.151
Activity 3: Converting from a non-cyclic to a cyclic form of the molecule									
1 Adding a bond	0.032	0.015	0.079	0.203	0.241	–0.096	0.259	0.106	0.059
2 Chg. bond type	–0.034	0.069	0.115	0.261	0.162	0.046	0.031	0.408[b]	0.130
4 Rotating a branch	0.015	0.198	–0.029	0.267	–0.022	0.152	0.228	0.293[a]	0.250
3,5 Geom. optim.	–0.394[b]	0.061	0.180	0.198	–0.034	0.070	0.123	0.315[a]	–0.185
6 Creating image	0.012	0.071	–0.350[a]	0.066	–0.196	–0.084	0.123	–0.050	–0.058
Mean	–0.0724	0.169	0.026	0.299[a]	0.169	0.021	0.296[a]	0.313[a]	0.176

[a]$p < 0.05$, [b]$p < 0.01$

recognizing the correct action and performing the action correctly. Action status could help with the first part. The tutorial video could help with the second part. Only for branch rotation difficulties was there a low correlation with multiple video views.

4. Conclusions and Implications for Teaching

The experience of undergraduate students in construction and editing of molecular models of small organic compounds aimed to equip them with the knowledge and ability to create their own presentations and to proceed with further exploration and analysis of model properties in chemistry courses beyond introductory chemistry. The success of the course also depends on the design of the course and the teacher, which would be worth of further study.

Manipulation of 3D molecular models has been associated with the development of representational skills, particularly when used to support learning.[12,13] Students of all ages encounter problems and misunderstandings when asked to explain chemical phenomena at the submicroscopic level.[73] Molecular modeling has long been used to support experimental work, and to teach fundamental concepts.[39] Previous studies have also shown that software usability, expressed as perceived meaningfulness and ease of use, has an impact on learning.[74] Spatial ability is another factor involved in learning science.[75] Its active promotion in college-level chemistry and biochemistry has increased, but not to the same extent as other cognitive skills.[76]

The *3DChemMol* molecular editor for building/editing 3D molecular models was used in the study. Features implemented in the user interface allowed for ease of use: a toolbar; separation of the editing function from other functions; the ability to undo and redo changes for multiple steps; various types of help, including video tutorials, button hovering, action status display, and help menu.

The *3DChemMol* molecular editor incorporating an editing toolbar was tested in a group of 54 university students using three model building/editing activities of varying difficulty: 1) building a simple model, 2) splitting a model into two, 3) creating a cyclic from a non-cyclic structure.

In relation with **first research question (RQ1)**, it was found that students were successful overall in using the tool and graphical interface and in completing the activities. They were excellent on the first two activities and good on the third activity. As expected, the more time they spent on an activity, the more difficult it appeared to them. When they were unable to complete the activity, they perceived it to be more difficult. No relationship was found between time spent and success rate.

As expected, the average step difficulty of the activity correlated inversely with activity completion and directly with perceived activity difficulty. The more difficulties students encountered, the more difficult the activity seemed to them; more difficulties also meant more time spent on the activity.

When it comes to the **second research question (RQ2)**, it was found that actions for direct model manipulation (atoms, bonds) caused more difficulties than using the toolbar buttons. There were more difficulties interacting with the model by dragging than by clicking. Steps that involved changing the model configuration or required changing the working mode of the interface were more problematic. It was also found that actions were perceived as easier if they were preceded by a clear mode change. This means that a lot of emphasis needs to be placed on displaying the state of the system so that the user is immediately aware of the actions available.

The most difficult individual actions reported were 1) rotating a branch around a bond, 2) adding a bond between two existing atoms, and 3) manually adding a hydrogen atom, but also 4) changing a bond type, 5) creating an image, and 6) adding heteroatoms. Issue #5 was technical in nature. Actions 2 and 3 involved dragging the mouse on or between model atoms. Issues 2–4 had a common denominator: the actions were not implicitly given in the toolbar but were available as part of the default add/change action mode, so students could not discover them without either watching the video tutorial or reading the available actions displayed at the bottom of the screen. Correct addition of bonds and heteroatoms probably requires good spatial orientation, which could be especially true for branch rotation. Action 1 required repeated clicking on a bond until a satisfactory configuration was achieved. The latter was done in 60-degree increments.

Difficulties related to the user interface will be addressed in future improvements of the tool, such as highlighting the action state or even separating actions. Difficulties related to spatial abilities could be mitigated by simple video tutorials and exercises focusing on a single issue.

Related to the **third research question (RQ3)**, the study indicated that among the four types of help provided, and regardless of reported difficulties, students most frequently watched video tutorials once or used hovering over buttons to indicate button meanings. Use of other forms of help increased only on the third activity, which was perceived as most difficult. Use of the multiple undo feature was high, indicating that it was absolutely necessary, and increased with activity difficulty. Similarly, free rotation compensated for the use of the undo function on the second activity. The most difficult and complex activity was found to have a relatively high rate of restarting the activity and re-watching the learning video.

When difficulties occurred, students most often used the help menu and the undo/redo actions. Use of the undo function increased for the most difficult steps. For activities/steps that required a mode change, more students consulted the action state that contained the correct answer. Individual activities were associated with multiple video views, with video views generally increasing on the most difficult activity. Mouse hovering over the toolbar was used more often when students could not visually identify the correct button. Sometimes the wrong type of help was consulted, such as button hovering (looking for an appropriate action) when no toolbar interaction was required. Reading the action status would have helped there. In other cases, consulting the action status did not contain the answer and the tutorial video should be watched. Negative correlations between difficulties and single video views may indicate that the video was a sufficient aid in activity completion for many students.

Despite using all the help available (multiple tutorial video views and restarting the activity), some students were not able to complete the most difficult activity. This could be related to the difficulty of the activity and the need for good spatial orientation and/or mean that the help menus and system status were not fully utilized.

Some of the lessons learned in this work, particularly the shortcomings of the user interface for editing, have already been implemented and further improvements are planned. Video tutorials became an important part of the help menu. Bond change methods will be unified so that they always include hydrogen adjustment. The toolbar will be upgraded with additional buttons, e.g., for actions that were part of the working modes but were not explicitly present. The action status display will be improved, and video tutorials for individual actions that proved most difficult will be added and immediately available. Alternative help display could be considered, e.g., when you hover over the model parts.

The **implications for teaching** of this study are multifaceted. Using the new tool, students successfully created 3D models with the help of video tutorials and various types of help. In general, the availability of tools is not yet sufficient for students to use them for learning. Their use must to be encouraged through pedagogical approaches. We suggest that the tool is suitable for direct instruction or self-study. Students can easily use this tool to visualize the structure of chemical compounds during their studies and create images of 3D models to include in their own products, such as seminar works, reports, and theses.

3DChemMol could also be used to improve students' development of chemistry knowledge and representation-

al skills. Some students may be afraid of special chemistry visualization software because they think it requires special skills. Because of its simplicity, even students who were not previously familiar with molecular modeling tools and may not have had experience drawing 3D representations or molecules can use it after studying short tutorials. Using *3DChemMol* allows students to construct molecular models to visualize the structure of compounds and understand their properties, rather than memorizing facts and writing about them.

The accessibility of the *3DChemMol* tool makes it easy to incorporate into various educational settings. The models created form the basis for further investigation and study of chemistry concepts through display of chemical properties. Teachers can use the tool directly in the classroom during lectures or prepare study materials for students in electronic or printed form. For example, visualizations created in *3DchemMol* can be part of lectures on various topics. Moreover, it can be used in students' individual work when they can check their understanding on new examples. Different levels of task difficulty can be accommodated in the tool by the teacher.

We are aware that our observational study has some limitations. One of them is the self-reporting nature of the questionnaires. Further insight into students' behavior and efficiency in building molecular models could be gained by using additional recording and analysis methods, such as eye-tracking, video recording during activity performance, and structured interviews afterwards. Another limitation was that the study was focused only on the editing feature of the tool. Future research could include experimental studies such as comparing the usability and effectiveness of other features of the tool (e.g. molecular property display and exploration), comparing it with other 2D and 3D model editing tools, and with building physical models, investigating correlations with other internal or external factors such as students' spatial skills, representational competence, chemistry knowledge and teaching methods. However, this is already beyond the scope of this study.

In further development of *3DChemMol* more interactive online tutorials and exercises tailored to specific chemistry courses could be prepared.

Acknowledgements

This study was co-financed by University of Ljubljana (grant no. 704-8/2016-229). The authors would like to thank all of the students who participated in the survey.

5. References

1. K. L. Vavra, V. Janjic-Watrich, K. Loerke, L. M. Phillips, S. P. Norris, J. Macnab, *Alta. Sci. Educ. J.* **2011**, *41*, 22–30.
2. I. Vekiri, *Educ. Psychol. Rev.* **2002**, *14*, 261–312. **DOI:**10.1023/A:1016064429161
3. S. R. Hinze, D. N. Rapp, V. M. Williamson, M. J. Shultz, G. Deslongchamps, K. C. Williamson, *Learn. Instr.* **2013**, *26*, 12–21. **DOI:**10.1016/j.learninstruc.2012.12.002
4. J. K. Gilbert, D. F. Treagust, in: J. K. Gilbert and D. Treagust (Eds.): Multiple Representations in Chemical Education, Springer Netherlands, **2009**, pp. 1–8. **DOI:**10.1007/978-1-4020-8872-8_1
5. A. H. Johnstone, *Sch. Sci. Rev.* **1982**, *64*, 377–379. **DOI:**10.1017/S0035336100178700
6. A. H. Johnstone, *J. Comput. Assist. Learn.* **1991**, *7*, 75–83. **DOI:**10.1111/j.1365-2729.1991.tb00230.x
7. V. Ferk Savec, I. Sajovic, K. S. W. Grm, in: Multiple representations in chemical education, Springer Netherlands, **2009**, pp. 309–331. **DOI:**10.1007/978-1-4020-8872-8_14
8. R. Kozma, J. Russell, in: J. K. Gilbert (Ed.): Visualization in Science Education, Springer Netherlands, **2005**, pp. 121–145. **DOI:**10.1007/1-4020-3613-2_8
9. M. Stieff, A. Origenes, D. DeSutter, M. Lira, L. Banevicius, D. Tabang, G. Cabel, *J. Educ. Psychol.* **2018**, *110*, 1160–1174. **DOI:**10.1037/edu0000258
10. N. A. Kiernan, A. Manches, M. K. Seery, *Chem. Educ. Res. Pract.* **2021**, *22*, 626–639. **DOI:**10.1039/D0RP00354A
11. M. Stieff, S. Scopelitis, M. E. Lira, D. Desutter, *Sci. Educ.* **2016**, *100*, 344–363. **DOI:**10.1002/sce.21203
12. A. T. Stull, M. Gainer, S. Padalkar, M. Hegarty, *J. Chem. Educ.* **2016**, *93*, 994–1001. **DOI:**10.1021/acs.jchemed.6b00194
13. A. T. Stull, M. Hegarty, *J. Educ. Psychol.* US, **2016**, *108*, 509–527. **DOI:**10.1037/edu0000077
14. Y. J. Dori, M. Barak, *J. Educ. Technol. Soc.* **2001**, *4*, 61–74.
15. S. R. Hinze, V. M. Williamson, M. J. Shultz, K. C. Williamson, G. Deslongchamps, D. N. Rapp, *Cogn. Process.* **2013**, *14*, 129–142. **DOI:**10.1007/s10339-013-0539-3
16. E. Francoeur, *Soc. Stud. Sci.* **1997**, *27*, 7–40. **DOI:**10.1177/030631297027001002
17. D. Gabel, D. Briner, D. Haines, *Sci. Teach.* **1992**, *59*, 58–63. **DOI:**10.1038/s41578-019-0146-8
18. A. M. Ingham, J. K. Gilbert, *Int. J. Sci. Educ.* **1991**, *13*, 193–202. **DOI:**10.1080/0950069910130206
19. N. Barnea, in: J. K. Gilbert and C. J. Boulter (Eds.): Developing Models in Science Education, Springer Netherlands, Dordrecht, **2000**, pp. 307–323. **DOI:**10.1007/978-94-010-0876-1_16
20. H. Hugel, *Chem. Aust.* **2005**, *72*, 31.
21. H.-K. Wu, J. S. Krajcik, E. Soloway, *J. Res. Sci. Teach.* **2001**, *38*, 821–842. **DOI:**10.1002/tea.1033
22. W. L. DeLano, *CCP4 Newsl. Protein Crystallogr.* **2002**, *40*, 82–92.
23. Free Molecular Modeling Software, **1999**, https://www.edinformatics.com/mathmol/free-molecular-modeling-software.html, (accessed: December 20, 2021)
24. A. Moll, A. Hildebrandt, H.-P. Lenhof, O. Kohlbacher, *Bioinformatics* **2006**, *22*, 365–366. **DOI:**10.1093/bioinformatics/bti818
25. E. F. Pettersen, T. D. Goddard, C. C. Huang, G. S. Couch, D. M. Greenblatt, E. C. Meng, T. E. Ferrin, *J. Comput. Chem.*

2004, *25*, 1605–1612. **DOI:**10.1002/jcc.20084
26. R. A. Sayle, E. J. Milner-White, *Trends Biochem. Sci.* **1995**, *20*, 374–376. **DOI:**10.1016/S0968-0004(00)89080-5
27. M. D. Casselman, J. F. Eichler, K. Atit, *Sci. Educ.* **2021**, 1–30. **DOI:**10.1002/sce.21675
28. Erlina, C. Cane, D. P. Williams, *J. Chem. Educ.* **2018**, *95*, 991–995. **DOI:**10.1021/acs.jchemed.7b00687
29. B. Mohamed-Salah, D. Alain, *Chem. Educ. Res. Pract.* **2016**, *17*, 862–877. **DOI:**10.1039/C5RP00180C
30. A. T. Stull, M. J. Gainer, M. Hegarty, *Learn. Instr.* **2018**, *55*, 80–92. **DOI:**10.1016/j.learninstruc.2017.09.008
31. A. Taly, F. Nitti, M. Baaden, S. Pasquali, *Interface Focus* **2019**, *9*, 1–11. **DOI:**10.1098/rsfs.2018.0065
32. C. A. Terrell, M. A. Franzen, T. Herman, S. Malapati, D. L. Newman, L. K. Wright, in: T. J. Bussey, K. Linenberger Cortes and R. C. Austin (Eds.): Biochemistry education : from theory to practice, American Chemical Society, Washington, DC, **2019**, pp. 43–62. (ACS Symposium Series; vol. 1337). **DOI:**10.1021/bk-2019-1337.ch003
33. T. Thayban, H. Habiddin, Y. Utomo, M. Muarifin, *Acta Chim. Slov.* **2021**, *68*, 736–743. **DOI:**10.17344/acsi.2021.6836
34. V. Ferk Savec, M. Vrtacnik, J. K. Gilbert, in: J. K. Gilbert (Ed.): Visualization in Science Education, Springer Netherlands, **2005**, pp. 269–297. **DOI:**10.1007/1-4020-3613-2_14
35. M. Barak, in: J. P. Suits and M. J. Sanger (Eds.): Pedagogic Roles of Animations and Simulations in Chemistry Courses, Amer Chemical Soc, Washington, **2013**, pp. 273–291. **DOI:**10.1021/bk-2013-1142.ch011
36. M. T. Springer, *J. Chem. Educ.* **2014**, *91*, 1162–1168. **DOI:**10.1021/ed400054a
37. R. Kelly, S. Akaygun, *Chem. Educ. Res. Pract.* **2019**, *20*, 657–658. **DOI:**10.1039/C9RP90009H
38. T. J. José, V. M. Williamson, *J. Chem. Educ.* **2005**, *82*, 937–943. **DOI:**10.1021/ed082p937
39. W. J. Hehre, A. J. Shusterman, J. E. Nelson, The molecular modeling workbook for organic chemistry, Wavefunction, Irvine, CA, **2004**.
40. A. D. Clauss, S. F. Nelsen, *J. Chem. Educ.* **2009**, *86*, 955–958. **DOI:**10.1021/ed086p955
41. K. J. Linenberger, R. S. Cole, S. Sarkar, *J. Chem. Educ.* **2011**, *88*, 962–965. **DOI:**10.1021/ed100727r
42. J. Raiyn, A. Rayan, *World J. Chem. Educ.* **2015**, *3*, 1–4. **DOI:**10.12691/wjce-3-1-1
43. E. Rothe, W. Zygmunt, *Chem. Eng. Educ.* **2016**, *50*, 125–129. **DOI:**10.1007/s10749-016-0672-0
44. Y. J. Dori, M. Barak, N. Adir, *J. Chem. Educ.* **2003**, *80*, 1084–1092. **DOI:**10.1021/ed080p1084
45. J. B. Ealy, *J. Sci. Educ. Technol.* **2004**, *13*, 461–471. **DOI:**10.1007/s10956-004-1467-x
46. R. Kozma, *Learn. Instr.* **2003**, *13*, 205–226. **DOI:**10.1016/S0959-4752(02)00021-X
47. J. Lundell, *Educ. Quím.* **2017**, 33–36. **DOI:**10.2436/20.2003.02.157
48. K. Kolar, R. Dolezal, N. Karaskova, N. Maltsevskaya, S. Krizkova, *Chem.-Didact.-Ecol.-Metrol.* Warsaw, **2019**, *24*, 45–51. **DOI:**10.2478/cdem-2019-0003
49. L. L. Winfield, K. McCormack, T. Shaw, *J. Chem. Educ.* Washington, **2019**, *96*, 89–92. **DOI:**10.1021/acs.jchemed.8b00145
50. S. S. Johnson, L. Winfield, S. H. Sung, *J. Chem. Educ.* **2021**, *98*, 982–985. **DOI:**10.1021/acs.jchemed.0c01134
51. L. Soulère, *J. Chem. Educ.* **2021**, *98*, 2709–2713. **DOI:**10.1021/acs.jchemed.1c00017
52. A. Grushow, M. S. Reeves, in: Using Computational Methods To Teach Chemical Principles, American Chemical Society, **2019**, pp. 1–10. (ACS Symposium Series; vol. 1312). **DOI:**10.1021/bk-2019-1312.ch00110.1021/bk-2019-1312.ch001
53. J. Rodríguez-Becerra, L. Cáceres-Jensen, T. Díaz, S. Druker, V. B. Padilla, J. Pernaa, M. Aksela, *Chem. Educ. Res. Pract.* **2020**, *21*, 638–654. **DOI:**10.1039/C9RP00273A
54. M. Aksela, J. Lundell, *Chem. Educ. Res. Pract.* **2008**, *9*, 301–308. **DOI:**10.1039/B818464J
55. M. Aksela, J. Pernaa, P. Blomgren, I. Rautiainen, Collaborative science education at the University of Helsinki: ChemistryLab Gadolin: a science lab as an inspiring environment for learning, development and research since 2008, Unigrafia Oy, Helsinki, **2018**.
56. J. Pernaa, M. Aksela, S. P. Ghulam, Introduction to Molecular Modeling in Chemistry Education, e-Oppi Ltd. & Edumendo Publishing, Jokioinen, **2017**.
57. J. Pernaa, *LUMAT Int. J. Math Sci. Technol. Educ.* **2015**, *3*, 960–975. **DOI:**10.31129/lumat.v3i7.977
58. D. Dolničar, B. Boh Podgornik, in: I. Devetak (Ed.): Eurovariety 2021: 9th European Variety in University Chemistry Education Conference: 7-9 July 2021, Ljubljana, Slovenia, online conference: book of abstracts, University of Ljubljana, Faculty of Education, **2021**, p. 74. http://pefprints.pef.uni-lj.si/id/eprint/6794
59. L. A. Abriata, *Inform.-Basel* **2017**, *4*, 1–18. **DOI:**10.3390/informatics4030028
60. S. Pirhadi, J. Sunseri, D. R. Koes, *J. Mol. Graph. Model.* **2016**, *69*, 127–143. **DOI:**10.1016/j.jmgm.2016.07.008
61. M. C. Burger, *J. Cheminformatics* **2015**, *7*, 1–7. **DOI:**10.1186/s13321-015-0085-3
62. B. Rayan, A. Rayan, *World J. Chem. Educ.* **2017**, *5*, 136–141. **DOI:**10.12691/wjce-5-4-4
63. R. M. Hanson, *J. Appl. Crystallogr.* **2010**, *43*, 1250–1260. **DOI:**10.1107/S0021889810030256
64. N. Rego, D. Koes, *Bioinformatics* **2015**, *31*, 1322–1324. **DOI:**10.1093/bioinformatics/btu829
65. H. Bergwerf, *ACS CHED CCCE Newsl.* **2015**, https://confchem.ccce.divched.org/2015FallCCCENLP9, (accessed: December 20, 2021)
66. R. M. Hanson, J. Prilusky, Z. Renjian, T. Nakane, J. L. Sussman, *Isr. J. Chem.* **2013**, *53*, 207–216. **DOI:**10.1002/ijch.201300024
67. O. Rothenberger, Virtual Molecular Model Kit, https://chemagic.org/molecules/amini.html, (accessed: December 20, 2021)
68. J. H. Jensen, J. C. Kromann, *J. Chem. Educ.* **2013**, *90*, 1093–1095. **DOI:**10.1021/ed400164n
69. B. Nevo, *J. Educ. Meas.* **1985**, *22*, 287–293. **DOI:**10.1111/j.1745-3984.1985.tb01065.x

70. J. Kim, *Inf. Res.* **2008**, *13*, 13–14. **DOI:**10.1111/j.1469-8749.1971.tb03071.x
71. M. Harle, M. Towns, *J. Chem. Educ.* **2011**, *88*, 351–360. **DOI:**10.1021/ed900003n
72. H. Van der Meij, J. Van Der Meij, *Comput. Educ.* **2014**, *78*, 150–159. **DOI:**10.1016/j.compedu.2014.06.003
73. M. Slapničar, V. Tompa, S. A. Glažar, I. Devetak, J. Pavlin, *Acta Chim. Slov.* **2020**, *67*, 904–915. **DOI:**10.17344/acsi.2020.5908
74. Z. Merchant, E. T. Goetz, W. Keeney-Kennicutt, O. Kwok, L. Cifuentes, T. J. Davis, *Comput. Educ.* **2012**, *59*, 551–568. **DOI:**10.1016/j.compedu.2012.02.004
75. M. Tanweer, *Eur. J. Phys. Educ. Sport Sci.* **2019**, *4*, 145–151. **DOI:**10.5281/zenodo.3407001
76. M. Oliver-Hoyo, M. A. Babilonia-Rosa, *J. Chem. Educ.* **2017**, *94*, 996–1006. **DOI:**10.1021/acs.jchemed.7b00094

Povzetek

V članku je predstavljena študija, v kateri je 54 univerzitetnih študentov preizkusilo in ovrednotilo *3DChemMol* - novo razviti, brezplačni spletni urejevalnik modelov molekul z orodno vrstico. Namen orodja je povečanje reprezentacijske kompetence v povezavi s submikroskopskimi predstavitvami. Študenti so programsko opremo uporabili prvič. Z orodjem za gradnjo/urejanje modelov so izdelali modele molekul v naslednjih treh aktivnostih z različnimi stopnjami težavnosti: 1) gradnja preprostega modela (butanojska kislina), 2) pretvorba enega modela (heksan) v dva modela, 3) pretvorba iz neciklične v ciklično obliko (glukoza). Študenti so za izvedbo vsake od aktivnosti potrebovali od dveh do 15 minut. V orodni vrstici urejevalnika *3DChemMol* je bilo na voljo več vrst pomoči, ki so študentom olajšale izvajanje aktivnosti, vključno z video vodnikom, prikazom pomoči ob preletu gumbov orodne vrstice z miško, prikazom statusa/načina dela in menijem pomoči. Na voljo so bile tudi možnosti razveljavitve in ponovne uveljavitve posameznih korakov ter ponovnega začetka celotne aktivnosti. Stopnjo dokončanja aktivnosti, težave in uporabo pomoči smo preučevali s pomočjo vprašalnikov za samoocenjevanje študentov. Urejevalnik molekul *3DChemMol* se je izkazal kot koristna podpora študentom pri preprostih kemijskih aktivnostih. Študenti so bili pri gradnji modelov uspešni, čeprav so naleteli na nekatere specifične težave, zlasti pri korakih, ki so vključevali prostorske operacije, kot je vrtenje izbranega dela modela molekule okoli vezi. Po mnenju študentov so bila video navodila najprimernejša in najpogosteje uporabljena vrsta pomoči, funkcija razveljavitve pa je bila pri delu bistvenega pomena. Rezultati kažejo, da lahko urejevalnik modelov molekul *3DChemMol* učinkovito uporabljamo pri osnovnih predmetih kemije na terciarni ravni izobraževanja, bodisi za poučevanje, samostojno učenje študentov ali druge oblike podpore v pedagoškem procesu. Rezultati in ugotovitve študije bodo uporabljeni tudi za nadaljnjo optimizacijo uporabniškega vmesnika v prihodnjih različicah ovrednotenega orodja.

Except when otherwise noted, articles in this journal are published under the terms and conditions of the Creative Commons Attribution 4.0 International License

Scientific paper

Synthesis of New Regioisomers of 5-Nitro-1,4-Naphthoquinone, Evaluation of Antioxidant and Catalase Inhibition Activities

Aesha F. SH. Abdassalam,[1] Nahide Gulsah Deniz,[1] Cigdem Sayil,[1,*] Mustafa Ozyurek,[2] Emin Ahmet Yesil[3] and Huseyin Salihoglu[1]

[1] *Istanbul University-Cerrahpasa, Engineering Faculty, Department of Chemistry, Division of Organic Chemistry, Avcilar, 34320, Istanbul, Turkey*

[2] *Istanbul University-Cerrahpasa, Engineering Faculty, Department of Chemistry, Division of Analytical Chemistry, Avcilar, 34320, Istanbul, Turkey*

[3] *Istanbul Gedik University, Vocational School, Polymer Technology Programme, Pendik, Istanbul, Turkey*

* *Corresponding author: E-mail: sayil@istanbul.edu.tr*

Received: 09-04-2021

Abstract

The studies on nitronaphthoquinone derivatives are rare in the literature, and the nitro group associated with the aromatic ring in the quinone system is known to increase the biological activity of naphthoquinone due to its electron-withdrawing properties. In the course of quinone derivatives, the new N(H)-substituted-5-nitro-1,4-naphthoquinones (NQ) as regioisomers were synthesized by reactions of 2,3-dichloro-5-nitro-1,4-naphthoquinone with some heterocyclic ring substituted nucleophiles such as anilines, piperazines, or morpholines, according to a Michael 1,4-addition mechanism. Five NQ regioisomer couples having different functional group (2-chloro-isomers **3**, **5**, **7**, **9** and **13**; 3-chloro-isomers **2**, **4**, **6**, **8** and **12**) are reported here. All new synthesized compounds were characterized by spectroscopic methods and two-dimensional NMR techniques $^{1}H–^{1}H$ correlated spectroscopy (COSY).

The synthesized NQ regioisomers were evaluated for catalase enzyme inhibitory activities and antioxidant efficiency. The synthesized regioisomers were screened for their antioxidant capacity using the cupric-reducing antioxidant capacity (CUPRAC) method. 2-Chloro-3-((2,4-dimethoxyphenyl)amino)-5-nitronaphthalene-1,4-dione (**5**) showed the highest antioxidant capacity with a 1.80±0.06 CUPRAC-trolox equivalent antioxidant capacity (TEAC) coefficient. Compound **5** also showed strongest catalase enzyme inhibitory activity. The antioxidant capacity results of all 2-chloro regioisomers are higher than the 3-chloro regioisomers. Likewise, also catalase enzyme inhibitory activities results were determined in the same way, except for one regioisomer pair. The catalase was effectively inhibited by the newly synthesized compounds, with % inhibition values in the range of 0.71–0.86%. Some of these NQ compounds also showed remarkable antioxidant capacities.

Keywords: 5-Nitro-1,4-naphthoquinone; heterocyclic ring; CUPRAC method; Catalase inhibition activity

1. Introduction

Naphthoquinone derivatives have been used as antibacterial agents for several years already, there are many reports in the 1960s of chemical compounds synthesized with 1,4-naphthoquinone structure and having antibacterial properties.[1] Later, in the 1980s, there were studies on inhibition of bacteria, along with vitamin K and 1,4-naphthoquinone. It has been suggested that pharmaceuticals compete in the electronic transport system. Another suggestion was the production of ROS and radical semiquinone and cytotoxicity of naphthoquinone.[2,3] It has been shown that amino derivatives such as anilines, piperazines, or morpholines of naphthoquinone improve the biological properties of these derivatives.[4] 2,2′-[1-(2-Aminoethyl) piperazin-1-yl]-3,3′-dichloro-bis(1,4-naphthoquinone) has showed remarkable antioxidant capacity by using the cupric-reducing antioxidant capacity (CUPRAC) methods and cytotoxic activity against A549 (lung), MCF-7 (breast), DU145 (prostate), and HT-29 (colon) cancer cell lines.[4]

Furthermore, the amino-1,4-naphthoquinone derivative has been used as synthetic key intermediate or as starting material for synthesis of many compounds.[5–10] Some literature reports point to the pro-oxidative effect of 5-hydroxy-1,4-naphthoquinone (juglone).[11,12] Also it has been reported that pyridine, 4*H*-pyran and thiazolopyrimidine derivatives of 3-hydroxynaphthoquinone have high antioxidant activity.[13]

There are two main ways describing how to prepare the alkyl or arylamino naphthoquinone derivatives. In the first type, the reaction requires a Michael 1,4-addition reaction between the amino compound and 1,4-naphthoquinone ring to produce 2-amino-1,4-naphthoquinone. The second type involves a nucleophilic substitution reaction between the nucleophile with a mono or dihalogenated derivative of 1,4-naphthoquinone to generate the corresponding amino derivative.[14]

The studies on nitronaphthoquinone derivatives are rare in the literature, and the nitro group associated with the aromatic ring in the quinone system is known to increase the biological activity of naphthoquinone due to its electron-withdrawing properties and it has been reported that the 2,3-dichloro-5-nitro-1,4-naphthoquinone derivative is more active towards amines and the reaction provides a mixture of two regioisomers.[15] Blackburn (2005) has treated 2,3-dichloro-5-nitro-1,4-naphthoquinone with linked resin amine to give very colorful products in high yields.[11] The resin under some reducing process and reacted with 2,3-dichloro-5-nitro-1,4-naphthoquinone in the presence of 2,6-di(*tert*-butyl)pyridine to give the red resin-quinone. Treatment with trifluoroacetic acid led to the rapid formation of regioisomeric mixtures of nitroquinones. As a comparison between the regioisomers the retention factor (R_f) of the 5-nitro isomer was found to be higher than for the 8-nitro isomer. Also, in the ^{1}H NMR, the proton signals of naphthoquinone ring for the first isomer are shifted more downfield than the naphthoquinone peaks of the second isomer.[15] In a later study, some derivatives of 5-nitro-2/3-aminonaphthalene-1,4-dione have been synthesized, studied and tested for biological activities by Samant *et al.* (2013).[16] They found that two regioisomers of nitronaphthoquinone derivatives, 3-chloro-5-nitro-2-((2-(trifluoromethyl)phenyl)amino)naphthalene-1,4-dione and 2-chloro-5-nitro-3-((2-(trifluoromethyl)phenyl)amino)naphthalene-1,4-dione demonstrated strong activity against the sleeping sickness disease (African human trypanosomiasis) with low cytotoxicity *in vitro*.[16] In addition to this, we have previously reported that some regioisomers of 5-nitro-1,4-naphthoquinone containing *N*-substituted group have been synthesized from 2,3-dichloro-5-nitro-1,4-naphthoquinone.[10]

Catalase (EC 1.11.1.6) as an antioxidant metalloenzyme capable of degradation of H_2O_2 is present in many cell types. Lack or malfunction of this class of enzyme may lead to severe disorders such as apoptotic cell death, anemia, some dermatological disorders, cardiovascular diseases, Wilson disease, hypertension and Alzheimer's diseases.[17] Some drugs bind to catalase and elicit enzyme inhibition; led to H_2O_2 accumulation and cytotoxicity in cancer cells.[18] So, it is important to measure catalase inhibition activity in the presence of new catalase inhibitor.

In this study, new regioisomeric compounds of 5-nitro-1,4-naphthoquinone were synthesized by the reactions of 2,3-dichloro-5-nitro-1,4-naphthoquinone with some heterocyclic ring substituted nucleophiles such as amines, piperazines, or morpholines, according to a Michael 1,4-addition mechanism. Their structures were characterized by using Fourier transform infrared spectroscopy (FTIR), ^{1}H nuclear magnetic resonance (^{1}H NMR) and two-dimensional techniques (^{1}H–^{1}H correlated spectroscopy (COSY)), attached proton test nuclear magnetic resonance (APT-NMR), mass spectrometry (MS) and elemental analyses. Secondly, these compounds were also tested for their antioxidant capacity *in vitro* by CUPRAC method and catalase inhibition activities.

2. Experimental

2. 1. Materials and Methods

Melting points were measured on a Büchi B-540 melting point apparatus. FTIR spectra (cm^{-1}) were recorded as KBr pellets in nujol mulls on a Shimadzu IR Prestige 21 model Diamond spectrometer (ATR method). ^{1}H NMR and APT-NMR spectra were obtained using a Varian Unity Inova (500 MHz) spectrometer by using TMS as the internal standard and deuterated chloroform as the solvent. Mass spectra were obtained on a Thermo Finnigan LCQ Advantage MAX LC/MS/MS spectrometer according to ESI probe. Elemental analyses were performed with a Thermo Finnigan Flash EA 1112 elemental analyzer. Products were isolated by column chromatography on silica gel (Fluka Silica gel 60, particle size 63–200 μm). Kieselgel 60 F-254 plates (Merck) were used for thin layer chromatography (TLC). All chemicals were of reagent grade and were used without further purification. Moisture was excluded from the glass apparatus with $CaCl_2$ drying tubes. Solvents, unless otherwise specified, were of reagent grade and distilled once prior to use.

2. 2. CUPRAC Assay of Total Antioxidant Capacity

The CUPRAC total antioxidant capacity measurement method[19] depends on the oxidation of an antioxidant by cupric neocuproine complex (Cu(II)-Nc) generating yellow-orange colored product (cuprous chelate: Cu(I)-Nc). To a test tube 1 mL $CuCl_2{\cdot}2H_2O$ (10 mM), 1 mL Nc (7.5 mM), 1 mL NH_4Ac buffer solution (1.0 M, pH 7), x mL newly synthesized compound, and H_2O (1.1 – x mL) (total volume: 4.1 mL) were added in this order and mixed well. The absorbance at 450 nm was recorded

against a reagent blank using a Perkin–Elmer Lambda 35 UV–Vis spectrophotometer with a pair of matched quartz cuvettes of 1 cm thickness after 30 min incubation period at room temperature. The calibration graph was then constructed by plotting the final concentration of each compound against the absorbance values which were measured. The result of antioxidant efficiency was expressed as trolox equivalent antioxidant capacity (TEAC) coefficient, mean ±SD of three determinations.

2. 3. Catalase Enzyme Inhibition Activity

The catalase enzyme inhibition activity was evaluated by using a modified CUPRAC method described by Bekdeser *et al.*[20] To a test tube 0.5 mL H_2O_2 (1.0 mM), 1.8 mL H_2O, 0.1 mL catalase solution (3.691 U mL^{-1}), and 0.2 mL synthesized compound (1.0 mM, total volume 2.6 mL) were added in this order, mixed and incubated at room temperature for 30 min. After this period, the optical CUPRAC sensor (Cu(II)-Nc-impregnated nafion membrane) was taken out and immersed in a test tube consisting of 2 mL incubation mixture + 6.2 mL EtOH. After 30 min agitation period, the yellow-orange colored nafion membrane was taken out and its absorbance was measured at 450 nm against that of a blank membrane excluding analyte.

2. 4. Synthesis

2. 4. 1. General Synthesis Procedure 1 for 2,3-Dichloro-5-nitro-1,4-naphthoquinone (1)

2,3-Dichloro-5-nitro-1,4-naphthoquinone (**1**) was prepared *via* the following method.[21] First, a mixture of the isomer, in which nitro group is substituted at five and six positions, was obtained. These isomers were separated by using column chromatography. The physical properties and characterization methods have been described before.[21–23] A complete and unambiguous assignment of ^{1}H shifts was based on a combination of one- and two-dimensional techniques (^{1}H and ^{1}H–^{1}H correlated spectroscopy (COSY)), see Figures 2–4.

2. 4. 2. General Synthesis Procedure 2 for Regioisomeric Compounds 2–13

Regioisomeric compounds **2**–**13** were synthesized by a known previous method.[9] 2,3-Dichloro-5-nitro-1,4-naphthoquinone (**1**) and nucleophiles (anilines, piperazines, etc.) **1a**–**f** were stirred in 25 mL of absolute ethanol for 3–4 h in the presence of Na_2CO_3 at room temperature. The reaction mixture was monitoring by TLC to establish the end of the reaction. 30 mL of chloroform was added to the reaction mixture. The organic layer was washed with water (3 × 30 mL), and dried with Na_2SO_4. Evaporator system was used to remove the extra amount of solvent, the residue was then purified by column chromatography (Table 1). In the ^{1}H NMR spectra of compounds **1**–**13**, the signals for protons represented H_{1-3} belong to the naphthoquinone ring (Figure 1).

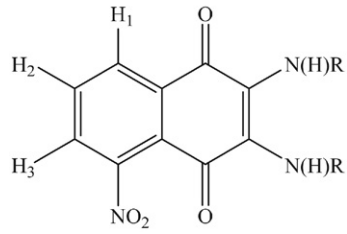

Figure 1. Characterization of quinonoid protons H_{1-3} of N(H)-substituted 5-nitro-1,4-naphthoquinones **1**–**13**

Synthesis of 2,3-Dichloro-5-nitro-1,4-naphthoquinone (1)

Dark yellow crystals, yield: 12 g (42%); R_f 0.3 (EtOAc/Hexane) (1:6 v/v). M.p. 151–152 °C (lit.[19] 156–157 °C); ^{1}H NMR (499.74 MHz, $CDCl_3$) δ 7.81 (dd, H_1, J = 9.2, 0.98 Hz, 1H, H_{naphth}), 7.98 (t, H_2, J = 7.8 Hz, 1H, H_{naphth}), 8.42 (dd, H_3, J = 8.6, 0.98 Hz, 1H, H_{naphth}). ^{13}C(APT) NMR (125.66 MHz, $CDCl_3$) δ 121.95, 128.26, 130.04, 131.75, 135.53 (CH_{arom}, C_{arom}), 143.35 (=C-Cl), 143.82 (C-NO_2), 172.63, 174.29 (C=O). $C_{10}H_3Cl_2NO_4$ (M_w 272.04 g/mol). MS [+ESI]: m/z = 271.2 $[M]^+$.

Synthesis of 2-(4-(Benzo[*d*][1,3]dioxol-5-ylmethyl)piperazin-1-yl)-3-chloro-5-nitronaphthalene-1,4-dione (2)[9] and 3-(4-(Benzo[*d*][1,3]dioxol-5-ylmethyl)piperazin-1-yl)-2-chloro-5-nitronaphthalene-1,4-dione (3)[10]

Isomer compounds of **2** and **3** were obtained by reaction between 2,3-dichloro-5-nitro-1,4-naphthoquinone (**1**) and 1-piperonylpiperazine (**1a**) according to the general procedure 2. The mixture was purified by using column chromatography and mixture of ethyl acetate with hexane (1:3 ratio) was used as the mobile phase.

Isomer **2**: Red solid, R_f 0.80 (EtOAc /Hexane) (1:3 v/v). M.p. 131–132 °C.

Isomer **3**: Pink solid, R_f 0.73 (EtOAc /Hexane) (1:3 v/v). M.p. 89–91 °C.

Isomer **2**: Red solid, yield: 0.110 g (20%); R_f 0.80 (EtOAc/Hexane) (1:3 v/v). M.p. 131–132 °C (lit.[10] 131–132 °C); FTIR (cm^{-1}) ν 3094 (C-H_{arom}), 2912, 2809, 2772, 2659 (C-H_{aliph}), 1679, 1640 (C=O), 1590, 1555 (C=C), 1494, 1438 (C-NO_2). ^{1}H NMR (499.74 MHz, $CDCl_3$) δ 2.56 (br s, 4H, H_{piper}), 3.52 (s, 2H, CH_2), 3.64 (br s, 4H, H_{piper}), 5.96 (s, 2H, O-CH_2-O), 6.79–6.91 (m, 3H, CH_{arom}), 7.76–7.82 (m, 2H (H_1,H_2), H_{naphth}), 8.34 (dd, J = 9.27, 1.46 Hz, 1H (H_3), H_{naphth}). ^{13}C(APT) NMR (125.66 MHz, $CDCl_3$) δ 51.15, 53.31 (N-CH_2)$_{piper}$, 62.43 (CH_2), 101.12 (O-CH_2-O), 108.01, 109.56, 122.60, 127.07, 129.42, 130.49, 132.64, 134.17 (CH_{arom}, C_{arom}), 148.40 (C-NO_2), 150.40 (=C-N), 175.74, 179.07 (C=O). Anal. Calcd. for $C_{22}H_{18}N_3O_6Cl$ (M_w

455.85 g/mol): C, 57.97; H, 3.98; N, 9.22. Found: C, 58.31; H, 3.59; N, 9.12. MS [+ESI]: m/z = 456.0 $[M]^+$.

Isomer **3**: Pink solid, yield: 0.223 g (44 %); R_f 0.73 (EtOAc/Hexane) (1:3 v/v). M.p. 89–91°C (lit.[10] 89–91°C); FTIR (cm^{-1}) ν 3079 (C-H_{arom}), 2905, 2811, 2772 (C-H_{aliph}), 1676, 1644 (C=O), 1590, 1537 (C=C), 1492, 1439 (C_{arom}-NO_2). ^{1}H NMR (499.74 MHz, $CDCl_3$) δ 2.52 (br s, 4H, H_{piper}), 3.62 (s, 2H, CH_2), 3.64 (br,s, 4H, H_{piper}), 5.97 (s, 2H, O-CH_2-O), 6.81–6.92 (m, 3H, CH_{arom}), 7.67 (dd, J = 9.2, 1.4 Hz, 1H (H_1), H_{naphth}), 7.81 (t, J = 7.8 Hz, 1H (H_2), H_{naphth}), 8.21 (dd, J = 9.2, 1.4 Hz, 1H (H_3), H_{naphth}). ^{13}C(APT) NMR (125.66 MHz, $CDCl_3$) δ 53.26 (N-CH_2), 62.39 (CH_2), 101.08 (O-CH_2-O), 108.07, 109.73, 122.67, 127.63, 129.16, 132.32, 133.70 (CH_{arom}, C_{arom}), 148.35 (C-NO_2), 149.33 (=C-N), 173.97, 179.84 (C=O). Anal. Calcd. for $C_{22}H_{18}N_3O_6Cl$ (M_w 455.85 g/mol): C, 57.97; H, 3.98; N, 9.22. Found: C, 58.21; H, 3.54; N, 9.15. MS [+ESI]: m/z = 456.0 $[M]^+$.

Synthesis of 3-Chloro-2-((2,4-dimethoxyphenyl)amino) -5-nitronaphthalene-1,4-dione (4) and 2-Chloro-3-((2,4-dimethoxyphenyl)amino)-5-nitronaphthalene-1,4 -dione (5)

According to the general procedure 2, 0.50 g (1.8 mmol) of 2,3-dichloro-5-nitro-1,4- naphthoquinone (**1**) was reacted with 0.30 g (2 mmol) of 2,4-dimethoxyaniline (**1b**) in 25 mL of ethanol at room temperature for 4 hours. The mixture was purified by column chromatography and mixture of ethyl acetate with hexane (1:4 ratio) was used as the mobile phase. Compounds **4** and **5** were obtained as a new regioisomer compounds.

Isomer **4**: Red solid, R_f 0.52 (EtOAc/Hexane) (1:4 v/v). M.p. 205–206 °C.

Isomer **5**: Red solid, R_f 0.35 (EtOAc/Hexane) (1:4 v/v). M.p. 198–199 °C.

Isomer **4**: Red solid, yield: 0.251 g (32%); R_f 0.52 (EtOAc/Hexane) (1:4 v/v). M.p. 205–206 °C; FTIR (cm^{-1}) ν 3316 (N-H), 3083 (C-H_{arom}), 2967, 2917 (C-H), 1675 (C=O), 1585, 1554 (C=C), 1534, 1370 (C-NO_2). ^{1}H NMR (499.74 MHz, $CDCl_3$) δ 3.84 (s, 6H, O-CH_3), 6.42–6.52 (m, 2H, H_{arom}), 6.93–7.02 (m, 2H, H_{arom}), 7.40 (s, 1H, N-H), 7.73 (d, J = 7.8 Hz, 1H, (H_1)H_{naphth}), 8.02 (t, J = 7.3 Hz, 1H, (H_2), H_{naphth}), 8.40 (d, J = 7.8 Hz, 1H, (H_3) H_{naphth}). ^{13}C(APT) NMR (125.66 MHz, $CDCl_3$) δ 55.58 (O-CH_3), 98.65, 103.54 (CH_{arom}), 113.79 (=C-Cl), 119.17, 126.85, 128.30, 128.87, 130.88, 131.73, 135.60 (CH_{arom}, C_{arom}), 143.34 (C-NO_2), 148.93 (=C-N), 154.57, 159.64 (=**C**-OCH_3), 172.65, 174.28 (C=O). Anal. Calcd. for $C_{18}H_{13}ClN_2O_6$ (M_w 388.73 g/mol): C, 55.61; H, 3.37; N, 7.21. Found: C, 55.31; H, 3.49; N, 7.12. MS [+ESI]: m/z = 387.2 $[M–H]^+$.

Isomer **5**: Red solid, yield: 0.357 g (46%); R_f 0.35 (EtOAc/Hexane) (1:4 v/v). M.p. 198–199 °C; FTIR (cm^{-1}) ν 3308 (N-H), 3090 (C-H_{arom}), 2970 (C-H), 1679, 1640 (C=O), 1590, 1563 (C=C), 1455, 1339 (C-NO_2). ^{1}H NMR (499.74 MHz, $CDCl_3$) δ 3.82 (s, 6H, O-CH_3), 6.48 (dd, J = 6.9, 2.4 Hz, 2H, H_{arom}), 6.98–7.20 (m, 1H, H_{arom}), 7.54 (s, 1H, N-H), 7.69 (dd, J = 9.2, 1.4 Hz, 1H, (H_1), H_{naphth}), 7.87 (t, 7.8 Hz, 1H, (H_2), H_{naphth}), 8.29 (dd, J = 8.8, 1.2 Hz 1H, (H_3), H_{naphth}). ^{13}C(APT) NMR (125.66 MHz, $CDCl_3$) δ 55.68 (O-CH_3), 98.67, 103.60 (CH_{arom}), 113.34 (=C-Cl), 119.17, 123.71, 126.84, 128.95, 131.05, 133.37, 135.24 (CH_{arom}, C_{arom}), 142.86 (C-NO_2), 148.72 (=C-N), 154.11, 159.49 (=**C**-O-CH_3), 173.29, 178.67 (C=O). Anal. Calcd. for $C_{18}H_{13}ClN_2O_6$ (M_w 388.73 g/mol): C, 55.61; H, 3.37; N, 7.21. Found: C, 55.83; H, 3.71; N, 7.41. MS [+ESI]: m/z = 387.5 $[M–H]^+$.

Synthesis of 3-Chloro-2-((4-methoxyphenyl)amino)-5-nitronaphthalene-1,4-dione (6) and 2-Chloro-3-((4-methoxyphenyl)amino)-5-nitronaphthalene-1,4-dione (7)

According to the general procedure 2, 0.50 g (1.8 mmol) of 2,3-dichloro-5-nitro-1,4- naphthoquinone (**1**) was reacted with 0.22 g (1.8 mmol) of 4-methoxyaniline (**1c**) in 25 mL of ethanol at room temperature for 4 hours. The mixture was purified by column chromatography and mixture of ethyl acetate with hexane (1:4 ratio) was used as the mobile phase. Compounds **6** and **7** were obtained as a new regioisomer compounds.

Isomer **6**: Red solid, R_f 0.51 (EtOAc/Hexane) (1:4 v/v). M.p. 167–168 °C.

Isomer **7**: Red solid, R_f 0.33 (EtOAc/Hexane) (1:4 v/v). M.p. 129–131 °C.

Isomer **6**: Red solid, yield: 0.157 g (24%); R_f 0.51 (EtOAc/Hexane) (1:4 v/v). M.p. 167–168 °C; FTIR (cm^{-1}) ν 3226 (N-H), 3084 (C-H_{arom}), 2919, 2850 (C-H), 1684, 1636 (C=O), 1590, 1563 (C=C), 1532, 1376 (C-NO_2). ^{1}H NMR (499.74 MHz, $CDCl_3$) δ 3.85 (s, 3H, O-CH_3), 5.38 (br s, 1H, NH), 6.85–6.94 (m, 2H, H_{arom}), 7.04–7.10 (m, 2H, H_{arom}), 7.91 (dd, J = 7.9, 1.2 Hz, 1H, (H_1), H_{naphth}), 7. 97 (t, J = 7.8 Hz, 1H, (H_2), H_{naphth}), 8.33–8.42 (m, 1H, (H_3), H_{naphth}). ^{13}C(APT) NMR (125.66 MHz, $CDCl_3$) δ 55.53 (O-CH_3), 111.70 (CH_{arom}), 113.36 (=C-Cl), 119.17, 123.17, 126.84, 127.14, 128.95, 131.37, 135.24 (CH_{arom}, C_{arom}), 144.86 (C-NO_2), 148.93 (=C-N), 158.64 (=C-OCH_3), 173.29, 178.91 (C=O). Anal. Calcd. for $C_{17}H_{11}ClN_2O_3$ (M_w 358.73 g/mol): C, 56.92; H, 3.09; N, 7.81. Found: C, 56.79; H, 2.93; N, 7.63. MS [+ESI]: m/z = 357.1 $[M–H]^+$.

Isomer **7**: Red solid, yield: 0.355 g (54%); R_f 0.33 (EtOAc/Hexane) (1:4 v/v). M.p. 129–131 °C; FTIR (cm^{-1}) ν 3289 (N-H), 3102, 3002 (C-H_{arom}), 2918, 2843 (C-H), 1680, 1644 (C=O), 1590, 1542 (C=C), 1500, 1329 (C -NO_2). ^{1}H NMR (499.74 MHz, $CDCl_3$) δ 3.86 (s, 3H, O-CH_3), 6.15 (s, 1H, N-H), 6.74–6.98 (m, 2H, H_{arom}), 7.06–7.17 (m, 2H, H_{arom}), 7.63–7.74 (m, 2H, (H_1,H_2), H_{naphth}), 8.26-8.41 (m, 1H, (H_3), H_{naphth}). ^{13}C(APT) NMR (125.66 MHz, $CDCl_3$) δ 55.49 (O-CH_3), 112.04 (=C-Cl), 113.66 (CH_{arom}), 123.12, 126.60, 128.46, 129.17, 131.90, 132.01, 134.60 (CH_{arom}, C_{arom}), 144.25 (C-NO_2), 148.23 (=C-N), 157.36 (=C-O-CH_3), 173.66, 178.92 (C=O). Anal. Calcd. for $C_{17}H_{11}ClN_2O_3$ (M_w 358.73 g/mol): C, 56.92; H, 3.09; N, 7.81. Found: C, 57.13; H, 3.25; N, 7.52. MS [+ESI]: m/z = 357.2 $[M–H]^+$.

Synthesis of 3-Chloro-2-((2-morpholinoethyl)amino)-5-nitronaphthalene-1,4-dione (8) and 2-Chloro-3-((2-morpholinoethyl)amino)-5-nitronaphthalene-1,4 -dione (9)

According to the general procedure 2, 0.50 g (1.8 mmol) of 2,3-dichloro-5-nitro-1,4- naphthoquinone (**1**) was reacted with 0.24 g (1.8 mmol) of 4-(2-aminoethyl) morpholine (**1d**) in 25 mL of ethanol at room temperature for 4 hours. The mixture was purified by column chromatography and mixture of ethyl acetate with hexane (1:2 ratio) was used as the mobile phase. Compounds **8** and **9** were obtained as a new regioisomer compounds.

Isomer **8**: Red solid, R_f 0.50 (EtOAc/Hexane) (1:2 v/v). M.p. 178–179 °C.

Isomer **9**: Red solid, R_f 0.33 (EtOAc/Hexane) (1:2 v/v). M.p. 173–174 °C.

Isomer **8**: Red solid, yield: 0.231 g (34%); R_f 0.50 (EtOAc/Hexane) (1:2 v/v). M.p. 178–179 °C; FTIR (cm^{-1}) ν 3292 (N-H), 3096 (C-H_{arom}), 2918, 2852, 2813 (C-H), 1690 (C=O), 1591, 1561 (C=C), 1519, 1338 (C-NO_2). ^{1}H NMR (499.74 MHz, $CDCl_3$) δ 2.50 (t, *J* = 6.1 Hz, 4H, (CH_2-N-CH_2)$_{morph}$), 2.58 (t, *J* = 6.0 Hz, 2H, N-CH_2CH_2), 3.75 (t, *J* = 6.1 Hz, 4H, CH_2-O-CH_2), 3.85 (q, *J* = 6.1 Hz, 2H, HN-CH_2), 6. 94 (br s, 1H, N-H), 7.65 (dd, *J* = 7.9, 0.98 Hz, 1H, (H_1) H_{naphth}), 7.86 (t, *J* = 7.8 Hz, 1H, (H_2) H_{naphth}), 8.36 (dd, *J* = 7.8, 1.5 Hz, 1H, (H_3) H_{naphth}). ^{13}C(APT) NMR (125.66 MHz, $CDCl_3$) δ 40.87 (NH-**C**H_2-CH_2), 52.93 (CH_2-N-CH_2)$_{morph}$, 56.50 (NH-CH_2-**C**H_2), 66.94 (CH_2-O-CH_2)$_{morph}$, 110.36 (=C-Cl), 123.22, 126.09, 129.02, 133.54, 135.24 (CH_{arom}, C_{arom}), 152.16 (C-NO_2), 158.93 (=C-N), 178.69, 181.51 (C=O). Anal. Calcd. for $C_{16}H_{16}N_3O_5Cl$ (M_w 365.77 g/mol): C, 52.54; H, 4.41; N, 11.49. Found: C, 52.67; H, 4.70; N, 11.50. MS [+ESI]: *m/z* = 366.2 $[M]^+$.

Isomer **9**: Red solid, yield: 0.221 g (32%); R_f 0.33 (EtOAc/Hexane) (1:2 v/v). M.p. 173–174 °C; FTIR (cm^{-1}) ν 3275 (N-H), 3080 (C-H_{arom}), 2957, 2894, 2822 (C-H), 1679, 1640 (C=O), 1609, 1572 (C=C), 1535, 1330 (C-NO_2). ^{1}H NMR (499.74 MHz, $CDCl_3$) δ 2.62 (br s, 4H, (CH_2-N-CH_2)$_{morph}$), 2.73 (br s, 2H, N-CH_2-CH_2), 3.70 (br s, 4H, CH_2-O-CH_2), 3.80–3.94 (m, 2H, HN-CH_2), 7. 06 (br s, 1H, N-H), 7.66 (dd, *J* = 7.9, 0.98 Hz, 1H, (H_1), H_{naphth}), 7.81 (t, *J* = 7.8 Hz, 1H, (H_2), H_{naphth}), 8.23 (dd, *J* = 7.8, 1.5 Hz, 1H, (H_3), H_{naphth}). ^{13}C NMR (125.66 MHz, DMSO-d_6) δ 40.49 (NH-CH_2-CH_2), 53.28 (CH_2-N-CH_2)$_{morph}$, 57.13 (NH-CH_2-CH_2), 66.45 (CH_2-O-CH_2)$_{morph}$, 98.63 (=C-Cl), 122.98, 128.71, 129.50, 133.30, 134.24 (CH_{arom}, C_{arom}), 148.83 (C-NO_2), 160.45 (=C-N), 175.26, 176.76 (C=O). Anal. Calcd. for $C_{16}H_{16}N_3O_5Cl$ (M_w 365.77 g/mol): C, 52.54; H, 4.41; N, 11.49. Found: C, 52.83; H, 4.13; N, 11.08. MS [+ESI]: *m/z* = 366.5 $[M]^+$.

Synthesis of 3-Chloro-5-nitro-2-((2-(pyrrolidin-1-yl) ethyl)amino)naphthalene-1,4-dione (10) and 2-Chloro-5-nitro-3-((2-(pyrrolidin-1-yl)ethyl)amino)naphthalene-1,4-dione (11)

According to the procedure 2, 0.50 g (1.8 mmol) of 2,3-dichloro-5-nitro-1,4- naphthoquinone (**1**) was reacted with 0.24 g (1.8 mmol) of 2-(pyrrodin-1-yl)ethane-1-amine (**1e**) in 25 mL of ethanol at room temperature for 4 hours. The mixture was purified by column chromatography and mixture of ethyl acetate with hexane (1:2 ratio) was used as the mobile phase. Compounds **10** and **11** were obtained as a new regioisomer compounds.

Isomer **10**: Red solid, R_f 0.71 (EtOAc/Hexane) (1:2 v/v). M.p. 146–147 °C

Isomer **11**: Red solid, R_f 0.33 (EtOAc/Hexane) (1:2 v/v). M.p. 132–133 °C

Isomer **10**: Red solid, yield: 0.280 g (46%); R_f 0.71 (EtOAc/Hexane) (1:2 v/v). M.p. 146–147 °C; FTIR (cm^{-1}) ν 3281 (N-H), 3112 (C-H_{arom}), 2958, 2851 (C-H), 1681 (C=O), 1591, 1559 (C=C), 1525, 1335 (C-NO_2). ^{1}H NMR (499.74 MHz, $CDCl_3$) δ 1.72 (br s, 4H, (CH_2-CH_2)$_{pyrro}$), 2.51 (br s, 4H, (CH_2-N-CH_2)$_{pyrro}$), 2.61–2.70 (m, 2H, CH_2-N), 3.82 (br s, 2H, HN-CH_2), 6.96 (br s, 1H, N-H), 7.61 (d, *J* = 7.8 Hz, (H_1), 1H, H_{naphth}), 7.79 (t, *J* = 7.8 Hz, 1H, (H_2), H_{naphth}), 8.32 (d, *J* = 7.8 Hz, 1H, (H_3), H_{naphth}). ^{13}C(APT) NMR (125.66 MHz, $CDCl_3$) δ 23.34 (CH_2-CH_2)$_{pyrro}$, 43.24 (**N**-CH_2), 54.11 (CH_2-N-CH_2)$_{pyrro}$, 55.32 (HN-CH_2), 109.98 (=C-Cl), 126.02, 128.88, 130.91, 133.43, 135.37 (C_{arom}, CH_{arom}), 148.23 (=C-N) 173.95, 177.32 (C=O). Anal. Calcd. for $C_{16}H_{16}ClN_3O_4$ (M_w 363.80 g/mol): C, 54.94; H, 4.61; N, 12.01. Found: C, 54.64; H, 4.39; N, 11.77. MS [+ESI]: *m/z* = 349.5 $[M]^+$.

Isomer **11**: Red solid, yield: 0.220 g (35%); R_f 0.33 (EtOAc/Hexane) (1:2 v/v). M.p. 132–133 °C. FTIR (cm^{-1}) ν 3241 (N-H), 3072 (C-H_{arom}), 2968 (C-H), 1681 (C=O), 1590 (C=C), 1531, 1372 (C-NO_2). ^{1}H NMR (499.74 MHz, $CDCl_3$) δ 1.50 (br s, 4H, CH_2-CH_2)$_{pyrro}$, 2.48 (br s, 4H, CH_2-N-CH_2)$_{pyrro}$, 2.58–2.69 (m, 2H, (CH_2-N), 3.60 (br s, 2H, HN-CH_2), 6.73 (br s, 1H, N-H), 7.47 (d, *J* = 7.8 Hz, 1H, (H_1), H_{naphth}), 7.76 (t, *J* = 7.8 Hz, 1H, (H_2), H_{naphth}), 8.29 (d, *J* = 7.8 Hz, 1H, (H_3), H_{naphth}). ^{13}C NMR (125.66 MHz, DMSO-d_6) δ 23.83 (**C**H_2-**C**H_2)$_{pyrro}$, 45.17 (**N**-CH_2), 54.05 (**C**H_2-N-**C**H_2)$_{pyrro}$, 60.90 (HN-**C**H_2), 103.93 (=C-Cl), 122.02, 126.05, 128.16, 131.35, 136.42 (C_{arom}, CH_{arom}), 148.03 (=C-N), 166.72 (C-NO_2), 172.46, 181.90 (C=O). Anal. Calcd. for $C_{16}H_{16}ClN_3O_4$ (M_w 349.77 g/mol): C, 54.94; H, 4.61; N, 12.01. Found: C, 55.03; H, 4.81; N, 12.29. MS [+ESI]: *m/z* = 348.5 $[M]^+$.

Synthesis of 2-(4-Benzylpiperidin-1-yl)-3-chloro-5-nitronaphthalene-1,4-dione (12) and 3-(4-Benzylpiperidin-1-yl)-2-chloro-5-nitronaphthalene-1,4-dione (13)

According to the general procedure 2, 0.50 g (1.8 mmol) of 2,3-dichloro-5-nitro-1,4- naphthoquinone (**1**) was reacted with 0.32 g (1.8 mmol) of 4- benzylpiperidine (**1f**) in 25 mL of ethanol at room temperature for 4 hours. The mixture was purified by column chromatography and mixture of chloroform with petroleum ether (1:1 ratio) was used as the mobile phase. Compounds **12** and **13** were obtained as a new regioisomer compounds.

Isomer **12**: Red solid, R_f 0.46 ($CHCl_3$/PE) (1:1 v/v). M.p. 153–154 °C.

Isomer **13**: Red oil, R_f 0.37 ($CHCl_3$/PE) (1:1 v/v).

Isomer **12**: Red solid, yield: 0.332 g (44 %); R_f 0.46 ($CHCl_3$/PE) (1:1 v/v). M.p. 153–154 °C; FTIR (cm^{-1}) ν 2952, 2920, 2853 (C-H), 1718 (C=O), 1606, 1594 (C=C), 1453, 1375 (C-NO_2). ^{1}H NMR (499.74 MHz, $CDCl_3$) δ 1.46–1.59 (m, 2H, $(CH_2)_{piperi}$), 1.66–1.93 (m, 3H, $(CH_2$-$CH)_{piperi}$), 2.53–2.71 (m, 2H, (CH_2), 3.12–3.19 (m, 2H, (N-$CH_2)_{piperi}$), 3.69–3.81 (m, 2H, (N-$CH_2)_{piperi}$, 7.07–7.25 (m 5H, H_{arom}), 7.70–7.74 (m, 2H, (H_1,H_2), H_{naphth}), 8.26–8.37 (dd, J = 2.4, 6.8 Hz, 1H, H_{naphth}). ^{13}C(APT) NMR (125.66 MHz, $CDCl_3$) δ 33.06 ($\mathbf{C}H_2$-CH-$\mathbf{C}H_2)_{piperi}$, 37.65 (CH_2-$\mathbf{C}H$-$CH_2)_{piperi}$, 42.95 (CH_2), 52.20 (CH_2-N-$CH_2)_{piperi}$, 119.98 (=C-Cl), 125.79, 126.95, 128.27, 129.08, 130.02, 132.80, 135.51, 140.00 (C_{arom}, CH_{arom}), 151.10 (=C-N), 175.69, 179.36 (C=O). Anal. Calcd. for $C_{22}H_{19}ClN_2O_4$ (M_w 410.85 g/mol): C, 64.32; H, 4.66; N, 6.82. Found: C, 64.64; H, 5.02; N, 6.72. MS [+ESI]: m/z = 411.1 $[M]^+$, 433.2 $[M+Na]^+$.

Isomer **13**: Red oil, yield: 0.226 g (30 %); R_f 0.37 ($CHCl_3$/PE) (1:1 v/v). FTIR (cm^{-1}) ν 3060 (C-H_{arom}), 2970, 2919 (C-H), 1717, 1664 (C=O), 1592, 1561 (C=C), 1452, 1329 (C-NO_2). ^{1}H NMR (499.74 MHz, $CDCl_3$) δ 1.38–1.43 (m, 2H, $(CH_2)_{piper.}$), 1.69–1.81 (m, 3H, $(CH_2$-$CH)_{piper.}$), 2.50–2.55 (m, 2H, (CH_2), 3.12–3.18 (m, 2H, (N-$CH_2)_{piper.}$), 3.77–3.80 (m, 2H, (N-$CH_2)_{piper.}$, 7.05–7.25 (m 5H, H_{arom}), 7.62–7.70 (m, 1H, (H_1), H_{naphth}), 7.75–7.85 (m, 1H, (H_2)H_{naphth}) 8.22 (d, J = 7.8 Hz, 1H, (H_3), H_{naphth}). ^{13}C(APT) NMR (125.66 MHz, $CDCl_3$) δ 33.05 (CH_2-CH-$CH_2)_{piperi}$, 37.60 (CH_2-$\mathbf{C}H$-$CH_2)_{piper.}$, 42.92 (CH_2), 52.20 (CH_2-N-$CH_2)_{piperi}$, 119.90 (=C-Cl), 122.70, 126.08, 127.01, 128.33, 129.63, 133.61, 134.14, 139.87 (C_{arom}, CH_{arom}), 148.23 (C-NO_2), 151.11 (=C-N), 173.89, 179.35 (C=O).

Table 1. The reaction pathway and obtained regioisomeric products **2**–**13**

Reactions and conditions	**Colour, R_f, yield (%), m.p. (°C)**
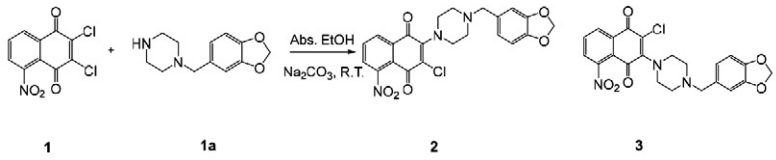 **1** **1a** **2** **3**	**(2):** Red solid, R_f: 0.80, yield 20%, m.p. 131–132 **(3):** Pink solid, R_f: 0.37, yield 44%, m.p. 89–91
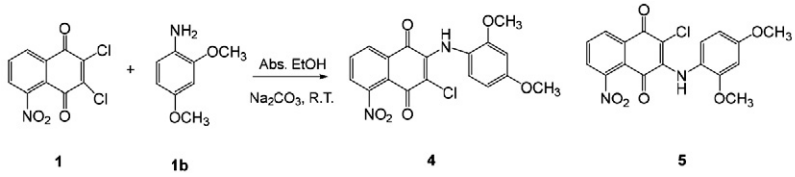 **1** **1b** **4** **5**	**(4):** Red solid, R_f: 0.52, yield 32%, m.p. 205–206 **(5):** Red solid, R_f: 0.35, yield 46%, m.p. 198–199
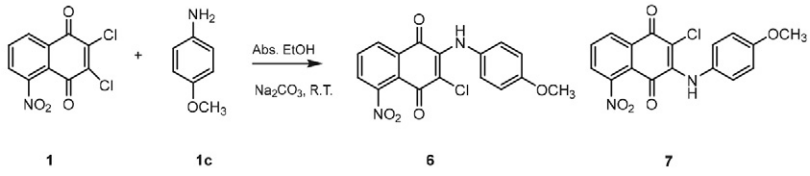 **1** **1c** **6** **7**	**(6):** Red solid, R_f: 0.51, yield 24%, m.p. 167–168 **(7):** Red solid, R_f: 0.33, yield 54%, m.p. 129–131
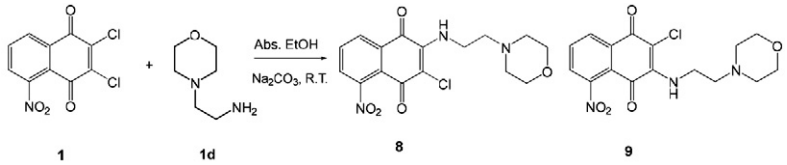 **1** **1d** **8** **9**	**(8):** Red solid, R_f: 0.50, yield 34%, m.p. 178–179 **(9):** Red solid, R_f: 0.33, yield 32%, m.p. 173–174
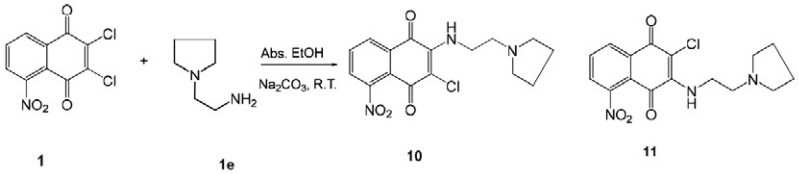 **1** **1e** **10** **11**	**(10):** Red solid, R_f: 0.71, yield 46%, m.p.146–147 **(11):** Red solid, R_f: 0.33, yield 35%, m.p.132–133
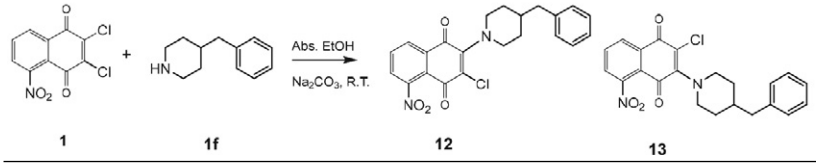 **1** **1f** **12** **13**	**(12):** Red solid, R_f: 0.46, yield 44%, m.p.153–154 **(13):** Red oil R_f: 0.37, yield 30%

Anal. Calcd. for $C_{22}H_{19}ClN_2O_4$ (M_w 410.85 g/mol): C, 64.32; H, 4.66; N, 6.82. Found: C, 64.60; H, 4.66; N, 7.16. MS [+ESI]: m/z = 411.2 $[M]^+$, 433.1 $[M+Na]^+$.

3. Results and Discussion

3. 1. Chemistry and Spectral Study

The new regioisomers **2**–**13** were synthesized by the reactions of 2,3-dichloro-5-nitro-1,4-naphthoquinone (**1**) with some nucleophiles such as amines, piperazines, or morpholines (**1a**–**f**) according to a Michael 1,4-addition mechanism and reaction pathways of synthesizes are illustrated in Table 1. The regioisomers were separated by column chromatography by using a different ratio of solvents. The obtained regioisomers have different color, melting point, retention factor (R_f) and chemical shifts of naphthoquinone ring protons in ^{1}H NMR spectra.

The ^{1}H NMR spectra of the synthesized new regioisomers indicate that the peaks of the 2-N-substituted-3-chloro-5-nitro-naphthalene-1,4-dione isomer of aromatic protons (H_{1-3}) are shifted more downfield than the aromatic protons of the 3-N-substituted-2-chloro-5-nitro-naphthalene-1,4-dione isomer. Also, it has been found that in the case of mixture of regioisomers, the higher R_f component was shown to be the 2-N-substituted-3-chloro-5-nitro-naphthalene-1,4-dione isomer and the lower R_f component the 3-N-substituted-2-chloro-5-nitro-naphthalene-1,4-dione isomer. The comparison of R_f values is compatible with similar values published in the literature.[15–16, 24] As a comparison between the ^{1}H NMR spectra of the synthesized new regioisomers **4** and **5**; we found that the protons of the naphthoquinone (H_{1-3}) peaks (δ 7.73–8.40 ppm) for the first isomer 3-chloro-2-((2,4-dimethoxyphenyl)amino)-5-nitronaphthalene-1,4-dione (**4**) are shifted more downfield than the naphthoquinone peaks (δ 7.69–8.29 ppm) of the second isomer 2-chloro-3-((2,4-dimethoxyphenyl)amino)-5-nitronaphthalene-1,4-dione (**5**). Also, it was found that the isomer **4** has a higher R_f component than the isomer **5**. The comparison of R_f values is consistent with the related literature.[15] In APT-NMR spectra signals of methoxy group (CH_3-O) and carbonyl group for isomer **4** were detected at δ 55.58 and δ 172.65, 174.28 ppm, while in isomer **5** at δ 55.68 and δ 173.29, 178.67 ppm, respectively.

3. 2. ^{1}H–^{1}H Correlated Spectroscopy (COSY)

The structures of these 5-nitro-1,4-naphthoquinone (**1**) and regioisomers of 5-nitro-1,4-naphthoquinone (**2** and **3**) were elucidated by using one- and two-dimensional NMR techniques in which the differences of positions of nitro group on the naphthalene ring were detected. The three hydrogen signals at the quinone ring of 2,3-dichloro-5-nitro-1,4-naphthoquinone (**1**) were assigned in the ^{1}H NMR spectrum (Figure 2) and confirmed by the ^{1}H–^{1}H COSY (Figure 3). In the ^{1}H NMR spectrum of compound **1**, a doublet of doublet (dd) at 7.81 ppm corresponding to H_1 that are coupled to H_2 (t, 7.98, 1H, $^3J_{H,H}$ = 9.27 Hz), and to H_3 (dd, 8.42, 1H, $^3J_{H,H}$ = 9.27 Hz) (Figure 2).

All these hydrogens were assigned on the basis of the ^{1}H–^{1}H COSY spectrum, where can be observed that H_1 is coupled to H_2 and H_3, H_2 to H_1 and H_3, and H_3 to H_2 and H_1. From ^{1}H–^{1}H COSY contour map these hydrogens are coupled to each other (Figure 3).

The hydrogen signals at the quinone and piperonylpiperazine ring of compounds **2** and **3** were assigned in the ^{1}H NMR spectrum (Figures 4 and 7) and also confirmed by the ^{1}H–^{1}H COSY spectrum (Figures 5, 6 and 8,

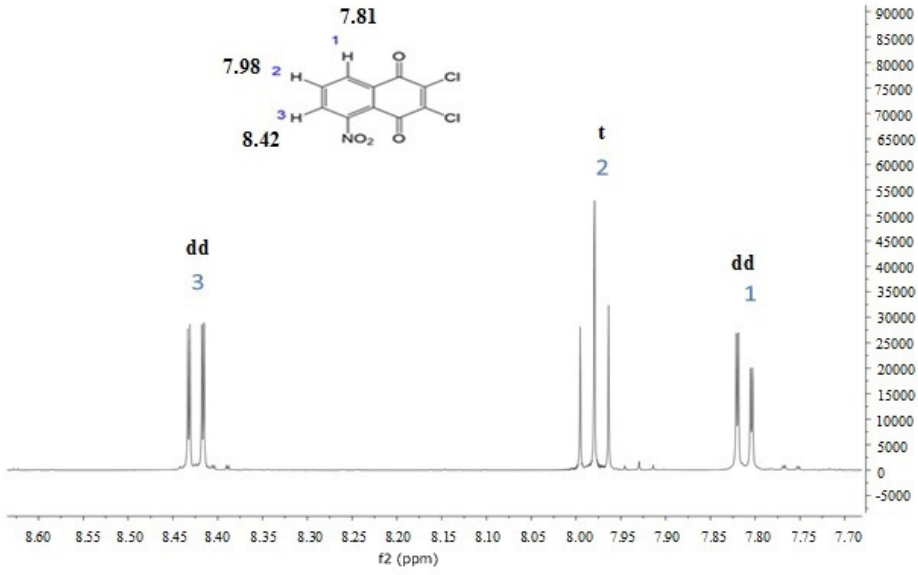

Figure 2. ^{1}H NMR spectrum of compound **1**

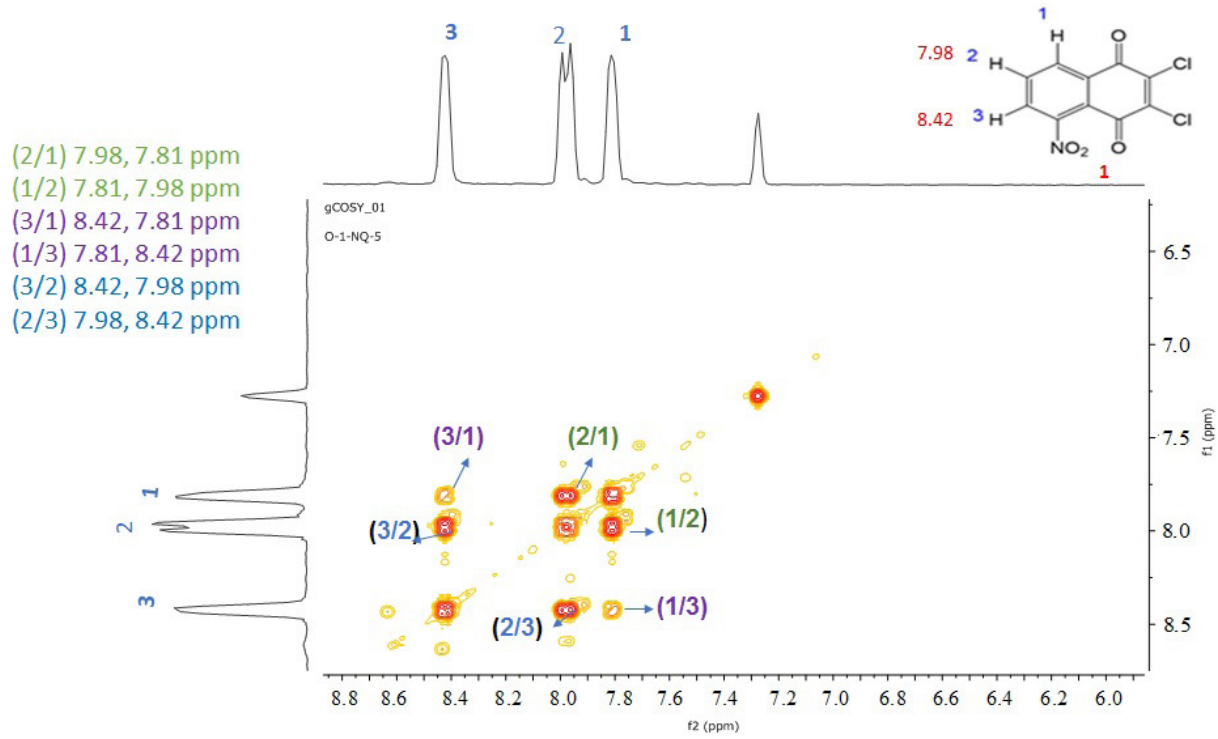

Figure 3. ^{1}H–^{1}H COSY contour map of compound **1**

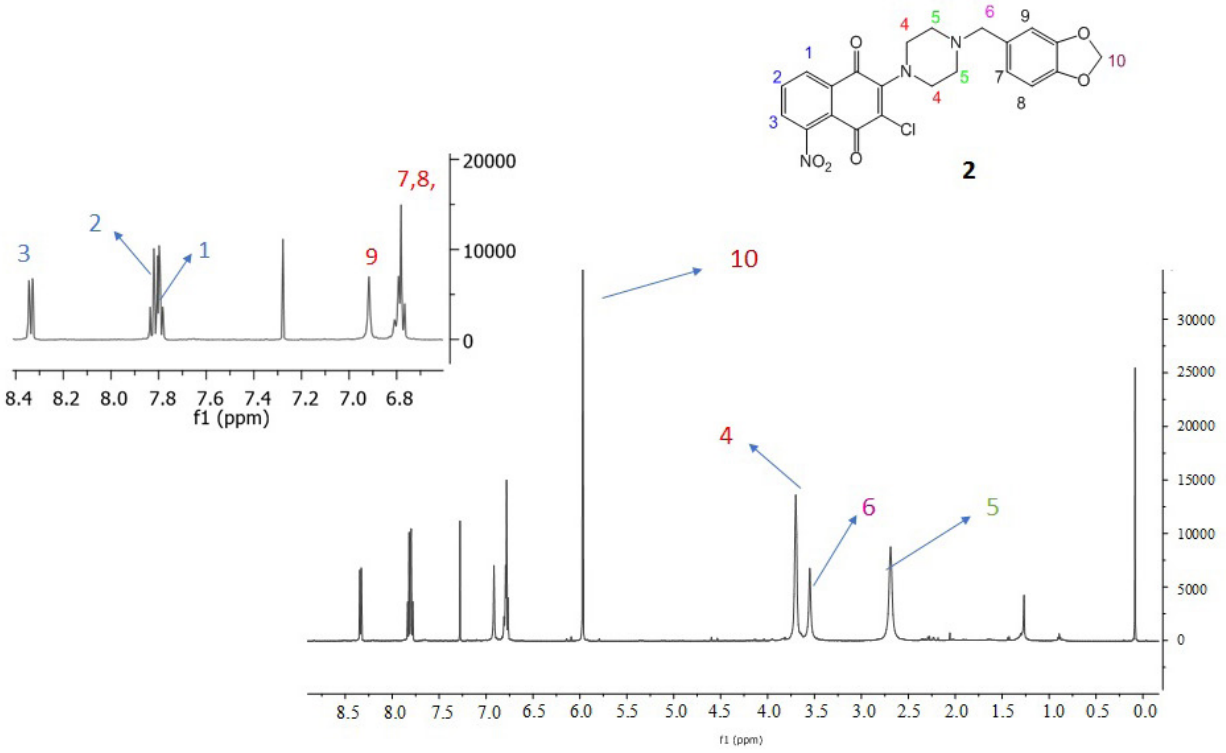

Figure 4. The hydrogen signals at the quinone and piperonylpiperazine ring of compound **2** in ^{1}H NMR spectrum

9). For compound **2** a multiplet at 7.76–7.82 corresponding to H_1 and H_2 that are coupled to H_3 (8.34, dd, $^{3}J_{H,H}$ = 9.27 Hz). As expected, H_4 and H_5 at piperizine ring appear as broad singlets at 3.64 and 2.56 ppm, respectively. A multiplet at 6.79–6.91 ppm corresponds to H_7 and H_8, respectively. In the ^{1}H NMR spectrum of compound **3**, a doublet of doublet (dd) at 7.67 ppm corresponding to H_1 that is coupled to H_2 (t, 7.81, 1H, $^{3}J_{H,H}$ = 7.8 Hz), and to H_3 (dd,

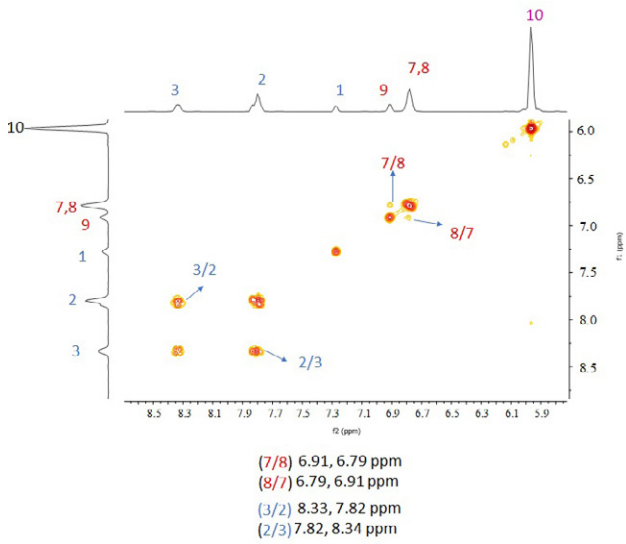

Figure 5. ^{1}H–^{1}H COSY contour map of aromatic protons of compound **2**

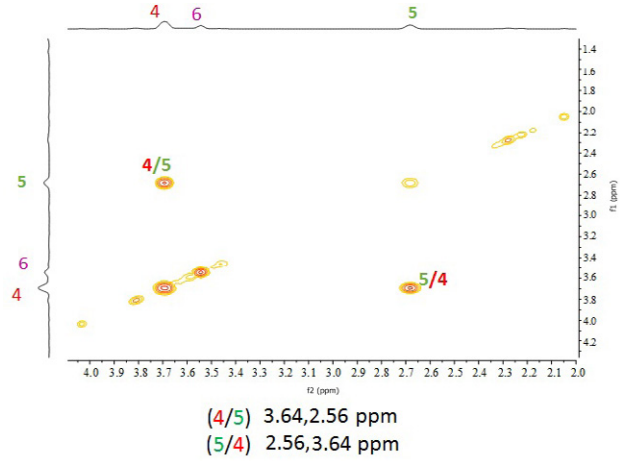

Figure 6. ^{1}H–^{1}H COSY contour map of piperazine ring protons of compound **2**

8.21, 1H, $^{3}J_{H,H}$ = 9.20 Hz) was observed. H_4 and H_5 appear as broad singlets at 3.64 and 2.52 ppm, respectively. A multiplet at 6.81–6.92 ppm corresponds to H_7 and H_8, respectively (Figures 4 and 7).

The interaction of hydrogens of 1, 2, 3, 7, 8 and 4, 5 in compound **2** and **3** were observed on the basis of the ^{1}H–^{1}H COSY spectrums, as can be seen from Figures 5, 8 and Figures 6, 9. H_3 is coupled to H_2, H_2 to H_3, and H_7 is coupled to H_8, H_8 to H_7 and H_4 is coupled to H_5, H_5 to H_4 for compound **2** (Figures 5, 6). As can be observed from Figure 8, H_3 is coupled to H_1 and H_2, H_2 to H_3 and H_1, and H_1 is coupled to H_2 and H_3 also H_7 coupled to H_8, H_8 to H_7. As can be seen in Figure 9, H_4 is coupled to H_5 and H_5 to H_4 for compound **3**. Chemical shifts in ppm of the above mentioned hydrogens are indicated in the figures.

3. 3. CUPRAC Antioxidant Capacities

NQ compounds were assayed using the normal CUPRAC assay (at 25 °C) against trolox (TR) as the reference standard.[18] $TEAC_{CUPRAC}$ coefficients are defined as the ratio of the slope of the curve of the tested compounds to that of TR (Table 2). LODs for synthesized compounds with respect to CUPRAC method were established between 0.74–7.37 μM (n = 10) and RSD% were found to be

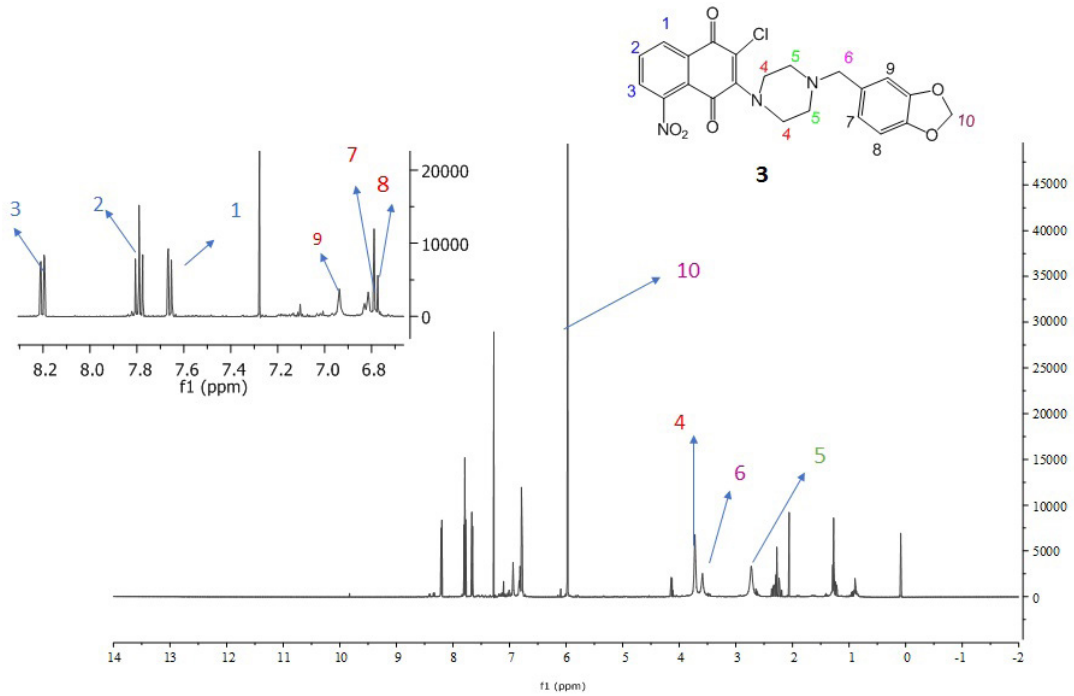

Figure 7. The hydrogen signals at the quinone and piperonylpiperazine ring of compound **3** in ^{1}H NMR spectrum

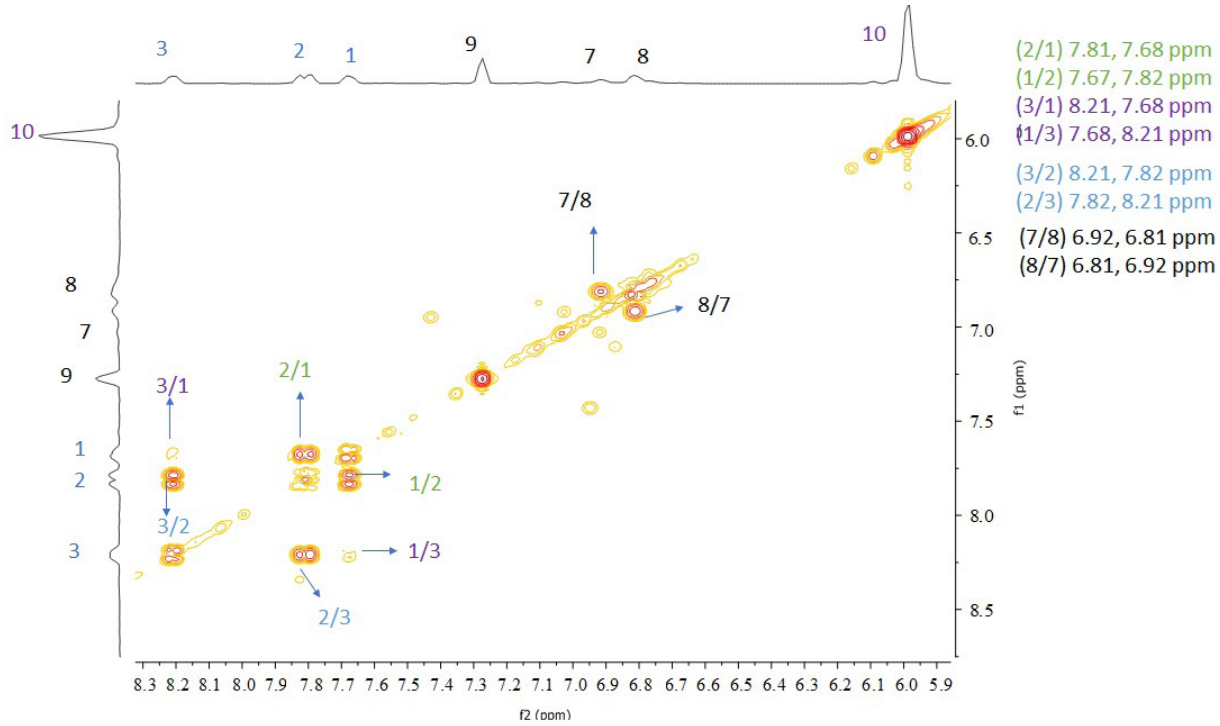

Figure 8. ^{1}H–^{1}H COSY contour map of aromatic protons of compound **3**

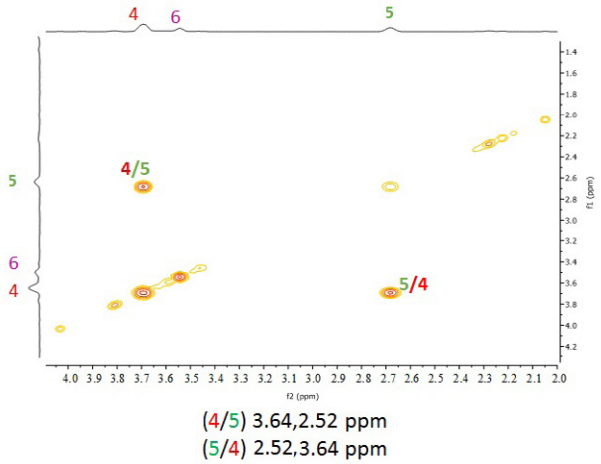

Figure 9. ^{1}H–^{1}H COSY contour map of piperazine ring protons of compound **3**

less than 4%. Among all the compounds synthesized, compound **5** showed the highest antioxidant potency ($TEAC_{CUPRAC}$ = 1.80±0.06). The $TEAC_{CUPRAC}$ coefficient of compound **5** was also higher than unity ($TEAC_{TR}$ = 1.0). Since $TEAC_{CUPRAC}$ coefficient of ascorbic acid (for comparison)[19] and compound **7** is close to 1.0, their antioxidant power are approximately equal to that of TR.

Five NQ regioisomer couples having different functional group (2-chloro-isomers **3**, **5**, **7**, **9** and **13**, as well as 3-chloro-isomers **2**, **4**, **6**, **8** and **12**) are reported here (Table 2). Although all isomer couples are just regioisomers, very interesting and dramatic differences in biological activities have been observed. Antioxidant capacity result of isomers showed that it is directly related to the bonding of N-nucleophiles at the 2 or 3 position on the naphthoquinone ring. As can be seen from the Table 2, the capacity results of all 2-chloro regioisomers are higher than the 3-chloro regioisomers. Surprisingly, two isomer pairs having –OCH_3 functional group also attracted attention in these results. Interestingly, despite having the same functional group, isomer **6** and **7**, if we compare the antioxidant result of the two isomers, we see that the difference is more than two times. Likewise, there is a remarkable difference in capacity result of isomers **4** and **5**. As shown in Table 2, **4** and **5** had stronger antioxidant capacity than **6** and **7**. These results may be related to that the larger the number of the –OCH_3 groups in the same structure, the higher is the antioxidant capacity of a molecule.[25]

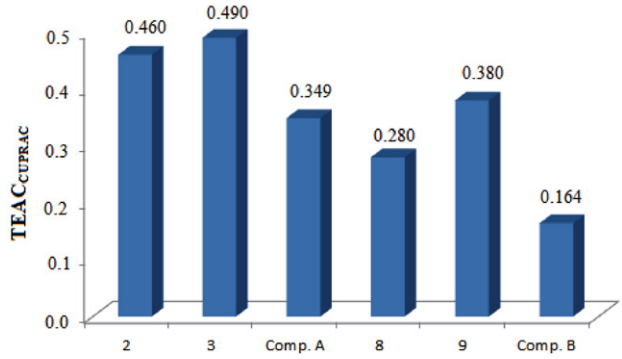

Figure 10. The comparison of TEAC coefficients of derivatives with and without NO_2 substituents (**2**, **3**, compound **A**, **8**, **9** and compound **B**)

Table 2. The linear calibration equations, correlation coefficients, linear concentration ranges, and TEAC coefficients of the NQ compounds using CUPRAC method.

Compounds	Linear range (mol L^{-1})	Calibration equation	r	$TEAC_{CUPRAC}$[a]
2	3.28×10^{-5} – 1.05×10^{-4}	$A = 7.60\times10^{3}\ c + 0.12$	0.992	0.46±0.02
3	1.23×10^{-6} – 1.42×10^{-4}	$A = 8.10\times10^{3}\ c + 0.05$	0.988	0.49±0.02
4	4.09×10^{-6} – 4.75×10^{-5}	$A = 2.44\times10^{4}\ c + 0.04$	0.989	1.46±0.07
5	1.26×10^{-6} – 3.51×10^{-5}	$A = 3.16\times10^{4}\ c + 0.09$	0.992	1.80±0.06
6	2.89×10^{-6} – 1.63×10^{-4}	$A = 6.90\times10^{3}\ c + 0.07$	0.990	0.41±0.01
7	4.45×10^{-6} – 6.88×10^{-5}	$A = 1.57\times10^{4}\ c + 0.06$	0.991	0.94±0.04
8	2.13×10^{-6} – 2.47×10^{-4}	$A = 4.68\times10^{3}\ c + 0.04$	0.989	0.28±0.01
9	2.05×10^{-5} – 1.61×10^{-4}	$A = 6.32\times10^{3}\ c + 0.18$	0.991	0.38±0.02
10	3.77×10^{-6} – 1.40×10^{-4}	$A = 7.95\times10^{3}\ c + 0.08$	0.990	0.48±0.03
12	1.39×10^{-5} – 2.54×10^{-4}	$A = 4.29\times10^{3}\ c + 0.11$	0.988	0.26±0.01
13	1.76×10^{-6} – 2.03×10^{-4}	$A = 5.69\times10^{3}\ c + 0.04$	0.991	0.34±0.02

[a] $TEAC_{compound} = \varepsilon_{compound} / \varepsilon_{TR}$ $\varepsilon_{TR} = 1.67\times10^{4}$ $Lmol^{-1}cm^{-1}$ (DMSO).

A few years ago, our research group synthesized two derivatives not substituted with nitro groups on the aromatic skeleton (compounds **A** and **B**) and reported their antioxidant results.[4] Comparing these results with those for the regioisomers **2**, **3** and **8**, **9** (Table 3 and Figure 10), it is evident that the effect of the electron-withdrawing nitro group in the system is directly reflected on the antioxidant results and higher antioxidant capacities were obtained for nitro derivatives. Regiosomers **8** and **9** showed approximately twice as high antioxidant activity, while regioisomers **2** and **3** showed approximately half times higher antioxidant activity than compounds **B** and **A**, respectively.

3. 4 Catalase Activity

The screening of NQ compounds against the catalase revealed that most of the compounds have moderate inhibition activity of this enzyme (> 0.7 U/mL, Figure 11). Enzyme activity results were determined in accordance with the antioxidant activity results. As can be seen in Figure 11, generally the enzyme inhibitory activities results of 2-chloro regioisomers are higher than for the 3-chloro regioisomers except for one regioisomer pair and compounds **5** and **7** revealed significant inhibition activity.

Table 3. Comparison of antioxidant results of substituted NO_2 and unsubstituted NO_2 derivatives of NQ according to CUPRAC method

Compounds	$TEAC_{CUPRAC}$[a]	Compounds	$TEAC_{CUPRAC}$[a]
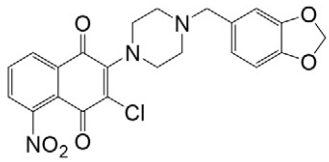 **2**	0.46±0.02	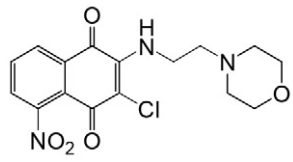 **8**	0.28±0.01
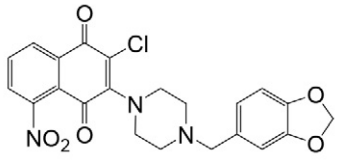 **3**	0.49±0.02	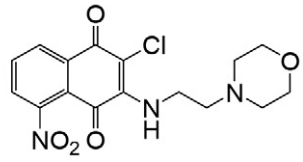 **9**	0.38±0.02
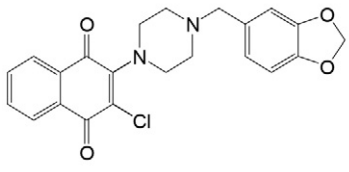 Compound **A**[22]	0.349±0.02[22]	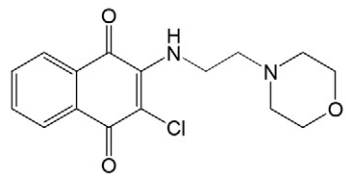 Compound **B**[22]	0.164±0.02[22]

[a] $TEAC_{compound} = \varepsilon_{compound} / \varepsilon_{TR}$ $\varepsilon_{TR} = 1.67\times10^{4}$ $Lmol^{-1}cm^{-1}$ (DMSO).

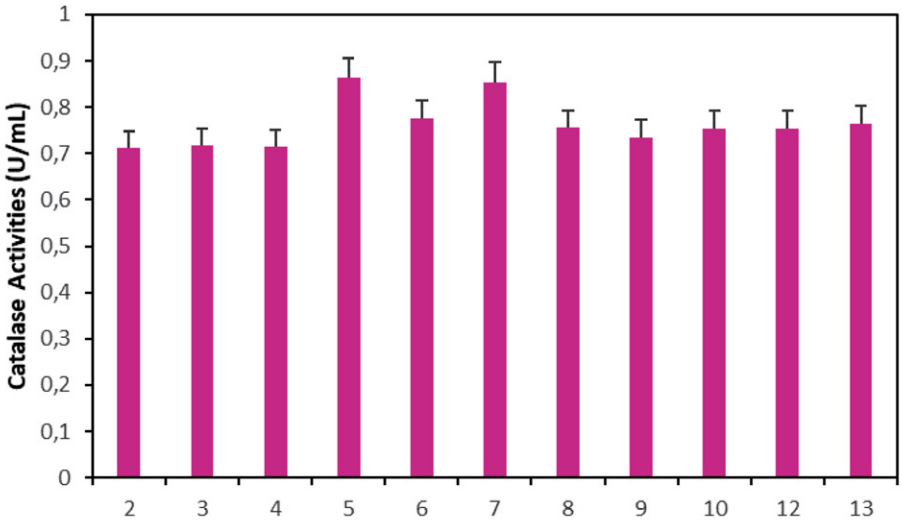

Figure 11. Catalase enzyme activities (U mL^{-1}) of the novel NQ compounds.

4. Conclusions

The studies on nitronaphthoquinone derivatives are rare in the literature and the nitro group associated with the aromatic ring in the quinone system is known to increase the biological activity of naphthoquinone due to its electron-withdrawing properties. For this reason, 2,3-dichloro-5-nitro-1,4-naphthoquinone (**1**) was used as the starting material in this study. The new regioisomeric compounds of 5-nitro-1,4-naphthoquinone **2**–**13** were synthesized by the reactions of 2,3-dichloro-5-nitro-1,4-naphthoquinone with some heterocyclic ring substituted nucleophiles according to a Michael 1,4-addition mechanism. All newly synthesized compounds were characterized by electrospray ionisation mass spectrometry (ESI-MS), Fourier transform infrared spectroscopy (FTIR), ^{1}H nuclear magnetic resonance (^{1}H NMR), attached proton test nuclear magnetic resonance (APT-NMR). Two-dimensional technique ^{1}H–^{1}H correlated spectroscopy (COSY) was used for characterization of compound **1** and regioisomers **2** and **3**. Their *in vitro* antioxidant capacity and catalase enzyme inhibition activity were investigated. The effect of the electron-withdrawing nitro group in the system was directly reflected on the antioxidant results and higher antioxidant capacities were obtained. The compounds **4** and **5** showed comparable antioxidant potency to ascorbic acid. The antioxidant capacity results of all 2-chloro regioisomers are higher than for the 3-chloro regioisomers. Likewise, also catalase enzyme inhibitory activities results were determined in the same way, except for one regioisomer pair.

Supplementary Information (SI)

Supplementary information for this article is available at the journal web site.

Acknowledgements

We gratefully thank the Research Fund of Istanbul University-Cerrahpasa for financial support of this work (Project Numbers: FDK-2017-24871, FYL-2018-30488, FBA-2019-30472, FBA-2019-32783).

Conflict of Interest

No potential conflict of interest was reported by the authors.

5. References

1. R. F. Silver, H. Holmes, *Can. J. Chem.* **1968**, *46*, 1859–1864. **DOI:**10.1139/v68-309
2. H. Tomozane, Y. Takeuchi, T. Choshi, S. Kishida, M. Yamato, *Chem. Pharm. Bull.* **1990**, *38*, 925–929. **DOI:**10.1248/cpb.38.925
3. K. Oogose, Y. Hafuri, E. Takemori, E. Nakata, Y. Inouye, S. Nakamura, A. Kubo, *J. Antibiot.* **1987**, *40*, 1771–1778. **DOI:**10.7164/antibiotics.41.1471
4. N. G. Deniz, C. Ibis, Z. Gokmen, M. Stasevych, V. Novikov, O. Komarovska-Porokhnyavets, M. Ozyurek, K. Guclu, D. Karakas, E. Ulukaya, *Chem. Pharm. Bull.* **2015**, *63*, 1029–1039. **DOI:**10.1248/cpb.c15-00607
5. S. Kurban, N. G, Deniz, C. Sayil, *Bulg. Chem. Comm.* **2016**, *48*, 43–47.
6. C. Sayil, C. Ibis, *Russ. J. Org. Chem.* **2010**, *46*, 216–221. **DOI:**10.1134/S1070428010020119
7. C. Sayil, S. Kurban, C. Ibis, *Phosphorus Sulfur Silicon Relat. Elem.* **2013**, *188*, 1855–1867. **DOI:**10.1080/10426507.2013.796475
8. A. Kacmaz, N. G. Deniz, S. G. Aydinli, C. Sayil, E. Onay-Ucar, E. Mertoglu, N. Arda, *Open Chem.* **2019**, *17*, 337–345.

DOI:10.1515/chem-2019-0030
9. S. Kurban, N. G. Deniz, C. Sayil, M. Ozyurek, K. Guclu, M. Stasevych, V. Zvarych, O. Komarovska-Porokhnyavet, V. Novikov, *Heteroat. Chem.* **2019**, *2019*, 1–12. **DOI:**10.1155/2019/1658417
10. A. Abdassalam, S. Kurban, N. G. Deniz, C. Sayil, *J. Chem. Soc. Pak*. **2019**, *41*, 834–840.
11. V. Chobot, F. Hadacek, *J. Chem. Ecol.* **2009**, *35*, 383–390. **DOI:**10.1007/s10886-009-9609-5
12. C. Soto-Maldonado, M. Vergara-Castro, J. Jara-Quezada, E. Caballero-Valdés, A. Müller-Pavez, M. E. Zúñiga-Hansen, C. Altamirano, *Electron. J. Biotechnol.* **2019**, *39*, 1–7. **DOI:**10.1016/j.ejbt.2019.02.001
13. M. A. Berghot, E. M. Kandeel, A. H. Abdel-Rahman, M. Abdel-Motaal, *Med. Chem.* **2014**, *4*, 381–388. **DOI:**10.4172/2161-0444.1000169
14. A. A. Kutyrev, V. V. Moskva, *Russ. Chem. Rev.* **1991**, *47*, 72–88. **DOI:**10.1070/RC1991v060n01ABEH001032
15. C. Blackburn, *Tetrahedron Lett.* **2005**, 46, 1405–1409. **DOI:**10.1016/j.tetlet.2005.01.049
16. B. S. Samant, C. Chakaingesu, *Bioorganic Med. Chem. Lett*. **2013**, *23*, 1420–1423. **DOI:**10.1016/j.bmcl.2012.12.075
17. A. Nandi, L. J. Yan, C. K. Jana, N. Das, *Oxid. Med. Cell. Longev*. **2019**, *2019*, 1–20. **DOI:**10.1155/2019/9613090
18. L. Yang, X. L. Zheng, H. Sun, Y. J. Zhong, Q. Wang, H. N. He, X. W. Shi, B. Zhou, J. K. Li, Y. Lin, L. Zhang, X. Wang, *Cancer Sci.* **2011**, *102*, 870–876. **DOI:**10.1111/j.1349-7006.2011.01874.x
19. R. Apak, K. Guclu, M. Ozyurek, S. E. Karademir, *J. Agric. Food Chem.* **2004**, *52*, 7970–7981. **DOI:**10.1021/jf048741x
20. B. Bekdeser, M. Ozyurek, K. Guclu, F. Ustun Alkan, R. Apak, *Spectrochim. Acta Part A* **2014**, *132*, 485–490. **DOI:**10.1016/j.saa.2014.04.178
21. G. M. Neelgund, M. L. Bundni, *Spectrochim. Acta A Mol. Biomol. Spectrosc.* **2004**, *60* 1793–1803. **DOI:**10.1016/j.saa.2003.09.017
22. T. S. Gwon, B. W. Lee, *Bull. Korean Chem.* **1998**, *19*, 1337–1341.
23. G. H. Jones, J. M. Young, Naphthoquinone anti-psoriatic agents, US Patent Number 4,442,127, date of patent April 10, **1984**.
24. J. E. Egleton, C. C. Thinnes, P. T. Seden, N. Laurieri, S. P. Lee, K. S. Hadavizadeh, A. R. Measuresn, A. M. Jones, S. Thompson, A. Varney, G. M. Wynne, A. Ryan, E. Sim, A. J. Russell, *Bioorg. Med. Chem.* **2014**, *22*, 3030–3054. **DOI:**10.1016/j.bmc.2014.03.015
25. J. Chen, J. Yang, L. Ma, J. Li, N. Shahzad, C. K. Kim, *Sci. Rep*. **2020**, *10*, 2611–2620. **DOI:**10.1038/s41598-020-59451-z

Povzetek

Raziskave nitronaftakinonskih derivatov so v literaturi redke, čeprav je znano, da prisotnost nitro skupine na aromatskem obroču zaradi svojih elektron-privlačnih lastnosti skupaj s kinonskim sistemom poveča biološko aktivnost tovrstnih naftokinonskih sistemov. Z reakcijo med 2,3-dikloro-5-nitro-1,4-naftokinonom in različnimi nukleofili, substituiranimi s heterocikličnimi fragmenti, kot so anilini, piperazini in morfolini, smo s pomočjo Michaelove 1,4-adicije sintetizirali nove regioizomere N(H)-substituiranih-5-nitro-1,4-naftokinonov (NQ). Poročamo o petih regioizomernih parih NQ z različnimi funkcionalnimi skupinami, ki se ločijo po položajih klorovega substituenta (2-kloro izomeri **3**, **5**, **7**, **9** in **13** ter 3-kloro izomeri **2**, **4**, **6**, **8** in **12**). Vse nove spojine smo karakterizirali s spektroskopskimi metodami in dvodimenzionalno NMR tehniko ^{1}H–^{1}H korelacijske spektroskopije (COSY).

Pripravljenim NQ regioizomerom smo določili inhibitorne aktivnosti na encimu katalaza. S pomočjo metode bakrove redoks antioksidativne kapacitete (CUPRAC) smo določili njihovo antioksidativno delovanje. 2-Kloro-3-((2,4-dimetoksifenil)amino)-5-nitronaftalen-1,4-dion (**5**) se je izkazal z najvišjo antioksidativno kapaciteto in sicer je koeficient CUPRAC-troloks antioksidativne kapacitete (TEAC) znašal 1.80±0.06. Spojina **5** je izkazala tudi najmočnejšo inhibitorno aktivnost na encim katalaza. Ugotovili smo, da je antioksidativna kapaciteta za vse 2-kloro regioizomere večja kot za 3-kloro regioizomere. Za vse spojine, razen za en regioizomerni par, so bili analogni tudi rezultati za inhibitorno aktivnost na encim katalaza. Nove spojine so učinkovito inhibirale katalazo, odstotek inhibicije je bil v območju 0.71–0.86 %. Nekatere izmed teh NQ spojin so pokazale precejšnje antioksidativne kapacitete.

Except when otherwise noted, articles in this journal are published under the terms and conditions of the Creative Commons Attribution 4.0 International License

DOI: 10.17344/acsi.2021.7182 *Acta Chim. Slov.* **2022,** *69,* 200–216
creative commons

Scientific paper

Metal Based Bioactive Nitrogen and Oxygen Donor Mono and Bis Schiff Bases: Design, Synthesis, Spectral Characterization, Computational Analysis and Antibacterial Screening

Sajjad Hussain Sumrra,[1,*] Wardha Zafar,[1] Sabaahatul Ain Malik,[1] Khalid Mahmood,[2] Syed Salman Shafqat[3] and Saira Arif[1]

[1] *Department of Chemistry, University of Gujrat, Gujrat 50700, Pakistan;*

[2] *Institute of Chemical Sciences, Bahauddin Zakariya University, Multan, Pakistan;*

[3] *Department of Chemistry, Division of Science and Technology, University of Education, Lahore, Pakistan*

* *Corresponding author: E-mail: sajjadchemist@gmail.com/sajjadchemist@uog.edu.pk*

Received: 09-30-2021

Abstract

The scientific interest in developing the advanced metal based compounds to inhibit and control bacterial infections is continuously rising. Keeping in view their pharmacological significance, two new bioactive symmetrical phenylenediamine mono- and bis-Schiff bases, *2-{[(4-aminophenyl)imino]methyl}-6-methoxyphenol* **(L^1)** and *2,2'-{benzene-1,2-diylbis[nitrilomethylylidene]}bis(6-methoxyphenol)* **(L^2)** have been synthesized and characterized by using physical techniques, spectral methods, elemental and DFT based computational analysis with B3LYP/6-311++G(d, p) basis set. Furthermore, the synthesized ligands were complexed with VO, Mn, Co, Ni, Cu and Zn ions in ratio [M:L,1:2 and 1:1], respectively. All the complexes exhibited significant antibacterial action against all tested bacterial strains. But overall, the zinc complexes possessed higher antibacterial activity. These results concluded that metal complexes might be promising induction in the upcoming time for medical purposes.

Keywords: Symmetrical phenylenediamine mono and bis-Schiff bases; computational study; chelation; bidentate and tetradentate; antibacterial activity.

1. Introduction

Schiff base ligands occupy significant importance in coordination chemistry as they have potential to form medicinally important metal complexes.[1] They have attained greater attention in biological and coordination chemistry because of their facile preparation, structural variability and diversity.[2] They are significantly involved in the development of chelates. Particularly, the Schiff bases having –OH, –SH and $–NH_2$ nucleophilic substituents at *ortho* position to the azomethine group have appropriate structures for coordination with metal ions forming more stable metal chelates.[3] Schiff base ligands with electron donors such as nitrogen and oxygen atoms have been extensively investigated because of their competent therapeutic potentials.[4] They are also significant for their biological action against fungi, bacteria[5] and certain types of tumors.[6]

Nowadays, the design and development of new compounds for dealing with resistant microbes have become an important area of antifungal and antibacterial research, as resistance of pathogenic microbes towards already existing antimicrobial drugs is rapidly becoming a worldwide problem. And the discovery of novel metal based antimicrobial agents is one of the most challenging demands for pharmacologists and chemists today.[7] The work highlights the bioactivity of those compounds of first-row divalent and tetravalent transition metals which are non-toxic, economical as well as readily available for pharmacology. Most of the first-row transition metals are essential for biological processes[8] such as respiration, cell division, photosynthesis and nitrogen fixation.[9] Apart from choice of transition metals, it is also important to properly design the ligand framework as it has the ability to modify the systematic/oral bioavailability of metals, se-

cure some selective target enzymes or DNA, protect as well as supply metal ions at targeted sites.[10]

Slight modifications in the structure of ligand could significantly increase the pharmacological properties of metal complexes through the endorsement of bioactive metal ions.[11] The metal complexes of Schiff bases have been known to possess different biological activities like antifungal,[12] enzyme inhibition,[13] anticancer,[14] anticonvulsant,[15] antitumor,[16] anti-proliferative,[17] antibacterial,[18] antioxidant,[19] anti-inflammatory,[20] cytotoxic,[21] DNA binding[22] and antiviral.[23] Literature reveals that extensive work have been done on the preparation of various symmetrical tetradentate Schiff bases from 1,2-diamines with *ortho*-hydroxyketones/aldehydes.[24] The metal complexes of 1,2-diamine have a vital role in both structural and synthetic research,[25] related to analytical, pharmaceutical, biological and clinical fields.[26]

With the expansion of our research work describing the synthesis, structure elucidation and pharmacological properties of chemical scaffolds prepared by the condensation of phenylenediamine with aromatic carbonyls,[27] here we report the facile synthesis of two new phenylenediamine derived mono- and bis-Schiff bases, *2-{[(4-aminophenyl)imino]methyl}-6-methoxyphenol* **(L^1)** and *2,2'-{benzene-1,2-diylbis[nitrilomethylylidene]}bis(6-methoxyphenol)* **(L^2)** and their complexes with VO(IV), Mn(II), Co(II), Ni(II), Cu(II) and Zn(II) metals. All the synthesized compounds have been studied in detail for their structure, physicochemical and *in vitro* antibacterial properties against one Gram positive bacteria (GPB) and one Gram negative bacteria (GNB). Density functional parameters have been utilized for analysing the molecular designs, active sites, molecular interactions along with biochemical activity. The experimental findings have been compared to their computed results.

2. Experimental

2. 1. Materials

Chemicals of analytical grade were used during the research work. *o*-Phenylenediamine, *p*-phenylenediamine and 2-hydroxy-3-methoxybenzaldehyde were purchased from Sigma Aldrich which were extremely pure so they were used without further purification. Ethanol and dioxane were distilled for the additional refinement because they have been used as solvents in the reaction media for the synthetic reactions of ligands and their corresponding metal chelates, respectively.

2. 2. Instrumentation

The melting temperatures of ligands and decomposition temperatures of metal complexes were determined using Stuart apparatus. FT-IR spectra were documented using Nicolet FT-IR Impact 400D infrared Spectrophotometer in working range (4000–400 cm^{-1}). Proton NMR spectra of the mono- and bis-Schiff bases were obtained through Bruker Advance 300 MHz using DMSO (dimethyl sulfoxide) solvent. The mass spectra of ligands were taken on JEOL MS Route instrument. UV-Vis spectra were recorded on Hitachi UV-3200 spectrophotometer using DMF (dimethyl formamide) solvent. Magnetic moment values for the metal complexes were recorded with the Magnetic Susceptibility Balance (MSB Mk-1) using $MnCl_2$ as a reference. Molar conductivity measurements of metal complexes (0.001M solutions in DMF) were carried out using Inolab Cond 720 Conductivity Bridge at room temperature. The antibacterial activity was performed using DMSO solvent on ESCO Laminar Flow Cabinet and Memmert incubator at the Department of Biochemistry, University of Gujrat, Gujrat, Pakistan.

2. 3. Synthesis of Ligands

The phenylenediamine based ligands, *2-{[(4-aminophenyl)imino]methyl}-6-methoxyphenol* **(L^1)** and *2,2'-{benzene-1,2-diylbis[nitrilomethylylidene]}bis(6-methoxyphenol)* **(L^2)** have been synthesized by adopting already published path[28] as shown in Scheme 1. The *p*-phenylenediamine ligand **(L^1)** was synthesized by adding the equimolar amount of ethanolic solution of 2-hydroxy-3-methoxybenzaldehyde (10 mmol, 1.52 g) over a stirred ethanolic solution of *p*-phenylenediamine (10 mmol, 1.08 g). Change in colour and precipitate formation in the reaction mixture was the first indication of the successful reaction. The reaction mixture was continuously stirred and the advancement in the reaction mixture was checked by taking comparative thin layer chromatography (TLC). The finishing point of the reaction was evidenced through a single spot of ligand on the TLC. The precipitates of ligand were then filtered out, rinsed with warm ethanol, dried off and then recrystallized by 1:2 ratio of ethanol and ether to obtain the pure product. The *o*-phenylenediamine ligand **(L^2)** was also synthesized by the same pathway through refluxing instead of stirring the ethanolic solution of *o*-phenyl-

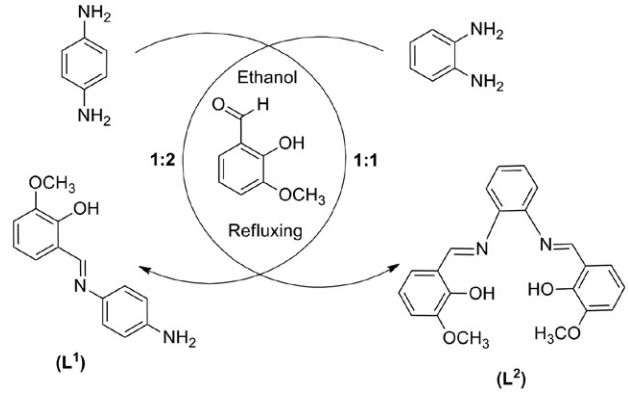

Scheme 1. Synthesis of phenylenediamine Schiff base ligands **(L^1)** & **(L^2)**

enediamine (5 mmol, 0.54 g) with same 2-hydroxy-3-methoxybenzaldehyde (10 mmol, 1.52 g) in 1:2 molar ratio.

2. 3. 1. *2-{[(4-Aminophenyl)imino]methyl}-6-methoxyphenol* (L^1)

Yield (%): 82; m.p. (°C): 256; colour: light yellow; IR (KBr, cm^{-1}): 3427 (OH), 3020 (NH_2), 2930 (OCH_3), 1640 (HC=N), 1389 (C-O); ^{1}HNMR (DMSO-d_6, 300 MHz) δ (ppm): 3.82 (s, 3H, OCH_3), 6.90-7.26 (m, 7H, Ar-H), 7.53 (s, 2H, NH_2), 9.01 (s, 1H, HC=N), 13.17 (s, 1H, OH); MS (ESI) *m/z* (%): 241.1 ([M]$^+$, 100), 227.1 (24), 209.1 (09), 197.0 (08), 183.0 (05), 154.0 (10), 135.0 (04); Anal. calcd. for $C_{14}H_{14}N_2O_2$ (%) C, 69.4; N, 11.56; H, 5.82; found: C, 69.35; N, 11.49; H, 5.78.

2. 3. 2. *2,2'-{Benzene-1,2-diylbis[nitrilomethylylidene]}bis(6-methoxyphenol)* (L^2)

Yield (%): 73; m.p. (°C) 173; colour: dark orange; IR (KBr, cm^{-1}): 3431 (OH), 3100 (C-H), 2918 (OCH_3), 1638 (HC=N), 1396 (C-O); ^{1}HNMR (DMSO-d_6, 300 MHz,) δ (ppm): 3.92 (s, 3H, OCH_3), 6.88-6.93 (t, 1H, C_8-H, C_{18}-H), 6.95-6.97 (d, 1H, C_9-H, C_{19}-H), 7.07-7.13 (dd, 1H, C_7-H, C_{23}-H), 7.23-7.28 (d, 1H, C_3-H), 7.38-7.46 (m, 1H, C_1-H, C_2-H), 7.60-7.64 (d, 1H, C_6-H), 8.91 (s, 1H, HC=N), 12.97 (s, 1H, OH); MS (ESI) *m/z* (%): 376.4 ([M]$^+$, 100), 361.2 (36), 253.1 (25), 240.1 (62), 222.1 (28), 211.1 (22), 197 (14). Anal. Calcd. for $C_{22}H_{20}N_2O_4$ (%): C, 70.20; N, 7.44; H, 5.36; found: C, 69.96; N, 7.38; H, 5.31.

2. 4. Synthesis of Transition Metal Complexes

All the transition metal complexes of *p*-phenylenediamine ligand (**L^1**) were synthesized using 1:2 molar ratio of metal to ligand by accomplishing previously reported protocol.[28] The ligand (20 mmol) was dissolved in 10 mL dioxane and magnetically refluxed until the ligand was completely dissolved. Then, the respective metallic salt (vanadyl sulphate hydrate, manganese(II) chloride, cobalt(II) chloride hexahydrate, nickel(II) chloride hexahydrate, copper(II) chloride dihydrate and anhydrous zinc(II) chloride) solution (10 mmol) was gradually added in the ligand solution with continual stirring. After that, the reaction mixture was further refluxed for 6 hours. The reaction was observed by using TLC at regular intervals. Desired products were obtained in the form of the precipitates, which were filtered, washed with hot dioxane, dried and then recrystallized using dioxane and ether (1:2) to obtain the pure product. For the synthesis of metal complexes of *o*-phenylenediamine ligand (**L^2**), same procedure was fallowed except that ligand (**L^1**) was replaced with ligand (**L^2**) and equimolar ratio of ligand and metal salts were used. All complexes were synthesized according to above mentioned procedure and their structures are shown in Scheme 2.

2. 5. Computational Study

Both the ligands (**L^1**) and (**L^2**) and their selected 3*d*-metal complexes have been optimized by density functional theory (DFT) to insight their geometries in absence of their well resolved SC-XRD data. For this computational study, the Gaussian 09 program[29] was employed to execute all the theoretical simulations for molecular dynamics with the help of DFT. Based on the B3LYP method with 6-311++G(d, p) basis sets, the molecular geometries of compounds were thoroughly optimized at their ground state energy levels. The HOMO-LUMO energies together with their energy differences for optimized structures were

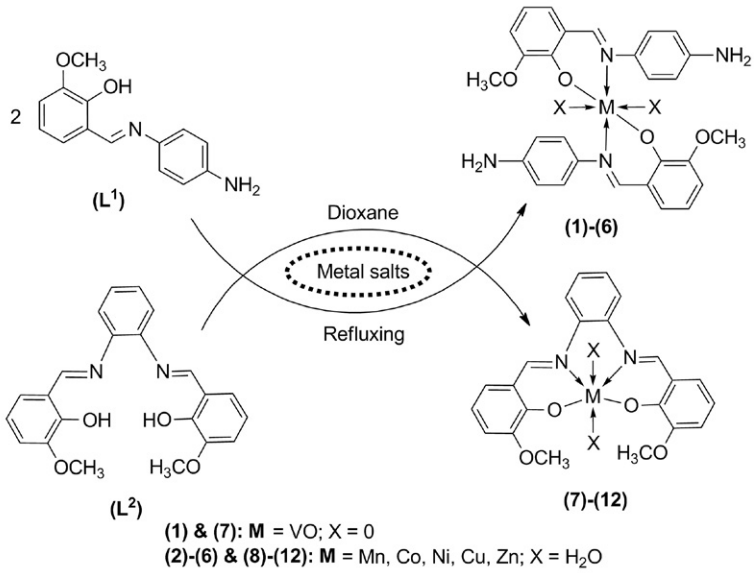

Scheme 2. Synthesis of phenylenediamine metal based compounds (**1**)–(**12**)

calculated to analyse their quantum chemical parameters. The structural characteristics, stability and molecular quantities *i.e.,* chemical softness, hardness and electronegativity, electrophilicity were determined satisfactorily.[30] The computed FT-IR spectra of the studied molecular systems have also been established from their optimized geometrical structures through B3LYP/6-311++G(d, p) functions. The natural bond orbital (NBO) analysis, Mulliken atomic charges (MAC) and molecular electrostatic potential (MEP) maps of the studied molecules have been assessed at the same functional, whereas UV–Vis spectra have been computed employing the TD-DFT (time-dependent density functional theory) accompanied by the afore-mentioned functional. Furthermore, all the input data files were structured using Gaussview 5.0.[31] While GaussSum,[32] Avogadro,[33] Chemcraft[34] and Gaussview 5.0 programs have been utilized to interpret and visualize the outcomes of the optimized structures, computed spectra along with the summary of their geometrical parameters like bond lengths and bond angles.

2. 6. Antibacterial Study

Anti-bacterial action of the prepared compounds was evaluated against three G- bacteria (GNB) *i.e., Salmonella typhi*, *Klebsiella pneumonia, Escherichia coli* and one Gram+ bacteria (GPB) *i.e., Staphylococcus aureus* through disc diffusion method.[35] Standard drugs ampicillin and streptomycin were used to compare the results. Equivalent quantity of both nutrient broth and agar-agar were mixed up in distilled water. The synthesized media, filter paper strips and petri dishes were autoclaved for about 30 minutes at 121 °C for sterilization. Then, the semi-liquid media was transferred to petri dishes and allowed to solidify. After that, the bacterial inoculum was spread over the media by means of glass spreader. Later on, the filter paper strips were placed at the regular distance on the solidified media. Then, 10 µL of DMSO, sample solutions and standards having same concentration (2 mM in DMSO) were poured onto the strips *via* micropipette. In this analysis, DMSO and standards acted as negative and positive controls, correspondingly. The plates were properly labelled for each sample and standard, tightly wrapped and placed in incubator at 37 °C temperature for 24 hours. Finally, the inhibition zones of the tested samples and standards were checked and recorded in millimetre (mm) against each bacterial strain.

3. Results and Discussion

The symmetrical Schiff base ligands **(L^1)** and **(L^2)** were prepared in 1:1 and 1:2 molar ratio by condensation reaction of *o*-vanillin with *p*-phenylenediamine and *o*-phenylenediamine, respectively. The synthesized ligands

Table 1. Physical, analytical and elemental details of metal complexes **(1)**–**(12)**

No	Compound M.P (°C)	Formula Colour	M.W (g/mol) Yield (%)	Calculated (%) (Found) C	H	N	M
(1)	$VO(L^1)_2$	$C_{28}H_{26}N_4O_5V$	547.47	61.20	4.77	10.20	9.27
	300+	Pine green	65	(61.08)	(4.65)	(10.11)	(9.14)
(2)	$Mn(L^1)_2(H_2O)_2$	$C_{28}H_{30}N_4O_6Mn$	573.50	58.64	5.27	9.77	9.58
	283–285	Dark brown	78	(58.59)	(5.21)	(9.68)	(9.45)
(3)	$Co(L^1)_2(H_2O)_2$	$C_{28}H_{30}N_4O_6Co$	577.49	58.23	5.24	9.70	10.20
	277–279	Russet Brown	70	(58.18)	(5.19)	(9.64)	(10.07)
(4)	$Ni(L^1)_2(H_2O)_2$	$C_{28}H_{30}N_4O_6Ni$	577.25	58.26	5.24	9.71	10.17
	289–291	Cyan	72	(58.18)	(5.16)	(9.63)	(10.09)
(5)	$Cu(L^1)_2(H_2O)_2$	$C_{28}H_{30}N_4O_6Cu$	582.11	57.77	5.19	9.62	10.92
	293–295	Olive green	82	(57.65)	(5.08)	(9.53)	(10.88)
(6)	$Zn(L^1)_2(H_2O)_2$	$C_{28}H_{30}N_4O_6Zn$	583.94	57.59	5.18	9.59	11.20
	264–266	Off–white	72	(57.51)	(5.07)	(9.50)	(11.06)
(7)	$VO(L^2)$	$C_{22}H_{18}N_2O_5V$	441.33	59.87	4.11	6.35	11.54
	265–267	Greenish black	72	(59.73)	(4.05)	(6.31)	(11.47)
(8)	$Mn(L^2)(H_2O)_2$	$C_{22}H_{22}N_2O_6Mn$	465.37	56.78	4.77	6.02	11.81
	276–278	Brownish green	68	(56.64)	(4.72)	(5.96)	(11.76)
(9)	$Co(L^2)(H_2O)_2$	$C_{22}H_{22}N_2O_6Co$	469.35	56.30	4.72	5.97	12.56
	248–250	Dark violet	77	(56.17)	(4.67)	(5.90)	(12.50)
(10)	$Ni(L^2)(H_2O)_2$	$C_{22}H_{22}N_2O_6Ni$	469.1	56.33	4.73	5.97	12.51
	260–262	Dark grey	83	(56.18)	(4.68)	(5.93)	(12.43)
(11)	$Cu(L^2)(H_2O)_2$	$C_{22}H_{22}N_2O_6Cu$	473.97	55.75	4.68	5.91	13.41
	230–232	Greenish black	82	(55.65)	(4.64)	(5.88)	(13.47)
(12)	$Zn(L^2)(H_2O)_2$	$C_{22}H_{22}N_2O_6Zn$	475.83	55.53	4.66	5.89	13.74
	239–241	Off–white	81	(55.41)	(4.60)	(5.83)	(13.66)

were moisture and air stable. Both the ligands were completely soluble in DMSO, DMF and dioxane at room temperature. Both these ligands were then reacted with metallic salts $VOSO_4 \cdot H_2O$, $MnCl_2 \cdot 2H_2O$, $NiCl_2 \cdot 6H_2O$, $CoCl_2 \cdot 6H_2O$, $CuCl_2 \cdot 2H_2O$ and $ZnCl_2$ to synthesize 3*d*-metal complexes in metal to ligand molar ratio of 1:2 and 1:1, respectively (Scheme 1). All the as-synthesized metal chelates were microcrystalline solids having intense colours except zinc complexes which were colourless. The metal complexes exhibited greater range of decomposition points with regard to their respective ligands as a result of strong bonding in metal chelates. The structures of synthesized phenylenediamine Schiff bases and their corresponding 3*d*-metal chelates were explored on the basis of their spectral, physical and micro-analytical results. The non-electrolytic behaviour of the metal chelates was specified by their minor conductance values. The spectral results together with elemental analysis agreed well with the proposed structures of the as-synthesized compounds, verifying their high purity (given in Table 1).

3. 1. FT-IR Spectra

The IR spectra of both ligands showed a typical peak of azomethine linkage (HC=N) at 1638-1640 cm^{-1} that gave a clue about the condensation of amine (-NH_2) group of phenylenediamine with carbonyl (C=O) group of 2-hydroxy-3-methoxybenzaldehyde. Moreover, the ligands also exhibited different bands at 3427–3431, 2918–2930 and 1389–1396 cm^{-1} because of the existence of ν(OH), ν(OCH_3) and ν(C-O) groups, respectively.[36] The vibrational spectrum of ligand **(L^1)** demonstrated a peak at 3020 cm^{-1} (Figure S1) signifying the non-participation of one amino (NH_2) group of *p*-phenylenediamine moiety in the condensation process, consequently validating the synthesis of mono-Schiff base **(L^1)**. While the characteristic peaks of both amino (NH_2) groups of *o*-phenylenediamine moiety were missing in the spectrum of ligand **(L^2)** confirming the synthesis of bis-Schiff base (Figure S2).

IR spectra of the phenylenediamine Schiff bases **(L^1)** and **(L^2)** have been compared with metal complexes and showed that the Schiff bases were bonded with metal ions in bidentate and tetradentate mode, respectively (Table 2). Coordination of both ligands with 3*d*-metallic ions occurred *via* oxygen atom of benzaldehyde by the deprotonation of phenolic group and nitrogen atom of azomethine (Figure S3-S4). The coordinating action of the azomethine-N with the metal atoms was confirmed from the shifting of the IR band of azomethine (CH=N) linkage from 1638-1640 cm^{-1} to lower frequency at 1620–1630 cm^{-1}.[37] The absence of band at 3427–3431 cm^{-1} because of ν(OH) group accompanied by the shifting of ν(C–O) band from 1389-1396 cm^{-1} to 1381–1388 cm^{-1} indicated the deprotonation of phenolic group of the ligands and its coordination with metal ions.[38]

Existence of new weak bands at 431–440 and 523–539 cm^{-1} in the metal complexes, were allocated to ν(M–O) and ν(M–N) vibrations, correspondingly[39] and these vibrational bands were not observed in the spectra of the uncomplexed ligands. A peak was emerged at 968–972 cm^{-1} only in the vibrational spectra of VO(IV) complexes **(1)** and **(7)** which was owing to ν(V=O). New broad peaks appearing in all the complexes except vanadium complexes at 3423–3479 cm^{-1} were due to existence of H_2O molecules.[40] There was no change in IR bands of methoxy (OCH_3) group indicating that it was not involved in the complexation.[41] All these evidences confirmed that the ligands bonded with the respective metal cations by azomethine-N along with benzaldehydic-O by the deprotonation of phenolic group.

3. 2. UV-Vis Spectra

The experimental UV-Vis spectra of all the as-synthesized complexes were recorded in dimethylformamide using 10^{-1} M concentration. The UV–Vis spectra of ligands have shown a band at 282–297 nm attributed to π–π* electronic structure of aromatic ring system. However, the

Table 2. Magnetic, conductivity and IR spectral data of metal complexes **(1)**–**(12)**

No.	μ_{eff} (B.M)	Ω_M ($\Omega^{-1}cm^2mol^{-1}$)	ν (cm^{-1})
(1)	1.72	13.5	3153 (NH_2), 1625 (C=N), 972 (V=O), 538 (V-N), 434 (V-O)
(2)	5.78	12.9	3479 (H_2O), 3128 (NH_2), 1622 (C=N), 535 (Mn-N), 432 (Mn-O)
(3)	4.34	15.4	3477 (H_2O), 3140 (NH_2), 1626 (C=N), 547 (Co-N), 445 (Co-O)
(4)	3.07	17.6	3467 (H_2O), 3152 (NH_2), 1620 (C=N), 528 (Ni-N), 440 (Ni-O)
(5)	1.81	19.2	3423 (H_2O), 3167 (NH_2), 1621 (C=N), 540 (Cu-N), 439 (Cu-O)
(6)	Dia	15.6	3470 (H_2O), 3145 (NH_2), 1627 (C=N), 549 (Zn-N), 435 (Zn-O)
(7)	1.76	12.7	1622 (C=N), 972 (V=O), 528 (V-N), 439 (M-O)
(8)	5.85	17.2	3429 (H_2O), 1620 (C=N), 535 (Mn-N), 431 (Mn-O)
(9)	4.21	14.8	3475 (H_2O), 1628 (C=N), 537 (Co-N), 437 (Co-O)
(10)	3.11	22.3	3445 (H_2O), 1625 (C=N), 528 (Ni-N), 440 (Ni-O)
(11)	1.87	15.4	3470 (H_2O), 1623 (C=N), 539 (Cu-N), 437 (Cu-O)
(12)	Dia	18.3	3473 (H_2O), 1630 (C=N), 530 (Zn-N), 433 (Zn-O)

other absorption bands were documented as λ_{max} at the 339–364 and 395–407 nm owing to n–π* electronic transitions by the azomethine linkage together with charge transfer, correspondingly.[42] The vanadium(IV) complexes, **(1)** and **(7)** exhibited their characteristic bands in the range of 374–387, 529–536 and 733–747 nm as a result of the electronic transitions that were referred to $B_2 \rightarrow E_\pi$, $B_2 \rightarrow B_1$ and $B_2 \rightarrow A_1$ thus validating their predicted square pyramidal geometry.[43] The three bands in the UV-Vis spectra of manganese(II) complexes **(2)** and **(8)** were observed at 221–233 nm 251–267 nm and 342–356 nm due to intra-ligand electronic transitions and $^6A_{1g} \rightarrow {}^4E_g$ therefore verifying their proposed octahedral geometry.

The cobalt(II) complexes **(3)** and **(9)** had shown a high energy band of 327-348 nm along with the low energy absorption bands ranging from 506-586 and 1135-1157 nm because of $^4T_{1g}(F) \rightarrow {}^4T_{1g}(P)$ and $^4T_{1g}(F) \rightarrow {}^4T_{2g}(F)$ electronic transitions evidencing their anticipated octahedral geometrical structure.[44] The three electronic bands of nickel(II) complexes **(4)** and **(10)** were observed in the range of 389–425, 617–645 and 1024–994 nm owing to $^3T_{2g}(F) \rightarrow {}^3T_{1g}(P)$, $^3A_{2g}(F) \rightarrow {}^3T_{1g}(F)$ and $^3A_{2g}(F) \rightarrow {}^3T_{2g}(F)$ electronic transitions proving their estimated octahedral geometry. The copper(II) complexes, (**5**) and (**11**) demonstrated two absorption bands at 518–524 and 631–674 nm due to $^2B_{1g} \rightarrow {}^2E_g$ and $^2B_{1g} \rightarrow {}^2A_{1g}$ excitations as well as a highly intense band as a result of metal→ligand charge transfer (MLCT) at 338–345 nm suggesting their octahedral geometry.[45] Only a strong band owed to MLCT at 322–336 nm was recorded for zinc(II) complexes **(6)** and **(12)**, signifying the absence of d–d transitions and confirming their anticipated octahedral geometry.[46]

3. 3. ^{1}H-NMR Spectra

^{1}HNMR spectra of the phenylenediamine Schiff bases **(L^1)** and **(L^2)** were determined in DMSO-d_6. All the aromatic as well as heteroaromatic protons were observed in their estimated ranges. In the spectra of both ligands, the distinctive singlet peak of imine (HC=N) proton was spotted at 8.91–9.01 ppm. While in the spectrum of ligand **(L^1)**, the singlet peak of two amino (NH_2) protons was observed at 7.53 ppm, signifying that only one amino group of *p*-phenylenediamine was condensed with *o*-vanillin, indicating the synthesis of mono-Schiff base ligand (Figure S5). While the absence of both amino (NH_2) group of *o*-phenylenediamine (Figure S6) specified the synthesis of bis-Schiff base ligand **(L^2)**. The peaks of methoxy (OCH_3) group protons of both Schiff bases were observed as singlet at 3.82-3.92 ppm. The aromatic protons were appeared in the range 6.88–7.64 ppm. Furthermore, the phenolic (OH) group protons were found at 12.97–13.17 ppm as singlet. Absence of aldehydic (CH=O) group protons in the spectra of both ligands, confirmed that the condensation phenomenon was occurred between phenylenediamine and *o*-vanillin.

3. 4. Mass Spectra

The mass spectra of both phenylenediamine Schiff bases showed the molecular weights (*m/z*) and base peaks (%). The base peak as well as molecular ion peak of the ligand **(L^1)** was found at *m/z* 241.1 due to $[C_{14}H_{13}N_2O_2]^+$ fragment (Figure S7). While the ligand **(L^2)** displayed molecular ion peak of $C_{22}H_{20}N_2O_4$ fragment at *m/z* 376.4 that was equivalent to its molecular weight (Figure S8). This was also the most stable fragment. Similarly, all the daughter fragments were obtained by the cleaving action of exocyclic as well as endocyclic (C=N) and (C=C) groups. The results of mass spectra evidently confirmed the synthesis of both phenylenediamine Schiff bases with their proposed structures.

3. 5. Molar Conductivity and Magnetic Moment Measurements

The molar conductivity measurements of the synthesized metal complexes have been carried out at room temperature using dimethylformamide solvent and the conductivity readings are depicted in Table 2. The complexes were found to be non-electrolytes in nature as their molar conductance values were observed in the range 12.7–22.3 $\Omega^{-1}cm^2mol^{-1}$.[47] The findings of molar conductivity analysis declared all the metal complexes as neutral having no free anions outside the coordination sphere.

Magnetic moments have contributed valuable details regarding the number of unpaired electrons together with stereochemistry of metal cations, leading towards the determination of the appropriate geometries of the complexes. Depending on the magnetic influence of the unpaired electrons, some metal complexes have shown greater values of magnetic moments while others presented lesser magnetic moments (as given in Table 2). The vanadyl complexes **(1)** and **(7)** had the magnetic moment values of 1.72–1.76 B.M which showed one unpaired electron and thus confirmed a square pyramidal configuration for both VO(IV) complexes.[48] The Mn(II) complexes **(2)** and **(8)** have exhibited 5.78–5.85 B.M that pointed towards the presence of five unpaired electrons suggesting octahedral arrangement.[49] The Co(II) complexes **(3)** and **(9)** displayed the magnetic moments at 4.21–4.34 B.M, signifying complexes have high spins with three unpaired electrons present in an octahedral geometry.[50] The measured magnetic moments of nickel complexes **(4)** and **(10)** were found at 3.07–3.11 B.M representing the existence of two unpaired electrons thus signifying an octahedral configuration for Ni(II) complexes.[51] The magnetic moments for Cu(II) complexes **(5)** and **(11)** have been observed as 1.81-1.87 B.M representing only one unpaired electron for each copper metal ion with d^9-system indicating octahedral geometry for copper complexes.[52] The Zn(II) complexes **(6)** and **(12)** had zero magnetic moment showing no unpaired electron thus both the complexes were found to be diamagnetic in nature as expected.[53]

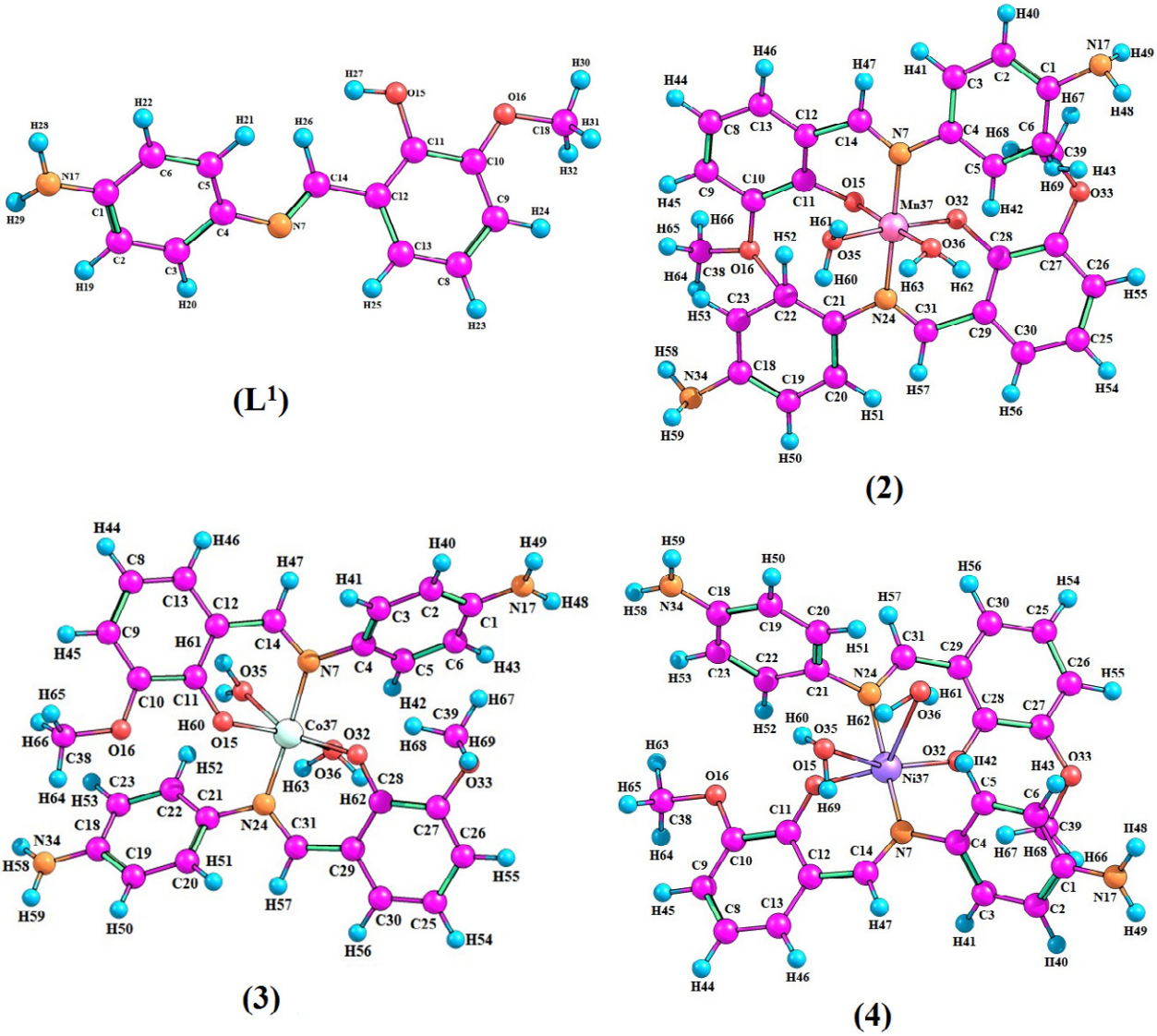

Figure 1. View of optimized geometrical structures of *p*-phenylenediamine ligand (**L¹**) and its derived metal complexes (**2**), (**3**) and (**4**)

3. 6. Molecular Geometric Parameters

Complete process of geometry optimization has been accomplished without any symmetry restriction by employing B3LYP level of DFT in combination with basis set 6-311++G(d, p). The vibrational analysis employing DFT/B3LYP/6-311++G(d, p) level of theory has also been carried out to further validate the stability related with optimized geometrical structures. No hypothetical frequency was detected from the vibrational scrutiny of investigated compounds, which signified the completion of their geometry optimization. Figures 1 & 2 illustrate the molecular structure of all the studied compounds with atom numbering. The optimized geometrical elements including bond angles together with bond lengths were estimated with DFT study by the B3LYP level, and the representative outcomes are given in Table S1 (Supplementary Information).

For complexes (**2**), (**3**) and (**4**), the bond lengths of C4-N7, N7-C14 and C11-O15 were increased, because of the reason that the chelation occurred *via* N7, O15 with metallic centres (Mn, Co and Ni). Similarly for complexes (**7**), (**11**) and (**12**), increase in C5-N13, N13-C15, C4-N14, N14-O24, O16-C11 and O25-C21 bond lengths was observed as a result of the complexation *via* N13, N14, O16, O25 with metallic centres (V, Cu and Zn). This increase in bond lengths signified that the ligands (**L¹**) and (**L²**) coordinated *via* N7, O15 and N13, N14, O16, O25 with divalent and tetravalent metallic centres, respectively. The formations of the M–N and M–O bonds resulted in the weakness of C–N and C–O bonds, correspondingly.

All the bond lengths of ligands (**L¹**) and (**L²**), which were involved in coordination have shown an increase in the lengths signifying the establishment of M–N and M–O bonds in all the studied metal complexes. Moreover, the

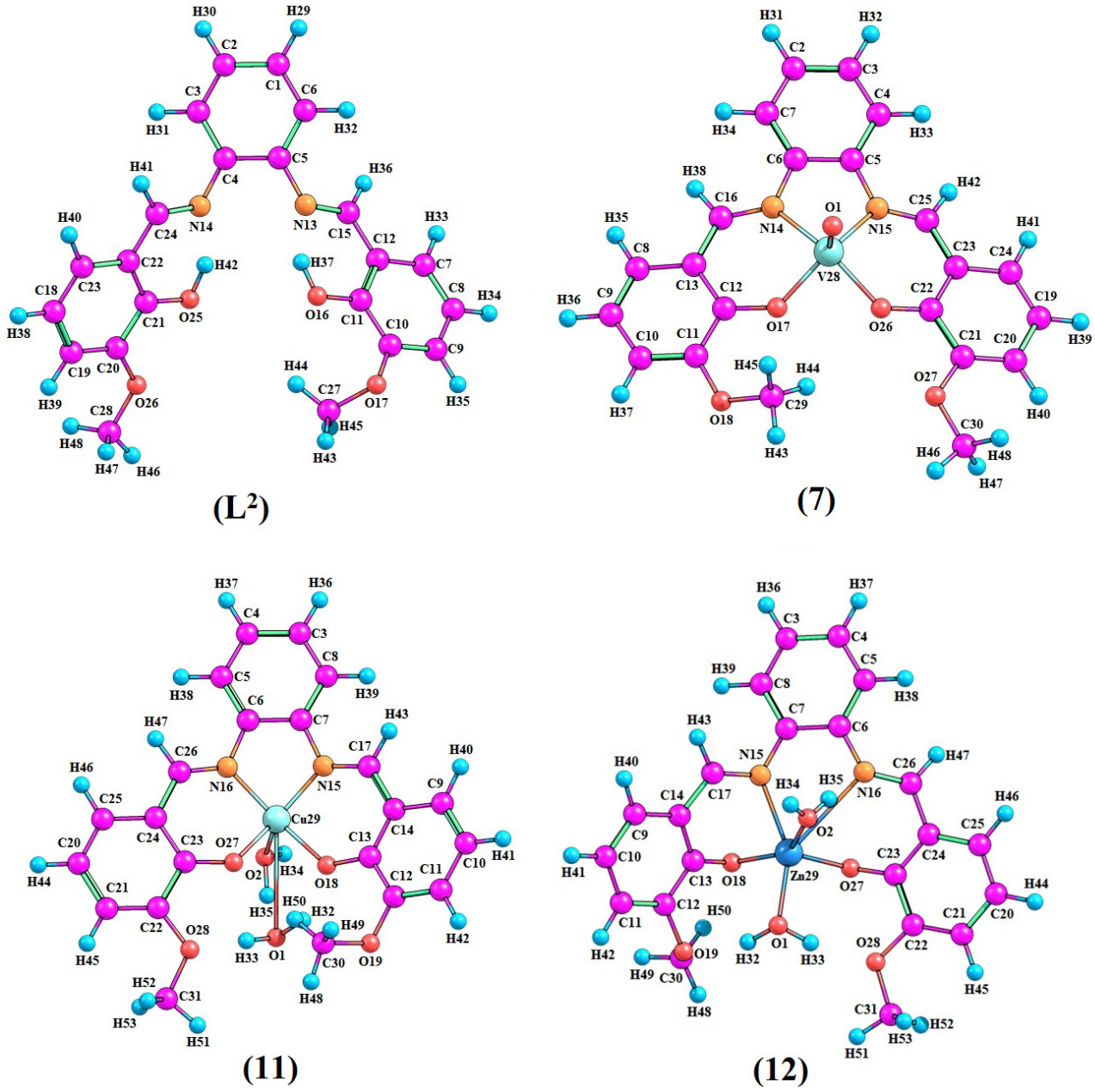

Figure 2. View of optimized geometrical structures of *o*-phenylenediamine ligand (**L²**) and its derived metal complexes (**7**), (**11**) and (**12**)

other bond lengths of the ligands were also significantly influenced by the coordination. Bond lengths of M–N bonds were greater than that of M–O bonds that gave the indication for stronger coordination of metal centers with oxygen atom of benzaldehyde by the deprotonation of phenolic group rather than nitrogen atom of azomethine linkage.

3. 7. Frontier Molecular Orbitals (FMOs) Analysis

The highest occupied molecular orbital (HOMO) designates the electron donation while the lowest unoccupied molecular orbital (LUMO) designates electron acceptance aptitude. The electronic transitions produced in consequence of the dipole moments arising amongst the ground and excited states of studied chemical entities are responsible for the optical features, electrical attributes and molecular chemical stability together with reactivity. In most of the cases, a transitions occur from HOMO to LUMO. Furthermore, the energy gap (ΔE) between these molecular orbitals is the main parameter to assign and explain reactivity and stability of the studied compounds.[54]

For newly synthesized phenylenediamine ligands (**L¹**)–(**L²**) and their selective metal complexes, the energies

of molecular orbitals including LUMO and HOMO, along with their energy differences have been computed by employing B3LYP/6-311++G(d, p) basis sets (as shown in Table 3). While the FMO's interpreting the distribution of electron charge density are illustrated in Figure 3. The DFT obtained results have shown that ligands **(L¹)** and **(L²)** exhibited 491 and 749 molecular orbitals, respectively. From these orbitals, 64-65 and 99–100 were established as HOMO-LUMO for both ligands, correspondingly. It is evaluated that the FMO energy gap calculated for HOMO→LUMO in ligand **(L¹)** was more than that in ligand **(L²)**. The FMO energy gap HOMO→LUMO was 3.693 eV for **(L¹)**, which decreased to 3.653 eV in **(L²)**. This reduction in the band difference for **(L²)** may be because of the presence of noncovalent attraction as well as extended conjugation in contrast to **(L¹)**.

In both studied structures of the ligands, an evident intramolecular transfer of charge occur from the middle part (HOMO) to the ultimate part (LUMO), therefore giving appropriate explanations to use these studied ligands in phenomenon of charge transfer. Overall, the acquired details signified that the ligand **(L²)** has shown small energy difference contrary to other ligand **(L¹)**, which describes greater intra-molecular charge transfer (ICT) communication within the ligand **(L²)**. The trend for $\Delta E_{HOMO \rightarrow LUMO}$ was obtained as; **(L¹)** 3.693 > **(L²)** 3.654 > **(3)** 3.085 > **(12)** 2.967 > **(11)** 2.926 > **(4)** 2.912 > **(7)** 2.847 > **(2)** 1.728. The molecules having minor frontier orbital band difference are highly chemical reactive as well as more polarizable. The calculated values of $\Delta E_{HOMO \rightarrow LUMO}$ suggested that the studied complexes have small band gap. Therefore, the complexes were found to be more reactive than the ligands.

It could be observed from figure that for both ligands **(L¹)** and **(L²)**, the electron density of HOMO and LUMO is concentrated on the entire structures with the exception of methoxy groups. Likewise, in LUMO of complex **(2)**, the charge density is only accomulated at half part of the complex. Whie in the LUMO of all the other stidied complexes, the charge density is distributed over the entire complex structure. But in the HOMO of complex **(2)** and **(7)**, the charge density is only focused at central part, mainly at the central metal ions and phenylenediamine-azomethine fragments. Whereas in the HOMO of all the other studied complexes, the charge density is dispersed over the complete complex structure.

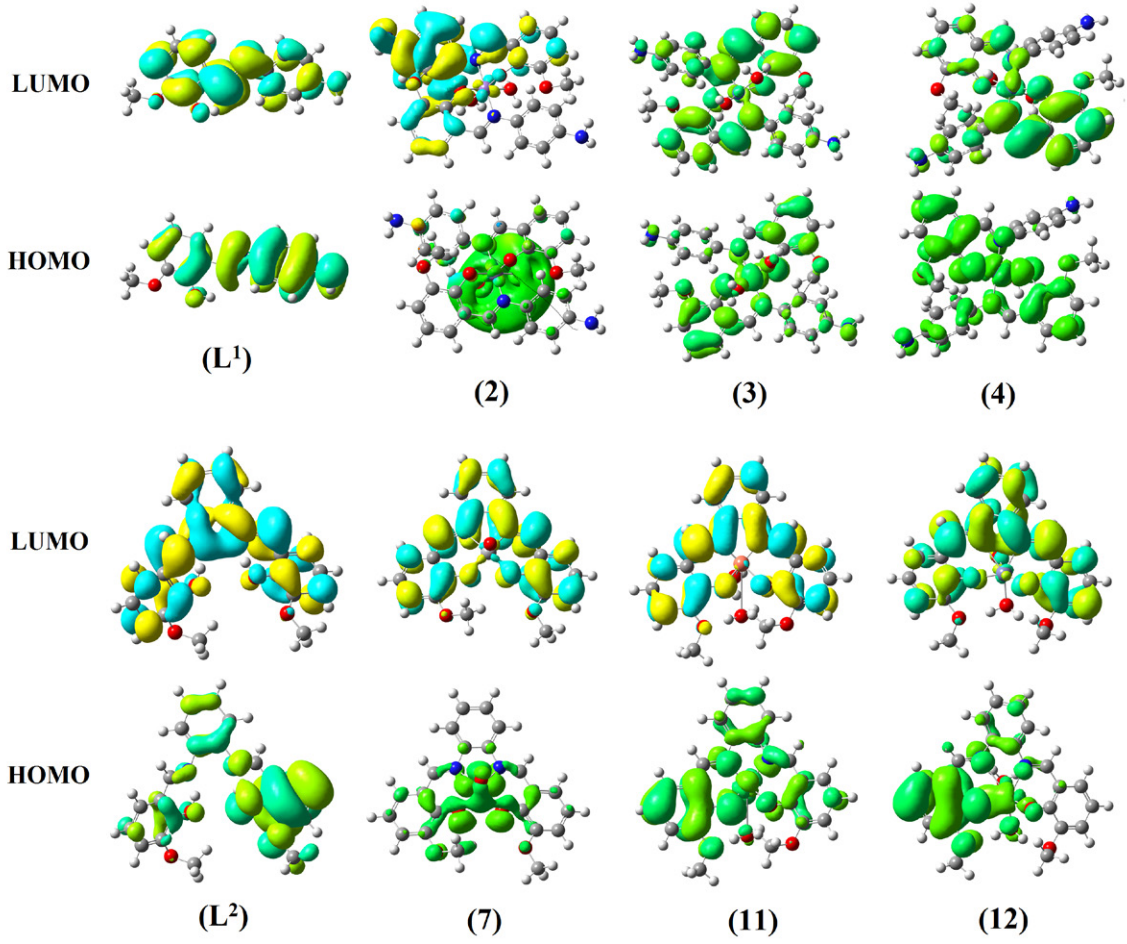

Figure 3. Frontier molecular orbitals (FMOs') illustrating distribution of electronic charge density in ligands and their selected metal complexes

Table 3. FMO energies and their energy gaps (ΔE) for phenylenediamine based ligands and their selected metal complexes

Descriptor (eV)	Compounds							
	(L^1)	**(L^2)**	**(2)**	**(3)**	**(4)**	**(7)**	**(11)**	**(12)**
E_{LUMO}	−1.796	−2.232	−1.483	−1.039	−1.484	−2.235	−1.891	−1.860
E_{HOMO}	−5.489	−5.886	−3.211	−4.124	−4.396	−5.082	−4.817	−4.827
$\Delta E_{HOMO \rightarrow LUMO}$	3.693	3.654	1.728	3.085	2.912	2.847	2.926	2.967
Ionization Potential (*IP*)	5.489	5.886	3.211	4.124	4.396	5.082	4.817	4.827
Electron Affinity (*EA*)	1.796	2.232	1.483	1.039	1.484	2.235	1.891	1.860
Global Hardness (η)	1.847	1.827	0.864	1.543	1.456	1.424	1.463	1.484
Chemical Potential (μ)	−3.643	−4.059	−2.347	−2.582	−2.940	−3.659	−3.354	−3.344
Global Softness (*S*)	0.271	0.274	0.579	0.324	0.343	0.351	0.342	0.337
Electronegativity (χ)	3.643	4.059	2.347	2.582	2.940	3.659	3.354	3.344
Electrophilicity (ω)	3.593	4.509	3.188	2.160	2.968	4.701	3.845	3.768

3. 8. Chemical Reactivity Parameters

The FMO band gap (ΔE) is a remarkable factor to investigate and describe the chemical reactivity parameters such as the accepting and donating ability of the studied molecules along with their hardness and softness.[55] Molecules with a high FMO energy difference are kinetically least reactive and more stable, which makes them chemically hard in nature. While the molecules with small FMO band gaps are kinetically more reactive in nature which makes them chemically soft and less stable with more polarizability. Global reactivity parameters[56] like electron affinity (*EA*), ionization potential (*IP*), global softness (σ), chemical potential (μ), global hardness (η), global electrophilicity (ω) in addition to electronegativity (χ) can be determined using FMO energy gap employing equations S1–S6 and the values are shown in Table 3. Electronegativity is considered as the most important chemical parameter that describes the competency of any chemical system for attracting the electrons. The stability of any molecule is specified by the negative readings of the chemical potential (μ). This remarkable study could play an imperative impact in the domain of experimental investigation and particularly in the biological assay of chemical systems.[57] It can be witnessed from the table that the ionization potential (5.886 eV) in ligand **(L^2)** is more, having most negative chemical potential (−4.059 eV), greater values of electron affinity (2.232 eV) and electronegativity (4.059 eV) than **(L^1)**. In addition, there exist a straight link between the FMO energy gap and the hardness, consequently the compound with a more FMO energy difference is the chemically less reactive. As a result, the calculated FMO energy differences and hardness are greater, while softness readings are smaller for **(L^1)** in comparison to **(L^2)**, signifying that **(L^2)** is more reactive and less stable. The detailed comparison of global reactivity parameters for all the studied compounds is illustrated by Figure 4.

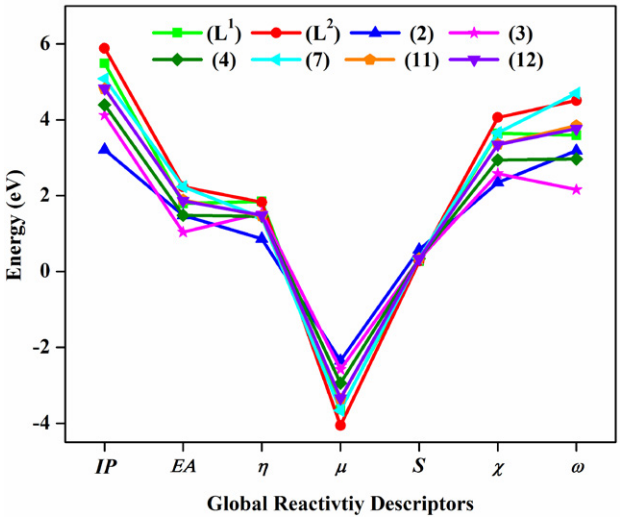

Figure 4. Comparison of global reactivity parameters for ligands vs metal complexes

3. 9. Molecular Electrostatic Potential (MEP) Analysis

Molecular electrostatic potential (MEP) map is linked to electronic charge density and with the help of it, the chemical reactivity and noncovalent interactions such as nucleophilic and electrophilic attack sites can be comprehend. MEP map is the graphical interpretation of the three dimensional electronic charge. With the help of this 3D map, the physical as well as chemical characteristic features of any chemical structure can also be elucidated.[58] In the MEP map, the charge is distributed around the molecule in space which helps to understand the hydrogen bonding, reactive positions for the attack by electrophiles and nucleophiles as well and biological recognition procedures. It is known as supportive parameter that provides assistance to characterize the zone, size, positive, negative and shape of an investigated chemical structure. The electrostatic potential values are assessed with different shades. The negative region of electrostatic potential is denoted by red colour, while the blue and green colours represent the positive and less positive region of MEP respectively. Different code colours in the terms of potential fallows following order; blue > green > yellow > orange > red.

By using density functional B3LYP/6-311++G(d, p) basis set, MEP is designed over optimized geometrical structures of the studied compounds and the MEP plots are displayed in Figure 5. An analysis of the MEP plots suggested that in the investigated compounds, the red colour (negative region) was localized around $O_{hydroxyl}$ and $O_{methoxy}$ atoms. Hence, it is an electron rich part and could be potential place for the attack by electrophile. In contrast, the blue colour (positive region) defining the electron deficient area was localized around N_{amino} and $N_{azomethine}$ atoms together with some of the hydrogen alongside carbon atoms could be a favourable site for the attack by nucleophiles. Whereas, the green zone indicated the average potential, *i.e.,* the part in the middle of two margins. From blue, green and red colours, it was obvious that all these different reaction positions were present in all studied compounds. The studied metal complexes possess electron deficient sites with smaller electronegativity which are the preferred positions for an attack by nucleophilic species. The computed MEP plots were found to be in agreement with the computed atomic charges contained by studied chemical molecules. Thus, signifying that on complexation, the intra-molecular charge dispersal produced an electropositive zone at the central metal atoms that might influence their various physicochemical properties.

3. 10. Natural Bond Orbital (NBO) Analysis

NBO analysis is an effective practice that proficiently interprets the intramolecular interactions and delocalization of electronic charge density. It provides proper details to analyse and explain the intra-molecular hydrogen bonding as well as transfer of electronic charge from the filled orbitals to free orbitals by employing the second-order Fock matrix. By means of equation 1, the stabilization energies of the investigated molecules have been calculated, and some significant NBO interactions are depicted in Table S2. NBO analysis indicated the existence of resonance/π-conjugation attributable to delocalization of π-electrons in addition to strong intra-molecular primary or secondary hyper-conjugative interactions in the investigated compounds. From the findings attained in valence hybrids of NBO's, the NBO analysis also provides significant perceptions about the polarity of different bonds within the studied molecular systems. The NBO results also signify the involvement of extra valence orbitals in the composition of natural bond orbitals that has notable contribution regarding the stabilization energy within the examined molecules.[59] The NBO analysis is also important as it explains the nature of any definite bond through evaluating the interactions between donating and accepting orbitals.

$$E^{(2)} = q_i \frac{(F_{i,j})^2}{\varepsilon_i - \varepsilon_j} \quad (1)$$

In this equation, $E^{(2)}$ defines the stabilization energy, q_i symbolizes the vacancy of the contributor orbital, $F_{(i,j)}$ denotes the diagonal while ε_i and ε_j indicate the off diagonal NBO Fock matrix features. In this NBO study, interactions between electron donating and accepting orbitals are exposed by the stabilization energy $E^{(2)}$ value. The larger value of stabilization energy $E^{(2)}$ indicates that greater interaction is found between electron acceptors and donors. The overlapping of σ(C-C) with σ*(C-C) bonding orbitals causes molecular interaction, that is producing the intramolecular charge to stabilize the system. When there is higher electronic charge density in C-C antibonding orbital, these interactions are observed which weakens corresponding bonds.[60] The electron density due to single and double bond of the conjugated ring exhibits strong delocalization within the chemical systems. The interaction energy inferred from second order perturbation theory analysis of Fock Matrix. The analysis was performed for

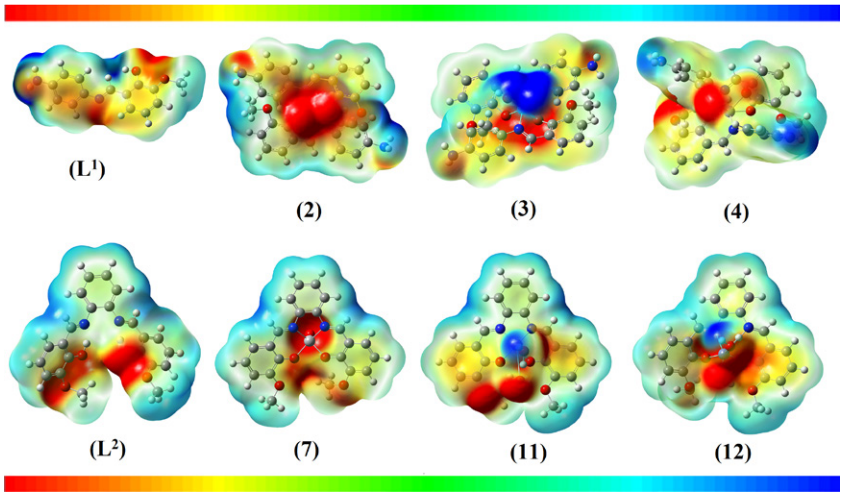

Figure 5. MEPs and colour pattern for the investigated ligands and their selected metal complexes

studied compounds by investigating all the promising interactions regarding occupied Lewis style donors and vacant non Lewis type acceptor, while their status of energies is estimated by second order perturbation theory.

Usually, four major types of electronic transitions including σ→σ*, LP→σ*, π→π*, along with LP→π* are seen for any studied molecule. The observed π→π* type of transitions have an additional estimation, while transitions such as LP→σ* as well as LP→π* demonstrated quite appropriate values for stabilization energy $E^{(2)}$. Moreover, the least $E^{(2)}$ values were shown by σ→σ* electronic transitions. The highest readings for π→π* transitions were π(C_2–C_3)→π*(C_1–C_6), π(C_{21}–C_{22})→π*(N_{14}–C_{24}) with stabilization energies of 21.46 and 21.54 kcal/mol in ligands **(L¹)** and **(L²)**, correspondingly. Although, some other π→π* electronic transitions having significant values of stabilization energy were also observed like π(C_8–C_{13})→π*(C_9–C_{10}), π(C_4–C_5)→π*(C_1–C_6), π(C_{11}–C_{12})→π*(N_7–C_{14}), π(C_9–C_{10})→π*(C_8–C_{13}) and π(C_1–C_6)→π*(C_2–C_3) in **(L¹)** with 18.68, 18.67, 18.38, 17.77 and 16.25 kcal/mol, whereas π(C_3–C_4)→π*(C_1–C_2), π(C_5–C_6)→π*(C_1–C_2), π(C_7–C_8)→π*(C_9–C_{10}), π(C_1–C_2)→π*(C_3–C_4), π(C_{18}–C_{23})→π*(C_{19}–C_{20}), π(C_{19}–C_{20})→π*(C_{18}–C_{23}) and π(C_9–C_{10})→π*(C_7–C_8) in **(L²)** with stabilization energy of 20.54, 20.54, 20.54, 20.09, 18.30, 17.61 and 17.34 kcal/mol, respectively. These electronic transitions strongly stabilize both the ligands **(L¹)** and **(L²)**.

Similar type of interaction linked to resonance in the structure was observed between the oxygen lone pair O_{15}, O_{12} and the anti-periplanar C_{11}–C_{12}, C_7-C_8 antibond which gave 27.24 and 65.17 kcal/mol energy of stabilization in **(L¹)** and **(L¹)**, respectively. It is evident from the NBO analysis that strong interactions, charge transfer properties, stabilization energies, coordination tendency and stability exist in the studied ligands **(L¹)** and **(L²)**. Likewise, the foremost π→π* interactions including; π(C_{29}-C_{30})→π*(N_{24}-C_{31}), π(C_{29}-C_{30})→π*(N_{24}-C_{31}), π(C_2-C_3)→π*(C_4-C_5), π(C_{24}-C_{25})→π*(N_{16}-C_{26}) and π(C_{20}-C_{21})→π*(C_{24}-C_{25}) produced 18.39, 38.68, 10.64, 17.72 and 23.42 kcal/mol stabilization energies for complexes **(2)**, **(4)**, **(7)**, **(11)** and **(12)** correspondingly. In addition, the LP→π* transitions were observed as; C_{10}→π*(C_8-C_9), C_{12}→π*(N_7-C_{14}), C_{23}→π*(N_{15}-C_{25}), C_{22}→π*(C_{20}-C_{21}) and O_{14}→π*(C_9-C_{10}) with higher stabilization energies of 39.85, 125.84, 69.47, 41.41 and 64.55 kcal/mol for complexes **(2)**, **(4)**, **(7)**, **(11)** and **(12)** respectively. This NBO analysis showed extended hyperconjugation and notable intramolecular interactions of studied compounds.

3. 11. Mulliken Atomic Charge (MAC) Analysis

In chemistry, chemical reactivities, electromagnetic spectra accompanied by NMR chemical shifts, electric potentials and dipole moments are considered as recognizable parameters of molecules which could have direct association with atomic charges in the chemical systems. Various theories regarding the structural features of chemical systems entirely depend on the concept of Mulliken atomic charges. The calculation of atomic charges for the preferred chemical systems by computational chemistry play supportive role to evaluate and explain the experimental data. It is particularly important to deeply comprehend the characterization of atomic charges to understand and describe the applications of any chemical system.[61] The Mulliken atomic charges of investigated compounds were determined by employing B3LYP level and 6–311++G(d, p) basis set. The Mulliken charges are listed in Tables S3 & S4, while their histograms are presented in Figure 6 & 7. The charge dispersion of the studied compounds displayed that the all oxygen and nitrogen atoms in addition to the carbon atoms linked with oxygen and nitrogen atoms were negatively charged. Whereas, greater positive values were found for the other carbon and hydrogen atoms together

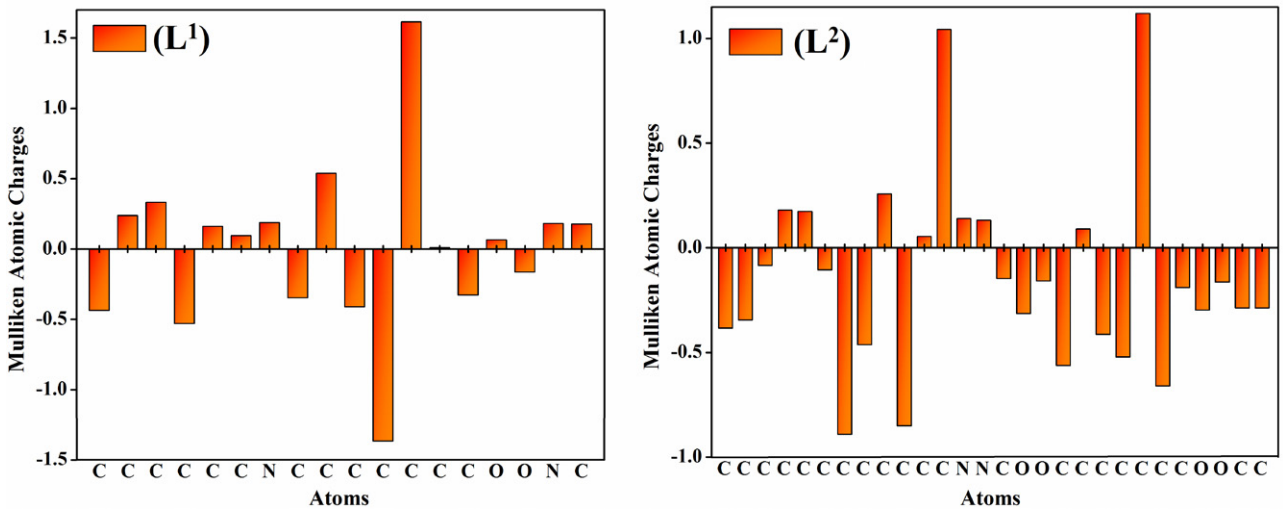

Figure 6. Histogram for Mulliken atomic charges of ligands **(L¹)** & **(L²)**

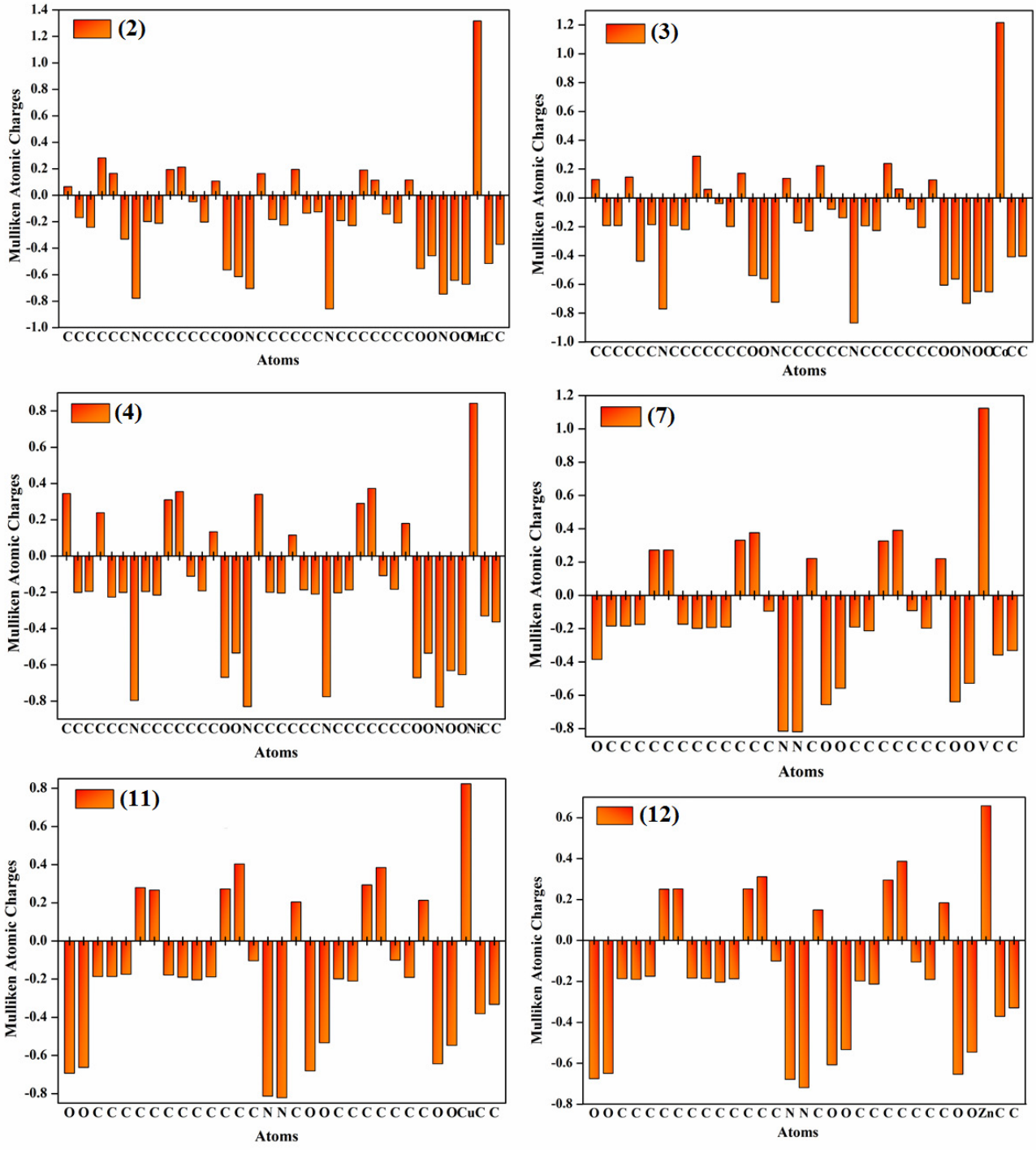

Figure 7. Histogram for Mulliken atomic charges of studied metal complexes

with metals (Mn, Co, Ni, V, Cu and Zn) in the studied metal complex **(2)**, **(3)**, **(4)**, **(7)**, **(11)** and **(12)**.

3. 12. Computed UV–Vis Analysis

UV–Visible spectroscopy gave valuable explanation on the charge transfer potentials of the investigated compounds. To get the insights concerning the theoretical UV-Vis spectra of the ligands together with their selected metal complexes, TD-DFT calculation were executed at B3LYP/6-311++G(d, p) level. The transition energy values, maximum absorption wavelength (λ_{max}), oscillator strength (f_{os}) together with minor and major molecular orbital transitions of the studied compounds are tabulated in Table S5. Whereas, the theoretical UV-Vis spectra are shown in Figure S9.

3. 13. Computed IR Analysis

The synthesized ligands **(L[1])** and **(L[2])** having 32 and 48 atoms correspondingly comprising carbon, oxygen, hydrogen and nitrogen atoms. The harmonic vibrational frequencies of both ligands were computed using B3LYP/6-311++G(d, p). Both the ligands contain 90 and 138 vibrational modes correspondingly with singlet spin and point group symmetry C1. The calculated vibrational modes of atoms were assigned using the animation option of Gauss View software. All the vibrational assignments associated with theoretical infrared spectral values were taken into consideration while only the most prominent vibrational frequencies with high accuracy are listed in Tables S6 & S7. Figure 8 illustrates the theoretically simulated scaled infrared spectra of all studied compounds. The theoretical frequencies were found to be greater than the experimentally observed values and the obvious reason would be the overestimation of the computed vibrational modes because of the negligence of anharmonicity in the actual chemical system.

With the aim to reduce the frequency values analogous to that of experimental values, electron correlation would be included in density functional theory. The overall practice is to scale down the computed vibrational frequencies to compare the frequency values obtained after the experiment. The scaling factor approach is very valuable for correlating the theoretical vibrational frequencies to the practically investigated frequencies. Thus, the scaling factor (0.9742) of B3LYP/6-311++G(d, p) was utilized to precise the systematic defects *i.e.,* to neglect of basis set defects along with some enharmonic effects.[62] Experimental infrared spectra of ligands were compared with the theoretically simulated scaled infrared spectra, followed by comprehensive frequency assignments. The important functional groups are described here in detail:

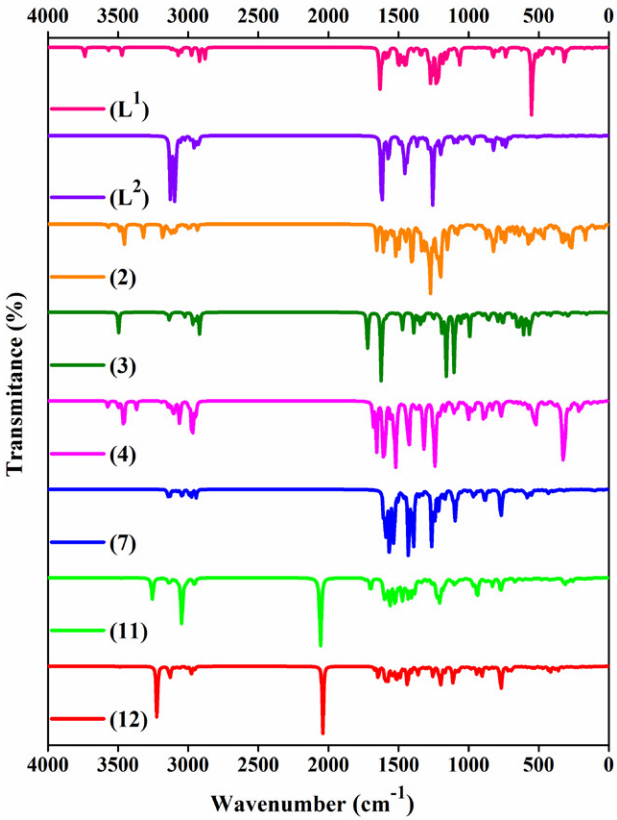

Figure 8. Computed IR spectra for phenylenediamine Schiff base ligands and their selected metal complexes

O-H vibrations: The O–H stretching vibration was found at 3744, 3123 cm^{-1} (theoretical) and 3427, 3230 cm^{-1} (experimental) for ligand **(L[1])** and **(L[2])**, respectively.

NH_2 vibrations: The vibrational modes for NH_2 were observed at 3478 and 3574 cm^{-1} (theoretical) and 3020 cm^{-1} (experimental).

HC=N vibration: The HC=N vibrations were detected at 1617, 1619 cm^{-1} (theoretical) and 1640, 1638 cm^{-1} (experimental) for ligand **(L[1])** and **(L[2])**, correspondingly.

The DFT-based theoretical vibrational modes have obtained to be consistent with the practically determined findings.

3. 14. Antibacterial Activity

The as-synthesized compounds were investigated for *in vitro* antibacterial activity against three G- bacteria (GNB) *i.e., Salmonella typhi*, *Klebsiella pneumonia, Escherichia coli* along with one G+ bacteria (GPB) *i.e., Staphylococcus aureus*. Two reference drugs *i.e.,* ampicillin **(SD[1])** and streptomycin **(SD[2])** were used to compare the results of antibacterial activity of investigated compounds (Table 4, Figure 9). The results showed that DMSO had no interference on antibacterial activity of the compounds. Both the uncomplexed ligands exhibited antibacterial activity against all bacteria except **(L[2])** that showed no activity against *Klebsiella pneumonia.* Overall, ligand **(L[1])** exhibited more activity. It showed maximum and minimum activity against *Staphylococcus aureus* and *Klebsiella pneumonia* with 17 and 05 mm zones of inhibition, respectively. While **(L[2])** exhibited highest activity against *Escherichia coli* with 18 mm zone of inhibition.

All the complexes exhibited significant antibacterial activity against all bacteria except complexes **(2)** and **(4)** that were inactive against *Klebsiella pneumonia* and *Staphylococcus aureus,* correspondingly. Among all the complexes, the zinc complexes were found to be the most active. The complexes **(12)** and **(6)** displayed the maximum activity of 29 and 28 mm against *Staphylococcus aureus*. While both complexes **(12)** and **(6)** exhibited moderate inhibitory activity of 23 mm against *Escherichia coli,* correspondingly. The complex **(3)** inhibited 23, 22, 21 and 16 mm zones of *Klebsiella pneumonia, Salmonella typhi, Escherichia coli* and *Staphylococcus aureus,* respectively. The complexes **(7)** and **(8)** demonstrated least antibacterial profile with 6 and 7 mm inhibition zones against *Staphylococcus aureus* and *Salmonella typhi*, correspondingly.

Table 4. Antibacterial activity (inhibition zone/mm) of ligands and their metal complexes

Compounds	*Salmonella typhi* (G-)	*Klebsiella pneumonia* (G-)	*Escherichia coli* (G-)	*Staphylococcus aureus* (G+)
(L^1)	15	05	15	17
(L^2)	17	0	18	16
(1)	14	22	06	19
(2)	21	23	11	0
(3)	22	23	16	21
(4)	21	0	21	0
(5)	19	15	17	20
(6)	20	23	19	28
(7)	14	20	05	06
(8)	07	16	23	23
(9)	21	09	07	09
(10)	18	21	22	19
(11)	22	18	15	20
(12)	19	22	23	29
(SD^1)	29	38	35	30
(SD^2)	35	39	37	40

SD^1 = Ampicillin, SD^2 = Streptomycin

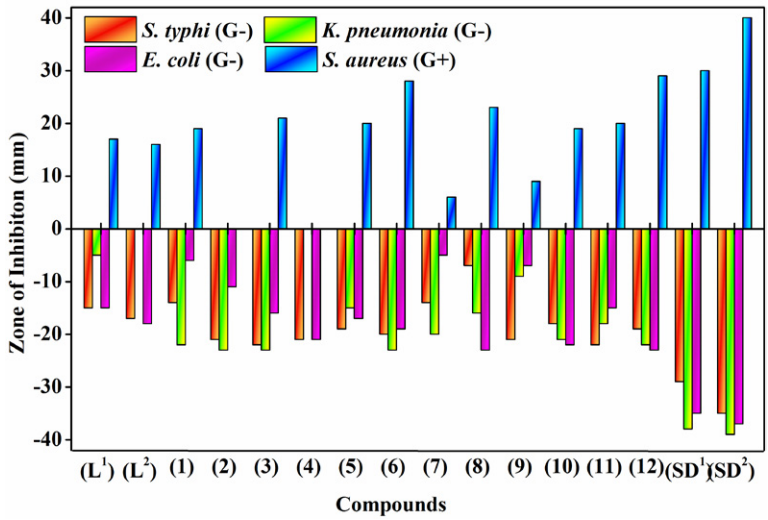

Figure 9. Antibacterial activity of phenylenediamine Schiff base derived compounds against Gram-positive and Gram-negative bacteria

4. Conclusion

In the current situation of increasing global drug resistance coupled with the scarcity of efficient antibacterial drugs, two new symmetrical ligands **(L^1)–(L^2)** and their derived metal chelates were synthesized and experimentally characterized through physical, elemental, spectral data along with computational study by DFT/B3LYP/6-311++G(d,p) approach. The spectral assignments of all the metal based phenylenediamine compounds confirmed that the deprotonated bidentate and tetradentate Schiff base ligands bonded with 3*d*-metal cations through phenolic oxygen and azomethine nitrogen along with two water molecules resulting in the formation of a stable six-membered chelate ring. Based on the magnetic moments and electronic spectra, an octahedral geometry was recommended for all the divalent metal complexes except for tetravalent vanadyl complexes that exhibited square pyramidal geometry, thus correlating accurately with the assessed molecular formula. On the basis of molar conductivity, all the metal complexes formed were declared as neutral having no free anions outside the coordination sphere. The theoretically obtained structural features accorded effectively with experimentally determined structural findings. This reasonable constancy validated that the chosen DFT method might be a realistic approach to comprehend some other characteristic features of the studied compounds. The charge transfer properties, kinetic stability and chemical reactivity of the studied compounds were evaluated by FMO analysis. Antibacterial activity of all the

phenylenediamine derived compounds was evaluated. The results of bioactivity concluded that both the phenylenediamine ligands have shown significant antibacterial potential which was further intensified upon chelation owing to the transference of charge from metal to ligand. Overall, the Zn(II) complex possessed higher antibacterial activity. The results conclude that these metal based compounds have the aptitude to be converted into drug candidates and this study will be valuable to design and develop promising metal-based drugs to treat microbial infections.

Acknowledgements

The authors are grateful to the Higher Education Commission (HEC) of Pakistan for providing financial assistance through the NRPU Project # 7800.

Conflict of Interest

All authors declared that they have no conflict of interest.

5. References

1. W. Zafar, S. H. Sumrra, Z. H. Chohan, *Eur. J. Med. Chem.* **2021**, *222*, 113602. **DOI:**10.1016/j.ejmech.2021.113602
2. H. Kargar, R. Behjatmanesh-Ardakani, V. Torabi, M. Kashani, Z. Chavoshpour-Natanzi, Z. Kazemi, V. Mirkhani, A. Sahraei, M. N. Tahir, M. Ashfaq, K. S. Munawar, *Polyhedron*, **2021**, *195*, 114988. **DOI:**10.1016/j.poly.2020.114988
3. S. A. Beyramabadi, M. Saadat-Far, A. Faraji-Shovey, M. Javan-Khoshkholgh, A. Morsali, *J. Mol. Struct.* 2020, *1208*, 127898. **DOI:**10.1016/j.molstruc.2020.127898
4. H. Kargar, V. Torabi, A. Akbari, R. Behjatmanesh-Ardakani, M. N. Tahir, *J. Mol. Struct.* 2019, *1179*, 732–738. **DOI:**10.1016/j.molstruc.2018.11.066
5. A. Sahraei, H. Kargar, M. Hakimi, M. N. Tahir, *J. Mol. Struct.* **2017**, *1149*, 576–584. **DOI:**10.1016/j.molstruc.2017.08.022
6. P. Sen, T. Nyokong, *Polyhedron*, **2019**, *173*, 114135. **DOI:**10.1016/j.poly.2019.114135
7. S. H. Sumrra, Z. Arshad, W. Zafar, K. Mahmood, M. Ashfaq, A. U. Hassan, E. U. Mughal, A. Irfan, M. Imran, *R. Soc. Open Sci.* **2021**, *8*, 210910. **DOI:**10.1098/rsos.210910
8. H. Kargar, A. A. Ardakani, M. N. Tahir, M. Ashfaq, K. S. Munawar, *J. Mol. Struct.* **2021**, *1233*, 130112. **DOI:**10.1016/j.molstruc.2021.130112
9. X. H. Qi, Z. M. Wu, S. B. Wang, B. X. Wang, L. L. Wang, H. Li, Q. Guo, *J. Coord. Chem.* **2019**, *14*, 2310–2325. **DOI:**10.1080/00958972.2019.1647535
10. S. H. Sumrra, U. Habiba, W. Zafar, M. Imran, Z. H. Chohan, *J. Coord. Chem.* **2020**, *73*, 2838–2877. **DOI:**10.1080/00958972.2020.1839751
11. Y. J. Ren, J. L. Zhu, L. X. Zhang, Y. X. Xu, S. S. Qian, *Acta Chim. Slov.* 2017, *64*, 825–831. **DOI:**10.17344/acsi.2017.3315
12. S. Yasmeen, S. H. Sumrra, M. S. Akram, Z. H. Chohan, *J. Enzyme Inhib. Med. Chem.* 2017, *32*, 106–112. **DOI:**10.1080/14756366.2016.1238363
13. K. Buldurun, N. Turan, E. Bursal, A. Mantarcı, F. Turkan, P. Taslimi, İ. Gülçin, *Res. Chem.* Intermed. **2020**, *46*, 283–297. **DOI:**10.1007/s11164-019-03949-3
14. M. Kumbar, S. A. Patil, S. S. Toragalmath, S. S. Jawoor, A. Shettar, *Inorg. Chim. Acta.* **2020**, *500*, 119210. **DOI:**10.1016/j.ica.2019.119210
15. X. S. Cui, J. Chen, K. Y. Chai, J. S. Lee, Z. S. Quan, *Med. Chem. Res.* **2009**, *18*, 49–58. **DOI:**10.1007/s00044-008-9106-3
16. S. S. Hassan, S. M. Gomha, *Chem. Pap.* **2018**, *73*, 331–344. **DOI:**10.1007/s11696-018-0592-6
17. D. Śmiłowicz, N. Metzler-Nolte, *J. Inorg. Biochem.* **2020**, *206*, 111041. **DOI:**10.1016/j.jinorgbio.2020.111041
18. H. Kargar, F. Aghaei-Meybodi, R. Behjatmanesh-Ardakani, M. R. Elahifard, V. Torabi, M. Fallah-Mehrjardi, M. N. Tahird, M. Ashfaq, K. S. Munawar, *J. Mol. Struct.* **2021**, *1230*, 129908. **DOI:**10.1016/j.molstruc.2021.129908
19. S. H. Sumrra, W. Zafar, H. Javed, M. Zafar, M. Z. Hussain, M. Imran, M. A. Nadeem, *BioMetals*, **2021**, 1-23. **DOI:**10.1007/s10534-021-00345-6
20. Z. D. Petrović, J. Đorović, D. Simijonović, S. Trifunović, V. P. Petrović, *Chem. Pap.* **2018**, *72*, 2171–2180. **DOI:**10.1007/s11696-018-0419-5
21. Z. Shokohi-Pour, H. Chiniforoshan, M. R. Sabzalian, S. A. Esmaeili, A. A. Momtazi-borojeni, *J. Biomol. Struct. Dyn.* **2018**, *36*, 532–549. **DOI:**10.1080/07391102.2017.1287006
22. A. Jamshidvand, M. Sahihi, V. Mirkhani, M. Moghadam, I. Mohammadpoor-Baltork, S. Tangestaninejad, H. A. Rudbari, H. Kargar, R. Keshavarzi, S. Gharaghanic, *J. Mol. Liq.* **2018**, *253*, 61–71. **DOI:**10.1016/j.molliq.2018.01.029
23. Jarrahpour, D. Khalili, E. D. Clercq, C. Salmi, J. M. Brunel, *Molecules*, **2007**, *12*, 1720–1730. **DOI:**10.3390/12081720
24. S. N. Shukla, P. Gaur, M. L. Raidas, B. Chaurasia, *J. Mol. Struct.* **2020**, *1202*, 127362. **DOI:**10.1016/j.molstruc.2019.127362
25. A. A. Abdel-Aziz, S. H. Seda, *J. Fluoresc.* **2017**, *27*, 1051–1066. **DOI:**10.1007/s10895-017-2039-9
26. S. S. Wu, W. B. Yuan, H. Y. Wang, Q. Zhang, M. Liu, K. B. Yu, *J. Inorg. Biochem.* **2008**, *102*, 2026–2034. **DOI:**10.1016/j.jinorgbio.2008.08.005
27. S. Khalid, S. H. Sumrra, Z. H. Chohan, *Sains Malays.* 2020, *49*, 1891–1904. **DOI:**10.17576/jsm-2020-4908-11
28. Z. H. Chohan, S. H. Sumrra, *Appl. Organomet. Chem.* 2010, *24*, 122–130. **DOI:**10.1002/aoc.1590
29. M. J. Frisch et al. (2009) Gaussian 09, Revision D.01; Gaussian, Inc.: Wallingford, CT.
30. N. Prabavathi, A. Nilufer, V. Krishnakumar, *Spectrochim. Acta A Mol. Biomol. Spectrosc.* **2013**, *114*, 449–474. **DOI:**10.1016/j.saa.2013.05.011
31. R. Dennington, T. Keith, J. Millam (2009) GaussView, Version 5; Semichem, Inc.: Shawnee Mission, KS.
32. N. M. O'boyle, A. L. Tenderholt, K. M. Langner, *J. Comput. Chem.* **2008**, *29*, 839–845. **DOI:**10.1002/jcc.20823

33. M. D. Hanwell, D. E. Curtis, D. C. Lonie, T. Vandermeersch, E. Zurek, G. R. Hutchison, *J. Cheminform.* **2012**, *4*, 1–17. **DOI:**10.1186/1758-2946-4-17
34. G. A. Andrienko, (2010) Chemcraft. Graphical Software for Visualization of Quantum Chemistry Computations.
35. A. Sahraei, H. Kargar, M. Hakimi, M. N. Tahir, *Transit. Met. Chem.* **2017**, *42*, 483–489. **DOI:**10.1007/s11243-017-0152-x
36. P. Gull, A.A. Hashmi, *J. Mol. Struct.* **2017**, *1139*, 264–268. **DOI:**10.1016/j.molstruc.2017.03.053
37. M. Hanif, Z. H. Chohan, *Spectrochim. Acta A Mol. Biomol. Spectrosc.* **2013**, *104*, 468–476. **DOI:**10.1016/j.saa.2012.08.026
38. G. Ramesh, S. Daravath, N. Ganji, A. Rambabu, K. Venkateswarlu, *J. Mol. Struct.* 2**020**, *1202*, 127338. **DOI:**10.1016/j.molstruc.2019.127338
39. M. A. Diab, G. G. Mohamed, W. H. Mahmoud, A. Z. El-Sonbati, S. M. Morgan, S. Y. Abbas, *Appl. Organomet. Chem.* 2019, *33*, e4945. **DOI:**10.1002/aoc.4945
40. M. R. Hasan, M. A. Hossain, M. A. Salam, M. N. Uddin, *J. Taibah* Univ. Sci. **2016**, *10*, 766–773. **DOI:**10.1016/j.jtusci.2015.11.007
41. A. U. Hassan, S. H. Sumrra, M. N. Zafar, M. F. Nazar, E. U. Mughal, M. N. Zafar, M. Iqbal, *Mol. Divers.* 2021, 1–22. **DOI:**10.1007/s11030-020-10157-4
42. H. Kargar, *Transit. Met. Chem.* **2014**, *39*, 811–817. **DOI:**10.1007/s11243-014-9863-4
43. R. C. Maurya, D. Sutradhar, M. H. Martin, S. Roy, J. Chourasia, A. K. Sharma, P. Vishwakarma, *Arab. J. Chem.* 2015, *8*, 78–92. **DOI:**10.1016/j.arabjc.2011.01.009
44. A. A. Abou-Hussein, W. Linert, *Spectrochim. Acta A Mol. Biomol. Spectrosc.* 2014, *117*, 763–771. **DOI:**10.1016/j.saa.2013.06.078
45. G. G. Mohamed, M. A. Zayed, S. M. Abdallah, *J. Mol. Struct.* **2010**, *979*, 62–71. **DOI:**10.1016/j.molstruc.2010.06.002
46. M. S. Nair, D. Arish, R. S. Joseyphus, *J. Saudi Chem. Soc.* **2012**, *16*, 83–88. **DOI:**10.1016/j.jscs.2010.11.002
47. Y. Xu, L. Xue, Z. G. Wang. Russ, *J. Coord. Chem.* **2017**, *43*, 314–319. **DOI:**10.1134/S1070328417050098
48. T. Sedaghat, M. Yousefi, G. Bruno, H. A. Rudbari, H. Motamedi, V. Nobakht, *Polyhedron*, **2014**, *79*, 88–96. **DOI:**10.1016/j.poly.2014.04.061
49. N. H. Al-Shaalan, *Molecules*, 2011, *16*, 8629-8645. **DOI:**10.3390/molecules16108629
50. E. Pahonțu, M. Proks, S. Shova, G. Lupașcu, D. C. Ilieș, Ș. F. Bărbuceanu, L. Socea, M. Badea, V. Păunescu, D. Istrati, A. Gulea, D. Drăgănescu, C. E. D. Pîrvu, *Appl. Organomet. Chem.* **2019**, *33*, e5185. **DOI:**10.1002/aoc.5185
51. O. A. Dar, S. A. Lone, M. A. Malik, M. Y. Wani, M. I. A. Talukdar, A. S. Al-Bogami, A. A. Hashmi, A. Ahmad, *Appl. Organomet. Chem.* 2019, *33*, e5128. **DOI:** doi.org/10.1002/aoc.5128
52. G. P. Dharsini, C. Thanaraj, R. Velladurai, *J. Inorg. Organomet. Polym. Mater.* **2020**, *30*, 2315. **DOI:**10.1007/s10904-019-01413-8
53. Z. H. Chohan, M. Hanif, *Appl. Organomet. Chem.* 2011, *25*, 753–760. **DOI:**10.1002/aoc.1833
54. R. C. Maurya, B. A. Malik, J. M. Mir, P. K. Vishwakarma, D. K. Rajak, N. Jain, *J. Coord. Chem.* **2015**, *68*, 2902–2922. **DOI:**10.1080/00958972.2015.1064526
55. I. Seghir, N. Nebbache, Y. Meftah, S. E. Hachani, S. Maou, *Acta Chim. Slov.* **2019**, *66*, 629–637. **DOI:**10.17344/acsi.2019.5044
56. A. R. Simović, R. Masnikosa, I. Bratsos, E. Alessio, *Coord. Chem. Rev.* **2019**, *398*, 113011. **DOI:**10.1016/j.ccr.2019.07.008
57. K. A. Moltved, K. P. Kepp, *J. Phys. Chem. C.* **2019**, *123*, 18432–18444. **DOI:**10.1021/acs.jpcc.9b04317
58. S. Guidara, H. Feki, Y. Abid, *Spectrochim. Acta A Mol. Biomol. Spectrosc.* **2014**, *133*, 856–866. **DOI:**10.1016/j.saa.2014.06.021
59. R. P. Gangadharana, S.S. Krishnan, *Acta. Phys. Pol. A.* **2014**, *125*, 18–22. **DOI:**10.12693/APhysPolA.125.18
60. A. S. G. El-hak, A. A. Mohammed, A. F. A. Hakiem, R. M. Mahfouz, *Spectrochim. Acta A Mol. Biomol. Spectrosc.* **2019**, *222*, 117200. **DOI:**10.1016/j.saa.2019.117200
61. A. S. Athmani, F. Madi, I. Laafifi, M. Cheriet, N. Issaoui, L. Nouar, R. Merdes, *J. Struct. Chem.* **2019**, *60*, 1906–1916. **DOI:**10.1134/S0022476619120060
62. V. S. Kumar, Y. S. Mary, K. Pradhan, D. Brahman, Y. S. Mary, R. Thomas, M. S. Roxy, C. V. Alsenoy, *J. Mol. Struct.* **2020**, *1199*, 127035. **DOI:**10.1016/j.molstruc.2019.127035

Povzetek

Zanimanje za razvoj naprednih spojin na osnovi kovin, ki zavirajo in kontrolirajo bakterijske okužbe, neprestano narašča. Sintetizirali smo dve novi bioaktivni simetrični mono- in bis- Schiffovi bazi na osnovi fenilendiamina, *2-{[(4-aminofenil) imino]metil}-6-metoksifenol* **(L^1)** in *2,2'-{benzen-1,2-diilbis[nitrilometililiden]}bis(6-metoksifenol)* **(L^2)**. Spojini smo karakterizirali s fizikalnimi metodami, spektroskopijo, elementno analizo in DFT računalniško analizo z metodo B3LYP/6-311++G(d, p). Sintetizirali smo koordinacijske spojine obeh novih ligandov z VO, Mn, Co, Ni, Cu in Zn v množinskih razmerjih [M:L, 1:2 in 1:1]. Vse tako pripravljene koordinacijske spojine imajo dobro antibakterijsko delovanje, z najboljšim delovanjem v primeru cinkovih kompleksov. Rezultati kažejo, da so tovrstne spojine obetavne za medicinske aplikacije.

Except when otherwise noted, articles in this journal are published under the terms and conditions of the Creative Commons Attribution 4.0 International License

Scientific paper

Metal and Non-Metal Modified Titania: the Effect of Phase Composition and Surface Area on Photocatalytic Activity

Boštjan Žener,[1] Lev Matoh,[1] Martin Reli,[2] Andrijana Sever Škapin[3,4] and Romana Cerc Korošec[1,*]

[1] *Faculty of Chemistry and Chemical Technology, University of Ljubljana, Večna pot 113, 1000 Ljubljana, Slovenia;*

[2] *Institute of Environmental Technology, VŠB-Technical University of Ostrava, 17. listopadu 15/2172, Ostrava-Poruba, Czech Republic;*

[3] *Slovenian National Building and Civil Engineering Institute, Dimičeva 12, 1000 Ljubljana, Slovenia*

[4] *Faculty of Polymer Technology - FTPO, Ozare 19, 2380, Slovenj Gradec, Slovenia*

* *Corresponding author: E-mail: romana.cerc-korosec@fkkt.uni-lj.si*

Received: 10-11-2021

Abstract

The application of TiO_2 photocatalysis in various environmental fields has been extensively studied in the last decades due to its ability to induce the degradation of adsorbed organic pollutants. In the present work, TiO_2 powders doped and co-doped with sulfur and nitrogen and modified with platinum were prepared by particulate sol-gel synthesis. PXRD measurements revealed that the replacement of HCl with H_2SO_4 during synthesis reduced the size of the crystallites from ~ 30 nm to ~20 nm, increasing the surface area from ~44 m^2/g to ~80 m^2/g. This is consistent with the photocatalytic activity of the samples and the measured photocurrent behavior of the photocatalysts. The results showed that the properties of the powders (i.e., surface area, crystallite size, photocurrent behavior) depend strongly not only on the type but also on the amount of acid and dopants used in the synthesis. Doping, co-doping and modification of TiO_2 samples with nitrogen, sulfur and platinum increased their photocatalytic activity up to 6 times.

Keywords: Titanium dioxide; powders; doping; photocatalysis; photocurrent; SEM

1. Introduction

Titanium dioxide is considered to be one of the most contemporary important materials. It occurs in nature in three polymorphic modifications: anatase, rutile and brookite, among which rutile is the most abundant and thermodynamically stable. On the contrary, anatase has the highest photocatalytic activity, which can be attributed to the highest number of hydroxyl groups on the surface.[1] Furthermore, three metastable phases can be produced synthetically, one of which is β-TiO_2, which crystallizes in a monoclinic crystal system.[2,3] Due to its favourable properties, including its high chemical stability, non-toxicity, low price and high refractive index (value of μ is 2.70 for rutile and 2.55 for anatase) TiO_2 is used for a wide number of applications in a variety of fields, for example as a white pigment in paints, plastic, paper, toothpastes and chewing gums, replacing the toxic lead oxides.[4] It is also used in the fields of photovoltaics, electrochemistry and photocatalysis.[5–9]

Due to its ability to mineralize adsorbed organic pollutants to CO_2 and H_2O, photocatalysis has been researched extensively with regard to its application in the fields of water remediation and air purification.[10–12] Oxidation of adsorbed organic pollutants can occur directly on the surface of the photocatalyst.[13] In the case that adsorption is not favourable due to the same electric charge on both pollutant and catalyst itself, reactive hydroxyl radical, formed via oxidation of water with holes, can start degradation reactions of pollutants in a solution. To enhance photocatalytic efficiency, it is necessary to prevent recombination between holes and electrons on route to the surface or on the surface sites.[14]

Various studies have been aimed at increasing the photocatalytic activity of TiO_2, which can be achieved by increasing the surface area of TiO_2, or through metal and non-metal doping. The surface area of the photocatalyst can be increased by decreasing its particle size.[15,16] Samples with a smaller crystallite size have a larger number of surface active sites, which should also increase its photocatalytic activity. Wang *et al.,* however, concluded that an optimum particle size of 11 nm exists for the degradation of chloroform in water. This was attributed to an increased recombination rate, which offsets the ultra-high surface area.[17,18] Maira *et al.* found an optimum particle size of 7 nm for gas phase photooxidation of trichloroethylene. The diminished activity for samples with crystallites, smaller than 7 nm, was attributed to changes in electronic and structural properties.[19] The surface area of the photocatalyst can also be increased by adding polymers during the synthesis. The calcination that follows removes the polymer chains, leaving behind a mesoporous framework of TiO_2, with an increased surface area.[20–23]

Doping TiO_2 with metals also increases its photocatalytic activity, by facilitating free electron capture and thus extending the lifetime of photogenerated electron-hole pairs.[24] The capture results in an efficient separation of electron-hole pairs, thus inhibiting recombination and increasing the photocatalytic activity of TiO_2 by enhancing the mass transfer of holes and possibly electrons to the surface.[25] It has to be mentioned, however, that metal centres can also act as recombination centres and thus lower the photocatalytic activity. TiO_2 is usually doped with noble metals, such as Ag, Pt and Pd.[26–28] Other metals include Cu, V, Cr, Ni, as well as In.[29–31]

TiO_2 can be synthesized using various synthetic procedures, including hydrothermal, microwave-assisted and sonochemical methods, and miniemulsion techniques.[32–35] Sol-gel synthesis offers many benefits compared to the synthetic methods mentioned above, including low cost, simplicity and low preparation temperatures. Because of this, it is a well-established procedure for the preparation of metal oxide nanoparticles.[36] The method is based on initial hydrolysis of a precursor (e.g. $TiCl_4$, titanium alkoxides), which is followed by reactions of condensation (oxolation and olation). Reactions result in the formation of sols, which are defined as stable suspensions of colloidal particles that can polymerize to form gels under certain conditions. On the other hand, stable sol can be deposited by dip- or spin coating onto a substrate and is then subjected to a drying process. During this process, the free –OH groups begin to link together, resulting in xerogels.[37]

In this work, we focussed on the preparation and characterization of sulfur and nitrogen doped and co-doped and platinum modified TiO_2 powders. Synthesis, structural properties and photocatalytic efficiency of the corresponding thin film was already published.[38] Since chemically equivalent thin films and powders often behave in different way, we have also systematically studied powdered samples, which is the main focus of the presented paper. Different analytical methods were used for their characterization and determination of the photocatalytic activity. Prepared samples were characterized by X-ray diffraction (XRD), specific surface area (BET) and photocurrent measurements. Morphology of the powders was examined using a field emission scanning electron microscopy. The photocatalytic activity of the powders was determined by monitoring the rate of oxidation of isopropanol to acetone using FTIR spectroscopy.

2. Experimental

2. 1. Synthesis

The method of synthesis, as used to synthesize metal and non-metal doped and co-doped TiO_2 powders, has been described previously in detail elsewhere.[38] The synthesis procedure is described in the supplementary material.

Sample names, types and amounts of dopants and acids added during the synthesis are presented in Table 1.

Table 1. Sample names, types and amounts of dopants and acids added during the synthesis.

Sample	Dopant; dopant source	Nominal amount of dopant relative to TiO_2 (atom %)	Amount (mL) and type of acid added
REF	/	/	18; HCl
Urea_15	N; urea	15	18; HCl
Thiourea_15	S; Thiourea	15	18; HCl
S2	S; H_2SO_4	/	3.3; H_2SO_4
S3	S; H_2SO_4	/	4.95; H_2SO_4
S3_N0.5	S; H_2SO_4 N; NH_4NO_3	/ 0.5	4.95; H_2SO_4
S3_N2	S; H_2SO_4 N; NH_4NO_3	/ 2	4.95; H_2SO_4
S3_urea15	S; H_2SO_4 N; urea	/ 15	4.95; H_2SO_4
S3_thiourea15	S; H_2SO_4 S; Thiourea	/ 15	4.95; H_2SO_4
S3_N0.5+1%Pt	S; H_2SO_4 N; NH_4NO_3 Pt; H_2PtCl_6	/ 0.5 1	4.95; H_2SO_4
S3_N0.5+2%Pt	S; H_2SO_4 N; NH_4NO_3 Pt; H_2PtCl_6	/ 0.5 2	4.95; H_2SO_4
S3_N0.5+3%Pt	S; H_2SO_4 N; NH_4NO_3 Pt; H_2PtCl_6	/ 0.5 3	4.95; H_2SO_4
S3_urea15+1%Pt	S; H_2SO_4 N; urea Pt; H_2PtCl_6	/ 15 1	4.95; H_2SO_4
S3_urea15+2%Pt	S; H_2SO_4 N; urea Pt; H_2PtCl_6	/ 15 2	4.95; H_2SO_4

The measured amounts of different dopants were determined with XPS measurements and are given in.[38]

2. 2. Characterization

XRD patterns were measured using a PANalytical X'Pert PRO MPD instrument in the 2θ range of 20–80° with a step of 0.034° using CuKα1 radiation. The average diameters of crystallites and phase compositions (amounts of polymophic modifications in %) of the samples and corresponding error values were calculated with Rietveld analysis using TopasR software.[39] Structural model (ICSD codes 92363 for anatase and 171670 for β-TiO_2) was used for the calculations.

The specific surface area of the powders was determined through the measurement of nitrogen adsorption-desorption isotherms by a Tristar 3000, Micromeritics (USA) instrument. The measurements were performed at –196 °C (77 K). The samples were outgassed under vacuum for 16 h at 110 °C (383 K). The mass of the samples in the analyser was ≈ 0.1 g. The specific surface area was calculated from the adsorption measurements in the relative pressure ($p/p0$) range of 0.05–0.25.

Photocurrent responses were recorded using a three electrode system, where Ag/AgCl and a Pt wire were used as reference and counter electrodes, respectively. The working electrode was prepared by depositing the measured sample on the conductive side of an ITO foil. 0.1 M KNO_3 was used as an electrolyte. The measurements were carried out in the range of wavelengths from 250 nm to 450 nm at an applied external potential of 1 V. This ensures that the highest number of photogenerated electrons travel to the working electrode. In this way the charge carriers (free electrons and holes) were successfully separated, thus preventing recombination. Before each measurement, the cell was purged with argon in order to ensure an oxygen free environment.[40,41] In the measured range from 250 nm to 450 nm, the wavelength is being changed by 10 nm step. The photocurrent signal drops down when the shutter closes to switch the wavelength for another 10 nm.

The morphology and the size of the particles of prepared powders were examined using a field-emission scanning electron microscope FE-SEM (FEI Inspect^{TM} F50 and Ultra Plus Zeiss). Accelerating voltage was set to 2 kV. Images were obtained with detection of secondary electrons.

2. 3. Photocatalytic Activity Tests

The photocatalytic activity of the powder samples under UV and visible light exposure was determined by measuring the rate constant of oxidation of isopropanol to acetone and further oxidation leading to CO_2 and H_2O as the final products using FTIR spectroscopy. Commercially available Hombikat UV 100 (DE) – anatase nanopowder, with a primary crystal size <10 nm and specific surface area >250 m^2/g was used for comparison. The reactions are presented in Equation (2):[42]

$$isopropanol \overset{k_0}{\rightarrow} acetone \overset{k_1}{\rightarrow} further\ oxidation\ products \quad (2)$$

Generally, the first step (k_0) is considered to be a zero order reaction, whereas the second step (k_1) is considered to be first order reaction. The method is presented in detail elsewhere.[43] In the first step, approximately 50 mg of the powder was suspended in 3 mL of 1-butanol. This suspension was then evenly distributed in a standard Petri dish and dried for 2 hours at 50 °C. Each dried sample was then put in a sealed gas-solid flow reactor system and then injected with 8 μL of isopropanol. Once the adsorption equilibrium was reached, as indicated by flat line in the isopropanol concentration profile, the sample was illuminated with a 300 W Xe lamp (Newport Oriel Instrument) with an infrared filter. The spectrum of this Xe lamp is similar to sun illumination. The working distance between the Petri dish and the lamp was 6 cm. The temperature and relative humidity were set to 23 ± 2 °C and 25 ± 5 %, respectively. The isopropanol degradation and acetone formation and degradation processes (see equation 2) were followed by monitoring the calculated area of their characteristic peaks at 951 cm^{-1} and 1207 cm^{-1}, respectively, in the IR spectra obtained by a FT-IR spectrometer (Perkin-Elmer Spectrum BX II). The examples of characteristic FTIR output at three diferent reaction times with related explanations are presented in Figure S1 (Supplementary material).

3. Results and Discussion

3. 1. X-Ray diffraction (XRD)

XRD patterns of the prepared powders are presented in Figure 1. It can be seen from the results that anatase is the only polymorphic modification present in samples synthesized with HCl (REF, Urea_15 and Thiourea_15). On the contrary, patterns of samples synthesized with H_2SO_4 include peaks of β-TiO_2, which crystallizes in a monoclinic crystal system and cannot be found in nature. Table 2 shows the share of polymorphic phases and calculated diameters of crystallites (both were calculated using the *Rietveld analysis*) in characterized samples. The results show that the amount of β-TiO_2 in samples synthesized with H_2SO_4 varies from 15.6 ± 0.3 % to 45.4 ± 0.3 %. The highest amounts are present in samples S3_urea15 and S3_thiourea15 (38.7 ± 0.3 % and 45.4 ± 0.3 %), whereas samples S3 exhibits the lowest (15.6 ± 0.3 %). Moreover, crystallites found in samples synthesized with H_2SO_4 (15.1 ± 0.3 – 23.5 ± 0.2 nm) were smaller compared to samples synthesized with HCl (26.9 ± 0.7 – 30.7 ± 0.8 nm). The same trend was observed in our previously published work, which focused on thin films.[38] As with thin film sys-

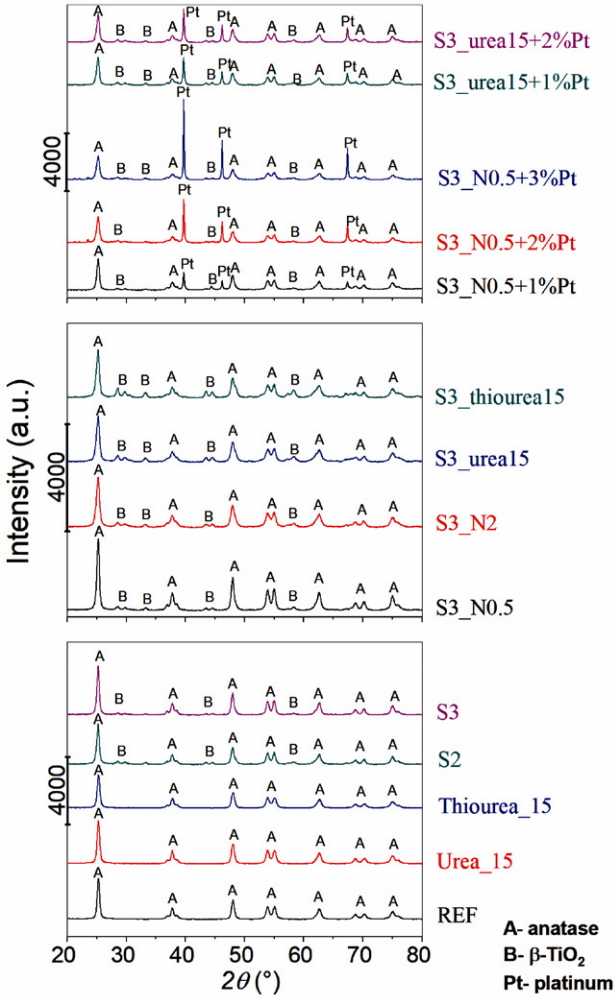

Figure 1. X-Ray diffraction patterns of powders. The designations A, B and Pt indicate the peaks for the corresponding TiO_2 polymorphic modifications and platinum.

tems, this can be attributed to the formation of $TiOSO_4$ in samples synthesized with H_2SO_4, which inhibits the crystallization of anatase. The smallest crystallites were found in samples S3_N2 and S3_urea15 (15.1 ± 0.3 to 17.5 ± 0.2 nm). Decreasing the crystallite size of TiO_2 usually results in an increase in surface area, which can have a positive effect on the photocatalytic activity of the samples. In most samples, the calculated crystallite sizes of β-TiO_2 are smaller to those of anatase.

When comparing the size of crystallites in powders to those in thin films (as published in our previous work), we observed an interesting phenomenon. In the case of samples synthesized with H_2SO_4 we found larger crystallites in powder form (sizes of ~ 15 – 23 nm in powders compared to 8–12 nm in thin films). This can be explained by the unlimited growth of crystallites in powders, unlike in thin films, where growth is limited by the thickness of the film and the substrate. In direct contrast, when analysing samples synthesized with HCl we found larger crystallites in thin film samples compared to powders (sizes of 40 – 60 nm and ~ 27 – 31 nm, respectively). We attribute this to the partial crystallization and subsequent growth of TiO_2 nanoparticles during the thermal treatment after each deposition (the final layer was prepared from three successive depositions, after each deposition thermal treatment was performed at 300 °C).[38]

Samples with added platinum also exhibit peaks at 40, 47.5 and 67.5° *2θ*, which correspond to metallic platinum.

3. 2. Specific Surface Area (BET)

Results of surface area measurements are presented in Table 2. Measurements for six of these samples (REF, Urea_15, Thiourea_15, S3, S3_N0.5 and S3_N0.5+1% Pt)

Table 2. The share of different polymorphic modifications, sizes of crystallites in powder samples calculated from XRD patterns using Rietveld refinement and the specific surface areas for examined samples.

Sample	Amount of anatase (wt%)	Calculated diameters of anatase crystallites (nm)	Amount of β-TiO_2 (wt%)	Calculated diameters of β-TiO_2 crystallites (nm)	BET specific surface area (m^2/g)
REF	100	30.7 ± 0.8	/	/	44.1 ± 0.4
Urea_15	100	29.6 ± 0.7	/	/	24.2 ± 0.2
Thiourea_15	100	26.9 ± 0.7	/	/	49.5 ± 0.3
S2	75.1 ± 0.3	21.1 ± 0.1	24.9 ± 0.3	19.0 ± 0.5	63.2 ± 0.3
S3	84.4 ± 0.3	23.5 ± 0.2	15.6 ± 0.3	19.0 ± 0.7	80.2 ± 0.2
S3_N0.5	81.1 ± 0.4	22.3 ± 0.2	18.9 ± 0.4	18.8 ± 0.6	84.5 ± 0.3
S3_N2	69.9 ± 0.3	16.8 ± 0.1	30.1 ± 0.3	15.1 ± 0.3	103.4 ± 0.4
S3_urea15	61.3 ± 0.3	17.5 ± 0.2	38.7 ± 0.3	16.5 ± 0.3	101.7 ± 0.4
S3_thiourea15	54.6 ± 0.3	18.7 ± 0.2	45.4 ± 0.3	19.3 ± 0.3	92.1 ± 0.3
S3_N0.5+1%Pt	82 ± 1	21.0 ± 0.4	18 ± 1	18 ± 1	83.7 ± 0.2
S3_N0.5+2%Pt	77 ± 2	17.9 ± 0.6	23 ± 2	20 ± 3	80.5 ± 0.4
S3_N0.5+3%Pt	74 ± 2	17.1 ± 0.8	26 ± 2	20 ± 3	84.1 ± 0.4
S3_urea15+1%Pt	69 ± 1	21.0 ± 0.6	31 ± 1	22 ± 2	82.3 ± 0.3
S3_urea15+2%Pt	73 ± 1	20.7 ± 0.6	27 ± 1	23 ± 2	84.2 ± 0.4

have already been published in our previous article. This study expands on those results.[38]

In general, samples synthesized with H_2SO_4 have higher surface areas (63.2 ± 0.3 to 103.4 ± 0.4 m^2/g) compared to samples synthesized with HCl (24.2 ± 0.2 to 49.5 ± 0.3 m^2/g). The higher surface area can be attributed to smaller crystallites found in samples synthesized with the addition of H_2SO_4, which is also observed from the XRD measurements.

It can be seen from the results presented in Table 2 that the addition of urea (sample Urea_15 has specific surface area of 24.2 ± 0.2 m^2/g) significantly decreases the surface area compared to the undoped sample REF (44.1 ± 0.4 m^2/g). By increasing the volume of H_2SO_4 added we also increase the surface area of the sample (63.2 ± 0.3 m^2/g for S2, 80.2 ± 0.2 m^2/g for S3). The addition of NH_4NO_3 (samples S3_N0.5 and S3_N2), urea (sample S3_urea15) and thiourea (sample S3_thiourea15) to sample S3 also increase the surface area of the samples (surface areas 84.5 ± 0.3 to 103.4 ± 0.4 m^2/g). This can be explained by an additional decrease in the size of crystallites in these samples as compared to those in sample S3.

The specific surface area does not change significantly when adding 1 % and 3 % of Pt to sample S3_N0.5. On the contrary, a decrease in surface area is observed when adding 2 % of Pt to sample S3_N0.5 (from 84.5 ± 0.3 m^2/g for sample S3_N0.5 to 80.5 ± 0.4 m^2/g for sample S3_N0.5+2%Pt) and when adding 1 % or 2 % of Pt to sample S3_urea15 (from 101.7 ± 0.4 m^2/g for S3_urea15 to 82.3 ± 0.3 m^2/g and 84.2 ± 0.4 m^2/g for sample S3_urea15+1%Pt and S3_urea15 + 2%Pt, respectively).

3. 3. Scanning Electron Microscopy (SEM)

Figure 2 shows FE-SEM micrographs of samples REF, S3_N0.5 and S3_thiourea15. Substituting HCl (sample REF) with H_2SO_4 (samples S3_N0.5 and S3_thiourea15) during the synthesis has resulted in the formation of more porous powders, which is in agreement with the results of BET specific surface area measurements. Furthermore, we have observed crystallites of sizes 31–35 nm in the SEM image of sample REF, which confirms the results of the XRD measurements. SEM images of samples synthesized with H_2SO_4 show crystallites ranging in size from 20–22 nm (sample S3_N0.5) and 18–23 nm (sample S3_thiourea15), which is also in agreement with the results of XRD measurements. We can also observe pores with sizes ranging from 70-100 nm (sample S3_N0.5) and 70-80 nm (sample S3_thiourea15).

3. 4. Photocurrent Measurements

Figure 3 shows the results of photocurrent measurements for different samples. The reason why there is a very low photocurrent response in UV region is due to the fact 150 W Xe lamp was used as the light source. Xe lamps have very low intensity in UV region below 300 nm.

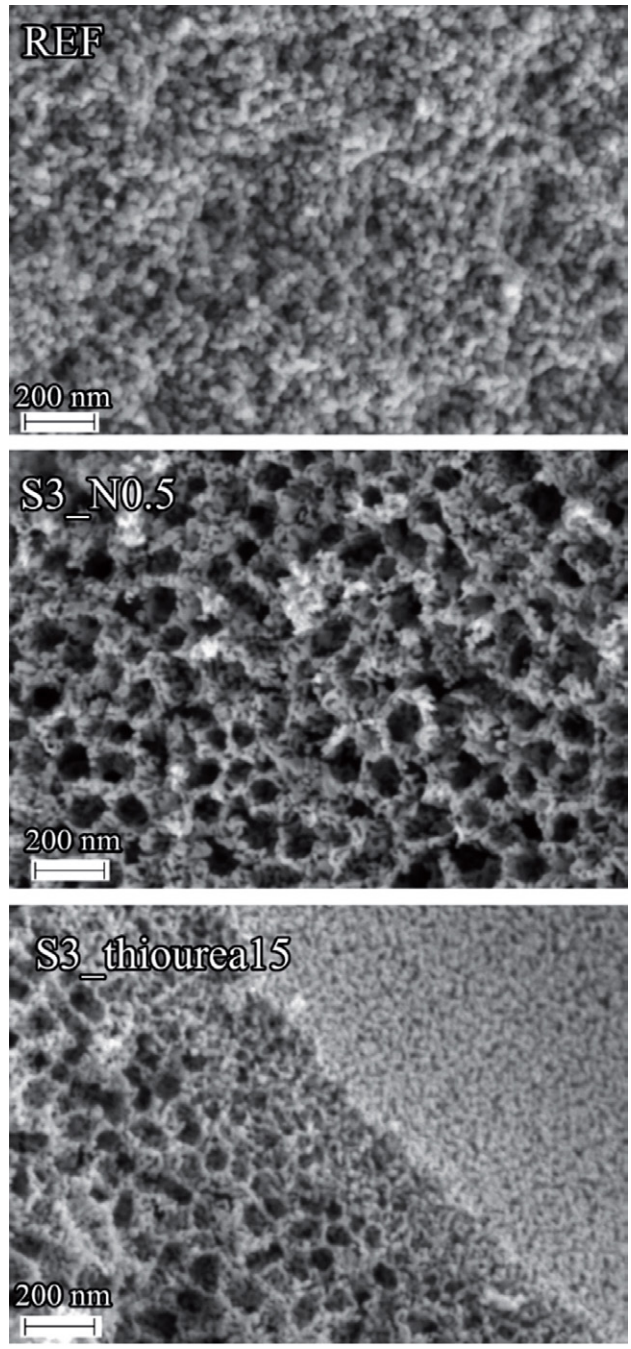

Figure 2. FE-SEM micrographs of powders: REF, S3_N0.5 and S3_thiourea15 at 200,000x magnification. Accelerating voltage was set to 2 kV. Images were obtained with detection of secondary electrons.

By adding urea (sample Urea_15) to the undoped sample REF, the photocurrent response has decreased. We can attribute this to the lower surface area of sample Urea_15, which was observed from BET measurements. Contrarily, the addition of thiourea (sample Thiourea_15) has resulted in an increase in photocurrent response, which is attributed to the higher surface area of the sample Thiourea_15.

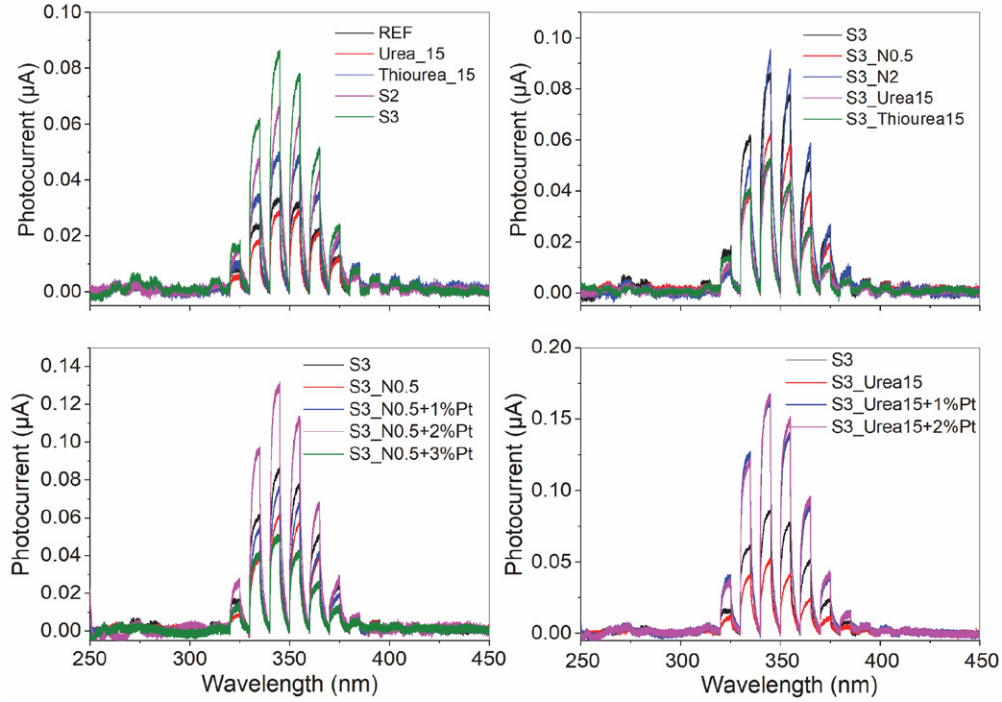

Figure 3. Photocurrent responses recorded under applied external potential of 1 V.

By substituting HCl with H_2SO_4 during the synthesis (samples S2 and S3) the current has increased. As with sample Thiourea_15, this can be explained by the higher surface area of samples S2 and S3 compared to the samples synthesized with HCl. Because sample S3 has a higher surface area than sample S2, a higher photocurrent is induced when irradiating the former. The results, as presented in Figure 3b, show that the addition of 0.5 % of NH_4NO_3 (sample S3_N0.5), urea (sample S3_urea15) or thiourea (sample S3_thiourea15) to sample S3 has resulted in a decrease in photocurrent response, despite the increase in surface area. The response has increased when adding 2 % of NH_4NO_3 (sample S3_N2), which also has the highest surface area of all the samples. From this we can deduce that the amount of induced photocurrent depends not only on the surface area, but also on the amount of added dopants. Band gap energies for selected samples have already been measured and published by Žener et al. [38]

Results for samples with added Pt are presented in Figures 3c and 3d. When comparing these samples with those without the added Pt (samples S3_N0.5 and S3_urea15), we can see that the addition of 1 % and 2 % of Pt had a positive effect on the photocatalytic response, despite the lower surface area of these samples. When irradiating the sample with 3 % of added Pt (sample S3_N0.5 + 3%Pt) the amount of induced photocurrent has decreased dramatically, which could be due to the increased Pt blocking light to the photocatalyst. Moreover, platinum particles can also act as recombination centres.

3. 5. Photocatalytic Activity

Concentration profiles for isopropanol and acetone for selected samples are presented in Figure 4. The photocatalytic activity of powders under UV and visible light irradiation was tested by monitoring the oxidation of isopropanol to acetone. It can be seen that the isopropanol curve is unstable before the UV and visible light is switched on, which can be attributed to the adsorption of isopropanol onto the surface of the sample and reactor system. After the UV and visible light is switched on the acetone concentration increases, while the isopropanol concentration decreases. Reactions are presented in Equation (2) in the experimental section. In the initial steps of the photocatalysis, we can approximate the reaction to be of zero order, because the photocatalytic oxidation of isopropanol to acetone is faster than the subsequent oxidation of acetone. Zero order kinetics can be described with Equation (3):

$$c = k_0 t + c_0 \quad (3)$$

In this equation c and c_0 represent concentration of acetone and the initial concentration of acetone, respectively in ppm, while t is time in hours and k_0 is the zero-order rate constant (units ppm/h). Therefore, the initial slope of the acetone concentration curve is equal to k_0 (Equation (3)), which was determined from line equations in Figure 4. This presents a good basis to compare photocatalytic activity of different TiO_2 powders.[43] Zero order rate constants (k_0) for different samples are presented in Table 3.

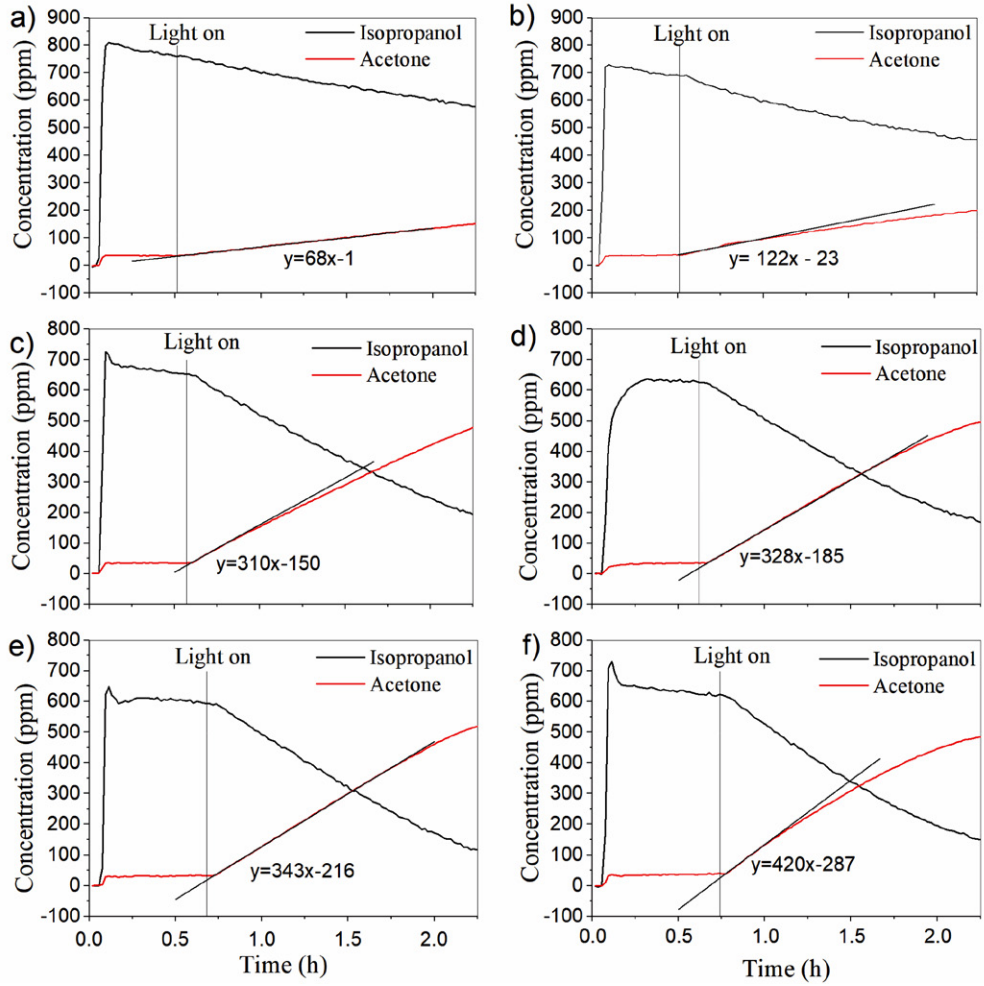

Figure 4. Concentration profiles of isopropanol and acetone for: (a) REF; (b) Urea_15; (c) S3; (d) S3_N2; (e) S3_N0.5 + 1%Pt and (f) S3_urea15 + 1%Pt; y in the line equation represents concentration of acetone (in ppm) and x represents time of experiment in reactor (in hours)

Table 3. Photocatalytic activities of different samples, determined by observing the oxidation of isopropanol to acetone (rate constant k_0).

Sample	Activity under UV and visible light exposure - k_0 (ppm/h)
HOMBIKAT UV 100	337 ± 2
REF	68 ± 1
Urea_15	122 ± 4
Thiourea_15	50 ± 2
S2	183 ± 2
S3	310 ± 3
S3_N0.5	260 ± 2
S3_N2	328 ± 3
S3_urea15	304 ± 2
S3_thiourea15	225 ± 2
S3_N0.5+1%Pt	343 ± 2
S3_N0.5+2%Pt	251 ± 3
S3_N0.5+3%Pt	260 ± 3
S3_urea15+1%Pt	420 ± 3
S3_urea15+2%Pt	420 ± 2

The addition of urea (sample Urea_15) to the undoped sample REF has resulted in an increase in the photocatalytic activity (k_0 = 122 ± 4 ppm/h and 68 ± 1 ppm/h for sample Urea_15 and REF, respectively). In our previously published work, we reported a very high band-gap value in sample REF (3.44 eV). The addition of urea narrows the band-gap due to nitrogen doping, and consequently increases photocatalytic activity even under UV light.[38,44] On the contrary, addition of thiourea (sample Thiourea_15) decreases the photocatalytic activity of the sample (k_0 = 50 ± 2 ppm/h) when compared to REF, despite the former having a higher surface area (49.5 ± 0.3 m^2/g for sample Thiourea_15 and 44.1 ± 0.4 m^2/g for REF) and higher photocurrent response. This could be explained by higher recombination rates of the charge carriers in sample Thiourea_15. Additional measurements would, however, be needed to confirm this theory.

By using H_2SO_4 instead of HCl in the synthesis (samples S2 and S3) we obtained samples with smaller-sized crystallites, which results in higher porosity (24.2 ± 0.2 to 49.5 ± 0.3 m^2/g for samples synthesized with HCl; 63.2 ± 0.3

and 80.2 ± 0.2 m^2/g for samples S2 and S3, respectively) and a far higher photocurrent response. For these reasons, samples S2 and S3 show much higher activity than samples synthesized with HCl (k_0 = 183 ± 2 ppm/h for sample S2 and 310 ± 3 ppm/h for sample S3). S3 has a higher surface area and higher photocurrent response compared to S2, and consequently much higher photocatalytic activity.

The addition of NH_4NO_3 (samples S3_N0.5 and S3_N2), urea (sample S3_urea15) and thiourea (sample S3_thiourea_15) to sample S3 increases the specific surface areas (84.5 ± 0.3 to 103.4 ± 0.4 m^2/g). Despite this, only one sample has a higher photocatalytic activity than the sample without additions (sample S3, k_0 = 310 ± 3 ppm/h, sample S3_N2, k_0 = 328 /h). This can be explained by the results of the photocurrent measurements, which have shown decreased responses (compared to sample S3) in all but sample S3_N2, which also has the highest surface area (103.4 ± 0.4 m^2/g). Higher activity can also be attributed to the addition of nitrogen, which increases the amount of oxygen vacancies and reduces the band gap energy, resulting in higher photocatalytic activity.[38] The decreased activity in samples S3_urea15 and S3_thiourea15 can be attributed to higher percentages of β-TiO_2, found in these two samples, since the photocatalytic activity of β-TiO_2 is generally much lower than that of anatase.[45–47]

The addition of Pt to sample S3_N0.5 does not increase its surface area, in fact in the case of the sample with 2 % Pt added (sample S3_N0.5 + 2% Pt) it actually decreases (84.5 ± 0.3 m^2/g for sample S3_N0.5 and 80.5 ± 0.4 m^2/g for sample S3_N0.5 + 2% Pt). Despite this, the sample S3_N0.5 + 1%Pt shows much higher photocatalytic activity (k_0 = 343 ± 2 ppm/h), compared to sample S3_N0.5 (k_0 = 260 ± 2 ppm/h). We attribute this to Pt acting as an efficient trap for free electrons, thus inhibiting recombination (confirmed with photocurrent measurements), whilst also improving the free electron transfer to adsorbed pollutants. The activity of sample S3_N0.5+3%Pt is equal to the activity of sample S3_N0.5, but the activity of sample S3_N0.5 + 2%Pt has reduced slightly.

Doping the sample S3_urea15 with Pt (samples S3_urea15 + 1%Pt and S3_urea15+2%Pt) significantly lowers its surface area (82.3 ± 0.3 m^2/g for sample S3_urea15 + 1%Pt and 84.2 ± 0.4 m^2/g for sample S3_urea15 + 2%Pt). Furthermore, results of the photocurrent measurements have shown that the addition of Pt significantly increases the photocurrent response, resulting in far higher photocatalytic activity in samples S3_urea15 + 1%Pt (k_0 = 420 ± 3 ppm/h) and S3_urea15 + 2%Pt (k_0 = 420 ± 2 ppm/h) compared to sample S3_urea15 (k_0 = 304 ± 2 ppm/h). It was found out that metal and non-metal doping, as well as addition of HPC significantly increase the photocatalytic activity of powders under UV and visible light irradiation. In the case of samples S3_urea15 + 1%Pt and S3_urea15 + 2%Pt the photocatalytic activity is even higher than that of selected anatase sample available on the market: HOMBIKAT UV 100 (k_0 = 337 ± 2 ppm/h) (see Table 3).[48]

4. Conclusions

In the present work TiO_2 powders, doped with sulfur and nitrogen and modified with platinum were prepared by means of particulate sol-gel synthesis in order to increase the photocatalytic activity of undoped sample, while the organic polymer hydroxypropyl cellulose (HPC) was added to increase the surface area of the photocatalyst. By substituting HCl with H_2SO_4 during the synthesis, the resulting samples contained smaller crystallites (26.9 ± 0.7 – 30.7 ± 0.8 nm for samples synthesized with HCl; 15.1 ± 0.3 – 23.5 ± 0.2 nm nm for samples synthesized with H_2SO_4). We attributed the smaller crystallite size to the formation of $TiOSO_4$, which inhibits the crystallization of TiO_2. Additionally, we observed the presence of β-TiO_2 in samples synthesized with H_2SO_4. The highest percentage of β-TiO_2 was found in sample S3_thiourea15 (45.4 ± 0.3 %). The afore-mentioned decrease in the size of crystallites led to a higher specific surface area for samples synthesized with H_2SO_4 (63.2 ± 0.3 to 103.4 ± 0.4 m^2/g) compared to those synthesized with HCl (24.2 ± 0.2 to 49.5 ± 0.3 m^2/g). The addition of NH_4NO_3, urea and thiourea to sample S3 increased its porosity. Sample S3_N2 had the highest surface area (103.4 ± 0.4 m^2/g) and the smallest crystallites of anatase (16.8 ± 0.1 nm). The addition of Pt did not increase the sample's porosity, in some cases it even decreased it. FE-SEM images confirmed the increased porosity of samples synthesized with H_2SO_4. Additionally, smaller crystallites were found in samples synthesized with H_2SO_4, confirming the results of X-Ray diffraction.

The increased porosity of the samples synthesized with H_2SO_4 also resulted in greater photocurrent responses in these samples compared to those synthesized with HCl. Despite increasing the specific surface area, the addition of NH_4NO_3, urea and thiourea to S3 yielded a lower photocurrent response, with the exception of sample S3_N2, which also had the highest surface area. In all but one case the addition of platinum resulted in greater photocurrent responses.

Samples synthesized with H_2SO_4 exhibit higher photocatalytic activity compared to samples synthesized with HCl, which can be explained by larger surface areas and higher photocurrent responses. Out of all the samples with added NH_4NO_3, urea or thiourea, only sample S3_N2 has a higher photocatalytic activity compared to sample S3. This is also the only sample in this group which exhibit a greater photocurrent response than sample S3. The addition of platinum to sample S3_urea significantly increased its photocatalytic activity, which is in agreement with the results of photocurrent measurements. Out of all the samples, samples S3_urea15 + 1%Pt and S3_urea15 + 2%Pt showed the highest photocatalytic activity (k_0 = 420 ± 3 and 420 ± 2 ppm/h), which was even higher than the activity of the well-known pure anatase photocatalyst HOMBIKAT UV 100 (k_0 = 337 ± 2 ppm/h). We were able to significantly increase the photocatalytic activity of pow-

ders under UV and visible light irradiation by increasing the surface area and photocurrent response with non-metal and metal doping.

Acknowledgements

The authors acknowledge the financial support from the Slovenian Research Agency (research core funding Nos. P1-0134 and P2-0273, while part of the work was conducted under project No. NC-0002). B. Ž. is grateful to Slovenian Research Agency for the position of young researcher enabling him the doctoral study. M. R. also acknowledges the Operational Programme Research, Development and Education, project No. CZ.02.1.01./0.0/0.0/17 _049/0008419 „COOPERATION". The authors thank to Mojca Opresnik from the National Institute of Chemistry for BET measurements and to Edi Kranjc (also from the National Institute of Chemistry) for performing XRD measurements. The authors also acknowledge dr. Amalija Golobič for her help with Rietveld analysis.

5. References

1. R. Fagan, D. E. McCormack, D. D. Dionysiou, S. C. Pillai, *Mater. Sci. Semicond. Process.* **2016**, *42*, 2–14. **DOI:**10.1016/j.mssp.2015.07.052
2. R. Marchant, L. Brohan, M. Tournox, *Mater. Res. Bull.* **1980**, *15*, 1129–1133. **DOI:**10.1016/0025-5408(80)90076-8
3. S. León-Ríos, R. Espinoza González, S. Fuentes, E. Chávez Ángel, A. Echeverría, A. E. Serrano, C. S. Demergasso, R. A. Zárate, *J. Nanomater.* **2016**, *2016*, 1–8. **DOI:**10.1155/2016/7213672
4. T. Fröschl, U. Hörmann, P. Kubiak, G. Kučerová, M. Pfanzelt, C. K. Weiss, R. J. Behm, N. Hüsing, U. Kaiser, K. Landfester, M. Wohlfahrt-Mehrens, *Chem. Soc. Rev.* **2012**, *41*, 5313–5360. **DOI:**10.1039/c2cs35013k
5. M. Grätzel, *J. Sol- Gel Sci. Technol.* **2001**, *22*, 7–13. **DOI:**10.1023/A:1011273700573
6. M. Fitra, I. Daut, M. Irwanto, N. Gomesh, Y. M. Irwan, *Energy Procedia* **2013**, *36*, 278–286. **DOI:**10.1016/j.egypro.2013.07.032
7. M. Hassan, Y. Zhao, B. Xie, *Chem. Eng. J.* **2016**, *285*, 264–275. **DOI:**10.1016/j.cej.2015.09.093
8. M. Rozman, J. Cerar, M. Lukšič, M. Uršič, A. Mourtzikou, H. Spreizer, I. K. Škofic, E. Stathatos, *Electrochim. Acta* **2017**, *238*, 278–287. **DOI:**10.1016/j.electacta.2017.04.030
9. N. Amira Marfur, N. Farhana Jaafar, M. Khairuddean, N. Nordin, *Acta Chim. Slov.* **2020**, *67*, 361–374. **DOI:**10.17344/acsi.2019.5161
10. J.-M. Herrmann, C. Guillard, P. Pichat, *Catal. Today* **1993**, *17*, 7–20. **DOI:**10.1016/0920-5861(93)80003-J
11. H. Zhao, S. Chen, X. Quan, H. Yu, H. Zhao, *Appl. Catal. B Environ.* **2016**, *194*, 134–140. **DOI:**10.1016/j.apcatb.2016.04.042
12. J. Yu, P. Zhang, H. Yu, C. Trapalis, *Int. J. Photoenergy* **2012**, *2012*, 1–4. **DOI:**10.1155/2012/594214
13. Z. Xing, J. Zhang, J. Cui, J. Yin, T. Zhao, J. Kuang, Z. Xiu, N. Wan, W. Zhou, *Appl. Catal. B Environ.* **2018**, *225*, 452–467. **DOI:**10.1016/j.apcatb.2017.12.005
14. S. Zhu, D. Wang, *Adv. Energy Mater.* **2017**, *7*, 1–24. **DOI:**10.1002/aenm.201700841
15. C. B. Almquist, P. Biswas, *J. Catal.* **2002**, *212*, 145–156. **DOI:**10.1006/jcat.2002.3783
16. A. V. Vorontsov, E. N. Kabachkov, I. L. Balikhin, E. N. Kurkin, V. N. Troitskii, P. G. Smirniotis, *J. Adv. Oxid. Technol.* **2018**, *21*, 127–137. **DOI:**10.26802/jaots.2017.0063
17. C. C. Wang, Z. Zhang, J. Y. Ying, *Nanostructured Mater.* **1997**, *9*, 583–586. **DOI:**10.1016/S0965-9773(97)00130-X
18. Z. Zhang, C.-C. Wang, R. Zakaria, J. Y. Ying, *J. Phys. Chem. B* **2002**, *102*, 10871–10878. **DOI:**10.1021/jp982948+
19. A. J. Maira, K. L. Yeung, C. Y. Lee, P. L. Yue, C. K. Chan, *J. Catal.* **2000**, *192*, 185–196. **DOI:**10.1006/jcat.2000.2838
20. Y. Li, B. P. Bastakoti, M. Imura, S. M. Hwang, Z. Sun, J. H. Kim, S. X. Dou, Y. Yamauchi, *Chem. - A Eur. J.* **2014**, *20*, 6027–6032. **DOI:**10.1097/01.ccm.0000457553.95006.19
21. W. Dong, Y. Sun, C. W. Lee, W. Hua, X. Lu, Y. Shi, S. Zhang, J. Chen, D. Zhao, *J. Am. Chem. Soc.* **2007**, *129*, 13894–13904. **DOI:**10.1021/ja073804o
22. K. Kato, A. Tsuzuki, Y. Torii, H. Taoda, T. Kato, Y. Butsugan, *J. Mater. Sci.* **1995**, *30*, 837–841. **DOI:**10.1007/BF00356349
23. J. Zhang, Y. Deng, D. Gu, S. Wang, L. She, R. Che, Z. S. Wang, B. Tu, S. Xie, D. Zhao, *Adv. Energy Mater.* **2011**, *1*, 241–248. **DOI:**10.1002/aenm.201000004
24. J. Vargas Hernández, S. Coste, A. García Murillo, F. Carrillo Romo, A. Kassiba, *J. Alloys Compd.* **2017**, *710*, 355–363. **DOI:**10.1016/j.jallcom.2017.03.275
25. N. A. M. Barakat, M. A. Kanjwal, I. S. Chronakis, H. Y. Kim, *J. Mol. Catal. A Chem.* **2013**, *366*, 333–340. **DOI:**10.1016/j.molcata.2012.10.012
26. N. Sobana, M. Muruganadham, M. Swaminathan, *J. Mol. Catal. A Chem.* **2006**, *258*, 124–132. **DOI:**10.1016/j.molcata.2006.05.013
27. D. Hufschmidt, D. Bahnemann, J. J. Testa, C. A. Emilio, M. I. Litter, *J. Photochem. Photobiol. A Chem.* **2002**, *148*, 223–231. **DOI:**10.1016/S1010-6030(02)00048-5
28. S. Sakthivel, M. V. Shankar, M. Palanichamy, B. Arabindoo, D. W. Bahnemann, V. Murugesan, *Water Res.* **2004**, *38*, 3001–3008. **DOI:**10.1016/j.watres.2004.04.046
29. J. H. Kim, G. Kwon, H. Lim, C. Zhu, H. You, Y. T. Kim, *J. Power Sources* **2016**, *320*, 188–195. **DOI:**10.1016/j.jpowsour.2016.04.019
30. M. Tahir, N. A. S. Amin, *Appl. Catal. B Environ.* **2015**, *162*, 98–109. **DOI:**10.1016/j.apcatb.2014.06.037
31. R. Pol, M. Guerrero, E. García-Lecina, A. Altube, E. Rossinyol, S. Garroni, M. D. Baró, J. Pons, J. Sort, E. Pellicer, *Appl. Catal. B Environ.* **2016**, *181*, 270–278. **DOI:**10.1016/j.apcatb.2015.08.006
32. P. D. Cozzoli, A. Kornowski, H. Weller, *J. Am. Chem. Soc.* **2003**, *125*, 14539–14548. **DOI:**10.1021/ja036505h
33. X. Jia, W. He, X. Zhang, H. Zhao, Z. Li, Y. Feng, *Nanotechnology* **2007**, *18*, 075602. **DOI:**10.1088/0957-4484/18/7/075602

34. H. Xu, B. W. Zeiger, K. S. Suslick, *Chem. Soc. Rev.* **2013**, *42*, 2555–2567. **DOI:**10.1039/C2CS35282F
35. R. Rossmanith, C. K. Weiss, J. Geserick, N. Hüsing, U. Hörmann, U. Kaiser, K. Landfester, *Chem. Mater.* **2008**, *20*, 5768–5780. **DOI:**10.1021/cm800533a
36. B. G. Rao, D. Mukherjee, B. M. Reddy, in *Nanostructures Nov. Ther. Synth. Charact. Appl.* (Eds.: D. Ficai, A.M. Grumezescu), Elsevier Inc., Oxford, **2017**, pp. 1–31.
37. U. Schubert, N. Hüsing, *Synthesis of Inorganic Materials*, Wiley-VCH Verlag, Weinheim, **2012**.
38. B. Žener, L. Matoh, G. Carraro, B. Miljević, R. Cerc Korošec, *Beilstein J. Nanotechnol.* **2018**, *9*, 1629–1640. **DOI:**10.3762/bjnano.9.155
39. General Profile and Structure Analysis Software for Powder Diffraction Data, Topas version 2.1, Bruker AXS, Karlsruhe, Germany, **2000**.
40. M. Reli, I. Troppová, M. Šihor, J. Pavlovský, P. Praus, K. Kočí, *Appl. Surf. Sci.* **2019**, *469*, 181–191. **DOI:**10.1016/j.apsusc.2018.10.255
41. M. Reli, P. Huo, M. Šihor, N. Ambrožová, I. Troppová, L. Matějová, J. Lang, L. Svoboda, P. Kuśtrowski, M. Ritz, P. Praus, K. Kočí, *J. Phys. Chem. A* **2016**, *120*, 8564–8573. **DOI:**10.1021/acs.jpca.6b07236
42. M. Rutar, N. Rozman, M. Pregelj, C. Bittencourt, R. Cerc Korošec, A. Sever Škapin, A. Mrzel, S. D. Škapin, P. Umek, *Beilstein J. Nanotechnol.* **2015**, *6*, 831–844. **DOI:**10.3762/bjnano.6.86
43. T. Marolt, A. S. Škapin, J. Bernard, P. Živec, M. Gaberšček, *Surf. Coatings Technol.* **2011**, *206*, 1355–1361. **DOI:**10.1016/j.surfcoat.2011.08.053
44. B. Žener, Ž. Medoš, M. Bešter Rogač, R. Cerc Korošec, *ChemistrySelect* **2019**, *4*, 4112–4117. **DOI:**10.1002/slct.201900188
45. S. Yin, Y. Fujishiro, J. Wu, M. Aki, T. Sato, *J. Mater. Process. Technol.* **2003**, *137*, 45–48. **DOI:**10.1016/S0924-0136(02)01065-8
46. D. Yang, H. Liu, Z. Zheng, Y. Yuan, J. C. Zhao, E. R. Waclawik, X. Ke, H. Zhu, *J. Am. Chem. Soc.* **2009**, *131*, 17885–17893. **DOI:**10.1021/ja906774k
47. S. Yin, J. Wu, M. Aki, T. Sato, *Int. J. Inorg. Mater.* **2000**, *2*, 325–331. **DOI:**10.1016/S1466-6049(00)00034-9
48. D. M. Tobaldi, L. Gao, A. F. Gualtieri, A. S. Škapin, A. Tucci, C. Giacobbe, *J. Am. Ceram. Soc.* **2012**, *95*, 1709–1716. **DOI:**10.1111/j.1551-2916.2012.05135.x

Povzetek

Zaradi zmožnosti razgradnje adsorbiranih organskih onesnažil se fotokatalizator TiO_2 v zadnjih desetletjih veliko preučuje za različne okoljske aplikacije. V tem delu predstavljamo z žveplom in dušikom dopirane oz. kodopirane ter s platino modificirane prahove TiO_2, ki smo jih pripravili po koloidnem sol-gel postopku. PXRD meritve kažejo, da zamenjava HCl s H_2SO_4 med sinteznim postopkom zmanjša velikost kristalitov iz ~30 nm na ~20 nm, pri čemer se poveča tudi specifična površina iz ~44 m^2/g na ~80 m^2/g. Opažanja korelirajo z izmerjeno fotokatalitsko aktivnostjo vzorcev in izmerjenim fototokom. Rezultati kažejo, da so lastnosti prahov (specifična površina, velikost kristalitov, obnašanje fototoka) odvisne ne le od vrste uporabljene kisline, temveč tudi od njene količine in uporabljenega dopanta. Dopiranje z žveplom, kodopiranje z žveplom in dušikom in modifikacija prahov TiO_2 s platino povečajo fotokatalitsko aktivnost tudi do šestkrat.

Except when otherwise noted, articles in this journal are published under the terms and conditions of the Creative Commons Attribution 4.0 International License

Scientific paper

Synthesis, Crystal Structure and Separation Performance of *p-tert*-butyl(tetradecyloxy)calix[6]arene

Wei Zhang,[1] Zhi-qiang Cai,[1,*] Xiao-min Shuai,[1] Wei Li,[1] Qiu-chen Huang,[1] Ruo-nan Chen,[1] Qi-qi Zang,[2] Fei-fei Li[2] and Tao Sun[2,*]

[1] *Liaoning Province Professional and Technical Innovation Center for Fine Chemical Engineering of Aromatics Downstream, School of Petrochemical Engineering, Shenyang University of Technology, Liaoyang 111003, P. R. China.*

[2] *College of Chemistry and Chemical Engineering, Henan Key Laboratory of Function-Oriented Porous Materials, Luoyang Normal University, Luoyang 471934, P. R. China.*

* *Corresponding author: E-mail: kahongzqc@163.com; E-mail: suntao2226@163.com*

Received: 10-19-2021

Abstract

This work describes the investigation of separation performance of the *p-tert*-butyl(tetradecyloxy)calix[6]arene (C6A-C10-OH) as stationary phase for gas chromatography (GC) separations. Its structure was characterized by IR, ^{1}H NMR, ^{13}C NMR, MS and single-crystal X-ray diffraction analysis. The C6A-C10-OH column shows good separation capacity for aliphatic, aromatic and *cis-*/*trans-* isomers. Especially, it exhibits multiple molecular recognition interactions for the analytes with a wide range of polarity, including dispersion, π-π, H-bonding and dipole-dipole interactions. The present work provides experimental and theoretical basis for the designing of the new calixarene stationary phases in GC analyses.

Keywords: Calixarene; crystal structure; separation performance

1. Introduction

Calixarenes are the third generation of supramolecular compound after crown ethers and cyclodextrins.[1] These macrocyclic compounds have attracted extensive attention in the field of separation science because of it has unique physicochemical properties such as adjustable cavity size, good solubility, structural stability and so on.[2] Their hydrophobic cavities are composed of benzene ring units, and its upper and lower rims are *p-tert*-butyls and phenolic hydroxyl groups, respectively, which are easy to derivatize.[3] In recent years, calixarene derivatives with diverse structures have been widely used in various fields, such as catalysis, molecular recognition, energy and separation analysis.[4]

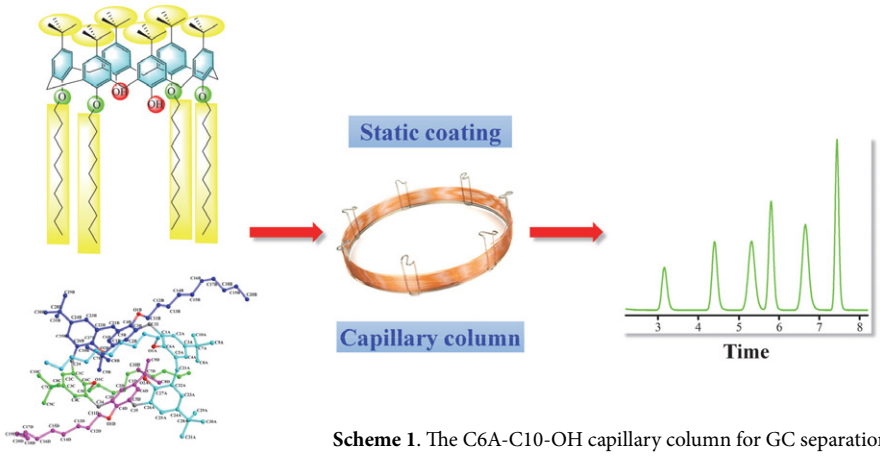

Scheme 1. The C6A-C10-OH capillary column for GC separation.

GC has widely applied in many fields including environmental analysis, petrochemical industry, food analysis and pharmaceutical analysis due to its excellent characteristics such as good selectivity, high sensitivity, rapid analysis and low cost.[5] In GC, it is the key to choose a suitable stationary phase for the separation of compounds with close nature. In recent years, our group has been engaged in the research of new calixarene chromatographic stationary phases. In 2019, we first reported the amphiphilic calixarene (C4A-NH_2) and used it to separate aromatic amine isomers.[6] Subsequently, we reported the study of calix[6]arene and calix[8]arene derivatives as stationary phases for GC.[7] These results indicated that calixarenes and their derivatives are suitable as GC stationary phases with good chromatographic selectivity.

First, we synthesized a new calixarene compound (C6A-C10-OH) in this work. The upper rim is *p-tert*-butyl, and the lower rim is long alkyl chain and phenolic hydroxyl. Second, we characterized the molecular structure of C6A-C10-OH by IR, ^{1}H NMR, ^{13}C NMR, MS and single-crystal X-ray diffraction analysis. Then, it was coated on the inner wall of capillary column by static method, and its chromatographic separation performance was investigated (Scheme 1).

2. Experimental

2. 1. Materials and Methods

An Agilent 7890A gas chromatograph was used for GC analyses. Thin layer chromatography (TLC) was performed on silica-gel plates (HF_{254}). ^{1}H NMR spectrum and ^{13}C NMR spectrum used TMS (tetramethylsilane) as the internal standard and exported on a Bruker BioSpin 400 MHz instrument. Chemical shifts (δ) were expressed in ppm. IR spectrum was reported on a Bruker Platinum ART Tensor II FTIR spectrometer. MALDI-TOF-MS was reported on a Bruker BIFLEX III mass spectrometer. Single Crystal data of C6A-C10-OH were gained on a Bruker D8 VENTURE X-ray diffractometer. All reagents and solvents were not further treated, and all from commercial way.

2. 2. Synthesis of the C6A-C10-OH

Firstly, NaH (1.24 g, 51.67 mmol), *p-tert*-butylcalix[6]arene (1.50 g, 1.54 mmol) and DMF (25 mL) were added to a 50 mL round bottom flask. The reactants were reacted at room temperature for 1 h. Afterwards, 1-bromodecane (4.30 g, 19.19 mmol) was added to mixed solution, raised the temperature to 85 °C and reacted for 10 h. After the reaction, the solvent was concentrated to obtain a yellow solid. Then, dichloromethane was used to dissolve the obtained yellow solid and rinsed three times with deionized water (15 mL). Then, the anhydrous magnesium sulfate was used to remove water and vacuum drying. Finally, a light yellow oily product was obtained. Using column chromatography [dichloromethane/petroleum ether (v/v = 1:4)] to purify the product of the previous step, and the final white solid product was gained with a yield of 85.34%. ^{1}H NMR (400 MHz, $CDCl_3$, ppm): δ 7.39 (s, 4H, CH), 7.04 (s, 8H, CH), 4.05 (m,8H, CH_2), 3.84 (s, 12H, CH_2), 1.60 (m, 8H, CH_2), 1.42 (m, 8H, CH_2), 1.27 (s, 54H, CH_3), 1.22 (m, 48H, CH_2), 0.86 (t,12H, CH_3); ^{13}C NMR (100 MHz, $CDCl_3$, ppm): δ 151.57, 151.15, 146.93, 142.79, 132.78, 126.23, 125.70, 77.48, 77.16, 76.84, 34.29–33.67, 32.19–31.90, 31.90–30.69, 30.16–29.01, 26.50, 23.05–22.74, 14.29; IR (KBr), cm^{-1}: ν(OH) 3373, ν(CH_3) 2955, ν(CH_2) 2929, ν(CH_2) 2858, ν(C=C) 1484, ν(C=C) 1460, ν(C-O-C) 1188, ν(CH_2) 722; ESI-MS(m/z): $[M+K]^+$calcd for $C_{106}H_{164}O_6$, 1572.253; found, 1572.166.

2. 3. X-Ray Structure Determination

Took a small amount of white solid of the C6A-C10-OH and dissolved it in dichloromethane. After two days, dichloromethane volatilizes completely, we gained the white crystal for single crystal diffraction analysis. The dimensions of white crystal ($C_{106}H_{164}O_6$) were 0.17mm × 0.12mm × 0.12mm, and which were measured on a Bruker D8 VENTURE diffractometer equipped with graphite-monochromatic Mo $K\alpha$ radiation (λ = 1.54178 Å) using an ω scan mode at 103(2) K. A total of 55912 reflections were gathered in the range of 2.457° < θ < 70.168° (index ranges: $-12 \le h \le 12$, $-43 \le k \le 42$ and $-30 \le l \le 30$) and 17547 were independent (R_{int} = 0.0745), of which 11531 observed reflections with $I > 2\sigma(I)$ were applied in the refinements and structure determination. Used the intrinsic phasing methods to confirm the structure with

Table 1. Crystal data of the C6A-C10-OH

Crystal size	0.170 × 0.120 × 0.120 mm^3
Formula	$C_{106}H_{164}O_6$
Molecular weight	1534.36
T (K)	103(2) K
Crystal system	Monoclinic
Space group	Cc
a (Å)	10.5965(5)
b (Å)	35.9665(16)
c (Å)	25.1721(11)
α (°)	90
β (°)	92.663(3)
γ (°)	90
V (Å)^3	9583.2(7)
Z	4
D_c (g/cm^3)	1.063
F(000)	3392
Goodness-of-fit on F^2	1.075
Reflection collected	55912
R_1, wR_2 [I > 2σ (I)]	0.0852, 0.2445
R_1, wR_2 (all data)	0.1135, 0.2743

$R_1 = \Sigma(||F_o|-|F_c||)/\Sigma|F_o|$ ... $wR_2 = (\Sigma w(F_o^2-F_c^2)^2/\Sigma w(F_o^2)^2)^{1/2}$

the SHELXT 2014 program and reported by the Fourier technique.[8] The non-hydrogen atoms were purified anisotropically. Through theoretical calculation, we reached the hydrogen atom combined with carbon atom. The structure was purged by the full-matrix least-squares techniques on F^2 with SHELXL-2017.[8] The final refinement gave R = 0.0852 and wR = 0.2743 ($w = 1/[\sigma^2(F_o^2)+(P)^2+P)]$, where $P = (F_o^2+2F_c^2)/3)$, S = 1.075, $(\Delta/\sigma)_{max}$ = 0.002, $(\Delta\rho)_{max}$ = 0.694 and $(\Delta\rho)_{min}$ = –0.278 e/Å^3. Other crystal structure data of C6A-C10-OH are shown in Table 1.

2. 4. Preparation of the Capillary Column

The static coating method was used to make the C6A-C10-OH capillary column.[9] Firstly, the dichloromethane was used to rinse the empty column (0.25 mm × 10 m) to remove impurities. The rinsed capillary column was filled by a NaCl-MeOH saturated solution to rough inner wall of capillary column. Then, it was rised from 40 °C to 200 °C and maintained at 200 °C for 3 h. Next, the C6A-C10-OH stationary phase was dissolved in dichloromethane (2 mL) and injected into the treated column. When the column was completely full of stationary phase solution, sealed one end of the chromatographic column and connected the other end to the vacuum environment at 40 °C to evaporate the excess dichloromethane solution. Temperature process started at 40 °C hold for 30 minutes rise to 160 °C at the rate of 1 °C/min and maintained at 160 °C for 7 h. The experimental process was operated in nitrogen atmosphere.

3. Results and Discussion

3. 1. Synthesis and Characterization

Scheme 2 exhibits the synthetic process of C6A-C10-OH and it was obtained by one-step reaction. Meanwhile, IR, ^{1}H NMR, ^{13}C NMR, MS and single-crystal X-ray diffraction analysis interpreted the molecular structure of C6A-C10-OH. In the IR, the peak value of 2955 cm^{-1} was C-H antisymmetric stretching vibration on the *p-tert*-butyl. The peak values of 1484 and 1460 cm^{-1} was the C=C stretching vibration on benzene ring units. The peak value of 1188 cm^{-1} was the C-O-C stretching vibration of ether, the peak value of 722 cm^{-1} was the CH_2 plane rocking vibration of alkyl chains in the compound. In the ^{1}H NMR, the proton absorption peaks of the aromatic rings were observed at 7.39 and 7.04 ppm in the low field, the proton absorption peaks of the bridged methylene in the benzene rings were discovered at 3.84 ppm, and the proton absorption peaks of methyl on *p-tert*-butyls and alkyl chains were found at 1.27 and 0.86 ppm, respectively. The integral area of each peak was consistent with the expected number of protons. Moreover, the structure of C6A-C10-OH was also characterized by ^{13}C NMR.

3. 2. Crystal Structure of the C6A-C10-OH

Fig. 1 presents the molecular structure of the C6A-C10-OH, the crystal data and selected bond lengths are listed in the Table 1 and the Table 2 respectively. Its molecular structure consisted of six benzene rings, the four alkyl chains and two phenolic hydroxyl groups at the lower of C6A. The torsion angle of C(5)B-C(21)B-C(22)B-C(27)B was –90.0(8)°, which suggested that the two blue benzene rings were perpendicular to each other in space. The torsion angle of C(4)B-C(5)B-C(6)B-C(1)B was 0.1(10)°, which further proved that the carbon atoms on the benzene ring were coplanar. In the Table 2, the bond lengths of C(23)B-C(24)B (1.387(10) Å) and C(22)B-C(23)B (1.391(11) Å) were almost equal because these two bonds were in the same benzene ring. The bond length of O(1)B-C(11)B (1.416(9) Å) is shorter than C(11)B-C(12)B (1.519(11) Å). This is because the electronegativity of oxygen atom was larger than that of carbon atom, so that the bond energy of C=O was stronger than that of C=C. Moreover, Fig. 2 depicts the molecular packing in the unit cell and Table 3 gives that the hydrogen bond lengths and bond angles in the structure.[10]

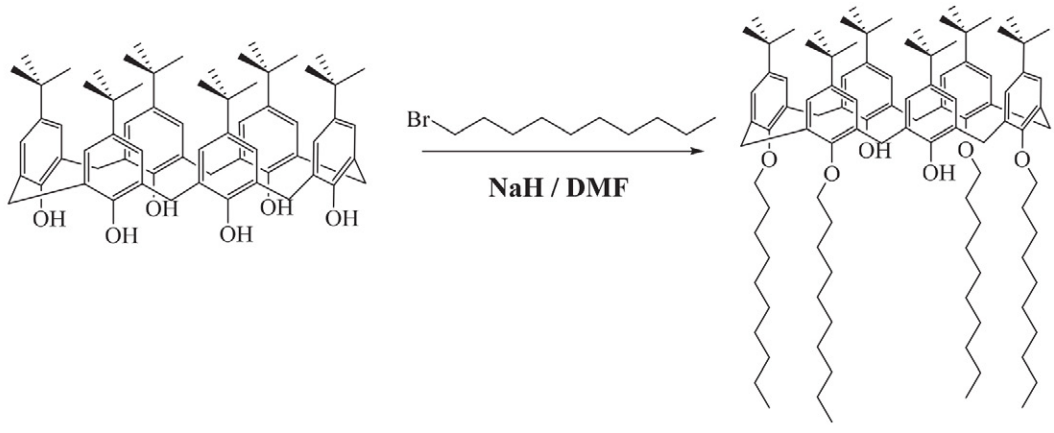

Scheme 2: Synthesis of the C6A-C10-OH

C6A-C10-OH

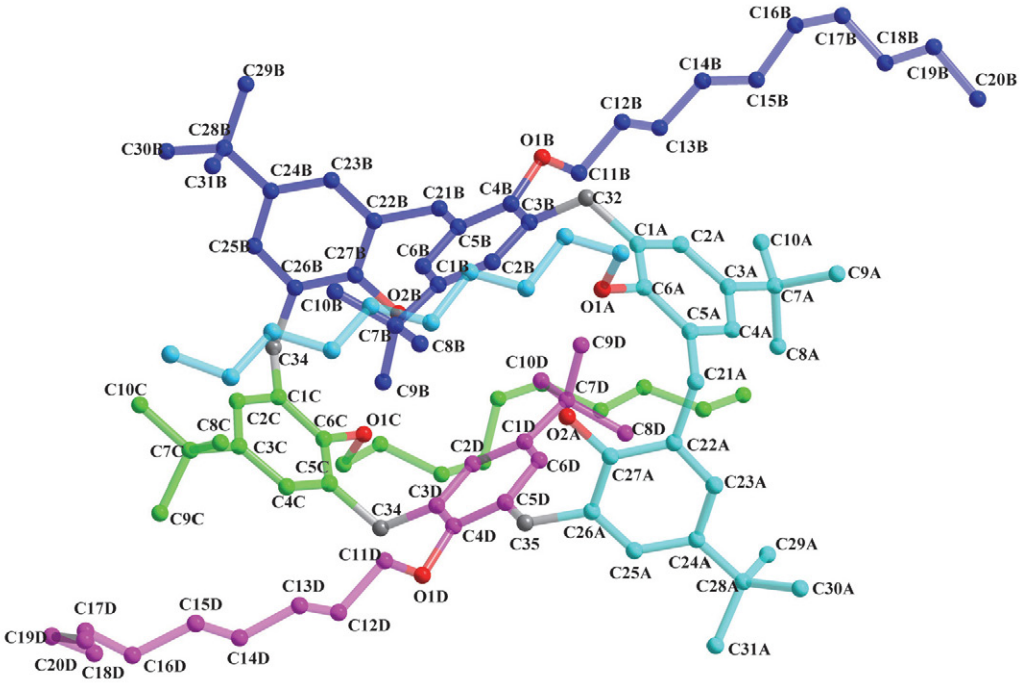

Fig. 1. Molecular structure of the C6A-C10-OH

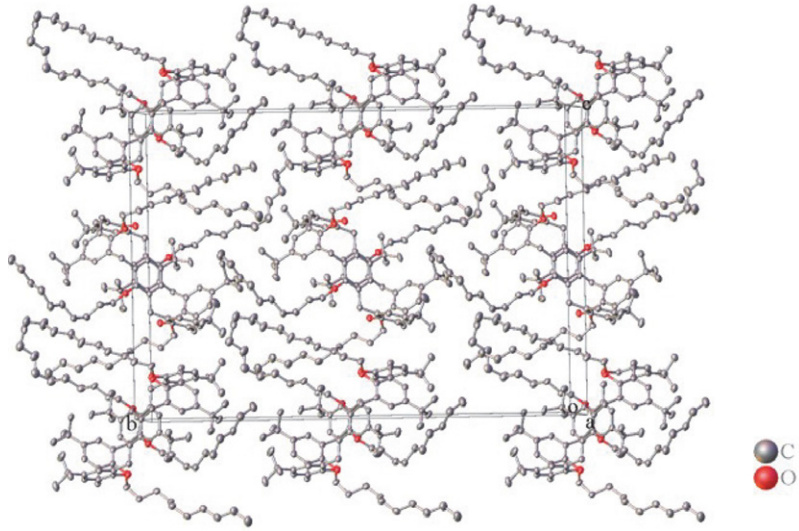

Fig. 2. Packing diagram of the C6A-C10-OH with 50% probability level ellipsoids

Table 2. Selected Bond Lengths (Å) and Bond Angles (°) for the C6A-C10-OH

Bond	**Dist.**	**Bond**	**Dist.**	**Bond**	**Dist.**
C(28)B-C(29)B	1.515(13)	C(21)B-C(22)B	1.522(9)	O(1)B-C(11)B	1.416(9)
C(24)B-C(28)B	1.526(11)	C(5)B-C(21)B	1.531(11)	C(11)B-C(12)B	1.519(11)
C(23)B-C(24)B	1.387(10)	C(4)B-C(5)B	1.399(9)	C(12)B-C(13)B	1.544(11)
C(22)B-C(23)B	1.391(11)	O(1)B-C(4)B	1.409(9)	C(13)B-C(14)B	1.449(13)
Angle	**(°)**	**Angle**	**(°)**	**Angle**	**(°)**
C(29)B-C(28)B-C(24)B	111.7(7)	C(22)B-C(21)B-C(5)B	111.5(6)	O(1)B-C(11)B-C(12)B	106.5(6)
C(23)B-C(24)B-C(28)B	122.8(7)	C(4)B-C(5)B-C(21)B	120.0(6)	C(11)B-C(12)B-C(13)B	113.6(7)
C(24)B-C(23)B-C(22)B	123.3(7)	C(5)B-C(4)B-O(1)B	120.8(7)	C(14)B-C(13)B-C(12)B	113.7(8)
C(23)B-C(22)B-C(21)B	119.7(6)	C(4)B-O(1)B-C(11)B	117.6(6)	C(13)B-C(14)B-C(15)B	118.5(9)

Table 3. Hydrogen Bond Lengths (Å)and Bond Angles (°) for the C6A-C10-OH

D-H...A	d(D-H)	d(H...A)	d(D...A)	<(DHA)
O(2)A-H(2)A...O(1)A	0.84	2.08	2.891(8)	162.9
O(2)B-H(2)B...O(1)C	0.84	2.04	2.874(7)	170.3

3. 3. Separation Performance of the C6A-C10-OH

The column efficiency of C6A-C10-OH column was 2400 plates/m. Afterwards, the aromatic and *cis*-/*trans*-isomers were used to study its separation performance. The results shown that the C6A-C10-OH column achieved baseline resolution for above analytes.

Fig. 3 shows the separation of aromatic isomers of different polarity on the C6A-C10-OH column, such as substituted benzenes, trimethylbenzene and trichloroben-

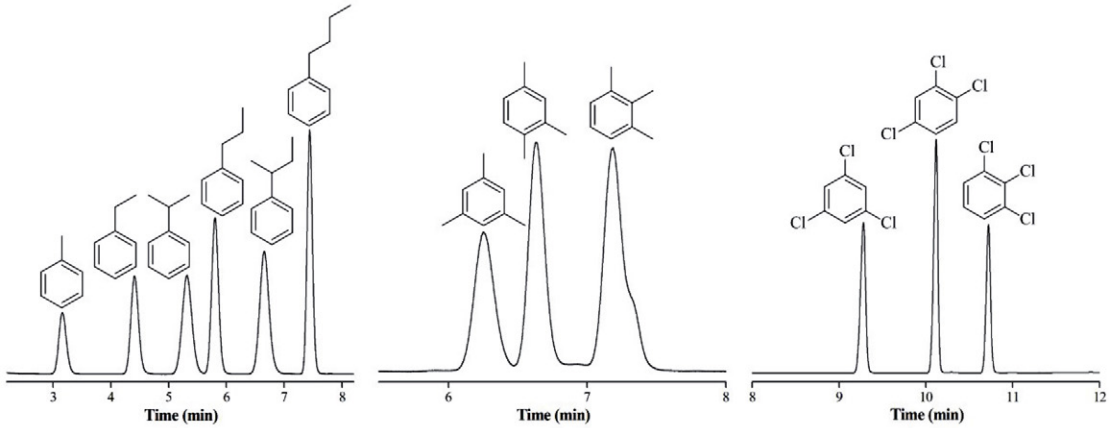

Fig. 3. GC separations of aromatic isomers. Temperature process: 40 °C (keep 1 min) up to 160 °C (keep 5 min) at 10 °C/min and gas flow rate at 0.6 mL/min.

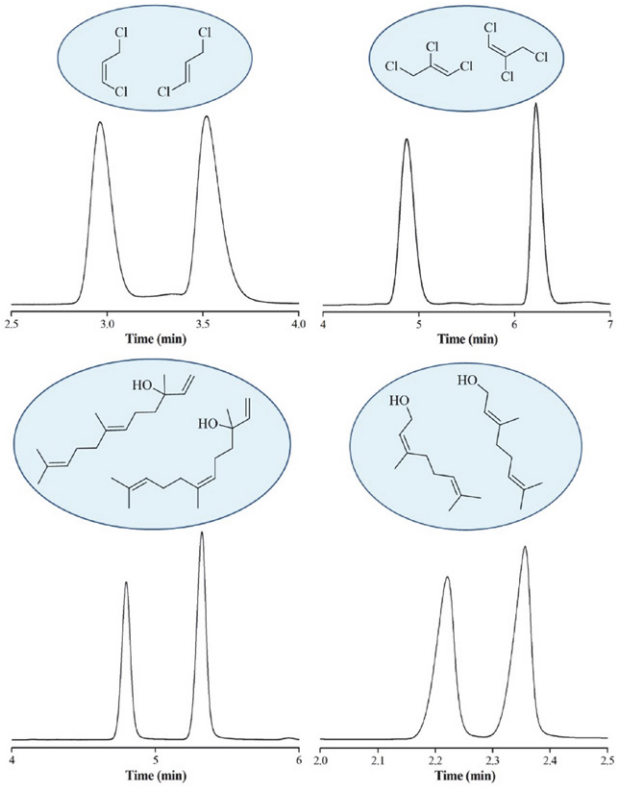

Fig. 4. GC separations of *cis*-/*trans*- isomers. Temperature process: 40 °C (keep 1 min) up to 160 °C (keep 5 min) at 10 °C/min and gas flow rate at 0.6 mL/min.

zene isomers. The C6A-C10-OH column presented excellent peak shapes for the benzene analytes and had a good resolution (R > 1.5). The C6A-C10-OH stationary phase had the good separation capacity for aromatic isomers due to its unique 3D cavity and aromatic framework, which can provide π-π interactions between stationary phase and aromatic analytes. In addition, *cis*-/*trans*- isomers were used to study the interaction mechanism between them in the C6A-C10-OH column.

Fig. 4 displays that the separations of *cis*-/*trans*- isomers on the C6A-C10-OH column, including 1,3-dichloropropene, 1,2,3-trichloropropene, nerolidol and nerol/geraniol. The results exhibited that the *cis*-/*trans*- isomers were well separated. It is worth to note that the C6A-C10-OH column had outstanding resolution for analytes with close boiling point, such as nerol (b.p. 226 °C)/geraniol (b.p. 229 °C), the boiling point difference was only 3 °C. This proved that the C6A-C10-OH column had excellent separation ability for the analytes of similar structure and physicochemical properties.

3. 4. Relationship Between Molecular Structure and Retention Behavior

In order to further study the relationship between molecular structure and retention behavior of the C6A-C10-OH stationary phase, we investigated its polarity and selectivity

in comparison to C6A-C10 stationary phase (the previous work of our group).[7] The McReynolds constants of the C6A-C10-OH and C6A-C10 stationary phases were determined by the five probe compounds at 120 °C. Their sum and average values were used to characterize their general polarity and average polarity. In general, it can be regarded as non-polar and moderately polar when the polarities of stationary phases are less than 100 and between 100 and 400 respectively.[11] As shown in table 4, the average value of C6A-C10 stationary phase was 89, belonging to nonpolar, but the average value of C6A-C10-OH stationary phase was 129, indicating its moderate polarity. This polarity difference may derive

Table 4. McReynolds constants of the C6A-C10-OH and C6A-C10 columns

Stationary phases	*X′*	*Y′*	*Z′*	*U′*	*S′*	General polarity	Average
C6A-C10-OH	68	153	99	165	161	645	129
C6A-C10	41	124	73	115	92	445	89

X′, benzene; *Y′*, 1-butanol; *Z′*, 2-pentanone; *U′*, 1-nitropropane; *S′*, pyridine. Temperature: 120 °C.

Table 5. The boiling point of alcohols and *n*-alkanes

Alcohols Compound	Molecular formula	Boiling point	*n*-Alkanes Compound	Molecular formula	Boiling point
1-nonanol	C9H20O	215 °C	*n*-dodecane	C12H26	216 °C
1-decanol	C10H22O	233 °C	*n*-tridecane	C13H28	235 °C
1-undecanol	C11H24O	241 °C	*n*-tetradecane	C14H30	254 °C
1-dodecanol	C12H26O	260 °C	*n*-pentadecane	C15H32	268 °C

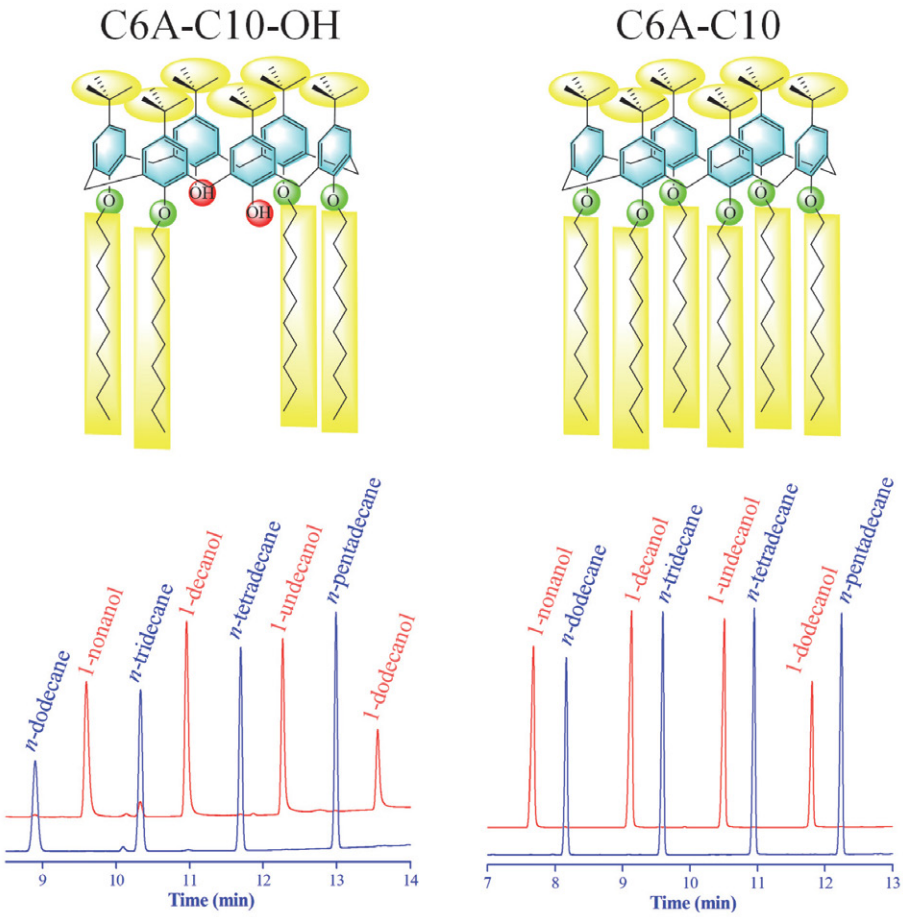

Fig. 5. GC separations of the alcohols and *n*-alkanes on the C6A-C10-OH and C6A-C10 columns. Temperature process: 40 °C (keep 1 min) up to 160 °C (keep 5 min) at 10 °C/min and gas flow rate at 0.6 mL/min.

from the different structures, the C6A-C10-OH stationary phase contained two unsubstituted phenolic hydroxyl groups, so its polarity was higher than C6A-C10 stationary phase and may offer H-bonding and dipole-dipole interactions for the separations of polar analytes.

Fig. 5 presents the separetions of the alcohols and *n*-alkanes on the C6A-C10-OH and C6A-C10 columns with the same separation conditions, respectively. The boiling points of analytes are listed in the Table 5. As shown, the C6A-C10-OH column exhibited the excellent resolving ability and good peak shapes for *n*-alkanes and alcohols. Interestingly, the C6A-C10-OH stationary phase exhibited stronger retention trend for the polar alcohols than the non-polar *n*-alkanes, such as the analyte pairs of *n*-dodecane/1-nonanol (b.p. 216 °C/b.p. 215 °C), *n*-tridecane/1-decanol (b.p. 235 °C/b.p. 233 °C), *n*-tetradecane/1-undecanol (b.p. 254 °C/b.p. 241 °C) and *n*-pentadecane/1-dodecanol (b.p. 268 °C/b.p. 260 °C).

However, the alcohols and alkanes were eluted in the order of boiling points on the C6A-C10 column. The above results showed that the retention behaviors of alcohols and alkanes in the two columns are quite different. This is because they have different molecular structures. C6A-C10-OH has two phenolic hydroxyl groups at the lower rim, so there are strong H-bonding and dipole-dipole interactions between the stationary phase and the polar analytes. The interactions between C6A-C10 and the linear analytes are mainly dispersion interactions, because the lower rim of its aromatic skeleton are all alkyl chain substituents. The above results proved that the C6A-C10-OH stationary phase had multiple molecular recognition interactions for different types of analytes due to its unique molecular structure, including dispersion, H-bonding and dipole-dipole interactions.

4. Conclusion

This work presents the investigation of the C6A-C10-OH stationary phase for GC separations. Its molecular structure was characterized by IR, ^{1}H NMR, ^{13}C NMR, MS and single-crystal X-ray diffraction analysis. As demonstrated, the C6A-C10-OH stationary phase presents good separation capacity for aliphatic, aromatic and *cis-*/*trans-* isomers. Importantly, it exhibits prolonged retention trend for alcohols mainly due to the H-bonding and dipole-dipole interactions with the phenolic hydroxyl groups. In short, this work illustrates the outstanding separation ability of the C6A-C10-OH stationary phase for diverse analytes owing to its distinct molecular structure and multiple interactions.

Supplementary Material

CCDC 2093329 contains the supplementary data for this paper. The data can be obtained free of charge from the Cambridge Crystallographic Data Centre via http://summary.ccdc.cam.ac.uk/structure-summary-form.

Acknowledgements

The authors thank the financial support of the Natural Science Foundation of Liaoning Province (20180550016) and the Scientific Research Foundation of the Education Department of Liaoning Province (LJGD2020015).

5. References

1. S. Shinkai, *Tetrahedron.***1993**, *49*, 8933–8968. **DOI:**10.1016/S0040-4020(01)91215-3
2. (a) H. J. Kim, M. H. Lee, L. Mutihac, J. Vicens, J. S. Kim, *Chem. Soc. Rev.* **2012**, *41*, 1173–1190. **DOI:**10.1039/C1CS15169J
   (b) C. Schneider, U. Menyes, T. Jira, *J. Sep. Sci.* **2010**, *33*, 2930–2942. **DOI:**10.1002/jssc.201000281
   (c) D. Guillaume, L. Roy, J. Ivan, A. Valerie, C. Pascal, *Curr. Org. Chem.* **2015**, *19*, 2237–2249.
3. (a) N. Y. Edwards, A. L. Possanza, *Supramol. Chem.* **2013**, *25*, 446–463. **DOI:**10.1080/10610278.2013.794277
   (b) N. Bregović, N. Cindro, L. Frkanec, V. Tomišić, *Supramol. Chem.* **2016**,*28*, 608–615. **DOI:**10.1080/10610278.2016.1154147
   (c) S. E. Matthews, P. D. Beer, *Supramol. Chem.* **2005**, *17*, 411–435. **DOI:**10.1080/10610270500127089
4. (a) M. Schulz, A. Gehl, J. Schlenkrich, H. A. Schulze, S. Zimmermann, A. Schaate, *Angew. Chem. Int. Ed.* **2018**, *57*, 12961–12965. **DOI:**10.1002/anie.201805355
   (b) K. Kurzątkowska, S. Sayin, M. Yilmaz, H. Radecka, J. Radecki, *Sens. Actuators B Chem.* **2015**, *218*, 111–121. **DOI:**10.1016/j.snb.2015.04.110
   (c) M. De Rosa, P. La Manna, A. Soriente, C. Gaeta, C. Talotta, P. Neri, *RSC Adv.* **2016**, *6*, 91846–91851. **DOI:**10.1039/C6RA19270J
   (d) M.Yilmaz, S. Erdemir, *Turk. J. Chem.* **2013**, *37*, 558–585. **DOI:**10.3906/vet-1210-33
   (e) P. M. Mareeswaran, D. Maheshwaran, E. Babu, S. Rajagopal, *J Fluoresc.* **2012**, *22*, 1345–1356. **DOI:**10.1007/s10895-012-1074-9
   (f) W. F. Zhang, Y. H. Zhang, Y. M. Zhang, C. Lan, Y. Miao, Z. F. Deng, X. Ba, W. D. Zhao, S. S. Zhang, *Talanta.* **2019**, *193*, 56–63. **DOI:**10.1016/j.talanta.2018.09.083
5. (a) B. J. Pollo, G. L. Alexandrino, F. Augusto, L. W. Hantao, *Trends Analyt. Chem.* **2018**, *105*, 202–217. **DOI:**10.1016/j.trac.2018.05.007
   (b) A. M. Muscalu, T. Górecki, *Trends Analyt. Chem.* **2018**, *106*, 225–245. **DOI:**10.1016/j.trac.2018.07.001
   (c) M. V. Russo, P. Avino, L. Perugini, I. Notardonato, *RSC Adv.* **2015**, *5*, 37023–37043. **DOI:**10.1039/C5RA01916H
   (d) C. Citti, D. Braghiroli, M. A. Vandelli, G. Cannazza, *J. Pharmaceut. Biomed.* **2018**, *147*, 565–579. **DOI:**10.1016/j.jpba.2017.06.003

6. T. Sun, L. R. Qi, W. W. Li, Y. Li, X. M. Shuai, Z. Q. Cai, H. P. Chen, X. G. Qiao, L. F. Ma, *J. Chromatogr. A.* **2019**, *1601*, 310–318. **DOI:**10.1016/j.chroma.2019.04.068
7. (a)T. Sun, X. M. Shuai, Y. J. Chen, X. Y. Zhao, Q. Q. Song, K. X. Ren, X. X. Jiang, S. Q. Hu, Z. Q. Cai, *RSC Adv.* **2019**, *9*, 38486–38495. **DOI:**10.1039/C9RA07798G
(b) X. M. Shuai, Z. Q. Cai, Y. J. Chen, X. Y. Zhao, Q. Q. Song, K. X. Ren, X. X. Jiang, T. Sun, S. Q. Hu, *Microchem. J.* **2020**, *157*, 105124. **DOI:**10.1016/j.microc.2020.105124
8. G. M. Sheldrick, *Acta Crystallogr A*. **2015**, *71*, 3–8. **DOI:**10.1107/S2053273314026370
9. L. Z. Qiao, K. Lu, M. L. Qi, R. N. Fu, *J. Chromatogr. A*. **2013**, *1276*, 112–119. **DOI:**10.1016/j.chroma.2012.12.039
10. (a) Q.Liu,J. H. Lin,J.Liu, W.Chen,Y. M. Cui, *Acta chim. Slov.* **2016**, *63*, 279–286.
(b) Q. A. Peng, X. P. Tan, Y. D. Wang, S.H. Wang, Y. X. Jiang, Y. M. Cui, *Acta chim. Slov.* **2020,** *67*, 644–650; **DOI:**10.17344/acsi.2019.5650
(c) S. S. Qian, X. L. Zhao, J. Wang, Z. L. You, *Acta chim. Slov.* **2015**, *62*, 828–833.
11. (a) P. Zhang, S. J. Qin, M. L. Qi, R. N. Fu, *J. Chromatogr. A*. **2014**, *1334*, 139–148. **DOI:**10.1016/j.chroma.2014.01.083
(b) X. M. Shuai, Z. Q. Cai, X. Y. Zhao, Y. J. Chen, Q. Zhang, Z. W. Ma, J. J. Hu, T. Sun, S. Q. Hu, *Chromatographia.* **2021**, *84*, 325–333. **DOI:**10.1007/s10337-021-04018-x
(c) T. Sun, B. Li, Y. Li, X. Y. Zhao, Q. Q. Song, X. X. Jiang, X. M. Shuai, Y. Y. Li, Z. Q. Cai, S. Q. Hu, *Chromatographia*. **2019**, *82*, 1697–1708. **DOI:**10.1007/s10337-019-03783-0

Povzetek

V prispevku opisujemo raziskave separacijskih lastnosti *p-tert*-butil(tetradeciloksi)calix[6] arena (C6A-C10-OH) kot stacionarne faze za plinsko kromatografijo (GC). Spojino smo karakterizirali z IR, ^{1}H NMR, ^{13}C NMR, MS in monokristalno rentgensko analizo. Kolona C6A-C10-OH ima dobre separacijske lastnosti za alifatske, aromatske in *cis*-/*trans*-izomere. Omogoča številne molekularne interakcije za analite s širokim razponom polarnosti, vključno z disperzijskimi silami, vodikovo vezjo, π-π in dipol-dipol interakcijami. Delo ponuja eksperimentalno in teoretsko podlago za razvoj novih stacionarnih faz na osnovi calixarenov v GC analizi.

Except when otherwise noted, articles in this journal are published under the terms and conditions of the Creative Commons Attribution 4.0 International License

Scientific paper

Two Oxidovanadium(V) Complexes with Hydrazone Ligands: Synthesis, Crystal Structures and Catalytic Oxidation Property

Yan Lei

School of Materials and Environmental Engineering, Chengdu Technological University, Chengdu 611730, P. R. China

** Corresponding author: E-mail: leiyan222@126.com*

Received: 11-23-2021

Abstract

Two new oxidovanadium(V) complexes, [VOL^1(aha)]DMF (**1**) and [VOL^2(mat)] (**2**), where L^1 and L^2 are the dianionic form of *N*'-(4-bromo-2-hydroxybenzylidene)-3-methyl-4-nitrobenzohydrazide and *N*'-(3,5-dibromo-2-hydroxybenzylidene) pivalohydrazide, respectively, and aha and mat are the monoanionic form of acetohydroxamic acid and maltol, respectively, have been synthesized and structurally characterized by physico-chemical methods and single crystal X-ray determination. X-ray analysis indicates that the V atoms in the complexes are in octahedral coordination. Crystal structures of the complexes are stabilized by hydrogen bonds. The catalytic property for epoxidation of styrene by the complexes was evaluated.

Keywords: Vanadium complex; hydrazone ligand; crystal structure; catalytic property

1. Introduction

Hydrazones bearing typical –CH=N–NH–C(O)– group are a kind of Schiff base compounds, which represent one of the most attractive series of ligands in coordination chemistry.[1] The hydrazone ligands can adopt both ketone and enol forms during the coordination with various transition and rare earth metal atoms, to form complexes with versatile structures and properties like antibacterial, enzyme inhibition, magnetism, catalytic and photoluminescence.[2] In the last few years, a number of complexes with hydrazone ligands have been reported to have fascinating catalytic properties, such as oxidation of sulfides, polymerization and asymmetric epoxidation.[3] Among the hydrazone complexes, those with V centers are of particular interest for their catalytic applications.[4] Maltol and acetohydroxamic acid are bidentate ligands in vanadium complexes.[4b,5] In pursuit of new maltolate and acetohydroxamate coordinated vanadium complexes with hydrazone ligands, we report herein two new oxidovanadium(V)

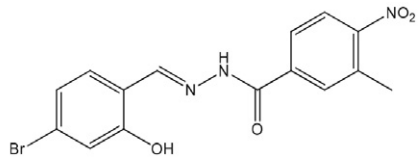

H_2L^1

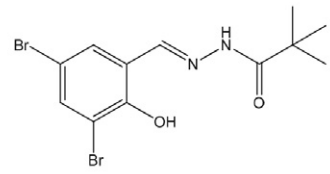

H_2L^2

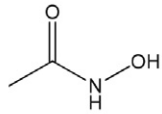

Haha

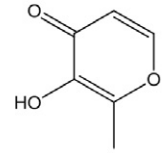

Hmat

Scheme 1. The ligands.

complexes, [VOL^1(aha)]DMF (**1**) and [VOL^2(mat)] (**2**), where L^1 and L^2 are the dianionic form of *N*'-(4-bromo-2-hydroxybenzylidene)-3-methyl-4-nitrobenzohydrazide (H_2L^1) and *N*'-(3,5-dibromo-2-hydroxybenzylidene) pivalohydrazide (H_2L^2), respectively, and aha and mat are the monoanionic form of acetohydroxamic acid (Haha) and maltol (Hmat), respectively (Scheme 1).

2. Experimental

2. 1. Materials

$VO(acac)_2$, 4-bromosalicylaldehyde, 3,5-dibromosalicylaldehyde, acetohydroxamic acid, and maltol were purchased from Aldrich. All other reagents with AR grade were used as received without further purification.

2. 2. Physical Measurements

Infrared spectra (4000–400 cm^{-1}) were recorded as KBr discs with a FTS-40 BioRad FT-IR spectrophotometer. The electronic spectra were recorded on a Lambda 35 spectrometer. Microanalyses (C,H,N) of the complex were carried out on a Carlo-Erba 1106 elemental analyzer. Solution electrical conductivity was measured at 298K using a DDS-11 conductivity meter. GC analyses were performed on a Shimadzu GC-2010 gas chromatograph.

2. 3. X-ray Crystallography

Crystallographic data of the complexes were collected on a Bruker SMART CCD area diffractometer with graphite monochromated Mo-Kα radiation (λ = 0.71073 Å) at 298(2) K. Absorption corrections were applied by using the multi-scan program.[6] The structures of the complexes were solved by direct methods and successive Fourier difference syntheses, and anisotropic thermal parameters for all nonhydrogen atoms were refined by full-matrix least-squares procedure against F^2.[7] All non-hydrogen atoms were refined anisotropically. The amino H atom of complex **1** was located from a difference Fourier map and refined isotropically, with N–H distance restrained to 0.90(1) Å. The remaining hydrogen atoms were located at calculated positions, and refined isotropically with U_{iso}(H) values constrained to 1.2 U_{iso}(C) and 1.5 U_{iso}(O and methyl C). The C20 and O8 atoms in complex **1**, and the C10 atom in complex **2** are refined as isotropic behavior due to their disorder manner. The crystallographic data and experimental details for the structural analysis are summarized in Table 1.

2. 4. Synthesis of H_2L^1

A methanol solution (20 mL) of 3-methyl-4-nitrobenzohydrazide (1.9 g, 0.010 mol) was added to a methanol solution (20 mL) of 4-bromosalicylaldehyde (2.0 g, 0.010

Table 1. Crystallographic data for the single crystal of the complexes

	1	**2**
Empirical formula	$C_{20}H_{21}BrN_5O_8V$	$C_{18}H_{17}Br_2N_2O_6V$
Formula weight	590.27	568.09
Temperature (K)	298(2)	298(2)
Crystal system	Monoclinic	Orthorhombic
Space group	$P2_1/n$	$Pca2_1$
a (Å)	8.6210(10)	14.6120(11)
b (Å)	26.9525(13)	15.6777(12)
c (Å)	10.5418(12)	9.4641(11)
α (°)	90	90
β (°)	98.528(1)	90
γ (°)	90	90
V (Å^3)	2422.4(4)	2168.1(3)
Z	4	4
F(000)	1192	1120
μ, mm^{-1}	2.114	4.179
R_{int}	0.0640	0.0910
Collected data	14312	19236
Unique data	4514	3834
Observed data [$I > 2\sigma(I)$]	2931	2731
Restraints	13	19
Parameters	323	267
Goodness-of-fit on F^2	0.994	1.031
R_1, wR_2 indices [$I > 2\sigma(I)$]	0.0507, 0.1162	0.0496, 0.0776
R_1, wR_2 indices (all data)	0.0893, 0.1357	0.0912, 0.0880
Large diff. peak and hole, *e* Å^{-3}	0.554, –0.425	0.655, –0.446

mol). The mixture was refluxed for 1 h, and three quarter of the solvent was evaporated to give yellow precipitate, which was filtered off and washed several times with methanol. The yield is 92%. Analysis calculated for $C_{15}H_{12}BrN_3O_4$: C, 47.64; H, 3.20; N, 11.11%; found: C, 47.47; H, 3.31; N, 11.25%. ^{1}H NMR (d_6-DMSO, 500 MHz): δ 2.62 (s, 3H, CH_3), 7.07 (d, 1H, ArH), 7.51 (s, 1H, ArH), 7.58 (d, 1H, ArH), 7.86 (d, 1H, ArH), 8.03 (s, 1H, ArH), 8.41 (d, 1H, ArH), 8.69 (s, 1H, CH=N), 10.76 (s, 1H, NH), 11.38 (s, 1H, OH). IR data (KBr, cm^{-1}): 3446 (br, w, ν_{OH}), 3222 (sh, w, ν_{NH}), 1657 (vs, $\nu_{\text{-C(O)-NH-}}$), 1602 (vs, $\nu_{C=N}$), 1520 (s, ν_{as} NO_2), 1338 (s, ν_s NO_2). UV-Vis data (λ_{max}, nm): 285, 345, 420.

2. 5. Synthesis of H_2L^2

A methanol solution (20 mL) of pivalohydrazide (1.1 g, 0.010 mol) was added to a methanol solution (20 mL) of 3,5-dibromosalicylaldehyde (2.8 g, 0.010 mol). The mixture was refluxed for 1 h, and three quarter of the solvent was evaporated to give colorless precipitate, which was filtered off and washed several times with methanol. The yield is 88%. Analysis calculated for $C_{12}H_{14}Br_2N_2O_2$: C, 38.12; H, 3.73; N, 7.41%; found: C, 38.31; H, 3.62; N, 7.32%. ^{1}H NMR (d_6-DMSO, 500MHz): δ 1.26 (s, 9H, $C(CH_3)_3$), 7.72 (s, 1H, ArH), 7.83 (s, 1H, ArH), 8.71 (s, 1H, CH=N), 11.22 (s, 1H, NH), 11.75 (s, 1H, OH). IR data (KBr, cm^{-1}): 3438 (br, w, ν_{OH}), 3121 (sh, w, ν_{NH}), 1653 (vs, $\nu_{\text{-C(O)-NH-}}$), 1605 (vs, $\nu_{C=N}$). UV-Vis data (λ_{max}, nm): 295, 305, 332, 400.

2. 6. Synthesis of [VOL^1(aha)]DMF (1)

H_2L^1 (1.0 mmol, 0.38 g) and [$VO(acac)_2$] (1.0 mmol, 0.26 g) were mixed and stirred in methanol (50 mL) for 30 min at 25 °C. Then, acetohydroxamic acid (1.0 mmol, 0.075 g) was added and the mixture was stirred for another 30 min. The brown solution was evaporated to remove three quarters of the solvents under reduced pressure, yielding deep brown solid of the complex. Yield: 65%. Well-shaped single crystals suitable for X-ray diffraction were obtained by re-crystallization of the solid from methanol. Analysis calculated for $C_{20}H_{21}BrN_5O_8V$: C, 40.70; H, 3.59; N, 11.86%; found: C, 40.54; H, 3.70; N, 11.95%. IR data (KBr, cm^{-1}): 3129 (sh, w, ν_{NH}), 1661 (vs, $\nu_{\text{-C(O)-NH-}}$), 1594 (vs, $\nu_{C=N}$), 1522 (s, ν_{as} NO_2), 1340 (s, ν_s NO_2), 973 (m, V=O). UV-Vis data (λ_{max}, nm): 260, 328, 410, 545.

2. 5. Synthesis of [VOL^2(mat)] (2)

H_2L^2 (1.0 mmol, 0.38 g) and [$VO(acac)_2$] (1.0 mmol, 0.26 g) were mixed and stirred in methanol (50 mL) for 30 min at 25 °C. Then, maltol (1.0 mmol, 0.13 g) was added and the mixture was stirred for another 30 min. The brown solution was evaporated to remove three quarters of the solvents under reduced pressure, yielding deep brown solid of the complex. Yield: 73%. Well-shaped single crystals suitable for X-ray diffraction were obtained by re-crystallization of the solid from methanol. Analysis calculated for $C_{18}H_{17}Br_2N_2O_6V$: C, 38.06; H, 3.02; N, 4.93%; found: C, 38.23; H, 2.95; N, 4.81%. IR data (KBr, cm^{-1}): 1611 (vs, $\nu_{C=N}$), 978 (m, V=O). UV-Vis data (λ_{max}, nm): 270, 340, 460.

2. 6. Styrene Epoxidation

The epoxidation reaction was carried out at room temperature in acetonitrile under N_2 atmosphere with constant stirring. The composition of the reaction mixture was 2.00 mmol of styrene, 2.00 mmol of chlorobenzene (internal standard), 0.10 mmol of the complexes (catalyst) and 2.00 mmol iodosylbenzene or sodium hypochlorite (oxidant) in 5.00 mL freshly distilled acetonitrile. When the oxidant was sodium hypochlorite, the solution was buffered to pH 11.2 with NaH_2PO_4 and NaOH. The composition of reaction medium was determined by GC with styrene and styrene epoxide quantified by the internal standard method (chlorobenzene). All other products detected by GC were mentioned as others. For each complex the reaction time for maximum epoxide yield was determined by withdrawing periodically 0.1 mL aliquots from the reaction mixture and this time was used to monitor the efficiency of the catalyst on performing at least two independent experiments. Blank experiments with each oxidant and using the same experimental conditions except catalyst were also performed.

3. Results and Discussion

3. 1. Chemistry

The hydrazones H_2L^1 and H_2L^2 were synthesized by reaction of 3-methyl-4-nitrobenzohydrazide with 4-bromosalicylaldehyde, and pivalohydrazide with 3,5-dibromosalicylaldehyde, respectively in methanol (Scheme 2). The complexes **1** and **2** were prepared by the reaction of the hydrazone ligands with $VO(acac)_2$ in the presence of acetohydroxamic acid and maltol (Scheme 3). The reaction progresses are accompanied by an immediate color change of the solution from colorless to deep brown. The hydrazones were deprotonated during the coordination. The oxidation of V(IV) in $VO(acac)_2$ to V(V) in both complexes during the reaction in air is not uncommon.[4c,8] The molar conductivities (Λ_M = 35 Ω^{-1} cm^2 mol^{-1} for **1** and 30 Ω^{-1} cm^2 mol^{-1} for **2**) are consistent with the values expected for non-electrolyte.[9]

3. 2. Crystal Structure Description of the Complexes

Selected bond lengths and angles for the complexes are listed in Table 2. Single crystal X-ray analysis indicates that the complexes are mononuclear oxidovanadium(V)

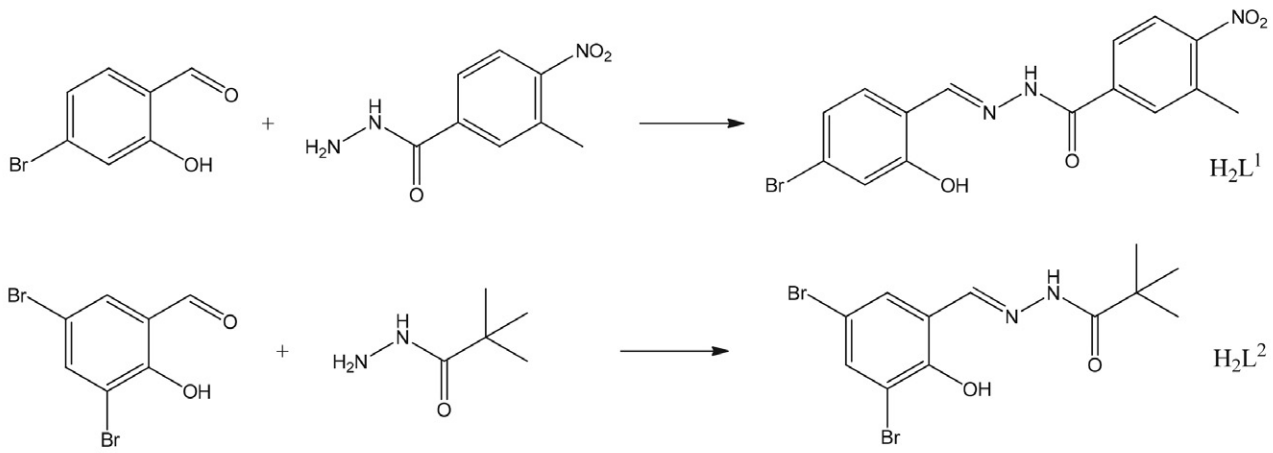

Scheme 2. The synthesis of the hydrazones.

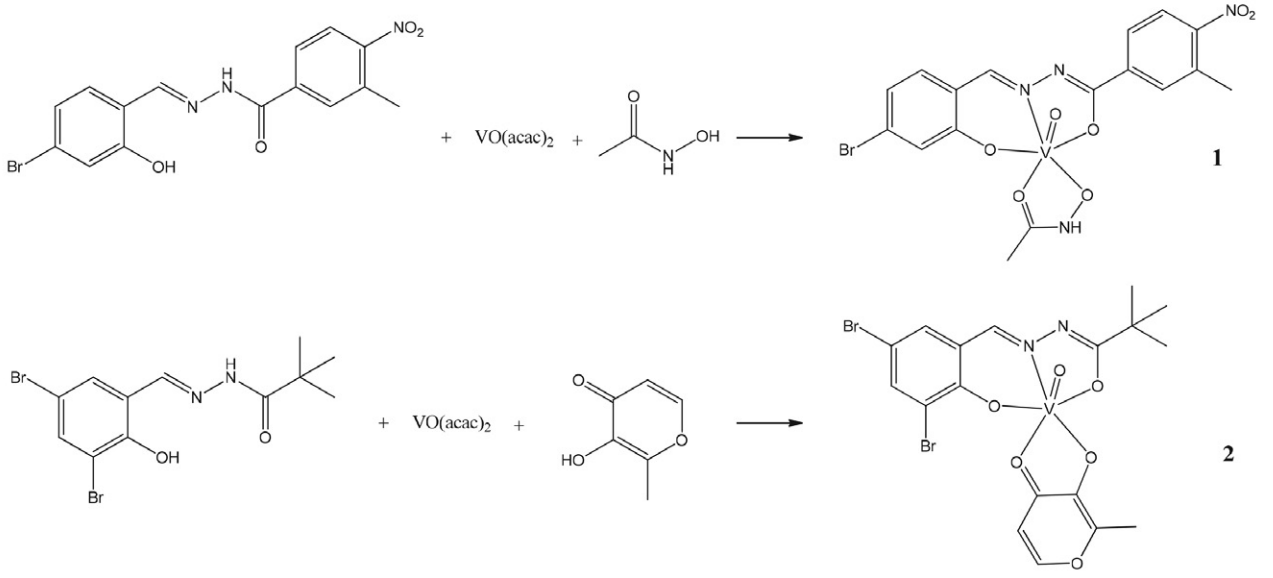

Scheme 3. The synthesis of the complexes.

compounds. The ORTEP plots of the complexes **1** and **2** are shown in Figs. 1 and 2, respectively. The V atoms in the complexes are in octahedral geometry. In complex **1**, the V atom is coordinated by the O_2N donor atoms of the hydrazone ligand L^1 and the hydroxyl O atom of the acetylhydroxamate ligand in the equatorial plane, and by the carbonyl O atom of the acetylhydroxamate ligand and the oxido O atom at the two axial positions. In complex **2**, the V atom is coordinated by the O_2N donor atoms of the hydrazone ligand L^2 and the hydroxyl O atom of the maltolate ligand in the equatorial plane, and by the carbonyl O atom of the maltolate ligand and the oxido O atom at the two axial positions. The V atoms displaced toward the axial oxido O atoms (O3) by 0.269(1) Å for **1**, and 0.322(1) Å for **2**, from the equatorial planes of both complexes. The distortion of the octahedral coordination of the complexes can be observed from the bond angles related to the V atoms. The *cis*- and *trans*- angles related to the V atoms at the equatorial planes are in the ranges of 75.22(15)–100.1(2)° and 154.24(16)–172.90(17)° for **1** and 74.6(2)–101.3(2)° and 153.6(2)–177.3(2)° for **2**. The deviations from the ideal octahedral geometry are mainly origin from the strain created by the five-membered chelate rings V1-N1-N2-C8-O2 and V1-O4-C17-N4-O5 for **1** or V1-O4-C13-C14-O5 for **2**. The bond lengths of V–O and V–N of both complexes are similar to each other, and comparable to those in other V complexes in literature.[4,10] The terminal V1–O3 [1.57–1.58 Å] bond distances of both complexes agree well with the corresponding values reported for related systems.[9] Because of the *trans* influence of the oxido groups, the distances to the O4 atoms (2.20–2.31 Å) are considerably elongated, making the O4 atoms weakly coordinated to the V atoms. Such elongation has previously been observed in other complexes with similar structures. The hydrazone ligands coordinate to the V atoms through dianionic form, which can be observed from the bond

Table 2. Selected bond distances (Å) and bond angles (°) for the complexes

	1	**2**
V1–O1	1.856(3)	1.841(7)
V1–O2	1.944(3)	1.901(7)
V1–O3	1.579(3)	1.575(6)
V1–O4	2.207(3)	2.309(7)
V1–O5	1.848(3)	1.856(6)
V1–N1	2.089(4)	2.098(7)
O3–V1–O5	96.46(16)	101.2(3)
O3–V1–O1	100.10(18)	98.1(3)
O5–V1–O1	98.23(14)	100.7(3)
O3–V1–O2	97.63(17)	99.5(3)
O5–V1–O2	98.18(14)	94.9(3)
O1–V1–O2	154.24(15)	153.7(3)
O3–V1–N1	98.39(16)	99.6(3)
O5–V1–N1	164.42(15)	158.0(3)
O1–V1–N1	83.78(14)	83.1(3)
O2–V1–N1	75.23(13)	74.8(3)
O3–V1–O4	172.88(16)	177.2(3)
O5–V1–O4	76.53(14)	76.9(3)
O1–V1–O4	82.37(14)	84.2(3)
O2–V1–O4	82.31(13)	78.7(3)
N1–V1–O4	88.50(13)	82.0(3)

lengths of C8–O2 and C8–N2. The bonds C8–O2 are obviously longer than typical double bonds, while the bonds C8–N2 are obviously shorter than typical single bonds.

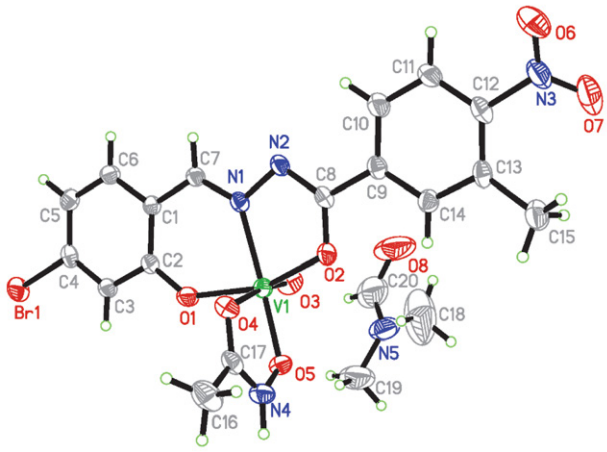

Fig. 1. ORTEP diagram of complex **1** with 30% thermal ellipsoid.

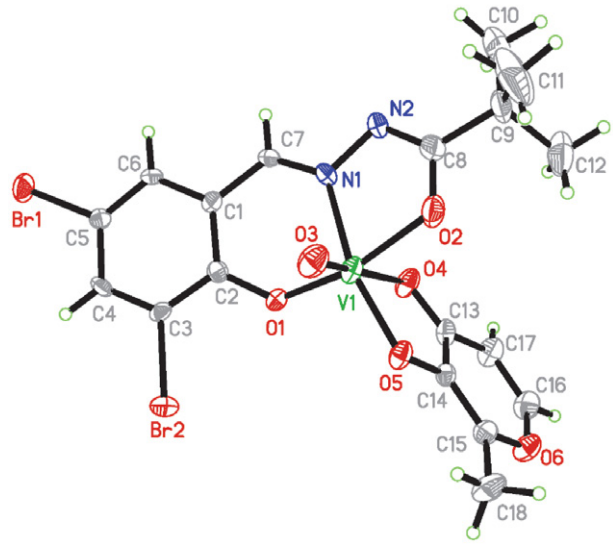

Fig. 2. ORTEP diagram of complex **2** with 30% thermal ellipsoid.

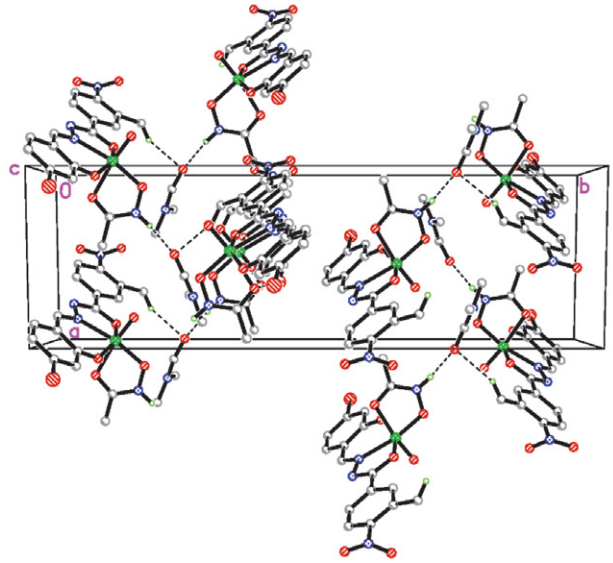

Fig. 3. Molecular packing structure of complex **1** linked by hydrogen bonds (dashed lines).

This phenomenon is not uncommon for hydrazone complexes.[4,5a,10]

The crystal structure of complex **1** is stabilized by N–H···N and C–H···O hydrogen bonds (Table 3), to gener-

Table 3. Hydrogen bond distances (Å) and bond angles (°) for the complexes

D*–H···*A	***d*(*D*–H)**	***d*(H···*A*)**	***d*(*D*···*A*)**	**Angle (*D*–H···*A*)**
1				
N4–H4···O8$^{\#1}$	0.90	1.83	2.698(4)	164(5)
C15–H15B···O8$^{\#2}$	0.96	2.44	3.334(4)	156(5)
2				
C6–H6···O4$^{\#3}$	0.93	2.54	3.404(5)	154(6)
C16–H16···O3$^{\#4}$	0.93	2.59	3.347(5)	139(6)

Symmetry codes: #1: 1½ + *x*, ½ – *y*, ½ + *z*; #2: 1 + *x*, *y*, *z*; #3: 1½ – *x*, *y*, ½ + *z*; #4: *x*, *y*, –1 + *z*.

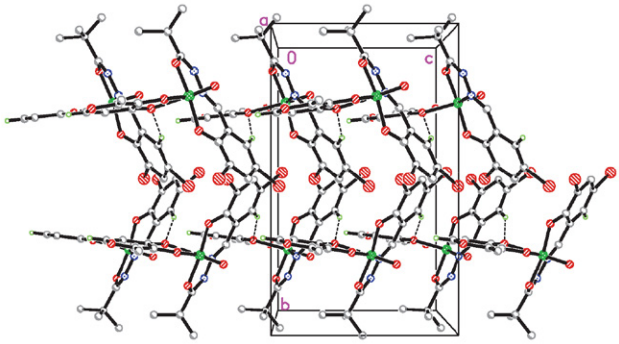

Fig. 4. Molecular packing structure of complex **2** linked by hydrogen bonds (dashed lines).

ate chains along the *a* axis (Fig. 3). The crystal structure of complex **2** is stabilized by C–H···O hydrogen bonds (Table 3), to generate chains along the *c* axis (Fig. 4).

3. 4. IR and UV-vis Spectra of the Compounds

The weak and broad absorptions in the region 3400–3500 cm^{-1} of the free hydrazones are attributed to the O–H bonds of the phenol groups. The weak absorptions at 3120–3230 cm^{-1} for the free hydrazones and complex **1** are assigned to the stretching vibrations of the N–H groups. The intense bands at 1657 cm^{-1} for H_2L^1, 1653 cm^{-1} for H_2L^2, and 1661 cm^{-1} for complex **1** are assigned to the vibrations of the C=O groups.[11] The typical bands for the azomethine groups, ν(C=N), are observed at 1590–1611 cm^{-1} for the compounds.[12] The characteristic of the spectra of both complexes is the exhibition of sharp bands at about 973 cm^{-1} for **1** and 978 cm^{-1} for **2**, corresponding to the V=O stretching vibration.[13] The appearance of a single band in this region indicates the existence of monomeric six-coordinated V=O units instead of the polymeric units.[14] This is approved by the single crystal structure determination. The weak bands in the range of 400–650 cm^{-1} are assigned to the vibrations of the V–O and V–N bonds.

In the UV-Vis spectra of the compounds, the bands at 320–350 nm are attributed to the azomethine chromophore π-π* transitions. The bands at higher energy (260–300 nm) are associated with the benzene π-π* transitions.[15] The weak bands at 545 nm for **1** and 460 nm for **2** are attributed to intramolecular charge transfer transitions from the p_π orbital on the nitrogen and oxygen to the empty *d* orbitals of the V atoms.[16]

3. 5. Catalytic Properties of the Complexes

The percentage of conversion of styrene, selectivity for styrene oxide, yield of styrene oxide and reaction time to obtain maximum yield using both the oxidants are given in Table 4. The data reveals that the complexes as catalysts convert styrene most efficiently in the presence of both oxidants. Nevertheless, the catalysts are selective towards the formation of styrene epoxides despite of the formation of by-products which have been identified by GC-MS as benzaldehyde, phenylacetaldehyde, styrene epoxides derivative, alcohols *etc.* From the data it is also clear that the complexes exhibit excellent efficiency for styrene epoxide yield. When the reactions are carried out with PhIO and NaOCl, styrene conversions of complexes **1** and **2** were about 85% and 81%, and 78% and 75%, respectively. It is evident that between PhIO and NaOCl, the former acts as a better oxidant with respect to both styrene conversion and styrene epoxide selectivity. The epoxide yields for the complexes **1** and **2** using PhIO and NaOCl as oxidants are 76% and 86%, and 74% and 81%, respectively.

Table 4. Catalytic epoxidation results of complexes **1** and **2***

	1	**1**	**2**	**2**
Oxidant	PhIO	NaOCl	PhIO	NaOCl
Conversion (%)	85	78	81	75
Epoxide yield (%)	76	74	86	81
Selectivity (%)	93	90	95	87

* The time is 2 h for PhIO, and 3 h for NaOCl.

4. Conclusion

Two new mononuclear oxidovanadium(V) complexes derived from hydrazone ligands have been synthesized and characterized. Single crystal X-ray analysis indicates that the V atoms in both complexes are in distorted octahedral coordination. The complexes have effective catalytic property for the epoxidation of styrene, with conversions over 75% and selectivities over 87%.

Supplementary Material

CCDC 2123401 for **1** and 2123402 for **2** contain the supplementary crystallographic data for this paper. These data can be obtained free of charge *via* http://www.ccdc.cam.ac.uk/conts/retrieving.html, or from the Cambridge Crystallographic Data Centre, 12 Union Road, Cambridge CB2 1EZ, UK; fax: (+44) 1223-336-033; or e-mail: deposit@ccdc.cam.ac.uk.

Acknowledgments

This work was financially supported by the Scientific Research Foundation of Chengdu Technological University (Grant No. 2021RC004).

5. References

1. (a) S. Kanchanadevi, F. R. Fronczek, V. Mahalingam, *Inorg. Chim. Acta* **2021**, *526*, 120532; (b) P. H. D. O. Santiago, E.

D. Duarte, E. C. M. Nascimento, J. B. L. Martins, M. S. Castro, C. C. Gatto, *Appl. Organomet. Chem.* **2021**, e6461; (c) A. M. Abu-Dief, R. M. El-khatib, S. M. El Sayed, S. Alzahrani, F. Alkhatib, G. El-Sarrag, M. Ismael, *J. Mol. Struct.* **2021**, *1244*, 131017; (d) A. V. Astashkin, R. D. Utterback, Y. S. Sung, E. Tomat, *Inorg. Chem.* **2020**, *59*, 11377–11384.

2. (a) T. Keskic, Z. Jaglicic, A. Pevec, B. Cobeljic, D. Radanovic, M. Gruden, I. Turel, K. Andelkovic, I. Brceski, M. Zlatar, *Polyhedron* **2020**, *191*, 114802; **DOI:**10.1016/j.poly.2020.114802
(b) N. Biswas, S. Saha, B. K. Biswas, M. Chowdhury, A. Rahaman, V. Junghare, S. Mohapatra, S. Hazra, E. Zangrando, R. R. Choudhury, *J. Coord. Chem.* **2021**, *74*, 1482–1504; **DOI:**10.1080/00958972.2021.1913128
(c) L. M. Balsa, V. Ferraresi-Curotto, M. J. Lavecchia, G. A. Echeverria, O. E. Piro, J. Garcia-Tojal, R. Pis-Diez, A. C. Gonzalez-Baro, I. E. Leon, *Dalton Trans.* **2021**, *50*, 9812–9826; **DOI:**10.1039/D1DT00869B
(d) K. S. Neethu, S. Sivaselvam, M. Theetharappan, J. Ranjitha, N. S. P. Bhuvanesh, N. Ponpandian, M. A. Neelakantan, M. V. Kaveri, *Inorg. Chim. Acta* **2021**, *524*, 120419; **DOI:**10.1016/j.ica.2021.120419
(e) S. Kanchanadevi, F. R. Fronczek, C. I. David, R. Nandhakumar, V. Mahalingam, *Inorg. Chim. Acta* **2021**, *526*, 120536. **DOI:**10.1016/j.ica.2021.120536

3. (a) H. Kargar, M. Fallah-Mehrjardi, R. Behjatmanesh-Ardakani, K. S. Munawar, M. Ashfaq, M. N. Tahir, *Polyhedron* **2021**, *208*, 115428; **DOI:**10.1016/j.poly.2021.115428
(b) H. Kargar, M. Fallah-Mehrjardi, R. Behjatmanesh-Ardakani, K. S. Munawar, *J. Mol. Struct.* **2021**, *1245*, 131259;
(c) Y. Tan, Y. Lei, *Acta Chim. Slov.* **2021**, *68*, 44–50; **DOI:**10.17344/acsi.2020.6044
(c) T. T. Adejumo, N. V. Tzouras, L. P. Zorba, D. Radanovic, A. Pevec, S. Grubisic, D. Mitic, K. K. Andelkovic, G. C. Vougioukalakis, B. Cobeljic, I. Turel, *Molecules* **2020**, *25*, 4043; **DOI:**10.3390/molecules25184043
(d) R. Bikas, M. S. Krawczyk, T. Lis, *ChemistrySelect* **2020**, 5, 6759–6764; **DOI:**10.1002/slct.202001032
(e) Y. Tan, *Acta Chim. Slov.* **2020**, *67*, 1233–1238. **DOI:**10.17344/acsi.2020.6136

4. (a) A. Kumar, S. D. Kurbah, I. Syiemlieh, S. A. Dhanpat, R. Borthakur, R. A. Lal, *Inorg. Chim. Acta* **2021**, *515*, 120068; **DOI:**10.1016/j.ica.2020.120068
(b) Y. M. Cui, Y. Q. Wang, X. X. Su, H. Huan, P. Zhang, *J. Struct. Chem.* **2019**, *60*, 1299–1305; **DOI:**10.1134/S0022476619080092
(c) Y.-J. Cai, Y.-Y. Wu, F. Pan, Q.-A. Peng, Y.-M. Cui, *Acta Chim. Slov.* **2020**, *67*, 896–903; **DOI:**10.17344/acsi.2020.5895
(d) L.-W. Xue, Y.-J. Han, X.-Q. Luo, *Inorg. Nano-Met. Chem.* **2020**, *50*, 654–660. **DOI:**10.1080/24701556.2020.1723629

5. (a) Z.-Q. Sun, S.-F. Yu, X.-L. Xu, X.-Y. Qiu, S.-J. Liu, *Acta Chim. Slov.* **2020**, *67*, 1281–1289; **DOI:**10.17344/acsi.2020.6236
(b) D.-L. Peng, *Russ. J. Coord. Chem.* **2020**, *46*, 276–282; **DOI:**10.1134/S1070328420040065
(c) S. H. Guo, N. Sun, Y. W. Ding, A. Li, Y. M. Jiang, W. Q. Zhai, Z. W. Li, D. Qu, Z. L. You, *Z. Anorg. Allg. Chem.* **2018**, *644*, 1172–1176; **DOI:**10.1002/zaac.201800060
(d) L. Li, K.-W. Lu, Y.-T. Li, G.-F. Jiang, Y. Xin, L. Ye, Y. Zhang, H. Liu, C.-N. Shang, Z.-L. You, *Chinese J. Inorg. Chem.* **2017**, *33*, 905–912; **DOI:**10.1007/s40242-017-7240-5
(e) L.-X. Li, Y. Sun, Q. Xie, Y.-B. Sun, K.-H. Li, W. Li, Z.-L. You, *Chinese J. Inorg. Chem.* **2016**, *32*, 369–376.

6. G. M. Sheldrick. SAINT (version 6.02), SADABS (version 2.03), Madison (WI, USA): Bruker AXS Inc, **2002**.

7. G. M. Sheldrick. SHELXL-97, A Program for Crystal Structure Solution, Göttingen (Germany): University of Göttingen, **1997**.

8. (a) D.-H. Zou, M. Liang, W. Chen, *Acta Chim. Slov.* **2021**, *68*, 441–446; **DOI:**10.17344/acsi.2020.6553
(b) Q. Yang, P. Wang, Y. Lei, *Acta Chim. Slov.* **2020**, *67*, 957–969;
(c) Q.-A. Peng, X.-P. Tan, Y.-D. Wang, S.-H. Wang, Y.-X. Jiang, Y. Cui, *Acta Chim. Slov.* **2020**, *67*, 644–650. **DOI:**10.17344/acsi.2019.5650

9. W. J. Geary, *Coord. Chem. Rev.* **1971**, *7*, 81–122. **DOI:**10.1016/S0010-8545(00)80009-0

10. (a) L.-Y. He, X.-Y. Qiu, J.-Y. Cheng, S.-J. Liu, S.-M. Wu, *Polyhedron* **2018**, *156*, 105–110; **DOI:**10.1016/j.poly.2018.09.017
(b) S.D. Kurbah, M. Asthana, I. Syiemlieh, A.A. Lywait, M. Longchar, R.A. Lal, *J. Organomet. Chem.* **2018**, *876*, 10–16. **DOI:**10.1016/j.jorganchem.2018.08.025

11. M.-L. Liu, J.-M. Dou, J.-Z. Cui, D.-C. Li, D.-Q. Wang, *J. Mol. Struct.* **2012**, *1011*, 140–144. **DOI:**10.1016/j.molstruc.2011.12.024

12. N. Mathew, M. Sithambaresan, M. R. Prathapachandra Kurup, *Spectrochim. Acta A* **2011**, *79*, 1154–1161. **DOI:**10.1016/j.saa.2011.04.036

13. (a) M. R. Prathapachandra Kurup, E. B. Seena, M. Kuriakose, *Struct. Chem.* **2010**, *21*, 599–605; **DOI:**10.1007/s11224-010-9589-7
(b) B. Mondal, M. G. B. Drew, T. Ghosh, *Inorg. Chim. Acta* **2009**, *362*, 3303–3308. **DOI:**10.1016/j.ica.2009.02.043

14. (a) R. Ando, S. Mori, M. Hayashi, T. Yagyu, M. Maeda, *Inorg. Chim. Acta* **2004**, *357*, 1177–1184; **DOI:**10.1016/j.ica.2003.09.033
(b) C. J. Chang, J. A. Labinger, H. B. Gray, *Inorg. Chem.* **1997**, *36*, 5927–5930; **DOI:**10.1021/ic970824q
(c) R. Ando, H. Ono, T. Yagyu, M. Maeda, *Inorg. Chim. Acta* **2004**, *357*, 2237–2244. **DOI:**10.1016/j.ica.2003.12.031

15. S. Mondal, M. Mukherjee, K. Dhara, S. Ghosh, J. Ratha, P. Banerjee, A. K. Mukherjee, *Cryst. Growth Des.* **2007**, *7*, 1716–1721. **DOI:**10.1021/cg060753i

16. (a) H. H. Monfared, S. Alavi, R. Bikas, M. Vahedpour, P. Mayer, *Polyhedron* **2010**, *29*, 3355–3362; **DOI:**10.1016/j.poly.2010.09.029
(b) L. Y. Xu, Y. M. Li, M. M. Duan, Y. X. Li, M. X. Han, J. H. Wu, Y. H. Wang, K. X. Dong, Z. L. You, *Polyhedron* **2019**, *165*, 138–142. **DOI:**10.1016/j.poly.2019.03.016

Povzetek

Sintetizirali smo dva nova oksidovanadijeva(V) kompleksa, [VOL^1(aha)]DMF (**1**) in [VOL^2(mat)] (**2**), kjer sta L^1 in L^2 dianionski obliki *N*'-(4-bromo-2-hidroksibenziliden)-3-metil-4-nitrobenzohidrazida in *N*'-(3,5-dibromo-2-hidroksibenziliden)pivalohidrazida ter aha in mat monoanionski obliki acetohidroksaminske kisline in maltola ter ju okarakterizirali s fizikalno-kemijskimi metodami in monokristalno rentgensko difrakcijo. Rentgenska analiza razkriva, da imajo V atomi v kompleksih oktaedrično koordinacijo. Kristalni strukturi kompleksov sta stabilizirani z vodikovimi vezmi. Proučili smo katalitske lastnosti kompleksov za epoksidacijo stirena.

Except when otherwise noted, articles in this journal are published under the terms and conditions of the Creative Commons Attribution 4.0 International License

Scientific paper

Crystallography and DFT Studies of Synthesized Tetraketones

Elma Veljović,[1] Krešimir Molčanov,[2] Mirsada Salihović,[1] Una Glamočlija,[1,3,4] Amar Osmanović,[1,*] Nevzeta Ljubijankić[5] and Selma Špirtović-Halilović[1]

[1] *University of Sarajevo, Faculty of Pharmacy, Zmaja od Bosne 8, 71 000 Sarajevo, Bosnia and Herzegovina*

[2] *Ruđer Bošković Institute, Bijenička 54, 10000 Zagreb, Croatia*

[3] *University of Mostar, School of Medicine, Bijeli Brijeg bb, 88000 Mostar, Bosnia and Herzegovina*

[4] *Bosnalijek JSC, Scientific-Research Unit, Jukićeva 53, 71 000 Sarajevo, Bosnia and Herzegovina*

[5] *University of Sarajevo, Faculty of Science, Department of Chemistry, Zmaja od Bosne 35, 71000 Sarajevo, Bosnia and Herzegovina*

** Corresponding author: E-mail: amar.osmanovic@ffsa.unsa.ba*

Received: 12-15-2021

Abstract

Two tetraketone derivatives, one previously reported and one novel, were synthesized, whose structures have been confirmed by elemental analyses, NMR, HPLC-MS, and IR spectroscopy. The crystal structures of synthesized tetraketones were determined using X-ray single-crystal diffraction. To analyze the molecular geometry and compare with experimentally obtained X-ray crystal data of synthesized compounds **1** (2,2'-((4-nitrophenyl)methylene)bis(5,5-dimethylcyclohexane-1,3-dione)) and **2** (2,2'-((4-hydroxy-3-methoxy-5-nitrophenyl)methylene)bis(5,5-dimethylcyclohexane-1,3-dione)), DFT calculations were performed with the standard 6-31G*(d), 6-31G**, and 6-31+G* basis sets. The calculated HOMO-LUMO energy gap for compound **1** was 4.60 eV and this value indicated that compound **1** is chemically more stable compared to compound **2** whose energy gap was 3.73 eV. Both compounds' calculated bond lengths and bond angles were in very good accordance to experimental values determined by X-ray single-crystal diffraction.

Keywords: Tetraketones; X-ray diffraction; DFT; HOMO-LUMO energies

1. Introduction

Tetraketones (2,2'-(arylmethylene)bis(5,5-dimethyl-2-cyclohexane-1,3-diones)) represent an important class of compounds that have shown beneficial pharmacological effects *in vitro*. They are widely used as important precursors in the synthesis of various acridindiones as laser dyes and some heterocyclic compounds, xanthendiones and thioxanthenes.[1] Tetraketones exhibit antioxidant, antibacterial and antiviral effects.[2] These compounds are well studied as the inhibitors of the enzyme lipooxygenase.[3] Tetraketones are being evaluated as prospective medicines in the treatment of inflammatory diseases, bronchiolitis, carcinoma, and autoimmune illnesses since lipooxygenases represent a potential target for rational drug design and identification of mechanism-based inhibitors for these conditions.[4,5]

These compounds were studied by X-ray crystallography (X-ray), nuclear magnetic resonance (NMR), and molecular modeling, revealing important information about structure and conformation, such as the presence of intramolecular hydrogen bonds.[6–9] One of the most important studies was conducted by Forsen *et al.* in 1969 when they determined by NMR that 2,2'-arylmethylene-bis(3-hydroxy-5,5-dimethyl-2-cyclohexene-1-ones) are found as dienol tautomers. As a result, these compounds are referred to as tetraketones in the literature (Figure 1).[10]

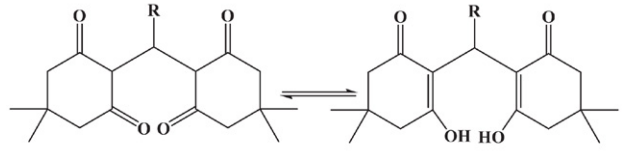

Figure 1. Tetraketones and their keto-enol tautomeric forms.

2. Materials and Methods

2. 1. Synthesis of Tetraketone (2,2'-(arylmethylene)bis(5,5-dimethyl -2-cyclohexane-1,3-dione)) Derivatives

Benzaldehyde (1 mmol), 5,5-dimethylcyclohexane-1,3-dione (2 mmol), and diazobicyclo[2.2.2]octane (DABCO) (0.05 g) were refluxed in water (20 mL). Thin-layer chromatography was used to monitor the reaction's flow and completion. Tetraketones are obtained approximately after 20 minutes of reflux. If the reflux is continued for longer (30 minutes or more), reaction leads toward formation of the 9-aryl substituted 3,3,6,6-tetramethyl-3,4,5,6,7,9-hexahydro-1*H*-xanthene-1,8(2*H*)-diones.[11] The mixture was cooled to room temperature, filtered, and rinsed with water once the reaction was completed. Recrystallization of the resulting compounds was performed from 96% ethanol.[12] All chemicals have been obtained from Merck (Germany).

Newly synthesized compounds were obtained through Knoevenagel condensation of aromatic aldehyde and Michael addition with 5,5-dimethylcyclohexandione-1,3-dione (Figure 2). In this article, we present two tetraketones, one previously reported (**1**)[13] and the other one novel (**2**), whose structures have been confirmed by elemental analysis, IR, NMR spectroscopy and HPLC-MS spectrometry.

2. 2. Characterization of Synthesized Products

Elemental analysis. For the synthesized tetraketone derivatives, elemental analysis was performed at the Institute of Chemistry, Technology and Metallurgy, Center for Chemistry in Belgrade, Serbia, on the Vario EL apparatus III C,H,N,S/O Elemental Analyzer, Elementar Analysensysteme GmbH, Hanau, Germany.

IR spectroscopy. IR spectra of the synthesized compounds were recorded at the Bosnalijek Pharmaceutical Company Ltd., Sarajevo, Bosnia and Herzegovina, on the Shimadzu IR Prestige 21 apparatus in the wavelength range from 4500 to 700 cm^{-1}.

NMR. ^{1}H NMR and ^{13}C NMR spectra for the synthesized compounds were recorded at the Faculty of Science in Novi Sad, Serbia, using a Bruker AC 250 E apparatus. Compounds were recorded in deuterated chloroform using TMS (tetramethylsilane) as a reference.

HPLC-MS spectra. The mass spectra were recorded on an HPLC-MS triple quadrupole 6420 autosampler (Agilent Technologies, Palo Alto, CA, USA). The recordings were made at a temperature of 573 K and a gas flow of 6 L min^{-1}. As the mobile phase, 0.1% formic acid in 50% methanol was used, at a flow rate of 0.2 mL min^{-1}. The spectra were processed using Agilent MassHunter software.

Melting point. The melting points of the synthesized compounds were determined at the Department of Pharmaceutical Chemistry, Faculty of Pharmacy in Sarajevo, Bosnia and Herzegovina, using the Melting point apparatus manufactured by Kruss Optronic, Germany.

X-ray diffraction. Single crystal measurements were performed on an Oxford Diffraction Xcalibur Nova R (microfocus Cu tube) at room temperature [293(2) K]. Program package CrysAlis PRO was used for data reduction.[14] The structures were solved using SHELXS97 and refined with SHELXL97.[15] The models were refined using the full-matrix least-squares refinement; all non-hydrogen atoms were refined anisotropically. Hydrogen atoms were modeled as riding entities using the AFIX command.

Molecular geometry calculations were performed by PLATON,[16] and molecular graphics were prepared using ORTEP-3,[17] and CCDC-Mercury.[18] Crystallographic and refinement data for the structures reported in this paper are shown in Table 1.

Supplementary crystallographic data can be obtained free of charge via www.ccdc.cam.ac.uk/conts/re-

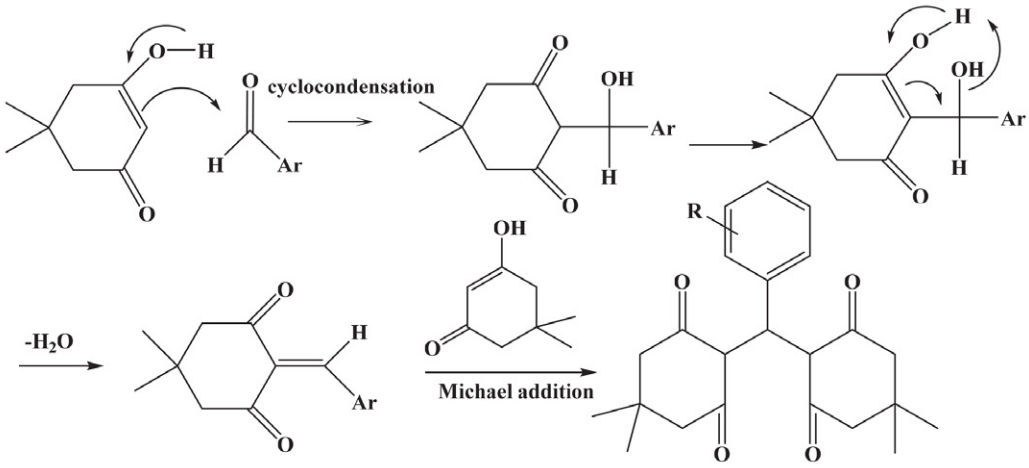

Figure 2. Synthesis of 2,2'-(arylmethylene)bis(5,5-dimethyl-2-cyclohexane-1,3-dione) derivatives.

Table 1. Crystallographic data collection and structure refinement details.

Compound	1	2
Empirical formula	$C_{23}H_{25}NO_6$	$C_{24}H_{27}NO_8$
Formula wt. / g mol^{-1}	411.45	457.47
Space group	$P\,bc2_1$	$P\bar{1}$
a / Å	23.5533(3)	8.9958(3)
b / Å	12.9754(1)	9.3891(4)
c / Å	28.1370(3)	13.9171(6)
α / °	90	98.814(4)
β / °	90	99.380(3)
γ / °	90	90.925(3)
Z	16	2
V / Å^3	8599.05(16)	1145.04(8)
D_{calc} / g cm^{-3}	1.271	1.327
μ / mm^{-1}	0.759	0.835
T / K	293(2)	293(2)
Radiation vawelength	1.54179 (Cu$K\alpha$)	1.54179 (Cu$K\alpha$)
Reflections collected	28964	10363
Independent reflections	13399	4692
Observed reflections ($I \geq 2\sigma$)	12660	4108
R_{int}	0.0212	0.0207
R (F)	0.0463	0.0488
R_w (F^2)	0.1313	0.1470
Goodness of fit	1.034	1.049
No. of parameters	1081	299
No. of restraints	1	0
Flack parameter	0.11(7)	–
$\Delta\rho_{max}$, $\Delta\rho_{min}$ (eÅ^{-3})	0.380; –0.199	0.338; –0.168

trieving.html (or from the Cambridge Crystallographic Data Centre, 12, Union Road, Cambridge CB2 1EZ, UK; fax: +44 1223 336033; or deposit@ccdc.cam.ac.uk). CCDC 1990310-1990311 contains the supplementary crystallographic data for this paper.[19]

2. 3. Computational Details

Quantum chemical computations were done for compounds **1** and **2** on a single molecule in vacuo, with comprehensive geometry optimizations using standard Spartan 14 software. At the B3LYP/6-31G*, 6-31G**, and 6-31+G* levels of theory, geometry optimization was performed.[20] The HOMO (highest occupied molecular orbital) and LUMO (lowest unoccupied molecular orbital) energy distributions, as well as the HOMO-LUMO energy gap, were calculated using these levels of theory. The results of the DFT analysis were compared to those experimentally obtained crystallographic data.

3. Results and Discussion

3. 1. Chemistry

According to described Knoevenagel condensation of aromatic aldehyde and Michael addition with 5,5-dimethyl-1,3-cyclohexandione, we synthesized compounds **1** (2,2'-((4-nitrophenyl)methylene)bis(5,5-dimethylcyclohexane-1,3-dione)) and **2** (2,2'-((4-hydroxy-3-methoxy-5-nitrophenyl)methylene)bis(5,5-dimethylcyclohexane-1,3-dione)) (Figure 3).

The characterization of synthesized compounds **1** and **2** was achieved by FT-IR, ^{1}H and ^{13}C NMR spectroscopy, and HPLC-MS spectrometry.

1: Yield: 81%. Mp 198–203 °C. Anal. Calcd for $C_{23}H_{27}N_1O_6$: C, 66.81; H, 6.58. Found: C, 66.74; H, 6.62. IR (KBr) ν 3000 (Ar-H), 1670 (C=O), 1480 (C=C), 1300 (C-O), 1500 (C=O), 1250 (NO_2) cm^{-1}. ^{1}H NMR (600 MHz, $CDCl_3$) δ 11.8 (br s, 1H, OH, disappears with D_2O), 8.13 (d, 2H, $J_{2',3'}$ = 8.9 Hz, H-3', H-5'), 7.24 (d, 2H, $J_{2',3'}$ = 8.9 Hz, H-2', H-6'), 5.53 (s, 1H, CH), 2.21–2.57 (m, 8H, 4 × CH_2), 1.11 and 1.23 (2 × s, 12 H, 4 × CH_3). ^{13}C NMR (150 MHz, $CDCl_3$) **δ** 190.82 (C=O), 189.46 (C-2), 146.49–146.03 (Ar-C), 127.56, 123.40 (Ar-CH), 114.81 (C-1), 46.91, 46.32 (CH_2), 33.18 (CH), 31.39 (C from $C(CH_3)_2$), 29.38, 27.38 (CH_3 from $C(CH_3)_2$). MS *m/z* (relative intensity): 412.2 (M+H).

2: Yield: 88%. Mp 230–232 °C. Anal. Calcd for $C_{24}H_{27}N_1O_8$: C, 62.73; H, 6.36. Found: C, 63.10; H, 6.08. IR (KBr) ν 3300–2500 (Ar-OH), 3042 (Ar-H), 1730 (C=O), 1607, 1588 (C=C), 1448 (O-CH_3), 1320 (C-O), 1200 (Ar-

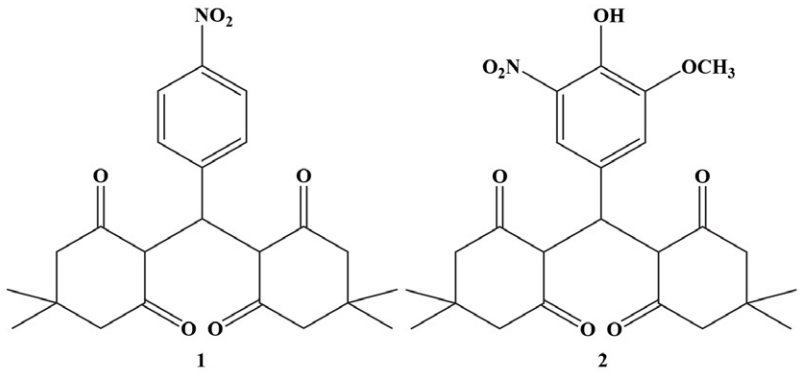

Figure 3. Structures of synthesized tetraketones **1** and **2**.

OH), 1595 (NO_2) cm^{-1}. ^1H NMR (600 MHz, $CDCl_3$) δ 10.60 (br s, 1H, OH, disappears with D_2O), 7.44 (s, 1H, H-6′), 6.90 (s, 1H, H-2′), 5.43 (s, 1H, H-13), 3.83 (s, 3H, OCH_3), 2.54–2.22 (m, 8H, H-3, H-11, H-5, H-9), 1.25 (s, 6H, H-15, H-17), 1.12 (s, 6H, H-14, H-16). ^{13}C NMR (150 MHz, $CDCl_3$) δ 190.94 (C-6, C-8), 189.45 (C-2, C-12), 149.59 (C-3′), 144.41 (C-5′), 133.60 (C-4′), 114.71 (C-1, C-7), 117.04 (C-2′), 114.01 (C-6′), 33.18 (C-13), 31.39 (C-4, C-10), 29.82 (C-15, C-17), 26.87 (C-14, C-16). MS *m/z* (relative intensity): 460 (M+H).

3. 2. Description of the Structures

The compound **1** crystallizes in a non-centrosymmetric space group $P\,bc2_1$ with four symmetry-independent molecules in the asymmetric unit (i.e. $Z' = 4$), labeled as **a**, **b**, **c**, and **d** (Figure 4).

There are two conformers, with a different conformation of the ring C2→C6: one is comprised of molecules **a** and **d**, and the other of **b** and **c**. The rest of the molecule differs less than 3 e.s.d.'s (least-squares overlay is shown in

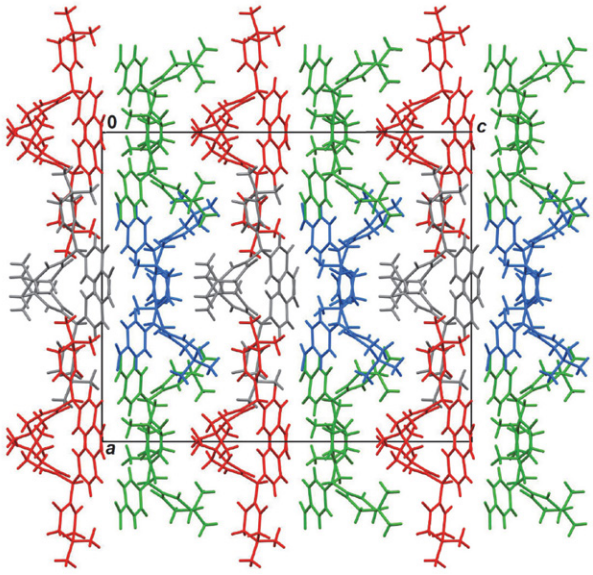

Figure 5. Crystal packing of **1** viewed in the direction [010]. Symmetry-independent molecules are shown in different colors: **a** are green, **b** are blue, **c** are red and **d** are gray.

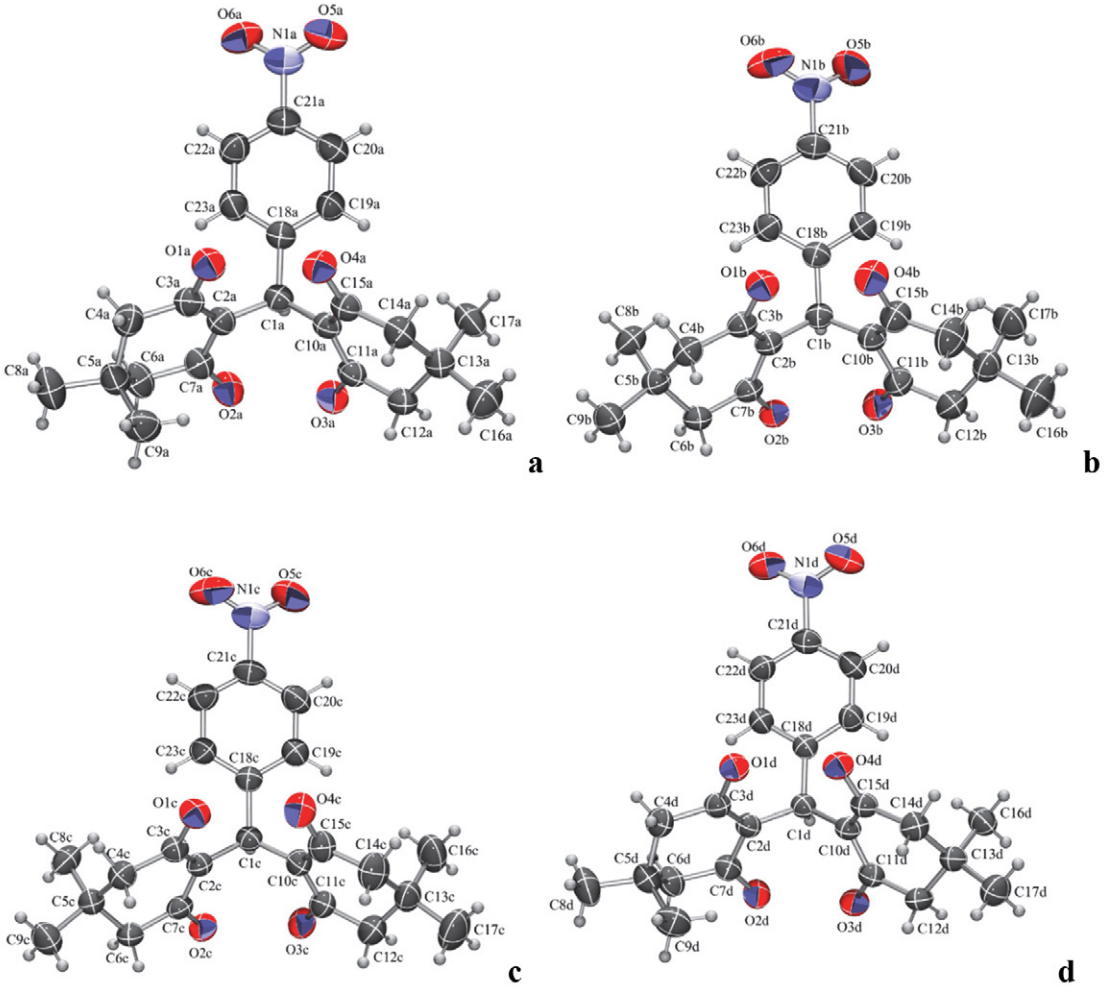

Figure 4. ORTEP-3 drawings of four symmetry-independent molecules in **1** with atom numbering schemes. Displacement ellipsoids are drawn for the probability of 50% and hydrogen atoms are shown as spheres of arbitrary radii.

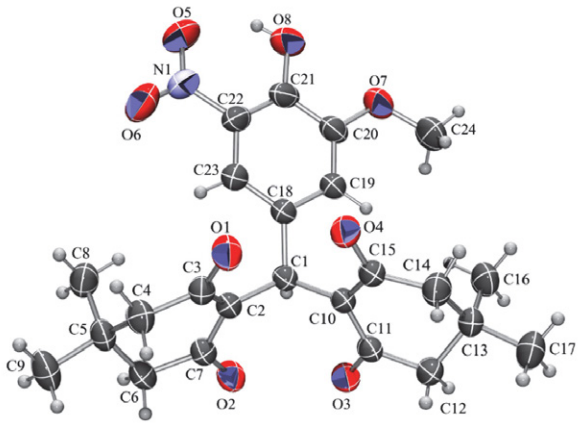

Figure 6. ORTEP-3 drawing of a molecule of **2** with the atom numbering scheme. Displacement ellipsoids are drawn for the probability of 50% and hydrogen atoms are shown as spheres of arbitrary radii.

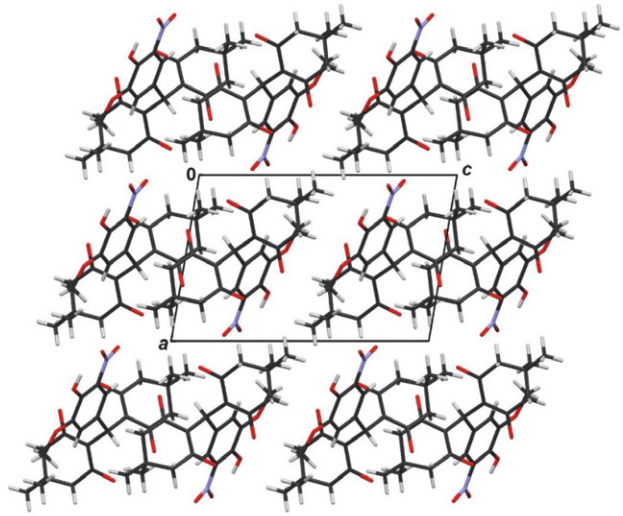

Figure 7. Crystal packing of **2** viewed in the direction [010].

Figure 8). The compound lacks proton donors and no π-stacking is observed, so 3D packing (Figure 5) is achieved mainly through dispersion interactions and weak C-H···O hydrogen bonds (Table 2).

The asymmetric unit of **2** contains one molecule (Figure 6), whose geometry and conformation are similar to those of **1** (Figure 8). The molecule possesses a single proton donor, the O8-H8 hydroxyl group, which forms an intermolecular hydrogen bond with atom O5 of the nitro group as an acceptor. Crystal data and structure refinement summary of compounds **1** and **2** are given in Tables 2 and 3. Dispersion interactions are responsible for the 3D packing (Figure 7).

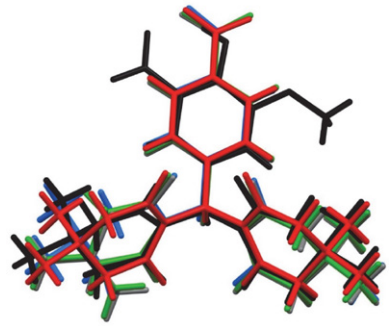

Figure 8. Least-squares overlay of four symmetry-independent molecules of **1** (**a** is green, **b** is blue, **c** is red and **d** is gray) and **2** (black).

Table 2. Geometric parameters of hydrogen bonds and angles.

Cpd (D–H···A)	d(D–H) (Å)		d(H···A) (Å)		d(D···A) (Å)		φ(D–H···A) (°)		
	Exp.	Calc.	Exp.	Calc.	Exp.	Calc.	Exp.	Calc.	Symm. op. on *A*
1									
C1A–H1A···O2A	0.98	1.01	2.41	2.38	2.855(3)	2.678	107	101	*x, y, z*
C1A–H1A···O3A	0.98	1.01	2.43	2.25	2.858(3)	2.680	106	109	*x,y, z*
C1B–H1B···O2B	0.98	1.01	2.42	2.53	2.871(3)	2.701	107	109	*x, y, z*
C1B–H1B···O3B	0.98	1.01	2.38	2.40	2.842(3)	2.710	108	110	*x, y, z*
C1C–H1C···O2C	0.98	1.01	2.41	2.47	2.863(3)	2.715	107	109	*x, y, z*
C1C–H1C···O3C	0.98	1.01	2.39	2.42	2.850(3)	2.370	108	110	*x, y, z*
C1D–H1D···O2D	0.98	1.01	2.38	2.45	2.842(3)	2.790	108	110	*x, y, z*
C1D–H1D···O3D	0.98	1.01	2.44	2.48	2.865(3)	2.800	106	109	*x, y, z*
C20B–H20B···O2A	0.93	0.99	2.54	2.60	3.295(4)	3.100	138	141	*x, −1+y,z*
C20D–H20D···O6A	0.93	0.99	2.53	2.58	3.434(4)	3.110	165	163	*x, 3/2−y, 1/2+z*
C22B–H22B···O6D	0.93	0.99	2.57	2.61	3.458(4)	3.120	160	161	*1−x, 1−y, −1/2+z*
C22D–H22D···O2D	0.93	0.99	2.51	2.56	3.199(3)	3.010	131	129	*1−x, 1/2+y, z*
2									
O8–H8···O5	0.82	0.99	1.89	1.84	2.578(3)	2.308	141	140	*x,y,z*
O8–H8···N1	0.82	0.99	2.50	2.41	2.911(2)	3.04	113	117	*x,y,z*
C1–H1···O2	0.98	1.09	2.35	2.35	2.843(18)	2.82	110	115	*x,y,z*
C1–H1···O3	0.98	1.09	2.40	2.44	2.8506(1)	2.81	108	106	*x,y,z*
C12–H12B···O1	0.97	1.09	2.53	2.84	3.480(2)	3.10	165	170	*1+x,y, z*

Table 3. Bond lengths [Å] and angles [°] of compounds **1** (molecule A, only) and **2**.

Bond length and angles	Compound 1		Compound 2	
	Exp.	Cal.	Exp.	Cal.
C1-C2	1.526(4)	1.548	1.5204(18)	1.548
C1-C10	1.528(3)	1.557	1.5246(19)	1.556
C10-C11	1.402(3	1.530	1.3944(19)	1.530
C11-C12	1.487(4)	1.520	1.499(2)	1.520
C2-C3	1.402(4)	1.546	1.395(2)	1.545
C21-O8	–	–	1.345(2)	1.340
C21-N1	1.470(4)	1.469	–	–
N1-O6	1.230(4)	1.232	1.211(3)	1.255
C7-O2	1.279(4)	1.211	1.285(19)	1.340
C11-O3	1.292(3)	1.215	1.297(19)	1.215
C2-C1-C10	113.6(2)	113.2	115.2(11)	118.0
C10-C11-O3	123.1(3)	124.0	123.0(13)	122.4
C10-C11-C12	122.2(2)	119.4	121.5(14)	121.1
C2-C3-O1	122.9(3)	120.0	123.3(13)	125.2
C2-C3-C4	122.0(2)	122.9	121.2(13)	119.9
C20-C21-C22	122.0(3)	122.7	116.9(14)	116.4
C21-N1-O5	118.4(3)	120.0	118.2(19)	119.0
C21-N1-O6	118.2(3)	119.8	119.8(16)	120.3

Compared calculated and experimentally obtained values in both Table 2 and 3 show very good accordance, differing mostly only in the second decimal place. Similar investigation and comparison of theoretical and experimental data, with good accordance for synthesized compounds, has been reported before.[21,22]

3. 3. Analysis of Molecular Orbital

The energy gap HOMO-LUMO of the molecules has a role in deciding their bioactivity and is an important parameter for quantum chemistry. The molecule becomes harder and more stable or less reactive when the HOMO-LUMO energy gap increases.[23] The HOMO energy distinguishes electron donor capacity, whereas the LUMO energy distinguishes electron acceptor capacity, and the gap defines chemical stability.[24] The energy gap HOMO-LUMO for the compounds **1** and **2** were calculated by 6-31G*, 6-31G**, and 6-31+G* basis sets and these values were –4.60, –4.57, and –4.58 for compound **1** and –3.73, –3.69, and –3.70 for compound **2**. The energies and energy gaps of HOMO and LUMO are shown in Table 4. The HOMO-LUMO orbital schemes for compounds **1** and **2** are shown in Figure 9 (the positive phases are red, and the negative phases are blue).

Compound **1** HOMO electron density demonstrates that the HOMO is localized on carbonyl carbons, methyl, and benzene, while compound **2** HOMO is concentrated on hydroxyl and methoxy groups. The HOMO-LUMO energy gap for compound **1** is 4.60 and for compound **2** is 3.73, indicating that electron density passes from carbonyl carbons, methyl, and methoxy groups to hydroxyl and nitro groups. Compound **1** has a larger HOMO-LUMO energy gap than compound **2**, making it less reactive and hence more stable. The descriptor of electron donor and acceptor is implicitly explained by the HOMO to LUMO transition to comprehend their interaction capabilities with their target molecules.

4. Conclusions

The tetraketones (compounds **1** and **2**) were successfully synthesized with excellent yield by condensation of aromatic aldehyde and Michael addition with 5,5-dimethylcyclohexane-1,3-dione. The synthesized compounds **1**

Table 4. Calculated HOMO and LUMO energy values for compounds **1** and **2**.

Parameters	Compound 1			Compound 2		
	B3LYP/6-31G*	B3LYP/6-31G**	B3LYP/6-31+G*	B3LYP/6-31G*	B3LYP/6-31G**	B3LYP/6-31+G*
E_{HOMO} (eV)	–6.85	–6.87	–6.84	–6.85	–6.87	–6.84
E_{LUMO} (eV)	–2.25	–2.30	–2.26	–2.53	–2.58	–2.54
Energy gap (Δ)	4.60	4.57	4.58	3.73	3.69	3.70

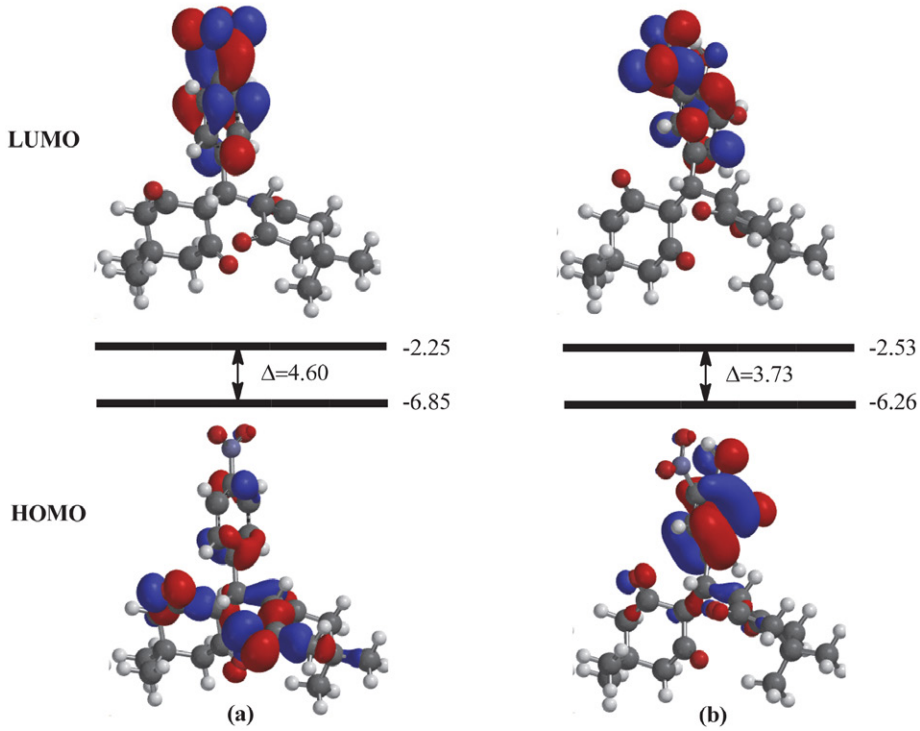

Figure 9. Frontier molecular orbitals of compound **1** (**a**) and compound **2** (**b**). All values are in eV.

and **2** were characterized using ^{1}H and ^{13}C NMR, FTIR, HPLC-MS methods, and elemental analysis. Using single-crystal X-ray diffraction data, we presented the structural details of tetraketone compounds **1** ($C_{23}H_{25}NO_6$) and **2** ($C_{24}H_{27}NO_8$). To analyze the molecular geometry and compare it to experimentally available X-ray crystal data of investigated compounds, DFT calculations were done using a standard 6-31G*(d), 6-31G**, and 6-31+G* basis sets. For compound **2**, the computed HOMO-LUMO energy gaps for basis sets 6-31G*(d), 6-31G**, and 6-31+G* were 3.73, 3.69, and 3.70, respectively. Compound **2** is chemically more reactive than compound **1** based on these smaller gap values. The theoretically determined HOMO-LUMO energy gaps can be employed to describe the biological activity of the title compounds. The crystal structure is stabilized by both intramolecular and intermolecular hydrogen bonds, with the intermolecular N–H···O hydrogen bond in compound **2** generating the N1 and O8 chain motif. The bond lengths and angles calculated for compounds **1** and **2** were in very good accordance with the experimental values obtained from X-ray crystal diffraction.

5. References

1. K. Khan, G. Maharvi, M. Khan, A. Jabbar Shaikh, S. Perveen, S. Begum, M. I. Choudhary, *Bioorg. Med. Chem.* **2006**, *14*, 344–351. **DOI:**10.1016/j.bmc.2005.08.029
2. R. W. Lambert, J. A. Martin, J. H. Merrett, K. E. B. Parkes, J. G. Thomas, PCT Int. Appl., WO 9706178 *Chem. Abstr.* **1997**, *126*, 212377y.
3. S. Ali, G. M. Maharvi, N. Riaz, N. Afza, A. Malik, A. U. Rehman, M. Lateef, L. Iqbal, *West Indian Med. J.* **2009**, *58*, 92–98.
4. G. M. Maharvi, S. Ali, N. Riaz, N. Afza, A. Malik, M. Ashraf, L. Iqbal, M, Lateef, *J. Enzyme Inhib. Med. Chem.* **2008**, *23*, 62–69. **DOI:**10.1080/14756360701408754
5. F. K. Rad, F. K. Behbahani, *Curr. Org. Synth.* **2017**, *14*, 22–39. **DOI:**10.2174/1570179413666160624112201
6. M. Bolte, M. A. Scholtyssik, *Acta Crystallogr., Sect. C: Cryst. Struct. Commun.* **1997**, *53*, 1869–1871. **DOI:**10.1107/S0108270197009438
7. M. Bolte, A. Degen, S. Rühl, *Acta Crystallogr., Sect. C: Cryst. Struct. Commun.* **2001**, *57*, 446–451. **DOI:**10.1107/S0108270101001792
8. J. N. Low, J. Cobo, S. Cruz, J. Quiroga, C. Glidewell, *Acta Crystallogr., Sect. C: Cryst. Struct. Commun.* **2003**, *59*, 666–668. **DOI:**10.1107/S0108270103023606
9. M. Sigalov, R. Vainer, V. Khodorkovsky, *J. Mol. Struct.* **2010**, *977*, 230–236. **DOI:**10.1016/j.molstruc.2010.05.039
10. S. Forsen, W. Frankle, P. Laszlo, J. Lubochinsky, *J. Magn. Reson.* **1969**, *1*, 327–338. **DOI:**10.1016/0022-2364(69)90071-7
11. S. Zukić, E. Veljović, S. Spirtović-Halilović, S. Muratović, A. Osmanović, S. Trifunović, I. Novaković, D. Zavrsnik, *Croat. Chem. Acta* **2018**, *91*, 1–9.
12. P. Paliwal, S. Jetti, A. Bhatewara, T. Kadre, S. Jain, *ISRN Org. Chem.* **2013**, Article ID 526173, 6 pages, **DOI:**10.1155/2013/526173

13. J. Safaei-Ghomi, S. Asadian, S. H. Nazemzadeh, H. Shahbazi-Alavi, *J. Chin. Chem. Soc. (Weinheim, Ger.)* **2018**, *65*, 430–434. **DOI:**10.1002/jccs.201700250
14. *CrysAlis PRO*, Oxford Diffraction Ltd., U.K., 2007.
15. G. M. Sheldrick, *Acta Crystallogr*. **2008***, 64*, 112–122. **DOI:**10.1107/S0108767307043930
16. A. L. Spek, *J. Appl. Cryst.* **2003**, *36*, 7–13. **DOI:**10.1107/S0021889802022112
17. L. J. Farrugia, *J. Appl. Cryst.* **1997**, *30*, 565. **DOI:**10.1107/S0021889897003117
18. C. F. Macrae, P. R. Edgington, P. McCabe, E. Pidcock, G. P. Shields, R. Taylor, M. Towler, J. ven de Streek, *J. Appl. Cryst.* **2006**, *39*, 453–457. **DOI:**10.1107/S002188980600731X
19. F. H. Allen, *Acta Crystallogr., Sect. B: Struct. Sci.* **2002**, *58*, 380–388. **DOI:**10.1107/S0108768102003890
20. M. Salihović, A. Osmanović, S. Špirtović-Halilović, S. Roca, A. Meščić, L. Vujisić, S. Trifunović, D. Završnik, E. Sofić, *J. Mol. Struct.* **2015**, *1091*, 170–176. **DOI:**10.1016/j.molstruc.2015.02.078
21. U. Glamočlija, S. Špirtović-Halilović, M. Salihović, I. Turel, J. Kljun, E. Veljović, S. Zukić, D. Završnik, *Acta Chim. Slov.* **2021**, *68*, 144–150. **DOI:**10.17344/acsi.2020.6237
22. M. Jayaraman, R. Balakrishnan, K. Muthu, M. Panneerselvam, V. Gnanasambandam, K. Ramadas, *J. Crystallogr.* **2014**, Article ID 369061, **DOI:**10.1155/2014/369061
23. A. A. Kadhum, A. A. Al-Amiery, M. Shikara, A. Mohamad, *Int. J. Phys. Sci.* **2011**, *6*, 6692–6697.
24. T. S. Xavier, I. H. Joe, *Spectrochim. Acta, Part A* **2011**, *79*, 332–337. **DOI:**10.1016/j.saa.2011.02.037

Povzetek

Sintetizirali smo dva tetraketonska derivata (enega novega in enega že znanega) ter njuni strukturi potrdili z elementno analizo, NMR, HPLC-MS in IR spektroskopijo. Kristalne strukture sintetiziranih tetraketonov smo določili z rentgensko difrakcijsko analizo monokristalov. S pomočjo DFT računskih metod s standardnimi baznimi seti 6-31G*(d), 6-31G** in 6-31+G* smo izvedli analizo molekulske geometrije in dobljene rezultate primerjali z eksperimentalnimi, ki so bili pridobljeni z rentgensko difrakcijo pripravljenih spojin **1** (2,2'-((4-nitrofenil)metilen)bis(5,5-dimetilcikloheksan-1,3-dion)) in **2** (2,2'-((4-hidroksi-3-metoksi-5-nitrofenil)metilen)bis(5,5-dimetilcikloheksan-1,3-dion)). Izračunana vrednost HOMO-LUMO energijske špranje za spojino **1** je 4.60 eV, kar kaže, da je spojina **1** kemijsko bolj stabilna kot spojina **2**, katere velikost energijske špranje je 3.73 eV. Izračunane dolžine vezi in koti se za obe spojini zelo dobro ujemajo z eksperimentalnimi vrednostmi, dobljenimi z rentgensko difrakcijo monokristala.

Except when otherwise noted, articles in this journal are published under the terms and conditions of the Creative Commons Attribution 4.0 International License

DRUŠTVENE VESTI IN DRUGE AKTIVNOSTI
SOCIETY NEWS, ANNOUNCEMENTS, ACTIVITIES

Vsebina

Doktorska in magistrska dela, diplome v letu 2021 ..... S3
Koledar važnejših znanstvenih srečanj s področja kemije in kemijske tehnologije S33
Navodila za avtorje S36

Contents

Doctoral theses, master degree theses, and diplomas in 2021 ..... S3
Scientific meetings – Chemistry and chemical engineering..... S33
Instructions for authors S36

UNIVERZA V LJUBLJANI
FAKULTETA ZA KEMIJO IN KEMIJSKO TEHNOLOGIJO
1. januar – 31. december 2021

DOKTORATI

DOKTORSKI ŠTUDIJSKI PROGRAM KEMIJSKE ZNANOSTI

KEMIJA

Antonio SCAFURI
Mentor: znan. sod. dr. Klemen Pirnat
Somentor: prof. dr. Robert Dominko
NAPREDNI ELEKTROLITI ZA KALCIJEVE AKUMULATORJE
Datum zagovora: 29. 3. 2021

Mateja MIHELAČ
Mentor: doc. dr. Martin Gazvoda
MEZOIONSKI PALADIJEV KOMPLEKS KOT KATALIZATOR ZA TVORBO VEZI C-N IN C-F
Datum zagovora: 6. 4. 2021

Urška JUG
Mentorica: viš. znan. sod. dr. Irena Vovk
KROMATOGRAFSKE IN MASNO SPEKTROMETRIČNE METODE ZA KARAKTERIZACIJO FENOLNIH SPOJIN V EKSTRAKTIH JAPONSKEGA DRESNIKA (*FALLOPIA JAPONICA* HOUTT.) IN DRUGIH RASTLINSKIH EKSTRAKTIH
Datum zagovora: 7. 4. 2021

Griša Grigorij PRINČIČ
Mentor: izr. prof. dr. Jernej Iskra
SINTEZA IN OPTIMIZACIJA AROMATSKO SUBSTITUIRANIH NESIMETRIČNIH 1,2,4,5-TETRAOKSANOV IN PEROKSI-BODIPY ANALOGOV
Datum zagovora: 9. 7. 2021

Isidora ČOBANOV MARINKOVIĆ
Mentorica: prof. dr. Marija Bešter Rogač
Somentor: izr. prof. dr. Milan Vraneš
TERMODINAMSKE RAZISKAVE MICELIZACIJE POVRŠINSKO AKTIVNIH IONSKIH TEKOČIN
Datum zagovora: 13. 7. 2021

Anja KRISTL
Mentor: prof. dr. Matevž Pompe
UPORABA KROMATOGRAFIJE Z MEŠANIMI REŽIMI ZA SEPARACIJO BIOLOŠKO POMEMBNIH MOLEKUL
Datum zagovora: 28. 9. 2021

Jure CERAR
Mentor: prof. dr. Matija Tomšič
PROSTORSKE KORELACIJE IN DINAMIKA V TEKOČINAH Z VODIKOVIMI VEZMI
Datum zagovora: 28. 9. 2021

Nejc PETEK
Mentor: prof. dr. Bogdan Štefane
FOTOREDOKS KATALITSKE PRETVORBE PIRAZOLOV
Datum zagovora: 29. 9. 2021

Damjan Jan PAVLICA
Mentor: prof. dr. Matevž Pompe
Somentor: doc. dr. Črtomir Podlipnik
KEMIJSKE PRETVORBE AEROSOLOV BIOGENEGA IZVORA
Datum zagovora: 30. 11. 2021

Nika VRTOVEC
Mentor: viš. znan. sod. dr. Matjaž Mazaj
OPTIMIZACIJA KOVINSKO-ORGANSKIH MIKROPOROZNIH MATERIALOV ZA ZAJEM IN PRETVORBO CO_2
Datum zagovora: 9. 12. 2021

Dino METARAPI
Mentor: znan. svet. dr. Johannes T. Van Elteren
Somentor: izr. prof. dr. Mitja Kolar
UPORABA SODOBNIH SLIKOVNIH ORODIJ PRI MASNOSPEKTROSKOPSKI ANALIZI PO VZORČENJU Z LASERSKO ABLACIJO
Datum zagovora: 23. 12. 2021

KEMIJSKO INŽENIRSTVO

Luka NOČ
Mentor: znan. sod. dr. Ivan Jerman
Somentor: izr. prof. dr. Boštjan Genorio
NANOSTRUKTURIRANE ČRNE, KERAMIČNE IN KOMPOZITNE VISOKOTEMPERATURNE SPEKTRALNO SELEKTIVNE PREVLEKE ZA SONČNE SPREJEMNIKE
Datum zagovora: 5. 2. 2021

Igor BOŠEVSKI
Mentorica: prof. dr. Andreja Žgajnar Gotvajn
RAZVOJ SISTEMA ZA ČIŠČENJE ODPADNIH VODA, KI VSEBUJEJO ANTIBIOTIČNE UČINKOVINE
Datum zagovora: 5. 10. 2021

BIOKEMIJA

Anja KRAJNC
Mentor: doc. dr. Miha Pavšič
ŠTUDIJE STRUKTURNIH LASTNOSTI IN INTERAKCIJ ČLOVEŠKIH PROTEOGLIKANOV TESTIKANOV
Datum zagovora: 7. 4. 2021

Metka STANTIČ
Mentor: prof. dr. Aleš Podgornik
Somentor: doc. dr. Gregor Gunčar
RAZVOJ KROMATOGRAFSKIH TEHNIK PROCESNO ANALITSKE TEHNOLOGIJE ZA DOLOČEVANJE IZOOBLIK MONOKLONSKIH PROTITELES
Datum zagovora: 26. 11. 2021

MAGISTRSKI ŠTUDIJ

MAGISTRSKI ŠTUDIJSKI PROGRAM 2. STOPNJE – KEMIJA

Žiga MLINAR
Mentor: izr. prof. dr. Drago Kočar
RAZGRADNJA KOFEINA IN TEOFILINA S FENTONOVIM REGENTOM V VODNIH RAZTOPINAH
Datum zagovora: 4. 1. 2021

Leja ERZIN
Mentor: prof. dr. Matevž Pompe
RAZVOJ KROMATOGRAFSKE METODE ZA DOLOČANJE SLADKORJEV S FLUORESCENČNO DETEKCIJO
Datum zagovora: 21. 1. 2021

Erik TROBEC
Mentor: izr. prof. dr. Uroš Grošelj
ORGANOKATALIZIRANA SINTEZA ALKILIRANIH DERIVATOV TETRAMSKE KISLINE
Datum zagovora: 29. 1. 2021

Deja ZUPANČIČ
Mentor: prof. dr. Janez Košmrlj
OPTIMIZACIJA SINTEZE MEZOIONSKEGA PALADIJEVEGA(II) KOMPLEKSA
Datum zagovora: 12. 3. 2021

Tjaša KLAVŽAR
Mentor: izr. prof. dr. Janez Cerkovnik
PRIPRAVA ORGANOKOVINSKIH HIDRIDOV KOVIN PREHODA IN ŠTUDIJ NJIHOVE OKSIDACIJE
Datum zagovora: 15. 3. 2021

Nina KRIŽAJ
Mentor: izr. prof. dr. Miha Lukšič
Somentor: doc. dr. Slavko Kralj
SINTEZA ANIZOTROPNIH SUPERPARAMAGNETNIH MIKRODELCEV ŽELEZOVEGA OKSIDA TER ŠTUDIJA NJIHOVE KOMPLEKSACIJE Z IONENI
Datum zagovora: 7. 4. 2021

Maša ČESNIK
Mentorica: prof. dr. Helena Prosen
OPTIMIZACIJA EKSTRAKCIJE POLICIKLIČNIH AROMATSKIH OGLJIKOVODIKOV IZ TAL
Datum zagovora: 31. 5. 2021

Jerneja ERHATIČ
Mentor: doc. dr. Andrej Pevec
SVINČEVE KOORDINACIJSKE SPOJINE Z NEKATERIMI TIOSEMIKARBAZIDI KOT LIGANDI
Datum zagovora: 7. 6. 2021

Mojca GRIŽNIK
Mentorica: znan. svet. dr. Barbara Malič
Somentorica: izr. prof. dr. Romana Cerc Korošec
ŠTUDIJ PRIPRAVE TANKIH PLASTI NATRIJEVEGA NIOBATA S SINTEZO V RAZTOPINI
Datum zagovora: 15. 6. 2021

Petra VIRANT
Mentor: doc. dr. Andrej Pevec
KOORDINACIJSKE SPOJINE Z N-ETOKSIKARBONIL-N'-(3-METILPIRIDIN-2-IL)TIOSEČNINO KOT LIGANDOM
Datum zagovora: 16. 6. 2021

Blaž SLABAJNA
Mentor: prof. dr. Robert Dominko
ELEKTROKEMIJSKA POLARIZACIJA MAGNEZIJEVE ANODE
Datum zagovora: 17. 6. 2021

Žan GOSTENČNIK
Mentor: izr. prof. dr. Janez Cerkovnik
SINTEZA KLEŠČASTIH LIGANDOV IN NJIHOVIH KOMPLEKSOV S KOVINAMI PREHODA
Datum zagovora: 17. 6. 2021

Deja ŠELIH
Mentor: prof. dr. Matevž Pompe
NADZOR KVALITETE IN STABILNOSTI IZDELKOV IZ NARAVNIH IN SINTETIČNIH KANABINOIDOV
Datum zagovora: 22. 6. 2021

Svit ŠMAJDEK
Mentor: izr. prof. dr. Drago Kočar
DOLOČITEV HLAPNIH KOMPONENT V MEDU Z GC-MS
Datum zagovora: 29. 6. 2021

Mariša KADIVEC
Mentorica: prof. dr. Irena Kralj Cigić
VPLIV NEVODNIH POSTOPKOV RAZKISLINJENJA Z NANO ALI MIKRO DELCI NA STABILNOST PAPIRJA
Datum zagovora: 5. 7. 2021

Eva KORENČIČ
Mentorica: prof. dr. Helena Prosen
SPREMLJANJE PRODUKTOV ELEKTROKEMIJSKE RAZGRADNJE BENZOTRIAZOLA
Datum zagovora: 5. 7. 2021

Aleksandar DJURDJEVIĆ
Mentor: prof. dr. Franc Požgan
PREUČEVANJE KATALITSKIH LASTNOSTI KOVINSKIH KOMPLEKSOV S HEKSAARILBENZENSKIMI LIGANDI
Datum zagovora: 5. 7. 2021

Neža LUPŠINA
Mentorica: prof. dr. Urška Lavrenčič Štangar
ELEKTROKEMIJSKO MODELIRANJE IN SIMULIRANJE LITIJ IONSKE BATERIJE
Datum zagovora: 6. 7. 2021

Ana PENKO
Mentorica: prof. dr. Irena Kralj Cigić
OPTIMIZACIJA EKSTRAKCIJE PROTEINOV ZA DETEKCIJO Z ENCIMSKOIMUNSKIM TESTOM (ELISA) V MODELNIH VZORCIH PROTEINSKIH BARV
Datum zagovora: 6. 7. 2021

Jan LOČNIŠKAR
Mentor: doc. dr. Črtomir Podlipnik
MOLEKULSKO MODELIRANJE INTERAKCIJ BCL-2 PROTEINOV IN PROTEINA E IZ VIRUSA SARS-CoV-2
Datum zagovora: 8. 7. 2021

Nejc KOLMAN
Mentor: izr. prof. dr. Janez Cerar
REOLOŠKE LASTNOSTI VODNIH RAZTOPIN IZBRANIH SOLI POLIALILAMINA
Datum zagovora: 13. 7. 2021

Mojca BAVČAR
Mentor: prof. dr. Matevž Pompe
VPLIV TEMPERATURE NA LOČBO BIOLOŠKIH MAKROMOLEKUL
Datum zagovora: 18. 8. 2021

Aljaž ŠINKOVEC
Mentor: doc. dr. Krištof Kranjc
SINTEZA RAZLIČNO SUBSTITUIRANIH BICIKLO[2.2.2]OKTENSKIH SISTEMOV Z UPORABO MALEINANHIDRIDA IN NJEGOVIH DERIVATOV
Datum zagovora: 31. 8. 2021

Uroš RAPUŠ
Mentor: doc. dr. Jakob Kljun
SINTEZA 4-HETEROARIL SUBSTITUIRANIH PIRIMIDINOV IN NJIHOVIH KOORDINACIJSKIH SPOJIN
Datum zagovora: 31. 8. 2021

Martin LJUBIČ
Mentor: znan. svet. dr. Jože Grdadolnik
Somentor: prof. dr. Jurij Lah
ŠTUDIJ MEHANIZMA TOPLOTNE IN KEMIČNE DENATURACIJE MODELNIH PROTEINOV S POMOČJO FTIR SPEKTROSKOPIJE
Datum zagovora: 2. 9. 2021

Peter OGRIN
Mentor: prof. dr. Tomaž Urbič
OBRAVNAVA PREPROSTEGA DVO-DIMENZIONALNEGA MODELA VODE S TEORIJO INTEGRALSKIH ENAČB IN TERMODINAMIČNO PERTURBACIJSKO TEORIJO
Datum zagovora: 2. 9. 2021

Mišel HOZJAN
Mentor: izr. prof. dr. Uroš Grošelj
UPORABA TETRAMSKIH KISLIN KOT IZHODNIH SUBSTRATOV V ORGANOKATALIZIRANIH PRETVORBAH
Datum zagovora: 3. 9. 2021

Vid RAVNIK
Mentor: izr. prof. dr. Miha Lukšič
MODELIRANJE VODE S POTENCIALOM CENTRALNE SILE V UTESNJENEM OKOLJU
Datum zagovora: 7. 9. 2021

Valentine DESTARKEET
Mentor: prof. dr. Miran Gaberšček
ADVANCED STRUCTURAL, CHEMICAL AND ELECTROCHEMICAL CHARACTERIZATION OF SODIUM LAYERED CATHODE
Datum zagovora: 13. 9. 2021

Luisa Larissa Arnaldo GOMES
Mentor: izr. prof. dr. Boštjan Genorio
FORMULATION OF FDM PRINTABLE POSITIVE ELECTRODE FILAMENT FOR Li-ion BATTERY
Datum zagovora: 13. 9. 2021

Aleksandra SUWALA
Mentor: izr. prof. dr. Mitja Kolar
CHEMICAL, PHYSICAL AND ELECTROCHEMICAL PROPERTIES OF ELECTROLYTE FOR SODIUM-ION BATTERIES
Datum zagovora: 13. 9. 2021

Armando AVILA CARDENAS
Mentor: izr. prof. dr. Boštjan Genorio
TOWARD THE FABRICATION OF A NASICON BASED ALL-SOLID-STATE BATTERY WORKING AT ROOM TEMPERATURE
Datum zagovora: 14. 9. 2021

Boluwatife IGBAROOLA
Mentor: prof. dr. Robert Dominko
DEVELOPMENT OF INDENTATION IN-SITU IN A SCANNING ELECTRON MICROSCOPE TO PROBE MECHANICAL PROPERTY EVOLUTION OF HARD CARBONS FOR SODIUM-ION BATTERIES.
Datum zagovora: 14. 9. 2021

David MATOH
Mentor: prof. dr. Matevž Pompe
DOLOČANJE FAKTORJEV OBČUTLJIVOSTI SORODNIH SUBSTANC AKTIVNIH FARMACEVTSKIH UČINKOVIN
Datum zagovora: 15. 9. 2021

Ana GORENC
Mentor: izr. prof. dr. Uroš Grošelj
UPORABA PIROLON VSEBUJOČIH SUBSTRATOV V ORGANOKATALIZIRANIH REAKCIJAH
Datum zagovora: 23. 9. 2021

Nik MASELJ
Mentor: izr. prof. dr. Jernej Iskra
Somentor: znan. sod. dr. Primož Jovanovič
ELEKTROKEMIJSKA SINTEZA HIPERVALENTNIH JODOVIH(I) SPOJIN
Datum zagovora: 27. 9. 2021

Jana KRUŠIČ
Mentor: prof. dr. Marjan Jereb
SINTEZA FLUORIRANIH SULFIDOV IN NEKATERE NJIHOVE PRETVORBE
Datum zagovora: 28. 9. 2021

David CIRIKOVIĆ
Mentor: izr. prof. dr. Miha Lukšič
MODELIRANJE VEZAVE ANTIRETROVIRUSNIH SPOJIN S HIV-1 INTEGRAZO IN REVERZNO TRANSKRIPTAZO
Datum zagovora: 28. 9. 2021

Eva KREJAN
Mentorica: prof. dr. Urška Lavrenčič Štangar
OPTIMIZACIJA DELOVNE ELEKTRODE V SONČNIH CELICAH ZA UPORABO BARVIL IZ INVAZIVNIH RASTLIN
Datum zagovora: 29. 9. 2021

Matic ROGAN
Mentor: prof. dr. Marjan Jereb
SINTEZA IN PRETVORBE IZBRANIH SUBSTITUIRANIH ALKINOV
Datum zagovora: 29. 9. 2021

David ZORKO
Mentor: izr. prof. dr. Mitja Kolar
DOLOČANJE VSEBNOSTI KOVIN IN PEKTINA V MOŠTU MED ALKOHOLNO FERMENTACIJO
Datum zagovora: 30. 9. 2021

Meta VRABEC
Mentor: prof. dr. Marjan Jereb
PRETVORBE A-OKSOKETEN DITIOACETALOV V PRISOTNOSTI JODA
Datum zagovora: 30. 9. 2021

Meta Špela KODERMAC
Mentor: prof. dr. Bogdan Štefane
OPTIMIZACIJA GRAFTIRANJA IN FUNKCIONALIZACIJE MONOLITNIH KROMATOGRAFSKIH NOSILCEV ZA UČINKOVITO IZOLACIJO PLAZMIDNE DNA
Datum zagovora: 1. 10. 2021

Klara KOČEVAR
Mentor: izr. prof. dr. Drago Kočar
DOLOČEVANJE FITINSKE KISLINE IN ŽELEZA V STROČNICAH
Datum zagovora: 4. 10. 2021

Klemen COTMAN
Mentor: doc. dr. Bojan Kozlevčar
SINTEZA IN KARAKTERIZACIJA BAKROVIH, NIKLJEVIH IN KOBALTOVIH SPOJIN Z ANIONI CITRONSKE KISLINE
Datum zagovora: 6. 10. 2021

Eva POGORELC
Mentorica: prof. dr. Marija Bešter Rogač
Somentor: prof. dr. Slobodan Gadžurić
TOKSIČNOST POVRŠINSKO AKTIVNIH SNOVI
Datum zagovora: 29. 10. 2021

Jernej IMPERL
Mentor: izr. prof. dr. Mitja Kolar
DOLOČEVANJE IN ODSTRANJEVANJE TEŽKIH KOVIN IZ REČNIH SEDIMENTOV
Datum zagovora: 2. 11. 2021

Aleksander KRAVOS
Mentorica: prof. dr. Helena Prosen
Somentorica: izr. prof. dr. Gabriela Kalčikova
KEMIJSKO IN EKOTOKSIKOLOŠKO SPREMLJANJE INDUCIRANIH IN NARAVNIH ABIOTSKIH RAZKROJNIH PROCESOV FENOLNIH ONESNAŽEVAL
Datum zagovora: 8. 11. 2021

Vasja VALETIČ
Mentor: viš. znan. sod. dr. Vasko Jovanovski
Somentorica: prof. dr. Urška Lavrenčič Štangar
SINTEZA IN UPORABA NANOSTRUKTURIRANEGA IRIDIJA ZA ELEKTROKEMIJSKO DETEKCIJO PEROKSO ZVRSTI
Datum zagovora: 12. 11. 2021

Martin TUŠEK
Mentor: izr. prof. dr. Miha Lukšič
TEORETIČNI PRISTOPI K ŠTUDIJU ELEKTROSTATSKIH LASTNOSTI GLOBULARNIH PROTEINOV
Datum zagovora: 26. 11. 2021

Samo KREVS
Mentor: prof. dr. Franc Požgan
RAZISKAVA PRETVORBE 2-HALOPIRIDINOV POD POGOJI KATALIZE S KOVINAMI PREHODA
Datum zagovora: 22. 12. 2021

MAGISTRSKI ŠTUDIJSKI PROGRAM 2. STOPNJE – KEMIJSKO INŽENIRSTVO

Ožbej BIZJAK
Mentor: prof. dr. Aleš Podgornik
VPLIV STRUKTURE POLIHIPE MATERIALOV NA NJIHOVE HIDRODINAMSKE LASTNOSTI
Datum zagovora: 13. 1. 2021

Elena SPASEVSKA
Mentor: izr. prof. dr. Boštjan Genorio
ELEKTROKEMIJSKE MERITVE LI-S AKUMULATORJEV IN KARAKTERIZACIJA PRIPRAVLJENIH KATOD
Datum zagovora: 20. 1. 2021

Neva IHANEC
Mentor: prof. dr. Robert Dominko
OGLJIKI SINTETIZIRANI IZ KAVNIH USEDLIN KOT ANODNI MATERIAL V Na-IONSKIH AKUMULATORJIH
Datum zagovora: 20. 1. 2021

Jošt HERMAN
Mentor: izr. prof. dr. Boštjan Genorio
KEMIJSKA IN ELEKTROKEMIJSKA ANALIZA KOMERCIALNIH LITIJ-IONSKIH BATERIJSKIH CELIC
Datum zagovora: 20. 1. 2021

Petra PRIVŠEK
Mentorica: doc. dr. Lidija Slemenik Perše
REOLOŠKE IN ČASOVNO ODVISNE MEHANSKE LASTNOSTI POLIMERNO-LESNIH KOMPOZITOV Z VISOKIM DELEŽEM LESNE MOKE
Datum zagovora: 22. 1. 2021

Matic ZIBELNIK
Mentorica: prof. dr. Andreja Žgajnar Gotvajn
UPORABA LIGNINOLITIČNIH ENCIMOV ZA RAZGRADNJO ORGANSKEGA ONESNAŽENJA V ODPADNIH VODAH
Datum zagovora: 11. 2. 2021

Rok NOVAK
Mentor: prof. dr. Marjan Marinšek
Somentorica: prof. dr. Violeta Bokan Bosiljkov
SAMOOBNOVA BETONA Z DOLOMITNIM AGREGATOM ZARADI PROCESA ALKALNO KARBONATNE REAKCIJE
Datum zagovora: 25. 2. 2021

Andreja PETROVIĆ
Mentorica: prof. dr. Polona Žnidaršič Plazl
BIOTEHNOLOŠKA PROIZVODNJA LAKAZ IN NJIHOVA UPORABA PRI RAZVOJU MIKROBIOSENZORJA
Datum zagovora: 3. 3. 2021

Aleksandar BLAGOJEVIĆ
Mentor: prof. dr. Robert Dominko
OPTIMIZACIJA ELEKTROKEMIJSKIH LASTNOSTI V PHBQS/CNT NANOKOMPOZITIH
Datum zagovora: 4. 3. 2021

Lucija POLAK
Mentorica: izr. prof. dr. Gabriela Kalčikova
UPORABA RAZLIČNIH METOD ZA ČIŠČENJE TEKSTILNIH ODPADNIH VOD
Datum zagovora: 31. 3. 2021

Leon OSTANEK JURINA
Mentorica: prof. dr. Polona Žnidaršič Plazl
RAZVOJ MIKROFLUIDNE PLATFORME ZA PRIPRAVO IN ANALIZO MIKROKAPLJIC
Datum zagovora: 12. 5. 2021

Alen ŠTROS
Mentor: prof. dr. Igor Plazl
NEVTRALIZACIJA ODPADNIH MEŠANIH ANORGANSKIH KISLIN Z APNENO SUSPENZIJO V INDUSTRIJSKEM MEŠALNEM REAKTORJU
Datum zagovora: 21. 5. 2021

Alenka FAJS
Mentorica: izr. prof. dr. Gabriela Kalčikova
OVREDNOTENJE UČINKOVITOSTI LABORATORIJSKE RASTLINSKE ČISTILNE NAPRAVE ZA ČIŠČENJE KOMUNALNIH ODPADNIH VODA
Datum zagovora: 3. 6. 2021

Anže ZALAR
Mentor: prof. dr. Robert Dominko
ELEKTROKEMIJA ULTRAMIKROPOROZNIH OGLJIKOV V Li- S AKUMULATORJIH
Datum zagovora17. 6. 2021

Silvo KOMATAR
Mentor: prof. dr. Igor Plazl
IMPLEMENTACIJA REOMETRIJE V MIKROKANALU IN ISKANJE PARAMETROV ZA NAPOVED VISKOZNOSTI PROTEINSKIH FORMULACIJ
Datum zagovora: 22. 6. 2021

Luka SKUBIC
Mentorica: prof. dr. Urška Šebenik
KOMPOZITNI HIDROGELI TEMPO MODIFICIRANE NANOCELULOZE Z DODATKOM GRAFENA
Datum zagovora: 5. 7. 2021

Tilen PILPAH
Mentorica: prof. dr. Polona Žnidaršič Plazl
RAZVOJ IN MATEMATIČNI OPIS MINIATURIZIRANEGA PRETOČNEGA SISTEMA ZA LOČEVANJE PRODUKTOV BIOKATALITSKE TRANSAMINACIJE
Datum zagovora: 9. 7. 2021

Teja ANTONČIČ
Mentorica: prof. dr. Andreja Žgajnar Gotvajn
OPTIMIZACIJA PROCESOV OZONACIJE ZA RAZGRADNJO ANTIBIOTIKOV
Datum zagovora: 9. 7. 2021

Žiga VIDRIH
Mentor: prof. dr. Marjan Marinšek
Somentor: znan. sod. dr. Ivan Jerman
MODIFIKACIJA SPEKTRALNO SELEKTIVNIH ABSORBERSKIH PREMAZOV NEODVISNIH OD DEBELINE ZA UČINKOVITEJŠO PRETVORBO SONČNE ENERGIJE V TOPLOTO
Datum zagovora: 16. 7. 2021

Anja VEHAR
Mentorica: prof. dr. Andreja Žgajnar Gotvajn
Somentorica: znan. svet. dr. Ester Heath
SPREMLJANJE UČINKOVITOSTI ODSTRANJEVANJA BISFENOLOV IZ ODPADNE VODE V KOMUNALNI ČISTILNI NAPRAVI
Datum zagovora: 8. 9. 2021

Blaž JAKLIČ
Mentor: doc. dr. Matjaž Spreitzer
Somentor: prof. dr. Marjan Marinšek
SINTEZA IN KARAKTERIZACIJA Li-Mn OKSIDOV ZA KATODNE MATERIALE V LITIJ-IONSKIH AKUMULATORJIH
Datum zagovora: 8. 9. 2021

Jan ŽUNTAR
Mentor: prof. dr. Miran Gaberšček
IMPEDANČNA SPEKTROSKOPIJA KATODNIH MATERIALOV NMC 811
Datum zagovora: 13. 9. 2021

Mark KOZAMERNIK
Mentor: izr. prof. dr. Boštjan Genorio
MEMBRANE NA OSNOVI GRAFENA ZA UPORABO V ETANOLNIH GORIVNIH CELICAH
Datum zagovora: 16. 9. 2021

Maša ARNŠEK
Mentor: prof. dr. Aleš Podgornik
HIDROTERMALNA SINTEZA KOSITROVEGA DIOKSIDA
Datum zagovora: 16. 9. 2021

Mark SMERDU
Mentor: prof. dr. Aleš Podgornik
HIDROTERMALNA SINTEZA NIOBIJEVEGA DIOKSIDA
Datum zagovora: 16. 9. 2021

Erik GREGORI
Mentor: izr. prof. dr. Boštjan Genorio
Somentor: znan. svet. dr. Anton Kokalj
MOLEKULSKO MODELIRANJE PREPUSTNOSTI INTRINZIČNIH TOČKOVNIH DEFEKTOV V GRAFENU ZA DIFUZIJO PREPROSTIH PLINOV.
Datum zagovora: 16. 9. 2021

Borut ŠKETA
Mentorica: prof. dr. Polona Žnidaršič Plazl
IMOBILIZACIJA TRANSAMINAZ NA PREPLETENA NANOVLAKNA V MIKROREAKTORJIH
Datum zagovora: 23. 9. 2021

Karmen PIRC
Mentor: prof. dr. Igor Plazl
VREDNOTENJE VPLIVA PROCESA MLETJA NA LASTNOSTI IZTISKANCA, IZDELANEGA S TEHNOLOGIJO IZTISKANJA TALIN
Datum zagovora: 28. 9. 2021

Klemen MOTALN
Mentor: prof. dr. Igor Plazl
ENCIMSKA MIKROKINETIKA V MIKROKANALU Z IMOBILIZIRANIM ENCIMOM V SLOJU GELA
Datum zagovora: 29. 9. 2021

Ajda RUS
Mentor: izr. prof. dr. Boštjan Genorio
ŠTUDIJ VPLIVA POLIMERNIH FUNKCIJSKIH DODATKOV NA APLIKACIJSKE LASTNOSTI KATAFOREZNEGA EPOKSI TEMELJNEGA PREMAZA
Datum zagovora: 15. 10. 2021

Miha KRAGELJ
Mentor: prof. dr. Marjan Marinšek
DODAJANJE ODPADNEGA PREMOGA IN ŽELEZOVE RUDE V SUROVINSKO MEŠANICO ZA PROIZVODNJO OPEČNIH IZDELKOV
Datum zagovora: 15. 10. 2021

Leja ZALETEL
Mentor: prof. dr. Robert Dominko
POLIMERNE PREVLEKE NA NMC KATODNEM MATERIALU
Datum zagovora: 20. 10. 2021

Eva ROVŠEK
Mentorica: prof. dr. Andreja Žgajnar Gotvajn
ZMANJŠEVANJE EMISIJ ANTIBIOTIKOV IZ ODPADNEGA BLATA Z OZONACIJO
Datum zagovora: 22. 10. 2021

Ana ČUJEŠ
Mentorica: prof. dr. Urška Šebenik
KARAKTERIZACIJA TEMPO MODIFICIRANIH NANOCELULOZNIH HIDROGELOV IN VPLIV NJIHOVE STRUKTURE NA HITROST SPROŠČANJA NIKOTINA V VODI
Datum zagovora: 22. 10. 2021

Špela KAPŠ
Mentorica: prof. dr. Andreja Žgajnar Gotvajn
KARAKTERIZACIJA BIOOGLJA ZA UPORABO V KMETIJSTVU
Datum zagovora: 3. 11. 2021

Elfi BIRSA
Mentor: prof. dr. Aleš Podgornik
TVORBA IN KARAKTERIZACIJA E. COLI BIOFILMOV V KONTINUIRNEM SISTEMU
Datum zagovora: 2. 12. 2021

Petra BAJEC
Mentorica: izr. prof. dr. Gabriela Kalčikova
MODIFIKACIJA ZLATIH IN OGLJIKOVIH ELEKTROD Z MEZOPOROZNO SILIKO IN AMINOKISLINAMI ZA ADSORPCIJO IN ELEKTROKEMIJSKO DETEKCIJO MIKROPLASTIKE
Datum zagovora: 7. 12. 2021

Matjaž ŠKEDELJ
Mentorica: prof. dr. Andreja Žgajnar Gotvajn
VPLIV OZONIRANJA NA UČINKOVITOST ANAEROBNE OBDELAVE Z ANTIBIOTIKI ONESNAŽENEGA ODPADNEGA AKTIVNEGA BLATA
Datum zagovora: 7. 12. 2021

Jan ZUPANČIČ
Mentorica: prof. dr. Polona Žnidaršič Plazl
RAZVOJ KONTINUIRNEGA PROCESA SINTEZE FARMACEVTSKEGA INTERMEDIATA V MIKROPRETOČNEM SISTEMU
Datum zagovora: 13. 12. 2021

Luka GORŠE
Mentor: izr. prof. dr. Aleš Ručigaj
KATIONSKA FUNKCIONALIZACIJA NANOCELULOZNIH VLAKEN ZA PRIPRAVO PH ODZIVNIH HIDROGELOV Z USTREZNIMI REOLOŠKIMI LASTNOSTMI
Datum zagovora: 17. 12. 2021

MAGISTRSKI ŠTUDIJSKI PROGRAM 2. STOPNJE – BIOKEMIJA

Urška KAŠNIK
Mentorica: izr. prof. dr. Nina Vardjan
Somentor: prof. dr. Einar Hallberg
VLOGA TRANSMEMBRANSKEGA PROTEINA JEDRNE OVOJNICE, SAMP1, PRI ORGANIZACIJI KROMATINA, DIFERENCIACIJI IN BOLEZNI
Datum zagovora: 15. 2. 2021

Natalija PUCIHAR
Mentorica: izr. prof. dr. Alja Videtič Paska
DOLOČANJE METILACIJE DNA GENA SLC6A4 PRI ŽRTVAH SAMOMORA S TEHNOLOGIJO SEKVENCIRANJA NASLEDNJE GENERACIJE
Datum zagovora: 22. 2. 2021

Jošt HOČEVAR
Mentor: doc. dr. Miha Pavšič
LIGAND-VEZAVNE LASTNOSTI HIDROFOBNEGA ŽEPA EpCAM IN NJEGOV VPLIV NA REGULIRANO INTRAMEMBRANSKO CEPITEV
Datum zagovora: 3. 3. 2021

Milena STOJKOVSKA
Mentor: izr. prof. dr. Marko Novinec
IDENTIFIKACIJA ČLOVEŠKIH CITOPLAZEMSKIH PROTEINOV, KI INTERAGIRAJO Z DVEMA DERIVATOMA PIRAZOLA
Datum zagovora: 21. 4. 2021

Ana OBAHA
Mentor: izr. prof. dr. Marko Novinec
PROTEINSKI INŽENIRING OLIGOMERNIH OBLIK KATEPSINA K
Datum zagovora: 25. 5. 2021

Vida ŠTRANCAR
Mentorica: doc. dr. Marina Klemenčič
BIOKEMIJSKA KARAKTERIZACIJA IN PRIMERJAVA LASTNOSTI TREH IZBRANIH REKOMBINANTNO IZRAŽENIH METAKASPAZ IZ ORGANIZMOV CHLAMYDOMONAS REINHARDTII IN GUILLARDIA THETA
Datum zagovora: 23. 6. 2021

Valentina NOVAK
Mentorica: doc. dr. Vera Župunski
VPLIV MALIH NEKODIRAJOČIH RNA IZ SKUPINE YRNA IN VTRNA NA RETROTRANSPOZICIJO LINE1
Datum zagovora: 2. 7. 2021

Elvira BORŠIĆ
Mentorica: viš. znan. sod. dr. Iva Hafner Bratkovič
Somentor: doc. dr. Gregor Gunčar
VPLIV KALIJEVIH IONOV IN VRSTE OLIGOMERA NLRP3 NA AKTIVACIJO INFLAMASOMA
Datum zagovora: 9. 7. 2021

Neža GAUBE
Mentor: prof. ddr. Boris Turk
VPLIV ODSOTNOSTI STEFINA B IN ANTIOKSIDANTOV NA OKSIDATIVNI STRES PRI PRIMARNIH MIŠJIH PyMT RAKAVIH CELICAH
Datum zagovora: 9. 7. 2021

Alen ŠADL
Mentor: prof. dr. Janez Plavec
NMR ŠTUDIJA S PURINI BOGATIH TANDEMSKIH PONOVITEV POVEZANIH S KOLAPSOM REPLIKACIJSKIH VILIC
Datum zagovora: 15. 7. 2021

Marina FILIPOVIĆ
Mentor: prof. dr. Gregor Anderluh
Somentorica: prof. dr. Brigita Lenarčič
OPREDELITEV VPLIVA IZBRANIH AMINOKISLINSKIH ZAMENJAV V HOLESTEROL-VEZAVNI DOMENI PERFRINGOLIZINA O
Datum zagovora: 27. 8. 2021

Jerneja SENICA
Mentor: prof. ddr. Boris Turk
VPLIV CISTATINA C IN STEFINA B NA PRISOTNOST MAKROFAGOV PRI MIŠJEM MODELU RAKA MLEČNE ŽLEZE MMTV-PyMT
Datum zagovora: 1. 9. 2021

Iza OBLAK
Mentorica: doc. dr. Vera Župunski
AGREGACIJSKE ŠTUDIJE PROTEINA ANEKSIN A11 TER NJEGOVIH MUTANTOV D40G IN Δ119
Datum zagovora: 1. 9. 2021

Anja KOBALE
Mentor: znan. svet. dr. Dušan Turk
Somentor: izr. prof. dr. Marko Dolinar
PRIMERJAVA METOD ZA OPTIMIZACIJO PREDKRISTALIZACIJSKIH POGOJEV PROTEINOV NA PRIMERU LIZOCIMA
Datum zagovora: 2. 9. 2021

Eva RAJH
Mentorica: doc. dr. Mojca Benčina
Somentor: doc. dr. Gregor Gunčar
OPTIMIZACIJA REAKCIJE RT-LAMP ZA DETEKCIJO SARS-CoV-2 V SLINI.
Datum zagovora: 2. 9. 2021

Andreja HABIČ
Mentor: doc. dr. Miha Pavšič
KARAKTERIZACIJA, OPTIMIZACIJA IN DOKAZ DELOVANJA SISTEMA ZA ODKRIVANJE INTERAKCIJSKIH PARTNERJEV DNA NA OSNOVI OZNAČEVANJA BLIŽNJIH MOLEKUL Z BIOTINOM
Datum zagovora: 2. 9. 2021

Mia ŽGANJAR
Mentor: prof. dr. Uroš Petrovič
POTRDITEV NOVIH INTERAKTORJEV VARIANT PROTEINA PIG1 KVASOVKE SACCHAROMYCES CEREVISIAE
Datum zagovora: 6. 9. 2021

Nina KOBE
Mentorica: prof. dr. Kristina Gruden
Somentor: izr. prof. dr. Marko Dolinar
OPTIMIZACIJA METODOLOGIJE ZA PROUČEVANJE AKTIVNOSTI PROMOTORJEV V KROMPIRJU
Datum zagovora: 7. 9. 2021

Kity POŽEK
Mentor: prof. dr. Igor Križaj
Somentorica: doc. dr. Vera Župunski
IZOLACIJA IN KARAKTERIZACIJA PROTEINA VAAMPIII-3 IZ MODRASOVEGA STRUPA
Datum zagovora: 8. 9. 2021

Tjaša SORČAN
Mentorica: prof. dr. Damjana Rozman
UGOTAVLJANJE KORELACIJE MED TRDNOSTJO CELIC IN MUTACIJAMI V KERATINIH V ČLOVEŠKIH KERATINOCITIH
Datum zagovora: 8. 9. 2021

Špela KOREN
Mentor: znan. sod. dr. Toni Petan
Somentorica: doc. dr. Marina Klemenčič
POVEZAVE MED LIPIDNIMI KAPLJICAMI IN AVTOFAGIJO V RAKAVIH CELICAH, IZPOSTAVLJENIH STRESU
Datum zagovora: 13. 9. 2021

Maksimiljan ADAMEK
Mentorica: izr. prof. dr. Marjetka Podobnik
Somentor: doc. dr. Miha Pavšič
STRUKTURNA IN FUNKCIJSKA PRIMERJAVA HOMOLOGOV ŠIROKOSPECIFIČNE FOSFOLIPAZE C IZ BAKTERIJE LISTERIA MONOCYTOGENES TER KARAKTERIZACIJA NJENE PROOBLIKE
Datum zagovora: 22. 9. 2021

David TITOVŠEK
Mentorica: prof. dr. Kristina Djinović Carugo
KONFORMACIJSKE SPREMEMBE ČLOVEŠKEGA A-AKTININA-1 OB VEZAVI KALCIJEVIH IONOV
Datum zagovora: 22. 9. 2021

Tanja ZUPAN
Mentorica: znan. sod. dr. Jerica Sabotič
Somentor: doc. dr. Gregor Gunčar
VPLIV KOKAPRINA IN MAKROCIPINA NA BIOFILM LISTERIJ
Datum zagovora: 30. 9. 2021

Petra HRUŠEVAR
Mentor: znan. sod. dr. Toni Petan
Somentor: izr. prof. dr. Marko Novinec
DINAMIKA TVORBE IN RAZGRADNJE LIPIDNIH KAPLJIC PRI METABOLIČNEM STRESU V RAKAVIH CELICAH
Datum zagovora: 8. 10. 2021

Roberta MULAC
Mentor: prof. dr. Peter Dovč
ANALIZA KANDIDATNIH REGIJ ZA EKTOPIČNI URETER V PASJEM GENOMU
Datum zagovora: 12. 10. 2021

Tina TUREL
Mentorica: izr. prof. dr. Nataša Debeljak
VPLIV NEKODIRAJOČIH REGULATORNIH REGIJ GENOV VKLJUČENIH V ERITROPOEZO NA RAZVOJ PRIROJENIH ERITROCITOZ
Datum zagovora: 3. 11. 2021

Patricija MIKLAVC
Mentor: doc. dr. Gregor Gunčar
BIOKOMPATIBILNI MAGNETNI NANODELCI KOT KONTRASTNA SREDSTVA ZA SLIKANJE Z MAGNETNO RESONANCO S PREVLEKO NA OSNOVI LIPOSOMOV IN ERITROCITNIH MEMBRAN
Datum zagovora: 16. 11. 2021

Jerneja NIMAC
Mentorica: doc. dr. Vera Župunski
PROTEINSKE INTERAKCIJE ČLOVEŠKEGA MATRINA 3
Datum zagovora: 30. 11. 2021

Benjamin MALOVRH
Mentor: prof. dr. Roman Jerala
Somentor: prof. dr. Janez Plavec
NAČRT IN KARAKTERIZACIJA INDUCIBILNE DIMERIZACIJE SVEŽNJA ŠTIRIH VIJAČNIC V SESALSKI CELIČNI LINIJI HEK293T
Datum zagovora: 17. 12. 2021

Ajda LENARDIČ
Mentorica: doc. dr. Vera Župunski
PRIPRAVA, GENSKI INŽENIRING IN KARAKTARIZACIJA CELIC ZA POVRNITEV IZRAŽANJA DISTROFINA V MIŠJEM MODELU DUCHENNOVE MIŠIČNE DISTROFIJE
Datum zagovora: 17. 12. 2021

Bor KLANČNIK
Mentor: prof. ddr. Boris Turk
KARAKTERIZACIJA BIOLUMINISCENČNE SONDE ZA GRANCIM B
Datum zagovora: 21. 12. 2021

MAGISTRSKI ŠTUDIJSKI PROGRAM 2. STOPNJE – TEHNIŠKA VARNOST

Anže HEINDLER
Mentorica: doc. dr. Barbara Novosel
PRIMERJAVA ORODIJ ZA SIMULACIJO NENADZOROVANEGA SPROŠČANJA PLINOV V OKOLICO
Datum zagovora: 18. 2. 2021

Tina LESJAK
Mentorica: doc. dr. Klementina Zupan
ERGONOMSKA ANALIZA DELOVNEGA MESTA V PODJETJU TALUM D.D. KIDRIČEVO
Datum zagovora: 23. 2. 2021

Loti BRUS
Mentor: prof. dr. Matevž Pompe
OCENA TVEGANJA NA DELOVNEM MESTU RAZVIJALCA ANALIZNIH METOD
Datum zagovora: 23. 2. 2021

Tajda BULOVEC
Mentor: izr. prof. dr. Simon Schnabl
UČINKOVITOST HEPTAFLUOROPROPANA PRI GAŠENJU POŽAROV Z ELEKTRO IZVOROM
Datum zagovora: 3. 3. 2021

Peter VIRŠEK
Mentorica: doc. dr. Barbara Novosel
OBVLADOVANJE TVEGANJA PRI OBRATOVANJU TERMINALOV UTEKOČINJENEGA ZEMELJSKEGA PLINA
Datum zagovora: 4. 3. 2021

Tina BREZAR
Mentor: izr. prof. dr. Luka Tičar
POMEN INŽENIRJA TEHNIŠKE VARNOSTI V DELOVNEM PROCESU
Datum zagovora: 17. 3. 2021

Anja MORAN
Mentor: izr. prof. dr. Simon Schnabl
VPLIV USPOSABLJANJA NA ZNANJE O POŽARNI VARNOSTI ZAPOSLENIH
Datum zagovora: 20. 4. 2021

Špela KRZNARIČ
Mentor: izr. prof. dr. Simon Schnabl
ANALIZA ZNANJA IZ VARSTVA PRED POŽAROM ZAPOSLENIH V ZDRAVILIŠČU
Datum zagovora: 3. 5. 2021

Matej VESEL
Mentorica: doc. dr. Klementina Zupan
PROUČEVANJE ERGONOMSKE UREDITVE PROSTOROV NA FAKULTETI UNIVERZE V LJUBLJANI
Datum zagovora: 14. 5. 2021

Miha PIRC
Mentor: doc. dr. Mitja Robert Kožuh
ANALIZA STANJA PREPREČEVANJA VEČJIH INDUSTRIJSKIH NESREČ V PREMAZNI INDUSTRIJI
Datum zagovora: 7. 7. 2021

Laura BOROŠ
Mentorica: doc. dr. Klementina Zupan
ANALIZA TVEGANJ SUŠ IN POPLAV
Datum zagovora: 5. 7. 2021

Peter KOČMAN
Mentor: izr. prof. dr. Simon Schnabl
Somentor: prof. dr. Robert Dominko
VARNOST LITIJ-IONSKIH BATERIJ
Datum zagovora: 8. 7. 2021

Laura HRKA
Mentorica: doc. dr. Klementina Zupan
ERGONOMIJA ŠOLAJOČE POPULACIJE
Datum zagovora: 11. 10. 2021

David KLANČIŠAR
Mentor: izr. prof. dr. Boštjan Genorio
RECIKLAŽA Li-Ion AKUMULATORJEV NA OSNOVI NMC KATOD
Datum zagovora: 15. 10. 2021

Tina BESAL
Mentorica: doc. dr. Barbara Novosel
OCENJEVANJE TVEGANJ PRI TRANSPORTU IN SKLADIŠČENJU METANOLA IN METANALA
Datum zagovora: 3. 11. 2021

Jan LIPOVŠEK
Mentor: izr. prof. dr. Simon Schnabl
ANALIZA EVAKUACIJE IN POTEKA POŽARA IZ KOMPLEKSNEGA OBJEKTA S PROGRAMOM PATHFINDER IN PYROSIM
Datum zagovora: 24. 11. 2021

DIPLOME - UNIVERZITETNI ŠTUDIJ

KEMIJA – 1. STOPNJA

Katharina Carola PAVLIN
Mentor: prof. dr. Franc Požgan
SINTEZA HEKSAARILBENZENOV Z DUŠIKOVIMI KOORDINIRAJOČIMI SKUPINAMI
Datum zagovora: 15. 6. 2021

Domen GOSTE
Mentorica: prof. dr. Marija Bešter Rogač
VODA V IONSKIH TEKOČINAH
Datum zagovora: 15. 6. 2021

Ana GOLOB
Mentor: izr. prof. dr. Uroš Grošelj
SINTEZA TETRAMSKE KISLINE IZ Cbz-Gly-OH IN UPORABA V ORGANOKATALIZIRANIH 1,4-ADICIJAH
Datum zagovora: 29. 6. 2021

Jakob HÖFFERLE
Mentor: prof. dr. Janez Košmrlj
SINTEZA IZBRANIH AROMATSKIH IN HETEROAROMATSKIH GEMINALNIH DIBROMOALKENOV
Datum zagovora: 30. 6. 2021

Tilen ZORKO
Mentor: prof. dr. Bogdan Štefane
FOTOKATALITSKE PRETVORBE NEKATERIH 3-(ALKILAMINO)PROPENOATOV
Datum zagovora: 30. 6. 2021

David RIBAR
Mentorica: prof. dr. Irena Kralj Cigić
RAZVOJ MODELA REVERZNO-FAZNIH KROMATOGRAFSKIH SEPARACIJ NA OSNOVI HANSENOVIH PARAMETROV TOPNOSTI
Datum zagovora: 1. 7. 2021

Anže HUBMAN
Mentor: prof. dr. Tomaž Urbič
ŠTUDIJ FOKUSIRANJA DELCEV V MIKROFLUIDNIH SISTEMIH Z UPORABO MREŽNE BOLTZMANNOVE METODE
Datum zagovora: 1. 7. 2021

Simon KEBELJ
Mentor: doc. dr. Krištof Kranjc
REGIOSELEKTIVNOST IN STEREOSELEKTIVNOST CIKLOADICIJ NA PRIMERIH SUBSTITUIRANIH 3-ACILAMINO-2H-PIRAN-2-ONOV
Datum zagovora: 1. 7. 2021

Klara KLEMENČIČ
Mentor: doc. dr. Krištof Kranjc
SINTEZE IN UPORABA 2H-PIRAN-2-ONOV PRI DIELS-ALDERJEVIH REAKCIJAH TER PREGLED ORGANOKATALIZE
Datum zagovora: 1. 7. 2021

Špela POK
Mentorica: prof. dr. Helena Prosen
PREIZKUS EKSTRAKCIJE BENZOTRIAZOLOV IZ TAL Z UPORABO VROČE VODE
Datum zagovora: 6. 7. 2021

Veronika GODEC
Mentor: prof. dr. Matevž Pompe
DOLOČEVANJE N-GLIKANOV Z MASNO SPEKTROMETRIJO
Datum zagovora: 7. 7. 2021

Ana ZIDAR
Mentorica: izr. prof. dr. Romana Cerc Korošec
UPORABA PLASTOVITIH DVOJNIH HIDROKSIDOV ZA ČIŠČENJE VODE
Datum zagovora: 8. 7. 2021

Nika ARTNAK
Mentor: izr. prof. dr. Mitja Kolar
DOLOČANJE pH IN VSEBNOSTI MAKROELEMENTOV V UMETNIH GNOJILIH
Datum zagovora: 8. 7. 2021

Amanda KAČAR
Mentor: izr. prof. dr. Uroš Grošelj
SINTEZA 5-SUBSTITUIRANIH Δ2-PIROLIN-4-ONOV
Datum zagovora: 17. 8. 2021

Sonja MAVRI
Mentor: izr. prof. dr. Drago Kočar
DOLOČANJE KINURENSKE KISLINE V MEDU S TEKOČINSKO KROMATOGRAFIJO Z UV IN FLUORESCENČNO DETEKCIJO
Datum zagovora: 18. 8. 2021

Dimitra ŠKREKOVSKI
Mentor: prof. dr. Bogdan Štefane
SINTEZA OKSALATA MORFOLINOETILETRA MIKOFENOLAT MOFETILA IN ŠTUDIJ KINETIKE NJEGOVE HIDROLIZE V KISLIH IN BAZIČNIH POGOJIH
Datum zagovora: 18. 8. 2021

Gabrijela PLETERSKI
Mentor: prof. dr. Janez Košmrlj
SINTEZA IN OPTIČNE LASTNOSTI NEKATERIH N,N-DIMETIL-4-(PIRIDIL)ANILINOV
Datum zagovora: 24. 8. 2021

Neža KRALJ
Mentor: izr. prof. dr. Mitja Kolar
ANALIZNE METODE V ARHEOLOGIJI
Datum zagovora: 24. 8. 2021

Kaja GLIHA
Mentor: izr. prof. dr. Mitja Kolar
LASTNOSTI GLOBOKIH EVTEKTIČNIH TOPIL IN NJIHOVA UPORABNOST ZA ANALIZO REALNIH VZORCEV
Datum zagovora: 24. 8. 2021

Katarina FABJAN
Mentor: prof. dr. Franc Perdih
VPLIV CINKA IN VITAMINOV NA COVID-19
Datum zagovora: 26. 8. 2021

Anja SEVER
Mentorica: doc. dr. Saša Petriček
3-HIDROKSIPIRIDIN V BAKROVIH KOMPLEKSIH
Datum zagovora: 26. 8. 2021

Lan SKOLIBER
Mentor: doc. dr. Andrej Pevec
KOFEIN KOT LIGAND V KOORDINACIJSKIH SPOJINAH S PLATINO
Datum zagovora: 26. 8. 2021

Teja PELKO
Mentor: doc. dr. Krištof Kranjc
SINTEZA SUBSTITUIRANIH BICIKLO[2.2.2]OKTENOV S CIKLOADICIJAMI MED 2H-PIRAN-2-ONSKIMI DERIVATI IN MALEINANHIDRIDOM TER NADALJNJE PRETVORBE Z DUŠIKOVIMI NUKLEOFILI
Datum zagovora: 30. 8. 2021

Blaž UŽMAH
Mentor: prof. dr. Marjan Jereb
PRETVORBE KARBONILNIH SPOJIN POD ZELENIMI POGOJI
Datum zagovora: 30. 8. 2021

Matej JARC RYDZI
Mentor: prof. dr. Jurij Svete
SINTEZA IMOBILIZIRANE 4-AMINOBENZOJSKE KISLINE IN NJENA UPORABA V PRIPRAVI IMOBILIZIRANIH Cu(II)-ENAMINON KATALIZATORJEV
Datum zagovora: 30. 8. 2021

Anja PEČKAJ
Mentorica: doc. dr. Marta Počkaj
PRIPRAVA IN KARAKTERIZACIJA KOORDINACIJSKIH SPOJIN KOBALTOVEGA(II) NITRATA IN 2-(HIDROKSIMETIL)PIRIDINA
Datum zagovora: 31. 8. 2021

Zala KOŽUH
Mentorica: doc. dr. Saša Petriček
SPOJINE 2-AMINOPIRIDIN-3-OLA S PREHODNIMI KOVINAMI
Datum zagovora: 1. 9. 2021

Petra ŠPORAR
Mentor: prof. dr. Marjan Jereb
NEKATERE PRETVORBE ALILNIH ALKOHOLOV
Datum zagovora: 1. 9. 2021

Marija KOVAČEVIĆ
Mentorica: prof. dr. Helena Prosen
DOLOČANJE ELEMENTNE SESTAVE IN IZOTOPSKEGA RAZMERJA 87Sr/ 86Sr V MEDU
Datum zagovora: 2. 9. 2021

Kristina BOŽIČ
Mentor: izr. prof. dr. Uroš Grošelj
SINTEZA SPOJINE NSC94914 KOT INHIBITORJA AKTIVNOSTI CISTEINSKE PEPTIDAZE KATEPSINA K
Datum zagovora: 2. 9. 2021

Tajda KURET
Mentor: izr. prof. dr. Mitja Kolar
MERJENJE SPROŠČENEGA HEKSANALA IZ MATERIALA Z VISOKO ZMOGLJIVO TEKOČINSKO KROMATOGRAFIJO (HPLC)
Datum zagovora: 2. 9. 2021

Jošt TRUČL
Mentor: izr. prof. dr. Drago Kočar
DOLOČEVANJE KATIONOV IN KATIONSKE KAPACITETE V OGLJU
Datum zagovora: 3. 9. 2021

Tilen ŠIMENKO LALIČ
Mentorica: prof. dr. Helena Prosen
DOLOČITEV FITOESTROGENOV V PIVU S HPLC
Datum zagovora: 3. 9. 2021

Žan ZAKOŠEK
Mentorica: izr. prof. dr. Amalija Golobič
KARAKTERIZACIJA IZBRANE KERAMIKE IZ TERNARNEGA SISTEMA La2O3-Ta2O5-TiO2
Datum zagovora: 3. 9. 2021

Tjaša STOPAR
Mentorica: doc. dr. Nataša Gros
METODE ZA DOLOČANJE SEČNINE
Datum zagovora: 3. 9. 2021

Sara ŠADL
Mentorica: doc. dr. Nataša Gros
DOLOČANJE HLAPNIH SNOVI V MINIATURIZIRANIH IN PRETOČNIH SISTEMIH
Datum zagovora: 3. 9. 2021

Vid KERMELJ
Mentorica: prof. dr. Urška Lavrenčič Štangar
ADSORPCIJA FENITOINA IN OKSITETRACIKLINA NA NANODELCE ZnO
Datum zagovora: 6. 9. 2021

Tine LIKOVIČ
Mentor: izr. prof. dr. Drago Kočar
DOLOČITEV IZBRANIH VITAMINOV IN MINERALOV PREHRANSKEGA DODATKA HERBALIFE NUTRITION
Datum zagovora: 6. 9. 2021

Gregor PUHAR
Mentor: prof. dr. Matevž Pompe
DOLOČEVANJE VEZAVNIH MEST DESNOSUČNIH AMINOKISLIN V PEPTIDIH IN PROTEINIH
Datum zagovora: 6. 9. 2021

Kaja CEGLAR
Mentor: izr. prof. dr. Miha Lukšič
MODELIRANJE STEREOSELEKTIVNOSTI PRI DIELS-ALDERJEVIH REAKCIJAH
Datum zagovora: 7. 9. 2021

Leja JELENKO
Mentor: prof. dr. Janez Košmrlj
SINTEZA IN UPORABA 2-NAFTOLNEGA DERIVATA
Datum zagovora: 7. 9. 2021

Daša KLANDER
Mentor: prof. dr. Janez Košmrlj
SINTEZA DERIVATA 1,2-DIFENILETINA S PODALJŠANO KONJUGACIJO
Datum zagovora: 7. 9. 2021

Ajda MIHELIČ
Mentor: izr. prof. dr. Miha Lukšič
UPORABA POLIMERNIH MATERIALOV PRI ČIŠČENJU ONESNAŽENIH VOD
Datum zagovora: 7. 9. 2021

Adela AVDIČEVIĆ
Mentor: izr. prof. dr. Miha Lukšič
VLOGA ELEKTROSTATSKIH INTERAKCIJ V PROTEINSKIH SISTEMIH
Datum zagovora: 7. 9. 2021

Neža SODNIK
Mentorica: prof. dr. Irena Kralj Cigić
EKSTRAKCIJA OCETNE KISLINE IN DIETIL FTALATA Z AKTIVNEGA OGLJA
Datum zagovora: 7. 9. 2021

Tanja TOPIĆ
Mentor: prof. dr. Janez Košmrlj
SINTEZA IZBRANIH ALIFATSKIH GEMINALNIH DIBROMOALKENOV
Datum zagovora: 7. 9. 2021

Klara ŠPARLEK
Mentor: prof. dr. Anton Meden
ANALIZA TABLET ZA POMIVALNI STROJ Z RENTGENSKO PRAŠKOVNO DIFRAKCIJO
Datum zagovora: 7. 9. 2021

Zala KOPČAVAR
Mentor: prof. dr. Matija Strlič
DOLOČANJE OCETNE KISLINE V MUZEJSKI ATMOSFERI
Datum zagovora: 7. 9. 2021

Andraž PEZDIRC
Mentor: prof. dr. Matija Strlič
DOLOČANJE ALDEHIDNIH ONESNAŽIL V NOTRANJOSTI ZGRADB
Datum zagovora: 7. 9. 2021

Katarina VELKOV
Mentor: prof. dr. Matija Strlič
DOLOČANJE KLORIDA V RAZGRAJENEM PVC
Datum zagovora: 7. 9. 2021

Jaka PRELOG
Mentor: prof. dr. Tomaž Urbič
MONTE CARLO SIMULACIJE MEHKIH DELCEV
Datum zagovora: 8. 9. 2021

Martin RIHTARŠIČ
Mentor: izr. prof. dr. Jernej Iskra
Z NATRIJEVIM NITRITOM KATALIZIRANO AEROBNO OKSIDATIVNO JODIRANJE AROMATSKIH SPOJIN
Datum zagovora: 8. 9. 2021

Simon PAVLIČ
Mentorica: doc. dr. Nataša Gros
METODE ZA IZDELAVO MIKROPRETOČNIH SISTEMOV
Datum zagovora: 8. 9. 2021

Andraž STARIHA
Mentorica: izr. prof. dr. Barbara Modec
PRIPRAVA AMIDINOV PROPIONITRILA IN BENZONITRILA
Datum zagovora: 8. 9. 2021

Larisa FILIP
Mentor: izr. prof. dr. Jernej Iskra
FOTOKEMIJSKE REAKCIJE FLUORIRANJA
Datum zagovora: 9. 9. 2021

Nika METELKO
Mentor: izr. prof. dr. Uroš Grošelj
SINTEZA PIRAZOLONOV IN NJIHOVA UPORABA V ORGANOKATALIZIRANIH PRETVORBAH
Datum zagovora: 10. 9. 2021

Ana CIZERL
Mentor: doc. dr. Jakob Kljun
SINTEZA HETEROCIKLIČNIH SPOJIN IZ TIOSEMIKARBAZIDOV IN ŠTUDIJA VEZAVE NA CINKOVE MODELNE SPOJINE AKTIVNIH MEST METALOPROTEINOV
Datum zagovora: 10. 9. 2021

Barbara DERGANC
Mentorica: prof. dr. Ksenija Kogej
TEMPERATURNA ODVISNOST SAMO-ASOCIACIJE ATAKTIČNE POLI(METAKRILNE KISLINE)
Datum zagovora: 10. 9. 2021

Jakob MUHIČ
Mentor: prof. dr. Bogdan Štefane
SINTEZA IN PRETVORBE 4-BENZILIDEN-2-FENILOKSAZOLONOV
Datum zagovora: 10. 9. 2021

Jan ŠILER HUDOKLIN
Mentor: prof. dr. Tomaž Urbič
IONSKE TEKOČINE
Datum zagovora: 10. 9. 2021

Ivana PODLIPNIK
Mentor: doc. dr. San Hadži
IZVOR SPREMEMBE TOPLOTNE KAPACITETE PRI ZVITJU DNK: VPLIV SPECIFIČNO VEZANIH MOLEKUL VODE
Datum zagovora: 10. 9. 2021

Žiga OGRIN
Mentor: izr. prof. dr. Janez Cerar
NAPAKE PRI MERJENJIH Z IONOSELEKTIVNIMI ELEKTRODAMI
Datum zagovora: 30. 9. 2021

Lara BREMEC KODELJA
Mentor: izr. prof. dr. Miha Lukšič
UPORABA KOLOIDNIH SISTEMOV PRI POSTOPKIH ČIŠČENJA PREDMETOV KULTURNE DEDIŠČINE S POUDARKOM NA POLI(VINIL ALKOHOLNIH) HIDROGELIH
Datum zagovora: 19. 10. 2021

Veronika BRAČIČ
Mentor: prof. dr. Franc Požgan
KOROZIJSKA ZAŠČITA ALUMINIJEVE ZLITINE S KONVERZIJSKO IN HIBRIDNO SOL-GEL PREVLEKO
Datum zagovora: 3. 11. 2021

Urška BERCKO
Mentor: prof. dr. Jurij Reščič
RAZISKAVE STRUKTURNIH IN TERMODINAMSKIH LASTNOSTI MEŠANIC NABITIH KOLOIDOV Z NEVTRALNIMI POLIMERI Z RAČUNALNIŠKIMI SIMULACIJAMI MONTE CARLO
Datum zagovora: 23. 11. 2021

Eva STERLE
Mentor: doc. dr. Krištof Kranjc
SUBSTITUIRANI CIKLIČNI DIENOFILI V DIELS-ALDERJEVIH REAKCIJAH POD OKOLJU PRIJAZNIMI POGOJI
Datum zagovora: 13. 12. 2021

KEMIJSKO INŽENIRSTVO – 1. STOPNJA

Nastja STRAŠEK
Mentor: prof. dr. Marjan Marinšek
BIOLOŠKO SAMOPOPRAVLJIVI BETONSKI SISTEMI
Datum zagovora: 15. 1. 2021

Maja KOŠAR
Mentorica: doc. dr. Lidija Slemenik Perše
FITOREMEDIACIJA ONESNAŽENIH TAL S TEŽKIMI KOVINAMI: GENSKI INŽENIRING ZA VEČJO UČINKOVITOST PROCESA
Datum zagovora: 22. 1. 2021

Tjaša UHELJ GRČA, TJAŠA
Mentorica: doc. dr. Lidija Slemenik Perše
VPLIV SESTAVE ČOKOLADE NA NJENE REOLOŠKE LASTNOSTI
Datum zagovora: 11. 2. 2021

Nik BRUDAR
Mentor: prof. dr. Miran Gaberšček
BATERIJE
Datum zagovora: 1. 4. 2021

Žan MOČNIK
Mentor: prof. dr. Igor Plazl
MIKROVALOVI IN MIKROFLUIDIKA
Datum zagovora: 8. 4. /2021

Tanja JELOVČAN
Mentor: izr. prof. dr. Blaž Likozar
HETEROGENA KATALITSKA OKSIDACIJA SLADKORJEV DO ALDARNIH KISLIN
Datum zagovora: 8. 4. /2021

Urban UDOVIČ
Mentorica: prof. dr. Urška Šebenik
PODALJŠEVANJE ŽIVLJENJSKE DOBE POLIMERNIH MATERIALOV ZA ZUNANJO UPORABO
Datum zagovora: 23. 4. /2021

Val SEVNIK
Mentor: prof. dr. Igor Plazl
OBNAŠANJE FLUIDOV IN MIKROFLUIDNE NAPRAVE V MIKROGRAVITACIJI
Datum zagovora: 13. 5. 2021

Nika MOČNIK
Mentorica: doc. dr. Lidija Slemenik Perše
PRIMERJAVA DVEH METOD ZA DOLOČANJE MULTI-ELEMENTNE SESTAVE TRDNIH DELCEV V ZRAKU: XRF IN ICP-QQQ
Datum zagovora: 3. 6. 2021

Lucija KORENČAN
Mentorica: prof. dr. Andreja Žgajnar Gotvajn
PREPOVEDANE DROGE V KOMUNALNIH ODPADNIH VODAH
Datum zagovora: 8. 6. 2021

Neli KUČIČ
Mentorica: prof. dr. Urška Šebenik
LAPONITNI HIDROGELI ZA ADSORPCIJO SNOVI
Datum zagovora: 5. 7. 2021

Teja BUH
Mentorica: doc. dr. Lidija Slemenik Perše
VPLIV NATRIJEVEGA LAVRIL ETER SULFATA IN SOLI NA VISKOZNOST DETERGENTA ZA ROČNO POMIVANJE POSODE
Datum zagovora: 16. 7. 2021

Katja TURK
Mentorica: izr. prof. dr. Gabriela Kalčikova
KVANTIFIKACIJA BIOFILMA NA MIKROPLASTIKI
Datum zagovora: 27. 8. 2021

Anej BLAŽIČ
Mentorica: izr. prof. dr. Gabriela Kalčikova
INTERAKCIJE MIKROPLASTIKE Z VODNIMI RASTLINAMI IN MOŽNOST UPORABE FITOREMEDIACIJSKIH TEHNOLOGIJ ZA NJENO ODSTRANJEVANJE IZ POVRŠINSKIH VOD
Datum zagovora: 27. 8. 2021

Neža VREČER
Mentorica: izr. prof. dr. Gabriela Kalčikova
UPORABA RASTLINSKIH ČISTILNIH NAPRAV ZA ODSTRANJEVANJE MIKROPLASTIKE IZ ODPADNIH VOD
Datum zagovora: 2. 9. 2021

Metod SPINDLER
Mentorica: prof. dr. Polona Žnidaršič Plazl
IMOBILIZACIJA BIOKATALIZATORJEV V MIKROREAKTORJE NA OSNOVI SAMOSESTAVLJIVIH HIDROGELOV
Datum zagovora: 6. 9. 2021

Isa SULJKANOVIĆ
Mentor: prof. dr. Matevž Dular
VPLIV SALICILNE KISLINE NA DINAMIKO KAVITACIJSKEGA TOKA V MIKROKANALIH
Datum zagovora: 6. 9. 2021

Vita MIHELIČ
Mentorica: doc. dr. Lidija Slemenik Perše
PROIZVODNJA PIVA TER DOLOČANJE REOLOŠKIH LASTNOSTI IN PARAMETROV KAKOVOSTI PIVA
Datum zagovora: 6. 9. 2021

Jernej JOZIČ
Mentorica: prof. dr. Urška Šebenik
SESTAVA IN DELOVANJE PNEVMATIK ZA DIRKANJE
Datum zagovora: 6. 9. 2021

Filip GEČ
Mentor: izr. prof. dr. Blaž Likozar
ENCIMSKA IN KISLINSKA KATALIZA ESTERIFIKACIJE MODELNIH KOMPONENT LIGNINA
Datum zagovora: 6. 9. 2021

Jurij GOLOBIČ
Mentor: izr. prof. dr. Aleš Ručigaj
MEHANIZMI SPROŠČANJA PROTEINOV IZ HIDROGELOV
Datum zagovora: 6. 9. 2021

Vesna PERNUŠ
Mentor: izr. prof. dr. Marko Hočevar
UPORABA INERCIJSKEGA SENZORJA V POVEZAVI S SISTEMOM ZA LASERSKO SKENIRANJE V VINOGRADIH
Datum zagovora: 7. 9. 2021

Urban JANJIČ
Mentor: prof. dr. Miran Gaberšček
GORIVNE CELICE
Datum zagovora: 7. 9. 2021

Jaka KOMAR
Mentor: izr. prof. dr. Blaž Likozar
IZBIRA TOPILA ZA EKSTRAKCIJO 5-HIDROKSIMETILFURFURALA IZ VODNE FAZE
Datum zagovora: 7. 9. 2021

Jovana ĐURĐEVIĆ
Mentor: prof. dr. Igor Plazl
RAZVOJ MATEMATIČNIH MODELOV ZA NAPOVED HITROSTNIH PROFILOV DVOFAZNEGA TOKA V MIKROKANALU
Datum zagovora: 7. 9. 2021

Blaž JANČIČ
Mentorica: prof. dr. Andreja Žgajnar Gotvajn
UČINKOVITOST NAPREDNIH OKSIDACIJSKIH PROCESOV PRI ODSTRANJEVANJU VIRUSOV IZ KOMUNALNE ODPADNE VODE
Datum zagovora: 7. 9. 2021

Monika NARTNIK
Mentor: izr. prof. dr. Blaž Likozar
UTEKOČINJANJE BIOMASE MIKROALG S KATALIZATORJEM
Datum zagovora: 7. 9. 2021

Jure BELEJ
Mentorica: prof. dr. Andreja Žgajnar Gotvajn
ODSTRANJEVANJE MIKROPOLUTANTOV IZ ODPADNE VODE Z ELEKTROKOAGULACIJO
Datum zagovora: 7. 9. 2021

Špela ČRV
Mentor: prof. dr. Igor Plazl
OPTIMIZACIJA HETEROGENE FOTOKATALIZE V ŠARŽNEM REAKTORJU Z RECIKLOM
Datum zagovora: 7. 9. 2021

Nikola POLJANEC
Mentor: prof. dr. Aleš Podgornik
VPLIV ORGANSKIH TOPIL NA MORFOLOGIJO EMULZIJSKO VTISNJENIH POROZNIH POLIMEROV
Datum zagovora: 7. 9. 2021

Vid OGRIZEK
Mentor: izr. prof. dr. Marko Hočevar
VPLIV VRTILNE FREKVENCE BOBNA NA POŠKODBE IN MEČKANJE PRI STROJNEM SUŠENJU PERILA
Datum zagovora: 7. 9. 2021

Nejc BUTINA
Mentor: izr. prof. dr. Marko Hočevar
VPLIV TEMPERATURE NA DEGRADACIJO IN MEČKANJE TEKSTILA PRI STROJNEM SUŠENJU PERILA
Datum zagovora: 7. 9. 2021

Mejrema NUHANOVIĆ
Mentorica: prof. dr. Polona Žnidaršič Plazl
UPORABA ZAMREŽENIH ENCIMSKIH AGREGATOV V BIOTRANSFORMACIJAH
Datum zagovora: 8. 9. 2021

Lan Julij ZADRAVEC
Mentorica: prof. dr. Polona Žnidaršič Plazl
UPORABA MIKROPRETOČNIH SISTEMOV ZA GOJENJE CELIC
Datum zagovora: 8. 9. 2021

Tjaša KNEZ
Mentor: izr. prof. dr. Blaž Likozar
VPLIV DOPIRANJA CuO/ZnO/Al2O3 KATALIZATORJEV NA SINTEZO METANOLA IN IZVAJANJE OBRATNE REAKCIJE VODNEGA PLINA.
Datum zagovora: 8. 9. 2021

Ana Kristina KLANČIČ
Mentorica: doc. dr. Lidija Slemenik Perše
RAZVOJ NOVIH BIORAZGRADLJIVIH POLIMEROV IZ OBNOVLJIVIH VIROV
Datum zagovora: 8. 9. 2021

Petra ZUPANČIČ
Mentorica: prof. dr. Andreja Žgajnar Gotvajn
PROIZVODNJA BIOPLINA IZ MIKROALG
Datum zagovora: 8. 9. 2021

Doroteja Marija NOVAK
Mentor: prof. dr. Robert Dominko
NADOMESTITEV LITIJA, IZGUBLJENEGA MED ZAČETNIM DELOVANJEM LI-IONSKEGA AKUMULATORJA
Datum zagovora: 9. 9. 2021

Aljaž URANKAR
Mentor: prof. dr. Igor Plazl
PROCES RAZTAPLJANJA TITANOVE RUDE PRI INDUSTRIJSKI PROIZVODNJI TITANOVEGA DIOKSIDA
Datum zagovora: 9. 9. 2021

Katja TRILER
Mentorica: doc. dr. Lidija Slemenik Perše
PRENOS PRAŠNIH DELCEV IN HLAPOV V ZRAK MED DELOM V ANALITSKEM LABORATORIJU
Datum zagovora: 9. 9. 2021

Robert BUH
Mentor: prof. dr. Marjan Marinšek
3-D TISKANJE TRAJNIH MAGNETOV
Datum zagovora: 10. 9. 2021

Zala VOLČANŠEK
Mentor: izr. prof. dr. Blaž Likozar
OKSIDACIJA GLUKOZE DO ALDARNIH KISLIN
Datum zagovora: 10. 9. 2021

Vita LETONJA
Mentor: izr. prof. dr. Boštjan Genorio
ELEKTROKEMIJSKI BIOSENZORJI ZA ZAZNAVANJE GLUKOZE Z GRAFENOM
Datum zagovora: 10. 9. 2021

Tine VOJSKA
Mentor: izr. prof. dr. Boštjan Genorio
Z DUŠIKOM DOPIRANI GRAFENSKI ELEKTROKATALIZATORJI ZA REDUKCIJO CO2
Datum zagovora: 10. 9. 2021

Jaka TRTNIK
Mentor: prof. dr. Aleš Podgornik
PRIPRAVA IN KARAKTERIZACIJA NANODELCEV ŽLAHTNIH KOVIN
Datum zagovora: 16. 9. 2021

Diana ŽNIDARŠIČ
Mentor: prof. dr. Aleš Podgornik
IZOLACIJA VIRUSOV Z LIPIDNO OVOJNICO
Datum zagovora: 16. 12. 2021

BIOKEMIJA – 1. STOPNJA

Lara HRVATIN
Mentor: prof. dr. Iztok Turel
VPLIV KOVINSKIH IONOV IN BIGVANIDNIH KOMPLEKSOV NA AKTIVNOST KATEPSINA K
Datum zagovora: 5. 3. 2021

Maja ŠKOF
Mentor: doc. dr. Jernej Ogorevc
PRIMERJAVA STRATEGIJ ZA OCENO UČINKOVITOSTI sgRNA NA PRIMERU TLR10.
Datum zagovora: 13. 4. 2021

Nika BOŠTIC
Mentorica: izr. prof. dr. Nina Vardjan
MERITVE ZNOTRAJCELIČNE KONCENTRACIJE KALCIJA IN cAMP V ASTROCITIH PO DODATKU LIGANDOV ZA ADHEZIJSKE RECEPTORJE GPCR
Datum zagovora: 2. 6. 2021

Neža BLAZNIK
Mentorica: prof. dr. Nina Gunde Cimerman
RAZGRADNJA RAZLIČNIH TIPOV PLASTIKE Z IZBRANIMI EKSTREMOFILNIMI GLIVAMI OSAMLJENIMI IZ GOSPODINJSKIH NAPRAV
Datum zagovora: 18. 6. 2021

Sonja GABRIJELČIČ
Mentor: izr. prof. dr. Marko Novinec
OVREDNOTENJE PROTIBAKTERIJSKIH LASTNOSTI IZBRANE SERIJE DERIVATOV 2-PIRIDONA
Datum zagovora: 17. 8. 2021

Barbara JAKLIČ
Mentorica: prof. dr. Tatjana Avšič Županc
RAZNOLIKOST ORTOBUNJAVIRUSOV V KOMARJIH V SLOVENIJI
Datum zagovora: 23. 8. 2021

Marko PAVLEKOVIĆ
Mentor: prof. dr. Janez Plavec
KARAKTERIZACIJA KRATKIH ZAPOREDIJ DNK, KI POVZROČAJO KOLAPS REPLIKACIJSKIH VILIC
Datum zagovora: 27. 8. 2021

Neža ŽERJAV
Mentor: doc. dr. Gregor Gunčar
FUNKCIONALIZACIJA MONODISPERZNIH DELCEV SILICIJEVEGA DIOKSIDA S KORONAVIRUSNIMA PROTEINOMA ORF8 IN N
Datum zagovora: 30. 8. 2021

Maks KUMEK
Mentor: doc. dr. Miha Pavšič
SISTEM ZA DETEKCIJO HOMOGENO GLIKOZILIRANIH PROTEINOV NA OSNOVI GLIKOZILTRANSFERAZE MGAT-1
Datum zagovora: 31. 8. 2021

Tina LOGONDER
Mentorica: prof. dr. Brigita Lenarčič
PRIPRAVA KONSTRUKTOV ZA IZRAŽANJE REKOMBINANTNEGA ZUNAJCELIČNEGA DELA ČLOVEŠKEGA PROTEINA EpCAM V SESALSKIH CELIČNIH LINIJAH
Datum zagovora: 1. 9. 2021

Nina VARDA
Mentor: izr. prof. dr. Marko Novinec
EVOLUCIJSKA ANALIZA DIPEPTIDIL PEPTIDAZE I
Datum zagovora: 2. 9. 2021

Nastja FEGUŠ
Mentor: izr. prof. dr. Marko Novinec
RAČUNALNIŠKA ANALIZA OLIGOMERNEGA STANJA IN FUNKCIJSKIH LASTNOSTI ČLOVEŠKEGA ISOC2
Datum zagovora: 2. 9. 2021

Anastasija NECHEVSKA
Mentor: prof. dr. Janez Plavec
ISKANJE VEZAVNIH MEST Mac3 DOMENE PROTEINA Nsp3 SARS-CoV-2
Datum zagovora: 2. 9. 2021

Tevž LEVSTEK
Mentor: prof. dr. Janez Plavec
ŠTUDIJA STRUKTURNIH MOTIVOV RNA ZAPOREDIJ S PONOVITVAMI ADENINA, GVANINA IN CITOZINA
Datum zagovora: 2. 9. 2021

Karmen MLINAR
Mentorica: izr. prof. dr. Nataša Debeljak
DOLOČITEV IZRAŽANJA KANABINOIDNIH RECEPTORJEV NA RAVNI INFORMACIJSKE RNA V CELIČNIH LINIJAH RAKA DOJKE
Datum zagovora: 6. 9. 2021

Tina ZAVODNIK
Mentor: prof. dr. Uroš Petrovič
DOLOČEVANJE INTERAKCIJ MED PROTEINOMA PMS2 IN NOVO VARIANTO MLH1
Datum zagovora: 6. 9. 2021

Polona SKRT
Mentor: prof. dr. Uroš Petrovič
MODELIRANJE BINARNIH KOMPLEKSOV SARS-CoV-2 PROTEINA ORF8 S TARČNIMI PROTEINI ČLOVEKA
Datum zagovora: 6. 9. 2021

Kim GLAVIČ
Mentor: izr. prof. dr. Marko Dolinar
BIOINFORMACIJSKA ANALIZA PAROV TOKSIN-ANTITOKSIN CIANOBAKTERIJE MICROCYSTIS AERUGINOSA PCC 7806 IN MOLEKULSKO KLONIRANJE ANTITOKSINOV BH695_0426 IN BH695_0430
Datum zagovora: 7. 9. 2021

Rebeka DAJČMAN
Mentor: prof. dr. Iztok Turel
VPLIV CINKOVIH SOLI IN PIRITIONSKIH DERIVATOV NA AKTIVNOSTI KATEPSINA L
Datum zagovora: 7. 9. 2021

Nika VEGELJ
Mentorica: prof. dr. Brigita Lenarčič
PRIPRAVA KONSTRUKTOV ZA IZRAŽANJE REKOMBINANTNEGA ZUNAJCELIČNEGA DELA ČLOVEŠKEGA PROTEINA EGFR V SESALSKIH CELIČNIH LINIJAH.
Datum zagovora: 7. 9. 2021

Eva GARTNER
Mentor: prof. dr. Boris Rogelj
PRIPRAVA CELIČNIH MODELOV S STABILNIM IZRAŽANJEM PROTEINOV Z DIPEPTIDNIMI PONOVITVAMI IN OVREDNOTENJE NJIHOVE VLOGE
Datum zagovora: 8. 9. 2021

Laura GAŠPERŠIČ
Mentor: prof. ddr. Boris Turk
PRIPRAVA REKOMBINANTNEGA PROTEINA BirA
Datum zagovora: 8. 9. 2021

Meta KODRIČ
Mentor: prof. ddr. Boris Turk
PRIPRAVA MIŠJEGA KATEPSINA S Z AVI OZNAKO IN NJEGOVA KARAKTERIZACIJA
Datum zagovora: 8. 9. 2021

Manca OSOLIN
Mentorica: doc. dr. Vera Župunski
MOLEKULSKO KLONIRANJE IN FILOGENETSKE ANALIZE PROTEINA MATRIN 3
Datum zagovora: 8. 9. 2021

Michelle OLETIČ
Mentorica: doc. dr. Marina Klemenčič
IZRAŽANJE IN ČIŠČENJE MUTIRANIH RAZLIČIC ANTITOKSINA 1067 IZ CIANOBAKTERIJE MICROCYSTIS AERUGINOSA PCC 7806
Datum zagovora: 8. 9. 2021

Tim NOGRAŠEK
Mentorica: doc. dr. Vera Župunski
MOLEKULSKO KLONIRANJE IN FILOGENETSKE ANALIZE NEKODIRAJOČIH VTRNA
Datum zagovora: 8. 9. 2021

Valeriya MUSINA
Mentorica: doc. dr. Tadeja Režen
VLOGA NONO IN PCBP2 V IZRAŽANJU IZBRANIH circRNA
Datum zagovora: 9. 9. 2021

Lara DRINOVEC
Mentor: izr. prof. dr. Mitja Kolar
RAZVOJ IN UPORABA ELEKTRODE Z OGLJIKOVO PASTO IN GLUKOZA OKSIDAZO ZA ZAZNAVANJE GLUKOZE
Datum zagovora: 9. 9. 2021

Maja MAHORIČ
Mentorica: doc. dr. Nada Žnidaršič
OVREDNOTENJE POSTOPKOV KONTRASTIRANJA BIOLOŠKIH VZORCEV Z ALTERNATIVNIMI KONTRASTNIMI SNOVMI ZA PRESEVNO ELEKTRONSKO MIKROSKOPIJO
Datum zagovora: 9. 9. 2021

Ana POTOČNIK
Mentor: doc. dr. Jernej Ogorevc
UPORABA SISTEMOV CRISPR/dCas9 ZA URAVNAVANJE IZRAŽANJA GENA TLR10 V PLJUČNI EPITELIJSKI CELIČNI LINIJI A549
Datum zagovora: 9. 9. 2021

Teo NOGRAŠEK
Mentor: prof. dr. Boris Rogelj
KLONIRANJE IN OPTIMIZACIJA IZRAŽANJA REKOMBINANTNIH PROTEINOV SKUPKOV Neat1 in G4C2 ZA IN VITRO OPAZOVANJE NJIHOVEGA NASTANKA
Datum zagovora: 10. 9. 2021

Tina ARNŠEK
Mentor: prof. dr. Peter Dovč
GENETSKA PESTROST NUKLEOTIDNEGA ZAPOREDJA KODOGENIH REGIJ PROTEINA ACE2 PRI PRAŠIČU (SUS SCROFA)
Datum zagovora: 10. 9. 2021

Sumeja KUDELIĆ
Mentorica: doc. dr. Marina Klemenčič
VZPOSTAVITEV METODE ZA VZBUJANJE OKSIDATIVNEGA STRESA V ALGI CHLAMYDOMONAS REINHARDTII S SVETLOBO UV
Datum zagovora: 13. 9. 2021

Anže ŠUMAH
Mentorica: doc. dr. Tadeja Režen
VLOGA hnRNPK IN RBM4 V IZRAŽANJU IZBRANIH mRNA IN circRNA
Datum zagovora: 17. 9. 2021

Gašper Anton KOMATAR
Mentor: doc. dr. Miha Pavšič
KLONIRANJE BIOTIN LIGAZE BioID2 IN PRIMERJAVA RAZLIČNIH BIOTIN LIGAZ ZA NAMEN ISKANJA INTERAKCIJSKIH PARTNERJEV
Datum zagovora: 17. 9. 2021

TEHNIŠKA VARNOST – 1- STOPNJA

Katja VALENKO
Mentorica: doc. dr. Marija Molan
ODNOS DO VARNOSTNE KULTURE MED ŠTUDENTI NA FAKULTETI ZA KEMIJO IN KEMIJSKO TEHNOLOGIJO
Datum zagovora: 12. 4. 2021

Peter KOŠIR
Mentorica: doc. dr. Barbara Novosel
ZAGOTAVLJANJE VARNOSTI IN ZDRAVJA DELAVCEV ZARADI IZPOSTAVLJENOSTI KEMIČNIM SNOVEM V OBRATU PIGMENTIRANI PREMAZI
Datum zagovora: 13. 5. 2021

Anka MERVAR
Mentorica: doc. dr. Klementina Zupan
ERGONOMSKA OCENA DELA PRODAJALKE
Datum zagovora: 16. 6. 2021

Niko VOLARIĆ
Mentor: prof. dr. Matija Tomšič
VARNOSTNI VIDIK DELA V MANJŠI BETONARNI
Datum zagovora: 18. 6. 2021

Anja KOČMAN
Mentorica: doc. dr. Klementina Zupan
VARNOST IN TVEGANJA PRI UPORABI NANOMATERIALOV
Datum zagovora: 9. 7. 2021

Tea BOŽIČ
Mentor: izr. prof. dr. Simon Schnabl
ANALIZA POŽAROV V NARAVI
Datum zagovora: 31. 8. 2021

Romana KRALJ
Mentorica: doc. dr. Barbara Novosel
DOLOČITEV TEŽKIH KOVIN V POTOČNEM SEDIMENTU IN OCENA NJIHOVIH VPLIVOV NA ZDRAVJE LJUDI
Datum zagovora: 6. 9. 2021

Anže GOLOB
Mentorica: doc. dr. Barbara Novosel
DOLOČANJE GORLJIVOSTI IN UPORABE IZOLACIJSKIH MATERIALOV, KOT ELEMENTI POŽARNE ODPORNOSTI, TER UGOTAVLJANJE NJIHOVIH VPLIVOV V PRIMERU POŽARA
Datum zagovora: 6. 9. 2021

Filip KOROŠEC
Mentor: izr. prof. dr. Simon Schnabl
AVTONOMNA KONTROLA EVAKUACIJE S POMOČJO IMPLEMENTACIJE SISTEMA FLUIDNIH EVAKUACIJSKIH POTI
Datum zagovora: 6. 9. 2021

Nastja STOVANJE
Mentorica: doc. dr. Barbara Novosel
DOLOČANJE EKSPLOZIJSKIH PARAMETROV PRI PRAŠNIH EKSPLOZIJAH
Datum zagovora: 8. 9. 2021

Tine VEREN
Mentorica: doc. dr. Klementina Zupan
ERGONOMIJA V AVTOMOBILIH
Datum zagovora: 8. 9. 2021

Ema JESENKO
Mentorica: doc. dr. Barbara Novosel
DOLOČANJE MINIMALNE VŽIGNE ENERGIJE LESNIH PRAHOV
Datum zagovora: 9. 9. 2021

Timotej BRUS
Mentor: izr. prof. dr. Simon Schnabl
SISTEMI ZA JAVLJANJE POŽAROV IN POŽARNA VARNOST ŠPORTNIH OBJEKTOV
Datum zagovora: 9. 9. 2021

Andraž ŠINKOVEC
Mentor: prof. dr. Matija Tomšič
PANDEMIJA COVID-19 IN OSEBNA VAROVALNA OPREMA V ZDRAVSTVU
Datum zagovora: 9. 9. 2021

David IVANČIČ
Mentor: izr. prof. dr. Simon Schnabl
VARNOSTNI VIDIKI PRI ORGANIZACIJI RALLY DIRK
Datum zagovora: 9. 9. 2021

Jure BEZELJAK
Mentor: prof. dr. Jurij Reščič
PRIMERJAVA SAR VREDNOSTI MOBILNIH TELEFONOV NA SLOVENSKEM TRGU
Datum zagovora: 30. 9. 2021

Monika CIMERMANČIČ
Mentorica: doc. dr. Sabina Huč
SIMULIRANJE POSLEDIC IZPUSTA NEVARNE SNOVI V PROGRAMU ALOHA
Datum zagovora: 30. 9. 2021

DIPLOME – VISOKOŠOLSKI STROKOVNI ŠTUDIJ

KEMIJSKA TEHNOLOGIJA – 1. STOPNJA

Neža DRNOVŠEK
Mentor: izr. prof. dr. Janez Cerkovnik
NOVE FORMULACIJE VODIKOVEGA PEROKSIDA
Datum zagovora: 15. 1. 2021

Diana OZMEC
Mentor: prof. dr. Anton Meden
RENTGENSKA PRAŠKOVNA DIFRAKCIJA ZDRAVIL PROTI DEPRESIJI
Datum zagovora: 22. 1. 2021

Jaka JENKO
Mentorica: doc. dr. Klementina Zupan
MATERIALI S FAZNO SPREMEMBO V GRADBENIŠTVU
Datum zagovora: 22. 1. 2021

Tajda RODE
Mentor: doc. dr. Bojan Kozlevčar
BAKROVE IN CINKOVE SPOJINE S 4-AMINOBENZOJSKO KISLINO
Datum zagovora: 29. 1. 2021

Sabina TRAKO
Mentor: prof. dr. Marjan Marinšek
DOLOČITEV KARAKTERISTIČNIH TEMPERATUR (LIKVIDUS IN SOLIDUS) NIKELJ-KROM-ŽELEZOVIH ZLITIN Z UPORABO DTA
Datum zagovora: 15. 2. 2021

Žiga PODBEVŠEK
Mentor: doc. dr. Bojan Šarac
POSTOPKI PRIDOBIVANJA ČISTE VODE
Datum zagovora: 8. 3. 2021

Eva KANALEC
Mentorica: doc. dr. Saša Petriček
KOORDINACIJA POLIETRA S TREMI O-DONORSKIMI ATOMI NA KOVINSKE IONE
Datum zagovora: 18. 3. 2021

Veronika KUMER
Mentor: prof. dr. Franc Perdih
DOLOČEVANJE BORA V TEKOČIH IN TRDNIH VZORCIH S POMOČJO MASNE SPEKTROMETRIJE Z VZBUJANJEM V INDUKTIVNO SKLOPLJENI PLAZMI
Datum zagovora: 23. 3. 2021

Lucija KUŽNIK
Mentor: doc. dr. Jakob Kljun
SINTEZA NOVIH TRIAZOLIDINOV IN NJIHOVIH CINKOVIH(II) KOORDINACIJSKIH SPOJIN
Datum zagovora: 23. 4. 2021

Ema ORAŽEM
Mentorica: doc. dr. Marija Zupančič
KEMIJSKA KARAKTERIZACIJA OBCESTNIH SEDIMENTOV IZ IDRIJE
Datum zagovora: 17. 5. 2021

Jusuf BOTONJIĆ
Mentorica: doc. dr. Saša Petriček
NIKLJEVI KOMPLEKSI S PIRIDIN-2-ONOM
Datum zagovora: 8. 6. 2021

Žana BANIČ
Mentorica: izr. prof. dr. Amalija Golobič
MINERALNA SESTAVA KAMNIN IN PRSTI S PODROČJA LESKOVCA
Datum zagovora: 17. 6. 2021

Jure LAVRIČ
Mentor: doc. dr. Martin Gazvoda
LOČEVANJE REGIOIZOMEROV FLUORIRANIH ORGANSKIH MOLEKUL Z USTREZNIMI KEMIJSKIMI METODAMI
Datum zagovora: 17. 6. 2021

Viktorija KUŽNIK
Mentorica: izr. prof. dr. Barbara Modec
PONOVLJIVOST REAKCIJ CINKOVEGA(II) KINALDINATA V PROPIONITRILU ALI BENZONITRILU
Datum zagovora: 21. 6. 2021

Lara KEBER
Mentor: doc. dr. Andrej Pevec
FLUORIDOOKSIDOVANADATI NEKATERIH PURINSKIH BAZ
Datum zagovora: 23. 6. 2021

Žan OCEPEK
Mentor: prof. dr. Matija Tomšič
ODSTRANJEVANJE AMFIFILNIH SNOVI IZ ODPLAK IN INDUSTRIJSKIH ODPADNIH VOD
Datum zagovora: 2. 7. 2021

Barbara PAJK KOVAČ
Mentor: viš. pred. dr. Branko Alič
POLIMERNI MATERIALI NAMENJENI ŠIROKI POTROŠNJI, NJIHOVO RECIKLIRANJE IN NJIHOV VPLIV NA OKOLJE
Datum zagovora: 5. 7. 2021

Tilen CELJER
Mentor: viš. pred. dr. Branko Alič
PROIZVODNJA PNEVMATIK
Datum zagovora: 5. 7. 2021

Jože DULAR
Mentorica: prof. dr. Helena Prosen
DOLOČANJE KPK V ODPADNI VODI
Datum zagovora: 6. 7. 2021

Nejc PAČNIK
Mentor: prof. dr. Matija Strlič
DOLOČANJE ŽELATINE V PAPIRJU
Datum zagovora: 6. 7. 2021

Tadeja ŽARN
Mentor: prof. dr. Franc Perdih
HALOGENSKA VEZ KOT ORODJE ZA TVORBO KOKRISTALOV
Datum zagovora: 7. 7. 2021

Klavdija BIJEK
Mentor: prof. dr. Franc Perdih
PERSPEKTIVE KOORDINACIJSKE KEMIJE ZA VEZAVO OGLJIKOVEGA DIOKSIDA
Datum zagovora: 7. 7. 2021

Eva KODRIČ
Mentorica: izr. prof. dr. Amalija Golobič
RENTGENSKA PRAŠKOVNA DIFRAKCIJA PRALNIH PRAŠKOV
Datum zagovora: 9. 7. 2021

Luka ROŽIČ
Mentor: doc. dr. Bojan Kozlevčar
BAKROVE(II) SPOJINE Z OKSALATNIM ANIONOM
Datum zagovora: 18. 8. 2021

Evgen KOZOLE
Mentorica: prof. dr. Helena Prosen
EKSTRAKCIJSKE METODE ZA POLARNE BENZOTRIAZOLE V TRDNIH OKOLJSKIH VZORCIH
Datum zagovora: 23. 8. 2021

Sara RUKLIĆ
Mentorica: doc. dr. Marta Počkaj
IDENTIFIKACIJA KRISTALINIČNIH SNOVI V TRDNIH ČISTILNIH SREDSTVIH Z RENTGENSKO PRAŠKOVNO DIFRAKCIJO
Datum zagovora: 23. 8. 2021

Zala TAVČER
Mentorica: prof. dr. Barbara Hribar Lee
BIOLOŠKI PUFRI
Datum zagovora: 25. 8. 2021

Lucija STRLE
Mentorica: izr. prof. dr. Romana Cerc Korošec
TOPLOTNA MODIFIKACIJA HRASTOVEGA LESA IN DOLOČITEV STOPNJE LE-TE S TERMOGRAVIMETRIJO
Datum zagovora: 27. 8. 2021

Klemen MATKO
Mentorica: doc. dr. Saša Petriček
KOMPLEKSI PREHODNIH KOVIN ČETRTE PERIODE IN 4-HIDROKSIPIRIDINA ALI 4-METOKSIPIRIDINA
Datum zagovora: 30. 8. 2021

Anže DEVJAK
Mentorica: doc. dr. Nives Kitanovski
KARAKTERIZACIJA KOORDINACIJSKE SPOJINE MOLIBDENA S PIRIDINSKIMI IN KLORIDNIMI LIGANDI
Datum zagovora: 2. 9. 2021

Tanja VIDIC
Mentor: doc. dr. Bojan Kozlevčar
BAKROVE(II) SPOJINE Z ADIPINSKO KISLINO IN DUŠIKOVIMI DONORSKIMI LIGANDI
Datum zagovora: 2. 9. 2021

Tajda FEMEC
Mentor: doc. dr. Bojan Kozlevčar
BAKROVE(II) SPOJINE Z GLUTARNO KISLINO IN DUŠIKOVIMI DONORSKIMI LIGANDI
Datum zagovora: 2. 9. 2021

Alenka GOLUB
Mentor: prof. dr. Iztok Turel
ANALIZA SINTEZNIH POSTOPKOV IN STRUKTUR BIZMUTOVIH KOORDINACIJSKIH SPOJIN Z DVOVEZNIMI DUŠIKOVIMI LIGANDI IN NAČRTOVANJE SINTEZ ANALOGNIH SPOJIN Z ESTRI PIRIDIN DIKARBOKSILATOV
Datum zagovora: 2. 9. 2021

Lara STIPANOVIĆ
Mentor: izr. prof. dr. Drago Kočar
DOLOČANJE MAGNEZIJA V PREHRANSKIH DOPOLNILIH
Datum zagovora: 2. 9. 2021

Maja MEGLEN
Mentorica: doc. dr. Nataša Gros
LABORATORIJ NA PAPIRJU V ANALIZNI KEMIJI
Datum zagovora: 3. 9. 2021

Taja AHLIN
Mentorica: prof. dr. Helena Prosen
SPEKTROFOTOMETRIČNO DOLOČANJE VITAMINOV V PREHRANSKIH DOPOLNILIH
Datum zagovora: 3. 9. 2021

Barbara ZORETIČ
Mentor: izr. prof. dr. Mitja Kolar
RAZVOJ IN UPORABA SPEKTROFOTOMETRIJE PRI DOLOČEVANJU GRENČICE V PIVU
Datum zagovora: 3. 9. 2021

Tjaša KOVAČIČ
Mentor: doc. dr. Krištof Kranjc
2H-PIRAN-2-ONI IN NJIHOVI DERIVATI KOT POMEMBNE NARAVNE SPOJINE TER GRADNIKI V ORGANSKI SINTEZI
Datum zagovora: 6. 9. 2021

Tjaša ČRNILOGAR
Mentor: doc. dr. Jakob Kljun
SINTEZA NOVIH TRIAZOLIDINOV IN NJIHOVIH SREBROVIH(I) KOORDINACIJSKIH SPOJIN
Datum zagovora: 6. 9. 2021

Nina LESJAK
Mentor: viš. pred. dr. Branko Alič
VPLIV MOLEKULSKIH MAS NA REOLOŠKE LASTNOSTI POLIMERNIH TALIN IN RAZTOPIN
Datum zagovora: 6. 9. 2021

Žiga ŠUBIC
Mentor: doc. dr. Krištof Kranjc
UPORABA PERICIKLIČNIH REAKCIJ V KLJUČNIH STOPNJAH SINTEZE NARAVNIH SPOJIN
Datum zagovora: 6. 9. 2021

Tilen MAGAŠ
Mentorica: prof. dr. Irena Kralj Cigić
DOLOČANJE ALDEHIDOV V NOTRANJIH PROSTORIH S PASIVNIMI VZORČEVALNIKI
Datum zagovora: 7. 9. 2021

Assya BELLAADEM
Mentor: prof. dr. Jurij Reščič
IZRAČUN PARNEGA TLAKA RAZKUŽIL ZA ROKE
Datum zagovora: 7. 9. 2021

Sara STANKO
Mentor: prof. dr. Matevž Pompe
DOLOČEVANJE NIKOTINAMIDA MONONUKLEOTIDA V PREHRANSKIH DOPOLNILIH
Datum zagovora: 7. 9. 2021

Mateja JELIĆ
Mentor: prof. dr. Matija Strlič
VSEBNOST AGRESIVNEGA CO2 V CELJSKEM VODOVODNEM OMREŽJU
Datum zagovora: 8. 9. 2021

Špela KLADNIK
Mentor: doc. dr. Martin Gazvoda
ORGANOKOVINSKI KOMPLEKSI KOVIN PREHODA Z ACETILENSKIMI LIGANDI
Datum zagovora: 8. 9. 2021

Tina JERETINA
Mentor: prof. dr. Marjan Jereb
PRETVORBA KARBONILNIH SPOJIN Z NEKATERIMI NUKLEOFILI
Datum zagovora: 9. 9. 2021

Urša SKUBE
Mentor: izr. prof. dr. Mitja Kolar
IONSKA KROMATOGRAFIJA KOT METODA ZA DOLOČANJE ANIONOV V LEBDEČIH (PM) DELCIH
Datum zagovora: 9. 9. 2021

Aljaž ZADRAŽNIK
Mentorica: doc. dr. Nives Kitanovski
KARAKTERIZACIJA DVEH KOORDINACIJSKIH SPOJIN MOLIBDENA
Datum zagovora: 10. 9. 2021

Nika MALEČKAR
Mentor: prof. dr. Jurij Lah
DOLOČITEV ELEKTROKINETIČNEGA POTENCIALA NA POVRŠINI MAGNETNIH NANODELCEV ZA UPORABO V SELEKTIVNI EKSTRAKCIJI POLIFENOLOV
Datum zagovora: 10. 9. 2021

Nina PAVLOVIČ
Mentor: prof. dr. Anton Meden
KVALITATIVNA FAZNA ANALIZA PROTIBOLEČINSKIH ZDRAVIL Z UPORABO RENTGENSKE PRAŠKOVNE DIFRAKCIJE
Datum zagovora: 16. 9. 2021

Branka HUDEJ
Mentor: prof. dr. Franc Perdih
SINTEZA METIL 6-(MORFOLIN-4-KARBONIL) PIKOLINATA IN MOŽNOSTI NJEGOVE UPORABE KOT LIGANDA V KOMPLEKSIH Z ANTIDIABETIČNIM DELOVANJEM
Datum zagovora: 17. 9. 2021

Nik MENCINGER
Mentor: izr. prof. dr. Miha Lukšič
INTRINZIČNO PREVODNI POLIMERI
Datum zagovora: 21. 9. 2021

Manca TURK
Mentor: viš. pred. dr. Andrej Godec
KEMIJSKA KINETIKA NEKATERIH DUŠIKOVIH OKSIDOV V ATMOSFERI
Datum zagovora: 27. 9. 2021

Maruša SKOZIT
Mentor: prof. dr. Bogdan Štefane
SINTEZE IN APLIKACIJE AZINOV
Datum zagovora: 30. 9. 2021

Manca ŽAGAR
Mentorica: prof. dr. Urška Lavrenčič Štangar
SINTEZA IN KARAKTERIZACIJA KOMPOZITOV g-C3N4/TiO2 ZA UPORABO V HETEROGENI FOTOKATALIZI
Datum zagovora: 30. 9. 2021

Tanja VADNJAL
Mentorica: doc. dr. Nataša Gros
DOBRE LABORATORIJSKE PRAKSE PRI ODMERJANJU VOLUMNA
Datum zagovora: 5. 10. 2021

Erika KOFALT
Mentorica: doc. dr. Nives Kitanovski
KARAKTERIZACIJA NEZNANEGA VZORCA DOBLJENEGA PRI REAKCIJI (pyH)5[MoOCl4(H2O)]3Cl2 IN KSCN
Datum zagovora: 6. 10. 2021

Patricija BERNOT
Mentor: izr. prof. dr. Janez Cerkovnik
PRIPRAVA KLEŠČASTIH KOMPLEKSOV Z NIKLJEM IN ŠTUDIJ NJIHOVE REAKTIVNOSTI
Datum zagovora: 7. 10. 2021

Nikol ČERNENŠEK
Mentor: doc. dr. Črtomir Podlipnik
STRUKTURA IN VLOGA PROTEINA E V VIRUSU SARS-CoV-2
Datum zagovora: 8. 10. 2021

Maja JERNEJČIČ
Mentorica: prof. dr. Urška Lavrenčič Štangar
RAZGRADNJA NEKATERIH MIKRO-ONESNAŽIL V VODI, OBOGATENI Z ULTRAFINIMI MEHURČKI OZONA
Datum zagovora: 8. 10. 2021

Jan SLOBODNIK
Mentorica: izr. prof. dr. Barbara Modec
PREGLED ENOSTAVNIH KOORDINACIJSKIH SPOJIN CINKA(II) Z 2,2'-BIPIRIDINOM, PIKOLINATOM ALI PIRAZINKARBOKSILATOM
Datum zagovora: 26. 10. 2021

Petra ZALOKAR
Mentor: prof. dr. Matija Tomšič
RECIKLIRANJE IN KEMIJSKA IZRABA ODPADNE PLASTIKE
Datum zagovora: 27. 10. 2021

David LAZIĆ
Mentorica: doc. dr. Marta Počkaj
REAKCIJE MED KOBALTOVIM(II) BROMIDOM IN 2-(HIDROKSIMETIL)PIRIDINOM
Datum zagovora: 28. 10. 2021

Sabina KLEMENC
Mentor: prof. dr. Franc Perdih
TVORBA KOKRISTALOV ORGANOKOVINSKIH SPOJIN Z JODOM IN JODOVIMI SPOJINAMI
Datum zagovora: 16. 11. 2021

David VERDEL
Mentor: izr. prof. dr. Janez Cerkovnik
NOVE FORMULACIJE VODIKOVEGA PEROKSIDA ZA UPORABO V PREHRAMBENI INDUSTRIJI IN ZA DEZINFEKCIJO
Datum zagovora: 23. 11. 2021

Boštjan HORVAT
Mentor: doc. dr. Bojan Šarac
KOLIGATIVNE LASTNOSTI V VSAKDANJEM ŽIVLJENJU
Datum zagovora: 3. 12. 2021

Karmen GROZNIK
Mentorica: prof. dr. Urška Lavrenčič Štangar
PRETOČNI FOTOKATALITSKI REAKTORJI ZA ČIŠČENJE VODE: TEORETIČNO OZADJE IN PRIMER LABORATORIJSKE IZVEDBE
Datum zagovora: 7. 12. 2021

Kristina JORDAN
Mentorica: prof. dr. Irena Kralj Cigić
DOLOČANJE MINERALOV V LISTNEM OHROVTU
Datum zagovora: 10. 12. 2021

Nataša HUDOKLIN
Mentor: izr. prof. dr. Janez Cerkovnik
RAZISKAVE NOVIH FORMULACIJ RAZREDČENIH RAZTOPIN VODIKOVEGA PEROKSIDA
Datum zagovora: 14. 12. 2021

Dejan HOČEVAR
Mentorica: izr. prof. dr. Romana Cerc Korošec
VPLIV VELIKOSTI DELCEV NA DOLOČITEV STOPNJE TOPLOTNE MODIFIKACIJE HRASTOVEGA LESA
Datum zagovora: 21. 12. 2021

Anže TEKAVC
Mentorica: prof. dr. Andreja Žgajnar Gotvajn
OBDELAVA TEKOČIH ODPADKOV Z ELEKTROKOAGULACIJO
Datum zagovora: 21. 12. 2021

Klara SMREKAR
Mentorica: prof. dr. Ksenija Kogej
ZETA POTENCIAL IN STABILNOST MIKROEMULZIJ NA PODROČJU FARMACIJE
Datum zagovora: 23. 12. 2021

UNIVERZA V MARIBORU
FAKULTETA ZA KEMIJO IN KEMIJSKO TEHNOLOGIJO
1. januar – 31. december 2021

DOKTORATI

DOKTORSKI ŠTUDIJ – 3. STOPNJA

Klavdija ZIRNGAST
SINTEZA FLEKSIBILNIH IN TRAJNOSTNIH (BIO) KEMIJSKIH PROCESOV IN MREŽ V POGOJIH NEGOTOVOSTI
Datum zagovora: 8. 7. 2021

Maja ČOLNIK
UPORABA POD- IN NADKRITIČNE VODE ZA PREDELAVO ODPADNE PLASTIKE
Datum zagovora: 31. 5. 2021

Sarah JURJEVEC
POLIELEKTROLITNI poliHIPE HIDROGELI ZA SANACIJO ONESNAŽENIH VODA
Datum zagovora: 30. 9. 2021

Petra UTROŠA
POROZNI POLIMERI, PRIPRAVLJENI S POLIMERIZACIJO Z ODPIRANJEM OBROČA V EMULZIJI
Datum zagovora: 10.9. 2021

Jozsef MURSICS
ENERGETSKA OPTIMIZACIJA VZPOREDNO DELUJOČIH PROCESOV ZA PROIZVODNJO FORMALDEHIDA IN ZMANJŠEVANJE EMITIRANIH KOLIČIN CO2
Datum zagovora: 26. 2. 2021

Mitja BUKOVEC
RAZVOJ IN ANALIZA FRIT ZA EMAJLIRANJE ALUMINIJEVIH ZLITIN
Datum zagovora: 2. 4. 2021

MAGISTERIJI

MAGISTRSKI ŠTUDIJ – 2. STOPNJA

Larisa SUHODOLČAN
ANALIZA POVRŠINSKE KISLOSTI IN HIDROKSILACIJE MAGNETNO IZLOEITVENEGA BEMITA IN S FTIR SPEKTROSKOPIJO
Datum zagovora: 20. 10. 2021

Klara JEZERNIK
OPTIMIZACIJA SESTAVE IN SITU ELEKTRODE IN METODE ZA IZBOLJŠANJE ANALITSKE UČINKOVITOSTI DOLOČANJA KOVIN V SLEDOVIH
Datum zagovora: 23. 6. 2021

Janez SMERKOLJ
RAZVOJ AFINITETNE KROMATOGRAFIJE S PROTEINOM A ZA DOLOČANJE STOPNJE OKSIDACIJE TERAPEVTSKIH MONOKLONSKIH PROTITELES RAZREDA IgG1, IgG2 IN IgG4
Datum zagovora: 30. 8. 2021

Mihaela TALJAN
ZAMREŽENJE ENCIMOV IZ GOBE PLEUROTUS OSTREATUS
Datum zagovora: 2. 6. 2021

Patricija BANDUR
KONTROLIRANO SPROŠČANJE RESVERATROLA V SIMULACIJSKIH TEKOČINAH
Datum zagovora: 22. 9. 2021

Tea DROBNIČ
REOLOŠKA IN FIZIKALNA KARAKTERIZACIJA PREMAZNEGA KOMPOZITA IN NJEGOVIH KOMPONENT
Datum zagovora: 23. 6. 2021

Urška OSTROŠKO
SINTEZA IN KARAKTERIZACIJA FUNKCIONALIZIRANIH NANODELCEV Fe3O4/APTES/CA IN Fe3O4/APTES/PAA
Datum zagovora: 9. 9. 2021

Primož TRŽAN
DOLOČITEV OPTIMALNIH POGOJEV SUPERKRITIČNE EKSTRAKCIJE S PROGRAMOM DESIGN EXPERT IN BIO-AKTIVNIH KOMPONENT ARNIKE (ARNICA MONTANA)
Datum zagovora: 9. 9. 2021

Eva KAUČIČ
UPORABA SEPARACIJSKIH PROCESOV PRI OBDELAVI MATIČNE LUŽNICE IZ PROCESA PROIZVODNJE PSEVDOBOEMITA
Datum zagovora: 15. 12. 2021

Laura PRŠA
ENCIMSKA RAZGRADNJA CIPROFLOKSACINA V ODPADNIH VODAH
Datum zagovora: 22. 12. 2021

Klara BERLAN
IZBIRA OPTIMALNEGA POSTOPKA EKSTRAHIRANJA SIVKE (LAVANDULA) IN DOLOČITEV BIOLOŠKO AKTIVNIH KOMPONENT TER ANTIMIKROBNEGA POTENCIALA
Datum zagovora: 9. 9. 2021

Špela SLAPNIČAR
RAZVOJ IN KARAKTERIZACIJA NANOVLAKEN S KAPSULIRANIMI PROBIOTIKI
Datum zagovora: 9. 9. 2021

Katja SVETEK
RAZVOJ KATALIZATORJEV ZA MAGNETNO SEGREVANO OKSIDACIJO PROPENA V PROPILEN OKSID Z MOLEKULARNIM KISIKOM
Datum zagovora: 15. 12. 2021

Anže PEKLAR
IZOLACIJA ENCIMOV IZ PLEUROTUS OSTREATUS
Datum zagovora: 15. 12. 2021

Anja HRIBERNIK
OPTIMIZACIJA IN VALIDACIJA METODE ZA DOLOČANJE STRANSKIH PRODUKTOV FERMENTACIJE V PIVU
Datum zagovora: 2. 9. 2021

Rene GOLE
FUNKCIONALIZACIJA POROZNIH POLIMERNIH MONOLITOV S CINHONIDINOM PREKO TIOL/EN KLIK REAKCIJ
Datum zagovora: 21. 9. 2021

Tamara SAVEC
PRIPRAVA LIPOSOMOV ZA UPORABO V KOZMETIČNI INDUSTRIJI
Datum zagovora: 15. 12. 2021

Tjaša DAMIJAN
VPLIV VELIKOSTI DELCEV NA VSEBNOST POLIFENOLOV IN KANABINOIDOV V EKSTRAKTIH INDUSTRIJSKE KONOPLJE
Datum zagovora: 15. 12. 2021

Jaka KUGLER
OPTIMIZACIJA POSTOPKOV KONČNE OBDELAVE V PROIZVODNJI PIGMENTA TiO2
Datum zagovora: 22. 9. 2021

Matej FUREK
OPTIMIZACIJA PROCESA EKSTRAKCIJE FARMACEVTSKE UČINKOVINE
Datum zagovora: 15. 9. 2021

Sandra MERTIK
UPORABA KLOROVEGA DIOKSIDA ZA RAZKUŽEVANJE VODE IN DOLOČANJE OSTANKA S TERENSKO METODO
Datum zagovora: 21. 4. 2021

Alain KERHE
PRIPRAVA TANKOSLOJNIH PLASTI NA OSNOVI TiO2 V NAMENE PROTIKOROZIJSKE ZAŠČITE
Datum zagovora: 17. 2. 2021

Klara ŽVAB
RAZVOJ IN OPTIMIZACIJA HPLC METODE ZA DOLOČANJE ANTIMIKROBNIH SUBSTANC V SUHEM EKSTRAKTU LIMONE
Datum zagovora: 20. 1. 2021

Jernej LIPOVEC
ANALIZA VARNOSTI OBRATA POLIMERIZACIJE
Datum zagovora: 24. 3. 2021

Katja ZEČEVIĆ
ESTERIFIKACIJA MAŠČOBNIH KISLIN Z BIOKATALIZATORJEM VEZANIM NA MEZOPOROZNI SILIKATNI NOSILEC
Datum zagovora: 24. 3. 2021

Medea BREČKO
ŠTUDIJA IZVEDLJIVOSTI OBDELAVE ODPADNE VODE MESNE INDUSTRIJE S FLOTACIJO IN BIOLOŠKIM ČIŠČENJEM
Datum zagovora: 24. 3. 2021

Ana AMBROŽ
ODSTRANJEVANJE NEODIMIJEVIH IONOV IZ VODNE RAZTOPINE Z MAGNETNIMI NANODELCI
Datum zagovora: 21. 4. 2021

Aljaž DEGEN
SINTEZA S SILIKO FUNKCIONALIZIRANIH MAGNETNIH NANODELCEV ZA IMOBILIZACIJO PROTEINOV
Datum zagovora: 19. 5. 2021

Teja ERMENC
VPLIV POSTOPKA IZOLACIJE UČINKOVIN IZ INDUSTRIJSKE KONOPLJE (KC DORA) NA METABOLNO AKTIVNOST ČLOVEŠKIH MELANOMSKIH CELIC (WM-266-4)
Datum zagovora: 20. 1. 2021

Simona GJORGIEVSKA
IZOLACIJA IN KARAKTERIZACIJA ETERIČNEGA OLJA IZ PEŠČENEGA SMILJA (HELICHRYSUM ARENARIUM)
Datum zagovora: 17. 2. 2021

Pia KERŠIČ
KONTROLIRANO SPROŠČANJE KLOROGENSKE KISLINE IN NJENIH FORMULACIJ V SIMULACIJSKIH RAZTOPINAH
Datum zagovora: 24. 3. 2021

Rebeka KOGELNIK
IZZIVI IN POTENCIALI UPORABE PROCESA OSMOZE PRI OBDELAVI TEKSTILNIH ODPADNIH VODA
Datum zagovora: 19. 5. 2021

Rolando KRIVEC
KINETIKA ESTERIFIKACIJE MIRISTINSKE KISLINE Z UPORABO KOVINSKEGA KATALIZATORJA
Datum zagovora: 19. 5. 2021

Marina MALIĆ
BIOLOŠKA AKTIVNOST ANTIOKSIDANTOV V KONOPLJINIH EKSTRAKTIH PRI RAKU PROSTATE
Datum zagovora: 19. 5. 2021

Anja SIHER
REAKCIJE METILAMINOV Z VODIKOVIMI HALOGENIDI IN NJIHOVA UPORABA V SINTEZI KOORDINACIJSKIH SPOJIN
Datum zagovora: 21. 4. 2021

Monika DOKL
SIMULACIJA IN OPTIMIRANJE ORGANSKEGA RANKINOVEGA CIKLA ZA IZKORIŠČANJE ODPADNE TOPLOTE PRI PROIZVODNJI ALUMINIJA
Datum zagovora: 8. 4. 2021

Jerneja BABIČ
ANTIMIKROBNO DELOVANJE GRANATNEGA JABOLKA IN ASIMINE
Datum zagovora: 4. 5. 2021

DIPLOME – UNIVERZITETNI ŠTUDIJ

UNIVERZITETNI ŠTUDIJ – 1. STOPNJA

Andraž OŠTIR
SINTEZA KOVINSKIH KATALIZATORJEV Z METODO MOKRE IMPREGNACIJE
Datum zagovora: 25. 8. 2021

Nina KOPŠE
PRIMERJALNA ŠTUDIJA POGOJEV FERMENTACIJE VODNEGA KEFIRJA
Datum zagovora: 17. 11. 2021

Nika KRAJNC
DINAMIČNO OPTIMIRANJE PROBLEMOV KEMIJSKEGA INŽENIRSTVA Z UPORABO PROGRAMSKEGA OKOLJA APMONITOR
Datum zagovora: 5. 7. 2021

Tina DŠUBAN
MED KOT INHIBITOR KOROZIJSKIH PROCESOV
Datum zagovora: 9. 9. 2021

Anja KOŠAK
BAKER IMOBILIZIRAN NA POROZEN POLIPIRIDIN KOT OBNOVLJIV KATALIZATOR
Datum zagovora: 7. 9. 2021

Katja GOLE
SINTEZA IN KARAKTERIZACIJA KOVINSKIH KISLINSKIH KATALIZATORJEV
Datum zagovora: 25. 8. 2021

Anej PEVEC
PREGLED IN OCENA POTENCIALA ENERGETSKE INTEGRACIJE MED RAZLIČNIMI INDUSTRIJSKIMI PODSEKTORJI
Datum zagovora: 22. 9. 2021

Blaž ŠKOF
DOLOČEVANJE IN IZBOLJŠEVANJE INDEKSA OPERABILNOSTI ZA PROCES HIDRODEALKILACIJE TOLUENA
Datum zagovora: 22. 9. 2021

Ana PERPAR
TANIN KOT ZAVIRALEC KOROZIJE NA JEKLU
Datum zagovora: 13. 7. 2021

Nina KUGL
DOLOČEVANJE AKTIVNOSTI ENCIMOV V PIRINI MOKI PO IZPOSTAVITVI V SUPERKRITIČNEMU CO2
Datum zagovora: 2. 9. 2021

Marcel ŽAFRAN
RAZVOJ IN VALIDACIJA KOLORIMETRIČNEGA SENZORSKEGA RECEPTORJA ZA ZAZNAVANJE KVARJENJA ŽIVIL
Datum zagovora: 9. 9. 2021

Iztok MAJCEN
VPLIV RAZMERJA FUNKCIONALNIH SKUPIN PRI TIOL/EN POLIMERIZACIJI NA TERMOMEHANSKE LASTNOSTI PRODUKTOV
Datum zagovora: 2. 9. 2021

Tinkara Marija PODNAR
ANALIZA VPLIVA SUŠENJA KEFIRNIH ZRN NA ČAS AKTIVACIJE IN KVALITETO PROBIOTIČNEGA NAPITKA
Datum zagovora: 9. 9. 2021

Domen SLEMENŠEK
IN SITU FUNKCIONALIZACIJA POROZNIH POLITIOLENOV S FUNKCIONALNIMI ALKENI
Datum zagovora: 7. 9. 2021

Zala SERIANZ
DOLOČEVANJE AKTIVNOSTI NEKATERIH ENCIMOV V OLUPKIH MANGA
Datum zagovora: 9. 9. 2021

Rok KRAMBERGER
TERMOKEMIJSKO SHRANJEVANJE ENERGIJE
Datum zagovora: 2. 9. 2021

Miha FERMIŠEK
TVORBA KOORDINACIJSKIH SPOJIN MED HIDROLIZIRAJOČIMI TANINI IN FE(II)
Datum zagovora: 9. 9. 2021

Rok PUČNIK
FUNKCIONALIZIRANI MAGNETNI NANODELCI ZA ODSTRANJEVANJE TEŽKIH KOVIN IZ ODPADNIH VOD
Datum zagovora: 2. 9. 2021

Lara PLOHL
VSEBNOST VITAMINA D V FARMACEVTSKIH PRIPRAVKIH
Datum zagovora: 9. 9. 2021

Nika HOČEVAR
MODELIRANJE PROCESA REGULACIJE NIVOJA S POVRATNO – ZANČNO KASKADNO REGULACIJO IN RAZVOJ SIMULACIJSKEGA VMESNIKA
Datum zagovora: 9. 9. 2021

Tamara GAVRIĆ
UPORABA SPLETNE PLATFORME SIMSCALE ZA SIMULACIJE MEHANIKE TEKOČIN IN PRENOSA TOPLOTE
Datum zagovora: 9. 9. 2021

Ana GORIČAN
EKSTRAKT ŠIPKA KOT ZELENI INHIBITOR KOROZIJSKIH PROCESOV
Datum zagovora: 9. 9. 2021

Teja CESAR
VPLIV SHRANJEVANJA STARTER KULTURE KOMBUČE NA HITROST AKTIVACIJE IN KAKOVOST FERMENTIRANEGA NAPITKA
Datum zagovora: 2. 9. 2021

Patricija POTISK
UPORABA MEŠANIH ŠABLON ZA PRIPRAVO HIERARHIČNO POROZNIH POLIMEROV
Datum zagovora: 2. 9. 2021

Anja MEŠL
IZOLACIJA KERATINA IZ ODPADNE BIOMASE IN SINTEZA KERATINSKIH NANODELCEV
Datum zagovora: 9. 9. 2021

Ema ŠUŠTERŠIČ
SEPARACIJA VREDNIH SPOJIN IZ LUPIN GRANATNEGA JABOLKA
Datum zagovora: 9. 9. 2021

Zala MESEC
IZOLACIJA KEFIRANA IZ KEFIRJA
Datum zagovora: 2. 9. 2021

Aleksander Saša MARKOVIČ
SINTEZA ? – KONJUGIRANIH POLIMERNIH PEN Z REAKCIJAMI PRIPAJANJA
Datum zagovora: 2. 9. 2021

Gal BJELOVUČIĆ
RAZVOJ KOLORIMETRIČNEGA SENZORSKEGA RECEPTORJA ZA ZAZNAVANJE BIOGENIH AMINOV
Datum zagovora: 9. 9. 2021

Jan GIMPELJ
IDENTIFIKACIJA PREVLADUJOČIH FUNKCIONALNIH SKUPIN V PROTIBAKTERIJSKIH UČINKOVINAH
Datum zagovora: 9. 9. 2021

Sven GRUBER
RAČUNALNIŠKA SIMULACIJA SUBKRITIČNIH IN TRANSKRITIČNIH TOPLOTNIH ČRPALK
Datum zagovora: 2. 9. 2021

Tinkara OŠLOVNIK
SIMULACIJA IN PRIMERJAVA REGULACIJSKIH MEHANIZMOV ZA REGULACIJO PROCESOV Z MRTVIM ČASOM
Datum zagovora: 9. 9. 2021

Klemen ROLA
PROIZVODNJA BIOETANOLA IZ LIGNOCELULOZNE BIOMASE
Datum zagovora: 2. 9. 2021

Maj VIRANT
INKORPORACIJA PROGRAMABILNEGA LOGIČNEGA KRMILNIKA V DINAMIČNI PROCES REGULACIJE PRETOKA
Datum zagovora: 9. 9. 2021

Dea SIMONIČ
SUBCELIČNA FRAKCIONACIJA HUMANIH MONONUKLEARNIH CELIC PERIFERNE KRVI IN IZOLACIJA PROTEINOV IZ RAZLIČNIH CELIČNIH KOMPARTMENTOV
Datum zagovora: 9. 9. 2021

Andreja BEŽAN
VPLIV TRANSGLUTAMINAZE NA ORGANOLEPTIČNE IN DRUGE LASTNOSTI JOGURTA
Datum zagovora: 2. 9. 2021

David HOMŠAK
ŠTUDIJA ADSORPCIJE LIPOFILNIH SNOVI NA BENTONIT
Datum zagovora: 22. 9. 2021

DIPLOME – VISOKOŠOLSKI STROKOVNI ŠTUDIJ

VISOKOŠOLSKI STROKOVNI ŠTUDIJ – 1. STOPNJA

Lucija DOLINŠEK
STABILNOST LIZOCIMA PRI EKSTREMNIH POGOJIH
Datum zagovora: 7. 7. 2021

Maja VERDEV
ZAMREŽENJE LIZOCIMA V ENCIMSKE SKUPKE
Datum zagovora: 9. 9. 2021

Nika ATELŠEK HOZJAN
EKSTRAKCIJA AMIGDALINA IZ JEDRC KOŠČIČASTEGA SADJA IN TESTIRANJE ANTIOKSIDATIVNE AKTIVNOSTI EKSTRAKTOV
Datum zagovora: 9. 9. 2021

Klemen GRADIŠNIK
SEPARACIJA VREDNIH SPOJIN IZ OREHOVIH LUPIN S POD- KRITIČNO VODO
Datum zagovora: 2. 9. 2021

Blaž VIDOVIČ
ODSTRANJEVANJE TEŽKIH KOVIN IZ ODPADNE VODE Z UPORABO GLINENEGA ADSORBENTA
Datum zagovora: 9. 9. 2021

Borut SOLINA
MODELIRANJE OGLJIČNEGA ODTISA METILIRANE MELAMINSKE SMOLE
Datum zagovora: 9. 9. 2021

Žan TURK
PROIZVODNJA GLIKOLNE KISLINE IZ ODPADNIH PLINOV
Datum zagovora: 7. 7. 2021

Eva ROZMAN
PROIZVODNJA SEČNINE IZ ODPADNIH PLINOV
Datum zagovora: 2. 9. 2021

Urška VTIČ
PINOCEMBRIN IZ MEDU KOT POTENCIALNI LOVILEC KEMIJSKIH KARCINOGENOV – RAČUNALNIŠKI PRISTOP
Datum zagovora: 9. 9. 2021

Nina BELINA
HIDROLIZA TRIACETINA Z UPORABO ENCIMA LIPAZE
Datum zagovora: 2. 9. 2021

UNIVERZA V NOVI GORICI
FAKULTETA ZA PODIPLOMSKI ŠTUDIJ

1. januar – 31. december 2021

DIPLOME

ŠTUDIJSKI PROGRAM OKOLJE – 1. STOPNJA

Milica ČVOROVIĆ
DIPLOMSKI SEMINAR
Datum zagovora: 13. 7. 2021

USTANAVLJANJE SEKCIJE ZA OKOLJE V OKVIRU SLOVENSKEGA KEMIJSKEGA DRUŠTVA

V okviru Slovenskega kemijskega društva (http://www.chem-soc.si) se vzpostavlja Sekcija za okolje, katere osnovno poslanstvo bo spodbujanje sodelovanja, povezovanja in izmenjave izkušenj med strokovnjaki z različnih področij kemije, ki se ukvarjajo z okoljskimi tematikami, z namenom ozaveščanja javnosti pri razumevanju aktualnih okoljskih vprašanj in dogodkov. Namen Sekcije za okolje bo tudi spodbujanje pravilne uporabe kemije za ocenjevanje in reševanje okoljskih vprašanj ter obravnava pomembnih vidikov okoljske kemije, ki potrebujejo regulacijo. Poleg tega bo Sekcija za okolje spodbujala vključitev novih vsebin s področja okoljske kemije v izobraževalni sistem ter sodelovala z mednarodnim okoljskimi organizacijami.

Mesto predsednika Sekcije za okolje prevzema dr. Marko Štrok (marko.strok@ijs.si), mesto pomočnice in tajnice pa dr. Janja Vidmar (janja.vidmar@ijs.si), oba sodelavca z Odseka za znanosti o okolju, Institut »Jožef Stefan«.

Ob tej priložnosti vabimo vse strokovnjake z različnih področij kemije, ki so zainteresirani za okoljsko tematiko, da se pridružijo Sekciji za okolje in v njej aktivno sodelujejo. Ob enem bi želeli povabiti študente s področja okolja k udeležbi na letošnjih Slovenskih kemijskih dnevih (https://skd2022.chem-soc.si/), na katerih bo sodelovala tudi novoustanovljena Sekcija za okolje.

KOLEDAR VAŽNEJŠIH ZNANSTVENIH SREČANJ S PODROČJA KEMIJE IN KEMIJSKE TEHNOLOGIJE

SCIENTIFIC MEETINGS – CHEMISTRY AND CHEMICAL ENGINEERING

2022

April 2022

4 – 7	NPM-6 (NEW PHOTOCATALYTIC MATERIALS FOR ENVIRONMENT, ENERGY AND SUSTAINABILITY)/PAOT-7 (PHOTOCATALYTIC AND ADVANCED OXIDATION TECHNOLOGIES FOR WATER, AIR, SOIL AND SURFACES Ljubljana, Slovenia
Information:	https://redoxtech.com/
26	THE NITROGEN ELEMENT – SUSTAINABLE FOOD PRODUCTION? Online
Information:	https://www.euchems.eu/events/nitrogen-workshop/
25 – 30	PETROMASS 2022 - XII INTERNATIONAL MASS SPECTROMETRY CONFERENCE ON PETROCHEMISTRY, ENVIRONMENTAL AND FOOD CHEMISTRY Crete, Greece
Information:	https://www.petromass2022.com/

May 2022

25 – 27	POLYMERS 2022: NEW TRENDS IN POLYMER SCIENCE: HEALTH OF THE PLANET, HEALTH OF THE PEOPLE Turin, Italy
Information:	http://polymers2022.sciforum.net

June 2022

6 – 10	11TH EUROPEAN CONFERENCE ON SOLAR CHEMISTRY AND PHOTOCATALYSIS: ENVIRONMENTAL APPLICATIONS - SPEA11 Turin, Italy
Information:	https://www.spea11.unito.it/home
6 – 10	10TH INTERNATIONAL CONFERENCE ON MECHANOCHEMISTRY AND MECHANICAL ALLOYING Cagliari, Italy
Information:	https://income2022.it/
9 – 10	58TH SERBIAN CHEMICAL SOCIETY CONFERENCE Belgrade, Serbia
Information:	https://www.shd.org.rs
12 – 16	XLVI »ATTILIO CORBELLA« INTERNATIONAL SUMMER SCHOOL ON ORGANIC SYNTHESIS Gargnano, Italy
Information:	https://corbellasummerschool.unimi.it/

13 – 15	SYMPOSIUM ON THE INTERACTIONS BETWEEN SEDIMENTS AND WATER Piran, Slovenia
Information:	https://www.iasws2022.si/
13 – 16	4TH TRAINING SCHOOL 'MECHANOCHEMICAL SYNTHESIS AND KINETICS' Cagliari, Italy
Information:	https://www.mechsustind.eu/
23 – 24	GREEN AND UNCONVENTIONAL SYNTHESIS, APPROACHES AND FUNCTIONAL ASSESSMENT AIM 2020 (AIM 2020 ADVANCED INORGANIC MATERIALS) Bari, Italy
Information:	http://www.unconventional-aim2020-bari.it/ž
28 – July 1	26TH INTERNATIONAL SYMPOSIUM ON SEPARATION SCIENCES - ISSS 2022 Ljubljana, Slovenia
Information:	https://isss2020.si/
30 – July 2	4TH INTERNATIONAL CONGRESS OF CHEMISTS AND CHEMICAL ENGINEERS OF B&H Sarajevo, Bosnia and Herzegovina
Information:	icccebih.dktks.ba

July 2022

4 – 8	CHEMISTRY FOR CULTURAL HERITAGE - CHEMCH-2020 Ravenna, Italy
Information:	https://eventi.unibo.it/chemch2022
11 – 13	EUROPEAN CONFERENCE OF RESEARCH IN CHEMISTRY EDUCATION (ECRICE 2020) Rehovot, Israel
Information:	https://www.weizmann.ac.il/conferences/ECRICE2020/
13 – 14	TOTAL FOOD 2022: MAXIMISING VALUE FROM THE FOOD CHAIN Nottingham, UK
Information:	https://www.nottingham.ac.uk/conference/fac-sci/biosciences/total-food/index.aspx
18 – 22	SECOND INTERNATIONAL CONFERENCE ON NONCOVALENT INTERACTIONS 2021-2022 - ICNI2021 Strasbourg, France
Information:	http://icni2021.unistra.fr/

August 2022

28 - Sept 1	8TH EUCHEMS CHEMISTRY CONGRESS (ECC8) Lisbon, Portugal
Information:	https://euchems2022.eu/

September 2022

5 – 9	9TH IUPAC INTERNATIONAL CONFERENCE ON GREEN CHEMISTRY - ICGC-9 Athens, Greece
Information:	greeniupac2020.org
21 – 23	19. RUŽIČKA DAYS Vukovar, Croatia
Information:	http://www.ruzickadays.eu
21 – 23	SCS ANNUAL MEETING 2022 Portorož-Portorose, Slovenia
Information:	https://skd2022.chem-soc.si/
27 – 30	11TH CENTRAL EUROPEAN CONGRESS ON FOOD AND NUTRITION Čatež ob Savi, Slovenia
Information:	https://cefood2022.si/

October 2022

5 – 7	7 MS FOOD DAY Florence, Italy
Information:	https://www.spettrometriadimassa.it/Congressi/7MS-FoodDay/index.html
23 – 26	31ST INTERNATIONAL SYMPOSIUM ON THE CHEMISTRY OF NATURAL PRODUCTS AND 11TH INTERNATIONAL CONGRESS ON BIODIVERSITY (ISCNP31 & ICOB11) Naples, Italy
Information:	https://www.iscnp31-icob11.org/index.php

November 2022

8 – 11	SOLUTIONS IN CHEMISTRY 2022 Sveti Martin na Muri, Croatia
Information:	https://solutionsinchemistry.hkd.hr/

Acta Chimica Slovenica

Author Guidelines

Submissions

Submission to ACSi is made with the implicit understanding that neither the manuscript nor the essence of its content has been published in whole or in part and that it is not being considered for publication elsewhere. All the listed authors should have agreed on the content and the corresponding (submitting) author is responsible for having ensured that this agreement has been reached. The acceptance of an article is based entirely on its scientific merit, as judged by peer review. There are no page charges for publishing articles in ACSi. The authors are asked to read the Author Guidelines carefully to gain an overview and assess if their manuscript is suitable for ACSi.

Additional information

- Citing spectral and analytical data
- Depositing X-ray data

Submission material

Typical submission consists of:

- full manuscript (PDF file, with title, authors, abstract, keywords, figures and tables embedded, and references)
- supplementary files
  - ***Full manuscript*** (original Word file)
  - ***Statement of novelty*** (Word file)
  - ***List of suggested reviewers*** (Word file)
  - ***ZIP file containing graphics*** (figures, illustrations, images, photographs)
  - ***Graphical abstract*** (single graphics file)
  - ***Proposed cover picture*** (optional, single graphics file)
  - ***Appendices*** (optional, Word files, graphics files)

Incomplete or not properly prepared submissions will be rejected.

Submission process

Before submission, authors should go through the checklist at the bottom of the page and prepare for submission.

Submission process consists of 5 steps.

Step 1: Starting the submission

- Choose one of the journal sections.
- Confirm all the requirements of the ***checklist.***
- Additional plain text comments for the editor can be provided in the relevant text field.

Step 2: Upload submission

- Upload full manuscript in the form of a Word file (with title, authors, abstract, keywords, figures and tables embedded, and references).

Step 3: Enter metadata

- First name, last name, contact email and affiliation for all authors, in relevant order, must be provided. Corresponding author has to be selected. Full postal address and phone number of the corresponding author has to be provided.
- ***Title and abstract*** must be provided in plain text.
- Keywords must be provided (max. 6, separated by semicolons).
- Data about contributors and supporting agencies may be entered.
- ***References*** in plain text must be provided in the relevant text filed.

Step 4: Upload supplementary files

- Original Word file (original of the PDF uploaded in the step 2)
- ***List of suggested reviewers*** with at least five reviewers with two recent references from the field of submitted manuscript must be uploaded as a Word file. At the same time, authors should declare (i) that they have no conflict of interest with suggested reviewers and (ii) that suggested reviewers are experts in the field of the submitted manuscript.
- All ***graphics*** have to be uploaded in a single ZIP file. Graphics should be named Figure 1.jpg, Figure 2.eps, etc.
- ***Graphical abstract image*** must be uploaded separately
- ***Proposed cover picture*** (optional) should be uploaded separately.
- Any additional ***appendices*** (optional) to the paper may be uploaded. Appendices may be published as a supplementary material to the paper, if accepted.
- For each uploaded file the author is asked for additional metadata which may be provided. Depending of the type of the file please provide the relevant title (Statement of novelty, List of suggested reviewers, Figures, Graphical abstract, Proposed cover picture, Appendix).

Step 5: Confirmation

- Final confirmation is required.

Article Types

Feature Articles are contributions that are written on Editor's invitation. They should be clear and concise summaries of the author's most recent work written with the broad scope of ACSi in mind. They are intended to be general overviews of the authors' subfield of research but should be written in a way that engages and informs scientists in other areas. They should contain the following (see also general guidelines for article structure below): (1) an introduction that acquaints readers with the authors' research field and outlines the important questions for which answers are being sought; (2) interesting, novel, and recent contributions of the author(s) to the field; and (3) a summary that presents possible future directions. Manuscripts should normally not exceed 40 pages of one column format (font size 12, 33 lines per page). Generally, experts who have made an important contribution to a specific field in recent years will be invited by the Editor to contribute a **Feature Article**. Individuals may, however, send a proposal (of no more than one page) for a **Feature Article** to the Editor-in-Chief for consideration.

Scientific articles should report significant and innovative achievements in chemistry and related sciences and should exhibit a high level of originality. They should have the following structure:

1. Title (max. 150 characters),
2. Authors and affiliations,
3. Abstract (max. 1000 characters),
4. Keywords (max. 6),
5. Introduction,
6. Experimental,
7. Results and Discussion,
8. Conclusions,
9. Acknowledgements,
10. References.

The sections should be arranged in the sequence generally accepted for publications in the respective fields and should be successively numbered.

Short communications generally follow the same order of sections as Scientific articles, but should be short (max. 2500 words) and report a significant aspect of research work meriting separate publication. Editors may decide that a Scientific paper is categorized as a Short Communication if its length is short.

Technical articles report applications of an already described innovation. Typically, technical articles are not based on new experiments.

Preparation of Submissions

Text of the submitted articles must be prepared with Microsoft Word. Normal style set to single column, 1.5 line spacing, and 12 pt Times New Roman font is recommended. Line numbering (continuous, for the whole document) must be enabled to simplify the reviewing process. For any other format, please consult the editor. Articles should be written in English. Correct spelling and grammar are the sole responsibility of the author(s). Papers should be written in a concise and succinct manner. The authors shall respect the ISO 80000 standard [1], and IUPAC Green Book [2] rules on the names and symbols of quantities and units. The Système International d'Unités (SI) must be used for all dimensional quantities.

Graphics (figures, graphs, illustrations, digital images, photographs) should be inserted in the text where appropriate. The captions should be self-explanatory. Lettering should be readable (suggested 8 point Arial font) with equal size in all figures. Use common programs such as MS Excel or similar to prepare figures (graphs) and ChemDraw to prepare structures in their final size. Width of graphs in the manuscript should be 8 cm. Only in special cases (in case of numerous data, visibility issues) graphs can be 17 cm wide. All graphs in the manuscript should be inserted in relevant places and **aligned left**. The same graphs should be provided separately as images of appropriate resolution (see below) and submitted together in a ZIP file (Graphics ZIP). Please do not submit figures as a Word file. In **graphs**, only the graph area determined by both axes should be in the frame, while a frame around the whole graph should be omitted. The graph area should be white. The legend should be inside the graph area. The style of all graphs should be the same. **Figures and illustrations** should be of sufficient quality for the printed version, i.e. 300 dpi minimum. **Digital images and photographs** should be of high quality (minimum 250 dpi resolution). On submission, figures should be of good enough resolution to be assessed by the referees, ideally as JPEGs. High-resolution figures (in JPEG, TIFF, or EPS format) might be required if the paper is accepted for publication.

Tables should be prepared in the Word file of the paper as usual Word tables. The captions should appear above the table and should be self-explanatory.

References should be numbered and ordered sequentially as they appear in the text, likewise methods, tables, figure captions. When cited in the text, reference numbers should be superscripted, following punctuation marks. It is the sole responsibility of authors to cite articles that have been submitted to a journal or were in print at the time of submission to ACSi. Formatting of references to published work should follow the journal style; please also consult a recent issue:

1. J. W. Smith, A. G. White, *Acta Chim. Slov.* **2008**, *55*, 1055–1059.
2. M. F. Kemmere, T. F. Keurentjes, in: S. P. Nunes, K. V. Peinemann (Ed.): Membrane Technology in the Chemical Industry, Wiley-VCH, Weinheim, Germany, **2008**, pp. 229–255.
3. J. Levec, Arrangement and process for oxidizing an aqueous medium, US Patent Number 5,928,521, date of patent July 27, **1999**.
4. L. A. Bursill, J. M. Thomas, in: R. Sersale, C. Collela, R. Aiello (Eds.), Recent Progress Report and Discussions: 5th International Zeolite Conference, Naples, Italy, 1980, Gianini, Naples, **1981**, pp. 25–30.
5. J. Szegezdi, F. Csizmadia, Prediction of dissociation constant using microconstants, http://www. chemaxon.com/conf/Prediction_of_dissociation _constant_using_microco nstants.pdf, (assessed: March 31, 2008)

Titles of journals should be abbreviated according to Chemical Abstracts Service Source Index (CASSI).

Special Notes

- Complete characterization, **including crystal structure**, should be given when the synthesis of new compounds in crystal form is reported.
- Numerical **data should be reported with the number of significant digits corresponding to the magnitude** of experimental uncertainty.
- **The SI system of units and IUPAC recommendations** for nomenclature, symbols and abbreviations should be followed closely. Additionally, the authors should follow the general guidelines when citing spectral and analytical data, and depositing crystallographic data.
- **Characters** should be correctly represented throughout the manuscript: for example, 1 (one) and l (ell), 0 (zero) and O (oh), x (ex), D7 (times sign), B0 (degree sign). Use Symbol font for all Greek letters and mathematical symbols.
- The rules and recommendations of the **IUBMB** and the **International Union of Pure and Applied Chemistry (IUPAC)** should be used for abbreviation of chemical names, nomenclature of chemical compounds, enzyme nomenclature, isotopic compounds, optically active isomers, and spectroscopic data.
- **A conflict of interest** occurs when an individual (author, reviewer, editor) or its organization is in-

volved in multiple interests, one of which could possibly corrupt the motivation for an act in the other. Financial relationships are the most easily identifiable conflicts of interest, while conflicts can occur also as personal relationships, academic competition, etc. **The Editors** will make effort to ensure that conflicts of interest will not compromise the evaluation process; potential editors and reviewers will be asked to exempt themselves from review process when such conflict of interest exists. When the manuscript is submitted for publication, **the authors** are expected to disclose any relationships that might pose potential conflict of interest with respect to results reported in that manuscript. In the Acknowledgement section the source of funding support should be mentioned. The statement of disclosure must be provided as Comments to Editor during the submission process.

- **Published statement of Informed Consent.** Research described in papers submitted to ACSi must adhere to the principles of the Declaration of Helsinki (***http://www.wma.net/e/policy/b3.htm***). These studies must be approved by an appropriate institutional review board or committee, and informed consent must be obtained from subjects. The Methods section of the paper must include: 1) a statement of protocol approval from an institutional review board or committee and 2), a statement that informed consent was obtained from the human subjects or their representatives.
- **Published Statement of Human and Animal Rights.**When reporting experiments on human subjects, authors should indicate whether the procedures followed were in accordance with the ethical standards of the responsible committee on human experimentation (institutional and national) and with the Helsinki Declaration of 1975, as revised in 2008. If doubt exists whether the research was conducted in accordance with the Helsinki Declaration, the authors must explain the rationale for their approach and demonstrate that the institutional review body explicitly approved the doubtful aspects of the study. When reporting experiments on animals, authors should indicate whether the institutional and national guide for the care and use of laboratory animals was followed.
- To avoid conflict of interest between authors and referees we expect that not more than one referee is from the same country as the corresponding author(s), however, not from the same institution.
- Contributions authored by **Slovenian scientists** are evaluated by non-Slovenian referees.
- Papers describing **microwave-assisted reactions** performed in domestic microwave ovens are not considered for publication in *Acta Chimica Slovenica.*
- *Manuscripts that are **not prepared and submitted** in accord with the instructions for authors are not considered for publication.*

Appendices

Authors are encouraged to make use of supporting information for publication, which is supplementary material (appendices) that is submitted at the same time as the manuscript. It is made available on the Journal's web site and is linked to the article in the Journal's Web edition. The use of supporting information is particularly appropriate for presenting additional graphs, spectra, tables and discussion and is more likely to be of interest to specialists than to general readers. When preparing supporting information, authors should keep in mind that the supporting information files will not be edited by the editorial staff. In addition, the files should be not too large (upper limit 10 MB) and should be provided in common widely known file formats to be accessible to readers without difficulty. All files of supplementary materials are loaded separately during the submission process as supplementary files.

Proposed Cover Picture and Graphical Abstract Image

Graphical content: an ideally full-colour illustration of resolution 300 dpi from the manuscript must be proposed with the submission. Graphical abstract pictures are printed in size 6.5 x 4 cm (hence minimal resolution of 770 x 470 pixels). Cover picture is printed in size 11 x 9.5 cm (hence minimal resolution of 1300 x 1130 pixels)

Authors are encouraged to submit illustrations as candidates for the journal Cover Picture*. The illustration must be related to the subject matter of the paper. Usually both proposed cover picture and graphical abstract are the same, but authors may provide different pictures as well.

* The authors will be asked to contribute to the costs of the cover picture production.

Statement of novelty

Statement of novelty is provided in a Word file and submitted as a supplementary file in step 4 of submission process. Authors should in no more than 100 words emphasize the scientific novelty of the presented research. Do not repeat for this purpose the content of your abstract.

List of suggested reviewers

List of suggested reviewers is a Word file submitted as a supplementary file in step 4 of submission process. Authors should propose the names, full affiliation (department, institution, city and country) and e-mail addresses of five potential referees. Field of expertise and at least two references relevant to the scientific field of the submitted manuscript must be provided for each of the suggested reviewers. The referees should be knowledgeable about the subject but have no close connection with any of the authors. In addition, referees should be from institutions other than (and countries other than) those of any of the authors. Authors declare no conflict of interest with suggested reviewers. Authors declare that suggested reviewers are experts in the field of submitted manuscript.

How to Submit

Users registered in the role of author can start submission by choosing USER HOME link on the top of the page, then choosing the role of the Author and follow the relevant link for starting the submission process.

Prior to submission we strongly recommend that you familiarize yourself with the ACSi style by browsing the journal, particularly if you have not submitted to the ACSi before or recently.

Correspondence

All correspondence with the ACSi editor regarding the paper goes through this web site and emails. Emails are sent and recorded in the web site database. In the correspondence with the editorial office please provide ID number of your manuscript. All emails you receive from the system contain relevant links. **Please do not answer the emails directly but use the embedded links in the emails for carrying out relevant actions.** Alternatively, you can carry out all the actions and correspondence through the online system by logging in and selecting relevant options.

Proofs

Proofs will be dispatched via e-mail and corrections should be returned to the editor by e-mail as quickly as possible, normally within 48 hours of receipt. Typing errors should be corrected; other changes of contents will be treated as new submissions.

Submission Preparation Checklist

As part of the submission process, authors are required to check off their submission's compliance with all of the following items, and submissions may be returned to authors that do not adhere to these guidelines.

1. The submission has not been previously published, nor is it under consideration for publication in any other journal (or an explanation has been provided in Comments to the Editor).
2. All the listed authors have agreed on the content and the corresponding (submitting) author is responsible for having ensured that this agreement has been reached.
3. The submission files are in the correct format: manuscript is created in MS Word but will be **submitted in PDF** (for reviewers) as well as in original MS Word format (as a supplementary file for technical editing); diagrams and graphs are created in Excel and saved in one of the file formats: TIFF, EPS or JPG; illustrations are also saved in one of these formats. The preferred position of graphic files in a document is to embed them close to the place where they are mentioned in the text (See ***Author guidelines*** for details).
4. The manuscript has been examined for spelling and grammar (spell checked).
5. The ***title*** (maximum 150 characters) briefly explains the contents of the manuscript.
6. Full names (first and last) of all authors together with the affiliation address are provided. Name of author(s) denoted as the corresponding author(s), together with their e-mail address, full postal address and telephone/fax numbers are given.
7. The ***abstract*** states the objective and conclusions of the research concisely in no more than 150 words.
8. Keywords (minimum three, maximum six) are provided.
9. ***Statement of novelty*** (maximum 100 words) clearly explaining new findings reported in the manuscript should be prepared as a separate Word file.
10. The text adheres to the stylistic and bibliographic requirements outlined in the ***Author guidelines***.
11. Text in normal style is set to single column, 1.5 line spacing, and 12 pt. Times New Roman font is recommended. All tables, figures and illustrations have appropriate captions and are placed within the text at the appropriate points.
12. Mathematical and chemical equations are provided in separate lines and numbered (Arabic numbers) consecutively in parenthesis at the end of the line. All equation numbers are (if necessary) appropriately included in the text. Corresponding numbers are checked.
13. Tables, Figures, illustrations, are prepared in correct format and resolution (see ***Author guidelines***).
14. The lettering used in the figures and graphs do not vary greatly in size. The recommended lettering size is 8 point Arial.
15. Separate files for each figure and illustration are prepared. The names (numbers) of the separate files are the same as they appear in the text. All the figure files are packed for uploading in a single ZIP file.
16. Authors have read ***special notes*** and have accordingly prepared their manuscript (if necessary).
17. References in the text and in the References are correctly cited. (see ***Author guidelines***). All references mentioned in the Reference list are cited in the text, and vice versa.
18. Permission has been obtained for use of copyrighted material from other sources (including the Web).
19. The names, full affiliation (department, institution, city and country), e-mail addresses and references of five potential referees from institutions other than (and countries other than) those of any of the authors are prepared in the word file. At least two relevant references (important recent papers with high impact factor, head positions of departments, labs, research groups, etc.) for each suggested reviewer must be provided. Authors declare no conflict of interest with suggested reviewers. Authors declare that suggested reviewers are experts in the field of submitted manuscript.
20. Full-colour illustration or graph from the manuscript is proposed for graphical abstract.
21. ***Appendices*** (if appropriate) as supplementary material are prepared and will be submitted at the same time as the manuscript.

Privacy Statement

The names and email addresses entered in this journal site will be used exclusively for the stated purposes of this journal and will not be made available for any other purpose or to any other party.

ISSN: 1580-3155

Koristni naslovi

Slovensko kemijsko društvo
www.chem-soc.si
e-mail: chem.soc@ki.si

Wessex Institute of Technology
www.wessex.ac.uk

SETAC
www.setac.org

European Water Association
http://www.ewa-online.eu/

European Science Foundation
www.esf.org

European Federation of Chemical Engineering
https://efce.info/

International Union of Pure and Applied Chemistry
https://iupac.org/

Novice europske zveze kemijskih društev EuChemS najdete na:

Brussels News Updates
http://www.euchems.eu/newsletters/

DONAU LAB Ljubljana
Member of LPPgroup

BINDER
Best conditions for your success

Komore za testiranje baterij

Vakuumski sušilniki

Klimatske komore

Donau Lab d.o.o., Ljubljana
Tbilisijska 85
SI-1000 Ljubljana
www.donaulab.si
office-si@donaulab.com

VITAMIN D3 Krka

ZAGOTOVITE SI SONCE. **PREPROSTO.**

- **EDINI** kot zdravilo brez recepta.
- **ZAGOTOVI** priporočeni dnevni odmerek vitamina D.
- **BREZ** konzervansov, barvil in glutena.

VITAMIN D3 Krka vsebuje holekalciferol.

www.vitamind3krka.si

KRKA

PRED UPORABO NATANČNO PREBERITE NAVODILO!
O TVEGANJU IN NEŽELENIH UČINKIH SE POSVETUJTE Z ZDRAVNIKOM ALI S FARMACEVTOM.

15th International Symposium on the Interactions Between Sediments and Water

June 12 – 15, 2022

Piran, Slovenia

https://www.iasws2022.si

Jožef Stefan Institute

IASWS

National Institute of Biology

Slovensko kemijsko društvo
Slovenian Chemical Society

SLOVENSKI KEMIJSKI DNEVI 2022

21.-23. SEPTEMBER 2022

SKD2022.CHEM-SOC.SI

KONGRESNI CENTER GRAND HOTELA BERNARDIN, PORTOROŽ

Acta Chimica Slovenica

Glucose-sensitive biosensors are known as glucose-oxidase, protein, and phenyl boronic acid based systems. Sugar-sensitive polymeric particles are produced via crosslinker and monomer in one step and surfactant-free emulsion polymerization technique. Sensitivity of the polymer particles to sugar molecules is monitored in glucose/fructose rich media

Year 2022, Vol. 69, No. 1